

GEOLOGIC FRAMEWORK OF THE GULF ISLANDS NATIONAL SEASHORE

A research report submitted to:
National Park Service

Prepared By:
Dr. Chris Houser

Department of Geography
Texas A&M University
810 O&M Building
College Station, Texas
77843-3147

TEXAS A&M UNIVERSITY

OVERVIEW

This final report presents the results of almost 5 years of research conducted by the University of West Florida and Texas A&M University for the Gulf Islands National Seashore (GUIS). The research was initiated by the National Park Service following extensive barrier island washover and erosion during Hurricanes Ivan (2004) and Katrina (2006). ***The broad objective of the study is to characterize the geologic framework of the Gulf Islands National Seashore with a primary focus on the Santa Rosa and Fort Pickens Units of the park***. The specific objectives of the study are:

> **Santa Rosa and Fort Pickens Sections of GUIS**: The purpose of the proposed study is to characterize the geologic framework of the Gulf Islands National Seashore, through a geophysical survey to locate and map the underlying strata, ancient sediments, historic inlets and seafloor characteristics. In this respect, this study will be able to address one of the most exciting research challenges of our time in the geosciences: the coupling of the processes that shape the terrestrial landscape with the processes responsible for sediment erosion, deposition, and redistribution within barrier island systems.
>
> **Mississippi Islands Section of GUIS:** Describe, qualitatively and quantitatively, the extent of coastal erosion and sediment redistribution by Hurricane Katrina. This study will include the types of sediment, the thickness and extent of sediment cover, and interpreting the method of emplacement of the sediment. Subaerial and subaqueous changes to the island will also be documented through the use of LiDAR and sonar data provided by the National Oceanographic and Atmospheric Association (NOAA), and post storm bathymetric data was collected with sonar following the storm. This information will be useful in planning facilities construction with future hurricanes in mind and in identifying the magnitude of stress to natural coastal communities.

Since a majority of the park consists of barrier islands an important focus of these studies was the impact and recovery of the island system to Hurricanes Ivan and Katrina. The impact of Hurricane Katrina and the recovery of the island from that storm was the primary focus of the study in the Mississippi Islands Units of the Park. The research conducted by the University of West Florida and Texas A&M University consists of 8 independent but related studies ranging from small-scale sediment transport studies along the backbarrier and Gulf shorelines, to the regional sub-surface geology. While the majority of these studies were funded directly from the National Park Service, other studies (Chapters 5 and 8 below) were completed with other funds to the PI, but nonetheless are part of the larger geologic and geomorphological state of the island.

The studies contained in this final report have either been published in a refereed journal, are in the review process or to be submitted in the near future:

1. **Controls on Coastal Dune Morphology, Shoreline Erosion and Barrier Island Response to Extreme Storms.** Houser**,** C., Hapke, C. and Hamilton, S., (2008) Controls on Coastal Dune Morphology, Shoreline Erosion and Barrier Island Response to Extreme Storms. *Geomorphology*, 100, 223-240.[1]

2. **Evolution of Overwash Deposits and Post-Hurricane Dune Recovery Following Hurricane Katrina.** Houser, C., Hobbs, C. and Saari, B. (2008) Post-hurricane airflow and sediment transport over a recovering dune. *Journal of Coastal Research*, 24, 944-953. [2]

3. **Post-Hurricane Beach and Dune Recovery.** Houser, C., and Hamilton, S. (2009) Sensitivity of post-hurricane beach and dune recovery to event frequency. *Earth Surface Processes and Landforms*, 34, 613-628.[1]

4. **Geomorphological controls on road damage during Hurricanes Ivan and Dennis** Houser, C. (2009) Geomorphological controls on road damage during Hurricanes Ivan and Dennis. *Journal of Coastal Research*, 25, 558-568.[1]

5. **Beachface Recovery Mechanisms** Houser, C. and Barrett, G. (2009). Wave-scale changes in bed elevation of an intermediate foreshore. *Journal of Coastal Research,* SI 56, 64-68.

6. **Geologic Framework of the GUIS**. Houser, C. (*in review)* Role of ridge and swale bathymetry in barrier island transgression. Submitted to *Geomorphology,* May, 2011.

7. **Impacts of Hurricane Katrina on the Geomorphology of the Mississippi Barrier Islands.** To be submitted for review and publication in late 2011.[2]

An additional paper that is the basis of a Ms thesis remains in progress:

8. **Post-Hurricane interactions between vegetation dynamics, dune recovery and physical gradients on barrier islands**. MS thesis (B. Saari) in progress at the University of West Florida.

With the exception of the above MS thesis, the papers listed above are provided in this report. Please note that there are slight variations in the formatting of each paper, reflecting the different formatting requirements of the journals to which they were submitted.

The raw data is archived at Texas A&M University and is available on request. While the formal

[1] Copy of draft and final paper submitted to and accepted by R. Hoggard of GUIS
[2] Previously submitted as and accepted by R. Hoggard as an interm report

study and contract with the National Park Service has come to an end, the geologic characterization of the GUIS and studies of extreme storm impact and recovery continue. Specifically, the results of the present study have been extended and form the basis for the following studies and review papers funded by the National Science Foundation and Florida SeaGrant:

1. **Houser**, C., and Ellis, J. (*in press*) Morphodynamic Systems: Beach and Dune Interaction. Accepted to *Treatise in Geomorphology*, March 2011.

2. **Houser,** C., Barrett, G., and Labude, D. (*In Press*) Alongshore variation in the rip current hazard at Pensacola Beach. Accepted to *Natural Hazards*, September 2010.

3. **Houser**, C., Caldwell, N., and Meyer-Arendt, K. (*In Press*) Hot times at Hot spots: The rip current hazard at Pensacola Beach, Florida. Invited submission to refereed book *Rip Currents: Beach Safety, Physical Oceanography and Wave Modelling*, edited by Steven Leatherman and John Fletemeyer. Accepted August 2010.

4. **Houser**, C., and Sojan, M. (*2011*) Variability in foredune height depends on the alongshore correspondence of transport potential and sediment supply. *Geomorphology*, 125, 62-72.

5. **Houser**, C. (2009) Synchronization of transport and supply in beach-dune interaction. *Progress in Physical Geography*, 33, 733-746. doi:10.1177/0309133309350120

These papers are provided at the end of this report in Appendix I while copies of a recent NPS Webinar (based on presentations at the American Geophysical Union, Geological Society of America and the American Association of Geographers) is presented in Appendix II. Follow-up studies planned in the next year by MS students at Texas A&M University include: 1) comparison of beach-dune morphology between ASIS, GUIS and PINS, 2) quantification of the ability of seagrass to provide shoreline protection along backbarrier shorelines, and 3) nearshore bar morphodynamics along Santa Rosa Island.

In addition to the papers and reports listed above, the results of these studies have been presented at both national and regional conferences:

1. **Houser**, C., Hamilton, S., Meyer-Arendt, K., and Oravetz, J. (2006) EOF analysis of barrier island morphological change during Hurricane Ivan. *Coastal Sediments '07*, May 2006.

2. **Houser**, C. Response and recovery of a barrier island to extreme storms. *Geological Society of America*, Denver, Colorado, October 31-November 4, 2010.

3. **Houser**, C., Linking beach-dune interaction with barrier island transgression. *American Geophysical Union Annual Meeting*, San Francisco, December 11-17, 2010.

4. **Houser,** C., Alongshore variation in dune morphology and storm impact in national seashores depends on the correspondence of transport potential and sediment supply. *Geological Society of America: Northeast*, Baltimore, March 13-15, 2010.

5. **Houser,** C., Rip Current Hazard at Pensacola Beach. *1st International Rip Current Symposium*, Miami, Florida, February 17-19, 2010.

6. **Houser,** C., Managing the natural recovery of coastal systems following extreme storms. *Annual Meeting of the George Wright Society*, Portland, Oregon, March 2-6, 2009.

7. **Houser,** C., Wave by wave changes in the swash zone. Annual Meeting of the *Geological Society of America*, Houston, Texas, October 5-10, 2008.

8. **Houser**, C., Post hurricane beach and dune recovery. *Association of American Geographers 104th Annual Meeting*, Boston, Massachusetts, April 15-19, 2008.

9. **Houser**, C., Linking Dune morphology on a barrier island to transverse Bars on the inner shelf. *Association of American Geographers 103rd Annual Meeting*, San Francisco, California, April 17-23, 2007.

10. Meyer-Arendt, K., Oravetz, J., and **Houser**, C., Response of the Mississippi barrier islands to Hurricane Katrina. *Association of American Geographers 103rd Annual Meeting*, San Francisco, California, April 17-23, 2007.

11. Hamilton, S., and **Houser**, C., LiDAR analysis of morphological changes from Hurricane Ivan *Association of American Geographers 103rd Annual Meeting*, San Fransisco, California, April 17-23, 2007.

12. **Houser**, C. Geologic controls on Hurricane Damage and Dune Recovery. *Geological Society of America, Southeast Division Annual Meeting*, Savannah, Georgia, March 29-30, 2007.

13. Houser, C., Hobbs, C., Saari, B. Post-hurricane airflow and sediment transport over a recovering dune. International Conference on Aeolian Research, University of Guelph, Guelph, Ontario, July 24-28, 2006.

14. **Houser**, C. and Hamilton, S., Geomorphological impacts of Hurricane Ivan on Santa Rosa Island, Pensacola, Florida. *Annual General Meeting of the Canadian Association of Geographers*, London, Ontario, May 31 – June 4, 2005.

TABLE OF CONTENTS

OVERVIEW ..... **ii**

TABLE OF CONTENTS ..... **vi**

LIST OF TABLES ..... **vii**

LIST OF FIGURES ..... **viii**

STUDY FINDINGS xix

CHAPTER 1: CONTROLS ON COASTAL DUNE MORPHOLOGY, SHORELINE EROSION AND BARRIER ISLAND RESPONSE TO EXTREME STORMS **1**

CHAPTER 2: EVOLUTION OF OVERWASH DEPOSITS AND POST-HURRICANE DUNE RECOVERY FOLLOWING HURRICANE KATRINA **40**

CHAPTER 3: POST-HURRICANE BEACH AND DUNE RECOVERY **103**

CHAPTER 4: GEOMORPHOLOGICAL CONTROLS ON ROAD DAMAGE DURING HURRICANES IVAN AND DENNIS **139**

CHAPTER 5: BEACHFACE RECOVERY MECHANISMS **168**

CHAPTER 6: GEOLOGIC FRAMEWORK OF THE GUIS **202**

CHAPTER 7: IMPACTS OF HURRICANE KATRINA ON THE GEOMORPHOLOGY OF THE MISSISSIPPI BARRIER ISLANDS **244**

LIST OF TABLES

Table 1. Results of cospectral analysis between the transverse ridges at the primary length scales of 475, 750, 1450 and 4550 m and variables describing the shoreline erosion, foredune height, overwash penetration and pre-storm dune morphology factors. Shown is the coherency and the phase relationship. Highlighted relationships are statistically significant at the 95% confidence level……28

Table 2. Canonical correlation coefficients (*r*) between the pre- and post-storm profiles, with the largest coefficients (strongest relationships) highlighted……64

Table 3. Definitions for the different levels of road damage and the percent length of road within each category based on aerial and ground-based assessments……..157

Table 4. Mean grain size (mm) and predicted fall velocity (m s^{-1}) for rising, high and falling tide collected adjacent to stations 1, 3, 5 and 7……189

Table 5. Canonical correlation coefficients (*r*) between the pre- and post-storm profiles for Petit Bois Island, with the largest coefficients (strongest relationships) highlighted……..…268

Table 6. Canonical correlation coefficients (*r*) between the pre- and post-storm profiles for Horn Island, with the largest coefficients (strongest relationships) highlighted……..…285

LIST OF FIGURES

Figure 1. Map of study site showing (a) location relative to the tracks of Hurricanes Ivan and Dennis and Tropical Storm Arlene and (b) large scale map of study site showing transect locations and cuspate forelands along Santa Rosa Sound……29

Figure 2. Alongshore variation in (a) the height of the foredune before and after Hurricane Ivan and (b) the cross-shore distance of overwash penetration at 35 m intervals alongshore. Also shown in (a) is the average surge elevation……30

Figure 3. Spectral plots for (a) bathymetry ratio (E1/E2) and island width, and for (b) pre-storm E2 and the historic rate of shoreline change (1858-2001)……31

Figure 4. Comparison of cross-island profiles for the pre- and post-storm eigenvalues with strong correlations identified through canonical correlation analysis……32

Figure 5. Comparison of factor scores for the pre- and post-storm eigenvalues with strong correlations identified through canonical correlation analysis……33

Figure 6. Alongshore variation in pre- and post-storm dune height with the variation in the pre-storm E2 and post-storm E4 amplitudes shown. Two areas that experienced lateral erosion of large pre-storm dunes (positive pre-storm E4) and overwash penetration (large post-storm E2) are shown……34

Figure 7. (a) Alongshore profile of a backbarrier dune pre- and post-Ivan with (b) a photograph of the dune showing erosion on the eastern side. The location of the photograph is shown with an arrow in the alongshore profile……35

Figure 8. Interpolated bathymetry for the western section of the study site to a minimum distance of ~2 km offshore. The post-Ivan LiDAR is overlain on a satellite image to show the location of the breaches in relation to the offshore ridges and troughs……36

Figure 9. (a) Characteristic bathymetry profiles based on the factor scores of the significant eigenmodes for bathymetry. Also shown (b) is the alongshore variation in the ratio of factor loadings for the eigenmodes. A large ratio represents a gently sloped shoreface and is associated with the crest of a transverse ridge……37

Figure 10: Shoreline change rates for east-central Santa Rosa Island. a) long-term rates from 1858 to May 2004 (pre-Ivan). The long-term rates are relatively low in this portion of the island, ranging from 0.0 to -0.35 (±0.1) m/yr; b) storm related shoreline change related to the hurricanes of 2004 and 2005. Note that the vertical scales are different to accommodate the two orders of magnitude difference in change rates from the long- to short-term. The average storm-related rate of change ranged from -19.6 to -54.4 (±1.4) m/yr……38

Figure 11. LiDAR images for a representative section of the study area for (a) the pre-Ivan and (b) the post-Ivan topography. Also shown are the largest (and most representative) factors for

the pre-Ivan and post-Ivan dune transects representatively. The location of the erosion hotspots, cuspate forelands and transverse ridges (large bathymetry ratio) are also shown for the 1450 m length scale…….39

Figure 12. Location of field site within the Gulf Islands National Seashore on Santa Rosa Island in Northwest Florida. Also shown are the tracks for Hurricanes Ivan and Dennis, Tropical Storm Arlene……53

Figure 13. Aerial photographs of a representative area (transects 380-400) on Santa Rosa Island before (a) and after (b) Hurricane Ivan made landfall. Big Sabine Point is identified for reference……54

Figure 14. Representative pre- and post-storm LIDAR images from the study area…….56

Figure 15. Alongshore variation in (a) the height of the foredune before and after Hurricane Ivan and (b) the cross-shore distance of overwash penetration. The dashed line is the surge elevation…….57

Figure 16. Pre- and post-storm average cross-island profiles with major morphological features identified……58

Figure 17. Alongshore variation in dune height modeled using a 9-point moving average and the volume change between the pre- and post-storm profiles. Also shown with the arrows are the locations where breaches were identified…….59

Figure 18. (a) Alongshore profile of a secondary dune pre- and post-Ivan with (b) a photograph of the dune showing erosion on the eastern side. The location of the photograph is shown with an arrow in the alongshore profile…….60

Figure 19. Factor weightings for the first 5 eigenmodes of the (a) pre-storm morphology and (b) the post-storm morphology……62

Figure 20. Comparison of cross-island profiles for the pre- and post-storm eigenvalues with strong correlations identified through canonical correlation analysis……64

Figure 21. Alongshore variation in pre- and post-storm dune height with the variation in the pre-storm E2 and post-storm E4 amplitudes shown. Two areas that experienced lateral erosion of large pre-storm dunes (positive pre-storm E4) and overwash penetration (large post-storm E2) are shown……66

Figure 22. Backbarrier transect data for February 14- April 4, 2006……71

Figure 23. Hydrodynamic and transport data from February 19, 2006 storm. Shown are (a) Cross-shore and alongshore current velocities, (b) sediment concentration and significant wave height, and (c) net cross-shore and alongshore sediment transport…….73

Figure 24. Shown are (a) change in predicted and observed (open circle) water depth relative to MLLW, (b) change in significant wave height and peak spectral period……..74

Figure 25. Time series of suspended sediment concentration at (a) 3:00, (b) 4:30, (c) 8:30 and (d) 11:00…….75

Figure 26. (a) Location of field site within the Gulf Islands National Seashore on Santa Rosa Island in Northwest Florida. Also shown are the tracks for Hurricanes Ivan and Dennis, Tropical Storm Arlene……..80

Figure 27. Profile of instrument transect showing location of the instrument stations (S1-S6). All profile stations (S1, S2, S4 and S6) were collocated with a cylinder trap over the entire study period and a Guelph-Trent sediment trap during certain storms……...81

Figure 28. Cross island transects at the study site showing the morphology before and after Hurricane Ivan (September, 2004) and at the start of the present study (March 2006). The pre- and post-Ivan transects were created from LIDAR data collected by the USGS, while the 2006 survey was completed by the authors using transect and level……..82

Figure 29. Photograph of remnant dune looking north (from the Gulf of Mexico) showing overwash fan developing in the swale between the berm and dune……..84

Figure 30. Velocity profiles for onshore winds within 15o of normal to the dune crest. Shown in the figure are the time-averaged profiles for winds between (a) 6-7 m s-1, (b) 8-9 m s-1 and (c) 10-11 m s-1 recorded at 2 m above the crest (S42.0 m)……85

Figure 31. Time-averaged amplification (speed-up) factors for onshore (a,b) and offshore winds (c,d). Shown are the amplification factors for the seaward slope (a,c) and the landward slope (b,d)……87

Figure 32. Cross-transect variations in vegetation cover (%) and net change in surface elevation…….88

Figure 33. Variation in sediment transport from each profile station towards the end of a frontal storm on April 29, 2006…….89

Figure 34. Time averaged sediment transport measured from cylinder traps expressed as a percent of the transport recorded at the first station in the direction of flow (S1 for onshore and S6 for offshore winds). Shown are the transport rates for (a) onshore winds on April 29 and (b) offshore winds on March 24. Also shown are the pre- and post-storm transects for each storm……91

Figure 35. Velocity profiles for offshore winds within 15^{o} of normal to the dune crest. Shown in the figure are the time-averaged profiles for winds between (a) 6-7 m s^{-1}, (b) 8-9 m s^{-1}, (c) 10-11 m s^{-1} and (d) 12-13 m s^{-1} recorded at 2 m above the crest ($S4_{2.0\ m}$)……..92

Figure 36. Map of study site showing location relative to the tracks of Hurricanes Ivan and Dennis and Tropical Storm Arlene, and the proximity of the Eastern and Western study areas……127

Figure 37. Oblique aerial photographs of storm impact from Hurricanes Ivan (2004), Dennis (2005) and Katrina (2005). Shown are photographs from a cuspate headland near the center of the Eastern study area and at a narrow section of the island immediately west of the headland. Note the different perspectives of the photographs, particularly those taken along the backbarrier……128

Figure 38. Spatially-averaged profiles for the (a) Eastern and (b) Fort Pickens Units of the study area. Shown are the average profiles for May 2004 (Pre-Ivan), September 2004 (Post-Ivan), September 2005 (Post-Katrina) and July 2006……..129

Figure 39. Oblique aerial photograph of the Fort Pickens Unit of the study area (looking west towards Fort Pickens), showing remnant dunes that were originally formed along the backbarrier shoreline. The road visible in the photograph was heavily damaged during Hurricane Ivan and moved behind the remnant dunes just before Hurricane Dennis……130

Figure 40. Change in profile volume within the Eastern study section during the hurricane season (May 2004-September 2005) and during the recovery period (September 2005-July 2006)……131

Figure 41. Characteristic profiles of the Eastern study section based on the significant eigenmodes for the September 2005 and July 2006 datasets. The profile combinations exhibit the strongest canonical correlations of alongshore factor scores…….132

Figure 42. Correspondence plot for the Eastern study section showing the structure of the primary factors for the characteristic recovery profiles relative to the island width, overwash penetration distance and the offshore bathymetry. The principal axis is described by factors 1 and 5 of the recovery dataset (shoreline recovery) and the secondary axis is described by island width……133

Figure 43. Oblique aerial photographs of the Fort Pickens Unit of the study area taken in October 2006. Shown are photographs from (a) the easternmost cuspate headland (foreground of Figure 4) and (b) the breach site west of the headland. The breaches are visible in Figure 39……..134

Figure 44. Overwash fan behind the storm berm that developed following Hurricane Katrina. This particular fan from the breached area shown in Figures 4 and 8 was created during a strong frontal storm on March 9, 2006, in the middle of the recovery period. This fan continued to develop during a later frontal storm and sediment was moved to the recovering dune field by onshore winds (see Houser et al., in press b)……135

Figure 45. Characteristic profiles of the Western study section based on the significant eigenmodes for the September 2004 and July 2006 datasets. The profile combinations exhibit the strongest canonical correlations of alongshore factor scores…….136

Figure 46. Schematic showing the observed variation in response and recovery alongshore within (a) the Santa Rosa Unit and (b) the Fort Pickens Unit of the study area. The response and recovery are shown with respect to the island width (ie. cuspate headlands), offshore bathymetry (reflective or dissipative) and pre-storm dune height…….137

Figure 47. Map of study site showing (a) location relative to the tracks of Hurricanes Ivan and Dennis and Tropical Storm Arlene and (b) alignment of County Road 399 within the Gulf Islands National Seashore relative to the cuspate forelands and study transects…….158

Figure 48. Representative photographs of the different levels of damage along County Road 399. Shown are a) no damage, b) ¼ damage (part of a lane), c) ½ damage (loss of an entire lane) and d) complete damage (loss of the entire road bed. In all of the photographs, the north side of the road is on the left of the image……...159

Figure 49. Aerial photographs of road damage showing (a) a transition from 1/4 damage to no damage (b) a transition from 1/2 damage to full damage (right to left). The photograph in (a) is from transects 25 to 27 and the photograph in (b) is from transects 22 to 24……160

Figure 50. Photograph showing asphalt and gravel debris north of the road (in the background), creating a lag surface that may limit aeolian sediment transport and dune recovery. The photograph was taken at transect 40……161

Figure 51. Alongshore variation for Hurricane Ivan in a) island width, b) ratio of gently sloped to steep offshore bathymetry factors, c) foredune height, d) distance between roadway and shoreline, and d) the categories of road damage……162

Figure 52. (a) Correspondence plot showing the pre-Ivan structure of the primary factors for the environmental variables of offshore bathymetry, island (foredune) elevation and island width. Also shown (b) is the Correspondence plot for the pre-Dennis structure for the environmental variables of offshore bathymetry, island elevation and island width…….163

Figure 53. Correspondence plot showing the structure of the primary factors for (a) Hurricane Ivan and (b) Hurricane Dennis. In both cases, the principal axis (Factor 1) is described by island elevation and the axis for Factor 2 is described by the offshore bathymetry……164

Figure 54. Alongshore variation in factor coordinates with the largest factor coordinate (whether positive or negative) providing the best description of the road damage and geological controls at each transect. Shown are the factor coordinates for (a) Hurricane Ivan and (b) Hurricane Dennis……165

Figure 55. Alongshore variation in (a) island elevation, (b) distance between roadway and shoreline, and (c) the categories of road damage for Hurricane Dennis…….166

Figure 56. Post Hurricane Ivan LiDAR surface and DOQ image of a representative section of road with the alongshore variation in road damage, island elevation and offshore slope labelled……167

Figure 57. Photograph showing cross-shore deployment of pressure transducers (S1-S8) and ultrasonic distance sensors (S1-S4). Note that the stations are spaced at ~ 1 m intervals from the lower limit of the foreshore……..190

Figure 58. Scatterplot and combined calibration equation relating sensor output to measured distance between the ultrasonic distance sensor and sediment and water surface……..191

Figure 59. Time series of pressure transducer and ultrasonic distance sensor measurements of water depth. Also shown (b) is a scatterplot of the water depth measurements from both sensors over a representative burst sample……192

Figure 60. (a) Cross-shore profile and elevation change of foreshore over sampled tidal cycle and (b) time series of elevation changed at S4 as measured using the ultrasonic distance sensor and the station post……193

Figure 61. Representative time series of bed elevation and swash depths from ultrasonic distance sensor at Station 4 (S4). Shown are time series from (a) rising, (b,c) high and (d) falling tide……194

Figure 62. Histogram of elevation change measured by the ultrasonic distance sensors following passage of all swash events over the sampled tidal cycle……195

Figure 63. Sequential photographs showing uprush and start of backwash for (a,b) an erosional wave and (d,e) an accretional wave. Also shown are the time series of bed and water level elevation for both waves measured at high tide……..196

Figure 64. Normalized and ensemble averaged time series of (a) water depth, (b) depth-averaged velocity and (c) upward suspension potential at S4 averaged over 'erosional' and 'accretional' waves……..……197

Figure 65. Scatterplots of bed elevation change relative to (a) skewness gradient across S4 and the local average velocity at S4……198

Figure 66. Representative time series of bed elevation and swash excursion with wavelet spectra shown in the inset graphs…….199

Figure 67. Variation in the relative importance of infragravity to gravity wave energy along with the variation in bed elevation and a 75 point running mean of bed elevation……..200

Figure 68. Scatterplot showing relationship between the local average velocity and the concentration of advected sediment predicted based on the balance of elevation change and upward suspension potential……201

Figure 69. Santa Rosa Island, a narrow Holocene barrier island in northwest Florida, which extends from East Pass in Destin (just off map) to Pensacola Pass in the west. Also shown are the transverse ridge and swale features on the inner-shelf fronting Santa Rosa Island. The highlighted area on the regional map defines the extent of the study area presented in the remainder of the paper……232

Figure 70. (a) Dominant eigenmodes (E1 and E2) of the shoreface bathymetry representing the average ridge and swale topography respectively. Also shown is the alongshore variation in (b) the eigenmodes, (c) the eigenmode ratio (E1/E2) and the depth at 500 m offshore, and (d) island width……233

Figure 71. Pre- and post-Hurricane Ivan LiDAR imagery of cupate headlands in the Santa Rosa Unit with elevations ranging from 0 m (msl) in white to 5 m in dark red. Shown are the cuspate headlands directly landward of ridges 18 and 19 on Figure 2c……..234

Figure 72. Map of alongshore and cross-shore seismic transects of ridge #6 (see Figure 2c) fronting Pensacola Beach……235

Figure 73. Map of alongshore and cross-shore seismic transects of ridge #4 (see Figure 2c) in the Fort Pickens Unit of the study area……236

Figure 74. Map of alongshore and cross-shore seismic transects along backbarrier shoreline of ridge #18 (see Figure 2c) in the Santa Rosa Unit of the study area…….237

Figure 75. Vibracore data from Ridge 6 fronting Pensacola Beach. Shown are vibrabore data, shown in terms of broad textural classifications, from the cross-shore and alongshore transects shown on the satellite image above……238

Figure 76. Vibracore data from Ridge 4 in the Fort Pickens Unit. Similar to Figure 7, the vicbracore data from the cross-shore and alongshore transects is presented in terms of broad textural classifications……..239

Figure 77. Ground-penetrating radar transects from the narrow and wide sections of the island in the Santa Rosa Island Unit of the study area. Note that the GPR surveys have not been corrected for the relatively small elevation variation of the transect areas……..240

Figure 78. Modeled (a) average wave heights and (b) total bed elevation change for Hurricane Ivan (2004) in the Pensacola Beach section of the study area. The erosion data is presented only as erosion (blue) and deposition (brown)…….241

Figure 79. (a) Comparison of NOAA and 2006 bathymetry over cross-shore and alongshore transects presented in the above figure. Also shown is the difference between the measured and modeled profile change along both transect……242

Figure 80. Conceptual model showing the translation of the island through with respect to the transverse ridges and swales. Also shown are transport vectors showing offshore erosion during extreme storms post-storm alongshore redistribution of sediment from areas of large dunes (LD) to small dunes (SD), and washover through the narrow sections of the island (Houser et al., 2008; Houser and Hamilton, 2010) responsible for the maintenance of island form……243

Figure 81. Relationship between average pre-storm elevation and (a) post-storm elevation and (b) elevation change (post-pre elevation) for Petit Bois, Ship and Horn Islands. Also shown is the relationship for Santa Rosa Island for Hurricane Ivan……246

Figure 82. Relationship between average pre-storm elevation and (a) volume change and (b) shoreline change (post-pre elevation) for Petit Bois, Ship and Horn Islands. Also shown is the relationship for Santa Rosa Island for Hurricane Ivan……..247

Figure 83. Pre- and post-storm bathymetry for the eastern end of Petit Bois Island showing the landward (northern) migration of the nearshore terrace and loss in elevation…….248

Figure 84. Hurricane Impact levels of Sallenger (2000)…….249

Figure 85. Map of the Mississippi barrier islands……..253

Figure 8**6.** Alongshore variation in wave height and surge height at (a0 Petit Bois Island, (b) Horn Island and (c) Ship Island…….255

Figure 87. (A) Alongshore variation (by transect) in volume change for Petit Bois Island from West to East. The alongshore variation has been smoothed using a 3-point moving average. Positive change represents accretion and negative change represents erosion. (B) Alongshore variation (by transect) in shoreline position for Petit Bois Island from West to East. The alongshore variation has been smoothed using a 3-point moving average. Positive change represents accretion and negative change represents erosion……259

Figure 88. Oblique aerial photographs of morphological change to Petit Bois Island following Hurricane Katrina. Photographs were taken November 30, 2005……..260

Figure 89. Pre-storm LiDAR data for Petit Bois Island……...261

Figure 90. Post-storm LiDAR data for Petit Bois Island…….262

Figure 91. Scatter plot of alongshore variation (by transect) in island volume change with shoreline position for Petit Bois. For both variables, a positive change represents accretion and negative represents erosion…….263

Figure 92. (a) Alongshore variation in pre- and post-storm elevation and (b) the relationship

between volume change and the change in average elevation (post-pre-storm elevation)……264

Figure 93. (a) Relationship between pre-storm elevation and elevation change. Also shown (b) is the relationship between pre-storm elevation and change in profile volume……265

Figure 94. (a) Relationship between pre-storm elevation and post-storm elevation. Also shown (b) is the relationship between pre-storm elevation and shoreline change…….266

Figure 95. Characteristic (a) pre-storm and (b) post-storm cross-shore profiles for Petit Bois Island……269

Figure 96. Alongshore factor scores for the pre-storm and post-storm characteristic profiles270

Figure 97. Comparison of cross-island profiles (factor scores) for the pre- and post-storm eigenvalues with strong correlations identified through canonical correlation analysis…….271

Figure 98. (a) Characteristic offshore profiles for Petit Bois Island and (b) alongshore factor scores for the characteristic profiles……272

Figure 99. Alongshore variation in the distance of the nearshore bar offshore relative to (a) the depth to the bar crest and (b) the average pre-storm elevation of the island……273

Figure 100. Alongshore variation in the distance of the nearshore bar offshore relative to (a) shoreline change and (b) the change in profile volume…….274

Figure 101. Alongshore variation (by transect) in volume change for Horn Island from West to East. The alongshore variation has been smoothed using a 3-point moving average. Positive change represents accretion and negative change represents erosion……..275

Figure 102. Oblique aerial photographs of morphological change to Horn Island following Hurricane Katrina. Photographs were taken November 30, 2005 and all photographs from the aerial survey are provided on the accompanying compact disc……..……..276

Figure 103. Pre-storm LiDAR data for Horn Island……277

Figure 104. Post-storm LiDAR data for Horn Island……278

Figure 105. Pre- and post-storm locations of beachface ridges……..279

Figure 106. Alongshore variation (by transect) in shoreline position for Horn Island from West to East. The alongshore variation has been smoothed using a 3-point moving average. Positive change represents accretion and negative change represents erosion…….……280

Figure 107. Scatter plot of alongshore variation (by transect) in island volume change with shoreline position for Horn Island. For both variables, a positive change represents accretion and negative represents erosion……..281

Figure 108. (a) Alongshore variation in pre- and post-storm elevation and (b) the relationship between volume change and the change in average elevation (post-pre-storm elevation)……282

Figure 109. (a) Relationship between pre-storm elevation and elevation change. Also shown (b) is the relationship between pre-storm elevation and change in profile volume……..283

Figure 110. (a) Relationship between pre-storm elevation and post-storm elevation. Also shown (b) is the relationship between pre-storm elevation and shoreline change…….284

Figure 111. Characteristic (a) pre-storm and (b) post-storm cross-shore profiles for Horn Island……286

Figure 112. Alongshore factor scores for the pre-storm and post-storm characteristic profiles…… 287

Figure 113. Comparison of cross-island profiles (factor scores) for the pre- and post-storm eigenvalues with strong correlations identified through canonical correlation analysis……..288

Figure 114. (a) Characteristic offshore profiles for Horn Island and (b) alongshore factor scores for the characteristic profiles……...290

Figure 115. Alongshore variation in the distance of the nearshore bar offshore relative to (a) the depth to the bar crest and (b) the average pre-storm elevation of the island……..291

Figure 116. Alongshore variation in the distance of the nearshore bar offshore relative to (a) shoreline change and (b) the change in profile volume…….292

Figure 117. Alongshore variation (by transect) in volume change for Ship Island from West to East. The alongshore variation has been smoothed using a 3-point moving average. Positive change represents accretion and negative change represents erosion……..293

Figure 118. Oblique aerial photographs of morphological change to Ship Island Island following Hurricane Katrina. Photographs were taken November 30, 2005 and all photographs from the aerial survey are provided on the accompanying compact disc……294

Figure 119. Pre-storm LiDAR data for Ship Island……..295

Figure 120. Post-storm LiDAR data for Ship Island……296

Figure 121. (a) Alongshore variation in pre- and post-storm elevation for Ship Island……297

Figure 122. Relationship between (a) profile volume change and the change in average elevation (post-pre-storm average elevation), and (b) pre-storm average elevation and volume change……298

Figure 123. (a) Relationship between pre-storm elevation and elevation change. Also shown (b) is the relationship between pre-storm elevation and change in profile volume……299

Figure 124. Characteristic (a) pre-storm and (b) post-storm cross-shore profiles for Ship Island……301

Figure 125. Characteristic (a) pre-storm and (b) post-storm cross-shore profiles for Ship Island…….302

STUDY FINDINGS

Following are overview statements about the research conducted in both sections of the Gulf Islands National Seashore (GUIS) and the individual studies completed within those areas.

Santa Rosa and Fort Pickens Units of GUIS: As noted, the majority of this study was completed within the Santa Rosa and Fort Pickens Units of the Gulf Islands National Seashore (GUIS). The study was initiated following Hurricanes Ivan and Dennis when it was noted (by the PI) that there was considerable alongshore variability in the response and recovery of the barrier island to the storms. The first part of the study was focused on the alongshore variability of island response and recovery to the storms using LiDAR data collected before and after Hurricanes Ivan, Dennis and Katrina (Chapter 1). Sections of the island with small dunes in narrow sections of the island experienced washover to the backbarrier shoreline and breaching in some locations. Adjacent and wider areas with larger dunes, experienced limited washover penetration with most beach and dune sediment eroded offshore. The washover sediment along the backbarrier shoreline was eroded by cold fronts following the storms, with sediment deposited at the backbarrier cuspate headlands through alongshore transport (Chapter 2). Despite early re-vegetation in some of these washover corridors, there is a limited sediment supply and the proto-dunes were unstable and eroding (Chapter 2; Chapter 8). The recovery of the island in the year(s) following the storm exhibits a similar alongshore pattern, with limited beach and dune recovery in the narrow sections of the island and more rapid recovery in the wider-sections of the island fronting the backbarrier cuspate headlands (Chapter 3). The recovery of the beachface, which ultimately supplies sediment to the dune, appears to be controlled by the cross-shore migration of the nearshore bars (Chapter 5). As the nearshore bars migrate landward, the swash becomes increasingly accretional in response to the change in wave transformation within the inner-surf zone. In this respect, the recovery of the dune system (the primary control on barrier island response to extreme storms) depends on the rate of cross-shore bar migration/recovery and the distance the bars were moved offshore during the previous storm. Ultimately, the response and recovery of the beach and dune system is controlled by transverse ridge and swale morphology on the inner-shelf that contains near-horizontal mud-layers similar to the backbarrier cuspate headlands that are characterized by seagrass, brackish marsh and maritime forest (Chapter 6). ***In other words, the response and recovery of the island is***

reinforced by the transverse ridges that are themselves created by the transgression of the island during extreme storms. This geologically controlled alongshore variation in island response and recovery should be used to determine where and how to develop park infrastructure and other capital outlay (Chapter 4).

Chapter 1 *Controls on Coastal Dune Morphology, Shoreline Erosion and Barrier Island Response to Extreme Storms*: The response of a barrier island to an extreme storm depends in part on the surge elevation relative to the height and extent of coastal dune development, which can exhibit considerable variability alongshore. The morphology of the foredune and backbarrier dunes along Santa Rosa Island in northwest Florida was characterized before and after Hurricane Ivan using empirical orthogonal function analysis and related through canonical correlation analysis. The height and extent of the foredune, and the presence and relative location of the backbarrier dunes varied alongshore at discrete length scales (of ~750, 1450 and 4500 m). Cospectral analysis suggests that the variation in dune morphology is coherent with transverse ridges on the inner shelf, the sound-side cuspate headlands, and the historical and recent trends in shoreline change. Sections of the coast with little to no dune development before Hurricane Ivan were observed in the narrowest portions of the island (between headlands) and along the western edge of the transverse ridges. Overwash penetration during Hurricane Ivan tended to be larger in these areas and island breaching was common, leaving the surface close to the watertable and covered by a lag of shell and gravel. In contrast, large foredunes and the backbarrier dunes were observed at the widest sections of the island (the cuspate headlands) and at crest of the transverse ridges. Due to the large dunes and the presence of the backbarrier dunes, these areas experienced less overwash penetration and most of the sediment from the beachface and dunes was deposited within the upper-shoreface. This sediment is returned to the beachface through nearshore bar migration following the storm, such that the areas with larger foredunes and backbarrier dunes have smaller rates of historical shoreline erosion compared to areas with smaller dunes and greater transfer of sediment to the washover terrace. Since the recovery of the dunes will vary depending on the availability of sediment from the washover and beachface, it is argued that the alongshore pattern of dune morphology and the response of the island to the next extreme storm is forced by the transverse ridges and island width through alongshore variations in storm surge and overwash gradients respectively.

Chapter 2 *Evolution of Overwash Deposits and Post-Hurricane Dune Recovery Following Hurricane Katrina*: The impact of an extreme storm on a barrier island depends on the vertical geometry of the coast, which in turn depends on the extent and height of foredune development (Sallenger, 2000; Morton, 2002). The impact of an extreme storm not only depends on the foredune height, but also on the presence and relative location of secondary dunes (Houser *et al.*, *in review*). Where the primary and secondary dunes are closely spaced, overwash is restricted and sediment erosion offshore increased, analogous to having a large wide foredune. As the separation between the primary and secondary dune increases, more sediment is deposited as overwash than is eroded offshore. This redistribution of sediment during an extreme storm is an important control on the rate of dune recovery, which will ultimately determine the height and extent of the coastal dune system during the next extreme storm.

The (limited) data set suggests that sediment is transported offshore during relatively weak storms, when the ratio of wave height to water depth is small. This promotes the development of an offshore-directed current along the upper-shoreface. In contrast, waves tend to break along the seaward edge of the terrace leading to strong skewed accelerations and weak offshore currents. While cross-shore currents were important during the observed storm, the alongshore currents are equally strong despite the almost shore-perpendicular winds. It is concluded that with more oblique winds, transport will become increasingly directed alongshore, in the direction of the cuspate forelands. This suggests that there is a link between the erosion of overwash sediment and the development (or at least maintenance) of the cuspate forelands

For both onshore and offshore winds the wind flow structure over the dune reflects a balance between topographic forcing towards the crest and increased drag from the vegetation. However, the non-uniform adjustment of onshore winds across the seaward slope suggests that there may be boundary layer adjustment seaward of the dune. Sediment transport is limited during onshore winds by elevated storm tides that overtop the berm and flood the (human-altered) swale immediately seaward of the dune. The sediment supply remains limited by the flooding and elevated watertable, despite the fresh supply of sediment provided in the overwash fans deposited during these events. The lack of sediment input from the beachface forces the saltation cascade to be initiated at the toe of the dune seaward slope, independent of variations in wind speed and vegetation cover over the seaward slope. This leads to sediment loss along the seaward slope and the migration of the dune to the north. Sediment is provided to the dune

during offshore winds, despite the presence of a lag surface on the overwash terrace. In this respect, the overwash terrace represents an important supply of sediment for the recovery of the dunes, at least in the time between the storm and the recovery of the beachface and backshore (not observed in this study), which will increase both the availability of sediment and the fetch for winds directly or obliquely onshore. While the results of this study are time and site-specific they do suggest that limits to sediment supply, including human-altered features, can delay post-hurricane dune recovery and can potentially lead to a destabilization of the remnant dunes.

Chapter 3 *Post-Hurricane Beach and Dune Recovery:* The recovery of Santa Rosa Island in northwest Florida is characterized following Hurricane Katrina (September 2005), which was preceded by Hurricanes Ivan (2004) and Dennis (2005), and Tropical Storm Arlene (2004) within the span of a year. Beach and dune recovery were quantified to the east and west of Pensacola Beach through a comparison of LiDAR data collected immediately following Hurricane Katrina and in July 2006 after almost a year of recovery. East of Pensacola Beach, the shoreline retreated by an average of 64 m during the 2004/2005 hurricane season and recovered by an average of 19 m. To the west of Pensacola Beach, the shoreline retreated by an average of 30 m, and while no significant shoreface recovery was observed, the presence of vegetation on low-profile dunes promoted backshore accretion. Using Empirical Orthogonal Function (EOF) analysis, it is found that shoreface recovery in the east and backshore accretion in the west occurred at the widest sections of the island where the pre-storm profile volume had been relatively large and overwash penetration was at a minimum. The narrow sections of the island (between cuspate headlands) had a smaller profile volume before the storms, leading to greater overwash penetration and in some cases island breaching, which limited the volume of sediment available for shoreface recovery. Through correspondence analysis it is found that the alongshore variation in recovery is not only related to the island width, but also the offshore bathymetry, height of the pre-storm dunes and the washover penetration. It is argued that the relative importance of vertical and horizontal accretion affects the recovery of the dune system, such that the recovery is forced and the alongshore variations in storm impact observed during Hurricane Ivan will be reinforced during subsequent storms.

Chapter 4 *Geomorphological controls on road damage during Hurricanes Ivan and Dennis*: County Road 399 along Santa Rosa Island in Northwest Florida was largely impassable following Hurricanes Ivan and Dennis, but the damage was highly variable alongshore, ranging from areas with little or no damage to areas where the road was completely breached. Damage was categorized and correspondence analysis was used to examine how these levels of damage were affected by the proximity of the road to the shoreline, the elevation and width of the island and the offshore bathymetry. The pre-storm elevation and offshore bathymetry exhibit a correspondence with island width but with an opposite relationship; a gently sloping shoreface does not correspond with a large pre-storm elevation. In this respect, the variables can have either a competing or a compounding impact on the road depending on the local combination. Sections of road with little to no damage were located close to the shoreline and associated with an above average island elevation (large foredunes or berm). These areas tended to be located in wider sections of the island and equally distributed between areas with a steep and a gentle offshore profile. During Hurricane Ivan, sections of the road that sustained major damage or were completely destroyed tended to be in narrow sections of the island where the offshore profile was steep, while half-damage was associated with a gently sloping bathymetry. In contrast, major damage during Hurricane Dennis occurred in areas where the road was located in the backbarrier where the pre-storm elevation of the island was relatively low and half-damage occurred in the narrow sections of the island where the offshore bathymetry was steep. Based on the observed relationships it is concluded that damage to the road is forced by the island geomorphology and that area where the road received extensive damage will continue to be areas of concern

Chapter 5 *Beachface Recovery Mechanisms:* Wave-scale changes in bed elevation are measured using ultrasonic distance sensors within the high tide swash zone of an intermediate foreshore. The calibrated distance sensors can measure changes in bed elevation of ~0.1 mm, thereby allowing for grain-scale changes to be recorded following the passage of individual swash events. Changes in bed elevation are examined relative to the depth-averaged Eularian flow velocity estimated using pressure transducers at 8 fixed stations equally spaced across the foreshore. Bed elevation is found to vary at infragravity frequencies but is dominated by much larger (centimeter-scale) variations at lower frequencies in response to the time-varying balance

of gravity and infragravity wave energy. No statistically significant relationship is observed between the change in bed elevation and the higher order moments of the velocity as would be expected from an energetics model for either bedload or suspended load. Balancing the bed elevation change with the suspension potential (u^3) provides an estimate of the advected sediment contribution, which is found to be on the same order of magnitude as the amount of locally suspended sediment. Accretion is associated with breaking on the innermost bar and lower foreshore, leading to swash bores with a relatively strong suspension potential during the uprush, and the landward advection of sediment with the time-averaged velocity. Erosion is associated with breaking on the foreshore and steeply faced swash bores that have a strong suspension potential during the uprush, but also have a strong seaward-directed transport of sediment with the backwash. In general, changes in bed elevation within the upper swash zone of this intermediate beach are a balance between the upward suspension potential (*S*) and the amount of sediment settling out of the water column after being advected landward with the advancing swash.

Chapter 6 *Geologic Framework of the GUIS*: As demonstrated in a number of recent studies, the shoreface of Santa Rosa Island in northwest Florida is characterized by a ridge and swale bathymetry that force an alongshore variation in beach and dune morphology. The alongshore variation in dune morphology in turn controls island response to and recovery from tropical storms and hurricanes, and is therefore, an important control on island transgression with relative sea level rise. A combination of field sampling, modeling and remote sensing is used in the present study to describe the geologic framework of Santa Rosa Island and to elucidate on the origins and maintenance of the shore-attached ridge and swale bathymetry. Shore-parallel seismic surveys reveal strong near-horizontal reflectors through the ridges at depths consistent with thick backbarrier muds extracted from vibracores taken across and along the ridges. Near-horizontal reflectors were also identified in ground-penetrating radar (GPR) surveys between the ridges and backbarrier cuspate headlands, but were not present in the narrow sections of the island landward of the swales. Continuation of the seismic surveys in the backbarrier also reveal near-horizontal reflectors at the cuspate headlands that are characterized by seagrass beds, salt marsh and maritime forest, and an absence of horizontal reflectors between headlands where the shoreline is dominated by washover deposits. Wave modelling suggests that the cuspate

headlands are the littoral endpoints for sediment eroded from the washover fans during frontal storms and transported alongshore as transverse bars. It is argued that the ridge and swale bathymetry is a transgressive surface resulting from the cuspate headlands along the backbarrier shoreline. Results of the wave modelling further suggest that the ridge and swale bathymetry is maintained through the transport of sediment from the swales to the ridges during large storms. In this respect, maintenance of the ridge and swale morphology reinforces the position of the backbarrier cuspate headlands ultimately responsible for the development of the ridge and swale morphology of the shoreface. The alongshore variation in beach and dune morphology on this island is the expression of this large-scale feedback and suggests a tow-down model in which meso-scale processes and landforms depend on the geologic context.

Chapter 7: *Impacts of Hurricane Katrina on the Geomorphology of the Mississippi Barrier Islands*: On all three islands, the morphological impact of Hurricane Katrina depended on the pre-storm average elevation as predicted by the Sallenger (2000) model of hurricane impacts. Specifically, the shoreline change, overwash penetration (see Morton, 2007) and volume change were inversely related to the pre-storm average elevation (Figures 1 and 2). The sediment eroded from the areas of higher average elevation (during swash and dune impact) was deposited on the shoreface as a nearshore bar. In these areas, the backbarrier island morphology remained intact, fronted by a short overwash terrace. In areas where the average pre-storm elevation was at a local minimum, the island experienced overwash early in the storm (ie. limited swash and dune impact), leading to sediment losses to the backbarrier, with some sediment deposited in the sound. These areas had limited bar development.

Some of the greatest change in island morphology occurred at the eastern ends of Horn and Petit Bois Islands and at both ends of Ship Island. The eastern end of each islands were eroded and there was a reorientation of the island to the dominant wave direction (from the SE). One of the most dramatic changes (outside the loss of land on Ship Island) was the migration of the spit terraces on the eastern end of Petit Bois Island. Based on 2001 NOAA bathymetry data, it appears that the spit terrace decreased in elevation by ~1.5 m and migrated to the north by ~315 m (Figure 3). As the nearshore bar on this terrace continues to migrate landward (to the north), it is anticipated that a small spit will emerge on the terrace as was present in the 2001

bathymetry. In contrast, the western end of Petit Bois and Horn Islands accreted (in volume and shoreline position) through alongshore sediment delivery from the east.

Based on the results of this study, there was little change in the sediment volume for Petit Bois and Horn Islands. Most of the sediment eroded from the beachface and dune systems was deposited on the shoreface as bars and recovery will depend on the onshore migration of these features. The length of time for bar migration and beachface recovery along the Gulf Coast remains poorly understood. Sediment volume on Petit Bois and Horn Islands was only lost from the islands were the overwash terraces extended to backbarrier shoreline. This sediment is most likely lost from the system through cold front erosion, although it is possible that the sediment is distributed alongshore. In contrast, significant changes in volume were observed on Ship Island due to the lower elevation of the island were it was eroded during Hurricane Camille and only partly recovered and due to the higher storm surge and wave height on the island. The sediment was deposited along the backbarrier shoreline and into Mississippi Sound, which will limit the potential for post-storm recovery.

Forthcoming Thesis*: Post-Hurricane interactions between vegetation dynamics, dune recovery and physical gradients on barrier islands:* [This is a draft abstract from B. Saari's MS thesis that will be completed in Fall 2011 and will be made available to the GUIS and submitted for peer review] Several hurricanes and tropical storms have made landfall in Northwest Florida in 2004 and 2005, significantly altering the morphology of the barrier island. The impact of the next storm depends on the ability of the dunes to re-develop in height and extent. The environmental gradients on Santa Rosa Island were examined after the island was overwashed and eroded during Hurricanes Ivan and Dennis. The environmental gradient in wind speed, salt spray and sediment movement were measured for a one month period at sites that are representative of the range of hurricane changes to the island morphology (from no impact to breeches). Preliminary results suggest that strong environmental gradients exist and that the gradients are significantly different between sites, largely in response to the pattern of vegetation. This suggests that the level of impact, and the resulting distribution of vegetation, affects the rate and pattern of dune recovery. In other words, the level of storm impact defines the aeolian transport gradients and the rate of dune recovery and thereby reinforces the geologic control on island morphology and transgression.

CHAPTER 1

Controls on Coastal Dune Morphology, shoreline erosion and Barrier Island Response to Extreme Storms

Chris Houser

Department of Environmental Studies
University of West Florida
11000 University Parkway
Pensacola, Florida
32514

Cheryl Hapke

U.S. Geological Survey, Coastal Field Station
339 Woodward Hall, Dept. of Geoscience
University of Rhode Island
Kingston, Rhode Island
02881

Stuart Hamilton

Department of Geography
University of Southern Mississippi
Walker Science Building
Hattiesburg, Mississippi 39406

ABSTRACT

The response of a barrier island to an extreme storm depends in part on the surge elevation relative to the height and extent of coastal dune development, which can exhibit considerable variability alongshore. The morphology of the foredune and backbarrier dunes along Santa Rosa Island in northwest Florida was characterized before and after Hurricane Ivan using empirical orthogonal function analysis and related through canonical correlation analysis. The height and extent of the foredune, and the presence and relative location of the backbarrier dunes varied alongshore at discrete length scales (of ~750, 1450 and 4500 m). Cospectral analysis suggests that the variation in dune morphology is coherent with transverse ridges on the inner shelf, the sound-side cuspate headlands, and the historical and recent trends in shoreline change. Sections of the coast with little to no dune development before Hurricane Ivan were observed in the narrowest portions of the island (between headlands) and along the western edge of the transverse ridges. Overwash penetration during Hurricane Ivan tended to be larger in these areas and island breaching was common, leaving the surface close to the watertable and covered by a lag of shell and gravel. In contrast, large foredunes and the backbarrier dunes were observed at the widest sections of the island (the cuspate headlands) and at crest of the transverse ridges. Due to the large dunes and the presence of the backbarrier dunes, these areas experienced less overwash penetration and most of the sediment from the beachface and dunes was deposited within the upper-shoreface. This sediment is returned to the beachface through nearshore bar migration following the storm, such that the areas with larger foredunes and backbarrier dunes have smaller rates of historical shoreline erosion compared to areas with smaller dunes and greater transfer of sediment to the washover terrace. Since the recovery of the dunes will vary depending on the availability of sediment from the washover and beachface, it is argued that the alongshore pattern of dune morphology and the response of the island to the next extreme storm is forced by the transverse ridges and island width through alongshore variations in storm surge and overwash gradients respectively.

Keywords: Hurricane Ivan, dune, shoreline erosion, overwash, barrier island

INTRODUCTION

The height and extent of foredune development relative to the storm tide elevation is a primary control on the response of a barrier island to extreme storms (Thieler and Young, 1991; Sallenger, 2000; Morton, 2002; Houser et al., 2007). The impact of Hurricane Alicia on Galveston Island, Texas was magnified by the absence of a protective foredune that had been eroded three years earlier during Hurricane Allen and had not had sufficient time to recover (Morton and Paine, 1985). The presence and relative location of backbarrier dunes also affects the impact of an extreme storm and the redistribution of sediment between overwash deposits and erosion offshore (Houser et al., 2007). Where the primary and backbarrier dunes are closely spaced, overwash penetration is reduced and eroded sediment is deposited on the shoreface - a situation that is analogous to having a large wide foredune. More sediment is deposited along the backbarrier by overwash as the separation distance between the primary and backbarrier dune increases. The ability of coastal dunes to recover and the morphological response to the next storm depends on the availability of sediment from the overwash (Leatherman 1976; Armon, 1979; Leatherman, 1979) and beachface (Psuty, 1992). Even if sediment is available from these sources, foredune recovery is only initiated when vegetation is able to re-establish with sufficient density and coverage to promote sediment deposition (Snyder and Boss, 2002).

The response and recovery of a barrier island is further complicated by alongshore variations in dune height (Wright et al., 1970; Morton, 2002; Gares and White, 2005l Stockdon et al., 2007) and island width (Morton, 2002), which can influence overwash and localize breaching. While dunes along Cape Hatteras are relatively continuous, variations in dune height (in excess of 8 m) have been noted at scales of kilometers to tens of kilometers (Elko et al., 2002). Similar variations in shoreline response (erosion and deposition) have also been documented (Terwindt and Battjes, 1990; Morton et al., 1995), but the mechanisms responsible for this variability remains poorly understood. Several studies suggest that localized coastal response can be forced by the geologic framework and offshore bathymetry (Demarest and Leatherman, 1985; Kraft et al., 1987; Pilkey et al., 1993; Riggs et al., 1995; Schwab *et al*., 2000; McNinch, 2004; Browder and McNinch, 2006; Schupp et al., 2006; Stockdon et al., 2007). For example, "hotspots" of shoreline change can develop in response to gradients in alongshore transport as a result of wave refraction/diffraction around bathymetric highs or lows (e.g. O'Reilly and Guza, 1993; Bender and Dean, 2003; Schupp et al., 2006). Schupp *et al*. (2006)

have shown that shoreline variability is highly correlated (with a lag) to shore-oblique ridges, which in turn are correlated with Pleistocene gravel outcrops. Since beach width and budget affect the availability of sediment to the foredune (Psuty, 1992; Bauer and Davidson-Arnott, 2003), it is reasonable to expect that local-scale variations in beach width will be mirrored in the dune morphology.

Spatial variation in island response to a storm can lead to similar variations in the supply of sediment and vegetation growth. In breached areas, the recovery of the dune system can be limited by the presence of moisture (Belly, 1964; Hotta et al., 1984; Sherman et al., 1998; Cornelis et al., 2004; Wiggs et al., 2004; Davidson-Arnott et al., 2005) and lag deposits (Nickling and McKenna Neuman, 1995; McKenna Neuman, 1998). Burial tolerant vegetation is preferentially selected within overwash and breach areas (Stallins and Parker, 2003), which promotes the development of dunes with limited relief (Stallins, 2005). As noted, surge water may be forced into the intervening areas of low elevation, which can become washover conduits (Wright et al., 1970; Morton, 2002; Gares and White, 2005), such that the dune field tends to develop as a mosaic of alongshore patches that vary in age and composition (Stallins and Parker, 2003). In this respect, the dunes can reinforce alongshore patterns in overwash and breaching during subsequent storms (Stockdon *et al.*, 2007; Gibeaut et al., 2002; Morton and Sallenger, 2003). Due to the importance of vegetation to topographic development, Stallins (2005) describes this biogeomorphic feedback as an adaptive system. This classification does not account for geologic controls on storm impact and dune development, which create a forced variation in dune morphology and vegetation.

While alongshore variations in coastal dune morphology have been described (Elko et al., 2002; Gibeaut et al., 2002; Stallins and Parker, 2003), the controls on this variations are not well understood. In recent years, Santa Rosa Island in northwest Florida has been impacted by Hurricane Ivan (2004), Tropical Storm Arlene (2005), Hurricane Dennis (2005) and Hurricane Katrina (2005). During Hurricane Ivan, Santa Rosa Island was within the Northeast quadrant of the storm and subject to surge heights in excess of 3 m. The island morphology changed from a discontinuous foredune backed by hummocky backbarrier dunes and maritime forest (at the bayside cuspate headlands) to washover terraces at the headlands and sheetwash corridors between headlands. However, the island response (Houser et al., 2007) and impact to infrastructure (Houser, *in review*) exhibited considerable variability alongshore at length scales

consistent with the spacing of the cuspate headlands. The aim of this study is to describe the statistical relationship between dune morphology, the historic and storm-related rates of shoreline retreat (hotspots) and bathymetric features alongshore Santa Rosa Island. The statistical relationship between offshore bathymetry and storm impact (including shoreline erosion) are well established in general (McNinch and Leuttich, 2000; Cooper and Navis, 2004; McNinch, 2004; Schupp et al., 2006), but have not been described along the Central Gulf Coast or in relation to coastal dune morphology.

STUDY SITE

Santa Rosa Island is a narrow sandy Holocene barrier island extending 96 km from East Pass near Destin to Pensacola Pass in the west (Figure 1). It is the second-longest barrier island on the U.S. Gulf Coast, and is separated from a higher standing barrier complex of late Pleistocene origin by Santa Rosa Sound. While the origin of the island has been attributed to the erosion of a central Pleistocene "core" and longshore redistribution of sediments (Otvos, 1982), others attribute longshore sediments derived by bluff erosion east of Destin as contributing most to the island's formation (Kwon, 1969; Stone, 1991; Stone et al., 1992; Stone & Stapor, 1996). Stone et al. (1992) argue that there is a second source of sediment near the center of the study site resulting from an increase in fetch length and wave energy. The island also experiences back-barrier shoreline erosion due to wind-driven waves generated by frontal winds between October and April. As a result, the roll-over effect commonly associated with transgressive island systems is largely absent. Overwash deposits that develop during intense hurricanes are quickly eroded by the frontal winds and redistributed alongshore within small littoral cells bounded by the cuspate headlands with a spacing of ~1400 m along Santa Rosa Sound (unpublished data). In spite of hurricanes in 1906, 1916, and 1926 (when Santa Rosa Island was unpopulated), the island's shoreline position remained relatively stable from 1920 to 1993 (Foster et al., 1999; Stapor, 1975), especially east of Pensacola Beach.

Prior to Hurricane Ivan, the dunes on the island formed a ridge and swale complex, with the primary dune parallel to the shoreline. The aeolian sediment drift potential (DP), calculated from the modified Fryberger Method (Lettau and Lettau, 1978), suggests that the resultant drift potential since Hurricane Ivan is oriented onshore (to the NW, 334^{o}). The ratio of the resultant drift potential to the total drift potential for this period is 0.24, which suggests an obtuse bimodal

wind regime (Fryberger, 1979) and is a reflection of the bimodal (NW-SE) frontal winds through the winter and spring and predominately south winds through summer. Winds from the Northwest have a relatively long fetch on the overwash fans, but transport by offshore winds is limited by a lag surface consisting of shells, gravel and road debris that develops following an extreme storm (Houser *et al*., *in press*).

Stone (1984) describes a series of offshore sinusoidal ridges and troughs oriented northwest-southeast, in alignment with the De Soto submarine canyon further to the east. While these features were also described by Hyne and Goodell (1967), little is known about how these shore-transverse ridges developed. Based on studies from Outer Banks (McNinch and Leuttich, 2000; Cooper and Navis, 2004; McNinch, 2004; Schupp et al., *in press)*, it is hypothesized that these bathymetric features affect the attenuation of wave energy incident to the coast and can lead to areas of high energy where the offshore profile is reflective (steep) and low energy where the offshore profile is dissipative (gentle).

METHODOLOGY

LiDAR data

LiDAR (Light Detection and Ranging) is a mapping technology that is increasingly used for coastal change studies. It is ideal for such analyses in that it provides spatially dense and accurate topographic data (see Irish & White, 1998; Woolard & Colby, 2002; Sallenger et al., 2004; Zhang et al., 2005). Data are collected with aircraft-mounted lasers capable of recording elevation measurements at a rate of 2000 to 5000 pulses per second and have a vertical precision of 15 cm. LiDAR data of Santa Rosa Island was collected before and (immediately) after Hurricane Ivan in May and September 2004 respectively. The pre-Ivan LiDAR dataset is a product of the USACE and Optech Inc., which is more commonly known as the Compact Hydrographic Airborne Rapid Total Survey (CHARTS). This system is a combination of a 1000 Hz hydrographic sensor, a 10,000 Hz topographic sensor and an image sensor working in unison. The post-Ivan LiDAR dataset is a product of the NASA sensor known as EAARL (Experimental Advanced Airborne Research LiDAR). The EAARL system was operated by a consortium of the USGS and NASA. Both datasets were obtained from the USGS Center for Coastal and Watershed Studies.

Analysis of the LiDAR data followed closely those of Young and Ashford (2006). All data was first converted from raw xyz data in ArcSDE feature classes. These feature classes were then combined into one feature class and clipped to the study area polygon. An inverse distance weighting operation (IDW) was utilized to interpolate the raw point data into pre-storm and post-storm elevation models. The IDW power was set to four to negate distant points and the search radius limited to the closest eight points, again to negate distant neighbors. The pre-Ivan IDW root-mean-square-error (RMSE) was 0.34 and the post-Ivan RMSE was 0.54. The post-storm RMSE is higher than the pre-storm error due to the lower density of survey points in the former. The RMSE should not be confused with the accuracy of the sensor; the vertical accuracy of LiDAR is approximately ±15 cm and the horizontal accuracy is < 1m (Sallenger et al., 2003).

Offshore Bathymetry

While the impact of Hurricane Ivan on the offshore bathymetry was not explored in this study, a series of shore-parallel and shore-perpendicular surveys were conducted using a 200 kHz fathometer to determine if the inner shelf morphology has changed as a result of Hurricanes Ivan, Dennis and Katrina. All data were spatially referenced in real-time using RTK-GPS and the seafloor depths were heave and tide-corrected to mean low water (MLW) using measured tides. The cleaned-data was interpolated using inverse distance weighting at a spacing of 1 m. Subsequent studies are planned to examine the characteristics of these ridges using high-resolution sidescan-sonar, seismic reflection and surface sediment analysis.

Historical and Recent Rates of Shoreline Change

The historical shoreline change rates used for this analysis are derived from both historical maps and recent LiDAR data, which were available for download from Miller et al. (2004). These data consist of three historical shorelines that were digitized from georeferenced NOS T-sheets, and represent the field interpretation of a high water line (HWL) on the beach (Shalowitz, 1964). The dates of the map-derived shorelines are 1858, 1934, and 1978. The modern shorelines are mean high water (MHW) shorelines derived from LiDAR data. For the long-term (~150 yr) shoreline change rate, the most recent shoreline position used is from May 2004 LiDAR data. Morton et al. (2004) used the historical and 2001 data to produce shoreline

change rates for the entire Gulf of Mexico, including Santa Rosa Island. However, there are several distinct differences between our analysis and theirs. We recalculated the shoreline change rates using the Digital Shoreline Analysis System (DSAS; Thieler et al., 2005), producing rates on shore-perpendicular transects spaced at 35 m intervals, instead of the 50m used by Morton et al. (2004), and included a fifth shoreline, from May 2004 in the analysis. Additionally, the earlier analysis did not account for the bias in the data that exists as a function of using different shoreline proxies, a HWL versus a MHW. A HWL shoreline is higher on the beach than the MHW shoreline which does not take total water level (wave run-up and tide height) into account. If a correction is not applied, the shoreline change rates will have an accretionary bias. The proxy bias was calculated using methods developed by Ruggiero et al. (2003) and Moore et al. (2006), and ranged from 5.0 – 10.2 m. The application of the proxy bias results in an overall increase in the erosion rate, which averaged -0.4 m/yr (-0.3 m/yr without the proxy-bias adjustment) for the portion of Santa Rosa Island extending from Pensacola Pass to Navarre Beach..

In order to assess storm-driven shoreline change, we acquired pre-Ivan (May 2004), post-Ivan (Sept. 2004) and post-Katrina (Sept. 2005) LiDAR data for Santa Rosa Island, from Pensacola Pass to Navarre Beach. Shorelines had been extracted from the pre- and post-Ivan LiDAR data by the USGS Center for Coastal and Wetland Studies (Stockdon, et al. 2002). The shoreline from the most recent (post-Katrina) LiDAR data was extracted by researchers at the USGS Woods Hole Science Center (WHSC) specifically for this analysis. We used the same 2300 transects to calculate short-term (May 2004 to September 2005) storm-driven shoreline change rates as were used in the long-term, pre-storms analysis. However, due to numerous gaps in the post-storm shoreline from island breaching and washover, only about 60% of the transects crossed all three LiDAR shorelines.

Statistical Analysis

Changes to the barrier morphology were quantified by comparing the LiDAR images collected immediately before and after landfall using cross-shore transects spaced 35 m alongshore. In order to provide overlap between the shoreline change, dune morphology and offshore bathymetry, cross-island profiles were extracted from the LiDAR data along 49 transects. EOF analysis was used to identify alongshore recurring patterns in the geometry of the

island, which includes both the height and width of the primary dune and the presence of backbarrier dunes. Only a limited number of factors are extracted from the data to explain most of the variance, and the variance explained by successive factors decreases monotonically. In this respect, EOFs can be used as a data reduction technique or a method to separate 'signal' and 'noise'. Data matrices *X* containing cross-island elevation and offshore bathymetric data (rows) from 49 transects (columns) are represented through matrices involving the eigenvalues and the spatial EOFs. The variance associated with the eigenmodes, which are the orthonormal column vectors in *E* and *A*, are given by the eigenvalue *L*. The EOFs are obtained by solving an eigenvalue problem involving the correlation matrix based on *X*.

The relationship between the primary modes of the pre- and post-storm topographic data is examined through canonical correlation analysis (CCA). This test is used to investigate whether or not there are patterns that occur simultaneously in two different data sets and to describe the nature of those patterns (see Larson et al., 2000; 2001). Using two data sets *Y* and *Z*, the transformed variables in matrices *U* and *V* have maximally correlated column vectors for the same index and zero correlation for differing indices. In the present study, the correlation between the spatial amplitudes (factor scores) from the pre- and post-storm variable sets is termed the canonical correlation. The first canonical correlation is the largest and the magnitudes decrease sequentially.

The relationship between the pre- and post-storm dune morphology and the offshore bathymetry and island width was examined using cross-correlation analysis (see Schupp et al., 2006). A negative lag between variables suggests that the response of the dependent variable (*e.g.* dune height) is to the east of the independent variable (*e.g.* island width), and a positive lag suggests that the dependent variable is to the west of the forcing variable. The 175 m spacing of transects used in the analysis is beyond the range of statistically significant ($\rho<0.05$) autocorrelation in the morphological data. While cross-correlation is commonly used to examine relationships between morphology alongshore (Schupp et al., 2006; Thornton et al., *in review*), the analysis is not sensitive to correlations at specific alongshore length scales, and it is unclear whether the correlation occurs at a single or all scales of variation; the results are an average of the correlation at all length scales. Cycles or regularly repeating patterns in the relationship between two variables are shown through cospectral analysis, in which the covariance between two variables is plotted as a function of wavenumber. As noted, peaks in the cospectrum

describe the relationship between two variables in a more sensitive way than conventional correlations, especially when the relationship between the two variables changes for different length scales.

RESULTS

Dune Morphology and Change

A comparison of the pre- and post-storm alongshore variation in foredune elevation is provided in Figure 2a. The average elevation was 4.3 m, but the foredune was discontinuous alongshore and varied in height from 2.1 to 9.3 m. The average elevation of the island within the foredune area was reduced to 2.3 m during Hurricane Ivan, with remnant dunes remaining only in areas where a relatively large continuous dune had been present before the storm. The pre-storm height of the foredune exhibits alongshore variations at length scales of 475 and 4500 m with secondary variations at length scales of 750 and 1450 m (Figure 3a). The variations at the 1450 and 4500 m length scales account for a larger part of the total variance (>50%) in post-storm elevation, while the percent variance at the 475 and 750 m length scales decreases from the pre-storm data. In general, the length of overwash penetration varied inversely with the pre-storm dune height (Figure 2b), and exhibited variations at the 475 and 1450 m length scales. The overwash penetration does not exhibit variations at length scales shorter than 475 m, although there are shorter variations in foredune height that appear to be both natural (vegetated) and beach access points.

Since the results of Houser et al. (2007) are the basis for this study, they are summarized here for the purpose of describing the dune morphology. EOF analysis was used in that study to identify characteristic structures for the cross-island morphology such as the height of the foredune and the presence and height of backbarrier dunes. The total variance in cross-island profile before and after the storm could be explained through 5 modes that describe different combinations of foredune elevation and the presence and relative location of the backbarrier dune (if present). Canonical correlation analysis between the factor scores for the pre- and post-storm morphology yields a correlation of 0.73 (ρ<0.05); the results of this analysis are presented graphically in Figure 4. The second eigenmode (E2) for the pre-Ivan data is characterized by a small foredune and is associated with the second eigenmode for the post-Ivan data. The negative correlation (-0.79) between the pre-storm E2 and post-storm E2 is a reflection of how overwash

penetration is inversely related to dune height and that significant overwash penetration and even breaching are observed in areas of low dune height (areas with a negative pre-storm E2). The fourth eigenmode for the pre-Ivan data is characterized by a backbarrier dune and a large foredune and is largely associated with the fifth eigenmode for the post-Ivan data, which shows little overwash deposition and some loss of backbarrier dune height. Correlations are also observed between the factor loadings of pre-storm E1, E3 and E5 and post-storm E1, E3 and E4 respectively.

The alongshore variation in the factor weightings for both the pre- and post-storm data is presented in Figure 5. Using spectral analysis it is found that the eigenmodes exhibit an alongshore variation (wavenumbers) similar to the distance of the overwash penetration, suggesting that the overwash penetration may be more sensitive to the alongshore variation in island morphology than just the height of the foredune. Specifically, the pre-storm factor loadings E2 and E4 exhibit variation at alongshore length scales of ~750 and 1450 m. E1 and E5 also exhibit an alongshore variation at a length scale of ~750 m, while E1, E3 and E5 have secondary spectral peaks at a length scale of ~1091 m. The variation at 1091 was not observed for any other variable except the pre-storm foredune height. All of the pre-storm and post-storm eigenmodes exhibit a variation around the 4500 m length scale. The island width also varies at length scales of 1450 and 4500 m, consistent with the spacing of the cuspate forelands and a general widening of the island in the middle of the study area respectively.

The weak but still significant correlation (r=0.18) between pre-storm E4 and post-storm E2 (see Figure 4f) suggests that (in fact) large dunes adjacent to smaller dunes can be eroded through lateral erosion. The alongshore variation in factor scores (EOF amplitudes) for a representative section of the study area showing areas of pre-storm E4 and strong post-storm E2 is provided in Figure 6. As a result of the lateral erosion, overwash penetration in these areas is greater than adjacent areas where the dune height was maintained and more sediment was lost offshore. Lateral erosion also caused a considerable loss in the volume of the backbarrier dunes, despite these dunes remaining largely intact after the storm. A representative alongshore profile of a backbarrier dune is provided in Figure 7a. The erosion was concentrated along the east and west slope, leading to steep slopes with exposed roots (Figure 7b). Many of the shrubs along the exposed slopes show (as of 2007) signs of stress and many are dying in response to the exposed roots and salt-spray exposure.

Offshore Bathymetry

The interpolated bathymetric surface is provided in Figure 8. The bathymetry exhibits a characteristic concave profile with semi-regular shore-oblique ridges of varying size oriented at an angle of ~65^{o} to the shoreline (to the SE). The ridges extend ~1700 km offshore at a depth of ~15 m and have a relief or ~3 m. A comparison of a 2006 bathymetric survey for a small section of the coast and the 1982 bathymetry shows little change in the morphology of these ridges. This suggests that these transverse ridges have persisted through a variety of storm activity (specifically Opal, Georges, Erin, Ivan, Dennis and Katrina). In the present study, the ridges do not appear to be discrete forms but part of larger field of overlapping ridges on the inner shelf (Figure 8). Only the innermost ridges are considered in this study.

EOF analysis of the offshore bathymetry along the study transects reveals 2 significant eigenmodes that represent a dissipative and a reflective profile (Figure 9a). The factor loadings for E1 and E2 suggest that the dissipative profile accounts for the greatest amount of the variation, but the ratio of eigenmodes (E1/E2) suggests that the offshore profile varies from reflective (E2) to highly dissipative (large E1). Using spectral analysis it is found that the factor loading ratio (E1/E2) varies at alongshore length scales of ~475, 750, 1450 and 4500 m (Figure 3). The peak of the bathymetry ratio is at the 1450 m length scale, consistent with the transverse ridges on the inner-shelf and the spacing of the cuspate forelands along Santa Rosa Sound. As presented in Figure 9b, the most dissipative sections of the island (large E1/E2 ratio) are adjacent to the cuspate forelands (to the west), while the reflective parts of the island (small E1/E2 ratio) are found to the west of the narrow sections of the island.

Shoreline Change

The historical (pre-2004/05 storms) shoreline change rates (1859 – May 2004) are shown in Fig. 10a, and were calculated using a linear regression method. Uncertainty estimates (±0.1 m/yr) on the rates were derived using the linear regression 90% confidence interval and the proxy-bias uncertainty, similar to methods outlined in Hapke et al. (2006). Figure 10a shows the variation in historical shoreline change rates along the same stretch of coast used in the elevation, bathymetry and island width analyses. The historical shoreline change rates in the study area are erosional, with a rate of -0.2±0.1 m/yr, averaged along 431 transects. The long-term erosion

rates are overall relatively low, especially as compared to other barrier island systems in the Gulf of Mexico (Morton et. al, 2004). Additionally, our results contrast with those described by Stone (1991), who found that the Gulf shoreline of Santa Rosa Island was generally stable. However, our rates include part of the period of increased storminess that began in 1995 with hurricane Opal and thus our rates reflect a more erosional, severe storm-driven regime. The highest historical erosion rates (-0.35±0.1 m/yr) were measured on the western end of the study area, where the island is somewhat narrower. Although the rates vary substantially, the most stable area is near the center of the study area where the average island width is the greatest, between the two largest cuspate forelands (Fig. 10a). The historic shoreline change exhibits statistically significant spectral peaks at length scales of ~4500 and 1450 m within the study area (see Figure 9). As noted, the 1450 m length scale is also observed in the recent (storm-related) shoreline change and is consistent with the alongshore variation in the bathymetry ratio (E1/E2), island width and dune morphology.

The storm-related shoreline change rate increased by two orders of magnitude from the historical, to -38.0±1.4 m/yr, and erosion was measured on all of transects in the study area. Due to data gaps associated with breaches and washover areas, the number of transects was 321 (as compared to 431 for the historical analysis. Figure 10b shows the spatial distribution of the erosion rates that occurred between May 2004 and September 09, 2005. Similar to the historic trend, the central portion of the study area was the most stable, and had the lowest erosion rates, although the specific transects do not spatially correlate between the two data sets. The maximum erosion rate was -53.3±1.4 m/yr was measured just east of the wide easternmost cuspate foreland in the study area (Fig. 10b). As shown in Figure 9, the storm-related shoreline change exhibits statistically significant spectral peaks at length scales of ~500, 750 and 1450 m. The variation at the 475 m length scale is only a small part of the total variance in storm-related shoreline change, but it is also observed in the E1/E2 bathymetry ratio, the historic erosion rate and dune height (pre-storm dune E2).

Cross-correlation and Co-spectral Analysis

While the dune morphology, bathymetry and shoreline change exhibit alongshore variations at similar length scales (475, 750, 1450 and 4500 m), it is possible that the variation is not in-phase between variables (with a lag of 0 alongshore). Through cross-correlation analysis

it is found that the pre-storm E2 is negatively correlated with the island width (ρ>0.95), such that areas with small foredunes and no backbarrier dunes (large E2) are found in the narrow sections of the island. A statistically significant cross-correlation between pre-storm E4 and island width was also observed. However, the largest dunes are not found at the widest sections of the island, but are ~350 m east of the cuspate forelands. The island width also exhibits a statistically significant cross-correlation with the bathymetry ratio (E1/E2) at a lag of ~175 m, such that the most dissipative offshore profiles are west of the widest sections of the island.

The cross-correlation analysis is not sensitive to correlations at the different length scales identified through spectral analysis and it is unclear whether the above correlations and lags are associated with all scales of variation. From the cospectral analysis, the dune height is coherent with the bathymetry ratio at the 475 m length scale at a lag of ~90 m (Table 1). The largest dunes (at this length scale) are east of the dissipative profiles and associated with pre-storm E4 dunes that change into pre-storm E3 dunes with increasing distance to the east. The historical shoreline change is in-phase with the offshore bathymetry, such that there are local erosion hotspots where the profile is more reflective and there are smaller dunes. A strongly coherent but out-of-phase relationship is observed between the length of overwash penetration and the bathymetry ratio. As a consequence of the smaller pre-storm dunes and reflective profile, overwash was able to penetrate to a greater distance on the island.

At the 750 m length scale, the pre-storm dune height is also coherent but out-of-phase with the bathymetry ratio; the largest dunes tend to be found ~350 m east of the dissipative profiles and are associated with the pre-storm E4 dunes. The pre-storm E3, E5 and E3 dune profiles (showing the presence of backbarrier dunes) were also coherent with the bathymetry ratio but at lags of ~190, 560 and 400 m to the west of the dissipative profile respectively. The bathymetry ratio exhibits a weak (but still significant) coherency with the historical rate of shoreline loss. These variables are out-of-phase, such that lower rates of shoreline retreat at this scale are associated with the reflective profiles. Interestingly the storm-related shoreline change is (weakly) coherent and in-phase with the bathymetry ratio, suggesting that lower rates of shoreline erosion are associated with dissipative profiles and that larger dunes and a reflective profile lead to greater shoreline retreat during the storms.

At the primary length scale for the offshore bathymetry (1450 m), the bathymetry ratio is coherent and in quadrature with the width of the island, such that dissipative profiles tend to be

found ~360 m west of the cuspate forelands. The ridges are also out-of-phase with the largest dunes (large pre-storm E4). The smallest dunes (large pre-storm E2) are lagged by ~360 m from the bathymetry ratio and out-of-phase with the island width. The recent and historic rates of shoreline erosion are also correlated with island width and the bathymetry ratio. At the 1450 m length scale, the recent rates of shoreline erosion are strongly coherent and in quadrature (270^{o}) with the island width and out-of-phase (180^{o}) with the bathymetry ratio. In this respect, higher (or more negative) rates of erosion are found 375 m west of the cuspate headlands in the vicinity of the transverse ridges and east of the breached sections of the island (large pre-storm E2). The lower (or less negative) rates of erosion are east of the headlands in the vicinity of the largest dunes (large pre-storm E4) and in the trough of the transverse ridges. In contrast, the rate of historic shoreline change is in quadrature with the bathymetry ratio. Higher (or more negative) rates of erosion are observed ~375 m west of the transverse ridges in the vicinity of the narrowest sections of the island (large pre-storm E2) and where there is a transition between a dissipative and reflective profile from east to west. A schematic showing the spatial relationship between variables at this length scale is provided in Figure 11.

The bathymetry ratio is coherent and in-phase with both the historical and storm-related rate of shoreline change at the 4500 m length scale. The broad area with a more dissipative profile is associated with a lower rate of shoreline erosion and a local area of accretion. This lower rate of historical erosion and the more dissipative profile is consistent with the location of the local sediment source described by Stone et al. (1992). Interestingly, the dune height is in quadrature with the bathymetry ratio at the 4500 m length scale, such that the broad dissipative profile is ~798 m east of the largest dunes on the island. The pre-storm E1 and E3 dune profiles are coherent but in quadrature with the bathymetry ratio. The E1 profiles are more common to the western part of the study site (~3400 m from the dissipative profile) and the E3 profiles are more common in the eastern part of the study site (~3200 m from the dissipative profile).

DISCUSSION

The impact of an extreme storm on a barrier island depends on the relative elevation of the storm surge and the foredune (Thieler and Young, 1991; Sallenger, 2000; Morton, 2002; Stockdon et al., 2007). To a lesser degree, the impact varies with the presence and relative location of backbarrier dunes (Houser et al., 2007), and alongshore variations in island width

(Morton, 2002) and dune height (Wright et al., 1970; Morton, 2002; Gares and White, 2005). Depending on the pre-storm dune morphology (both cross-shore and alongshore), sediment is redistributed between the nearshore where the dunes were relatively tall and overwash where the dunes are poorly developed. Overwash penetration was larger where the dune height was small and the island was narrow. Where the dunes are well developed or backbarrier dunes are present, overwash penetration is limited and more sediment is lost to the nearshore. This redistribution of sediment during an extreme storm is an important control on the rate of dune recovery, which will ultimately determine the height and extent of the coastal dune system during the next extreme storm. Variations in the availability of sediment can lead to considerable variability in the height and extent of dune development, which will reinforce the morphological response of the island to subsequent storms. Following the storm, the breach areas are at or close to the watertable and covered by a heavy lag of shell and gravel from the adjacent road bed (Houser et al., *in press*). Both the moisture and the lag create a supply-limited system in which dune recovery will be slow compared to those areas where the pre-storm dunes were well-developed and sediment was lost to the shoreface. As a result, burial tolerant vegetation is preferentially selected and dunes of limited relief and extent develop (Stallins and Parker, 2003; Stallins, 2005). During the next storm, surge water will be forced into these areas (Wright et al., 1970; Morton, 2002; Gares and White, 2005), such that the recovery of the dune field reinforces alongshore patterns in overwash and breaching during subsequent storms (Gibeaut et al., 2002; Morton and Sallenger, 2003).

Consistent with the alongshore variation in foredune morphology, the historic rate of shoreline retreat (at the 1450 m length scale) is strongly coherent and out-of-phase with the island width (see Figure 11). Higher rates of erosion are associated with the narrow sections of the island that are inundated early in a storm and (as noted) are characterized by a high concentration of shell lag and a high moisture content following the storm. The narrow sections of the island will also have larger gradients in the surge elevation (Morton, 2002), which would lead to significant overwash penetration and breaching. This would lead to a net loss of sediment from the Gulf of Mexico to Santa Rosa Sound, consistent with the observations of Stockdon et al. (2007) from the North Carolina coast. The overwash fans are eroded by frontal winds (Stone et al., 2004) and the transverse nearshore bars along the backbarrier suggest that sediment is transported alongshore towards the cuspate headlands (unpublished data). However,

further study is required to ascertain the link between the cuspate headlands and the erosion of the overwash fans in the breach areas.

Results of the cospectral analysis suggest that the alongshore variation in dune morphology is coherent with the bathymetry of the inner-shelf at a range of length scales (475, 750, 1450 and 4550; Table 1). Numerous studies suggest that transverse ridges will lead to alongshore variations in wave convergence and divergence as a result of wave refraction/diffraction around the bathymetric highs or lows (e.g. O'Reilly and Guza, 1993; Schwab et al., 2000; Bender and Dean, 2003; Schupp et al., 2006). It is reasonable to expect that the relative importance of the ridges at each length scale will vary with the ridge amplitude and the incident wave energy; smaller ridges (such as at the 475 m length scale) may be important during smaller storms and larger ridges during the storms such as Hurricane Ivan. As noted, the transverse ridges with the greatest amplitude and apparent control during Hurricane Ivan had an alongshore spacing of 1450 m and were oriented to the SE, which is the dominate direction of wave advance. While the formation of these features is beyond the scope of the present study, Niedoroda and Tanner (1970) suggest that ridges of this nature would be maintained by wave refraction towards the ridge crests. On average, the outermost nearshore bar in the vicinity of the transverse ridges is ~50 m further offshore and >1 m lower on the profile. This suggests that greater wave energy in these areas if it assumed that the equilibrium position of a nearshore bar is at the breakpoint (Plant et al., 2001; Houser and Greenwood, 2005). While Schwab et al. (2000) observed more stable shoreline segments at the crest of transverse bars, the results of the present study suggest that the long-term erosion hotspots are immediately west of the ridges at the 475 and 1450 m length scales. In contrast, the rate of historic shoreline change is coherent and in-phase with the bathymetry at the 4500 m length scale. Storm waves will experience greater energy dissipation where there is a broad dissipative profile, leading to lower rates of shoreline erosion. In fact, there is an area of historical accretion near the center of this broad dissipative region where there are also tends to be larger foredunes (pre-storm E4) and backbarrier dunes are more common (pre-storm E1). As discussed by Cooper and Navas (2004), areas with more dissipative profiles increase onshore-directed transport and are associated with foredune accretion. In this respect, the large scale bathymetric features may offset any regional erosion trends (see Stone et al., 1992) and force the alongshore variation in shoreline retreat and dune morphology.

The storm related rates of shoreline erosion were found to be greater (or more negative) east of the breached sections of the island, in the vicinity of the transverse ridges observed on the inner shelf. The lower (or less negative) rates of erosion are east of the headlands in the vicinity of the largest dunes (large pre-storm E4) where most sediment was deposited within the nearshore during the storm. Interestingly, the rate of storm related erosion was relatively muted near the breached areas of the island. Based on the model of Sallenger (2000) this may reflect the longer period of time that these areas are in the swash and collision regimes and the loss of sediment to the shoreface, compared to the low elevation areas that would be overwash and inundated earlier in the storm. This may also reflect greater wave set-up on the dissipative profile and greater focus of energy on the beachface, foredune and backbarrier dune compared to the low-elevation sections where the island would have been inundated relatively early in the storm. It is also reasonable to expect that there was an alongshore redistribution of the nearshore sediment following the storm, in a manner that is analogous to the lateral erosion of nourishment projects (Browder and Dean, 2000). The sediment deposited within the nearshore during the storm is moved to the west (with the prevailing southeasterly wind) and redeposited within the breached areas by the dominant southeast wind. This is potentially reinforced by the presence of the transverse ridges on the inner shelf that may lead to alongshore variations in wave convergence and divergence around the bathymetric highs or lows.

While the alongshore variation in dune morphology and the rate of historical shoreline retreat are coherent with the transverse ridges at a variety of length scales, the backbarrier dune profiles (pre-storm E1, E3 and E5) exhibit a secondary variation at a length scale of 1091 m that is not associated with the other variables. Prior to Hurricane Ivan, the hummocky backbarrier dunes were largely restricted to the sound-side cuspate headlands and were backed by maritime forest. While these dunes experienced considerable lateral erosion during the storm, they were already extremely steep and in some cases were already scarped before the storm. A recent study by Pries et al. (*in press*) suggests that the backbarrier dunes at the east end of Santa Rosa Island (~20 km east of the study site) did not recover following Hurricane Opal (1995) and were further reduced in number and aerial extent during Hurricanes Ivan and Dennis. In this respect, the presence and relative location of the backbarrier dunes may be a reflection of storm history and episodic erosion and not post-storm recovery. Pries et al. (*in press*) argue that with the recent increase in storm activity, Santa Rosa Island is changing towards a state where the dunes

are controlled by frequent overwash disturbance from one that is arranged by shore-normal environmental gradients in wind and wave energy (Stallins and Parker, 2003). Given sufficient time, the foredune will recover in both height and alongshore extent, but it is unclear whether the backbarrier dunes will recover and if the recovery is forced by the transverse ridges.

CONCLUSIONS

The results of this study provide greater insight into alongshore variations in coastal dune morphology, shoreline erosion and barrier island response to storms. While alongshore variation in the height and extent of coastal dunes has been identified in the literature (Carter, 1988; Carter and Wilson, 1990; Sarre, 1989; Hesp, 1989, 1999; Leys, 1991; Raupach et al., 1993; Hagen and Armbrust, 1994; Musick et al., 1996; Santos et al., 1996; Wilson et al., 1998), the controls on this variation remain poorly understood. It appears that the alongshore pattern in dune morphology, shoreline erosion and storm impact are controlled (at a range of length scales) by the transverse ridges on the inner-shelf and the cuspate forelands along Santa Rosa Sound (through the island width). Long-term rates of erosion are observed between cuspate headlands where the island is narrow and the low island elevation promotes overwash penetration, while storm-related rates of erosion are greatest at the headlands where the island elevation is greatest and more sediment is eroded offshore. In this respect, the supply of sediment for dune recovery (or lack thereof) varies in response to the storm impact, such that the height and extent of foredune development and the presence and relative location of the backbarrier dunes are geologically controlled and reinforced.

REFERENCES

Armon, J.W., 1980. Dune erosion and recovery on a northern barrier. In: Coastal Zone '80, Proceedings of the 2nd Symposium on Coastal and Ocean Management, Hollywood, Florida, November 1980, American Society of Civil Engineers, 2, pp. 1233-1250.

Bauer, B.O., and Davidson-Arnott, R.G.D., 2003. A general framework for modeling sediment supply to coastal dunes including wind angle, beach geometry, and fetch effects. Geomorphology, 49, 89-108.

Belly, P.Y., 1964. Sand movement by wind. United States Army, Corps of Engineers, Coastal Engineering Research Center, Washington DC, Technical Memorandum TM-1, 80 pp.

Bender, C.J. and Dean, R.G., 2003. Wave field modification by bathymetric anomalies and resulting shoreline changes: A review with recent results. Coastal Engineering, 49, 125-153.

Browder, A.E., and Dean, R.G., 2000, Monitoring and comparison to predictive models of the Perdido Key beach nourishment project, Florida, USA: Coastal Engineering, 39, 173-191.

Browder, A.G., McNinch, J.E., 2006. Linking framework geology and nearshore morphology: correlation of paleo-channels with shore-oblique sandbars and gravel outcrops. Marine Geology, 231, 141–162.

Cooper, J.A.G. & Navas, F., 2004. Natural bathymetry change as a control on century-scale shoreline behavior. Geology, 32, 513-516.

Cornelis, W.M., Gabriels, D. and Hartmann, R., 2004. A parameterisation for the threshold shear velocity to initiate deflation of dry and wet sediment. Geomorphology 59(1-4), 43-51.

Davidson-Arnott, R.G.D., MacQuarrie, K., and Aagaard, T., 2005. The effect of wind gusts, moisture content and fetch length on sand transport on a beach. Geomorphology, 68, 115-129.

Demarest, J.M., Leatherman, S.P., 1985. Mainland influence on coastal transgression: Delmarva peninsula. Mar. Geol. 63, 19–33.

Elko, N.A., Sallenger, A.H., Guy, K., & Morgan, K.L.M., (2002). Barrier island elevations relevant to potential storm impacts; 2, South Atlantic: U.S. Geological Survey, Open-File Report 2002-288, 1 folded sheet.

Foster, E.R., Spurgeon, D.L., and Cheng, J., 1999. Shoreline Change Rate Estimates: Escambia and Santa Rosa Counties. Florida Department of Environmental Protection, Office of Beaches and Coastal Systems, Report BCS-99-03, 85 p.

Fryberger, S.G. 1979. Dune forms and wind regime, Mauritania, West Africa; Implications for Past Climate. In: Sarnthien, M., Siebold, E. and Rognon, P. (eds), Van Zinderen Bakker, E.M.Sr. and Coetzee, J.A. (eds), Rotterdam: Balkema, Palaeoecology of Africa and the Surrounding Islands 12:79-96.

Gares, P., and White, S.A., 2005. Volumetric Analysis of Overwash Fans Resulting from Tropical Storms on North Hatteras Island, North Carolina. Southeastern Geographer 45, 1-15.

Hapke, Cheryl J., Reid, David, Richmond, Bruce M., Ruggiero Peter, and List, Jeff, 2006, National Assessment of Shoreline Change part 3; Historical shoreline change and associated coastal land loss along sandy shorelines of the California coast: U.S. Geological Survey Open-File Report 2006-1219, 79 pp.

Hotta, S., Kubota, S., Katori, S. and Horikawa, K. 1984. Sand transport by wind on a wet sand surface. In: Edge, B.L. (ed), Coastal Engineering 1984, Proceedings of the 19th International Conference, Houston, Texas, September 1984, American Society of Civil Engineers, 2, pp. 1265-1281.

Houser, C., Hamilton, S., Oravetz, J. & Meyer-Arendt, K., 2007. EOF Analysis of Morphological Change during Hurricane Ivan. Coastal Sediments 2007.

Houser, C., Hobbs, C. and Saari, B., *in press*. Post-hurricane airflow and sediment transport over a recovering dune. Journal of Coastal Research.

Hyne, N.J. & Goodell, H.G., (1967). Origin of the sediments and submarine geomorphology of the inner continental shelf off Choctawhatchee Bay, Florida. Marine Geology, 5, 299-313.

Irish, J.L. & White, T.E., (1998). Coastal engineering applications of high-resolution lidar bathymetry. Coastal Engineering, 35, 47-71.

Kraft, J.C., Chrzastowski, M.J., Belknap, D.F., Toscano, M.A., Fletcher, C.H., 1987. The transgressive barrier-lagoon coast of Delaware: morphostratigraphy, sedimentary sequences and responses to relative rise in sea-level. In: Nummedal, D., Pilkey, O.H., Howard, J.D. (Eds.), Sea-Level Fluctuation and Coastal Evolution. Society of Economic Paleontologists and Mineralogists, pp. 129–143.

Kwon, H.J., 1969, Barrier islands of the northern Gulf of Mexico coast: Sediment source and development. Coastal Studies Series 25. Baton Rouge: Louisiana State University Press.

Leatherman, S.P., 1976. Barrier island dynamics: overwash processes and eolian transport. In: Coastal Engineering 1976, Proceedings of the 15th International Conference, Honolulu, Hawaii, American Society of Civil Engineers, pp. 1958-1974.

Leatherman, S.P., 1979. Barrier dune systems: a reassessment. Sedimentary Geology, 24, 1-16.

Lettau, H.H., and Lettau, K., 1978. Exploring the World's Driest Climate. Madison, Wisconsin: Institute of Environmental Studies, University of Wisconsin.

McKenna-Neuman, C., 1998. Particle transport and adjustments of the boundary layer over rough surfaces with an unrestricted, upwind supply of sediment. Geomorphology, 25(1-2), 1-17.

McNinch, J.E., (2004). Geologic control in the nearshore: shore-oblique sandbars and shoreline erosional hotspots, Mid-Atlantic Bight, USA. Marine Geology, 211, 121-141.

McNinch, J.E., & Luettich, R.A., (2000). Physical processes around a cuspate foreland: implications to the evolution and long-term maintenance of a cape-associated shoal. Continental Shelf Research, 20, 2367-2389.

Miller, T.L., Morton, R.A., Sallenger, A.H., and Moore, L.J., 2004, The National Assessment of Shoreline Change: A GIS Compilation of Vector Shorelines and Associated Shoreline Change Data for the U.S. Gulf of Mexico: USGS Open File Report 2004-1089.

Moore, L., Ruggiero, P., and List. J., 2006, Comparing mean high water and high water line shorelines: Should proxy-datum offsets be incorporated in shoreline change analysis?: Journal of Coastal Research, v. 22, n. 4, p. 894-905.

Morton R.A., (2002). Factors controlling storm impacts on coastal barriers and beaches - a preliminary basis for near real-time forecasting. Journal of Coastal Research 18(3): 486- 501.

Morton, R. A., and Paine, J. G., (1985). Beach and vegetation-line changes at Galveston Island, Texas; Erosion, deposition, and recovery from Hurricane Alicia: The University of Texas at Austin, Bureau of Economic Geology Geological Circular 85-5, 39 p.Otvos, E.G., 1982, Santa Rosa Island, Florida panhandle: Origins of a composite barrier island, Southeastern Geology 23 (1): 15-24.

Morton, R.A., and Sallenger, A.H., 2003. Morphological impacts of extreme storms on sandy beaches and barriers. Journal of Coastal Research, 19, 560-573.

Morton, R.A., Paine, J.G., & Gibeaut, J.C., (1994). Stages and durations of post-storm beach recovery, southeastern Texas coast. Journal of Coastal Research, 10, 884-908.

Nickling, W.G., and McKenna-Neuman, C., 1995. Development of deflation lag surfaces. Sedimentology, 42, 403-414.

Otvos, E.G., 1982, Santa Rosa Island, Florida panhandle: Origins of a composite barrier island, Southeastern Geology 23, 15-24.

O'Reilly, W.C., Guza, R.T., 1993. A comparison of two spectral wave models in the Southern California Bight. Coast. Eng. 19, 263–282.

Pilkey, O.H., Young, R.S., Riggs, S.R., Smith, A.W., Wu, H., Pilkey, W.D., 1993. The concept of shoreface profile of equilibrium: a critical review. J. Coast. Res., 9, 255–278.

Psuty, N.P., 1992. Spatial variation in coastal fordune development. In: R.W.G. Carter, T.G.F. Curtis and M.J. Sheehy-Skeffington (Eds), Coastal Dunes: Geomorphology, Ecology and Management for Conservation. Balkema Rotterdam, pp. 3-13.

Riggs, S.R., Cleary, W.J., & Snyder, S.W., 1995. Influence of inherited geologic framework on barrier shoreface morphology and dynamics. Marine Geology, 126, 213-234.

Ruggiero, P., Kaminsky, G.M., and Gelfenbaum, G., 2003, Linking proxy-based and datum-based shorelines on a high-energy coastline: Implications for shoreline change analyses: Journal of Coastal Research Special Issue 38, p. 57-82.

Sallenger, A.H., Wright, C.W., & Lillycrop, J., 2004. Coastal Impacts of the 2004 Hurricanes Measured with Airborne LiDAR: Initial Results. Shore and Beach, 73, 10-15.

Sallenger, A. H., 2000. Storm impact scale for barrier islands. J. Coastal Research, 16, 890-895.

Sherman, D.J., Jackson, D.W.T., Namikas, S.L., and Jinkang, W., 1998. Wind-blown sand on beaches: an evaluation of models. Geomorphology, 22,113-133.

Schupp, C.A., McNinch, J.E., & List, J.H., 2006. Nearshore shore-oblique bars, gravel outcrops, and their correlation to shoreline change. Marine Geology, 233, 63-79.

Schwab, W.C., Thieler, E.RF., Allen, J.R., Foster, D.S., Swift, B.A., & Denny, J.F., 2000. Influence of inner-continental shelf geologic framework on the evolution and behaviour f the barrier-island system between Fire Island Inlet and Shinnecock Inlet, Long Island, New York. Journal of Coastal Research, 15, 408-422.

Snyder, R.A., and Boss, C.L., 2002. Recovery and stability of Barrier Island plant communities. Journal of Coastal Research, 18, 530-536.

Stallins, J.A., 2005. Stability Domains in Barrier Island Dune Systems. Ecological Complexity, 2, 410-430.

Stallins, J.A., and Parker, A.J., 2003. The influence of complex systems interactions on barrier island dune vegetation pattern and process. Annals of the Association of American Geographers, 93, 13-29.

Stockdon, H.F., Sallenger, A.H., List, J.H., Holman, R.A., 2002. Estimation of shoreline position and change from airborne scanning lidar data. J. Coast. Res. 18 (3), 502–513.

Shalowitz, A.L., 1964, Shore and sea boundaries. Publication 10-1, U.S. Department of Commerce, Washington, DC, 749 pp.

Stapor, F.W., Jr., 1975, Shoreline changes between Phillips Inlet and Pensacola Inlet, northwest Florida coast, Transactions, Gulf Coast Association of Geological Societies 25: 373-378.

Stockdon, H.F., Sallenger, A.H., Holman, R.A., and Howd, P.A., 2007. A simple model for the spatially-variable coastal response to hurricanes. Marine Geology, 238, 1-20.

Stone, G.W., 1991. Differential sediment supply and cellular nature of longshore sediment transport along coastal Northwest Florida and Southeast Alabama since the late Holocene. Ph.D. Dissertation, University of Maryland, College Park, MD.

Stone, G.W., 1984. Mathematical modeling of the nearshore and implications for coastal management, Northwest Florida. Unpublished MSc thesis, Department of Environmental Studies, University of West Florida, 140 pp.

Stone, G.W., Stapor, F.W., Jr., May, J.P., & Morgan, J.P., 1992. Multiple sediment sources and a cellular, non-integrated, longshore drift system: Northwest Florida and southeast Alabama coast, USA, Marine Geology, 105, 141-154.

Stone, G.W. & Stapor, F.W., Jr., 1996. A nearshore sediment transport model for the northeast Gulf of Mexico coast, USA, Journal of Coastal Research, 12, 786-792

Terwindt, J.H.J., Battjes, J.A., 1990. Research on large-scale coastal behaviour. Proc. 22nd Int. Conf. on Coastal Engineering, ASCE, New York, 1975– 1983.

Thieler, E. R., & Young, R. S., (1991). Quantitative evaluation of coastal geomorphological changes in South Carolina after Hurricane Hugo, Journal of Coastal Research, 8, 187–200.

Thieler, E.R., Himmelstoss, E.A., Zichichi, J.L., and Miller, T.L., 2005, Digital Shoreline Analysis System (DSAS) version 3.0; An ArcGIS© extension for calculating shoreline change: U.S. Geological Survey Open-File Report 2005-1304.

Wiggs, G.F.S. Baird, A.J. and Atherton, R.J., 2004, The dynamic effects of moisture on the entrainment and transport of sand by wind. Geomorphology, 59, 13-30.

Woolard, J.W. & Colby, J.D., (2002). Spatial characterization, resolution and volumetric change of coastal dunes using airborne LiDAR: Cape Hatteras, North Carolina. Geomorphology, 48, 268-287.

Zhang, K., Whitman, D., Leatherman, S., & Robertson, W., (2005). Quantification of Beach Changes caused by Hurricane Floyd along Florida's Atlantic coast using airborne Laser Surveys. Journal of Coastal Research, 21, 123-134.

Table 1. Results of cospectral analysis between the transverse ridges at the primary length scales of 475, 750, 1450 and 4550 m and variables describing the shoreline erosion, foredune height, overwash penetration and pre-storm dune morphology factors. Shown is the coherency (b_{xy}) and the phase relationship (ϕ_{xy}). Highlighted relationships are statistically significant at the 95% confidence level.

	475 m		**750 m**		**1450 m**		**4550 m**	
	b_{xy}	ϕ_{xy} (m)	b_{xy}	ϕ_{xy}(m)	b_{xy}	ϕ_{xy}(m)	b_{xy}	ϕ_{xy}(m)
Historic Erosion	0.46	-204	0.13		0.37	1156	0.29	275
Storm Erosion	0.17		0.28		0.16		0.14	
Pre-Storm Height	0.83	-125	0.17		0.53	-602	0.34	798
Post-Storm Height	0.49	-147	0.43	278	0.61	-586	0.44	532
Overwash Penetration	0.59	284	0.40	-370	0.53	760	0.17	
Pre Dune E1	0.61	82	0.78	208	0.15		0.57	-3449
Pre Dune E2	0.07		0.38	-566	0.70	426	0.25	
Pre Dune E3	0.37	-114	0.22		0.43	684	0.53	-3067
Pre Dune E4	0.69	-147	0.17		0.71	-728	0.37	2452
Pre Dune E5	0.01		0.47	-411	0.87	720	0.53	1653
Island Width	0.66	-174	0.65	-460	0.49	-397	0.11	

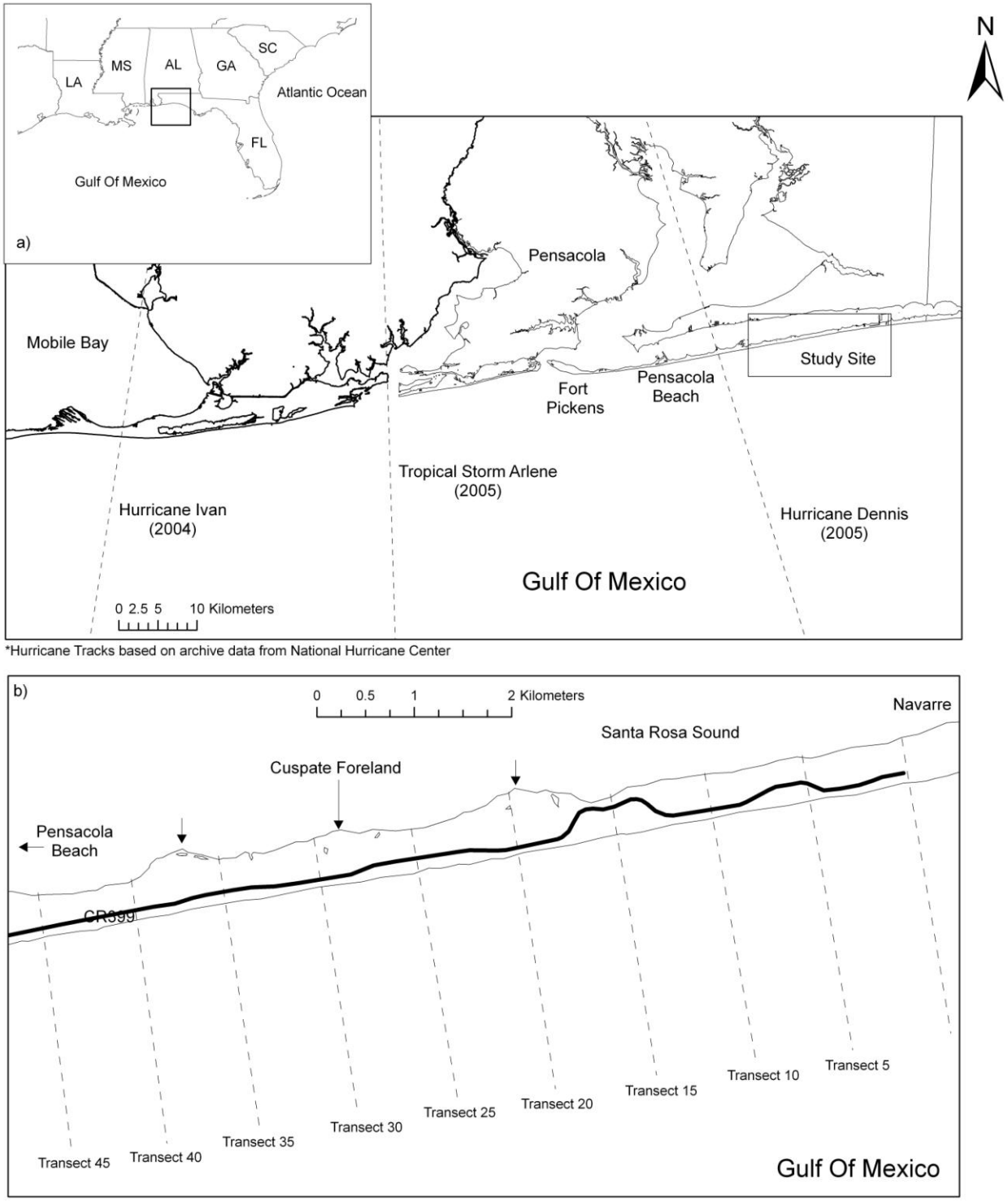


Figure 1. Map of study site showing (a) location relative to the tracks of Hurricanes Ivan and Dennis and Tropical Storm Arlene and (b) large scale map of study site showing transect locations and cuspate forelands along Santa Rosa Sound.

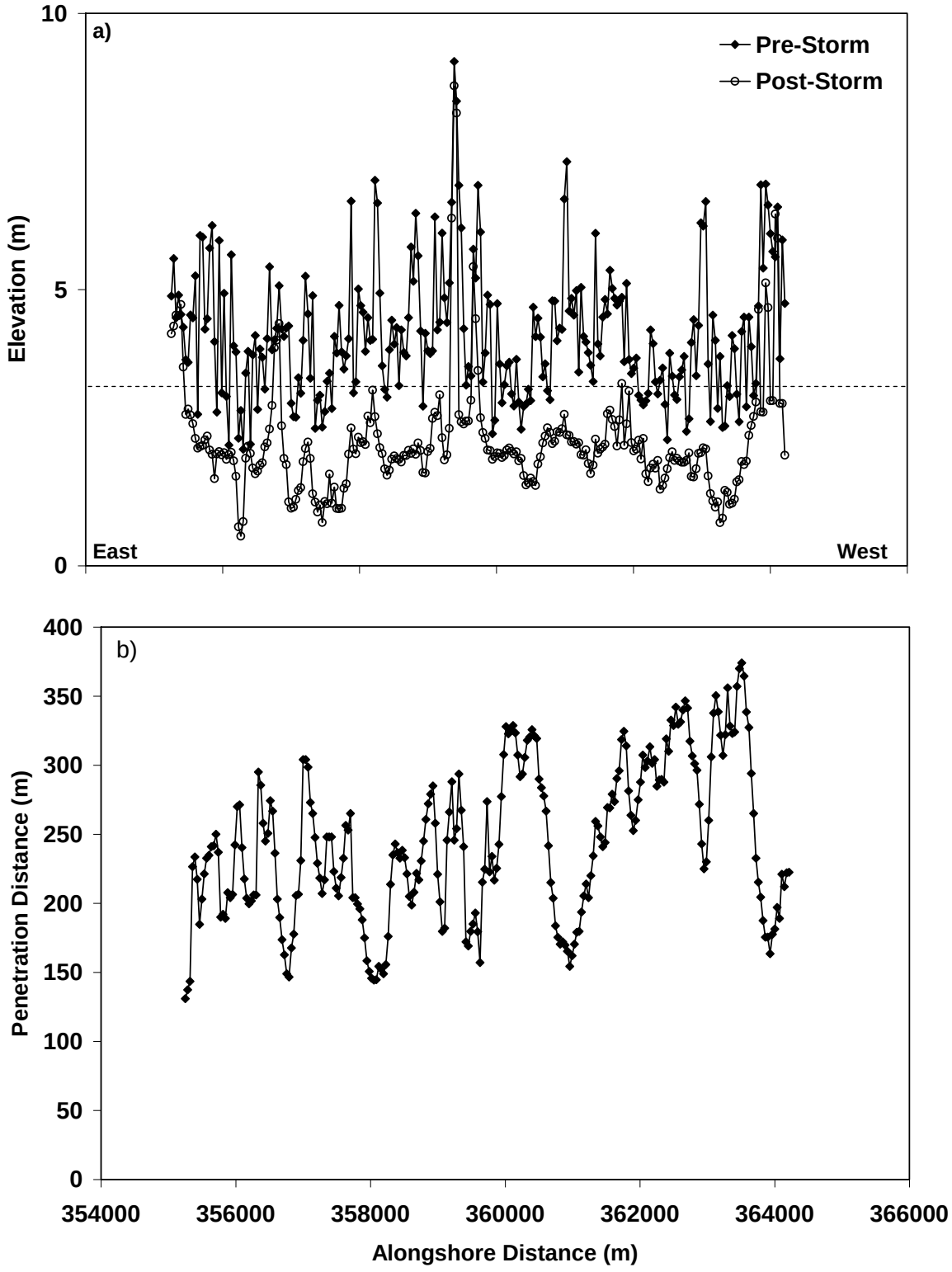


Figure 2. Alongshore variation in (a) the height of the foredune before and after Hurricane Ivan and (b) the cross-shore distance of overwash penetration at 35 m intervals alongshore. Also shown in (a) is the average surge elevation.

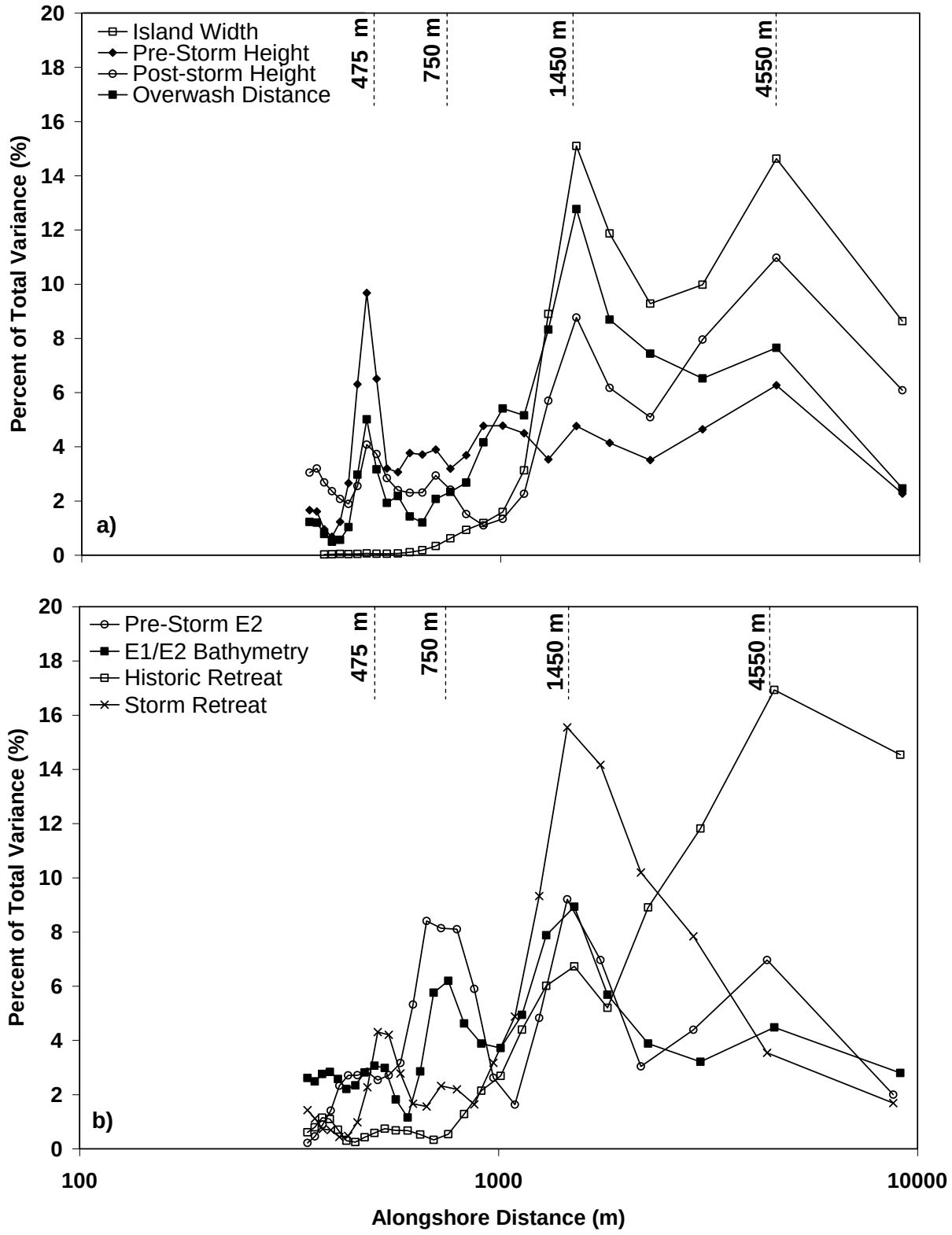


Figure 3. Spectral plots for (a) bathymetry ratio (E1/E2) and island width, and for (b) pre-storm E2 and the historic rate of shoreline change (1858-2001).

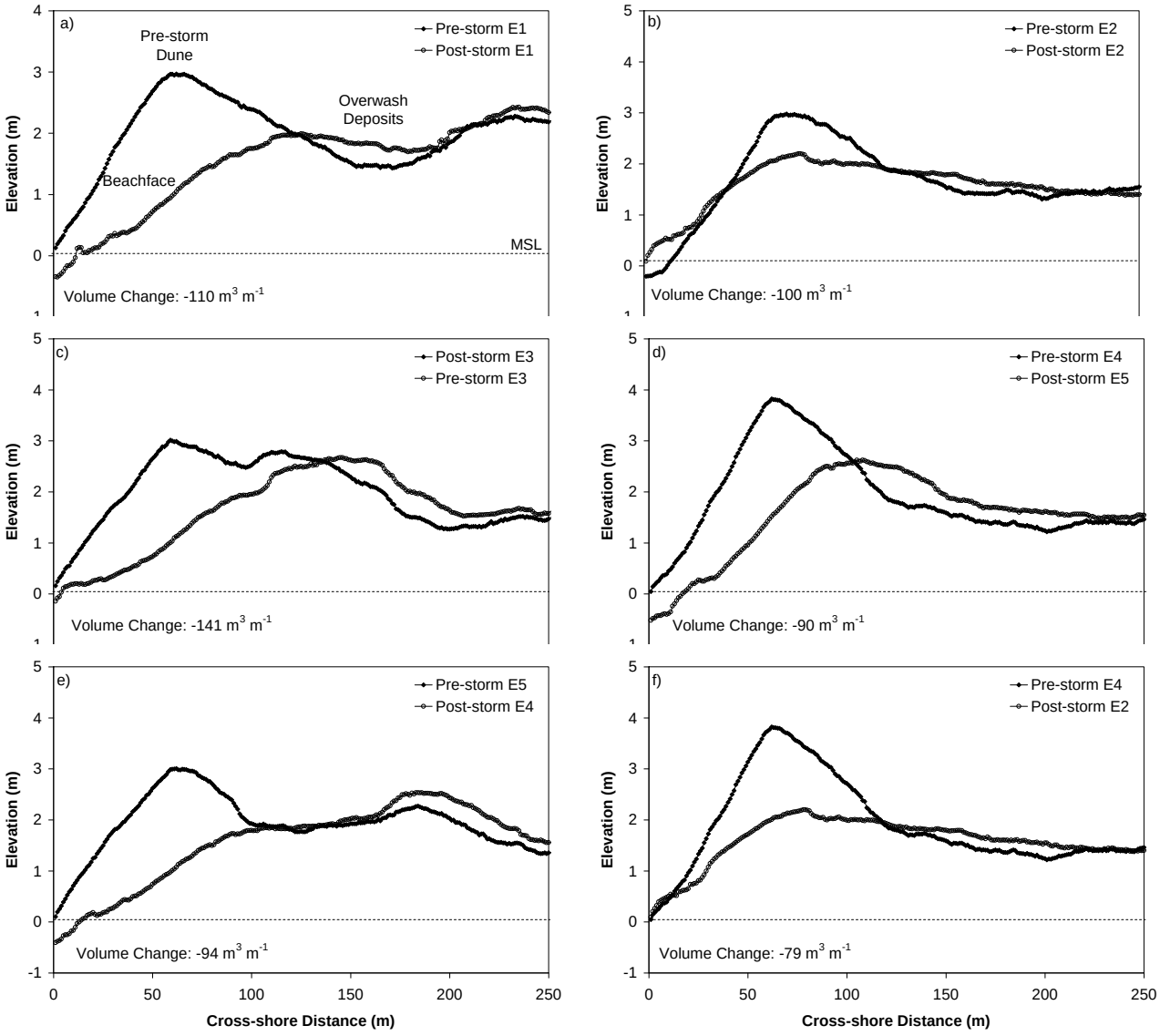


Figure 4. Comparison of cross-island profiles for the pre- and post-storm eigenvalues with strong correlations identified through canonical correlation analysis.

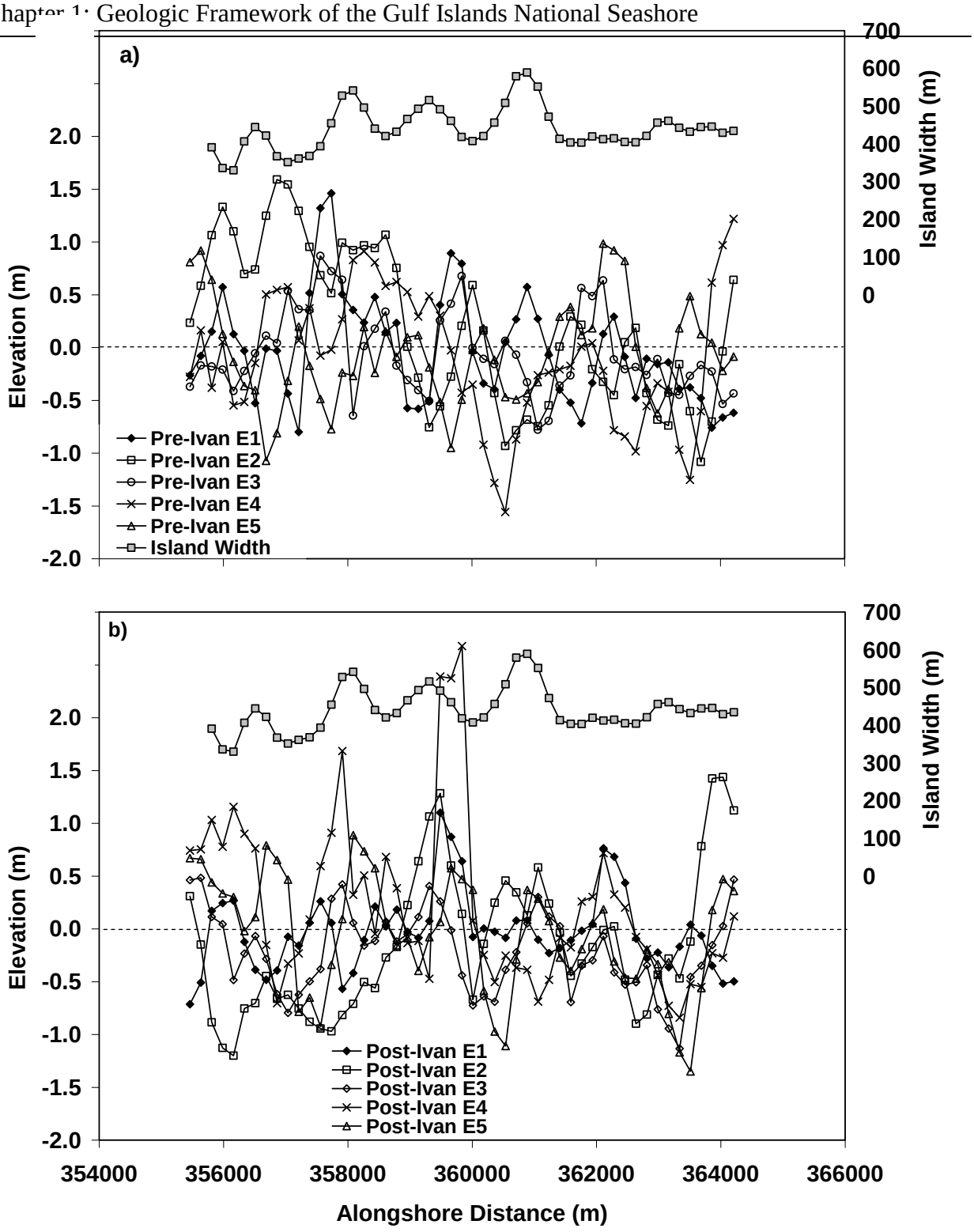


Figure 5. Comparison of factor scores for the pre- and post-storm eigenvalues with strong correlations identified through canonical correlation analysis.

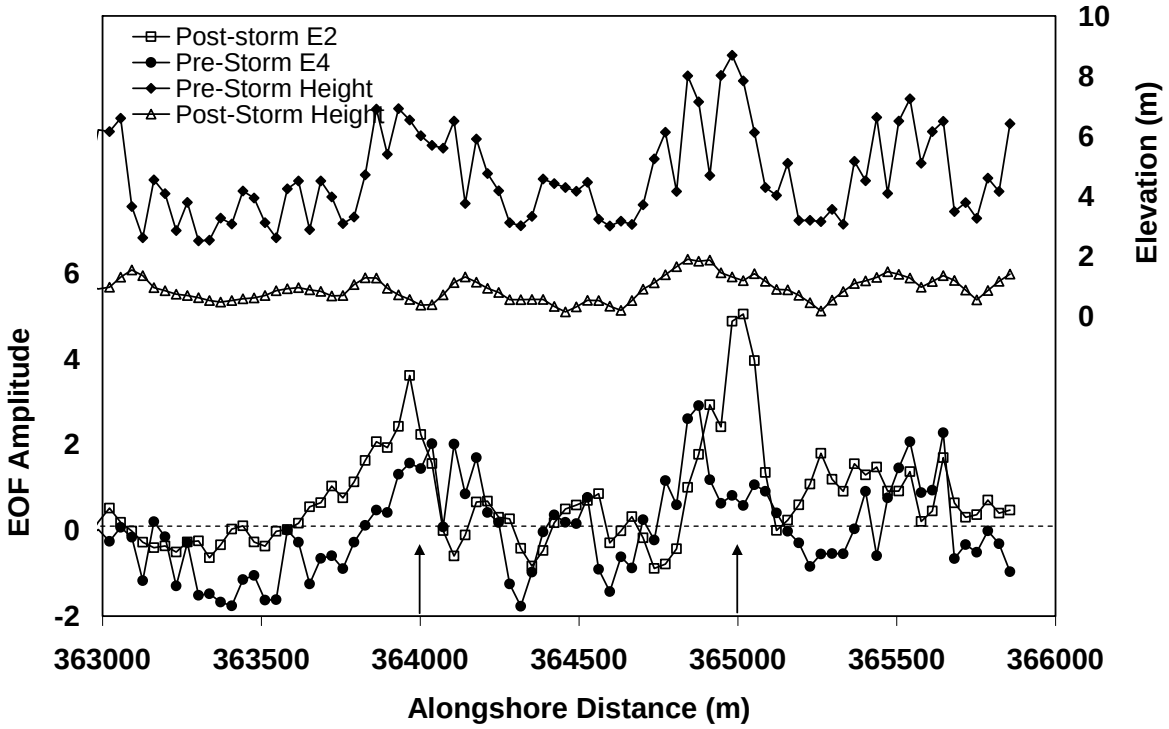


Figure 6. Alongshore variation in pre- and post-storm dune height with the variation in the pre-storm E2 and post-storm E4 amplitudes shown. Two areas that experienced lateral erosion of large pre-storm dunes (positive pre-storm E4) and overwash penetration (large post-storm E2) are shown.

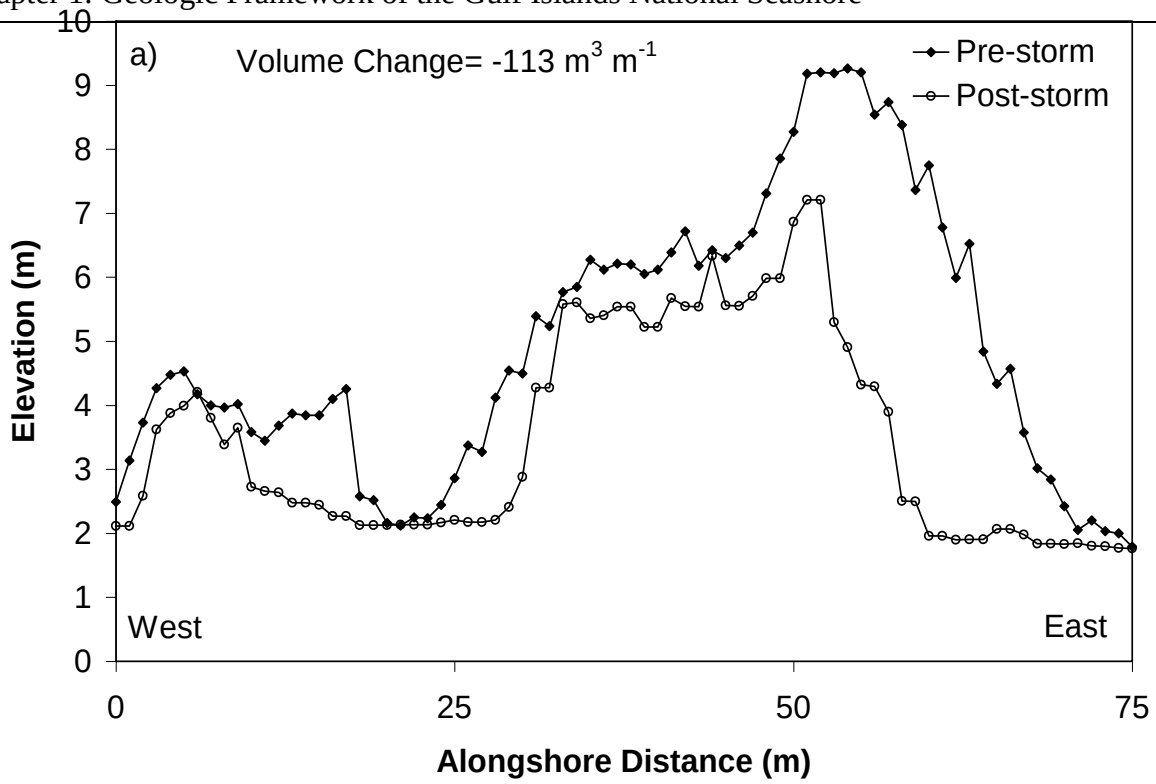




Figure 7. (a) Alongshore profile of a backbarrier dune pre- and post-Ivan with (b) a photograph of the dune showing erosion on the eastern side. The location of the photograph is shown with an arrow in the alongshore profile.

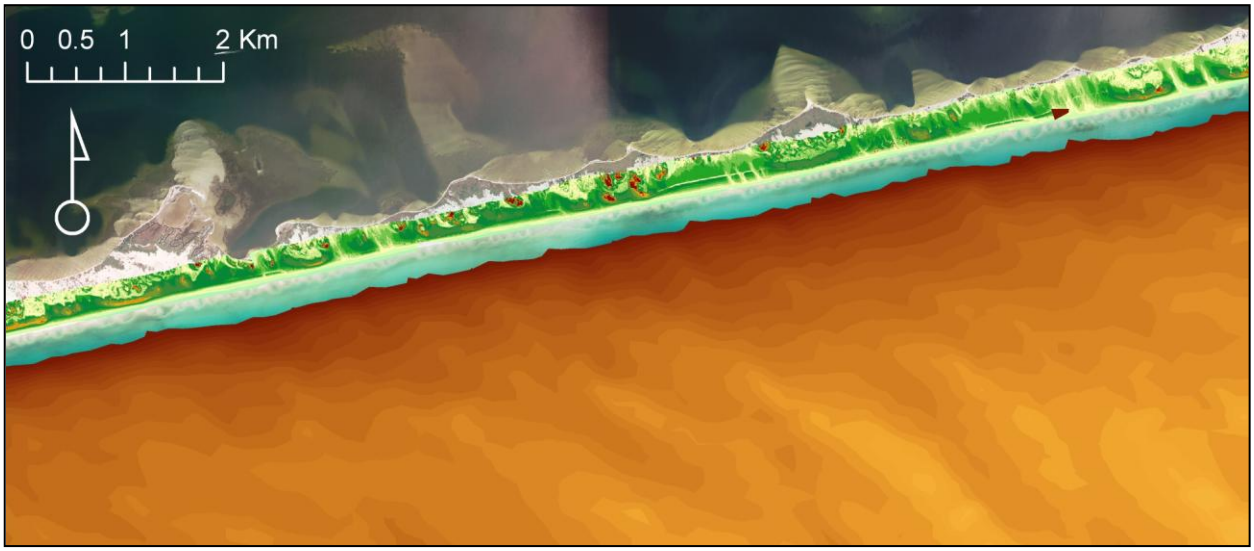


Figure 8. Interpolated bathymetry for the western section of the study site to a minimum distance of ~2 km offshore. The post-Ivan LiDAR is overlain on a satellite image to show the location of the breaches in relation to the offshore ridges and troughs.

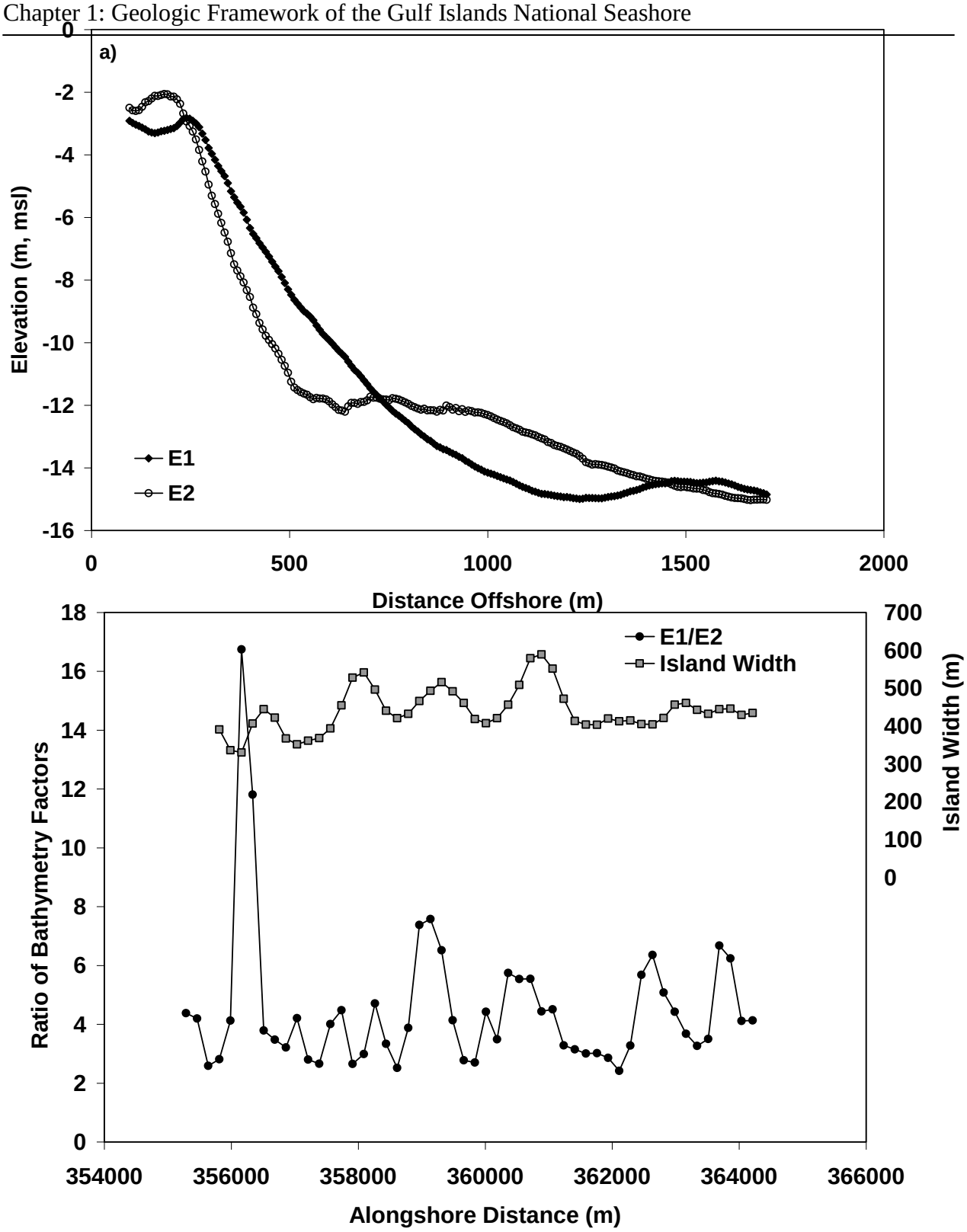


Figure 9. (a) Characteristic bathymetry profiles based on the factor scores of the significant eigenmodes for bathymetry. Also shown (b) is the alongshore variation in the ratio of factor loadings for the eigenmodes. A large ratio represents a gently sloped shoreface and is associated with the crest of a transverse ridge.

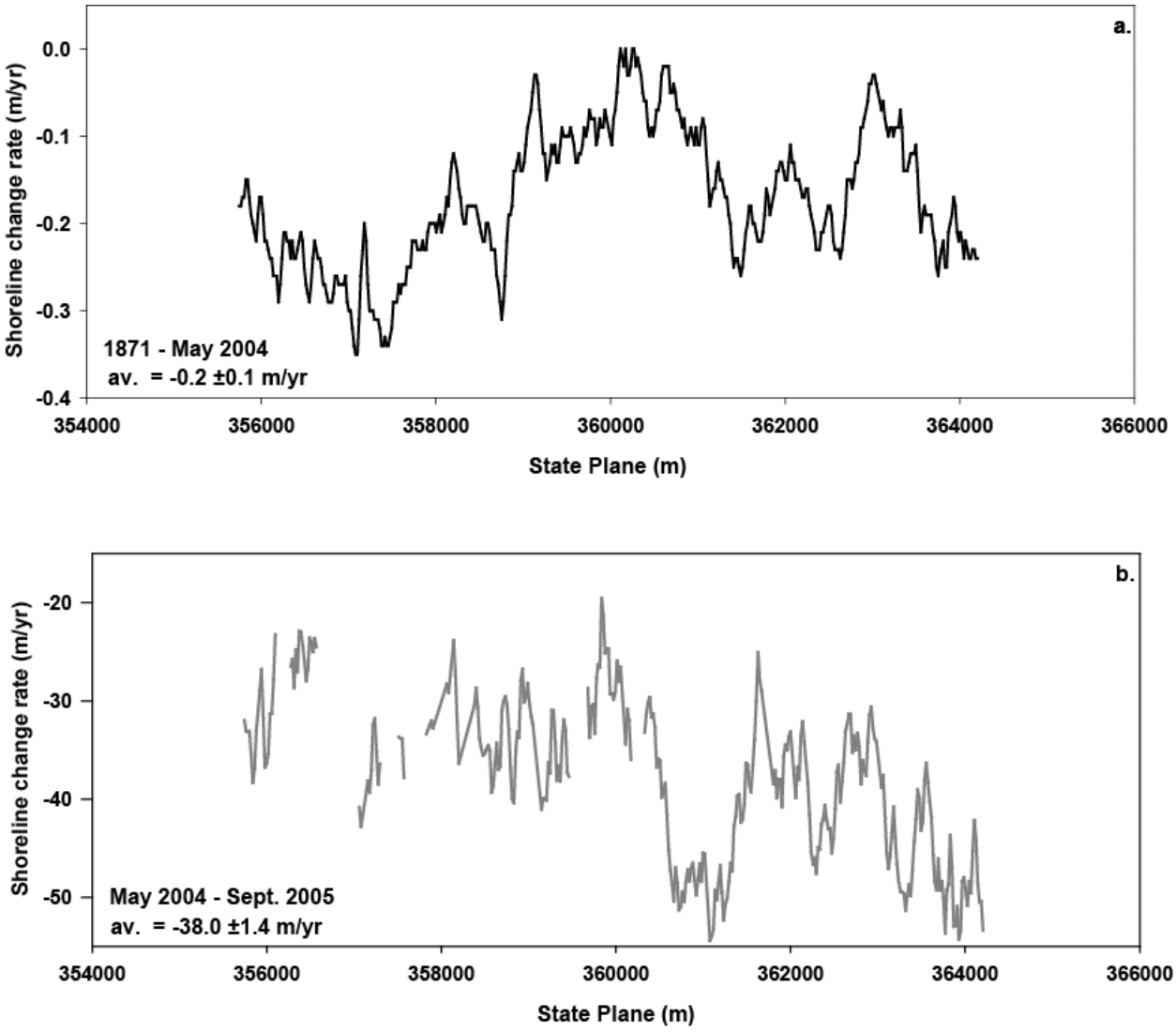


Figure 10: Shoreline change rates for east-central Santa Rosa Island. a) long-term rates from 1858 to May 2004 (pre-Ivan). The long-term rates are relatively low in this portion of the island, ranging from 0.0 to -0.35 (±0.1) m/yr; b) storm related shoreline change related to the hurricanes of 2004 and 2005. Note that the vertical scales are different to accommodate the two orders of magnitude difference in change rates from the long- to short-term. The average storm-related rate of change ranged from -19.6 to -54.4 (±1.4) m/yr.

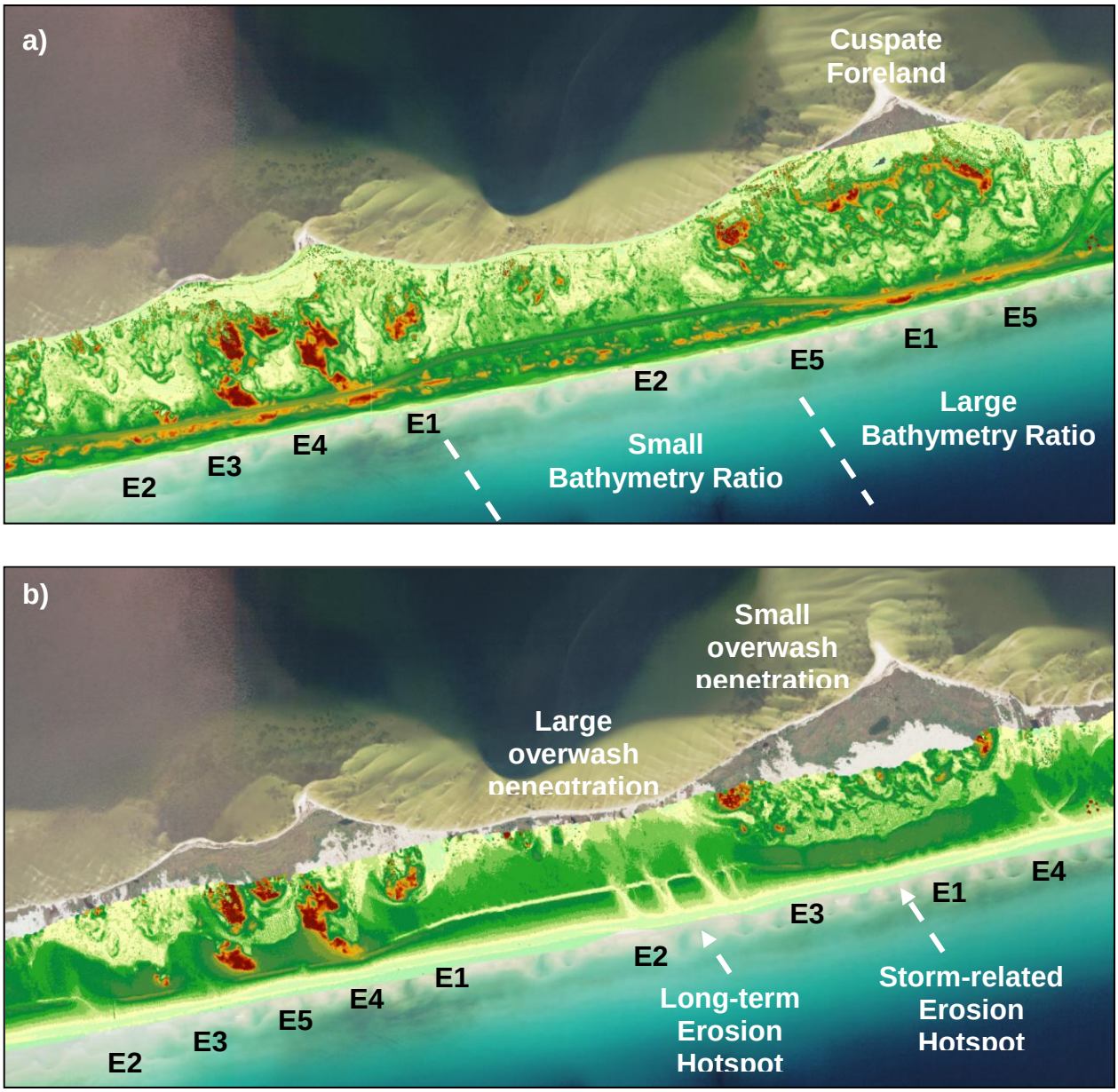


Figure 11. LiDAR images for a representative section of the study area for (a) the pre-Ivan and (b) the post-Ivan topography. Also shown are the largest (and most representative) factors for the pre-Ivan and post-Ivan dune transects representatively. The location of the erosion hotspots, cuspate forelands and transverse ridges (large bathymetry ratio) are also shown for the 1450 m length scale.

CHAPTER 2

Evolution of Overwash Deposits and Post-Hurricane Dune Recovery with Hurricane Katrina

Chris Houser

Department of Environmental Studies
University of West Florida
11000 University Parkway
Pensacola, Florida
32514

STUDY OVERVIEW

Hurricanes and tropical storms produce elevated water levels and large waves (heights >1 to 2 meters), capable of eroding the beachface and causing overwash and barrier breaching. The impact of a storm on a barrier island depends on the vertical geometry of the coast, which in turn depends on the extent and height of foredune development (Thieler and Young, 1991; Sallenger, 2000). This balance not only depends on the characteristics of the storm and its tracking, but also on the sequence of past storm events and the morphological response to those storms (Morton, 2002). For example, the impact of Hurricane Alicia on Galveston Island, Texas was magnified by the absence of a protective foredune that had been eroded three years earlier during Hurricane Allen and had not had sufficient time to recover (Morton and Paine, 1985). Similarly, the response of Santa Rosa Island during Hurricane Ivan (2004) was conditioned by the morphological changes that occurred during Hurricane Opal (1995). During Hurricane Opal, dunes in undeveloped sections of Santa Rosa Island were significantly reduced in height through direct wave erosion and the transfer of sediment to the backshore by overwashing. The dune system redeveloped from and within the overwash sediments and through sediment delivery to the beachface under fair-weather conditions. It is hypothesized that the response of Santa Rosa Island to Hurricane Katrina was conditioned by the lack of a foredune, which was not able to develop following Hurricanes Ivan and Dennis. As a result, the shoreline of the Gulf Islands National Seashore in the Florida Panhandle suffered beach erosion and widespread overwash and breaching, despite Hurricane Katrina making landfall along the border of Louisiana and Mississippi.

The warming of Atlantic sea-surface temperatures with the Atlantic Multidecadal Oscillation (AMO) has increased the frequency and magnitude of extreme storms (tropical storms and hurricanes) along the Gulf Coast (see Keim *et al.*, 2004). An increase in the frequency of extreme storms reduces the time available for the barrier island to recover and is therefore important to the long-term evolution of the barrier. In general, the recovery of the barrier island following a large storm depends not only on the local sand supply but also on the volume of sediment contained within the overwash deposit. Stone *et al.* (2004) found that the barrier islands along the northern Gulf of Mexico can conserve mass during catastrophic hurricanes through the generation of overwash fans. While the seaward shoreline of the barriers within the

National Seashore have been generally stable following these storms (Stone, 1991), the overwash deposits along the backbarrier shoreline have been eroding at an average rate of ~2 m yr^{-1} (Stone and Morgan, 1993; Armbruster *et al.*, 1995; Chaney and Stone, 1996; Armbruster, 1997; McBride and Byrnes, 1997) with event-based erosion of >10 m yr^{-1} (Stone *et al.*, 2004). The erosion has been linked to cold-front passage over the Northern Gulf of Mexico (Armbruster *et al.*, 1995; Chaney and Stone, 1996; Armbruster, 1997; Stone *et al.*, 2004), which generate strong northerly winds and steep high-frequency waves (Kraus *et al.*, 1991).

Following an extreme storm, dunes can redevelop from and within the overwash sediments (Leatherman 1976; Armon, 1979; Leatherman, 1979) and through sediment delivery to the beachface under fair-weather conditions and littoral drift (Psuty, 1992). The availability of sediment from both environments can be limited by the presence of moisture (Belly, 1964; Hotta *et al.*, 1984; Sherman *et al.*, 1998; Cornelis *et al.*, 2004; Wiggs *et al.*, 2004; Davidson-Arnott *et al.*, 2005), the wind regime (Tsoar and Werner, 1998), lag deposits (Nickling and McKenna Neuman, 1995; McKenna Neuman, 1998) and fetch length (Bauer and Davidson-Arnott, 2003; Davidson-Arnott *et al.*, 2005; Hesp *et al.*, 2005). The availability of sediment from the beachface will further depend on swash zone processes and the morphodynamics of intertidal and subtidal bars (Aagaard et al., 2004), which can limit dune develop even in the presence of suitable transport conditions.

The aeolian sediment drift potential, calculated from the Fryberger Method (Lettau and Lettau, 1978), suggests that the frontal storms responsible for overwash erosion are also responsible for renewed foredune development. In this respect, the sediment contained within the overwash deposit is important to the post storm recovery of the foredunes and therefore determines the response of the barrier island to subsequent storms. As the overwash deposits created during Hurricane Katrina are eroded, the availability of sediment for dune development is reduced. This limits the height and extent of the foredune and the barrier island becomes more susceptible to overwash and inundation during the next extreme storm (Sallenger, 2000). While Hurricane Katrina made landfall west of the Gulf Islands National Seashore in the Florida panhandle, overwash was extensive and the impact of this storm to the longer-term evolution of the island may be substantial.

Topographic forcing by remnant dunes is unclear, since the morphology of remnant dunes is more reflective of frontal and vertical erosion by surge water. The morphology of the dunes will vary alongshore depending on the elevation of the surge relative to the pre-storm dune morphology (Sallenger, 2000). Flow compression and acceleration by this morphology has the potential to increase sediment transport to the crest (Hesp, 2002; Hesp *et al.*, 2005). The increase in transport can be countered by vegetation, which increases momentum loss at the bed and promotes deposition, depending on the species type, cover, stem density, distribution and height. Dune recovery can be expected if there is an unlimited supply of sediment, but if the upwind sediment supply is limited, the accelerating flow can lead to erosion as saltation cascades over the stoss slope (Lancaster *et al.*, 1996), despite the presence of vegetation common in coastal environments.

The redistribution of sediment between the shoreface and overwash depends on the alongshore variations in the extent and height of the fronting dune morphology. The resulting dune development can reinforce alongshore patterns in overwash and breaching during subsequent storms (Morton and Sallenger, 2003). While dunes along Cape Hatteras are relatively continuous, variations in dune height (in excess of 8 m) have been noted at scales of kilometers to tens of kilometers (Elko et al., 2002). Wetzell (2003) showed that the alongshore variation in storm impact was consistent with the variation in dune height and the Storm Impact Scale of Sallenger (2000). In areas where there is frequent and extensive overwash the dune field tends to develop as a mosaic of alongshore patches that vary in age and composition (Stallins and Parker, 2003). While the dunes will obstruct overwash penetration, surge water may be forced into the intervening areas of low elevation, which can become washover conduits (Morton, 2002). It is reasonable to expect that the concentrated flows within these conduits could impact adjacent foredunes through lateral erosion, which could increase overwash penetration where dune height is variable.

Even if sediment is available, foredune recovery is only initiated when vegetation is able to re-establish with sufficient density and coverage to promote sediment deposition (Snyder and Boss, 2002). Vegetation can redevelop from existing seedbanks and through rhizome expansion,

which is partly determined by the impact of the extreme storm on the dune system. The growth in leaf area, height and coverage density can be initiated by fresh sand input and burial (Disraeli, 1984), although rapid rates of deposition and burial can inhibit growth of burial intolerant species (Morton and Sallenger, 2003). A preferential selection of burial tolerant vegetation will lead to a change in the stability domain of the dune system (Stallins, 2005) and the development of dunes with limited relief that promote overwash and breaching. Only in the absence of disturbance is vegetation able to reestablish and the dune height able to increase (Stallins, 2005; Snyder and Boss, 2002). Spatial variations in vegetation will be a response to the post-hurricane morphology (Stallins and Parker, 2003) and cross-island environmental gradients (Snyder and Boss, 2002), while the development of vegetation cover will depend on the frequency of disturbance.

Despite recent studies documenting the post-storm erosion of overwash deposits within the northern Gulf of Mexico (see Stone et al., 2004), the mechanisms responsible for changes in the overwash volume and the sediment transport pathways along the backbarrier have not been examined. Moreover, the relative rates of aeolian sediment transport from the overwash deposit and the loss of overwash area and volume have not been considered, despite the importance of this balance to the post-storm recovery of the island.

STUDY OBJECTIVES

The study examined the morphological evolution of an overwash fan during[1] and following Hurricane Katrina and the consequence of changes in overwash volume to aeolian transport and the post-storm recovery of the foredune. To accomplish the aims of this study, the following objectives were identified:

1. Characterize the aerial and volumetric development of the overwash deposit during Hurricane Katrina (or an extreme storm)

2. Examine the evolution of the overwash fan during frontal storms following Hurricane Katrina.

3. Examine the aeolian transport and resulting deflation across the evolving overwash deposit and to quantify changes in the supply of overwash sediment available for redevelopment of the foredunes

The results of this study are presented in 3 papers:

- **Controls on Overwash:** EOF Analysis of Morphological Response to Hurricane Ivan, Accepted to Coastal Sediments 2007.[1]

- **Evolution of Overwash Deposits:** Hydrodynamics and morphological response of an overwash fan following Hurricane Katrina. Not submitted for publication.

- **Dune recovery:** Post-hurricane Airflow and sediment transport over a recovering dune, Submitted to Journal of Coastal Research.

[1] The swath width of the Hurricane Katrina LiDAR data did not appear to provide sufficient detail on the size of the overwash fans. Due to the observed controls on overwash development (offshore transverse bars) and relative elevation of the storm surge and island elevation during both storms, the data from Hurricane Ivan provides a good substitute.

STUDY SITE

Santa Rosa Island is a narrow sandy Holocene barrier island extending over 80 km in length, from East Pass near Destin in the east to Pensacola Pass in the west. The second-longest barrier island on the U.S. Gulf Coast, Santa Rosa Island is separated from the Pleistocene mainland coast by Santa Rosa Sound, a continuous lagoon 3 km wide in the west and tapering to less than 400 m in the east (Kwon, 1969). Although some scholars ascribe the origin of the island to erosion of a central Pleistocene "core" and longshore redistribution of sediments (Otvos, 1982), others (Kwon, 1969; Stone, 1991; Stone et al., 1992; Stone & Stapor, 1996) attribute longshore sediments derived by bluff erosion east of Destin as contributing most to the island's formation. The island reached its present form by 3000 bp, and it has been characterized by overall transgression since then. On the basis of dated peat and tree stumps, Stone and Morgan (1993) estimated a landward shift of "one island width" over the past 800 years (cited in Otvos, 1997). This translates to a long-term shore retreat rate of about 2 ft/yr at the site of present-day Pensacola Beach.

Santa Rosa Island is microtidal, with an average tidal range of 0.43 m (Armbruster, 1997). In addition to strong wave action on the Gulf side, especially during tropical storms and hurricanes, the island experiences back-barrier shoreline erosion due to wind-driven waves generated by winter polar outbreaks(Armbruster *et al.*, 1995; Chaney and Stone, 1996; Armbruster, 1997; Stone *et al.*, 2004). The overwash deposits along the backbarrier shoreline have been eroding at an average rate of ~2 m yr^{-1} (Stone and Morgan, 1993; Armbruster *et al.*, 1995; Chaney and Stone, 1996; Armbruster, 1997), with event-based erosion of >10 m yr^{-1} (Stone *et al.*, 2004). As a result, the roll-over commonly associated with transgressive island systems is largely absent. Historically, Santa Rosa Island has been been struck by relatively few hurricanes, especially throughout most of the 20th century. In spite of hurricanes in 1906, 1916, and 1926 (when Santa Rosa Island was unpopulated), the island's shoreline position remained relatively stable from 1920 to 1993 (Foster et al., 1999).

Short-term shoreline changes have, on the other hand, been rather dramatic since 1995 because of the passage of several hurricanes and tropical storms (Hapke, *personal communication*), including Erin (1995), Opal (1995), Georges (1998), and various tropical storms. Such changes

have been well documented (e.g. Leadon et al., 1998; Leadon et al., 1999; Liebens, 2000, and unpublished analyses by Olsen & Associates). Due to the lack of a foredune following Hurricane Ivan (2004), this area of the Florida Panhandle suffered beach erosion and widespread overwash and breaching during Hurricane Katrina (2005), despite the storm making landfall along the border of Louisiana and Mississippi (a distance of ~150 km).

METHODOLOGY

Island Morphology and Analysis

Changes to the barrier morphology were quantified by comparing LIDAR images collected immediately before and after landfall using cross-shore transects spaced 50 m alongshore. The cross-shore geometry of the island was examined using empirical orthogonal function (EOF) analysis to identify and reduce the topographic data into common forms. EOF analysis is similar to principal component analysis, except that the variability of structure is examined through space rather than through time. The relationship between the primary modes of the pre- and post-storm topographic data was examined through canonical correlation analysis (CCA). This test is used to investigate whether or not there are patterns that occur simultaneously in two different data sets and to describe the nature of those patterns.

Nearshore Hydrodynamics and Sediment Transport

To monitor the wave and current hydrodynamics and flux of suspended sediment (cross-shore and alongshore), a sediment transport station was deployed along the outer margin of the overwash lobe. The station was equipped with a Nortek Vector Velocometer to measure the wave and current field and an optical backscatterance sensor for measuring suspended sediment concentration (D&A Instrument Company, Model OBS-3). The sensors were set to a nominal height of 0.10 m above the bed and aligned such that positive cross-shore flows are onshore and to the west. The collocation of current meters and concentration sensors permits the calculation of vertical and horizontal distributions of suspended sediment transport rates. Bedload (i.e. sediment transport in a thin layer in contact with the immobile bed) has not been considered, as measurement techniques remain beyond present technology.

The sensors were autonomously deployed and set to sample at 4 Hz for periods of 17 minutes every hour. Owing to a rather large and temporally variable background level of turbidity in Santa Rosa Sound, sensor field offsets were computed for each individual sampling record. To maintain uniformity in data analysis, the offset will be determined as the 10th percentile of the sample values. This threshold approximated the significant break in the cumulative frequency of signal values and best reflected the separation between the background signal and sediment suspension events. While this procedure may introduce some error in computing absolute cross products of velocity and concentration, we are mainly concerned with an examination of relative transport rates and offset errors are unimportant. Using the 'cleaned' and transformed data from both study sites, a no-slip condition between the fluid and sediment grains will be assumed in order to calculate the time-averaged net cross-shore and alongshore suspended sediment transport rate $\langle q_x \rangle_n$ given by:

$$\langle q_s \rangle_n = \frac{1}{n} \sum_{i=0}^{n} u_i c_i \qquad [1]$$

where n is the number of data points in the sample, u is the instantaneous velocity, and c is the sediment concentration. The time averaged net cross-shore transport of suspended sediment can also be expressed as:

$$\langle q_s \rangle_n = \overline{u}\,\overline{c} + \langle u' c' \rangle \qquad [2]$$

where $\overline{uc}$ is defined as the local mean sediment transport rate $\langle q_s \rangle_n$ and computed as the product of the time-averaged velocity and the time-averaged concentration. The term $\langle u'c' \rangle$ is a time-averaged measure of the correlation between fluctuations in the oscillatory current velocity and sediment concentration, which is typically non-zero in the surf zone (Jaffe *et al.*, 1985). This flux coupling term $\langle q_s \rangle_{osc}$ can also be computed using cross-spectral analysis (Huntley and Hanes, 1987), which attributes the total transport to the full range of wave frequencies:

$$\langle q_s \rangle_{osc} = \frac{\Delta f}{F} \sum C_{uc}(f) \qquad [3]$$

$C_{uc}(f)$ is the cospectral variance at a given frequency (f), Δf is the frequency resolution (in this study 0.00098 Hz) and F is the frequency range in the cospectrum. Cospectral density estimates will be separated into low (infragravity wave) and high-frequency (incident wave) components.

Univariate statistical descriptions of water surface elevation, velocity and sediment concentration were computed using Statistica™, with local significant wave heights calculated using the accepted convention of $H_s=4\eta_s$. Average (H_{avg}), root-mean square (H_{rms}), and significant wave heights (H_s) and peak periods (T_{pk}) were also determined from the water surface elevation records using a zero up-crossing approach, in which the wave height was defined as the difference of the maximum and minimum between two consecutive zero up-crossings. Oscillatory skewness at both incident and infragravity frequencies were computed as the normalised, time-averaged third moment about the mean of the cross-shore velocity, and do not incorporate any alongshore contribution or contributions from mean flows. In this way the mean velocity is a distinct component of the velocity field from the skewness. The acceleration skewness was computed by differentiating the velocity in the frequency domain and inverse Fourier transforming. The skewness was then calculated as the mean cube of the time series normalised by the variance.

Dune Morphological Response and Vegetation Cover

As noted, changes to the instrument transect as a result of Hurriance Ivan were quantified by comparing the LiDAR images collected immediately before and after landfall. The cross-island topography was resurveyed using a total station at the start of the study (March 9, 2006) to examine how Hurricanes Dennis (July 2005) and Katrina (September 2005) modified the post-Ivan topography. Changes to the dune morphology during the field study were quantified using a total of 66 erosion pins over the instrument transect at intervals of ~1 m. The rods were measured every week with additional measurements immediately before and after frontal storm activity. Height and percent cover of vegetation was measured in a 1 x 1 m grid centered on each of the erosion pins. The vegetation cover did not change substantially over the course of the study, but significant growth (largely in height) did occur after the study was completed.

This growth period was characterized by a decrease in transport events and a return of precipitation following an extended period of drought.

Wind Speed and Direction

Wind speed measurements were obtained at 4 profile locations across the dune: toe of the seaward slope (S1), mid-seaward slope (S2), crest (S4) and toe of the landward slope (S6). Each mast consisted of RM Young cup anemometers at 0.25, 0.5, 1.0 and 2.0 m, with a Gill Microvane on S6 at 2 m above the surface. Additional near-bed wind speed measurements (at stations S3 and S5) were obtained using Gill Windsonic 2-D anemometers mounted at 0.25 m above the surface. Data from all instruments were recorded continuously at 1 Hz on a Hobo™ data logger for the entire length of the study (March 9-July 1, 2006). Over this extended period, flow directions varied considerably, but only those winds that were within 15^{o} of the transect orientation (cross-shore) will be examined for this study. During these periods, wind speed was reduced to 10-minute averages to provide time-averaged windspeed profiles and 1-hour averages to examine the variation in wind during periods of trap monitoring.

Sediment Transport

Long-term measurement of sediment transport was completed using cylindrical traps at the instrument masts based on the design of Bennett and Olyphant (1998). The traps were 0.6 m in height and had an internal diameter of 0.10 m. Twelve 10 mm wide slots were put into the pipe at 30^{o} intervals. To stop sediment transfer through the trap a 0.04 m cylinder with four 10 mm wide slots was placed in the trap and wrapped with a 0.06 mm stainless steel wire mesh. Field testing of cylindrical traps (in general) suggests that they are similar to wedge-shaped traps in efficiency (Gares *et al.*, 1996; Jackson and Nordstrom, 1997).

During select frontal storms, sediment transport was also measured at all stations using Guelph-Trent sediment traps (Nickling and McKenna Neuman, 1997). The traps are wedged shaped and have a .015m opening at the front and a .115m opening in the back. The back opening is covered with 0.06 mm stainless steel wire mesh resulting in a nearly isokinetic trapping ability. Trap

sampling was initially completed at 30-minute intervals but was extended to hour-long intervals due to the small amount of sediment collected at all stations over the shorter sampling interval.

EOF ANALYSIS OF MORPHOLOGICAL RESPONSE TO HURRICANE IVAN

C. Houser, S. Hamilton, K Meyer-Arendt, J Oravetz

Department of Environmental Studies, University of West Florida, 11000 University Parkway, Pensacola, Florida, 32514.

Email: chouser@uwf.edu, shamilton@uwf.edu, kjma@uwf.edu, jro8@students.uwf.edu

ABSTRACT

Hurricane Ivan, a Category-3 hurricane, came ashore near Gulf Shores, Alabama, on September 16, 2004. Santa Rosa Island, Florida, was within the northeast quadrant of the storm and subject to surge heights in excess of 3 m. As a result the area suffered significant sediment loss (>200 m^3 m^{-1}) and widespread overwash and breaching. Morphological changes were quantified by comparing LiDAR images collected before and after landfall. In general, the morphological changes exhibited an alongshore variation at a range of scales (<1 km), consistent with the variation in foredune height prior to the storm. Overwash penetration is reduced and in some cases overwash is inhibited as the height of the foredune increases, leading to the redistribution of sediment offshore. However, overwash penetration was also observed to increase where lateral erosion was promoted by alongshore variability in dune height. The morphological response and resulting redistribution of sediment was also affected by the presence of secondary dunes. In general, overwash is inhibited and offshore erosion of the beachface is enhanced where a secondary dune was present, particularly where there is little cross-island separation between dunes.

RESULTS

Hurricane Ivan, a Category-3 hurricane, came ashore near Gulf Shores, Alabama, on September 16, 2004 (Figure 1). Santa Rosa Island was within the Northeast quadrant of the storm and subject to surge heights in excess of 3 m. In response, the area suffered significant beach erosion and widespread overwash and breaching. The cross-shore profile changed from a discontinuous foredune backed by hummocky secondary dunes and maritime forest (at the cuspate headlands) to washover terraces at the headlands and sheetwash corridors between headlands (Figure 2). In many cases, the sheetwash corridors developed into breaches that connected the Gulf with the Sound. Changes to the barrier morphology were quantified by comparing the LiDAR images collected

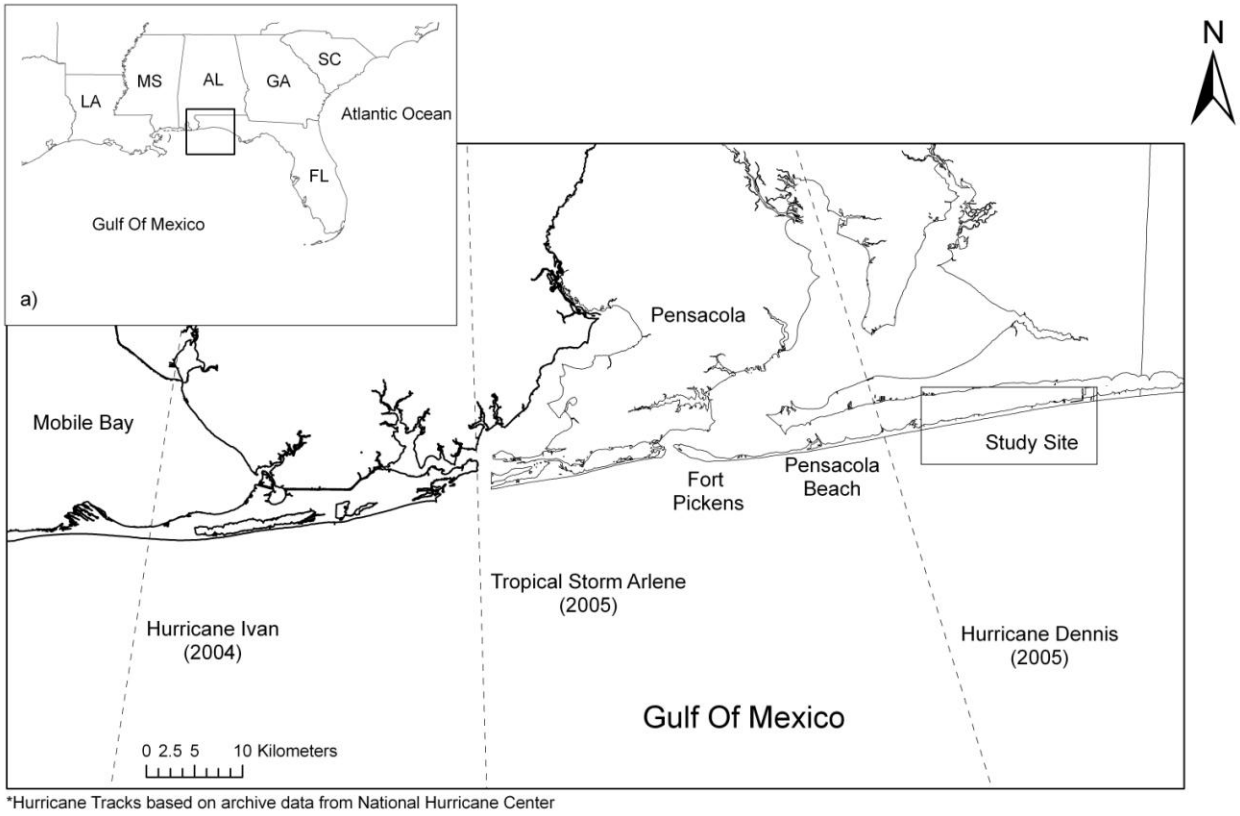


Figure 12. Location of field site within the Gulf Islands National Seashore on Santa Rosa Island in Northwest Florida. Also shown are the tracks for Hurricanes Ivan and Dennis, Tropical Storm Arlene.

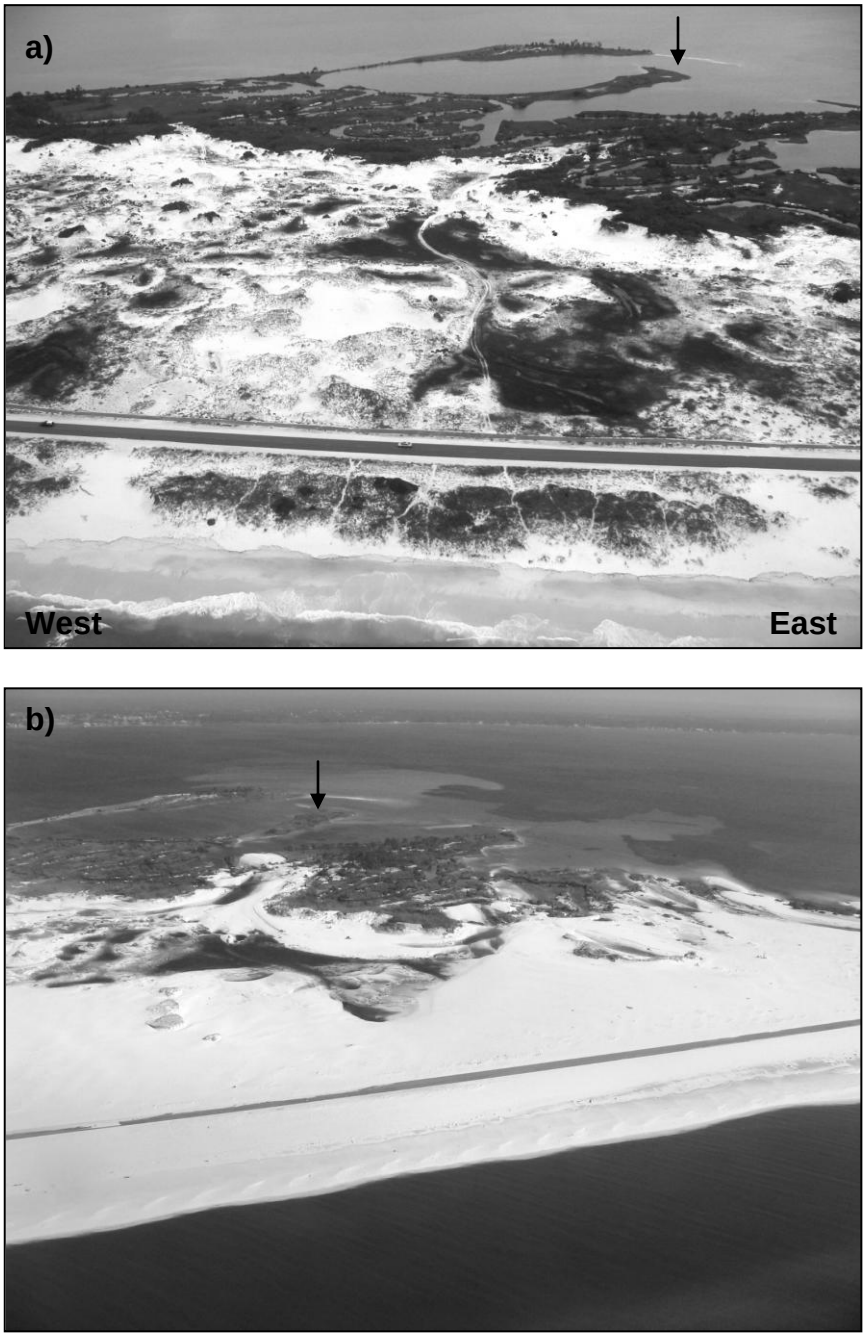


Figure 13. Aerial photographs of a representative area (transects 380-400) on Santa Rosa Island before (a) and after (b) Hurricane Ivan made landfall. Big Sabine Point is identified for reference.

immediately before and after landfall using cross-shore transects spaced 50 m alongshore. Representative pre- and post-storm LIDAR images are provided in Figure 3.

Morphological Changes

A comparison of the pre- and post-storm alongshore variation in foredune elevation is provided in Figure 4a. The foredune height exhibited considerable variability alongshore and was in some cases discontinuous with an average elevation above-sea-level of ~4.3 m prior to the storm. Through spectral analysis, it is found that the variation in dune height is periodic, with statistically significant spectral peaks at 9, 14, 31 and 76 transects. The average elevation within the foredune area was reduced to 2.3 m, with remnant dunes remaining only where relatively large continuous dunes had been present. The post-storm elevation data also exhibits an alongshore periodic variation at 31 and 76 transects and relatively muted variations at 9 and 14 transects. The length of overwash penetration varies inversely with the pre-storm dune height but only exhibits the larger-scale periodicity at 31 and 76 transects (Figure 4b). This suggests that overwash penetration is not sensitive to local-scale variations in the pre-storm dune height, which may reflect lateral transport of overwash sediments between transects. The length of overwash penetration exhibits signification autocorrelation at a lag of 7 transects, while the foredune height pre- and post-storm data exhibits significant autocorrelation at lags of 4 and 7 transects respectively.

The average pre- and post-storm cross-island profiles are presented in Figure 5. The net change in sediment volume ranged from an erosion of 238 to 43 m^3 per unit width of beach. The largest net losses of sediment (>150 m^3 per unit width of beach) were coincident with the location of breaches, which were observed where the dune crest elevation (based on a 9-point moving average) is at a minimum and close to the surge elevation (Figure 7). The crest of the dune at these locations would have been overtopped early in the storm and would have focused overwash that would eventually precipitate a breach. The breaches were reactivated during Hurricane Katrina (2005) and as documented by Houser et al. (*in prep.*) can be reactivated during frontal storms that coincide with high tide.

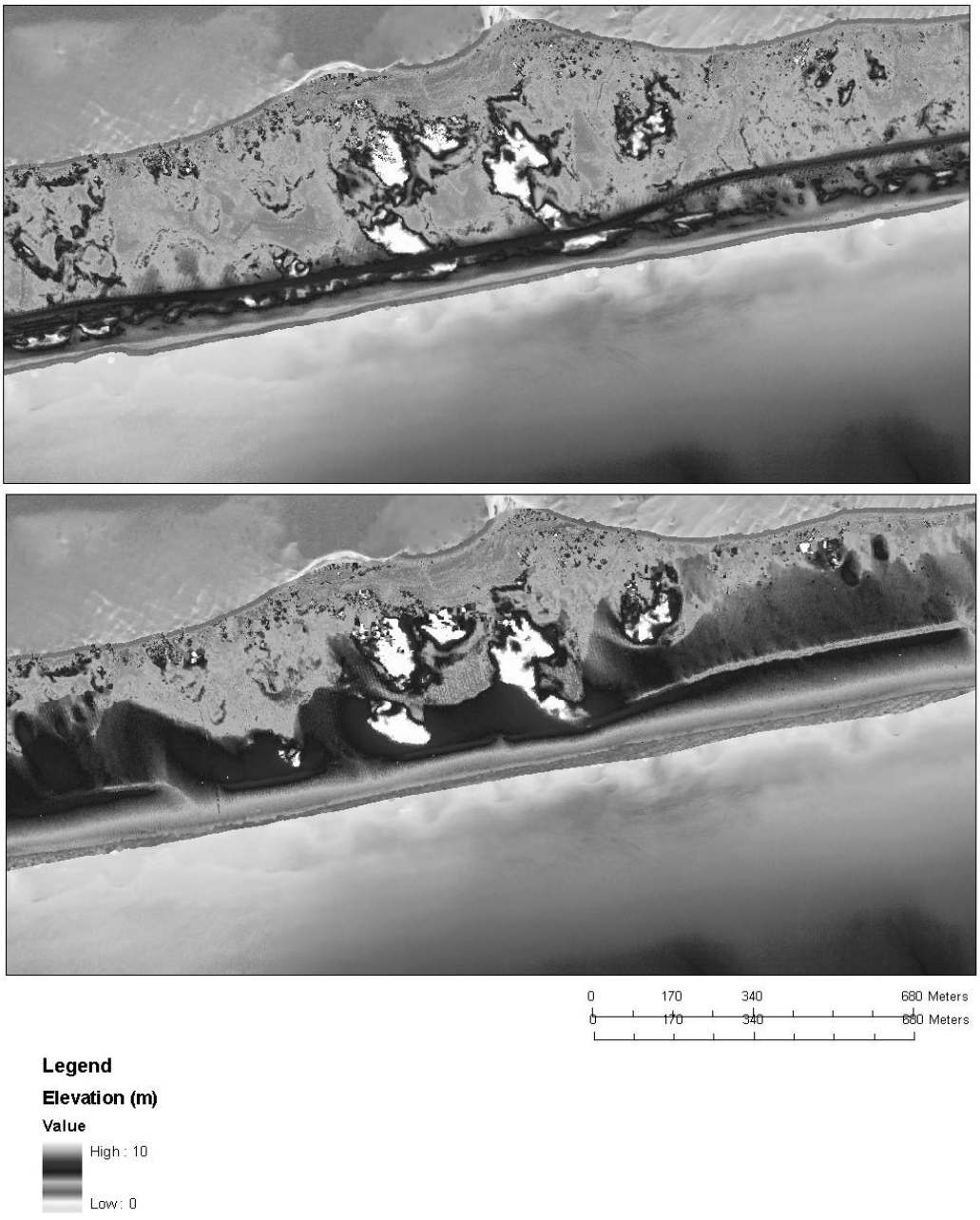


Figure 14. Representative pre- and post-storm LIDAR images from the study area.

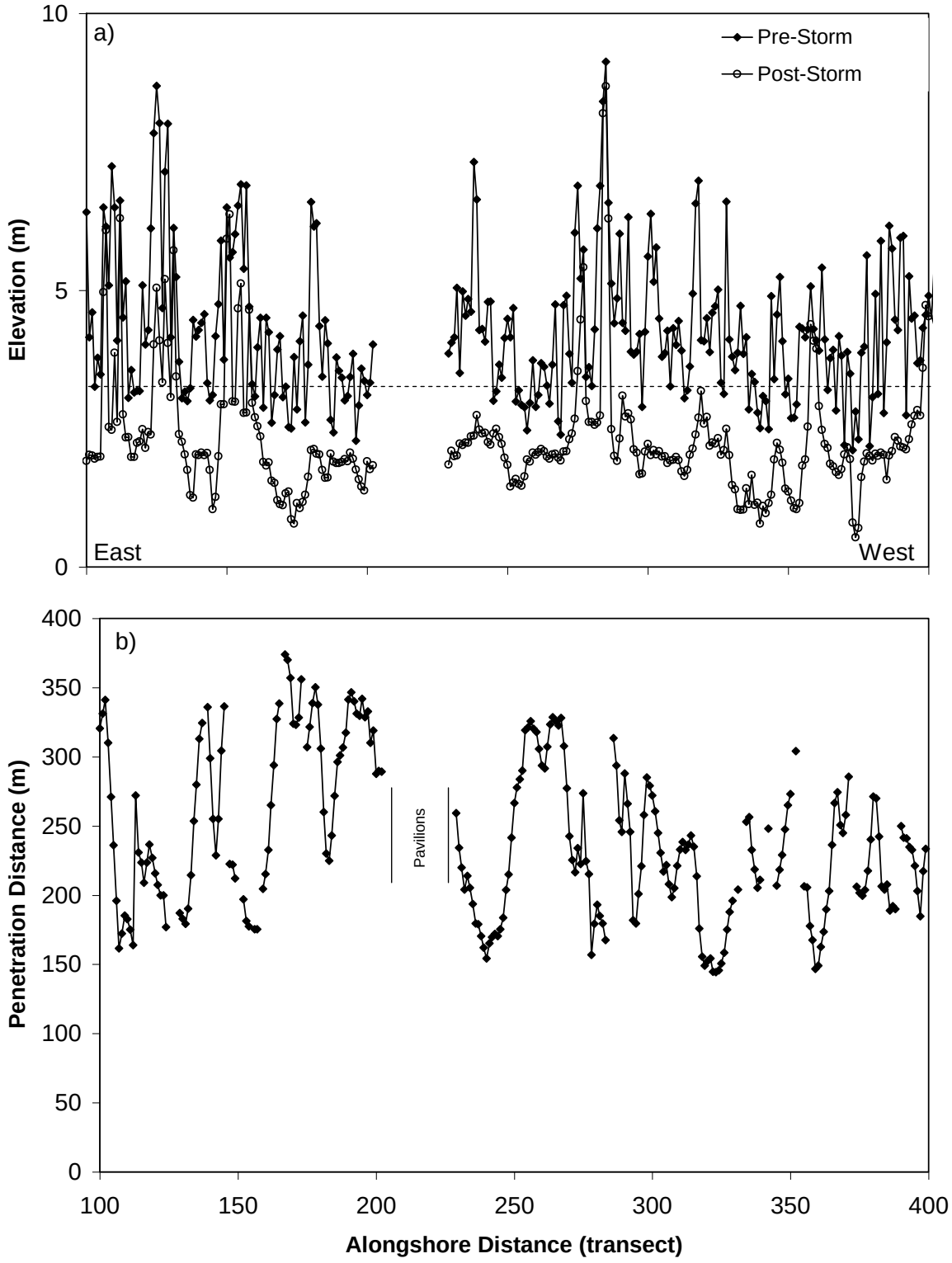


Figure 15. Alongshore variation in (a) the height of the foredune before and after Hurricane Ivan and (b) the cross-shore distance of overwash penetration. The dashed line is the surge elevation.

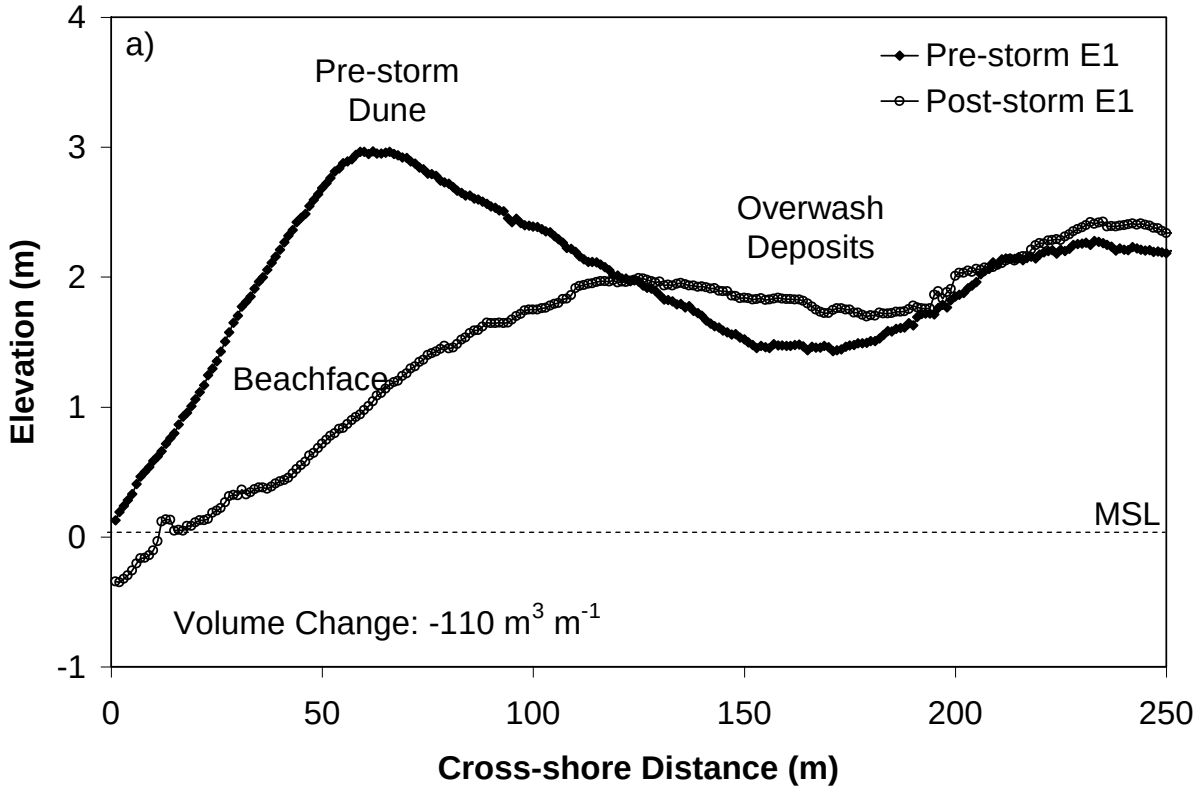


Figure 16. Pre- and post-storm average cross-island profiles with major morphological features identified.

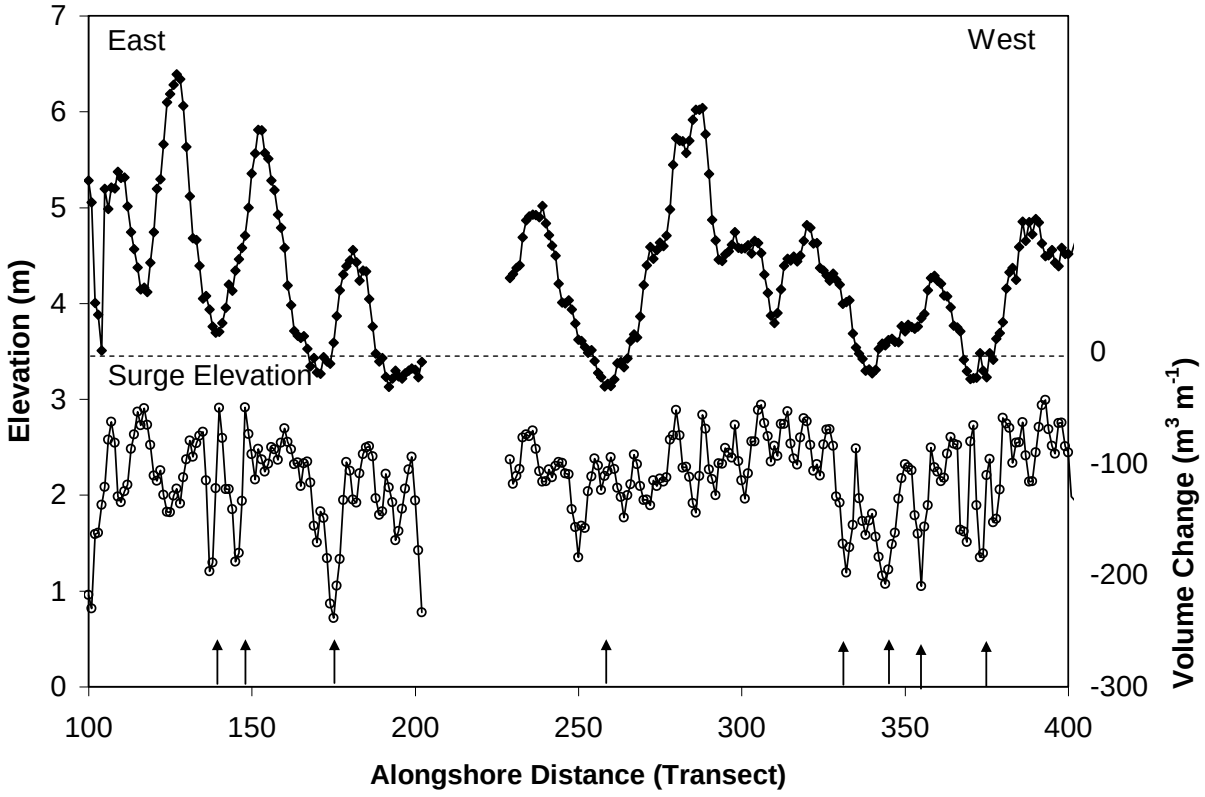


Figure 17. Alongshore variation in dune height modeled using a 9-point moving average and the volume change between the pre- and post-storm profiles. Also shown with the arrows are the locations where breaches were identified.

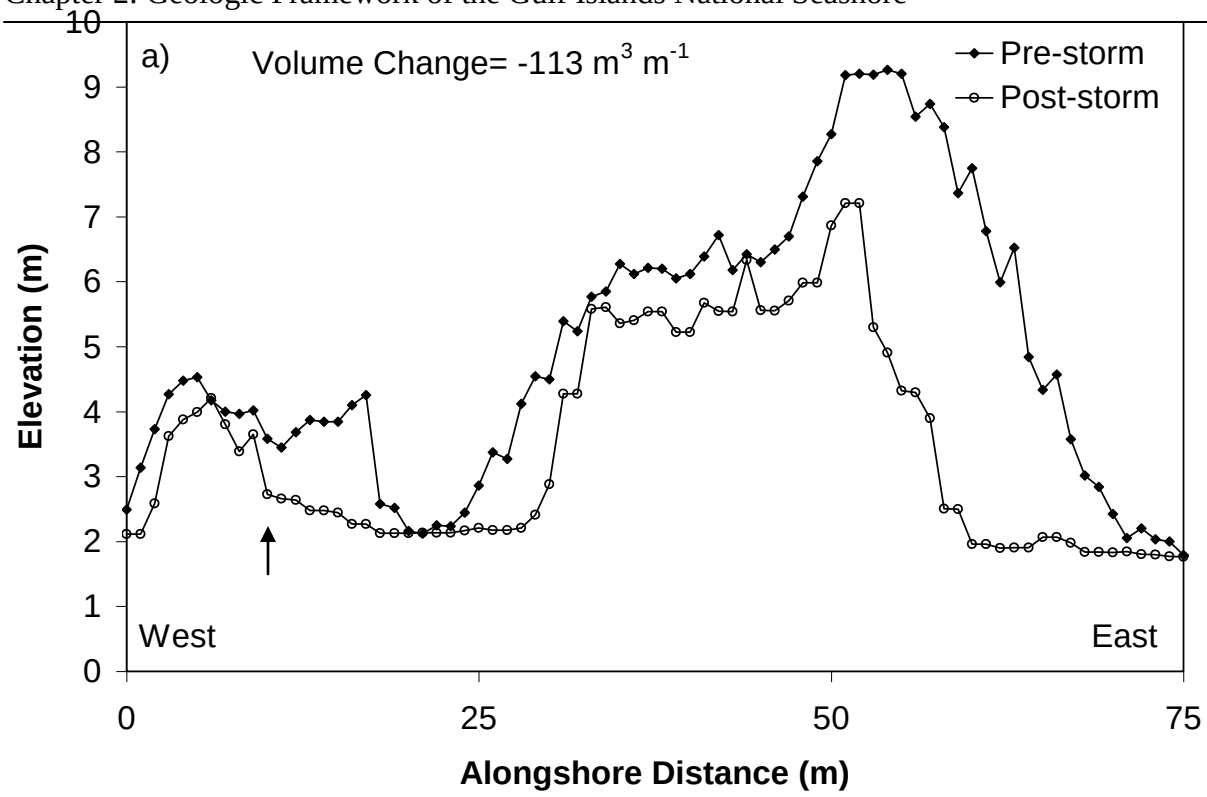




Figure 18. (a) Alongshore profile of a secondary dune pre- and post-Ivan with (b) a photograph of the dune showing erosion on the eastern side. The location of the photograph is shown with an arrow in the alongshore profile.

The amount of sediment removed per unit width of beach exceeded 45% at the breach sites and ~20% on average. The loss of sediment is considerably larger than the volumetric changes presented by Stone *et al.*, (2004) for Hurricane Opal, although sediment volumes in that study were considered to a depth of 1.5 m on both the Gulf and Sound side of the island. Except for the breach areas, the amount of sediment lost from the profile does not exhibit a clear relationship with the pre-storm elevation of the foredune. This suggests that the height of the foredune is not the only control on the redistribution of sediment between overwash and erosion offshore.

As shown in Figure 3, the secondary dunes were still apparent following the storm but exhibited considerable loss of volume, particularly along the east/west slopes. A representative alongshore profile of a secondary dune is provided in Figure 7a. A total of 113 m^3 of sediment was lost per unit width of profile. As shown in Figure 7b, the lateral erosion created cliffed slopes with exposed roots. Many of the shrubs along the exposed slopes shows signs of stress and many are dying in response to the exposed roots and salt-spray exposure.

Empirical Orthogonal Function (EOF) Analysis

EOF analysis was used to identify alongshore recurring patterns in the geometry of the island, which includes both the height and width of the primary dune and the presence of secondary dunes. In both the pre- and post-storm data, the first 5 modes were found to be statistically significant (ρ>0.05), with the percent of the total variance explained being 65 and 75% respectively. The primary eigenmode (E1) for the pre-storm morphology explains 21% of the variance and shows a secondary dune (positive factor weightings) ~170 m landward of the average primary dune (Figure 8a). Secondary dunes are also indicated by positive factor weightings for E3 and E5, at 67 and 117 m landward of the primary dune respectively. The second eigenmode (E2) explains 14% of the variance and exhibits negative factor weightings in the vicinity of the beachface and positive factor weightings on the landward slope of the primary dune. This profile is characterized by a single foredune that is ~20 m landward of the average foredune position and a relatively extensive foreshore and backshore. The fourth eigenmode (E4) has positive factor weightings at the crest of the foredune and is characteristic of a foredune that is ~0.80 m larger than the average dune (see Figure 5).

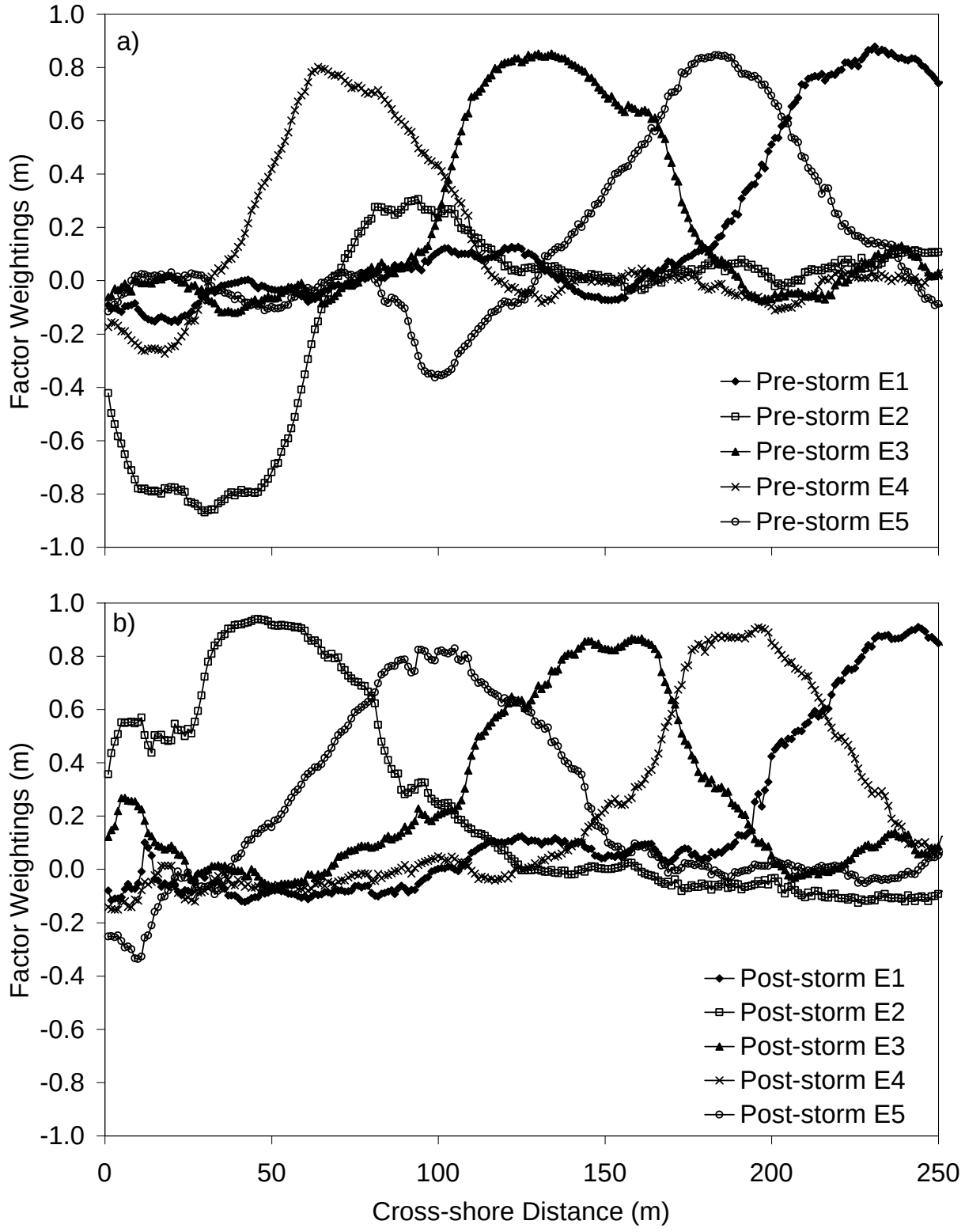


Figure 19. Factor weightings for the first 5 eigenmodes of the (a) pre-storm morphology and (b) the post-storm morphology.

In the post-storm morphology, 26% of the total variance is explained by E1 and 25% of the variance is explained by E2. The primary eigenmode (E1) for the post-storm morphology exhibits positive factor weightings in the backbarrier similar in position and amplitude to the primary eigenmode for the pre-storm morphology (Figure 8b). Remnant secondary dunes are also apparent, to varying degrees, in the profiles for E3 and E4. The location and amplitude of these dunes is consistent with E3 and E5 for the pre-storm morphology. The second eigenmode exhibits positive factor weightings and accretion in the vicinity of the beachface, characteristic of either less beachface erosion or accretion relative to the average post-storm profile (see Figure 5).

Canonical Correlation Analysis

As observed in the EOF analysis, there are similarities in the factor weightings of the pre- and post-storm morphology. Canonical correlation analysis between the factor scores for the pre- and post-storm morphology yields a correlation of 0.73 (ρ<0.05). Results of the analysis are presented in Table 1 and the profiles for pre- and post-storm eigenvalues with both strong negative and positive correlations are presented together in Figure 9. The negative correlation (-0.79) between the pre-storm E2 and post-storm E2 is a reflection of how overwash penetration is inversely related to dune height and that significant overwash penetration and even breaching are observed in areas of low dune height (areas with a negative pre-storm E2). The positive correlation between pre-storm E4 and post-storm E5 (Figure 9e) is a reflection of increased beachface erosion and sediment loss to the offshore with increasing dune height. Overwash penetration is relatively small and in some cases absent where there is a strong positive pre-storm E4 (large dunes). The additional correlation between pre-storm E4 and post-storm E2 (Figure 9f) suggests that large dunes adjacent to smaller dunes can be eroded through lateral erosion. The alongshore variation in factor scores (EOF amplitudes) for a representative section of the study area showing areas of pre-storm E4 and strong post-storm E2 is provided in Figure 10. In areas where there was a lateral erosion of large foredunes, overwash penetration was greater than adjacent areas where the dune height was maintained and sediment was lost offshore. The latter case is represented by the correlation between pre-storm E4 and post-storm E5.

Table 2. Canonical correlation coefficients (*r*) between the pre- and post-storm profiles, with the largest coefficients (strongest relationships) highlighted.

		Post-storm Profiles				
		E1	E2	E3	E4	E5
Pre-Storm Profiles	E1	0.66	-0.06	0.16	0.18	0.14
	E2	0.13	-0.79	-0.07	0.10	0.02
	E3	0.08	-0.06	0.63	0.24	-0.05
	E4	-0.03	0.21	0.23	0.07	0.72
	E5	0.20	0.03	0.04	0.52	-0.24

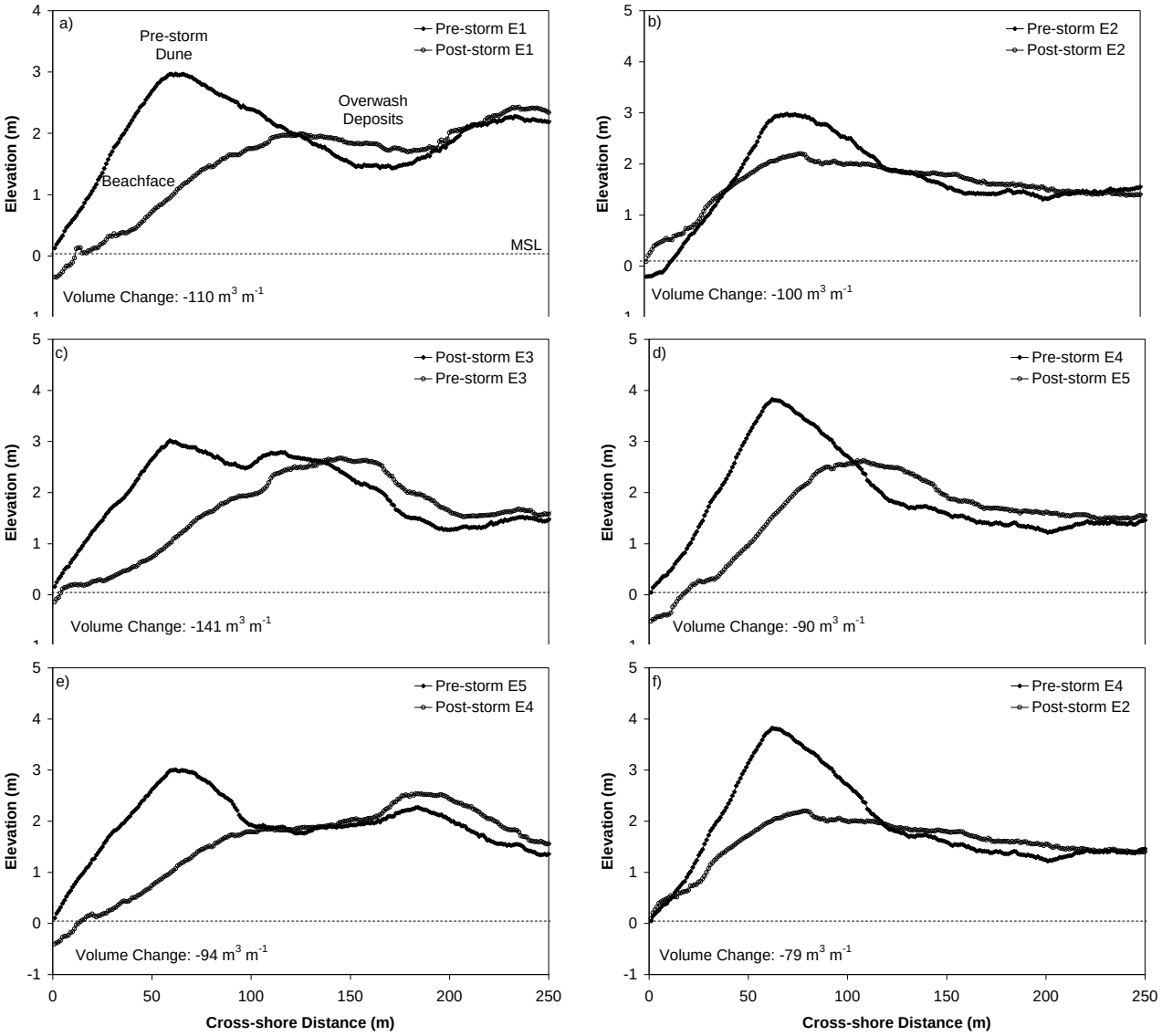


Figure 20. Comparison of cross-island profiles for the pre- and post-storm eigenvalues with strong correlations identified through canonical correlation analysis.

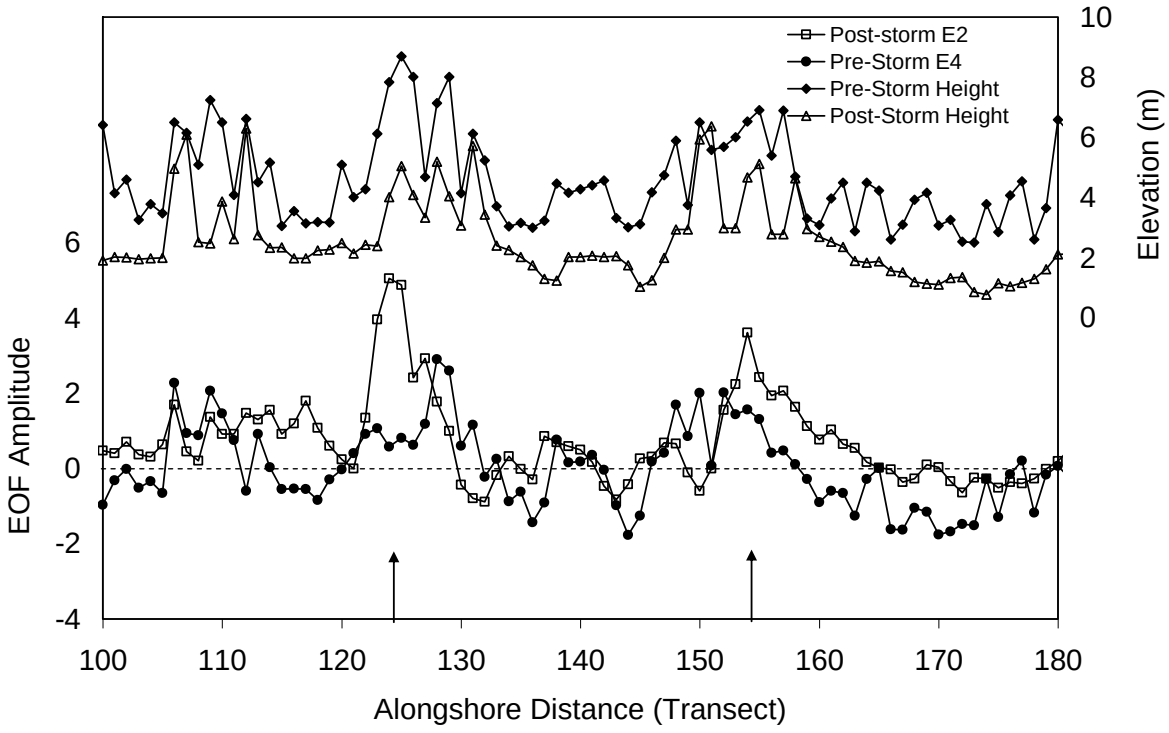


Figure 21. Alongshore variation in pre- and post-storm dune height with the variation in the pre-storm E2 and post-storm E4 amplitudes shown. Two areas that experienced lateral erosion of large pre-storm dunes (positive pre-storm E4) and overwash penetration (large post-storm E2) are shown.

DISCUSSION

It has been well demonstrated in previous studies that the response of a barrier island to an extreme storm depends not only the local magnitude of the storm but also the pre-storm morphology (e.g. Sallenger, 2000; Morton, 2002). The models developed in these studies provide reasonable estimates of storm impact (see Wetzell, 2003), but the models only provide a first approximation based largely on foredune height and there is a need for verification in the prototype. In the present study, LIDAR data is used to examine how the response of Santa Rosa Island to Hurricane Ivan was directed by the pre-storm geometry. Results suggest that the morphological response partly varied in response to the height of the foredune relative to the elevation of the storm surge, which supports the storm impact model of Sallenger (2000). As the height of the foredune increases, overwash penetration is reduced and sediment from the dune and beachface are eroded offshore. Overwash penetration is greater and less sediment is lost from the profie as the height of the foredune is reduced. Those areas where the pre-storm dune height was at or below the elevation of the storm surge would have been overwash early in the storm and continued to erode vertically throughout the storm. The breaches continue to be reactivated during frontal storms when wind speeds can reach 13 m s^{-1} from both the north and south. The breaches were also reactivated during Hurricane Katrina (September 200), despite the storm making landfall ~230 km west of the study site.

The pre-storm height of the foredune exhibited considerable variation alongshore and the variation in the morphological response and profile volume exhibited a similar variation. Prior to the storm, the alongshore variation in the foredune height exhibited periodic variations at 76, 31, 14 and 9 transects. The larger-scale variations remained strong following the storm while the smaller-scale variations were significantly weaker following the storm. If the impact of this storm depended only on the relative elevations of the dune and storm surge, then these small-scale variations would have been maintained and potentially reinforced with larger and sustained impacts where there were small dunes. It is reasonable to expect that the absence of these small-scale variations following the storm is a result of lateral dune erosion and that the scale of variation that is removed (or weakened) by the storm depends on the magnitude and duration of the storm. As noted in a number of studies, surge water can be forced into areas with low dune heights (Wright et al., 1970; Kah and Roberts, 1982; Morton, 2002; Gares and White, 2005) and

the fast flowing water within these conduits is capable of eroding the dunes laterally. As shown in Figure 10, large dunes that were eroded laterally experienced greater overwash penetration than would have been expected based on local dune height alone (see Sallenger, 2000). As a consequence, more sediment was transferred landward in the overwash than was eroded offshore.

The morphological response and redistribution of dune sediment was also found to depend on the cross-island geometry. Where there were no secondary dunes, overwash and sediment erosion offshore were primarily dependent on the height of the foredune (Sallenger, 2000), which was the general case in the eastern section of the study site (transects 115 through 181). Numerous secondary dunes were observed in the western section of the study site (transects 229 to 400) with a periodicity of 38 transects. Where the primary and secondary dunes were closely spaced overwash was restricted and sediment erosion offshore was increased (Figure 9c). This situation was analogous to having a large wide foredune (Thieler and Young, 1991). As the separation between the primary and secondary dune increased, overwash penetration was not restricted and the amount of sediment eroded offshore was reduced (Figures 9a and e). In all cases, the secondary dune exhibited lateral erosion that created cliffed slopes and exposed roots (Figure 7). The shrub vegetation along the edges of the dune are exhibiting signs of stress and many are dying in response to the root exposure and to exposure to salt spray during the storm and following the removal of the foredune.

While the island appears to be uniformly covered an overwash terrace, the results of this study have shown there to be considerable alongshore variability in the morphological response and redistribution of dune sediment. This variation will ultimately affect the recovery of the dune system, such that there will be alongshore variation in the height and extent of the next foredune (Carter, 1988; Carter and Wilson, 1990; Sarre, 1989; Hesp, 1989, 1999; Leys, 1991; Raupach et al., 1993; Hagen and Armbrust, 1994; Musick et al., 1996; Santos et al., 1996; Wilson et al., 1998). If the frequency of extreme storms increase, the alongshore variation will be reinforced and the dunes will develop a mosaic of alongshore patches that have a cross-island orientation (Stallins and Parker, 2003). The secondary dunes on Santa Rosa Island are remnant features that not only survived Hurricane Ivan but had also survived Hurricane Opal in 1995. The alongshore

periodicity of these features (~30 transects) is consistent with the alongshore periodicity in the height of the foredune, suggesting that the alongshore response of the island is directed by a persistent variation in the island geometry that is a reflection of the storm frequency (Stallins and Parker, 2003).

CONCLUSIONS

LIDAR data was used to examine the morphological response of Santa Rosa Island to Hurricane Ivan. Results suggest that, at first approximation, the storm impact was determined by the elevation of the foredune relative to the storm surge. The morphological response and redistribution of dune sediment is also found to vary in response to the local variability in dune height, and the presence of secondary dunes. Depending on the separation between the primary and secondary dune, overwash is restricted and more sediment is eroded offshore. These pre-storm morphological controls vary alongshore and the variation remains in the post-storm morphology and distribution of sediment. This persistent variation alongshore will direct the recovery of the dune system, which will direct the future response of the island and in turn reinforce the pattern.

HYDRODYNAMIC AND MORPHOLOGICAL EVOLUTION OF AN OVERWASH FAN FOLLOWING HURRICANE KATRINA

Department of Environmental Studies, University of West Florida, 11000 University Parkway, Pensacola, Florida, 32514.

Email: chouser@uwf.edu

ABSTRACT

This paper systematically examines the suspended sediment transport and morphodynamics of an overwash fan on the sound-side of Santa Rosa Island, Northwest Florida. Data from collocated concentration and velocity sensors indicate that the direction and magnitude of suspended sediment transport varies with the degree of local wave dissipation. While most of the erosion to the overwash fan occurred during the first cold front following Hurricane Katrina, significant reworking of sediment was still observed during subsequent storms through Spring 2006. The limited data set suggests that sediment is transported offshore during relatively weak storms, when the ratio of wave height to water depth is small, which promotes the development of an offshore-directed current along the upper-shoreface. In contrast, waves tend to break along the seaward edge of the terrace leading to strong skewed accelerations and weak offshore currents. While cross-shore currents were important during the observed storm, the alongshore currents are equally strong despite the almost shore-perpendicular winds. It is concluded that with more oblique winds, transport will become increasingly directed alongshore, in the direction of the cuspate forelands. This suggests that there is a link between the erosion of overwash sediment and the development (or at least maintenance) of the cuspate forelands.

RESULTS

Profile Variation

The most dramatic changes to the overwash fan occurred during the first frontal system following Hurricane Katrina, which was well before this study commenced (December 2005). The shoreface profile was initially characterised by a small berm near mean high water and a low amplitude bar at a distance of 15 m from the shoreline (Figure 11). Over the 2 month period of instrument deployment (February-April), the bar migrated ~7 m offshore and ~1.5 m^3 of

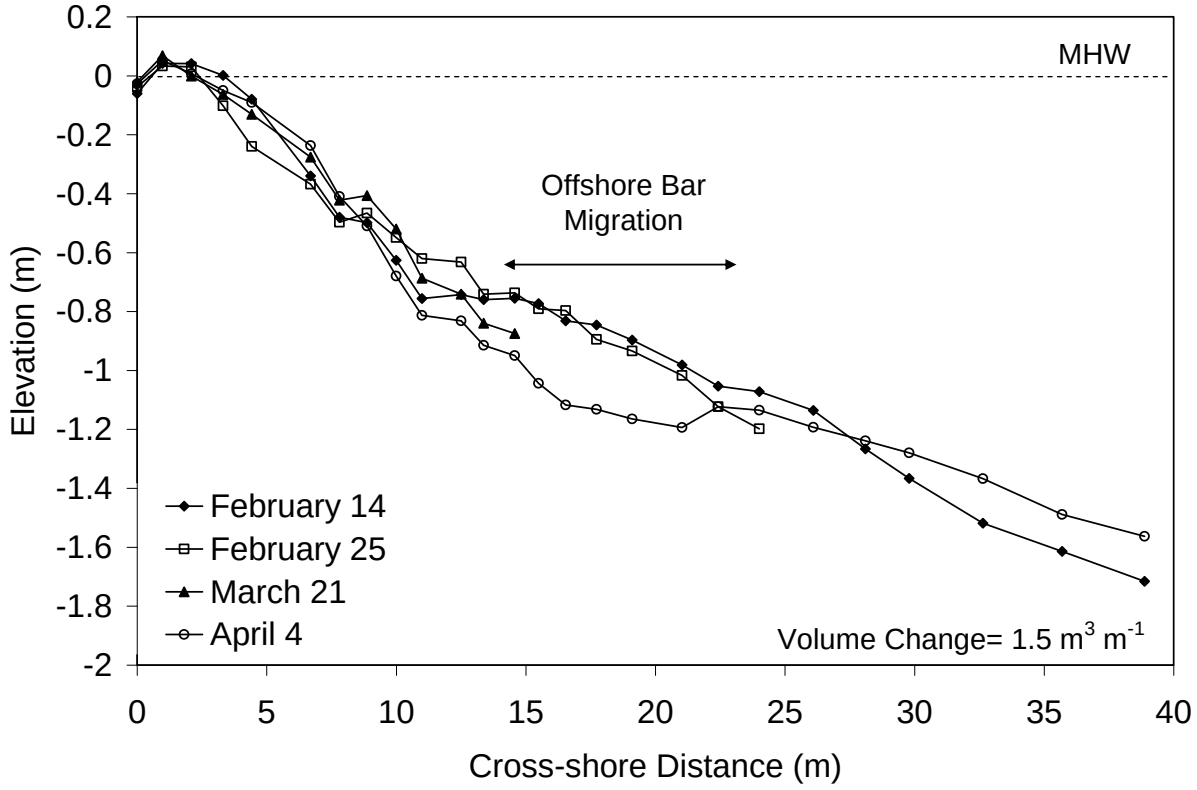


Figure 22. Backbarrier transect data for February 14- April 4, 2006.

sediment was lost per meter of shoreline. It appears that most of the sediment was transported offshore to the outer edge of the shoreface terrace.

Hydrodynamics and Sediment Transport

The time series of significant wave height, current velocities and sediment concentration (FTU) are presented in Figure 12 for a frontal storm on February 19, 2006. Winds from the north reached 6.7 m s^{-1} early on the 19th (2:53 am), diminishing to 1.3 m s^{-1} by 16:53. Despite this decrease, the significant wave height (at the 1 m isobath) persisted till the next day. Owing to the gently sloping shoreface, waves broke seaward of the terrace, creating a relatively wide surf zone throughout the storm. The surf zone was characterised by spilling breakers. The local significant wave height to depth ratio ($\gamma=H_s\ h^{-1}$) reached a maximum of 0.35 early in the storm and secondary maximum of 0.21 towards the end of the storm, when there was a temporary increase in wind speed and wave height offshore. This period was associated with an increase in the wave period from ~2.5 s early in the storm to ~5 s (Figure 13). Wave skewness was relatively strong (Houser, 2004), reaching a maximum of 0.76 m s^{-1} at 7:00 followed by a rapid decrease in skewness with the increase in wave height.

Suspended sediment concentrations reached a maximum in response to the second increase in wave height (9:00) and the largest wave periods and water depths (Figure 14). The cause of this increase could not be identified, although it is possible that there was a change in bed elevation. If there was (even temporary) accretion beneath the current meter, then the concentration of sediment will increase independent of changes to the water level and wave activity.

Through the early part of the storm there was a relatively strong onshore-directed mean current 0.13 m s^{-1} and an alongshore current <0.05 m s^{-1} (within the range of error). The strength of the cross-shore current fell within the error band of the sensor early in the storm, such that the mean currents represented a minor contribution to the transport. As a consequence, sediment transport at the height of the instrument was directed onshore, leading to the slight shoreface recovery through onshore bar migration between February 14 and 25. The burst-average sediment concentration reached a maximum of ~25,000 FTU at 9:30, apparently in response to rapid accelerations in the cross-shore velocity along the leading face of the incident waves.

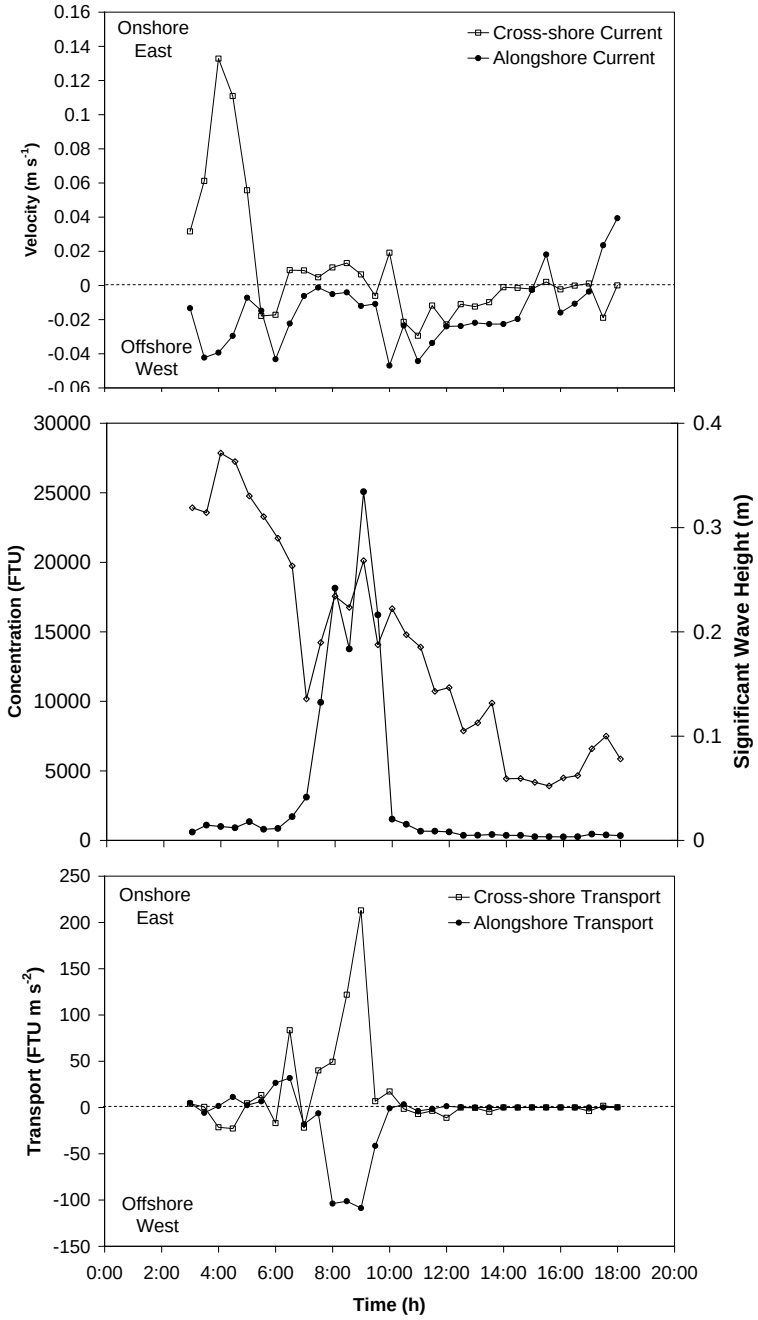


Figure 23. Hydrodynamic and transport data from February 19, 2006 storm. Shown are (a) Cross-shore and alongshore current velocities, (b) sediment concentration and significant wave height, and (c) net cross-shore and alongshore sediment transport.

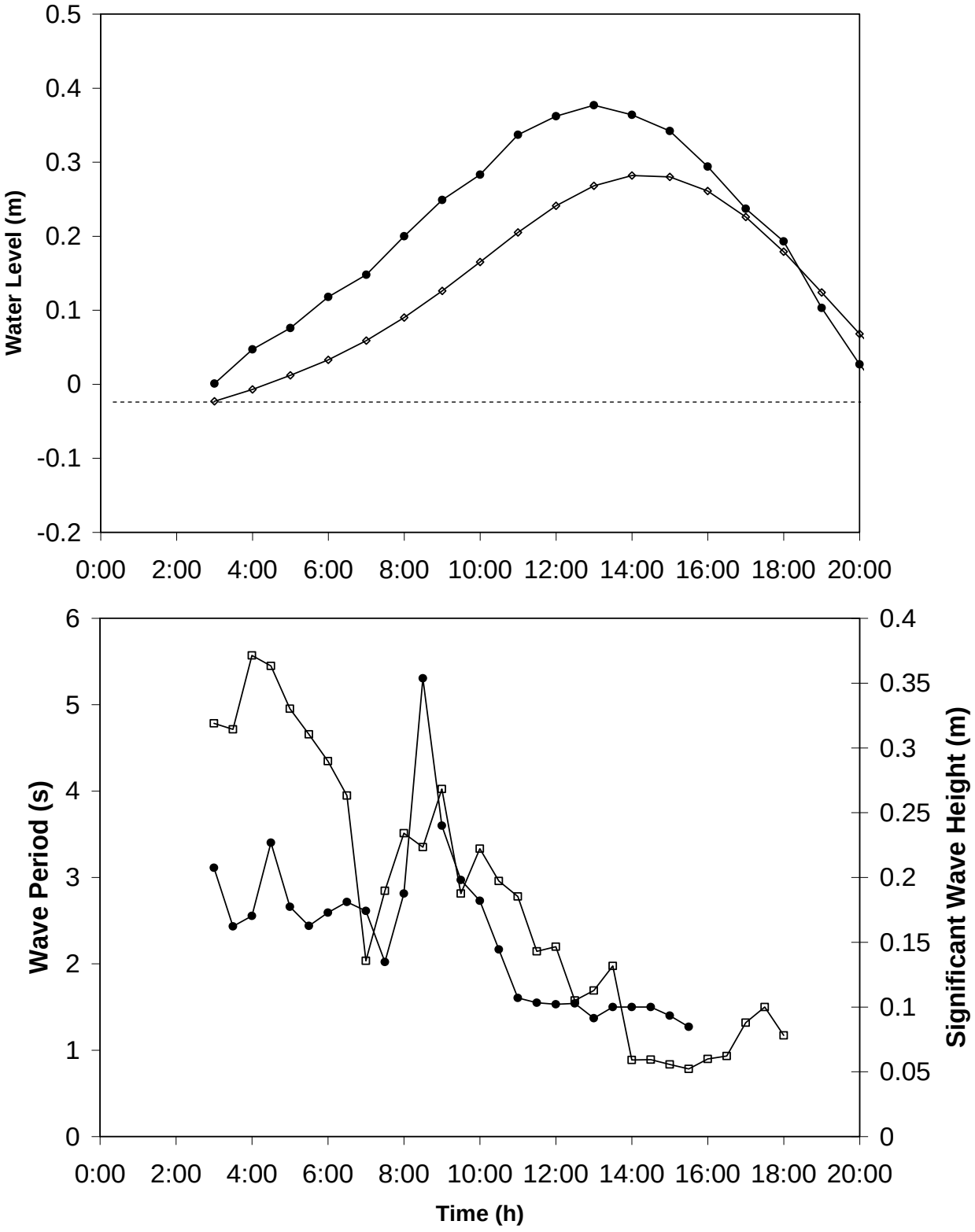


Figure 24. Shown are (a) change in predicted and observed (open circle) water depth relative to MLLW, (b) change in significant wave height and peak spectral period.

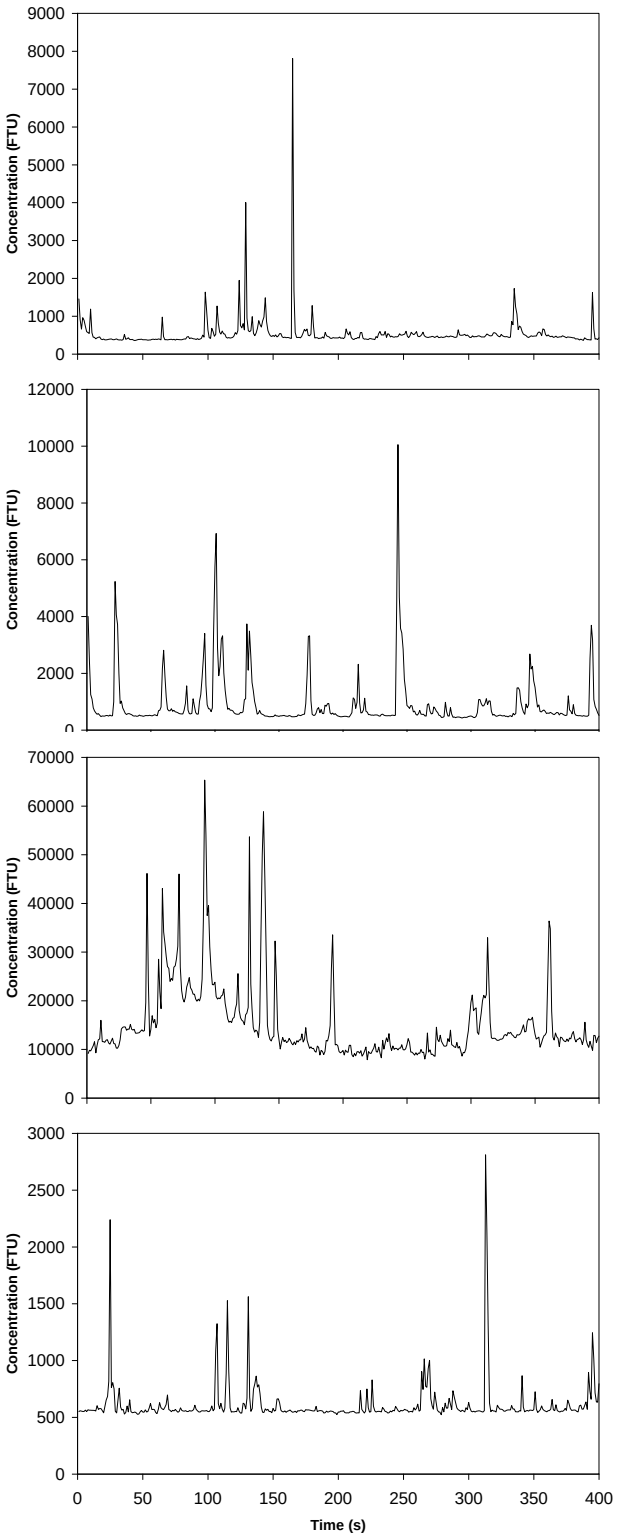


Figure 25. Time series of suspended sediment concentration at (a) 3:00, (b) 4:30, (c) 8:30 and (d) 11:00.

DISCUSSION

The results of this portion of the study were limited by instrument problems and in the inability to calculate water depth (gauge pressure) with the deployed instruments. While conclusions about the water depth and wave height controls on sediment transport could not be made, sediment transport was found to be largely directed onshore during a frontal storm. The mean currents (as described by Stone *et al.*, 2004) provided a relatively minor contribution to the total transport; most transport occurred at gravity wave frequencies and was associated with the strong accelerations at the leading edge of the wave. The fluid accelerations increase the amount of sediment that is brought into suspension (Huntley and Hanes, 1987; Nielsen, 1991; Osborne and Greenwood, 1993), which can then be carried shoreward by the skewed oscillatory velocities. While the relationship between acceleration and sediment transport could not be established in this study, the recovery of the shoreface (onshore bar migration) during the monitored storm seems to support this conclusion. The relative pre-dominance of onshore-directed transport, suggests that transport along the back-barrier beaches and terraces is similar to sand flats

As noted by Stone *et al.* (2004), the back-barrier beaches of Santa Rosa Island are fronted by a low-tide terrace that can extend up to several hundred meters into the bay/sound. The width of the terrace appears to exhibit an inverse relationship with the island width (or presence of the cuspate forelands). The terraces are widest where the island is narrow and susceptible to large overwash penetration distances and breaching. McNinch (*in review)* suggests that cuspate forelands and their associated terraces (shoals) behave as littoral cell endpoints, with sediment transport driven alongshore by oblique (or shore-parallel) winds. Transverse bars between the headlands support the transport of sediment alongshore between the overwash deposits and the headlands.

The larger fetch length for frontal winds within the Fort Pickens section of the GUIS, leads to less pronounced (or more linear) headlands. While there is the potential for the loss of sediment along the backbarrier, it appears that sediment volume is largely maintained through alongshore transport towards the headlands, particularly in the eastern sections of the park. The movement of sediment away from the overwash fans, creates a mechanism in which the narrow sections of

the island are reinforced[2]. Narrow sections of the island are more prone to strong overwash (independent of dune morphology) due to the strong hydraulic gradient that develops between the Gulf and Santa-Rosa Sound.

There remains a potential for offshore-directed sediment transport, as observed between March 21 and April 4. While there was little storm activity this period, it is not possible to describe the situation that would lead to offshore bar migration. However, it is reasonable to expect that the morphological response would depend on the ratio of the incident wave height to water depth, along the outer edge of the terrace. If wave heights are large compared to water depth (low tide or small surge), wave breaking will be initiated along the seaward edge of the terrace leading to an increase in the oscillatory skewness and little potential for offshore-directed mean currents. If the wave heights are small compared to the water depth (high tide or large surge), wave breaking will be initiated closer to the shore, potentially in the vicinity of the steeper beachface (Stone *et al.*, 2004). As a result of the steeper slope and narrow zone of wave breaking, offshore-directed mean currents are possible. Data from Stone *et al.* (2004) suggest that the offshore currents develop as wave heights decrease, which would focus wave breaking at the beachface. In this respect, weak frontal storms (small dissipation ratio) may promote offshore bar migration and beachface loss, while stronger storms (large dissipation ratio) may promote shoreface recovery.

[2] Results of a subsequent study (not included in this report) suggest that the location of the cuspate forelands, overwash fans, breaches and dune morphology are controlled by large transverse ridges along the Gulf.

POST-HURRICANE AIRFLOW AND SEDIMENT TRANSPORT OVER A RECOVERING DUNE

C. Houser, C. Hobbs

Department of Environmental Studies, University of West Florida, 11000 University Parkway, Pensacola, Florida, 32514.

Email: chouser@uwf.edu, cmh29@uwf.edu

ABSTRACT

During Hurricane Ivan, dunes in undeveloped sections of Northwest Florida were significantly reduced in height through direct wave erosion and the transfer of sediment to the backbarrier by overwash. The post-storm morphology of the island consists of a narrow beachface, multiple breach corridors, a wide overwash terrace and a remnant secondary dune that has been further eroded by Tropical Storm Arlene and Hurricanes Dennis and Katrina. The redevelopment of this dune will direct the response of the island to future storms, but the mechanisms of post-hurricane dune recovery are unclear, particularly in this low-energy coastal environment. The recovery is further complicated by a swale partly created during the removal of the access road to Fort Pickens in the Gulf Islands National Seashore. This study provides detailed measurements of airflow, sediment transport and elevation change over this low-profile dune.

Field observations suggest that sediment transport across the narrow beachface and berm is limited by a lag of shells and gravel from the pre-Ivan road bed. As a consequence, sediment input to the dune is relatively minor with onshore winds, despite the presence of overwash fans deposited during frontal storms in the swale behind the berm. The resulting sediment transport gradient across the seaward slope of the dune is more reflective of the expanding fetch than topographic acceleration and the drag imposed by the sparse vegetation. In contrast, there is a larger sediment input to the dune during offshore winds in response to the larger fetch across the overwash terrace, despite the presence of a lag. It is concluded that post-hurricane dune recovery in this area is strongly dependent on the deposition of overwash sediment during frontal storms and the resulting development of a sand ramp through the swale. This will increase both the availability of sediment and the fetch for winds directly or obliquely onshore.

RESULTS

Wind and sediment transport measurements for onshore and offshore winds were made on a low-profile (<1.0 m) remnant dune within the boundaries of the Gulf Islands National Seashore on Santa Rosa Island in Northwest Florida (Figure 15). The dune (Figure 16) has a length of ~60 m and aspect ratios of 1:34 and 1:23 for the gulf and sound side slopes respectively. The dunes do not have a "normal" morphology (see Arens, 1996 or Hesp *et al.*, 2005) due to erosion by surge water during Tropical Storm Arlene and Hurricanes Ivan, Dennis and Katrina. The dunes in this area are composed of medium sand with a mean grain size of 0.39 mm (1.35 ϕ) and a standard deviation of 0.54 ϕ. The surface south of the dune is typically saturated and consists of coarse sand (0.97 ϕ), while the overwash terrace north of the dune consists of medium sand (1.28 ϕ). Both surfaces are covered by a lag of shells and gravel.

Post-Hurricane Topography and Sediment Drift Potential

Hurricane Ivan, a Category-3 hurricane, came ashore near Gulf Shores, Alabama, on September 16, 2004 (see Figure 15). Santa Rosa Island was within the northeast quadrant of the storm ~40 km from the eye wall and subject to surge heights in excess of 3 m. In response, the area suffered significant beach erosion and widespread overwash and breaching. The cross-shore profile changed from a discontinuous foredune backed by hummocky secondary dunes and maritime forest (at the cuspate headlands) to washover terraces at the headlands and sheetwash corridors between headlands. In many cases, the sheetwash corridors developed into breaches that connected the Gulf with the Sound. As shown in Figure 17, the dune was further eroded by Tropical Storm Arlene (June 2005) and Hurricanes Dennis (July 2005) and Katrina (September 2005). While Hurricane Katrina made landfall along the Louisiana/Mississippi border (~150 km from the site), the lack of sufficient vertical geometry along the shoreline of the Gulf Islands National Seashore caused widespread overwash and breaching.

Based on the LIDAR images and extensive field and aerial surveys after Hurricane Ivan the barrier island can be divided into 4 morphological zones with different vegetation, sediment and surface roughness characteristics: beachface, overwash, breach corridors and vegetated remnant

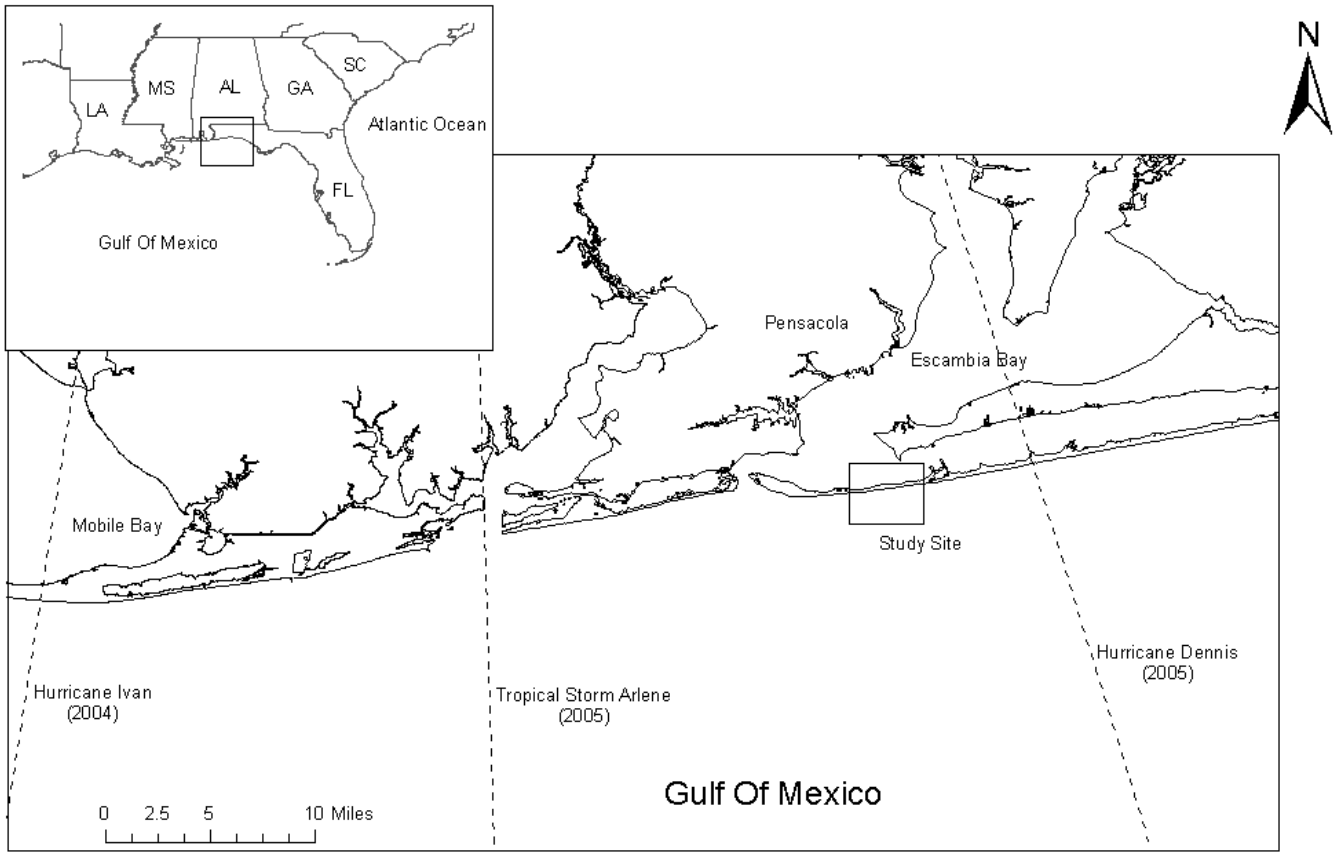


Figure 26. (a) Location of field site within the Gulf Islands National Seashore on Santa Rosa Island in Northwest Florida. Also shown are the tracks for Hurricanes Ivan and Dennis, Tropical Storm Arlene.

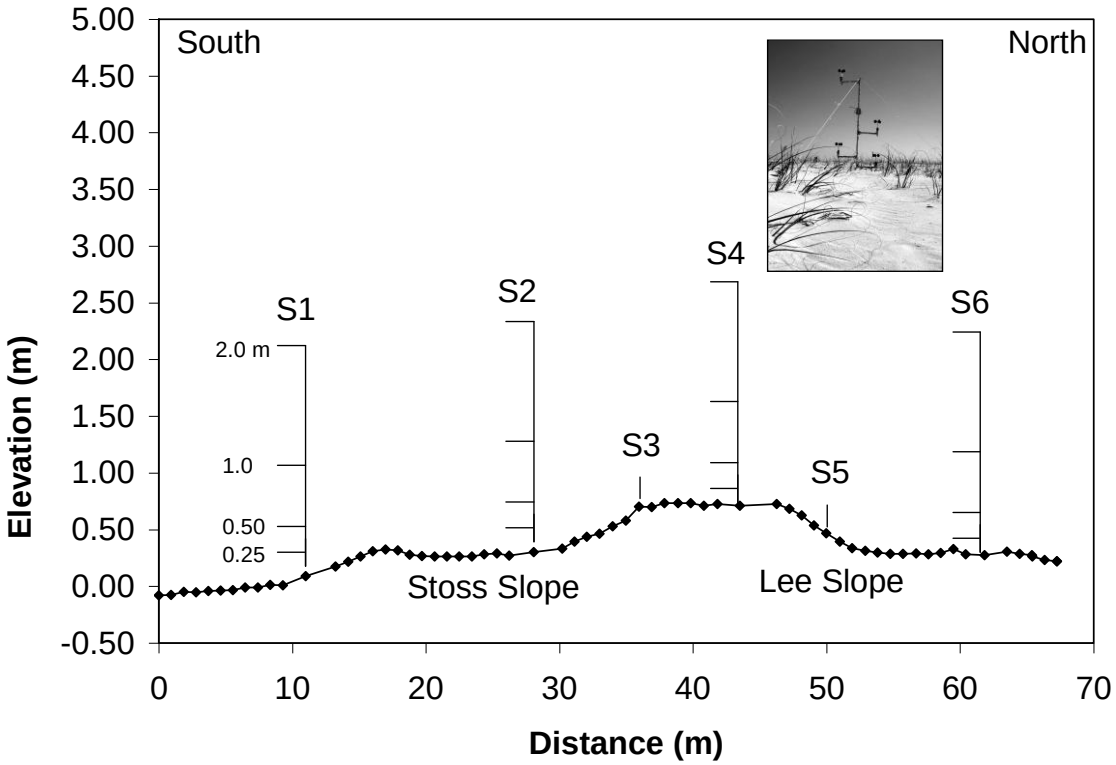


Figure 27. Profile of instrument transect showing location of the instrument stations (S1-S6). All profile stations (S1, S2, S4 and S6) were collocated with a cylinder trap over the entire study period and a Guelph-Trent sediment trap during certain storms.

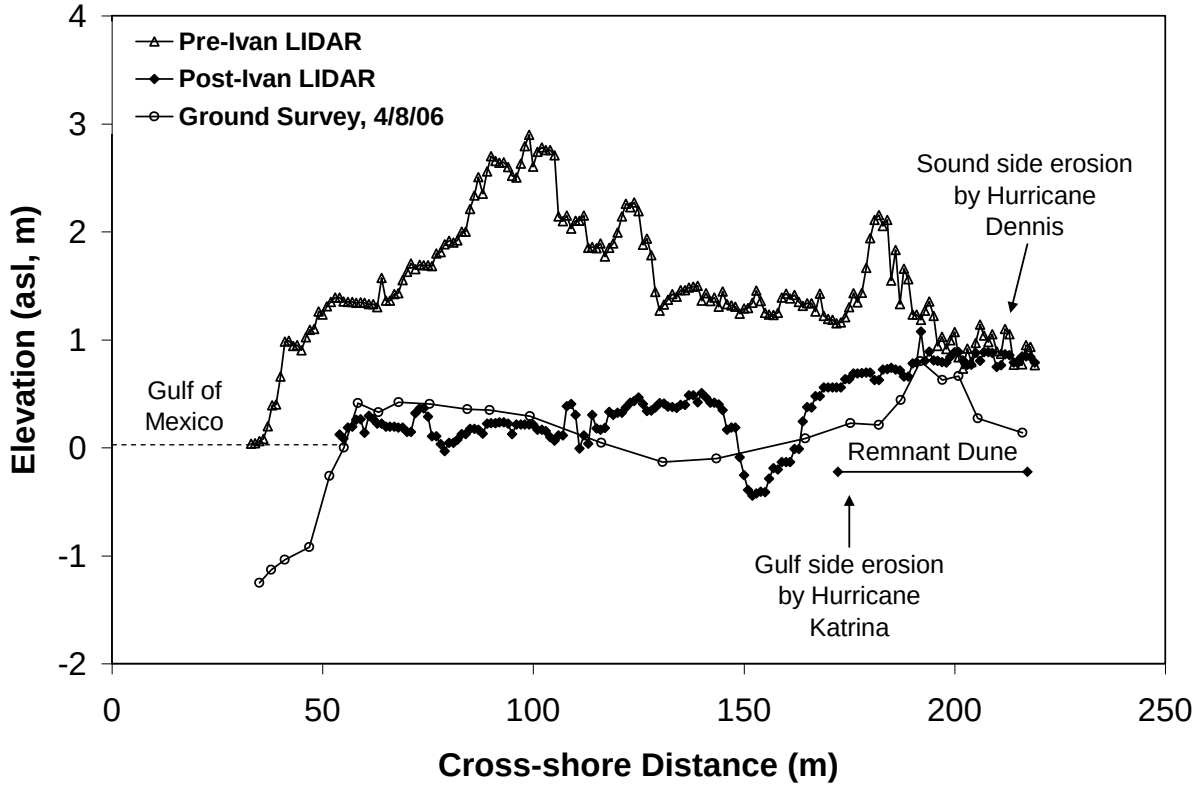


Figure 28. Cross island transects at the study site showing the morphology before and after Hurricane Ivan (September, 2004) and at the start of the present study (March 2006). The pre- and post-Ivan transects were created from LIDAR data collected by the USGS, while the 2006 survey was completed by the authors using transect and level.

dunes of low relief. Separating the beachface and the dunes is a large swale that initially developed through supercritical flows over the access road to Fort Pickens (Gulf Islands National Seashore), but expanded considerably when the road and its bed were removed. The aeolian sediment drift potential, calculated from the modified Fryberger Method (Lettau and Lettau, 1978), suggests that the resultant drift potential since Hurricane Ivan is oriented onshore (to the NW, 334^{o}), not including Hurricanes Dennis and Katrina. The RDP/DP ratio for this period is 0.24, which suggests an obtuse bimodal wind regime (Fryberger, 1979) and is a reflection of the bimodal (NW-SE) frontal winds through the winter and spring and predominately south winds through summer.

The resultant drift potential overestimates the relative importance of south winds, which are usually accompanied by precipitation as a frontal boundary approaches. Transport is further limited during strong onshore winds due to the ability of storm surge and increased wave run-up to reactivate the breach corridors created during Hurricane Ivan and to flood low elevation areas behind the berm. During storms with onshore winds, small overwash fans were deposited behind the berm and in some cases these fans extended within meters of the remnant dune (Figure 18). Visual observations suggest that there was no appreciable deflation of the overwash fans and that this potential supply of sediment is not available to the dune due to flooding and an elevated watertable that would persist for days after the storm tide had abated.

Sediment transport is observed with the north winds that followed the passage of a frontal boundary only after the sediment on the surface of the overwash terrace started to dry. Despite the long fetch, transport from these environments was also limited by the presence of a lag surface consisting of shells, gravel and debris. A large percentage (>70%) of the lag material is limestone that formed the bed of the pre-Ivan road, with secondary contribution (<10%) of oyster shells from the bed of an earlier road. Due to the human-alterations of this area (the lag surface and the swale seaward of the dune), the relative importance of both onshore and offshore winds in supplying sediment for dune recovery is not well described by the drift potential.



Figure 29. Photograph of remnant dune looking north (from the Gulf of Mexico) showing overwash fan developing in the swale between the berm and dune.

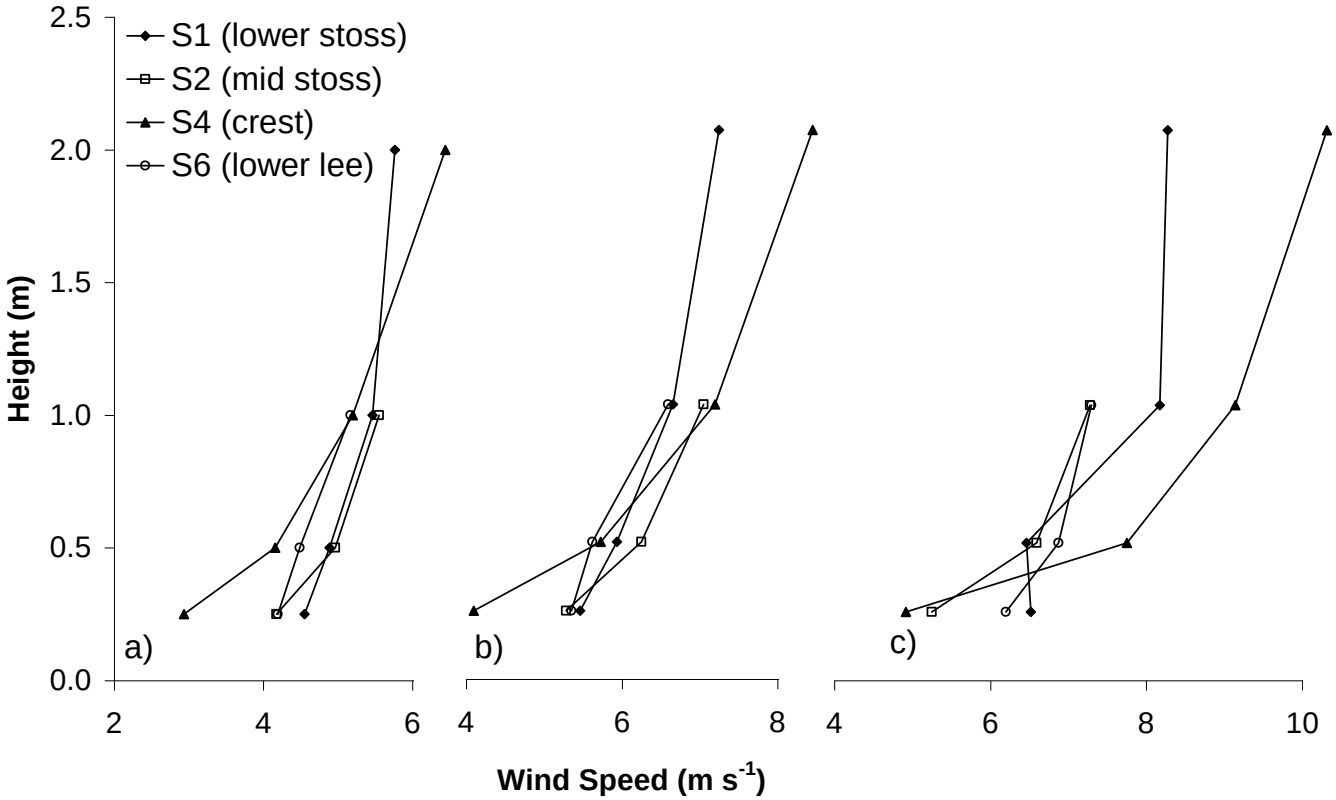


Figure 30. Velocity profiles for onshore winds within 15^{o} of normal to the dune crest. Shown in the figure are the time-averaged profiles for winds between (a) 6-7 m s^{-1}, (b) 8-9 m s^{-1} and (c) 10-11 m s^{-1} recorded at 2 m above the crest ($S4_{2.0\ m}$).

Time-Averaged Flow and Sediment Transport During South (Onshore) Winds

Time-averaged velocity profiles are provided in Figure 19 for all onshore winds within 15^{o} of normal to the dune crest. This figure shows time-averaged velocity profiles over the dune for reference wind speeds between (a) 6-7 m s^{-1}, (b) 8-9 m s^{-1} and (c) 10-11 m s^{-1} recorded at 2 m above the crest ($S4_{2.0\ m}$). Clear flow acceleration between S1 and S4 is visible, particularly forthe upper-range of wind speeds and above the vegetation layer (Figure 19c). While winds measured at 2.0 m above the surface show a consistent speedup from 111% to 124%, speedup is only observed (>100%) at the 1.0 m and 0.5 m anemometers when the reference wind speed exceeds 7 and 9 m s^{-1} respectively (Figure 20a). Since adjustments to changes in topography and surface roughness would begin in the lower part of the boundary, it appears that a larger-scale boundary adjustment is superimposed on the adjustments to this low-profile feature.

At the lowermost anemometer, there is a deceleration wind speed over the seaward slope over the entire range of reference wind speeds, despite flow compression towards the dune crest (Figure 20a). Assuming that this boundary is strictly a reflection of local roughness, the deceleration is most likely associated with the increase in vegetation cover towards the crest. Within the vegetation cover, a local acceleration of the near-surface flow is observed between S2 and S3 as the reference wind speed exceeds 9 m s^{-1}. This acceleration is associated with the greater steepness of the upper-seaward slope, but a rapid deceleration is again observed between S3 and S4 as the vegetation cover increases (Figure 21). As the flow reemerges from the vegetation canopy (between S5 and S6) there is acceleration of the near-surface flow over all reference wind speeds despite the deceleration observed at the 0.5 m and 1.0 m (Figure 20b). This suggests that the low vegetation densities still provide sufficient momentum loss to counter the topographic forcing. While a separation cell landward of the dune is not expected based on the model results of Parsons *et al.* (2004), small flags attached to the erosion pins and observations of wind ripple migration were used to identify flow separation over the landward slope. Based on these observations and the measured aspect ratios, the dune in this study is similar to the Grainfall protodune observed by Kocurek *et al.* (1992).

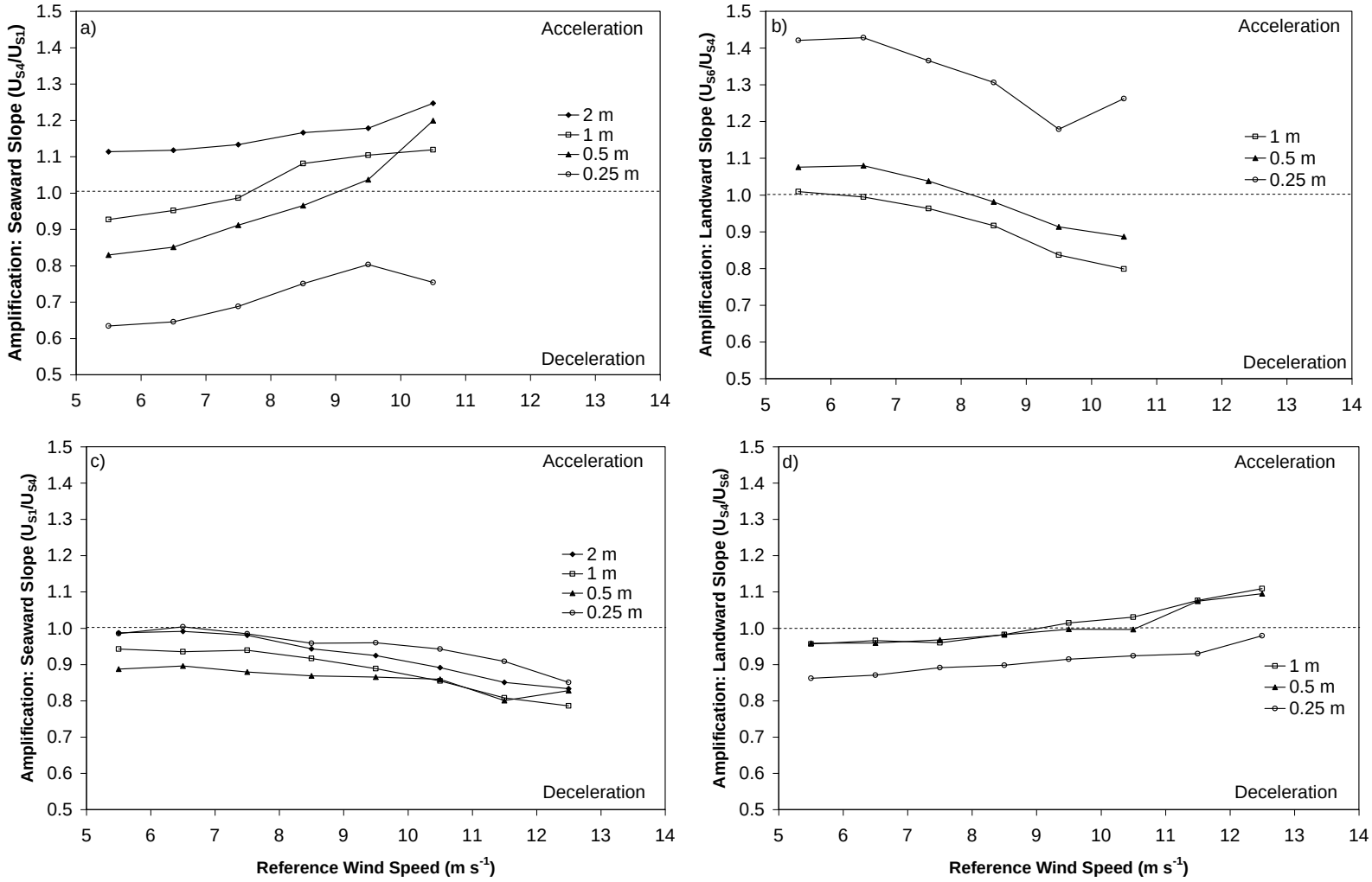


Figure 31. Time-averaged amplification (speed-up) factors for onshore (a,b) and offshore winds (c,d). Shown are the amplification factors for the seaward slope (a,c) and the landward slope (b,d).

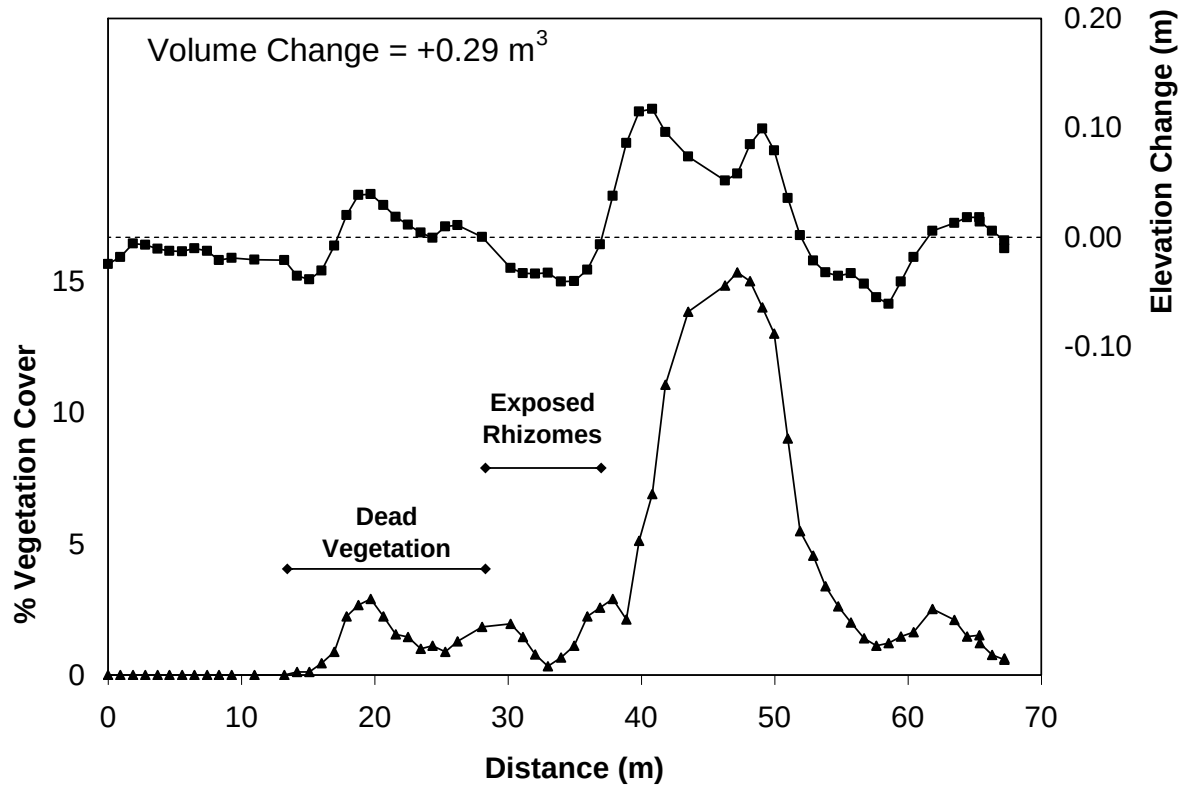


Figure 32. Cross-transect variations in vegetation cover (%) and net change in surface elevation.

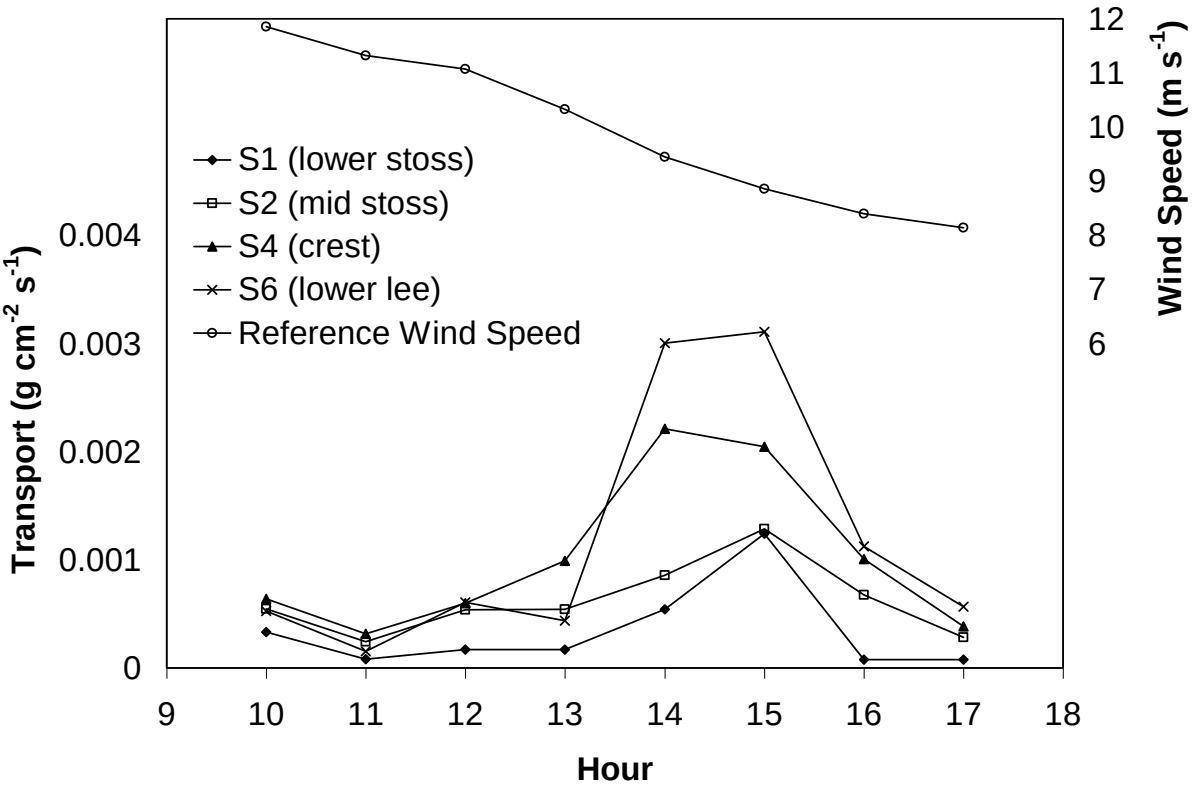


Figure 33. Variation in sediment transport from each profile station towards the end of a frontal storm on April 29, 2006.

Sediment transport was measured for 5 hours towards the end of a frontal storm with strong south winds (> 8 m s^{-1}) on April 29, 2006 (Figure 22). Due to the elevated storm tide, the berm was overtopped and the swale immediately seaward of the dune was flooded. As a consequence, measurements earlier in the storm were not possible due to flooding of the access road. Sediment transport at S1 was relatively small due to the short fetch length, creating an steep transport gradient across the seaward slope. The transport gradient reached a maximum at 14:00 h, as transport at the crest reaches a maximum before transport along the seaward slope. The lag in transport reflects drying of the dune surface following heavy precipitation earlier in the storm (~8:00 h). Transport at S1 drops dramatically at 16:00 h as the top layer of dry sediment is deflated exposing sediment saturated by the elevated watertable. At the other stations, transport is reduced as the wind speed decreases and the start of the saltation cascade is shifted up the seaward slope. Lancaster (1985) also observed the shift in transport towards the crest (of a barchan dune) as wind speeds approached the entrainment threshold.

If the transport was in equilibrium with the local wind speed, a net gain of sediment would be expected in the vicinity of the crest, which would in turn lead to an increase in dune height and volume. However, sediment transport (both integrated and event-based) across both the seaward and landward slopes was found to be independent of changes in the near-surface wind speed. The increase in transport across the seaward slope lead to the loss of sediment (erosion) by up to 0.10 m, which lead to the exposure of rhizomes immediately landward of S2 where vegetation density was relatively low (<5%). While the net gain in sediment along the landward slope suggests that sediment removed from the seaward slope was deposited in this region (Figure 23a), there was a net loss of sediment of ~1.08 m^3 per meter width of dune (alongshore). A large part of the sediment lost from the dune is associated with erosion along the lower landward slope as the flow accelerated out of the vegetation cover. The net result of this storm was a migration of ~1 m to the north and an increase in crest height by ~0.12 m.

Time-Averaged Flow and Sediment Transport During North (Offshore) Winds

The time-averaged velocity profiles are provided in Figure 24 for all offshore winds within 15^o of normal to the dune crest. As shown for the onshore winds, this figure shows time-averaged velocity profiles over the dune for wind speeds between (a) 6-7 m s^{-1}, (b) 8-9 m s^{-1}, (c)

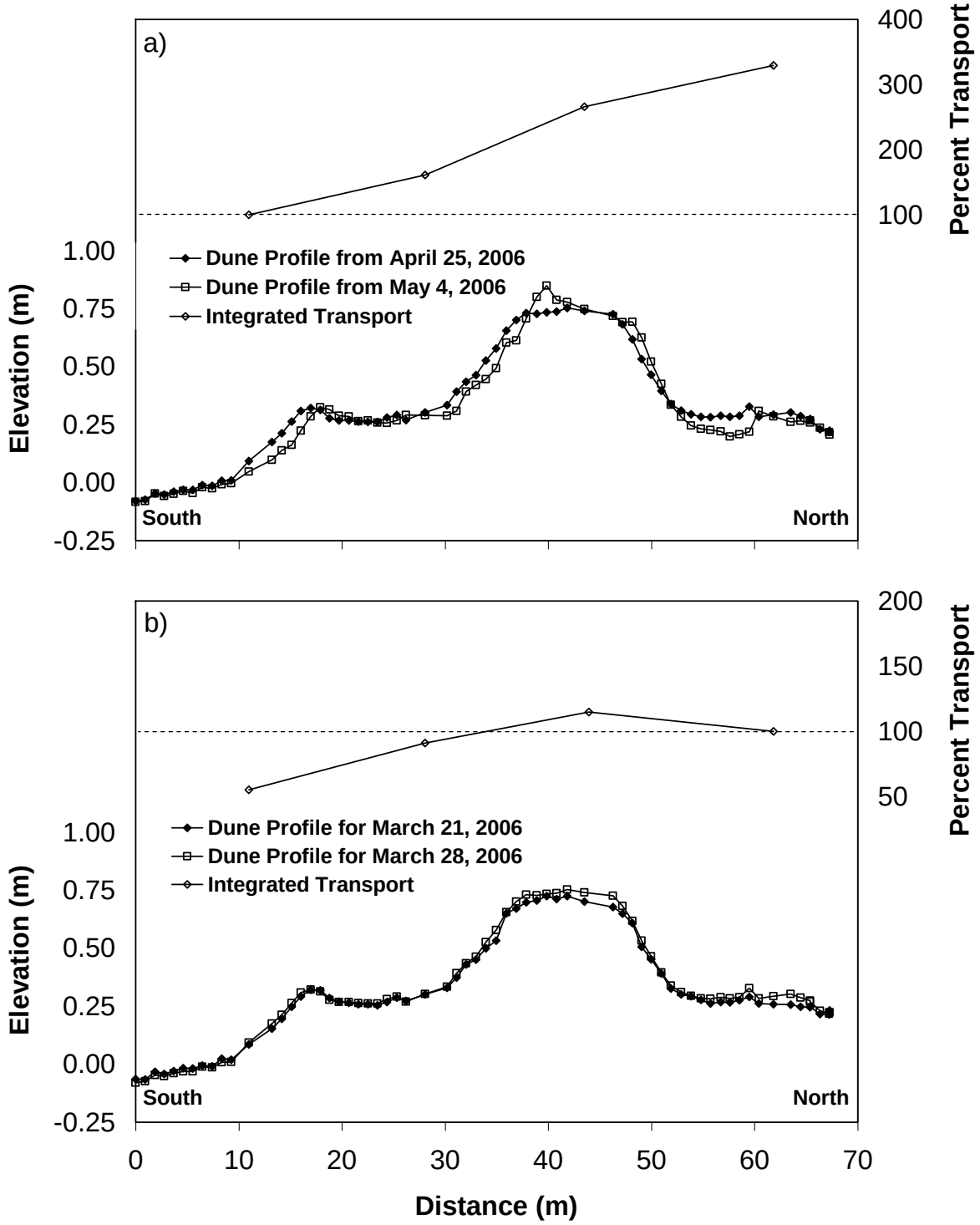


Figure 34. Time averaged sediment transport measured from cylinder traps expressed as a percent of the transport recorded at the first station in the direction of flow (S1 for onshore and S6 for offshore winds). Shown are the transport rates for (a) onshore winds on April 29 and (b) offshore winds on March 24. Also shown are the pre- and post-storm transects for each storm.

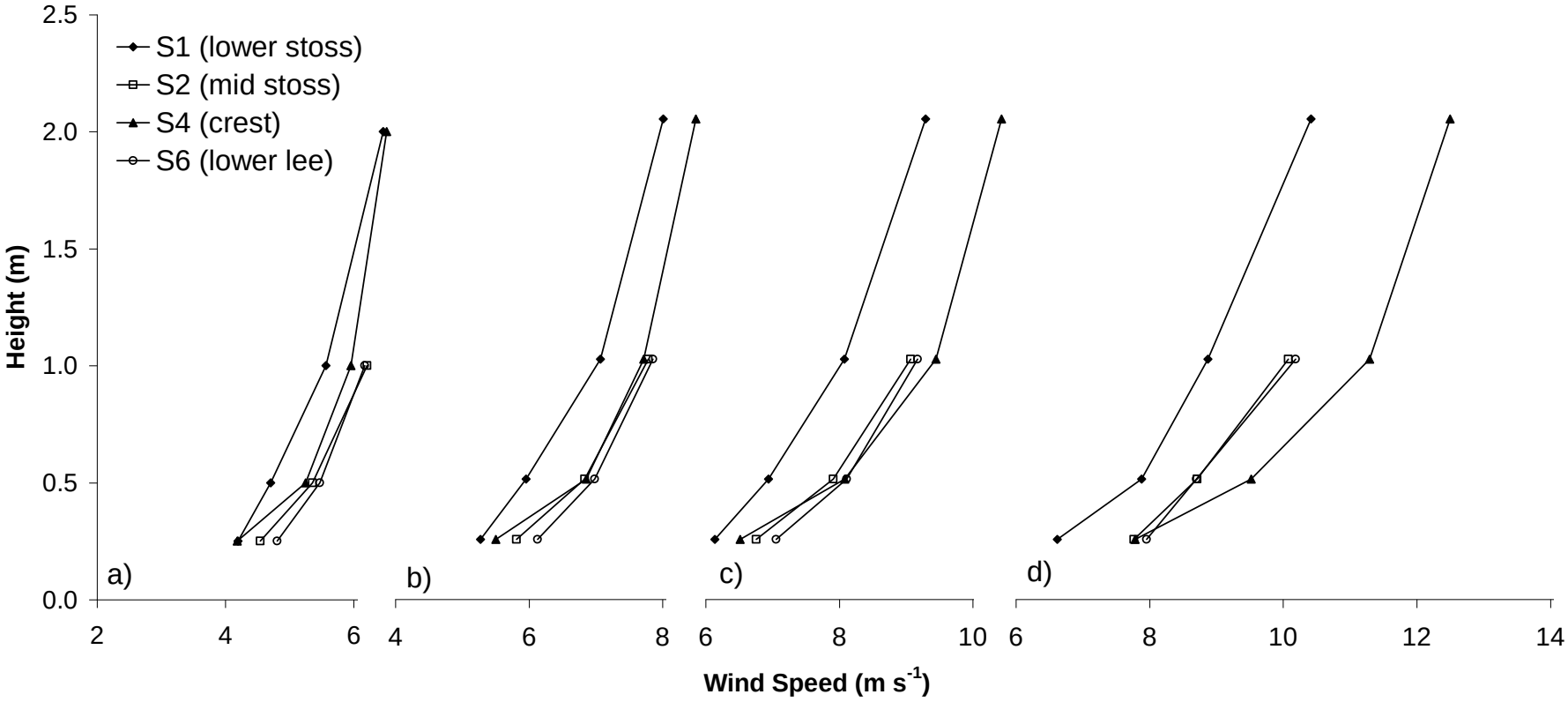


Figure 35. Velocity profiles for offshore winds within 15^{o} of normal to the dune crest. Shown in the figure are the time-averaged profiles for winds between (a) 6-7 m s^{-1}, (b) 8-9 m s^{-1}, (c) 10-11 m s^{-1} and (d) 12-13 m s^{-1} recorded at 2 m above the crest ($S4_{2.0\ m}$).

10-11 m s^{-1} and (d) 12-13 m s^{-1} recorded at 2 m above the crest ($S4_{2.0\ m}$). As wind speeds exceed 9 m s^{-1}, there is a clear acceleration of flow above the vegetation canopy (0.5 and 1.0 m) between S6 (lower landward slope) and S4 (crest). Due to the low dune height and aspect ratio, the speedup for winds measured at both 0.5 and 1.0 m above the surface reaches a maximum of only 112%, considerably less than observed over more "typical" coastal dunes (Arens *et al.*, 1995; Hesp *et al.*, 2005). The reason for the deceleration of flow when the reference wind speed is <9 m s^{-1} is not clear.

The near-surface flow is observed to decelerate between S6 and S4 (Figure 20c) over the entire range of reference wind speeds. However, this deceleration occurs between S6 and S5 asthe flow enters the vegetation canopy and a local acceleration is observed between S5 and S4 as the flow is compressed towards the crest. Seaward of the crest there is a deceleration of the flow (to varying degrees) at all sampling heights as the flow expands (Figure 20). The deceleration is most noticeable at the 0.50 m anemometer (winds at toe were 79% of crest speeds) and relatively muted at the lowermost anemometer. This suggests a balance between deceleration as the flow expands and acceleration as the flow reemerges from the vegetation canopy between S3 and S2.

The integrated transport for the storm on March 24, 2006 shows an increase up the landward slope and a decrease over the length of the seaward slope, consistent with the flow acceleration and deceleration observed on the respective slopes (Figure 23). In response, sediment deposition (>0.05 m) was observed at the crest on March 24, with a spatial extent that corresponded to the largest vegetation densities (see Figure 21). Deposition was also observed along the lower landward slope as the flow entered the vegetation canopy. There must still have been appreciable amount of sediment moving through this area to allow sediment transport to increase between S6 and S4 with no net change in surface elevation. Seaward of S6 the transport is observed to decrease as the flow decelerates, leading to an increase in crest elevation by ~0.06 m. The increase in crest elevation is associated with a minor increase in dune volume of ~0.5 m^3 per meter width of dune.

DISCUSSION

In general, coastal dunes can (re)develop from and within the overwash sediments (Leatherman 1976; Armon, 1979; Leatherman, 1979), but the recovery is more commonly associated with sediment delivery to the beachface under fair-weather conditions and littoral drift (Psuty, 1992). Field observations suggest that sediment transport across the narrow beachface and berm is limited by a lag of shells and gravel that limits the area of the transport surface (particularly for scallop shells) and expend available shear stress (Nickling and McKenna-Neuman, 1995). Sediment is also limited during onshore winds by elevated storm tides that overtop the berm and flood the (human-altered) swale immediately seaward of the dune. While the overwash fans deposited during strong onshore winds provide a fresh supply of sediment, the supply remains limited by the flooding and elevated watertable, which can persist for days after the storm has abated

Due to the limited availability of sediment, the input of sediment to the recovering dune was relatively minor during onshore winds and measurable sediment transport was only observed at the seaward edge of the dune. The sediment transport was observed to increase across the seaward slope, independent of the cross-dune variation in the near-bed wind speed. Over the lower-range of winds speeds observed, the near-bed wind speeds decreased towards the crest, consistent with the increase in vegetation cover towards the crest. Despite the low vegetation cover (<15%), it appears that the dune grass was capable of extracting momentum from the air flow. As the speed of the onshore wind increased ($U_{2.0}$>9 m s^{-1}), an acceleration of the near-bed flow was observed across the seaward slope with the largest speeds observed at the crest. This acceleration may reflect flow compression as is commonly observed over both desert (Walker and Nickling, 2002) and coastal dunes (e.g. Hesp *et al.*, 2005), despite the relatively low-profile of the dune in the present study.

It is interesting to note that there is no uniform speedup toward the dune crest over the observed range of wind speeds, unlike the relatively simple dune form examined by Hesp *et al.* (2005). It is possible that this is influenced by the uncharacteristic shape of the dune (Arens, 1997), which is more reflective of frontal and lateral erosion by surge water than aeolian processes. However,

it is reasonable to expect that variations in topography <0.10 m will not have a profound effect on the wind profiles, and that the profiles for offshore winds would exhibit a similar response to the topography. Further study is required to determine if there is internal boundary layer development and adjustment seaward of the dune (Bauer, 1991), as the flow over the surf zone encounters the steep beach, berm and swale. Each of these surfaces is associated with a change in surface roughness and availability of sediment that further complicates the input of sediment to the dune.

In contrast, the profiles for offshore winds show a more uniform acceleration over the landward slope and deceleration across the seaward slope as the reference wind speed exceeds 9 m s^{-1}. The near-bed flow exhibits a decrease in speed at the toe of the landward slope, which may reflect a stagnation of flow at the leading edge of the slope (e.g. Walmsely and Howard, 1985; Wiggs *et al.*, 1996; McKenna Neuman *et al.*, 1997; Walker and Nickling, 2002; Hesp *et al.*, 2005). However, given the low-profile and low aspect ratio of the dune it is more likely that the deceleration is a reflection of the increased vegetation cover on the landward slope. The flow over the dune reflects a balance between topographic forcing towards the crest and increased drag from the vegetation. In response, sediment transport is observed to increase over the landward slope towards a maximum at the crest and there is a net (but small) gain in sediment volume seaward of this point.

The closer relationship between the patterns in near-surface wind and sediment transport is a reflection of the greater availability of sediment from the wide overwash terrace. Despite the presence of a lag, the fetch appears to be sufficient for sediment to be transported from the overwash to the dune. As noted, sediment input to the dune is relatively minor during onshore winds, despite the presence of overwash fans deposited behind the berm during frontal storms. The substantial increase in sediment transport towards the crest, independent of variations in near-bed flow and vegetation cover, suggests that the fetch effect (see Gillette *et al.*, 1996; Bauer and Davidson-Arnott, 2003) is an important control on sediment transport and morphological response. This is similar to the transport patterns observed by Lancaster *et al.* (1996) over the seaward slope of an isolated barchan dune. In the present study, the saltation cascade is only initiated at the seaward edge of the dune and the transport along the seaward slope remains

below the potential transport capacity (Kocurek *et al.*, 1992) of the accelerating flow, even with presence the vegetation cover. The transport was found (in the trap data and through field observation) to continue to increase over the landward slope and the flow reemerged from the vegetation. Based on field studies the required fetch length to reach equilibrium saltation can exceed 30 m (Davidson-Arnott and Law, 1990; Nordstrom and Jackson, 1992, 1993; van der Wal, 1998; Davidson-Arnott *et al.*, 2005), which is greater than the length of either the seaward or landward slope lengths. This does not account for the influence of moisture (Davidson-Arnott *et al.*, 2005) or the presence of vegetation or boundary layer adjustments (Bauer, 1991), which can increase the saturation distance (Bauer and Davidson-Arnott, 2003). As a consequence, there was a net loss of sediment from the dune during onshore winds and particularly during the storm on April 29, 2006 when the dune was observed to migrate ~1 m to the north. The erosion on the seaward slope resulted in the exposure of rhizomes in areas where the vegetation density was relatively low.

Over the entire length of the field study there was a minor net gain in volume of 0.29 m^3 per m width of dune alongshore (Figure 21). The pattern of sediment gain and loss exhibits a similar pattern to the vegetation density, with erosion in areas devoid of vegetation and deposition in areas with vegetation cover. The results of the study suggest that offshore winds and the availability of sediment on the overwash terrace are critical to the recovery of the dune, which supports earlier findings by Leatherman (1979). However, it is difficult to transfer short-term transport studies such as this to the recovery of the dunes over longer timescales (Sherman, 1995; Davidson-Arnott and Law, 1996). Following Hurricane Opal, Stone *et al.* (2004) found that the dune system started to recover within a year, but it is reasonable to assume that the recovery process has been delayed by Tropical Storm Arlene and Hurricanes Dennis and Katrina. A recovery similar to the findings of Stone *et al.* (2004) may depend on the recovery of the beachface and the continued deposition of overwash sediment during frontal storms and the development of a sand ramp through the swale. This will increase both the availability of sediment and the fetch for transport by winds directly or obliquely onshore. However, it remains unclear the rate at which the beachface and backshore will develop in this relatively low-energy environment.

CONCLUSIONS

A number of conclusions can be drawn from the results of this study:

1. For both onshore and offshore winds the wind flow structure over the dune reflects a balance between topographic forcing towards the crest and increased drag from the vegetation. However, the non-uniform adjustment of onshore winds across the seaward slope suggests that there may be boundary layer adjustment seaward of the dune.
2. Sediment transport is limited during onshore winds by elevated storm tides that overtop the berm and flood the (human-altered) swale immediately seaward of the dune. The supply remains limited by the flooding and elevated watertable, despite the fresh supply of sediment provided in the overwash fans deposited during these events. The lack of sediment input from the beachface forces the saltation cascade to be initiated at the toe of the dune seaward slope, independent of variations in wind speed and vegetation cover over the seaward slope. This leads to sediment loss along the seaward slope and the migration of the dune to the north.
3. Sediment is provided to the dune during offshore winds, despite the presence of a lag surface on the overwash terrace. In this respect, the overwash terrace represents an important supply of sediment for the recovery of the dunes, at least in the time between the storm and the recovery of the beachface and backshore (not observed in this study), which will increase both the availability of sediment and the fetch for winds directly or obliquely onshore.
4. While the results of this study are time and site-specific they do suggest that limits to sediment supply, including human-altered features, can delay post-hurricane dune recovery and can potentially lead to a destabilization of the remnant dunes.

REFERENCES

Aagaard, T. Davidson-Arnott, R.G.D. Greenwood, B. Nielsen J., 2004. Sediment supply from shoreface to dunes- linking sediment transport measurements and long term morphological evolution. *Geomorphology,* 60, 205-224.

Arens, S.M., 1996. Patterns of sand transport on vegetated foredunes. *Geomorphology* 17(4), 339-350.

Armbruster, C.K., 1997 Morphologic responses of a low-energy micro-tidal beach to winter cold front passages: north shore Santa Rosa Island, Florida. M.S. Thesis, Department of Geography and Anthropology, Louisiana State University, Baton Rouge, Louisiana, 166 pp.

Armbruster, C.K., Stone, G.W., Xu, J.P., 1995. Episodic atmospheric forcing and bayside foreshore erosion: Santa Rosa Island Florida. Transactions-Gulf Coast Association of Geological Societies XLV, 31-37.

Armon, J.W. 1979. Dune erosion and recovery on a northern barrier. In: *Coastal Zone '80, Proceedings of the 2nd Symposium on Coastal and Ocean Management*, Hollywood, Florida, November 1980, American Society of Civil Engineers, 2, pp. 1233-1250.

Bauer, B.O. 1991. Aeolian decoupling of beach sediments. *Annals of the Association of American Geographers*, 81(2), 290-303.

Bauer, B.O. and Davidson-Arnott, R.G.D. 2003. A general framework for modeling sediment supply to coastal dunes including wind angle, beach geometry, and fetch effects. *Geomorphology*, 49(1-2), 89-108.

Belly, P.Y., 1964. *Sand movement by wind*. United States Army, Corps of Engineers, Coastal Engineering Research Center, Washington DC, Technical Memorandum TM-1, 80 pp.

Bennett, S.W. and Olyphant, G.A., 1998. Temporal and spatial variability in rates of eolian transport determined from automated sand traps: Indiana Dunes National Lakeshore, USA. *Journal of Coastal Research* 14(1), 283-290.

Chaney, P.L and Stone, G.W., 1996. Soundside shoreline erosion and implications for winter cold front forcing: West Ship Island, Mississippi. *Shore and Beach*, **64**, 27-33.

Cornelis, W.M., Gabriels, D. and Hartmann, R., 2004. A parameterisation for the threshold shear velocity to initiate deflation of dry and wet sediment. *Geomorphology* 59(1-4), 43-51.

Davidson-Arnott, R.G.D. and Law, M.N., 1990. Seasonal patterns and controls on sediment supply to coastal foredunes, Long Point, Lake Erie. *In*: Nordstrom, K., Psuty, N. and Carter, R.W.G. (eds), *Coastal dunes: processes and geomorphology*, New York: John Wiley and Sons, pp. 177-200.

Davidson-Arnott, R.G.D. MacQuarrie, K. and Aagaard, T., 2005. The effect of wind gusts, moisture content and fetch length on sand transport on a beach. *Geomorphology,* 68(1-2), 115-129.

Disraeli, D.J. 1984. The effect of sand deposits on the growth and morphology of Ammophila breviligulata. *The Journal of Ecology*, 72(1), 145-154.

Foster, E.R. Spurgeon, D.L. and Cheng, J., 1999. *Shoreline Change Rate Estimates: Escambia and Santa Rosa Counties*. Florida Department of Environmental Protection, Office of Beaches and Coastal Systems, Report BCS-99-03, 85 p.

Fryberger, S.G. 1979. Dune forms and wind regime, Mauritania, West Africa; Implications for Past Climate. In: Sarnthien, M., Siebold, E. and Rognon, P. (eds), Van Zinderen Bakker, E.M.Sr. and Coetzee, J.A. (eds), Rotterdam: Balkema, *Palaeoecology of Africa and the Surrounding Islands* 12:79-96.

Gares, P.A. Davidson-Arnott, R.G.D. Bauer, B.O. Sherman, D.J. Carter, R.W.G. Jackson, D. and Nordstrom, K.F., 1996. Longshore variations in aeolian sediment transport, sediment size and moisture at Carrick Finn Strand, Ireland. Journal of Coastal Research 12(3), 673-682.

Gillette, D.A. Herbert, G. Stockton, P.H. and Owen, P.R., 1996. Causes of the fetch effect in wind erosion. *Earth Surface Processes and Landforms,* 21(7), 641-660.

Hesp, P., 2002, Foredunes and blowouts: initiation, geomorphology and dynamics. *Geomorphology*, 48, 245-268.

Hesp, P.A. Davidson-Arnott, R. Walker, I.J. and Ollerhead, J., 2005. Flow dynamics over a foredune at Prince Edward Island, Canada. *Geomorphology* 65(1-2), 71-84

Hotta, S., Kubota, S., Katori, S. and Horikawa, K. 1984. Sand transport by wind on a wet sand surface. In: Edge, B.L. (ed), Coastal Engineering 1984, *Proceedings of the 19th International Conference*, Houston, Texas, September 1984, American Society of Civil Engineers, 2, pp. 1265-1281.

Houser, C. Hamilton, S. Meyer-Arendt, K. and Oravetz, J., 2006. EOF analysis of barrier island morphological change during Hurricane Ivan. Accepted to *Coastal Sediments '07.*

Huntley, D.A., and Hanes, D.M., 1987. Direct measurement of suspended sediment transport. *Proceedings of Coastal Sediments '87,* ASCE New York, 723-737.

Jackson, N.L. and Nordstrom, K.F., 1997. Effects of time-dependent moisture content of surface sediments on aeolian transport rates across a beach, Wildwood, New Jersey, USA. *Earth Surface Processes and Landforms*, 22, 611-621.

Keim, B.D., Muller, R.A., and Stone, G.W., 2004. Spatial and temporal variability of coastal storms in the North Atlantic Basin. *Marine Geology*, **210**, 7-15.

Kocurek, G. Townsley, M. Yeh, E. Sweet, M. and Havholm, K., 1992. Dune and dune-field development stages on Padre Island, Texas: Effects of lee airflow and sand saturation levels and implications for interdune deposition. *Journal of Sedimentary Petrology*, 62(4), 622-635.

Kraus, N.C., Larson, M., and Kriebel, D.L., 1991. Evaluation of beach erosion and accretion predictors. Proceedings of Coastal Sediments 1991. ASCE Press, New York, 572-587.

Lancaster, N., 1985. Variations in wind velocity and sand transport on the windward flanks of desert dunes. *Sedimentology,* 32(4), 581-593.

Lancaster, N. Nickling, W.G. McKenna Neuman, C.K. and Wyatt, V.E., 1996. Sediment flux and airflow on the stoss slope of a barchan dune. *Geomorphology,* 17(1-3), 55-62.

Leatherman, S.P., 1976. Barrier island dynamics: overwash processes and eolian transport. In: Coastal Engineering 1976, *Proceedings of the 15th International Conference*, Honolulu, Hawaii, American Society of Civil Engineers, pp. 1958-1974.

Leatherman, S.P., 1979. Barrier dune systems: a reassessment. *Sedimentary Geology,* 24(1), 1-16.

Lettau, H.H. and Lettau, K., 1978. Exploring the World's Driest Climate. Madison, Wisconsin: Institute of Environmental Studies, University of Wisconsin.

McBride, R.A. and Byrnes, M.R., 1997. Regional variations in shore response along barrier island systems of the Mississippi River Delta Plain; historical change and future prediction. *Journal of Coastal Research*, **13**, 628-655.

McKenna-Neuman, C., 1998. Particle transport and adjustments of the boundary layer over rough surfaces with an unrestricted, upwind supply of sediment. *Geomorphology*, 25(1-2), 1-17.

McKenna-Neuman, C. Lancaster, N. and Nickling, W.G., 1997. Relations between dune morphology, air flow, and sediment flux on reversing dunes, Silver Peak, Nevada. *Sedimentology,* 44(6), 1103-1113.

Morton, R.A. and Sallenger, A.H., 2003. Morphological impacts of extreme storms on sandy beaches and barriers. *Journal of Coastal Research,* 19, 560-573.

Musick, H.B., and Gillette. D.A., 1990. Field evaluation of relationships between a vegetation structural parameter and sheltering against wind erosion. Land Degradation Rehabilitation. **2**, 87–94.

Nickling, W.G. and McKenna-Neuman, C., 1995. Development of deflation lag surfaces. *Sedimentology,* 42(3), 403-414.

Nickling, W.G. and McKenna Neuman C., 1997. Wind tunnel evaluation of a wedge-shaped aeolian transport trap. *Geomorphology*, 18, 333-345.

Nordstrom, K.F. and Jackson, N.L., 1992. Effect of source width and tidal elevation changes on aeolian transport on an estuarine beach. *Sedimentology*, 39(5),769-778.

Nordstrom, K.F. and Jackson, N.L., 1993. The role of wind direction in eolian transport on a narrow sandy beach. *Earth Surface Processes and Landforms*, 18(8), 675-686.

Parsons, D.R., Walker, I.J. and Wiggs, G.F.S., 2004. Numerical modeling of flow structures over idealized transverse aeolian dunes of varying geometry. *Geomorphology*, 59, 149-164.

Psuty, N.P., 1992. Spatial variation in coastal fordune development. In: R.W.G. Carter, T.G.F. Curtis and M.J. Sheehy-Skeffington (Eds), *Coastal Dunes: Geomorphology, Ecology and Management for Conservation*. Balkema Rotterdam, pp. 3-13.

Sallenger, A. H., 2000, Storm impact scale for barrier islands. *J. Coastal Research*, **16,** 890-895.
Sherman, D.J., 1995. Problems of scale in the modeling and interpretation of coastal dunes. *Marine Geology*, 124(1-4), 339-349.

Sherman, D.J. Jackson, D.W.T. Namikas, S.L. and Jinkang, W. 1998. Wind-blown sand on beaches: an evaluation of models. Geomorphology 22(2):113-133.

Snyder, R.A. and Boss, C.L., 2002. Recovery and stability of Barrier Island plant communities. *Journal of Coastal Research*, 18, 530-536.

Stallins, J.A., 2005. Stability Domains in Barrier Island Dune Systems. *Ecological Complexity*, 2, 410-430.

Stallins, J.A. and Parker, A.J., 2003. The influence of complex systems interactions on barrier island dune vegetation pattern and process. *Annals of the Association of American Geographers*, 93, 13-29.

Stone, G.W., 1991. Differential sediment supply and the cellular nature of longshore sediment transport along coastal northwest Florida and southeast Alabama since the Late Holocene. PhD Dissertation, University of Maryland, 376 pp.

Stone, G.W. and Morgan, J.P., 1993. Implications for a constant rate of relative sea-level rise during the last millennium along the Northern Gulf of Mexico: Santa Rosa Island, Florida. *Shore and Beach*, 61, 24-28.

Stone, G.W. Liu, B. Pepper, D.A. and Wang, P., 2004. The importance of extratropical and tropical cyclones on the short-term evolution of barrier islands along the northern Gulf of Mexico, USA. *Marine Geology*, 210, 63-78.

Tsoar, H. and Werner, I., 1998. Reevaluation of sand dunes' mobility indices. *Journal of Arid Land Studies*, 7, 265-268.

van der Wal, D., 1998. The impact of the grain-size distribution of nourishment sand on aeolian sand transport. *Journal of Coastal Research*, 14(2), 620-631.

Walker, I.J. and Nickling, W.G. 2002. Dynamics of secondary airflow and sediment transport over and in the lee of transverse dunes. *Progress in Physical Geography*, 26(1), 47-75.

Walmsley, J.L. and Howard, A.D., 1985. Application of a boundary-layer model to flow over an eolian dune. *Journal of Geophysical Research*, 90(D6), 10631-10640.

Wiggs, G.F.S. Livingstone, I. Thomas, D.S.G. and Bullard, J.E., 1996. Airflow and roughness characteristics over partially vegetated linear dunes in the southwest Kalahari, Desert. *Earth Surface Processes and Landforms*, 21(1), 19-34.

Wiggs, G.F.S. Baird, A.J. and Atherton, R.J., 2004, The dynamic effects of moisture on the entrainment and transport of sand by wind. *Geomorphology*, 59(1-4), 13-30.

CHAPTER 3

Post-hurricane Beach and dune Recovery

Chris Houser

Department of Geography
Texas A&M University
College Station, Texas
77843

Stuart Hamilton

Department of Geography
University of Southern Mississippi
Walker Science Building
Hattiesburg, Mississippi 39406

Abstract

The recovery of Santa Rosa Island in northwest Florida is characterized following Hurricane Katrina (September 2005), which was preceded by Hurricanes Ivan (2004) and Dennis (2005), and Tropical Storm Arlene (2004) within the span of a year. Beach and dune recovery were quantified to the east and west of Pensacola Beach through a comparison of LiDAR data collected immediately following Hurricane Katrina and in July 2006 after almost a year of recovery. East of Pensacola Beach, the shoreline retreated by an average of 64 m during the 2004/2005 hurricane season and recovered by an average of 19 m. To the west of Pensacola Beach, the shoreline retreated by an average of 30 m, and while no significant shoreface recovery was observed, the presence of vegetation on low-profile dunes promoted backshore accretion. Using Empirical Orthogonal Function (EOF) analysis, it is found that shoreface recovery in the east and backshore accretion in the west occurred at the widest sections of the island where the pre-storm profile volume had been relatively large and overwash penetration was at a minimum. The narrow sections of the island (between cuspate headlands) had a smaller profile volume before the storms, leading to greater overwash penetration and in some cases island breaching, which limited the volume of sediment available for shoreface recovery. Through correspondence analysis it is found that the alongshore variation in recovery is not only related to the island width, but also the offshore bathymetry, height of the pre-storm dunes and the washover penetration. It is argued that the relative importance of vertical and horizontal accretion affects the recovery of the dune system, such that the recovery is forced and the alongshore variations in storm impact observed during Hurricane Ivan will be reinforced during subsequent storms.

Keywords: hurricane recovery, Santa Rosa Island, dune recovery

Introduction

It is well established that the impact of a hurricane or a tropical storm on a barrier island depends on the elevation of the storm surge relative to the geometry of the coast, which in turn depends on the extent and height of foredune development (Thieler and Young, 1991; Sallenger, 2000; Morton, 2002; Houser et al., 2007). Even a weak hurricane or tropical storm can lead to overwash and breaching if no protection is afforded by dunes. For example, Santa Rosa Island in northwest Florida suffered beach erosion and widespread overwash and breaching during Hurricane Katrina (2005), despite the storm making landfall along the border of Louisiana and Mississippi (~145 miles to the west). The relatively large impact of Katrina in this area was conditioned by the lack of a fronting dune, which had largely been eroded during Hurricane Ivan (2004). The dunes eroded during Ivan were still recovering from Hurricane Opal (1995) and had not achieved substantial height or extent. During Hurricane Opal, dunes in undeveloped sections of Santa Rosa Island were significantly reduced in height through direct wave erosion and the

transfer of sediment to the backshore by overwash. Stone et al. (2004) noted that post-storm recovery along the Gulf-facing beach/nearshore of Santa Rosa Island was not immediate and did not occur at the study site until approximately 6 years after the event. However, a net accumulation of sediment was apparent in the dune environment within the year following Hurricane Opal. A different assessment is made by Leadon (1999). Rapid beach recovery was generally observed within months throughout the Panhandle region, while dune recovery was found to be relatively slow in areas unaffected by assisted dune restoration activities.

The mechanisms and rate of barrier island recovery following an extreme storm have received relatively little attention in the literature, despite the importance of recovery conditioning the response of the island to subsequent storms. Through continuous monitoring of beaches along the Texas coast, Morton et al. (1994) found that recovery initially involved rapid forebeach accretion followed by backbeach aggradation, dune formation and dune expansion and vegetation recolonization. Foredune recovery is only initiated when vegetation is able to re-establish with sufficient density and coverage to trap sediment delivered to the forebeach during fair-weather conditions and transported to the backbeach by minor flooding and aeolian transport (Psuty, 1992; Morton *et al.*, 1994; Snyder and Boss, 2002). It is also possible that sediment is delivered to the dunes from the overwash fans during offshore winds (Leatherman 1976; Armon, 1979; Leatherman, 1979), which would allow for the recovery of the dunes before the recovery of the beachface (Stone et al., 2004). Regardless of the source, the availability of sediment can be limited by the presence of moisture (Belly, 1964; Hotta *et al.*, 1984; Sherman *et al.*, 1998; Cornelis *et al.*, 2004; Wiggs *et al.*, 2004; ; Davidson-Arnott *et al.*, 2005), the wind regime (Tsoar and Werner, 1998), lag deposits (Nickling and McKenna Neuman, 1995; McKenna Neuman, 1998) and fetch length (Bauer and Davidson-Arnott, 2003; Davidson-Arnott *et al.*, 2005; Hesp *et al.*, 2005). If sediment is not sufficiently available, then the dunes that survived the storm (to varying degrees) may not be stable and may continue to erode. Following Hurricane Katrina, Houser et al. (2007) found that a lack sediment (common in breaches and on washover fans) forces the saltation cascade to be initiated at the toe of the dune, leading to the loss of sediment and the migration of the dune.

The availability of sediment from the washover fans and the accreting beachface depends on how sediment is redistributed during the storm. As the foredune height increases or if closely spaced backbarrier dunes are present more sediment is eroded offshore then is transported to the

backbarrier as overwash (Sallenger, 2000; Houser et al., 2007). As a consequence, the forebeach can recover relatively fast through the onshore transport sediment that was stored directly offshore in the bars and in the upper-shoreface (Morton et al., 1994). As this sediment is delivered landward, the elevation of the backshore increases, leading to a lower frequency of flooding that promotes incipient dune formation. Assuming no alongshore redistribution of nearshore sediment and a limited availability of sediment from the washover fans, the rate of island recovery can mirror the level of impact and reinforce the alongshore variation in dune height and extent observed before the storm (see Stallins, 2005). Only in the absence of storm activity is vegetation able to be established and foredunes develop on a barrier island (Stallins and Parker, 2003; Stallins, 2005).

Considering the potential for change in the frequency and magnitude of extreme storms, the rate at which dune recovery occurs and the height that the recovered dunes can achieve is an important research question that remains poorly understood. This study examines the rate and alongshore variation in forebeach and backbeach recovery along Santa Rosa Island, Florida following Hurricanes Ivan (2004), Dennis (2005) and Katrina (2005). In a previous study, Houser et al. (in press a) found that the that the alongshore pattern of dune morphology and the response of the island to Hurricane Ivan was forced by transverse ridges on the inner-shelf and island width through alongshore variations in storm surge and overwash gradients respectively. In the present study, it is hypothesized that the alongshore variation in the beach and dune recovery also varies alongshore in manner that is coherent (statistically) with the shelf bathymetry and island width.

Study Site

The focus of this study is an approximately 35 km stretch of Santa Rosa Island in northwest Florida that was impacted by Hurricanes Ivan (2004), Dennis (2005) and Katrina (2005). Santa Rosa Island is a narrow sandy Holocene barrier island extending 96 km from East Pass near Destin to Pensacola Pass in the west (Figure 1). While there is evidence to suggest that the barrier is the result of longshore sediment transport from eroding bluffs east of Destin (Kwon, 1969; Stone, 1991; Stone et al., 1992; Stone and Stapor, 1996), the origin of the island has been attributed to the erosion of a central Pleistocene core and the redistribution of sediment alongshore (Otvos, 1982). On the inner-shelf fronting the island, Stone (1984) describes a series

of offshore sinusoidal ridges and troughs oriented northwest-southeast, in alignment with the De Soto submarine canyon further to the east. While these features were also described by Hyne and Goodell (1967), little is known about how these shore-transverse ridges developed.

The modern landscape is heavily developed in the communities of Pensacola Beach and Navarre, but a large part of the island (~26 km) is within the Gulf Islands National Seashore and managed by the National Park Service. Prior to Hurricane Ivan, the dunes east of Pensacola Beach formed a ridge and swale complex, with the primary dune parallel to the shoreline (see Houser et al., in press a). During the hurricane seasons of 2004 and 2005, the island morphology changed from a discontinuous foredune backed by hummocky backbarrier dunes and maritime forest (at the bayside cuspate headlands) to washover terraces at the headlands and washover corridors that reach Santa Rosa Sound between the headlands. The alongshore variation in the pre-Ivan dune morphology and hurricane impact has previously been described in companion studies by Houser et al. (2007) and Houser et al. (in press a); both studies examine the alongshore variation in morphological change during Hurricane Ivan. In these studies it was found that variation in dune morphology and hurricane impact was coherent with transverse ridges on the inner shelf (see Hyne and Goodell, 1967; Stone 1984), the sound-side cuspate headlands, and the historical and recent trends in shoreline change. Large foredunes and the backbarrier dunes were observed at the widest sections of the island (the cuspate headlands) and at crest of the transverse ridges. Due to the large dunes and the presence of the backbarrier dunes, these areas experienced less overwash penetration and most of the sediment from the beachface and dunes was deposited within the upper-shoreface (Figure 2). In contrast, sections of the coast with little to no dune development before Hurricane Ivan were observed in the narrowest portions of the island (between headlands) and along the western edge of the transverse ridges. Overwash penetration during Hurricane Ivan tended to be larger in these areas and island breaching was common, leaving the surface close to the watertable and covered by a lag of shell and gravel. As noted, Houser et al. (in press b) found that this limited the availability of sediment leading to dune erosion and migration following Hurricane Katrina. However, there was no significant recovery in island elevation before Hurricanes Dennis and Katrina leading to greater overwash penetration, particularly in the narrow sections of the island where washover fans were deposited into Santa Rosa Sound.

Based on the modified Fryberger Method (Lettau and Lettau, 1978), the aeolian sediment drift potential (DP) suggests that the resultant drift potential is directed onshore to the northwest (334^{o}). The ratio of the resultant drift potential to the total drift potential for this period is 0.24, which suggests a bimodal wind regime (Fryberger, 1980) and is a reflection of the (NW-SE) frontal winds through the winter and spring and predominately south winds through summer. Winds from the northwest have a relatively long fetch on the overwash fans, but transport by offshore winds is limited by a lag surface consisting of shells, gravel and road debris that developed following Hurricane Ivan and also after Hurricanes Dennis and Katrina (Houser et al., *in press* b). At and directly adjacent to the backbarrier headlands in the eastern study area, the backbarrier dunes that survived the storms and the maritime forest provide an effective barrier to offshore winds, thereby limiting the sediment transport potential.

To the east of the study site, within the boundaries of Eglin Air Force Base, Pries et al. (in press) reported on the impacts of Hurricanes Ivan and Dennis on coastal dunes along Santa Rosa Island. The authors specifically examine the spatial extent of the dunes and how the sequence of storm events leads to significant erosion of the secondary dunes, despite Hurricane Dennis being a relatively weak storm. Claudino-Sales et al. (in press) also describe the impact of Hurricanes Ivan and Dennis on Santa Rosa Island and note that dune survival is controlled by the characteristics of the storm and the morphology of the island and the height and extent of the foredunes. Depending on the specific combination of the controlling variables, there was considerable range in impact from complete inundation to minor scarping. However, the authors were not able to explain why the island response (and impact to infrastructure) exhibited considerable variability alongshore at length scales that appear to be consistent with the spacing of the cuspate headlands along Santa Rosa Sound (see Houser et al., in press a).

Methodology

LIDAR data

The alongshore variation in island recovery was examined using LIDAR, a mapping technology that is increasingly used for coastal change studies and provides a unique opportunity to systematically examine storm response and recovery over a large spatial scale. LIDAR involves the collection of spatially dense and accurate topographic data using aircraft-mounted lasers capable of recording elevation measurements with a vertical precision of ~0.15 m. LIDAR

data for Santa Rosa Island was collected by the USGS Center for Coastal and Watershed Studies before and (immediately) after Hurricane Ivan in May and September 2004 respectively with subsequent surveys completed after Hurricane Dennis (July, 2005) and Hurricane Katrina (September 2005). An additional survey was completed by Escambia County in July 2006 and included the Florida section of the Gulf Islands National Seashore. The pre-Ivan dataset is a product of the USACE and Optech Inc., which is more commonly known as the Compact Hydrographic Airborne Rapid Total Survey (CHARTS). This system is a combination of a 1000 Hz hydrographic sensor, a 10,000 Hz topographic sensor and an image sensor working in unison. The pre-Ivan LIDAR The post-Ivan LIDAR dataset is a product of the NASA sensor known as EAARL (Experimental Advanced Airborne Research LIDAR).

Following Young and Ashford (2006), all data was first converted from raw xyz data in ArcSDE feature classes. Raw point data was interpolated using inverse distance weighting (IDW) into pre-Ivan, post-Ivan, post-Katrina and recovery elevation models. The IDW power was set to four to negate distant points and the search radius limited to the closest eight points, again to negate distant neighbors. The root-mean-square-error (RMSE) was 0.34, 0.54, 0.67 and 0.62 for the pre-Ivan, post-Ivan, post-Katrina and July 2006 models respectively. Elevation models with larger error have a lower density of survey points. The RMSE should not be confused with the accuracy of the sensor; the vertical accuracy of LIDAR is approximately ±0.15 m and the horizontal accuracy is < 1m (Sallenger et al., 2004).

Offshore Bathymetry

As discussed by Houser et al. (*in* press a), the height of the pre-Ivan foredunes and the presence of backbarrier dunes were correlated but spatially lagged with transverse ridges on the inner-shelf. This study extends that analysis to the entire length of Santa Rosa Island using a 200 kHz fathometer along a series of shore-parallel and shore-perpendicular surveys. All data were spatially referenced in real-time using a ship-based GPS and the seafloor depths were heave and tide-corrected to mean low water (MLW) using measured tides. The cleaned-data was interpolated using inverse distance weighting at a spacing of 1 m. Consistent with the LIDAR profiles, the alongshore variation in the offshore bathymetry is examined using transects spaced at 35 m intervals.

Data Analysis

The recovery of the forebeach and backshore were characterized using Empirical Orthogonal Function Analysis. Cross-shore transects spaced at 35 m intervals were extracted from the LIDAR data for a total of 302 transects in Santa Rosa Unit and 184 transects in Fort Pickens Unit. As discussed by Houser et al. (*in press* a) and Houser et al. (2007), EOF analysis extracts a limited number of factors to explain most of the profile variance alongshore, with the variance explained by successive factors decreasing monotonically. The relationship between the primary modes for the different LIDAR surveys (pre-Ivan, post-Ivan, post-Katrina and recovery) was examined using Canonical Correlation Analysis (CCA). This test is used to investigate whether or not there are patterns that occur simultaneously in two different data sets and to describe the nature of those patterns (see Larson et al., 2000). The correlation between the spatial amplitudes (factor scores) from different combinations of the variable sets is termed the canonical correlation; the first canonical correlation is the largest and the magnitudes decrease sequentially.

Spectral analysis is used to decompose the spatial variation into sinusoidal components of varying frequency and amplitude in order to explore the nested controls on the recovery process. To avoid non-stationarity in the data, all variables were detrended through linear regression prior to analysis. The power spectrum gives the average spectral variance over the frequency interval (bandwidth) *B* centered on a given frequency:

$$B = \frac{2m+1}{N} \qquad [1]$$

where *N* are the discrete equally spaced intervals of the sample data and *m* is a smoothing coefficient that determines the degree of adjacent averaging of the periodogram. The choice of bandwidth to distinguish peaks was based on a compromise between the amount of detail required and the number of degrees of freedom. Small values of m help in locating periodic (deterministic) components, while larger values of m yield smoother curves for stochastic model fitting. Shumway (1988) recommends that the value of m is equal to 1/20 of sample points used in the analysis. A smoothing coefficient of 15 is used for the Santa Rosa Unit, while a coefficient of 9 is used for the Fort Pickens Unit where there are fewer transects. The statistical

significance of the peaks in the spectra compared to white noise was examined using an F variance-ratio test based on the ratio of variances. Only those spectral peaks that are identified as significantly different from white noise at the 95% confidence level are discussed.

Cycles or regularly repeating patterns in the relationship between two variables are shown through cospectral analysis, in which the covariance between two variables is plotted as a function of wavenumber. The correspondence between the two series is described by the squared-coherency spectrum, which is analogous to the r^2 in a simple linear regression analysis and measures the influence of noise at each frequency. As spatial noise increases in either spectrum there will be low correlation. The phase spectrum is used to describe the spatial delay (or lag) between variables as a function of the wavenumber. In this respect, cospectral analysis describes the relationship between two variables in a more sensitive way than conventional correlations, especially when the relationship between the two variables changes for different length scales.

While cospectral analysis can be used to examine the spatial relationship between variables, the observed hurricane impact and subsequent recovery may reflect several competing influences. Correspondence analysis is used to examine how the recovery relates to the island width (wide or narrow), offshore bathymetry (gentle versus steep offshore slope) and pre-Ivan dune height (high versus low). Correspondence analysis is an exploratory technique used to analyze two-way or multi-way tables containing some level of correspondence between the row and column categories (Hirschfel, 1935). The method is used to lower dimensionality in order to identify a smaller number of uncorrelated variates containing most of the variance of the raw data (Hill, 1974). In contrast to Principal Component Analysis, correspondence analysis uses Chi-square distances (rather than Euclidian distance) to arrange the categorical variables, relative to an axis in multidimensional space, according to their similarity (or association) to each other (Clausen, 1998). The closer the angle is to 0° (positive correlation) or 180° (negative correlation), the stronger the relationship. Angles near 90° and 270° show no relationship between variables. All variables were characterized based on whether the values were greater or less than the average for all 486 transects.

Results

Average Profile Change

Spatially-averaged island profiles are provided in Figure 3 for both the Eastern and Fort Pickens Units of the study area. Shown are the pre- and post-Ivan profiles, the post-Katrina profile and the "recovered" profile a year after Hurricane Katrina. The shoreline in the Santa Rosa Unit retreated by an average of 8 m during Hurricane Ivan but retreated a further ~57 m during Hurricanes Dennis and Katrina. The total change in profile volume ranged from -5 to -532 m^3 m^{-1} with an average change of -146 m^3 m^{-1}. The average profile changed from having a well-defined (but discontinuous) foredune with a height of 2.8 m to a steep foreshore backed by large washover sheets in the backshore. In the Fort Pickens Unit, the average shoreline retreated by an average of ~25 m during Hurricane Ivan (see Hapke and Christiano, 2007), although there were sections (the breached areas) where a welded bar was captured in the survey suggesting that the average shoreline (presented in Figure 3) extended seaward. The shoreline eroded by a further 13 m during Hurricanes Dennis and Katrina for a total retreat of ~38 m during the 2004/2005 hurricane season. The total change in profile volume ranged from (a gain of) 239 to -618 m^3 m^{-1} with an average change of -150 m^3 m^{-1}. The average profile changed from a wide foredune with a height of 2 m to an overwash terrace extending into a remnant dune field that had been a low-profile backbarrier dune field prior to Hurricane Ivan (Figure 4). Due to the continued presence of vegetation in the remnant dune system, the backshore accreted by an average of 0.20 m following Hurricane Katrina with most of the growth occurring in the summer of 2006, after the dune recovery study by Houser et al. (in press b).

Between September 2005 and July 2006, the shoreline in the Santa Rosa Unit recovered by ~19 m and the profile volume increased by an average of 28 m^3 m^{-1}. The recovered profile volume is only ~19% of the volume lost during the hurricane season. Consistent with the alongshore variation in island response to Hurricane Ivan (Houser et al., in press a), the "recovery" varied considerably alongshore. The change in profile volume ranged from a net loss of 72 m^3 m^{-1} to a gain of 160 m^3 m^{-1}. In general, areas with a larger loss in profile volume during the hurricanes had greater volumetric recovery. Those areas with a smaller profile volume before the storm experienced less recovery and in some cases continued erosion.

In an earlier study that focused on only the Santa Rosa Unit, Houser et al. (*in press* a) found that the impact of Hurricane Ivan along this stretch of coast was coherent, but spatially lagged, with the cuspate forelands and transverse ridges on the inner shelf. Both of these features exhibited an alongshore variation at a length scale of ~1400 m. The post-storm profile

also exhibits a statistically significant variation at a length scale of ~1400 m, with a secondary variation at a length scale of ~750 m. To highlight the variation at these scales, the alongshore variation in the post-storm profile change and pre-Ivan profile volume were smoothed using a 20-point (700 m) hamming low-pass filter (Figure 5). In general, there was an increase in both shoreline position and profile volume, characteristic of post-storm recovery, but there were also cases of shoreline gain but profile loss. Profiles with a large pre-Ivan volume tended to be at or west of the cuspate forelands where there is greater profile recovery compared to adjacent sites. In contrast, those areas with a relatively small pre-Ivan volume were observed east of the cuspate forelands where the island was breached during the storms. These areas tended to experience the smallest profile recovery.

Characteristic Change in the Santa Rosa Unit

To further examine the alongshore variation in recovery following Hurricane Katrina, Empirical Orthogonal Function Analysis was used to identify characteristic profiles. The relationship between the September 2005 and July 2006 profiles was examined using Canonical Correlation Analysis. In this section, five factors were found to be statistically significant for both datasets and their factors scores were correlated alongshore. The first combination of profiles (Figure 6a) is characterized by shoreline accretion by ~18 m, backshore accretion by ~0.31 m and a reduction in the foreshore slope without significant change in foreshore volume. The phase relationship between the factor scores for these profiles and the island width suggests that this combination is most commonly observed ~150 m west of the cuspate headlands. Adjacent to these sites and ~260 m west of the cuspate headlands, the profile change is characterized by a shoreline accretion by ~10 m, backshore accretion by ~0.27 m and a reduction in foreshore slope without a significant change in volume (Figure 6b). To the east of the cuspate headlands, the shoreline accreted by ~18 m but there was no significant change in the backshore elevation (Figure 6c). At the cuspate headlands, the profile change is characterized by ~14 m of shoreline accretion and ~0.17 m of backshore accretion (Figure 6d). Finally, at the narrowest sections of the island, the backshore accreted through the development of a storm berm with an average height of 0.60 m above the September 2004 profile (Figure 6f).

An additional correlation was observed between Factor 5 and Factor 3 of the September 2004 and October 2005 datasets respectively. This combination tended to be found within the

western portion of the Santa Rosa Unit in an area of the island managed by the University of West Florida. Following Hurricane Dennis a large berm of gravel and asphalt mixed with washover sediment was placed by the local county along the seaward edge of the road. This area exhibited no significant backshore accretion but considerable foreshore erosion that has lead to the development of a nearshore terrace. Ignoring this combination, the results of the correlation analysis suggest that there is an east-west transition in the relative proportion of vertical and horizontal profile accretion. Between headlands, where the island is narrow and the overwash penetration was greatest, the profile change during the recovery period has largely been vertical accretion in the backshore through the development of a storm berm. To the east the relative importance of horizontal foreshore accretion increases and the storm berm that developed during Hurricane Katrina largely disappears. East of the cuspate headlands there is considerable foreshore accretion but no significant backshore accretion.

The results of the EOF analysis suggest that there is an east-west variation in the relative amount of foreshore and backshore accretion, but it is not in-phase with either the island width, offshore bathymetry or the height of the foredunes before Hurricane Ivan. It is reasonable to expect that the influence of these variables may be additive or competing depending on specific combination. Correspondence analysis is used as a qualitative exploratory technique to identify how the recovered profiles are influenced by these controlling variables (Figure 7). The strong berm development described by Factor 3 from the July 2006 dataset tends to be associated with the narrow sections of the island where the offshore profile is relatively reflective and overwash penetration tended to be small. The relatively reflective profile west of the cuspate headlands, also appears to be responsible for the backshore accretion observed in Factor 1. The other profile factors (2, 4 and 5) are more strongly influenced by foredune height, with only minor influence from the offshore bathymetry and no control by island width. Where the foredunes were large and overwash penetration was small, the profile recovery is characterized by Factor 4, while those areas with smaller dunes and a dissipative offshore profile (Factor 5) had the largest overwash penetration and the largest foreshore recovery. The profile recovery represented by Factor 2 tends to be equally distributed with respect to offshore bathymetry and are associated with small foredunes and island width prior to Hurricane Ivan.

Characteristic Change in the Fort Pickens Unit

Despite being only separated by a distance of ~12 km, the response of the island to the storms and the post-storm recovery is very different for the Fort Pickens Unit of the island. As noted, the average profile changed from having a single wide foredune with a height of ~2 m to a relatively continuous overwash terrace extending into a remnant dune field that had been a low-profile backbarrier dune field prior to Hurricane Ivan (Figure 8). Large breach corridors developed in the narrow sections of the island where the pre-storm dune heights (~1 m) were less than the spatial average. The breaches were reoccupied during Hurricanes Dennis and Katrina, and during Tropical Storms Arlene and Cindy, but continue to be occupied by surge waters during relatively small frontal storms, particularly when those storms coincide with high tide. Based on these field observations, water levels created by winds of ~13 m s^{-1} (~30 mph) and energetic surf (H_o>1 m) are capable of exceeding the post-Ivan storm berm within the breach areas. Based on the July 2006 LiDAR, ~10.5 km (96%) of the FPU would be susceptible to overwash by an extreme storm with a storm tide elevation of 1 m, compared to only 36% of the SRU following Hurricane Katrina and 16% by July 2006. The resulting washover fans that develop behind the berm appear to be an important source of sediment for the recovery of the dunes (Houser et al., in press).

Consistent with the Santa Rosa Unit, the pre-storm height of the dunes and the response of the island to the sequence of storms seem to be related to the island width. To characterize the alongshore variation in storm recovery, the relationship between the September 2004 and July 2006 profiles was examined using Canonical Correlation Analysis. The recovery following Hurricane Katrina could not be examined due to the poor data quality and coverage within this section on that flight, so the July 2006 profiles are examined against the post-Ivan profiles. During Hurricane Dennis, this unit was west of the storm track and winds were offshore leading to a storm surge along the backbarrier that eroded the remnant dunes from behind (see Houser et al., *in press* b). During Hurricane Katrina, the lack of a foredune allowed the site to be overwashed but except for some erosion of the remnant dunes there was little change in island elevation but a further retreat of the shoreline (Hapke and Christiano, 2007). Over the 2004/2005 hurricane season, the shoreline of the Fort Pickens Unit retreated by an average of ~44 m (Hapke and Christiano, 2007). This suggests that there may have been <10 m of shoreline recovery within the Fort Pickens Unit between September 2005 and July 2006.

Based on the EOF analysis, five factors were found to be statistically significant for both datasets (September 2004 and July 2006) and their factors scores were found to be correlated alongshore (Figure 10). The first combination of profiles (Figure 10a) is characterized by no change in the shoreline position but the development of a large storm berm and a wide concave beach. The phase relationship between the factor scores for these profiles and the island width suggests that this combination is most commonly observed at the cuspate headlands. The profiles at the headlands are presented in Figure 10e and are characterized by no change in the shoreline position but significant accretion (~ 1 m) in the vicinity of the (former backbarrier) dunes that survived all of the storms. The erosion along the back of this profile is the result of backbarrier erosion during Hurricane Dennis (see Houser et al., *in press* b) and not a loss of sediment during the recovery period. Accretion at and to the east of the headlands is also represented through the profile combination presented in Figure 10d. These profiles are characterized by a retreat of the shoreline, loss of the beach berm and significant accretion (~0.75 m) within the remnant dune system.

In contrast to the vertical accretion within the remnant dunes at the headlands, little to no vertical or horizontal recovery is observed in the breach corridors between the headlands (Figure 10b and 9c). The breach corridors are represented by the relatively flat and featureless profiles in Figure 10b, which exhibit no change in shoreline position and a minor redistribution of sediment from the front of the island to the back. This redistribution of sediment is also observed immediately to the east of the breach corridors (Figure 10c). Since these areas are devoid of vegetation, it is reasonable to assume that the redistribution of sediment is more associated with Hurricanes Dennis and Katrina than change during the recovery period. While the lack of post-Katrina data for the Fort Pickens Unit limits our analysis of post-storm recovery, the results suggest that there is little shoreline recovery but relatively rapid dune growth at the headlands where there are remnant dunes and vegetation. This is consistent with the post-Opal observations of Stone et al. (2004) from the same area, while the beachface recovery and lack of backshore accretion in the Santa Rosa Unit are consistent with the observations of Leadon (1999).

Discussion

The impact of an extreme storm depends on elevation of the storm surge relative to the geometry of the coast (Thieler and Young, 1991; Sallenger, 2000; Morton, 2002; Houser et al.,

2007), which in turn depends on the extent and height of the foredunes. The response of the island to subsequent storms depends on the ability of the beachface and dunes to recover and the rate of recovery. The mechanisms and rates of beach and dune recovery following an extreme storm have received little attention in the literature, with the notable exceptions of Morton et al. (1994), Leadon (1999) and Stone et al. (2004). This may reflect the relatively slow rates of accretion compared to the dramatic change observed during the storm, particularly with respect to the dunes. In the present study, the recovery of Santa Rosa Island is examined following the 2004/2005 hurricane season when the island was impacted by Hurricanes Ivan (September 2004), Dennis (July 2005) and Katrina (September 2005). The availability of LIDAR data following a period of recovery allows for systematic evaluation of recovery and a unique opportunity for comparison with several other studies from the same region that describe the impact of the hurricanes (Claudino-Sales et al., 2007; Houser et al., 2007; Houser et al., in press a) and the recovery (Leadon, 1999; Stone et al., 2004).

Within a year of Hurricane Katrina, the shoreline recovered by ~19 m and the profile volume increased by an average of 28 m^3 m^{-1}. Accretion in the backshore was not a response to dune redevelopment but occurred through the deposition of sediment by storm surge that developed during frontal storms. The results are contrary to the observed recovery patterns observed by Stone et al., (1994) following Hurricane Opal (1996). In that study, foreshore recovery did not occur and the dunes started to recover within a year of the storm. The results from the Santa Rosa Unit of the present study are more consistent with those of Leadon (1999). That author noted foreshore recovery throughout most of the Panhandle following Hurricane Opal with little to no dune recovery within a year of the storm. The focus of Stone et al. (2004) is on the Fort Pickens Unit of the present study, where limited foreshore development but relatively strong dune recovery was also observed following Hurricane Katrina. The more rapid recovery can be attributed to the more extensive area covered by dune grass following Hurricane Ivan compared to the Santa Rosa Unit that is dominated by unvegetated washover terraces. Houser et al. (in press a) found that those remnant dunes were supplied by offshore winds that had a relatively large unobstructed fetch across the washover terrace. The sediment supply from onshore winds is limited by the narrow fetch covered in a lag of gravel and shells and the boundary adjustments caused by the steep beachface and berm (Houser et al., in press b), particularly in the narrow sections of the island that were breached The greater backbarrier

accretion in the Fort Pickens Unit can also be ascribed to the larger fetch across Escambia Bay and the lack of backbarrier dunes to obstruct the wind. Despite the presence of vegetation and readily available sediment from the beachface and foreshore, the dunes to the west of Pensacola Beach are much smaller, suggesting that the supply of sediment is ultimately limited. As shown by Stone et al. (2004), the washover fans in this region are readily eroded by the short-crested waves that are common in Escambia Bay following the passage of a cold front. The loss of island volume by these frontal storms is greater than observed during Hurricane Opal.

Within the Santa Rosa Unit of the study area, the hurricanes of 2004 and 2005 caused the island to change from a discontinuous foredune backed by hummocky backbarrier dunes and maritime forest (at the bayside cuspate headlands) to washover terraces at the headlands and washover corridors between headlands (Figure 2). The washover terraces showed little evidence of vegetation recovery following the storms and no recovery by the fall of 2007 (see Figure 2). The lack of vegetation has lead to relatively little backshore accretion with the exception of sediment deposited by overwash and aeolian transport from the beachface. As a consequence, the areas of the island characterized by large foreshore accretion and little to any storm berm development (Factors 4 and 5) require the recovery of the dunes, which in turn depends on the recovery of the dunes. In general, vegetation can redevelop from existing seedbanks and through rhizome expansion, both of which are determined by the impact of the extreme storm on the dune system. It appears that the overwash and later inundation experienced during Hurricane Ivan and the later storms redistributed the available supply of seeds to the backbarrier where the reestablishment of vegetation following the storm occurred relatively soon, but only in those areas lacking large backbarrier dunes. It appears that the narrow sections of the island and the western part of Santa Rosa Island in general are well adapted to the high frequency of storms and are able to recover relatively fast albeit with a smaller discontinuous dune system (Stallins and Parker, 2003).

In comparison, backshore accretion has been greater in the narrow sections of the island, characterized by Factors 1, 2 and 3. These profiles have almost reached the cross-shore average and maximum elevations observed in the pre-Ivan profiles, although the profile volumes of Factors 1 and 3 remain significantly smaller than their pre-Ivan volumes. For Factor 1 the lower profile volumes reflects the presence of foredunes before Hurricane Ivan, while the lower profile volume for Factor 3 is a consequence of erosion caused by inundation throughout most of the

storms and island breaching (see Houser et al., in press a). This ability to recover vertically suggests that the geometry of the island in these areas is dominated by storm berm development and that the lack of large and extensive dunes before Hurricane Ivan reflects a lack of available sediment from offshore. This would not only explain the lack of foredune development but also the larger historical rates of erosion observed in these areas where the island is narrow and the offshore profile is reflective (Houser et al., in press a). Sediment is further limited in the breached areas where the backbarrier elevation is at or close to the watertable and covered by a heavy lag of shell and gravel from the adjacent road bed (Houser et al., *in press*). Both the moisture and the lag create a supply-limited system in which dune recovery will be slow compared to those areas where the pre-storm dunes were well-developed and sediment was largely lost to the shoreface and the washover terraces are not covered by a lag.

The alongshore variation in the recovery and the relative importance of horizontal foreshore accretion and vertical accretion in the backshore is coherent with the bathymetry on the inner shelf. The transverse ridges will cause alongshore variations in wave convergence and divergence as a result of wave refraction/diffraction around the bathymetric highs and lows (e.g. O'Reilly and Guza, 1993; Schwab et al., 2000; Bender and Dean, 2003; Schupp et al., 2006). As noted by Houser et al. (in press a), the outermost nearshore bar in the vicinity of the transverse ridges is ~50 m further offshore and >1 m lower on the profile, characteristic of a more dissipative nearshore environment resulting from greater wave energy (Plant et al., 2001; Houser and Greenwood, 2005). Following from Wright and Short (1984) these dissipative environments will have limited berm development, compared to the reflective profiles in the narrow sections of the island. As noted, Houser et al. (in press b) found that the supply of sediment in these narrow reflective environments is limited by the narrow fetch covered in a lag of gravel and shells and the boundary adjustments caused by the steep beachface and berm. The larger beachwidth and lack of berm development in the wide dissipative sections of the island should be conducive to dune recovery once the vegetation is able to recovery (Hesp, 1988; Short and Hesp, 1982; Davidson-Arnott and Law, 1996). In this respect, the study provides a bridge between the process-based dune model of Short and Hesp (1982) and the sediment budget model that Psuty (1992) developed (in part) to explain variation in dune morphology to the west of the present study site.

The alongshore coherency between the rate and type of recovery, suggests that the recovery is forced and the alongshore variations in storm impact observed during Hurricane Ivan (see Houser et al., in press a) will be reinforced during subsequent storms (Figure 10). Assuming the recovery of vegetation and dunes before the next storm, the wide dissipative sections will have greater elevation than the narrow reflective areas where elevation appears to be limited to berm development. These areas will again have greater overwash penetration and potential for breaching compared to the wide dissipative sections. However, this pattern will only be reinforced if there is sufficient relaxation and the dunes are able to return to their pre-Ivan elevations. The dunes eroded during Ivan were still recovering from Hurricane Opal (1995) and had not achieved substantial height or extent leading to a significant reduction in height and greater overwash penetration than during Hurricane Opal. Prior to Hurricane Opal, the dunes had considerable time for development since the last major storms to directly impact the island in 1906, 1916 and 1926. The anticipated increase in the frequency of extreme storms with the warming of Atlantic sea-surface temperatures (Keim *et al.*, 2004) will reduce the time available for the dunes to redevelop. In this respect, the most vulnerable areas of the island are not those with a narrow dissipative profile and limited vertical accretion, but the wide-dissipative sections east of Pensacola Beach that require both vegetation and dune recovery.

Acknowledgements

This study was supported by a grant from the National Park Service (P5320060026). LIDAR survey data was prepared by Nathan McKinney, Amber Bloechle and John Oravetz of the University of West Florida Geodata Center. Field assistance was provided by Kevin Bradley and Chasidy Hobbs. Riley Hoggard, Resource Management Specialist for the Gulf Islands National Seashore provided important background information to the site and was helpful in providing access to the site. The shorelines from the pre- and post-Ivan LIDAR were graciously provided by Asbury Sallenger, Hilary Stockdon and Laura Fauver of the USGS Coastal and Marine Geology Program. Additionally, post-Katrina LIDAR coverage of Santa Rosa Island was made available by John Brock and Amar Nayegandhi of the USGS Center for Coastal and Watershed Studies and the July 2006 LIDAR data was provided by Escambia County.

References

Armon, JW. 1980. Dune erosion and recovery on a northern barrier. In: *Coastal Zone '80, Proceedings of the 2nd Symposium on Coastal and Ocean Management*. American Society of Civil Engineers: Hollywood, Florida; 1233-1250.

Bauer BO, Davidson-Arnott RGD. 2003. A general framework for modeling sediment supply to coastal dunes including wind angle, beach geometry, and fetch effects. *Geomorphology* **49:** 89-108.

Belly PY. 1964. *Sand movement by wind*. United States Army, Corps of Engineers, Coastal Engineering Research Center, Washington DC, Technical Memorandum TM-1, 80 pp.

Bender CJ, Dean RG. 2003. Wave field modification by bathymetric anomalies and resulting shoreline changes: A review with recent results. *Coastal Engineering* **49**: 125-153.

Claudino-Sales V, Wang P, Horwitz MH. *in press*. Factors controlling the survival of coastal dunes during multiple hurricane impacts in 2004 and 2005: Santa Rosa barrier island, Florida. *Geomorphology*.

Clausan SE. 1998. *Applied correspondence analysis: an introduction*. Sage University Papers Series on Quantitative Applications in the Social Sciences, 07-121. Thousand Oaks, California: Sage.

Cornelis WM, Gabriels D, Hartmann R. 2004. A parameterization for the threshold shear velocity to initiate deflation of dry and wet sediment. *Geomorphology* **59**: 43-51.

Davidson-Arnott RGD, Law MN. 1996. Measurement and prediction of long-term sediment supply to Coastal Foredunes. *Journal of Coastal Research* **12**: 654–663.

Davidson-Arnott RGD, MacQuarrie K, Aagaard T. 2005. The effect of wind gusts, moisture content and fetch length on sand transport on a beach. *Geomorphology* **68**: 115-129.

Fryberger SG. 1980. Dune forms and wind regime, Mauritania West Africa: implications for past climate. *Paleoecology of Africa* **12**: 79–96.

Hapke CJ, Christiano M. 2007, *Long-term and Storm-related Shoreline Change Trends in the Florida Gulf Islands National Seashore*. U.S. Geological Survey Open-file Report 2007-1392, 18p.

Hesp PA. 1988. Surfzone, beach and foredune interactions on the Australian southeast coast. *Journal of Coastal Research* **SI3:** 15–25.

Hesp PA, Davidson-Arnott R, Walker IJ, Ollerhead J. 2005. Flow dynamics over a foredune at Prince Edward Island, Canada. *Geomorphology* **65**: 71-84

Hill MO. 1974. Correspondence Analysis: A Neglected Multivariate Method. *Applied Statistics*, **23:** 340-354.

Hirschfel, HO. 1935. A connection between correlation and contingency. *Proceedings of the Cambridge Philosophical Society* **31**: 520-524.

Hotta S, Kubota S, Katori S, Horikawa K. 1984. Sand transport by wind on a wet sand surface. In: *Coastal Engineering 1984, Proceedings of the 19th International Conference*. American Society of Civil Engineers: Houston, Texas; 1265-1281.

Houser C, Greenwood B. 2005. Hydrodynamics and sediment transport within the inner surf zone of a lacustrine multiple-barred nearshore. *Marine Geology* **218**: 37-63.

Houser C, Hamilton S, Meyer-Arendt K, and Oravetz J. 2007. EOF analysis of barrier island morphological change during Hurricane Ivan. *Coastal Sediments* '07, 986-995.

Houser C, Hapke C, and Hamilton S. *in press* a. Controls on Coastal Dune Morphology, Shoreline Erosion and Barrier Island Response to Extreme Storms. *Geomorphology*.

Houser C, Hobbs C, Saari B. *in press* b. Post-hurricane airflow and sediment transport over a recovering dune. *Journal of Coastal Research*.

Hyne NJ, Goodell HG. 1967. Origin of the sediments and submarine geomorphology of the inner continental shelf off Choctawhatchee Bay, Florida. *Marine Geology* **5**: 299-313.

Kwon HJ, 1969. *Barrier islands of the northern Gulf of Mexico coast: Sediment source and development*. Coastal Studies Series 25. Baton Rouge: Louisiana State University Press.

Larson M, Capobianco M, Hanson H. 2000. Relationship between beach profiles and waves at Duck, North Carolina, determined by canonical correlation analysis. *Marine Geology* **163**: 275-288.

Leadon ME. 1999. Beach, Dune and Offshore Profile Response to a Severe Storm Event. In: *Proceedings of the ASCE Coastal Sediments 99 Conference*: Hauppauge, Long Island, NY; 2534-2549.

Leatherman SP. 1976. Barrier island dynamics: overwash processes and eolian transport. In: *Coastal Engineering 1976, Proceedings of the 15th International Conference*. American Society of Civil Engineers: Honolulu, Hawaii; 1958-1974.

Leatherman SP, 1979. Barrier dune systems: a reassessment. *Sedimentary Geology* **24**, 1-16.

Lettau HH, Lettau K. 1978. Exploring the World's Driest Climate. Madison, Wisconsin: Institute of Environmental Studies, University of Wisconsin.

McKenna-Neuman C. 1998. Particle transport and adjustments of the boundary layer over rough surfaces with an unrestricted, upwind supply of sediment. *Geomorphology* **25**: 1-17.

Morton RA. 2002. Factors controlling storm impacts on coastal barriers and beaches - a preliminary basis for near real-time forecasting. *Journal of Coastal Research* **18**, 486- 501.

Morton RA, Paine JG, Gibeaut JC. 1994. Stages and durations of post-storm beach recovery, southeastern Texas coast. *Journal of Coastal Research* **10**, 884-908.

Nickling WG, McKenna-Neuman C. 1995. Development of deflation lag surfaces. *Sedimentology* **42**, 403-414.

O'Reilly WC, Guza RT. 1993. A comparison of two spectral wave models in the Southern California Bight. *Coastal Engineering* **19**: 263–282.

Otvos EG. 1982, Santa Rosa Island, Florida panhandle: Origins of a composite barrier island. *Southeastern Geology* **23**: 15-24.

Plant NG, Freilich MH, Holman RA. 2001. The role of morphologic feedback in surf zone sand bar response. *Journal of Geophysical Research* **106**, 959-971.

Pries AJ, Miller DL, Branch, LC. *In press*. Identification of structural and spatial features that influence storm-related dune erosion along a barrier-island ecosystem in the Gulf of Mexico. *Journal of Coastal Research*.

Psuty NP. 1992. Spatial variation in coastal fordune development. In: *Coastal Dunes: Geomorphology, Ecology and Management for Conservation*, Carter RWG, Curtis TGF, Sheehy-Skeffington MJ. (eds.): Balkema Rotterdam; 3-13.

Sallenger AH. Wright CW, Lillycrop, J. 2004. Coastal Impacts of the 2004 Hurricanes Measured with Airborne LIDAR: Initial Results. *Shore and Beach* **73**: 10-15.

Sallenger AH. 2000. Storm impact scale for barrier islands. *Journal of Coastal Research* **16**: 890-895.

Schupp CA, McNinch JE, List JH. 2006. Nearshore shore-oblique bars, gravel outcrops, and their correlation to shoreline change. *Marine Geology* **233**: 63-79.

Schwab WC, Thieler ERF, Allen JR, Foster DS, Swift BA, Denny JF. 2000. Influence of inner-continental shelf geologic framework on the evolution and behaviour of the barrier-island system between Fire Island Inlet and Shinnecock Inlet, Long Island, New York. *Journal of Coastal Research* **15**: 408-422.

Sherman DJ, Jackson DWT, Namikas SL, Jinkang W. 1998. Wind-blown sand on beaches: an evaluation of models. *Geomorphology* **22**: 113-133.

Short A, Hesp PA. 1982. Wave–beach–dune interaction in southeast Australia. *Marine Geology* **48**: 259–284.

Shumway RH. 1988. Spectral analysis and filtering. In: *Applied statistical time series analysis*, Wichern RAJDW (ed.): Prentice Hall, Englewood Cliffs, NJ; 47-116.

Snyder RA, Boss CL. 2002. Recovery and stability of Barrier Island plant communities. *Journal of Coastal Research* **18**: 530-536.

Stallins JA. 2005. Stability Domains in Barrier Island Dune Systems. *Ecological Complexity* **2**: 410-430.

Stallins JA, Parker AJ. 2003. The influence of complex systems interactions on barrier island dune vegetation pattern and process. *Annals of the Association of American Geographers* **93**: 13-29.

Stone GW. 1991. *Differential sediment supply and cellular nature of longshore sediment transport along coastal Northwest Florida and Southeast Alabama since the late Holocene*. Ph.D. Dissertation, University of Maryland, College Park, MD.

Stone GW. 1984. *Mathematical modeling of the nearshore and implications for coastal management, Northwest Florida*. Unpublished MSc thesis, Department of Environmental Studies, University of West Florida, 140 pp.

Stone GW, Stapor FW, May JP, Morgan JP. 1992. Multiple sediment sources and a cellular, non-integrated, longshore drift system: Northwest Florida and southeast Alabama coast, USA. *Marine Geology* **105**: 141-154.

Stone GW, Stapor FW. 1996. A nearshore sediment transport model for the northeast Gulf of Mexico coast, USA. *Journal of Coastal Research* **12**: 786-792

Stone GW, Liu B, Pepper DA, Wang P. 2004. The importance of extratropical and tropical cyclones on the short-term evolution of barrier islands along the northern Gulf of Mexico, USA. *Marine Geology* **210**: 63-78.

Thieler ER, Young RS. 1991. Quantitative evaluation of coastal geomorphological changes in South Carolina after Hurricane Hugo. *Journal of Coastal Research* **8**, 187–200.

Tsoar H, Werner I. 1998. Reevaluation of sand dunes' mobility indices. *Journal of Arid Land Studies* **7**: 265-268.

Wiggs GFS, Baird AJ, Atherton RJ. 2004. The dynamic effects of moisture on the entrainment and transport of sand by wind. *Geomorphology* **59**: 13-30.

Wright LD, Short AD. 1984. Morphodynamic variability of surf zones and beaches: a synthesis. *Marine Geology* **56**: 93-118.

Young AP, Ashford S. 2006. Application of Airborne LIDAR for seacliff volumetric change and beach-sediment budget contributions. *Journal of Coastal Research* **22**: 307-318.

Figures

Figure 36. Map of study site showing location relative to the tracks of Hurricanes Ivan and Dennis and Tropical Storm Arlene, and the proximity of the Eastern and Western study areas.

Figure 37. Oblique aerial photographs of storm impact from Hurricanes Ivan (2004), Dennis (2005) and Katrina (2005). Shown are photographs from a cuspate headland near the center of the Eastern study area and at a narrow section of the island immediately west of the headland. Note the different perspectives of the photographs, particularly those taken along the backbarrier.

Figure 38. Spatially-averaged profiles for the (a) Eastern and (b) Fort Pickens Units of the study area. Shown are the average profiles for May 2004 (Pre-Ivan), September 2004 (Post-Ivan), September 2005 (Post-Katrina) and July 2006.

Figure 39. Oblique aerial photograph of the Fort Pickens Unit of the study area (looking west towards Fort Pickens), showing remnant dunes that were originally formed along the backbarrier shoreline. The road visible in the photograph was heavily damaged during Hurricane Ivan and moved behind the remnant dunes just before Hurricane Dennis.

Figure 40. Change in profile volume within the Eastern study section during the hurricane season (May 2004-September 2005) and during the recovery period (September 2005-July 2006).

Figure 41. Characteristic profiles of the Eastern study section based on the significant eigenmodes for the September 2005 and July 2006 datasets. The profile combinations exhibit the strongest canonical correlations of alongshore factor scores.

Figure 42. Correspondence plot for the Eastern study section showing the structure of the primary factors for the characteristic recovery profiles relative to the island width, overwash penetration distance and the offshore bathymetry. The principal axis is described by factors 1 and 5 of the recovery dataset (shoreline recovery) and the secondary axis is described by island width.

Figure 43. Oblique aerial photographs of the Fort Pickens Unit of the study area taken in October 2006. Shown are photographs from (a) the easternmost cuspate headland (foreground of Figure 4) and (b) the breach site west of the headland. The breaches are visible in Figure 4.

Figure 44. Overwash fan behind the storm berm that developed following Hurricane Katrina. This particular fan from the breached area shown in Figures 4 and 8 was created during a strong frontal storm on March 9, 2006, in the middle of the recovery period. This fan continued to develop during a later frontal storm and sediment was moved to the recovering dune field by onshore winds (see Houser et al., in press b).

Figure 45. Characteristic profiles of the Western study section based on the significant eigenmodes for the September 2004 and July 2006 datasets. The profile combinations exhibit the strongest canonical correlations of alongshore factor scores.

Figure 46. Schematic showing the observed variation in response and recovery alongshore within (a) the Santa Rosa Unit and (b) the Fort Pickens Unit of the study area. The response and recovery are shown with respect to the island width (ie. cuspate headlands), offshore bathymetry (reflective or dissipative) and pre-storm dune height.

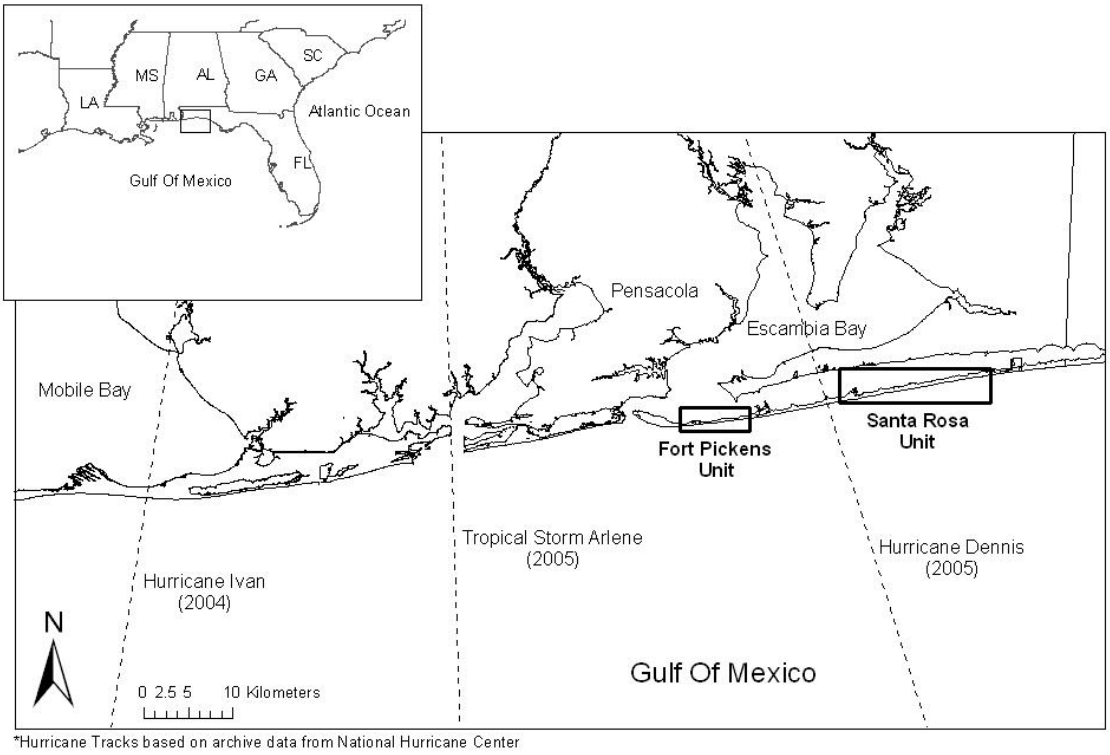
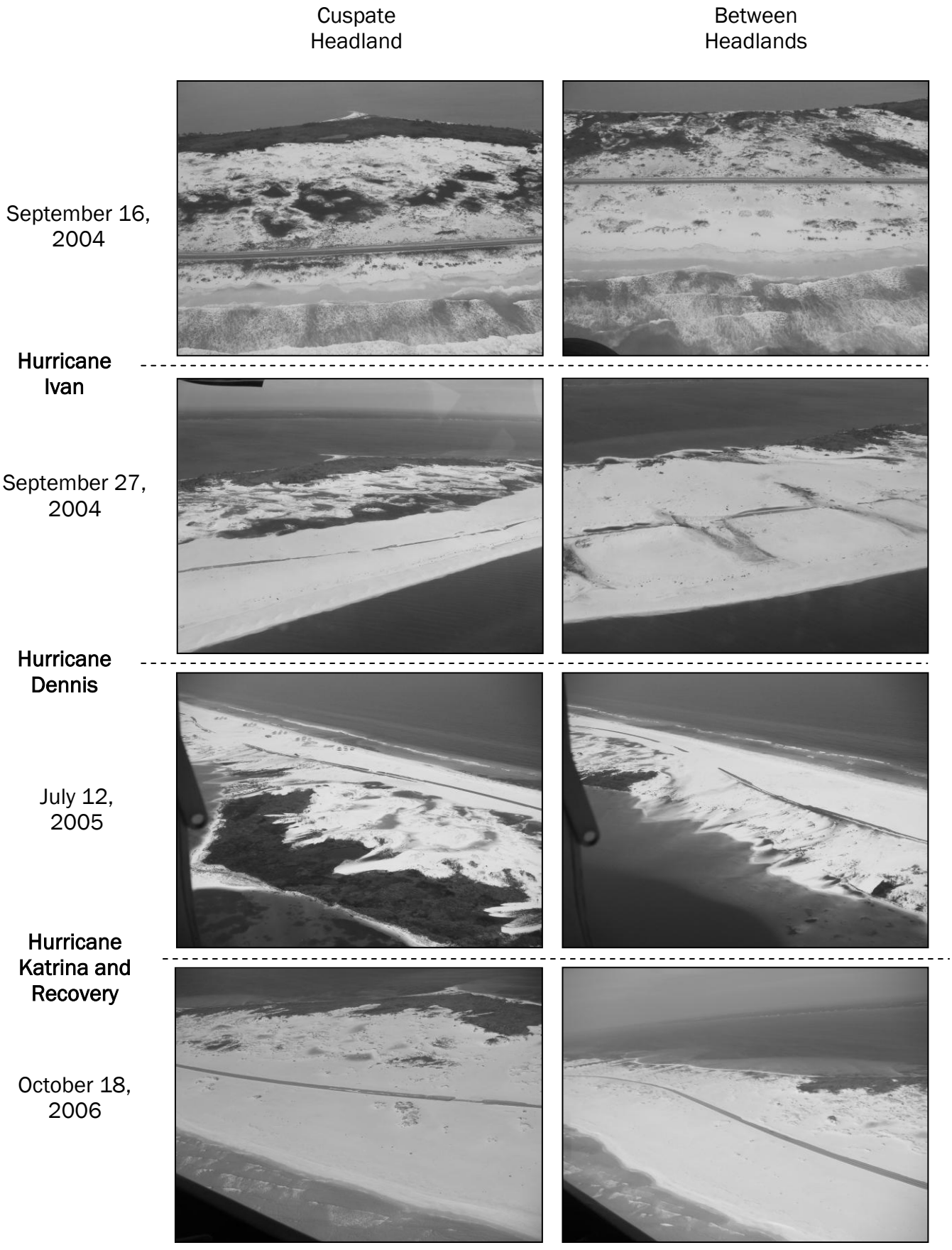

SC
MS
AL
GA
LA
Atlantic Ocean
FL
Gulf Of Mexico
Pensacola
Escambia Bay
Mobile Bay
Santa Rosa
Unit
Fort Pickens
Unit
Tropical Storm Arlene
(2005)
Hurricane Dennis
(2005)
Hurricane Ivan
(2004)
N
0 2.5 5 10 Kilometers
Gulf Of Mexico
*Hurricane Tracks based on archive data from National Hurricane Center

Figure 36.


Cuspate Headland
Between Headlands
September 16, 2004
Hurricane Ivan
September 27, 2004
Hurricane Dennis
July 12, 2005
Hurricane Katrina and Recovery
October 18, 2006

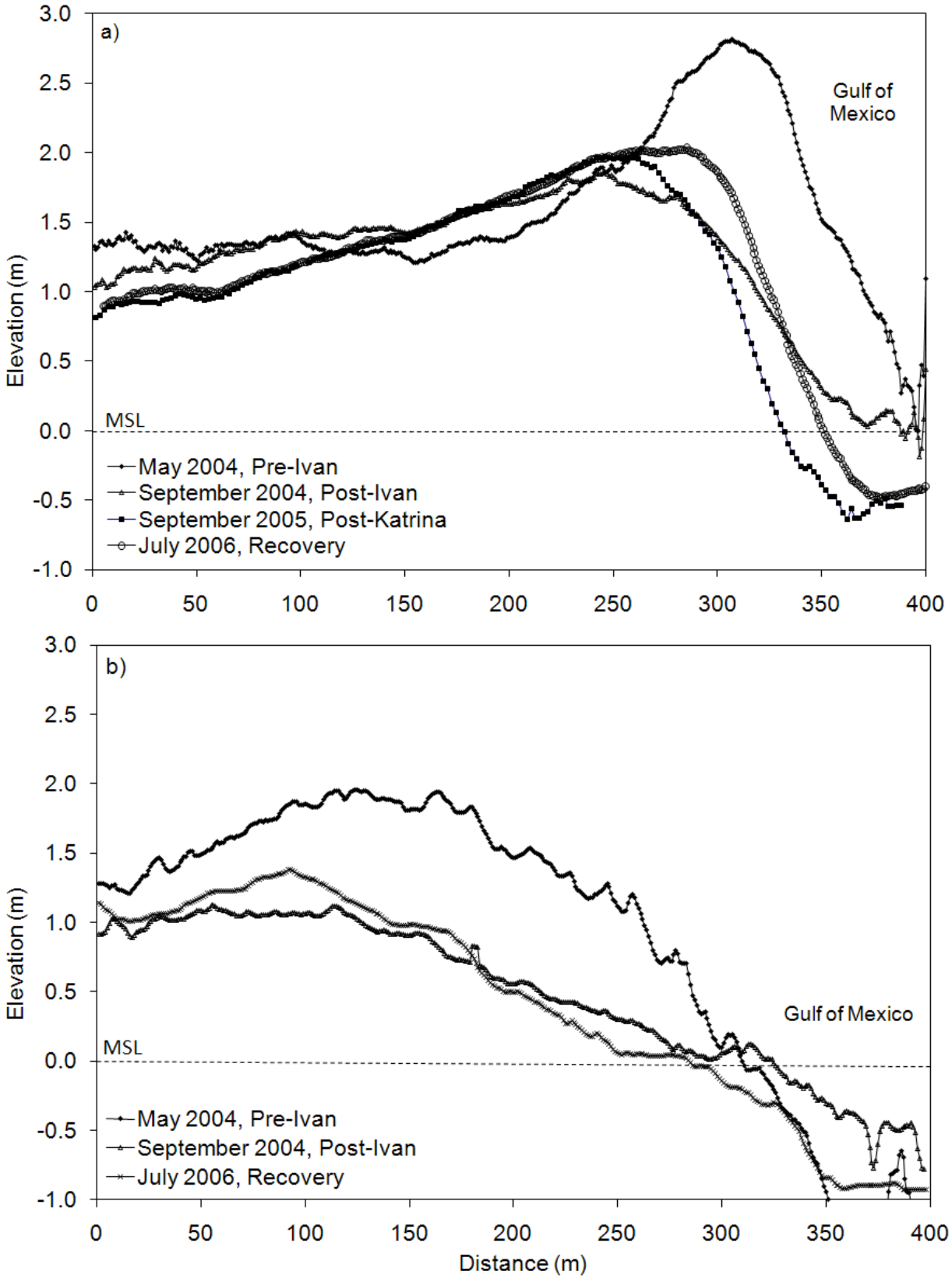

a)
Gulf of Mexico
MSL
May 2004, Pre-Ivan
September 2004, Post-Ivan
September 2005, Post-Katrina
July 2006, Recovery
Elevation (m)
b)
Gulf of Mexico
MSL
May 2004, Pre-Ivan
September 2004, Post-Ivan
July 2006, Recovery
Elevation (m)
Distance (m)

Figure 38.

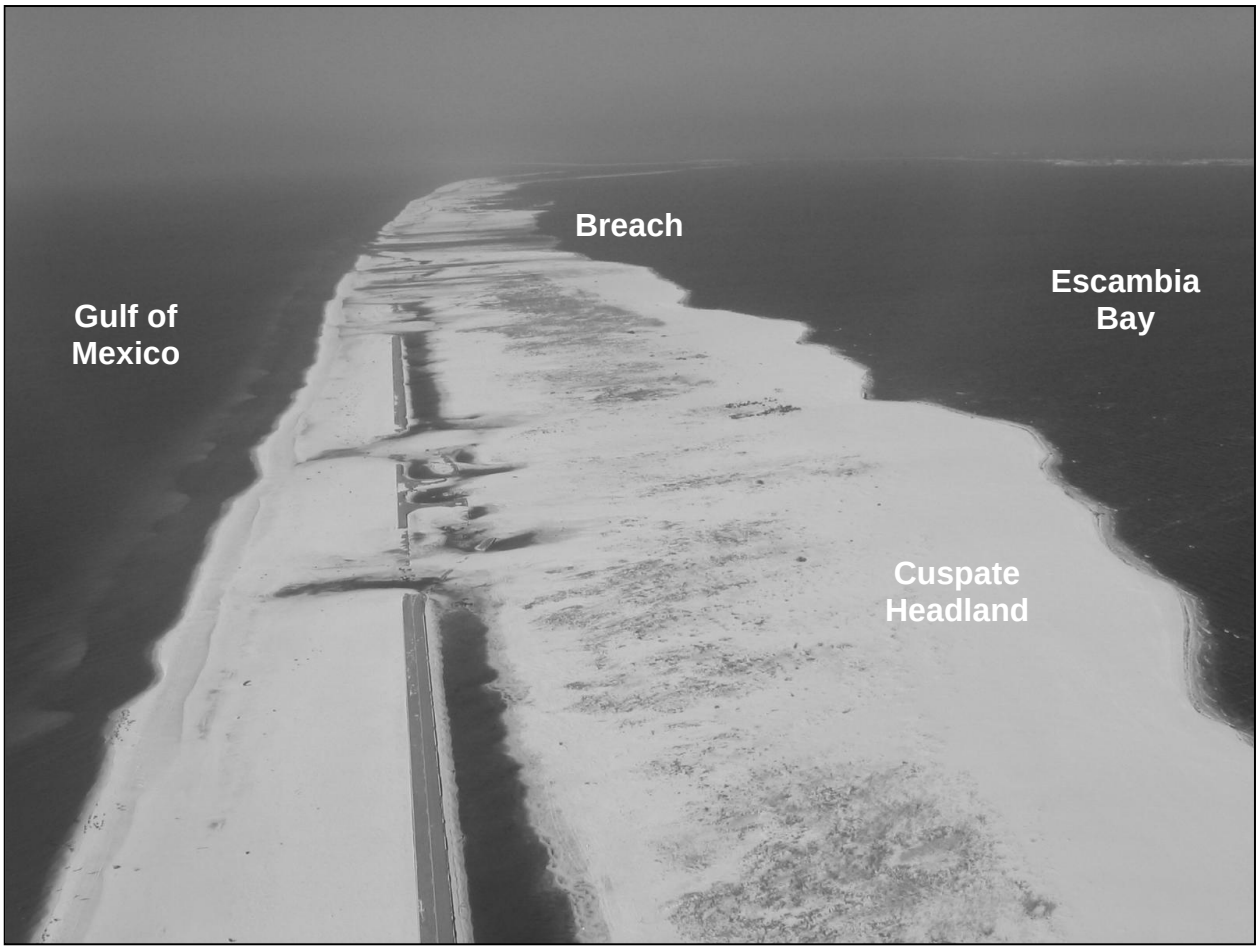


Figure 39.

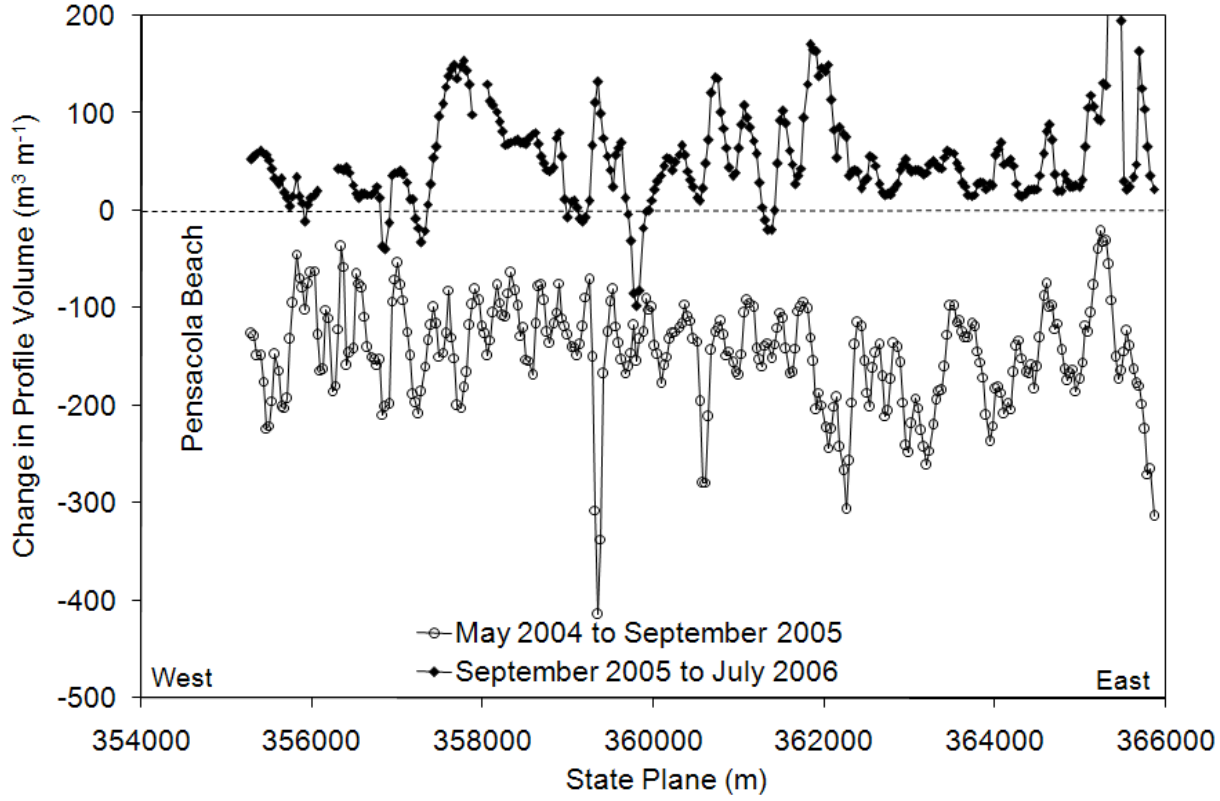

200
100
0
-100
-200
-300
-400
-500
Change in Profile Volume (m3 m-1)
Pensacola Beach
May 2004 to September 2005
September 2005 to July 2006
West
East
354000
356000
358000
360000
362000
364000
366000
State Plane (m)

Figure 40.

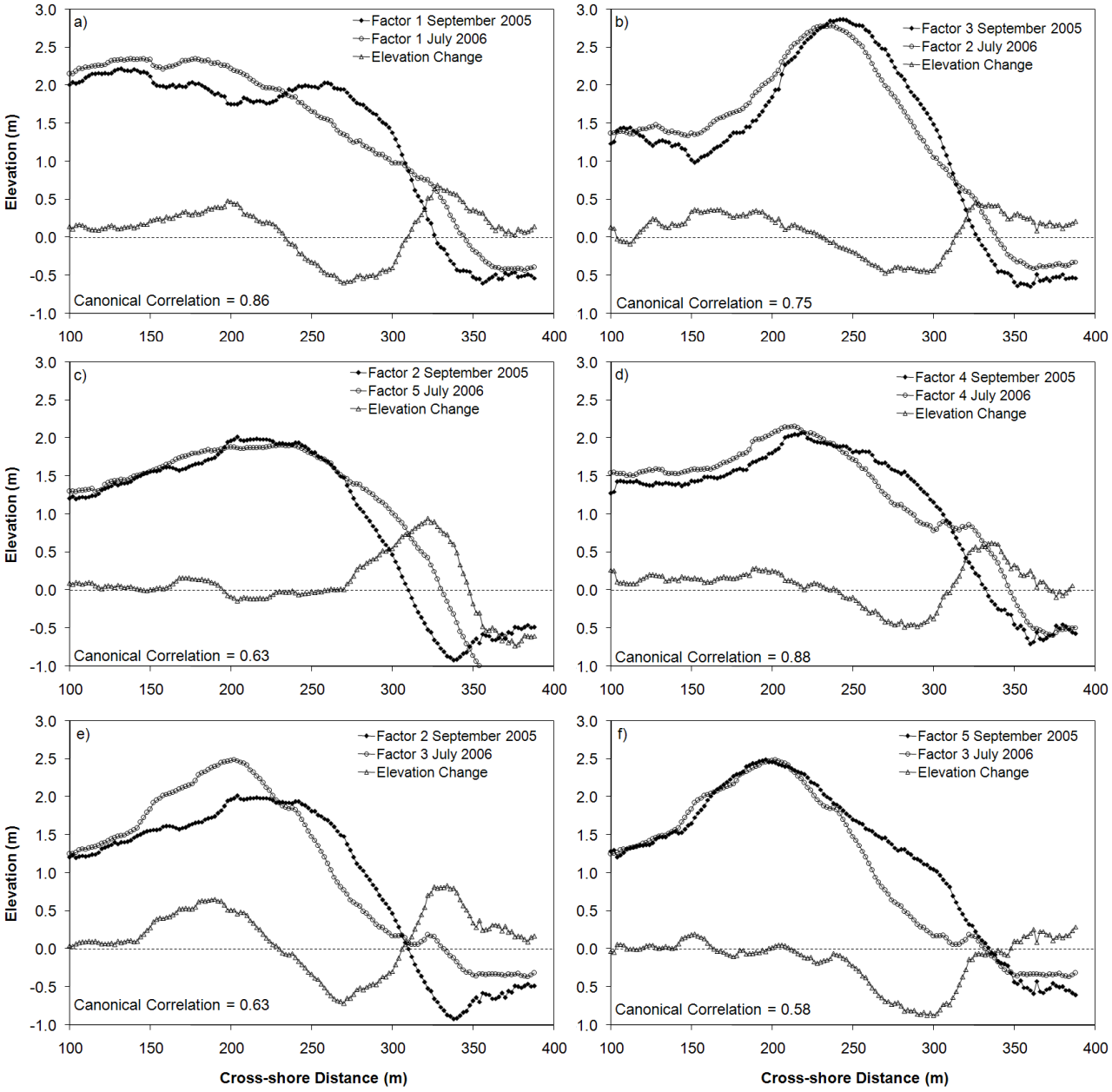

a)
Factor 1 September 2005
Factor 1 July 2006
Elevation Change
Canonical Correlation = 0.86
b)
Factor 3 September 2005
Factor 2 July 2006
Elevation Change
Canonical Correlation = 0.75
c)
Factor 2 September 2005
Factor 5 July 2006
Elevation Change
Canonical Correlation = 0.63
d)
Factor 4 September 2005
Factor 4 July 2006
Elevation Change
Canonical Correlation = 0.88
e)
Factor 2 September 2005
Factor 3 July 2006
Elevation Change
Canonical Correlation = 0.63
f)
Factor 5 September 2005
Factor 3 July 2006
Elevation Change
Canonical Correlation = 0.58
Elevation (m)
Cross-shore Distance (m)

Figure 41.

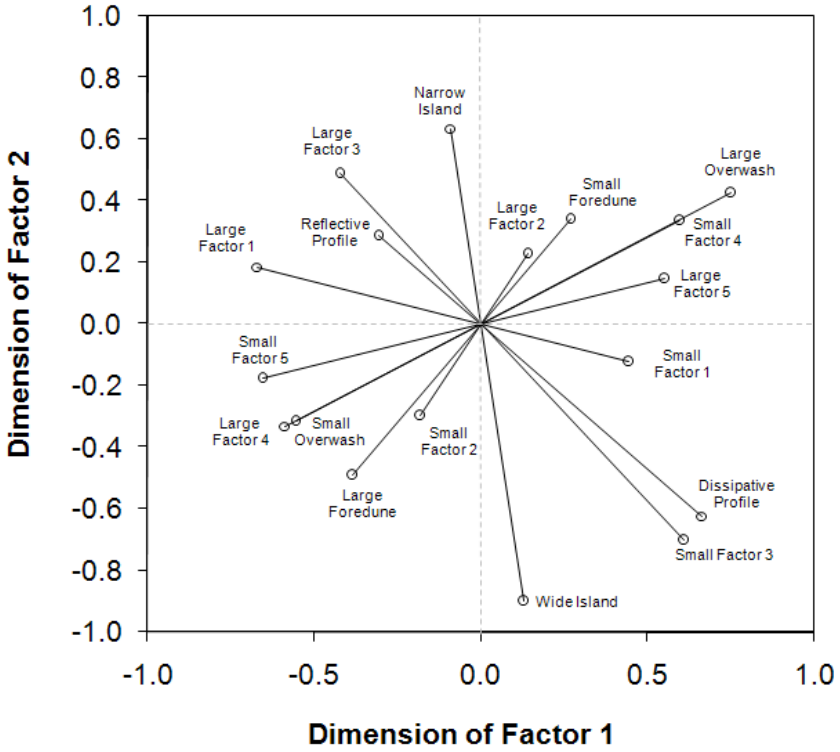

Dimension of Factor 2
Dimension of Factor 1
1.0
0.8
0.6
0.4
0.2
0.0
-0.2
-0.4
-0.6
-0.8
-1.0
-1.0
-0.5
0.0
0.5
1.0
Narrow Island
Large Factor 3
Large Overwash
Small Foredune
Large Factor 2
Small Factor 4
Reflective Profile
Large Factor 1
Large Factor 5
Small Factor 5
Small Factor 1
Large Factor 4
Small Overwash
Small Factor 2
Dissipative Profile
Large Foredune
Small Factor 3
Wide Island

Figure 42.

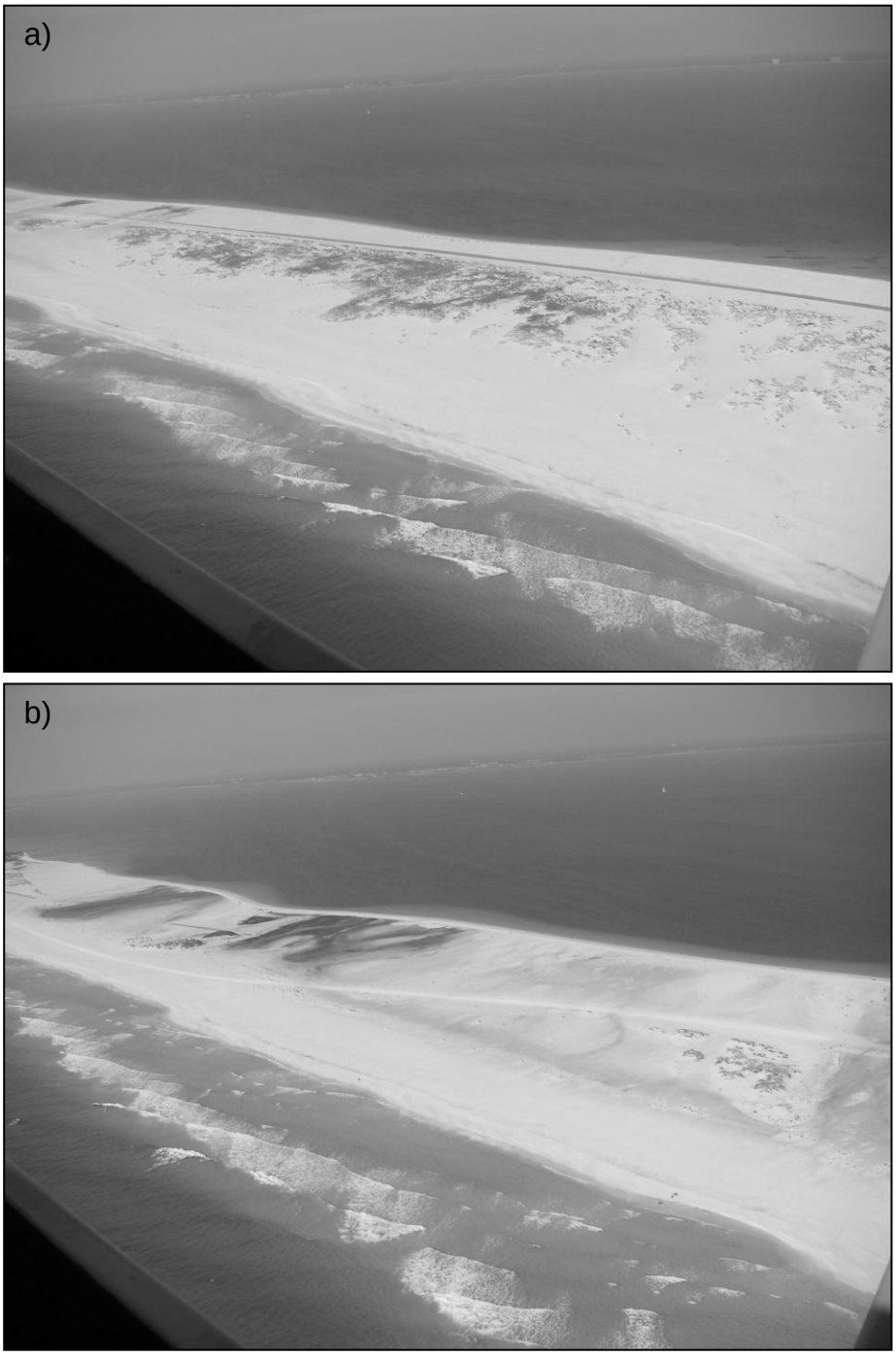


Figure 43.



Figure 44.

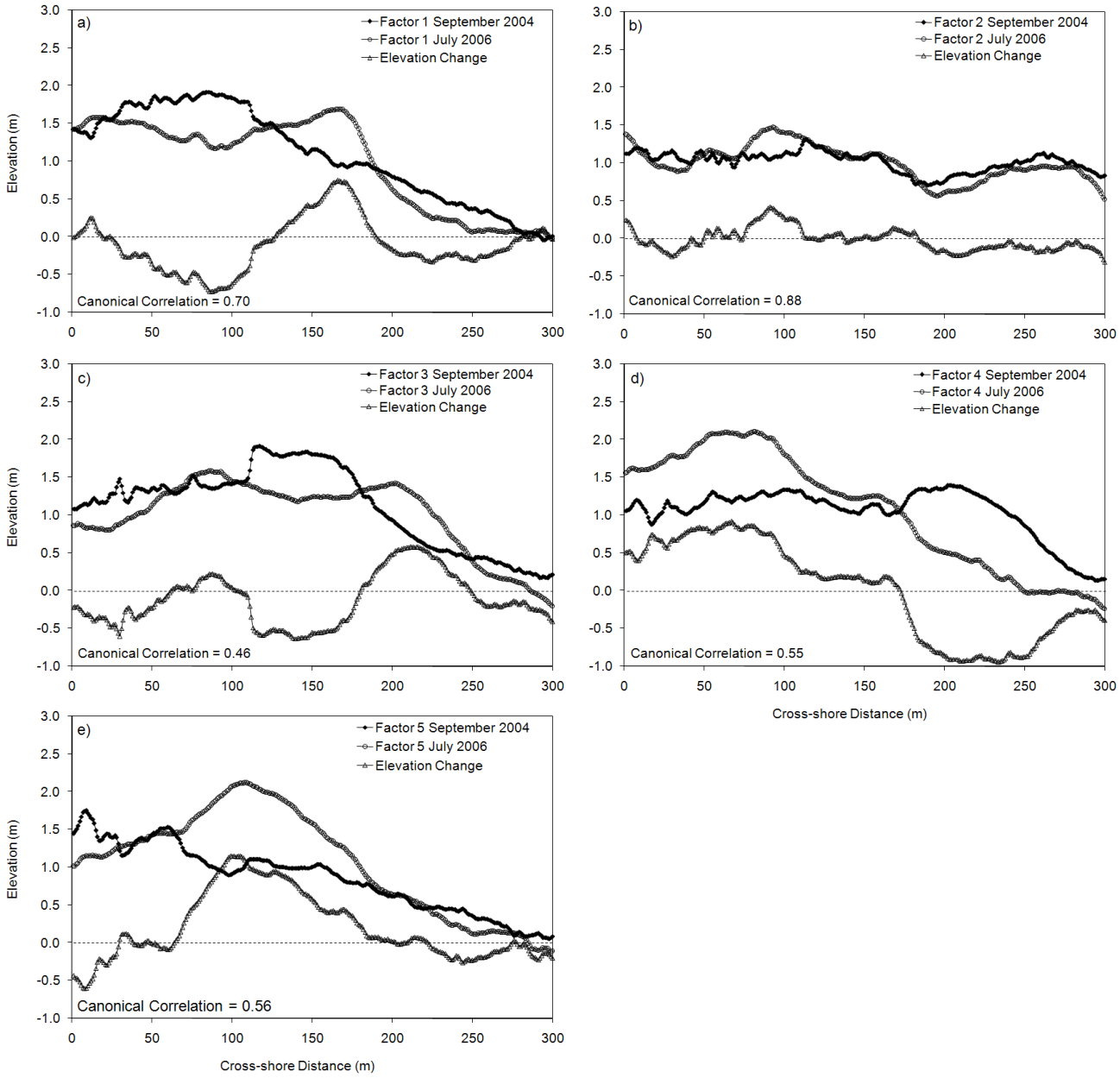

a)
Factor 1 September 2004
Factor 1 July 2006
Elevation Change
Canonical Correlation = 0.70
b)
Factor 2 September 2004
Factor 2 July 2006
Elevation Change
Canonical Correlation = 0.88
c)
Factor 3 September 2004
Factor 3 July 2006
Elevation Change
Canonical Correlation = 0.46
d)
Factor 4 September 2004
Factor 4 July 2006
Elevation Change
Canonical Correlation = 0.55
e)
Factor 5 September 2004
Factor 5 July 2006
Elevation Change
Canonical Correlation = 0.56
Elevation (m)
Cross-shore Distance (m)

Figure 45.

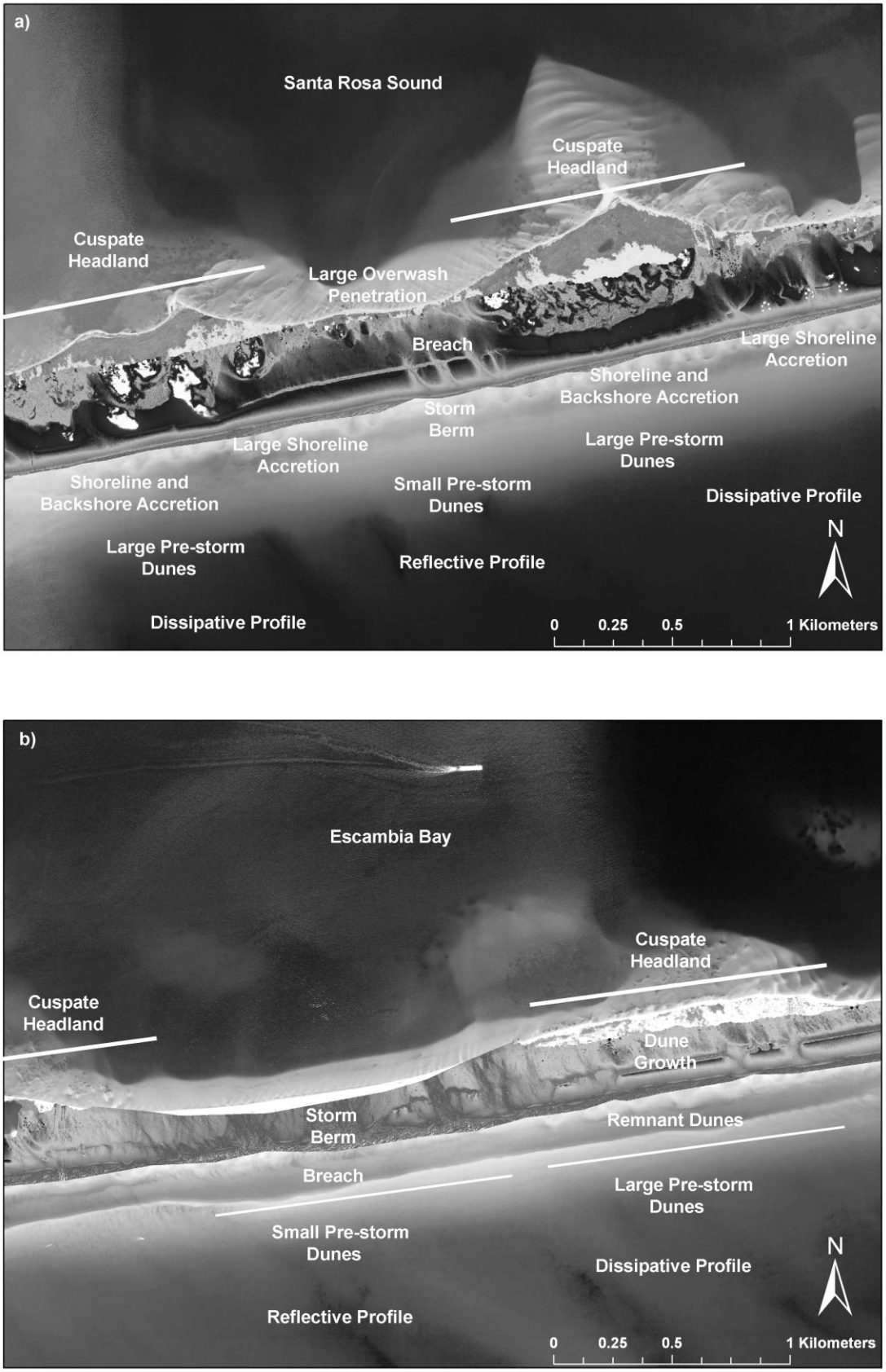

a)
Santa Rosa Sound
Cuspate Headland
Cuspate Headland
Large Overwash Penetration
Breach
Large Shoreline Accretion
Shoreline and Backshore Accretion
Storm Berm
Large Pre-storm Dunes
Large Shoreline Accretion
Shoreline and Backshore Accretion
Small Pre-storm Dunes
Dissipative Profile
N
Large Pre-storm Dunes
Reflective Profile
Dissipative Profile
0 0.25 0.5 1 Kilometers
b)
Escambia Bay
Cuspate Headland
Cuspate Headland
Dune Growth
Storm Berm
Remnant Dunes
Breach
Large Pre-storm Dunes
Small Pre-storm Dunes
Dissipative Profile
N
Reflective Profile
0 0.25 0.5 1 Kilometers

Figure 46.

CHAPTER 4

Geomorphological Controls on Road Damage during Hurricanes Ivan and Dennis

Chris Houser

Department of Environmental Studies
University of West Florida
11000 University Parkway
Pensacola, Florida
32514

ABSTRACT

County Road 399 along Santa Rosa Island in Northwest Florida was largely impassable following Hurricanes Ivan and Dennis, but the damage was highly variable alongshore, ranging from areas with little or no damage to areas where the road was completely breached. Damage was categorized and correspondence analysis was used to examine how these levels of damage were affected by the proximity of the road to the shoreline, the elevation and width of the island and the offshore bathymetry. The pre-storm elevation and offshore bathymetry exhibit a correspondence with island width but with an opposite relationship; a gently sloping shoreface does not correspond with a large pre-storm elevation. In this respect, the variables can have either a competing or a compounding impact on the road depending on the local combination. Sections of road with little to no damage were located close to the shoreline and associated with an above average island elevation (large foredunes or berm). These areas tended to be located in wider sections of the island and equally distributed between areas with a steep and a gentle offshore profile. During Hurricane Ivan, sections of the road that sustained major damage or were completely destroyed tended to be in narrow sections of the island where the offshore profile was steep, while half-damage was associated with a gently sloping bathymetry. In contrast, major damage during Hurricane Dennis occurred in areas where the road was located in the backbarrier where the pre-storm elevation of the island was relatively low and half-damage occurred in the narrow sections of the island where the offshore bathymetry was steep. Based on the observed relationships it is concluded that damage to the road is forced by the island geomorphology and that area where the road received extensive damage will continue to be areas of concern.

Keywords: Hurricane impact, barrier island, road damage, Hurricane Ivan, Hurricane Dennis, Gulf Islands National Seashore

INTRODUCTION

Human activity has become an integral part of barrier island landscapes, particularly in the United States where development often includes infrastructure to support recreation and navigation. Large-scale tourism and development along the barrier islands began in the second half of the nineteenth century (MEYER-ARENDT, 1990; EHLERS and KUNZ, 1993; NORDSTROM, 2000). Much of this expansion was associated with the expanded use of private vehicles (MEYER-ARENDT, 1991; NORDSTROM, 1994, 2000), and the roads have in turn become important links for commuting, shared community services and storm evacuation. Stabilization through hard structures and beach/dune nourishment is often used to defend the transportation infrastructure against changes to the island morphology, particularly during tropical storms and hurricanes. Despite these protective measures, elevated roads can be damaged during extreme storms, because the road acts as a weir during overwash (DOUGLASS et al., 2004; CHANEY, 2007). A hydraulic jump develops as the water flowing over the road hits the shoulder, scouring

the shoulder and undermining the road (CHANEY, 2007) similar to a fluvial knickpoint or what is seen at the base of a spillway (CHOW, 1959). The placement of a road can further alter the response of the island through direct alteration or removal of landforms and vegetation, disruption of seed dispersal and the transport of sediment (NORDSTROM, 2000), and by providing a pathway for overwash (HALL and HALSEY, 1991; FLETCHER et al., 1995). In this respect, the road can reinforce or even amplify its own vulnerability and that of the barrier island to storms.

In general, the impact of an extreme storm on a barrier island (and any roads on it) depends on the elevation of the storm surge relative to the vertical geometry of the coast, which in turn depends on the extent and height of foredune development (THIELER and YOUNG, 1991; SALLENGER, 2000) and the presence of secondary dunes (HOUSER *et al.*, 2007). This balance between island and storm surge elevation not only depends on the characteristics of the storm and its tracking, but also on the sequence of past storm events and the morphological response to those storms (MORTON, 2002). The vulnerability of a barrier island to subsequent overwash and inundation depends on the recovery of the foredune (*cf.* MORTON and PAINE, 1985). The impact also depends on the alongshore variability in dune height, which on Cape Hatteras can vary by ~8 m over scales of kilometers to tens of kilometers (ELKO et al., 2002). While dunes will obstruct overwash penetration, surge water may be forced into the intervening areas of low elevation, which can become washover conduits. WETZELL (2003) showed that the alongshore variation in storm impact was consistent with the variation in dune height and the Storm Impact Scale of SALLENGER (2000). Ultimately, the morphology of the barrier island and the response to extreme storms can be directed by the geologic framework (BELKNAP and KRAFT, 1985; RIGGS, et al., 1992; SNYDER, 1993; RIGGS et al., 1995; RIGGS et al., 1996; SCHWAB et al., 2000), which is commonly expressed through alongshore variations in the offshore bathymetry (MCNINCH and LEUTTICH, 2000; COOPER and NAVIS, 2004; MCNINCH, 2004; SCHUPP et al., 2007). Areas with steep (steep offshore) offshore profiles concentrate storm energy through wave refraction and reduced attenuation, in some cases leading to erosional hotspots (SCHUPP et al., 2007). In contrast, areas with a more gently sloped (or gently sloped) profile attenuate wave energy and provide more protection to the shoreline.

Post-storm rebuilding following an extreme storm often includes redesign and relocation without a proper understanding of how the island geomorphology and geology controlled the vulnerability of the road. County Road 399 between Navarre and Pensacola Beach in Northwest

Florida (Figure 1) was heavily damaged during Hurricane Ivan and again during Hurricane Dennis despite redesign and realignment following Hurricanes Opal and Ivan respectively. CHANEY (2007) provides a post-storm survey of road damage along Perdido Key (west of the present study) following Tropical Storm Isidore (2002), and argues that the collapse of the roadbed was caused overwash scouring where there were gaps in the dunes. In the present study, an assessment of road damage is completed immediately following Hurricanes Ivan and Dennis along County Road 399. The level of road damage is categorized using both aerial photographs and a ground-based assessment and the variation in damage along the length of the road is statistically related to the proximity of the road to the shoreline, the offshore bathymetry, and island width and elevation. The results of this study will demonstrate how damage to infrastructure on barrier islands is controlled (to a greater or lesser extent) by the island geomorphology, which will in turn can be used in future decisions on redesign and realignment.

STUDY SITE

The Florida district of Gulf Islands National Seashore is located close to highly populated areas of Florida, Alabama and Georgia (Figure 1) and receives approximately four million visitors per year. Access to this section of the park is by vehicle along County Road 399. Numerous visitor support facilities have been constructed, including campgrounds, restrooms, day-use structures, roads and parking lots, stores, and maintenance facilities to encourage and support this use and the associated tourism benefits. This development represents a significant capital outlay by the National Park Service and future development depends on an understanding of vulnerability to storm damage. In the past decade, the park infrastructure and County Road 399 have been repeatedly damaged by storm events, most recently during Hurricanes Ivan, Dennis and Katrina, and Tropical Storms Arlene and Cindy. The National Park Service and Florida Department of Transportation determined that additional measures should be investigated to protect County Road 399 so that damage to the roadway could be minimized from future storm events. Ground observations suggest that recent damage to the road is similar in degree and extent to past storms (*e.g.* Hurricane Opal, 1995), suggesting localized controls on road damage. As discussed in DOUGLASS et al. (2004), the road had been relocated to its present alignment after Hurricane Opal (1995) and only received minor damage during Hurricanes Georges (1998) and Tropical Storm Isadore (2002). Along a similar road on Perdido Key,

CHANEY (2007) noted that damage was concentrated along the northern edge of the road following Tropical Storm Isidore (2002).

County Road 399 was heavily damaged during Hurricane Ivan, a Category-3 hurricane that came ashore near Gulf Shores, Alabama, on September 16, 2004. Santa Rosa Island was within the Northeast quadrant of the storm and subject to surge heights reaching ~5 m. As a result, the area suffered significant sediment loss (>200 m^3 m^{-1}; HOUSER et al., 2007) and widespread overwash and breaching. Overwash penetration in the area was reduced and in some cases overwash was inhibited as the height of the foredune increased. However, overwash penetration was also observed to increase where lateral erosion occurred as a result of alongshore variability in dune height. The morphological response was also affected by the presence of secondary dunes. In the 10 months following the Hurricane Ivan, the beachface showed little recovery and no significant growth in island geometry (through dune growth) was observed before Tropical Storm Arlene (June, 2005), Tropical Storm Cindy (July, 2005), Hurricane Dennis (July, 2005) and Hurricane Katrina (August, 2005). Hurricane Dennis made landfall just west of the study site as a Category 3 storm, with a storm surge of ~2 m above normal tide levels. While the storm surge was smaller than the surge observed during Hurricane Ivan, the now reduced elevation of the island made it vulnerable to widespread overwash and erosion.

METHODOLOGY

Road Assessment

Damage to the road was examined using a combination of oblique aerial photographs and ground-based assessments, and was categorized as either no-damage, 1/4 damage, 1/2 damage and full damage (Table 1). Assessments were made at a regular alongshore (not road distance) spacing of 175 m (Figure 1b); these transects were also used for the geomorphological characterization of island elevation and offshore bathymetry discussed below. At each transect, the distance between the road and the shoreline (at mean sea level) and the width of the island were also measured.

Offshore Bathymetry

The relationships between offshore bathymetry and storm impact (including shoreline erosion) are well established in general (MCNINCH and LEUTTICH, 2000; COOPER and NAVIS,

2004; MCNINCH, 2004; SCHUPP et al., 2007), but have not been described along the Central Gulf Coast. Within the study area, STONE (1984) describes a series of offshore sinusoidal ridges and troughs oriented northwest-southeast, in alignment with the De Soto submarine canyon further to the east. While these features were also described by HYNE and GOODELL (1967), little is known about how these shore-transverse ridges developed. It is reasonable to expect that these bathymetric features affect the attenuation of wave energy incident to the coast and can lead to areas of high energy where the offshore profile is steep and low energy where the offshore profile is gentle, although a larger set-up is possible on more gently sloped profiles.

To characterize these ridges and examine how they may affect damage to the road, the offshore bathymetry was examined along each transect and analyzed using empirical orthogonal function (EOF). This form of analysis is commonly used to reduce variance within a dataset, and in the present study is used to reduce the topographic data into common (or characteristic) forms. EOF analysis is similar to principal component analysis, except that the variability structure is examined through space rather than over time (AUBREY, 1979). It is a powerful tool since it can identify a limited number of statistically significant descriptions of the data that can explain most of the variance in the data. In the present study, a data matrix X containing offshore bathymetry (rows) from 49 transects (columns) is represented through a matrix involving the eigenvalues (L) and the spatial EOF's (A):

$$X = ELA^T \quad [1]$$

The variance associated with the eigenmodes, which are the orthonormal column vectors in E and A, are given by the eigenvalue L. The EOF's are obtained by solving an eigenvalue problem involving the correlation matrix based on X. Since the explained variance typically decreases with the mode number, only a limited number of modes are required to explain most of the variance in the data. In this respect, EOFs can be used as a data reduction technique or a method to separate 'signal' and 'noise'. A more detailed description of EOF analysis is provided in studies by WIJNBERG (1995), LARSON et al. (2001), and HOUSER and GREENWOOD (2005).

Island Elevation

Topographic relief on a barrier island is largely a reflection of the height and extent of foredune development. The maximum elevation of the island (not including secondary dunes)

was calculated along each transect using LiDAR data collected by the USGS (2006) immediately before and after Hurricanes Ivan and Dennis. LiDAR (Light Detection and Ranging) is an increasingly used mapping technology that provides spatially dense and accurate topographic data (see IRISH and WHITE, 1998; WEHR and LOHR, 1999; WOOLARD and COLBY, 2002; SALLENGER et al., 2004; ZHANG et al., 2005). An overview of the changes in island elevation during Hurricane Ivan are presented in HOUSER et al. (*in press*) for the study site.

Correspondence Analysis

Correspondence analysis was used to identify how the different categories of damage (no damage, ¼ damage, ½ damage and full damage) were related to the proximity of the road and the geomorphological controls of offshore bathymetry (gentle versus steep offshore slope), island width (narrow and wide) and island elevation (high and low). Correspondence analysis is an exploratory technique used to analyze two-way or multi-way tables containing some level of correspondence between the row and column categories (HIRSCHFEL, 1935). The method is used to lower dimensionality in order to identify a smaller number of uncorrelated variates containing most of the variance of the raw data (HILL, 1974). In contrast to Principal Component Analysis, correspondence analysis uses Chi-square distances (rather than Euclidian distance) to arrange the cateogorical variables, relative to an axis in multidimensional space, according to their similarity (or association) to each other (CLAUSEN, 1998). The closer the angle is to 0° (positive correlation) or 180° (negative correlation), the stronger the relationship. Angles near 90° and 270° show no relationship between variables. All variables were characterized based on whether the values were greater or less than the average for all 49 transects.

RESULTS

Representative photographs of the different levels of damage are provided in Figure 2 and the percent length of road within each category of road damage is provided in Table 1. These levels of damage were not continuous but varied considerably alongshore, with areas of little to no damage near to areas where there was complete loss of the road and the island was breached (Figure 3). Where at least part of a lane was damaged, road material was deposited on the overwash fans, creating a debris field of gravel, shells and ashphalt (Figure 4). Consistent with the observations of Chaney (2007) from Hurricane Opal (1995) and Tropical Storm Isidore

(2002), only the northern edge of the road sustained significant damage. The roadbed material was scoured out from beneath the road surface causing the collapse of the road and in some cases the rafting of large sections of asphalt. Chaney (2007) argues that this form of damage is caused by a knickpoint effect commonly described in the fluvial literature. While this explanation remains untested and Bush et al. (1996) suggest that the scouring is associated with the ebb phase of the storm surge, the focus of the present study is not the mechanisms responsible for the damage, but rather on why certain areas were more heavily damaged than others.

Hurricane Ivan

The results of the EOF analysis suggest that the 49 bathymetry transects can be reduced to 2 characteristic profiles (modes) that account for 67% of the total variance. The first eigenmode explains 54% of the total variance and is characterized by a gently sloped offshore profile. The second eigenmode explains 7% of the total variance and is characterized by a steep offshore (steep) offshore profile. A large ratio of E1 to E2 is indicative of a gently sloped offshore profile, which tends to be associated with the widest parts of the island (Figure 5b). A similar pattern is observed in the alongshore variation in foredune height (not analyzed using EOF analysis). The foredune height ranged from 6.5 m at the cuspate headlands to 2.4 m in the narrowest sections of the island (Figure 5c). Correspondence analysis between these variables shows an alongshore correspondence around the primary factor of island width (Figure 6). For both storms, wider areas of the island tend to be associated with a gently sloped offshore profile and a larger than average pre-storm elevation, whereas narrow sections of the island tend to be associated with a small pre-storm elevation and a steep offshore profile. However, a small pre-storm elevation does not correspond with a steep offshore profile, nor does a large pre-storm elevation correspond to a gently sloped offshore profile. This suggests that these variables are spatially lagged. Smaller dunes are found west of the headlands despite the persistence of the gently sloped profile, and larger dunes are found east of the headlands despite the steep offshore profile.

The proximity of the road to the shoreline exhibits a similar alongshore pattern to the island width. Following Hurricane Opal, the road was placed near the back of the island between cuspate headlands and closer to the shoreline at the headlands (DOUGLASS et al., 2004). The road was positioned near the back of the island between headlands to allow for beach access points

where dunes were largely absent or poorly developed, and close to the shoreline at the headlands to avoid the secondary dunes that are common in these areas. A similar variation in is observed in the level of road damage during Hurricane Ivan (Figure 5e). The road was not damaged or received minor damage (1/4) where the road was near the back of the island or where the island is relatively wide. Comparison of Figure 5b and 5e, suggests that the road was completely destroyed in areas where the offshore profile was relatively steep (small E1/E2 ratio).

Correspondence analysis provides an objective means to examine the (above) relationships among the categories of road damage, the proximity of the road (close or far), offshore bathymetry (gentle versus steep offshore slope), island width (narrow and wide) and island elevation (high and low). The correspondence plot (Figure 7a) provides a graphical summary of the results and shows how the variables are grouped between the 2 statistically significant dimensions (factors). The graph shows a principal axis for Factor 1 based largely on the pre-storm elevation and equally distributed between areas with a steep and a gentle offshore slope. The difference between the small and large pre-storm elevation is related to the proximity of the road, island width and minor levels of road damage (1/4 and no damage). The road tended to undamaged in areas where the foredunes were tall and where the road was relatively close to the shoreline. The road experienced 1/4 damage in areas characterized by relatively small foredunes and where the road was near the back of the island. The larger foredunes and no damage tended to be found near the widest sections of the beach while the smaller foredunes and 1/4 damage were observed where the island was relatively narrow.

The principal axis for Factor 2 is a description of the offshore bathymetry and is related to the higher levels of road damage. The road tended to be completely destroyed in areas where the offshore profile was steep, but was only 1/2 damaged in areas where the offshore profile was gently sloped. Major damage to the road was equally distributed between areas with small and large pre-storm elevation, although complete loss of the road was more closely related to areas with a large pre-storm elevation than small. The post-storm elevation of these areas is close to the watertable (high moisture content) and the surface is characterized by asphalt and a heavy lag of shell and gravel (Figure 4). The gravel lag is primarily limestone and most likely originated from the roadbed. Consistent with field observations, this suggests that complete loss of the road occurred on the west side of the cuspate headlands adjacent to the area with larger dunes, which

experienced considerable lateral erosion (Houser et al., 2007). Areas that experienced 1/2 damage were east of the areas characterized by a smaller than average pre-storm elevation.

These variables can have either a competing or compounding impact on the road depending on their local combination. To characterize the road damage as a combination of factors, the alongshore variation in factor coordinates is provided in Figure 8a. The most continuous road damage occurred between transects 39 and 44 (875 to 1925 m alongshore), where a steep offshore profile was combined with a narrow section of the island and a small pre-storm elevation. Between transects 35 and 26 (2450 to 4025 m alongshore) the road exhibited the least amount of damage. This section of the island is relatively wide (middle of a cuspate foreland) and has a gently sloped profile and tall foredunes. In this respect, the most vulnerable section of the island is between the cuspate forelands and the least vulnerable is at the headlands. To the west of the headlands, where there are small dunes and a gently sloped profile, the road showed more damage than to the east of the headlands where there were larger dunes and a steep offshore profile.

Hurricane Dennis

With a few exceptions, the foredunes along this section of Santa Rosa Island were eroded during Hurricane Ivan, leaving a maximum island elevation of 4.3 m where the dunes had been relatively large and continuous alongshore before Hurricane Ivan. However, the average island elevation was 2.2 m (Figure 9a) and the pre-Ivan foredune had been replaced by a berm that formed within a couple of weeks of Hurricane Ivan. The breaches and complete loss of the road observed during Hurricane Ivan are coincident with the pre-storm sections of the island where the dune crest elevation is at a minimum and close to the average surge elevation. These breaches were reactivated in 2005 during Tropical Storms Arlene and Cindy, and Hurricanes Dennis and Katrina, causing damage to the roadway at similar locations to that observed during Hurricane Ivan (Figure 9c and Figure 8). It is interesting to note the similarity in degree and extent of damage in spite of the road being relocated following Hurricane Ivan and previously following Hurricane Opal (DOUGLASS et al., 2004).

The correspondence plot for the roadway damage observed during Hurricane Dennis is provided in Figure 7b and the alongshore variation in factor coordinates is provided in Figure 8b. Areas with no roadway damage were observed in close proximity to the shoreline and where the

pre-Dennis (post-Ivan) island elevation was below average. These areas were equally distributed between areas of wide and narrow island width, and areas with a steep and a gentle offshore profile. In contrast, areas with full roadway damage were in areas where the road was relatively far from the shoreline and where the island elevation was smaller than average. Similar to the results for Hurricane Ivan, the principal axis for Factor 1 suggests that island elevation is the primary control on road damage, and that a larger distance between the roadway and the shoreline does not prevent damage.

Areas with 1/4 damage were relatively far from the shoreline and tended to be associated with a gently sloped offshore profile. These areas were equally represented in wide and narrow sections of the island. Areas with 1/2 damage are associated with narrow sections of the island where the offshore profile was relatively steep and where the pre-storm elevation was small. This level of damage was equally represented in areas where the road was close and far from the beach. Unlike Hurricane Ivan, all levels of roadway damage during Hurricane Dennis are related to Factor 1 to varying degrees. Damage during this storm is largely controlled by pre-storm island elevation, with a relatively minor contribution from island width and offshore bathymetry.

DISCUSSION

County Road 399 along Santa Rosa Island in Northwest Florida was heavily damaged during Hurricanes Ivan and Dennis, limiting the sharing of emergency services between Pensacola Beach and Navarre, and reducing access to the Gulf Islands National Seashore. Using both aerial and ground-based assessments it was found that damage to the road was highly variable alongshore, but seemingly coherent with the width of the island. Through correspondence analysis it was found that damage to the road during both Hurricanes was controlled by the pre-storm elevation of the island, the width of the island and offshore bathymetry. Depending on the specific combination of variables at a location, they could either have a competing or a compounding impact on damage to the road. Sections of the road that were completely destroyed during Hurricane Ivan were in areas where there was a relatively steep offshore profile (Figure 10). This may allow for larger waves to reach the shore, which in turn allows for greater wave set-up (see McNinch, 2004; Schupp et al., 2007). These areas also tended to be found in areas where the island was narrow (between cuspate forelands), leading to steeper overwash gradients and stronger overwash currents (Morton, 2002). Despite a more

gently sloped offshore profile to the east of these sites, damage was still significant (~1/2 or road lost) due to the low pre-storm elevation of the island. In contrast, areas west of the breach sites had a steep offshore profile, but had larger dunes that minimized damage to the road despite the close proximity of the road to the shoreline. Not only would the pre-Ivan dunes have acted as a barrier to the surge for a large part of the storm, overwash would have buried the road and afforded protection once the dunes were breached.

The offshore bathymetry did not play as important of a role in controlling road damage during Hurricane Dennis as it did during Hurricane Ivan. Rather, the level of road damage was largely controlled by the pre-storm elevation of the island (the principal axis of Factor 1), which in turn was a result of Hurricane Ivan. Overwash depths and currents are weaker in areas with higher elevation, while overwash can become concentrated within areas of lower elevation (MORTON, 2002). DOUGLASS et al. (2004) suggest that a large part of the damage in the absence of sufficient island elevation is caused by water flow across the road. Similar to CHANEY (2007), the authors further suggest that this creates a "weir-like" flow that scours the north side of the road. Where dunes provide a barrier to overwash currents, the road may not be damaged during a storm. While the dunes were eventually breached during Hurricane Ivan, they would have remained above the elevation of the road, such that the overwash sediments would have covered and protected the road. Based on the results of the present study, these areas tend to be associated with a gently sloped offshore profile and the widest parts of the island, both of which provide additional protection to the road. The impact of the higher surge was tempered to the east of the headlands where the steep offshore profile was associated with relatively large dunes. To the west of the headlands, the gently sloped profile was associated with small dunes that provided little to no protection. As a result there was more road damage than expected and the north side of the road and shoulder were scoured, similar to the detailed observations of CHANEY (2007).

Due to the importance of County Road 399 to emergency services and access to the Gulf Islands National Seashore, it is likely that the road and associated infrastructure (parking lots, pavilions and facilities) will be rebuilt. In general, damage to infrastructure leads to considerations of redesign and realignment (WATANABE and HORIKAWA, 1983; NORDSTROM and JACKSON, 1995), but it many cases it also leads to increased levels of development (MEYER-ARENDT, 1985; 1990; 1991), without consideration of the vulnerability that lead to damage

during the first storm. For example, the road was relocated following Hurricanes Opal (1995) and Ivan (2004) but this did not significantly affect the level of road damage in subsequent storms (see CHANEY, 2007). Initially, the road was positioned near the shoreface in the widest parts of the island have a well-developed secondary dune system, the road had to be positioned behind the foredune and close to the shoreface in order to avoid the alteration or removal of the dunes. Where the foredunes were poorly developed and the secondary dunes were not present, the road could be positioned near the back of the island to allow for day-use structures and parking lots. Despite the road being located at the back of the island, it was still damaged during Hurricanes Ivan and Dennis respectively, because there were no protected dunes in these areas or the offshore profile made the island more vulnerable to storm surge.

The placement of the road and associated infrastructure (parking lots, etc) can reinforce or even amplify its own vulnerability through the loss of island elevation, which in turn provides a pathway for overwash (HALL and HALSEY, 1991; FLETCHER et al., 1995). Following both storms, areas where the road was completely destroyed were close to the watertable and characterized by a heavy lag of shell and gravel (limestone) from the road bed. The presence of a gravel lag and pieces of asphalt in the sediment are not only conspicuous features on the landscape (GUILCHER, 1985), but also lead to a supply-limited system in which dune recovery is slow (HOUSER et al., *in press*). In this respect, the historic presence of the road can ultimately lead to smaller dunes, which will reinforce the vulnerability of these areas to overwash and damage during subsequent storms (HOSIER and CLEARY, 1977; MORTON et al., 1994). Considering the importance of pre-storm island elevation in limiting road damage, it is reasonable to expect that the section of the road that were heavily damaged during Hurricanes Ivan and Dennis will continue to be areas of concern.

CONCLUSIONS

County Road 399 in Northwest Florida was heavily damaged during Hurricanes Ivan and Dennis, but the level of damage was highly variable alongshore ranging from complete loss of the road to minor shoulder damage. Through aerial and ground-based assessments the level of damage was found to be related to the height of the foredune, the width of the island and the offshore bathymetry. Areas with little to no road damage were observed along the widest parts of the island where the foredunes and secondary dunes were well-developed and the offshore

bathymetry was gently sloped. Major damage to the road was observed where the foredune system was not present or poorly developed, which was typically associated with a narrow island and a steep offshore profile. The results suggest that the vulnerability of the road (and the barrier island in general) is controlled by the island geomorphology and that the redesign and to a lesser extent realignment of the road needs to be based on this control.

ACKNOWLEDGEMENTS

This study was partly supported by a grant from the National Park Service (P5320060026). LiDAR survey transects were prepared by Stu Hamilton, Amber Bloechle and John Oravetz of the University of West Florida Geodata Center. Field assistance was provided by Klaus Meyer-Arendt (UWF), Chasidy Hobbs and Riley Hoggard (National Park Service).

LITERATURE CITED

AUBREY, D.G., 1979. Seasonal patterns of onshore/offshore sediment movement. *Journal of Geophysical Research*, 84, 6347-6354.

BELKNAP, D.F., and KRAT, J.C., 1985. Influence of antecedence geology on stratigraphic preservation potential and evolution of Delaware's barrier systems. *Marine Geology*, 63, 235-262.

BUSH, D.M., PILKEY, O.H., and NEAL, W.J., 1996. *Living by the Rules of the Sea.* Durham, North Carolina: Duke University Press, 179p.

CHANEY, P.L., 2007. Storm Overwash and the Knickpoint Effect: Northwest Florida Coast, USA. Journal of Coastal Research, 23, 247-254.

CLAUSAN, S.E., 1998. Applied correspondence analysis: an introduction. *Sage University Papers Series on Quantitative Applications in the Social Sciences*, 07-121. Thousand Oaks, California: Sage.

COOPER, J.A.G. and NAVAS, F., 2004. Natural bathymetry change as a control on century-scale shoreline behavior. *Geology*, 32, 513-516.

DOUGLASS, S. L., HUGHES, S., ROGERS , S. and CHEN, Q., 2004. *The impact of Hurricane Ivan to the coastal roads in Florida and Alabama : A preliminary report*. Coastal Transportation Engineering Research and Education Center , University of South Alabama.

EHLERS, J., and KUNZ, J., 1993. Morphology of the Wadden Sea: natural processes and human interference. In Hillen, R. and H.J. Verhagen editors, *Coastlines of the Southern North Sea.* New York: American Society of Civil Engineers, 65-84.

ELKO, N.A., SALLENGER, A.H., GUY, K., and MORGAN, K.L.M., 2002. Barrier island elevations relevant to potential storm impacts; 2, South Atlantic: U.S. Geological Survey, Open-File Report 2002-288, 1 folded sheet.

FLETCHER, C.H., RICHMOND, B.M., BARNES, G.M., and SCHROEDER, T.A., 1995. Marine flooding on the coast of Kaua'I during Hurricane Iniki: hindcasting inundation components and delineating washover. *Journal of Coastal Research*, 11, 188-204.

GUILCHER, A., 1985. Problems of shore and foreshore management exemplified by the French caosts. In *Coastal Planning: Realities and Perspectives*, Genoa: Comune di Genova, 91-124.

HALL, M.J. and HALSEY, S.D., 1991. Comparison of overwash penetration from Hurricane Hugo and pre-storm erosion rates for Myrtle Beach and North Myrtle Beach, South Carolina, U.S.A. *Journal of Coastal Research*, SI8, 229-235.

HILL, M.O., 1974. Corresdpondence Analysis: A Neglected Multivariate Method. *Applied Statistics*, 23, 340-354.

HIRSCHFEL, H.O., 1935. A connection between correlation and contingency. *Proceedings of the Cambridge Philosophical Society*, 31, 520-524.

HOSIER, P.E. and CLEARY, W.J., 1977. Cyclic geomorphic patterns of washover on a barrier island in southeastern North Carolina. *Environmental Geology*, 2, 23-31.

HOUSER, C., HAMILTON, S., ORAVETZ, J. and MEYER-ARENDT, K., 2007. EOF Analysis of Morphological Change during Hurricane Ivan. *Coastal Sediments 2007*.

HOUSER, C., and GREENWOOD, B., 2005. Profile response of a lacustrine multiple-barred nearshore to a sequence of storm events. *Geomorphology*, 69, 118-137.

HYNE, N.J. and GOODELL, H.G., 1967. Origin of the sediments and submarine geomorphology of the inner continental shelf off Choctawhatchee Bay, Florida. Marine Geology, 5, 299-313.

IRISH, J.L. and WHITE, T.E., 1998. Coastal engineering applications of high-resolution lidar bathymetry. *Coastal Engineering*, 35, 47-71.

LARSON, M., CAPOBIANCO, M. and HANSON, H., 2000. Relationship between beach profiles and waves at Duck, North Carolina, determined by canonical correlation analysis. Marine Geology, 163, 275-288.

MEYER-ARENDT, K.J., 1985. The Grand Isle, Louisiana resort cycle. *Annals of Tourism Research*, 12, 449-465.

MEYER-ARENDT, K.J., 1990. Recreational business districts in Gulf of Mexico seaside resorts. *Journal of Cultural Geography*, 11, 39-55.

MEYER-ARENDT, K.J., 1991. Tourism development on the north Yucatan coast: human response to shoreline erosion and hurricanes. *Geojournal*, 23, 327-336.

MCNINCH, J.E., 2004. Geologic control in the nearshore: shore-oblique sandbars and shoreline erosional hotspots, Mid-Atlantic Bight, USA. Marine Geology, 211, 121-141.

MCNINCH, J.E., and LUETTICH, R.A., 2000. Physical processes around a cuspate foreland: implications to the evolution and long-term maintenance of a cape-associated shoal. *Continental Shelf Research*, 20, 2367-2389.

MORTON R.A., 2002. Factors controlling storm impacts on coastal barriers and beaches - a preliminary basis for near real-time forecasting. *Journal of Coastal Research* 18(3): 486-501.

MORTON, R. A., and PAINE, J. G., 1985. Beach and vegetation-line changes at Galveston Island, Texas; Erosion, deposition, and recovery from Hurricane Alicia: The University of Texas at Austin, *Bureau of Economic Geology Geological Circula*r 85-5, 39 p.

MORTON, R.A., PAINE, J.G., and GIBEAUT, J.C., 1994. Stages and durations of post-storm beach recovery, southeastern Texas coast. *Journal of Coastal Research*, 10, 884-908.

NORDSTROM, K.F., 1994. Beaches and dunes of human altered coasts. *Progress in Physical Geography*, 18, 497-516.

NORDSTROM, K.F., 2000. *Beaches and Dunes of Developed Coasts.* Cambridge University Press, 338 pp.

NORDSTROM, K.F., JACKSON, N.L. and PRANZINI, E., 2004. Beach sediment alteration by natural processes and human actions: Elba Island, Italy. *Annals of the Association of American Geographers*, 94, 794-806.

NORDSTROM, K.F. and JACKSON, N.L., 1995. Temporal scales of landscape change following storms on a human-altered coasts, New Jersey, USA. *Journal of Coastal Conservation*, 1, 51-62.

RIGGS, S.R., YORK, L.L., WEHMILLER, J.F., and SNYDER, S.W., 1992. Depositional patterns resulting from high-frequency Quaternary sea-level fluctuations in northeastern North Carolina. In: Fletcher, C.H., Wehmiller, J.F. (Eds), Quaternary Coasts of the United States Marine and Lacustrine Systems. Society of Economic Paleontology and Mineralogy Special Publication, 48, 141-153.

RIGGS, S.R., CLEARY, W.J., and SNYDER, S.W., 1995. Influence of inherited geologic framework on barrier shoreface morphology and dynamics. Marine Geology, 126, 213-234.

RIGGS, S.R., SNYDER, S.W., HINE, A.C., and MEARNS, D.L., 1996. Hard-bottom morphology and relationship to the geologic framework: Mid-Atlantic continental shelf. *Journal of Sedimentary Research*, 66, 830-846.

SALLENGER, A. H., 2000. Storm impact scale for barrier islands. *Journal of Coastal Research*, 16, 890-895.

SALLENGER, A.H., WRIGHT, C.W., and LILLYCROP, J., 2004. Coastal Impacts of the 2004 Hurricanes Measured with Airborne LiDAR: Initial Results. *Shore and Beach*, 73, 10-15.

SCHUPP, C.A., MCNINCH, J.E., and LIST, J.H., 2007. Nearshore shore-oblique bars, gravel outcrops, and their correlation to shoreline change. *Marine Geology*.

SCHWAB, W.C., THIELER, E.RF., ALLEN, J.R., FOSTER, D.S., SWIFT, B.A., and DENNY, J.F., 2000. Influence of inner-continental shelf geologic framework on the evolution and

behaviour f the barrier-island system between Fire Island Inlet and Shinnecock Inlet, Long Island, New York. *Journal of Coastal Research*, 15, 408-422.

SNYDER, S.W., 1993. North Carolina Outer Banks beach nourishment sand resource study, first interim report; shallow, high-resolution seismic survey, offshore Nags Head area. Open-File Report 93-38. North Carolina Geological Survey, Raleigh, North Carolina.

STONE, G.W., 1984. Mathematical modeling of the nearshore and implications for coastal management, Northwest Florida. Unpublished MSc thesis, Department of Environmental Studies, University of West Florida, 140 pp.

THIELER, E. R., and YOUNG, R. S., 1991. Quantitative evaluation of coastal geomorphological changes in South Carolina after Hurricane Hugo, *Journal of Coastal Research* (Special Issue) 8, 187–200.

WATANABE, A. and HORIKAWA, K., 1983. Review of coastal stabilization works in Japan. *Proceedings of the International Conference on Coastal and Port Engineering in Developing Countries*, 186-200.

WEHR, A. and LOHR, U., 1999. Airborne laser scanning- an introduction and overview. *Journal of Photogrammetry and Remote Sensing*, 54, 68-82.

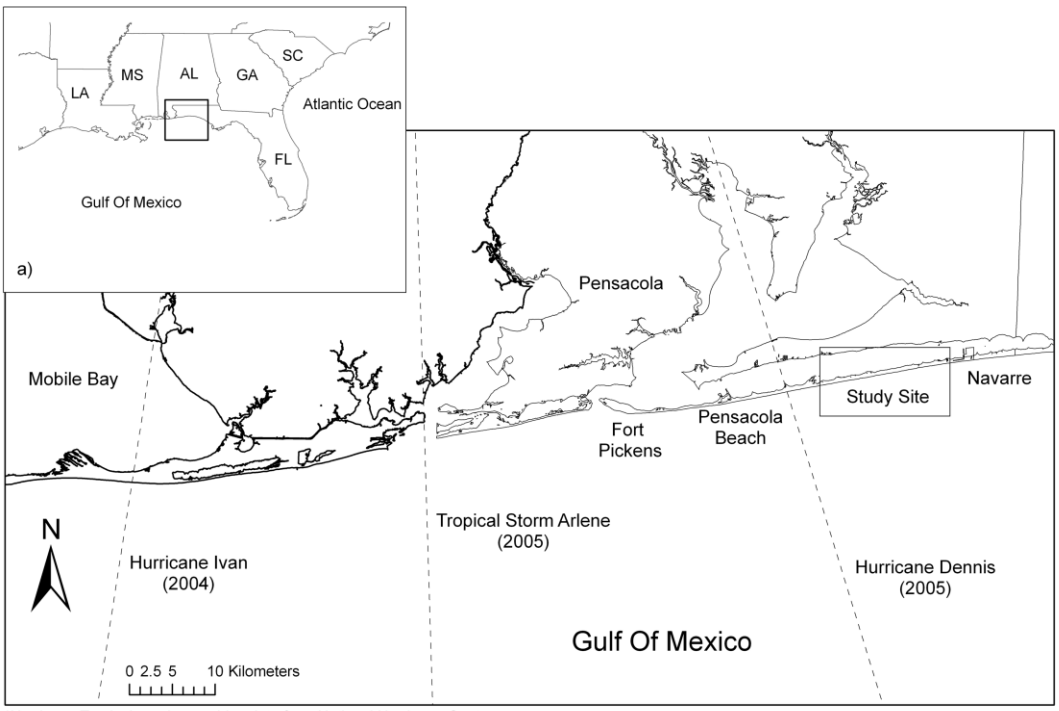
WIJNBERG, K.M., 1995. *Morphologic Behaviour of a Barred Coast over a Period of Decades*. Ph.D. Thesis, Proefschrift Universiteit Utrecht, 245 pp.

WOOLARD, J.W. and COLBY, J.D., 2002. Spatial characterization, resolution and volumetric change of coastal dunes using airborne LiDAR: Cape Hatteras, North Carolina. *Geomorphology*, 48, 268-287.

ZHANG, K., WHITMAN, D., LEATHERMAN, S., and Robertson, W., 2005. Quantification of Beach Changes caused by Hurricane Floyd along Florida's Atlantic coast using airborne Laser Surveys. *Journal of Coastal Research*, 21, 123-134.

Table 3. Definitions for the different levels of road damage and the percent length of road within each category based on aerial and ground-based assessments.

Level of Damage	Description	Percent Length	
		Hurricane Ivan	Hurricane Dennis
No Damage	No visible damage to the roadway	14	75
¼ Damage	The roadway was severely buckled or collapsed for less than ¼ of its width (one half of a travel lane)	31	9
½ Damage	The roadway was severely buckled or collapsed for less than ½ of its width (a full travel lane)	18	8
Full Damage	More than ½ of the roadway is severely buckled, collapsed or the roadway is completely washed out	37	8



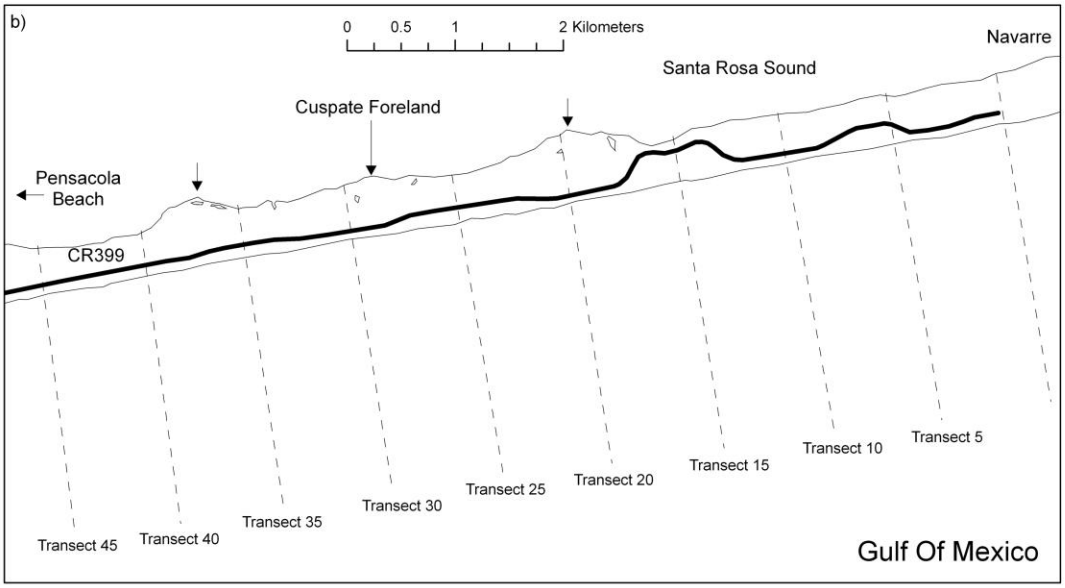


Figure 47. Map of study site showing (a) location relative to the tracks of Hurricanes Ivan and Dennis and Tropical Storm Arlene and (b) alignment of County Road 399 within the Gulf Islands National Seashore relative to the cuspate forelands and study transects.



Figure 48. Representative photographs of the different levels of damage along County Road 399. Shown are a) no damage, b) ¼ damage (part of a lane), c) ½ damage (loss of an entire lane) and d) complete damage (loss of the entire road bed. In all of the photographs, the north side of the road is on the left of the image.

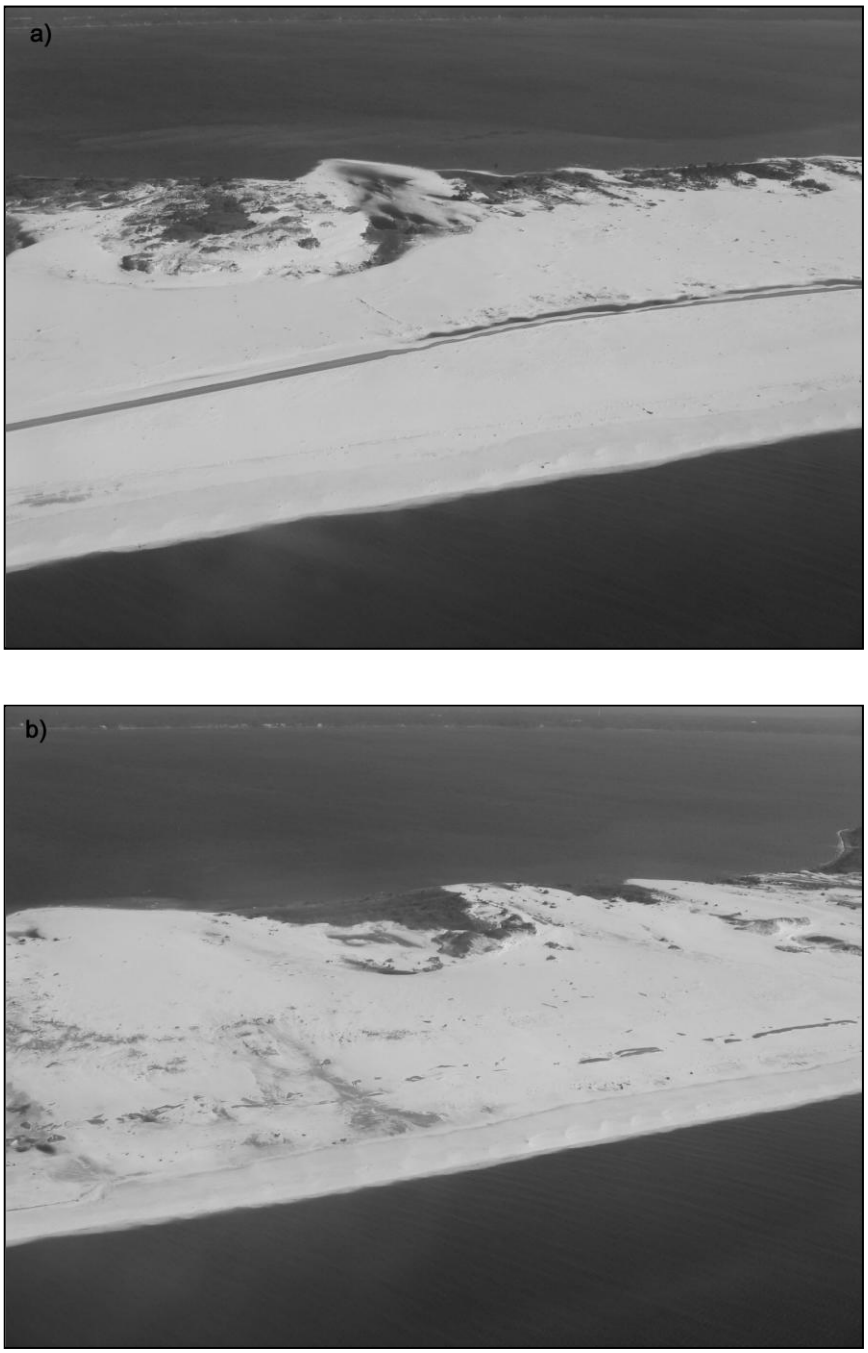


Figure 49. Aerial photographs of road damage showing (a) a transition from 1/4 damage to no damage (b) a transition from 1/2 damage to full damage (right to left). The photograph in (a) is from transects 25 to 27 and the photograph in (b) is from transects 22 to 24.



Figure 50. Photograph showing asphalt and gravel debris north of the road (in the background), creating a lag surface that may limit aeolian sediment transport and dune recovery. The photograph was taken at transect 40.

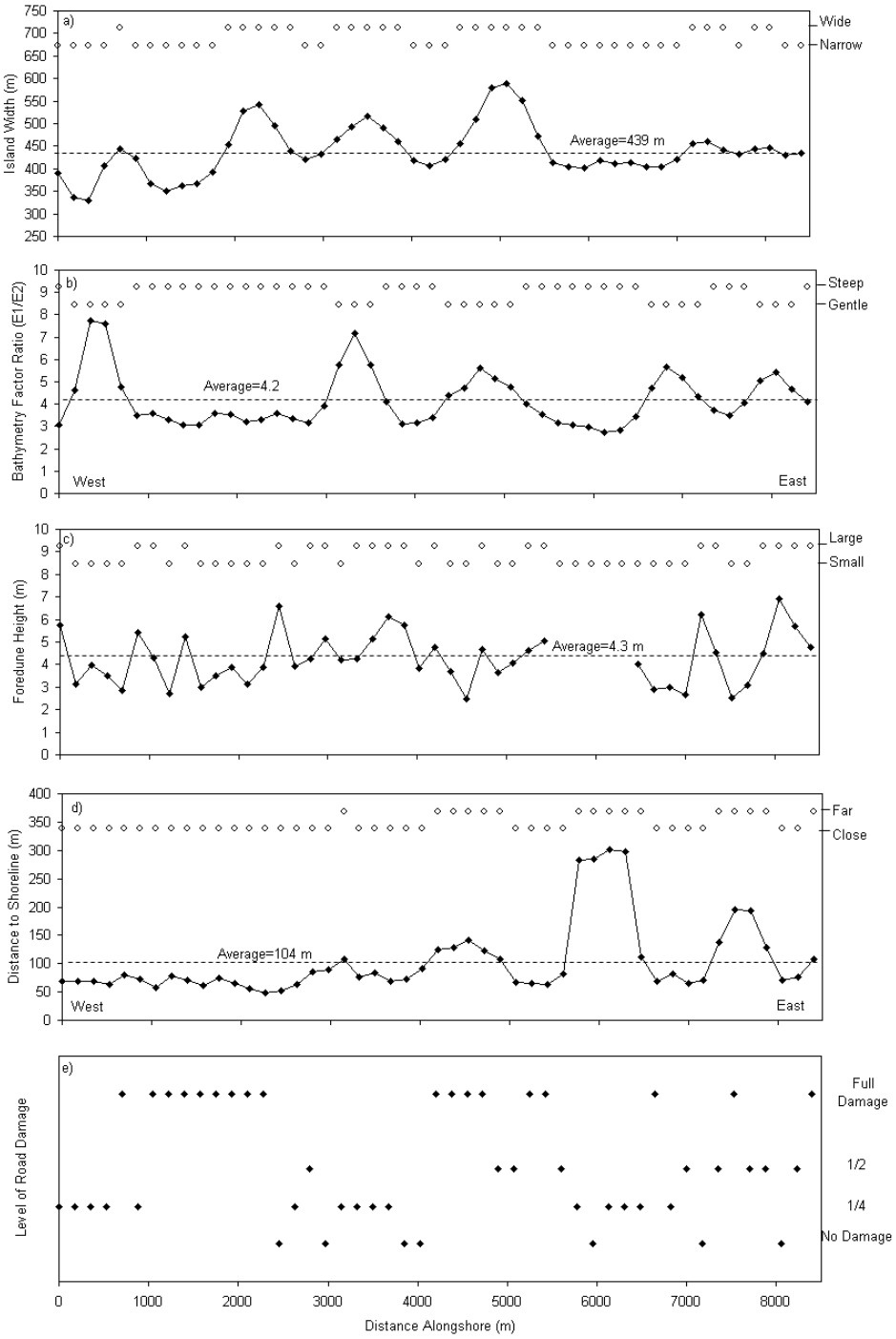


Figure 51. Alongshore variation for Hurricane Ivan in a) island width, b) ratio of gently sloped to steep offshore bathymetry factors, c) foredune height, d) distance between roadway and shoreline, and d) the categories of road damage.

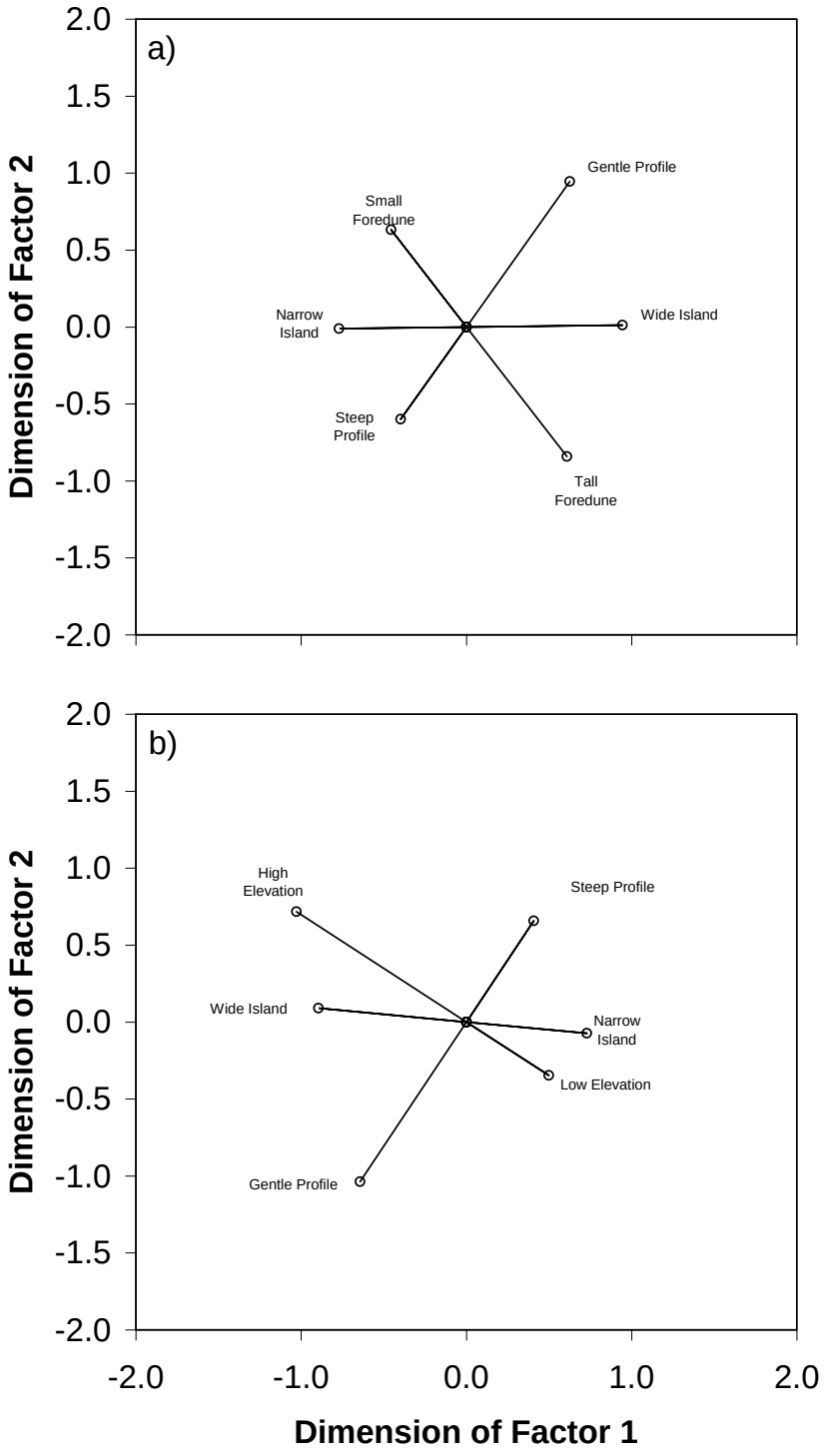


Figure 52. (a) Correspondence plot showing the pre-Ivan structure of the primary factors for the environmental variables of offshore bathymetry, island (foredune) elevation and island width. Also shown (b) is the Correspondence plot for the pre-Dennis structure for the environmental variables of offshore bathymetry, island elevation and island width.

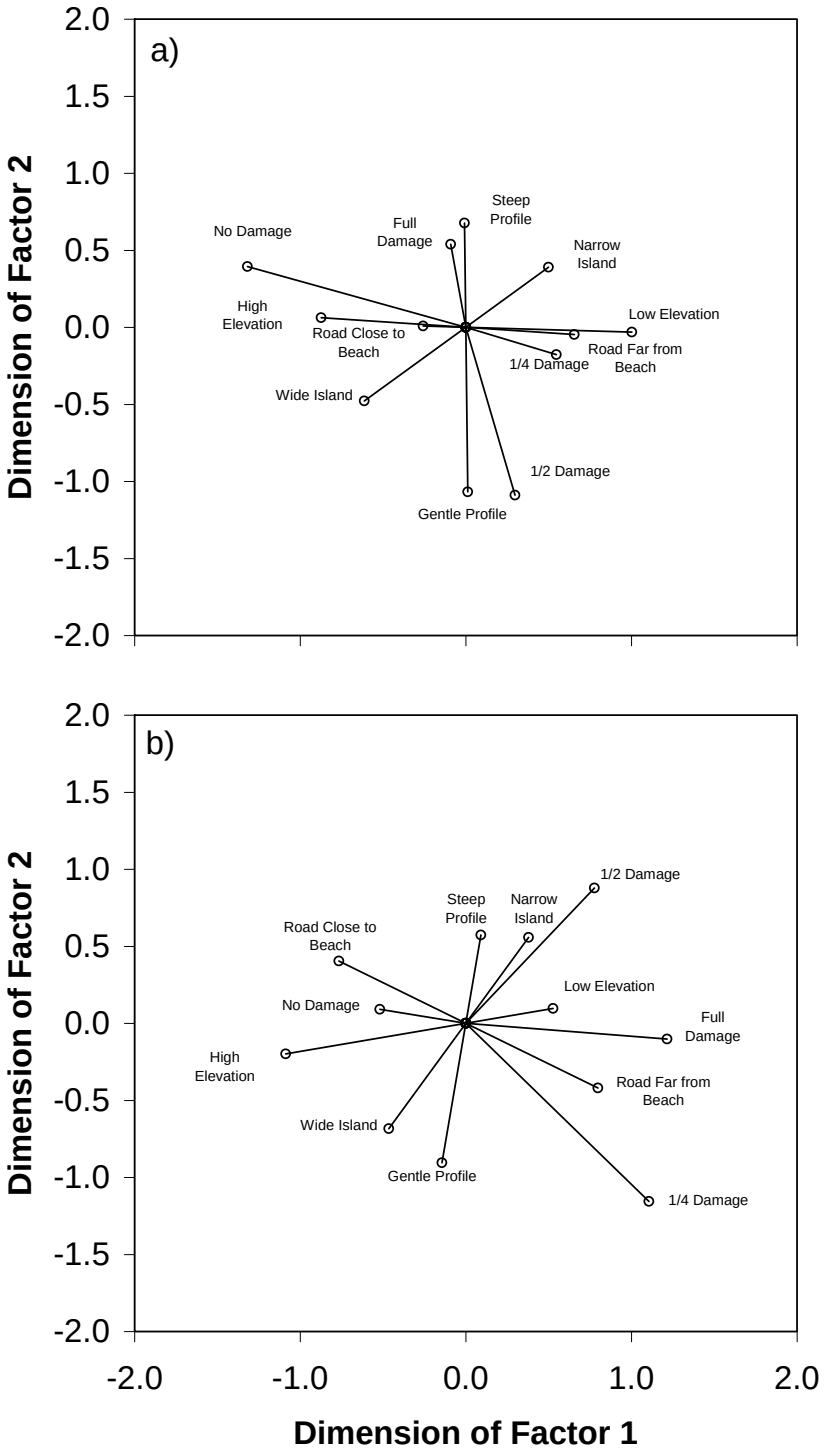


Figure 53. Correspondence plot showing the structure of the primary factors for (a) Hurricane Ivan and (b) Hurricane Dennis. In both cases, the principal axis (Factor 1) is described by island elevation and the axis for Factor 2 is described by the offshore bathymetry.

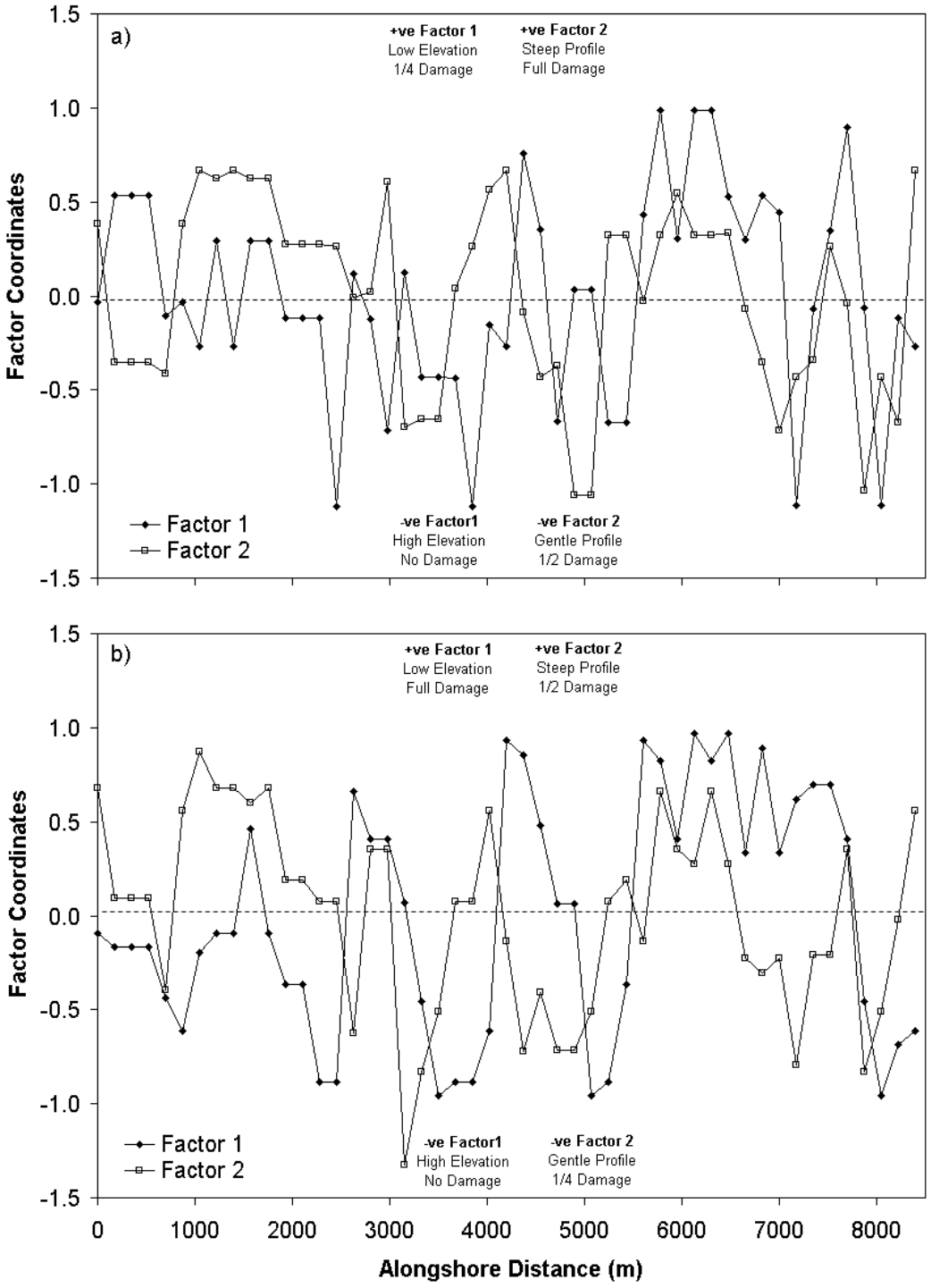


Figure 54. Alongshore variation in factor coordinates with the largest factor coordinate (whether positive or negative) providing the best description of the road damage and geological controls at each transect. Shown are the factor coordinates for (a) Hurricane Ivan and (b) Hurricane Dennis.

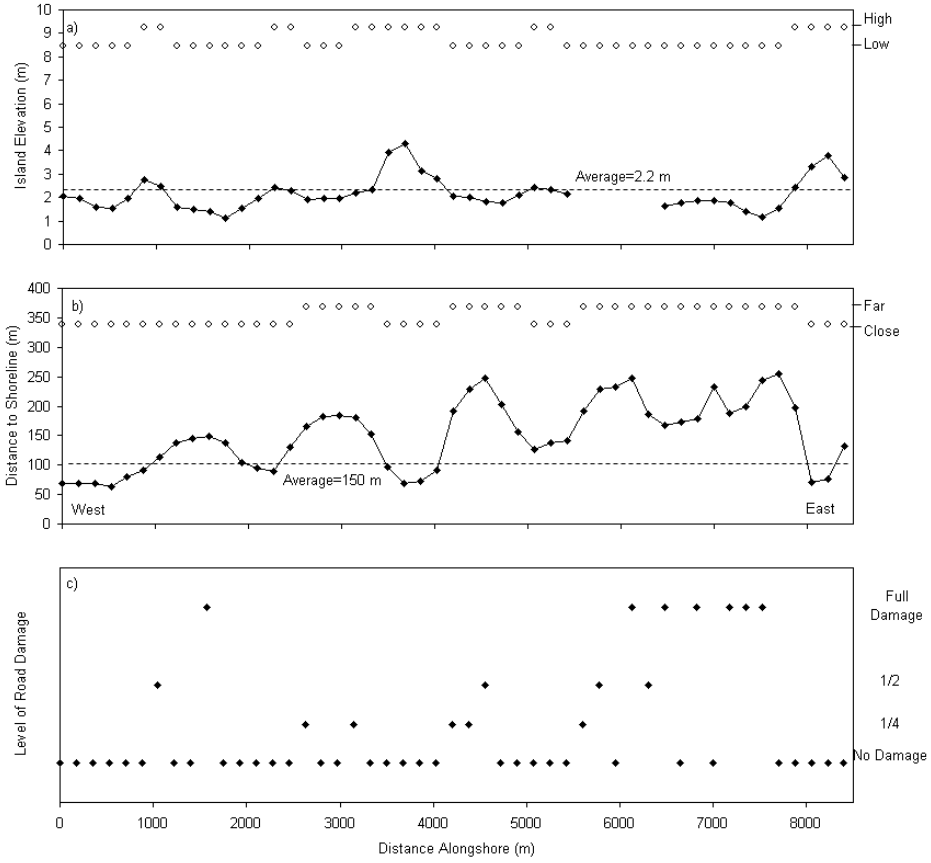


Figure 55. Alongshore variation in (a) island elevation, (b) distance between roadway and shoreline, and (c) the categories of road damage for Hurricane Dennis.

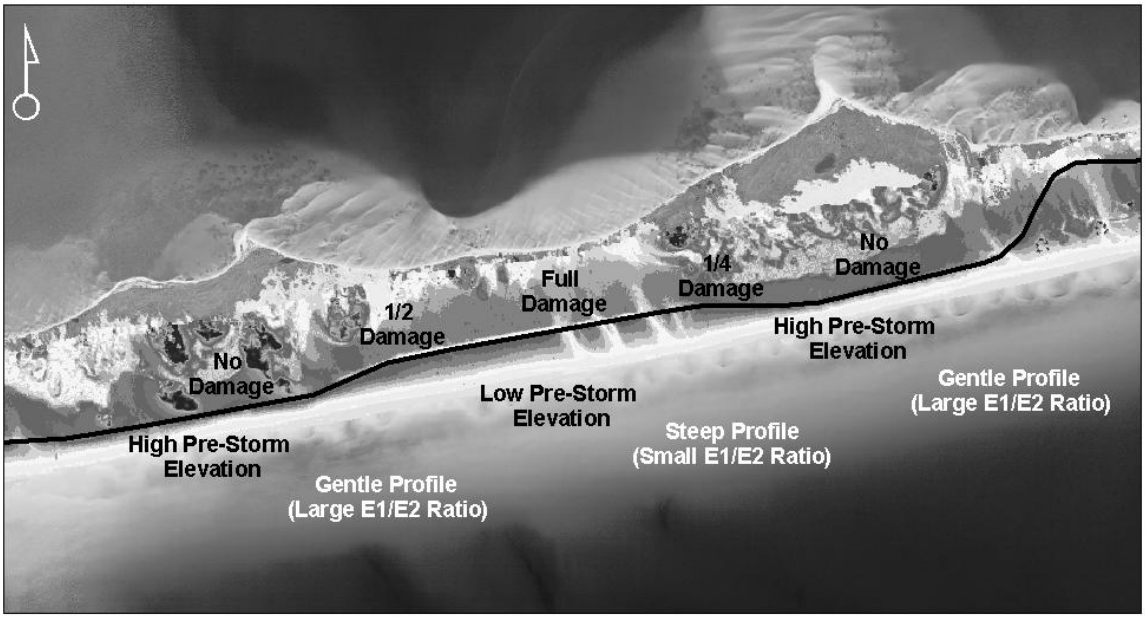


Figure 56. Post Hurricane Ivan LiDAR surface and DOQ image of a representative section of road with the alongshore variation in road damage, island elevation and offshore slope labeled.

CHAPTER 5

Wave-scale changes in bed elevation of an intermediate foreshore

Chris Houser

Department of Geography
Texas A&M University
810 O&M Building
College Station, Texas
77843-3147

Abstract

Wave-scale changes in bed elevation are measured using ultrasonic distance sensors within the high tide swash zone of an intermediate foreshore. The calibrated distance sensors can measure changes in bed elevation of ~0.1 mm, thereby allowing for grain-scale changes to be recorded following the passage of individual swash events. Changes in bed elevation are examined relative to the depth-averaged Eularian flow velocity estimated using pressure transducers at 8 fixed stations equally spaced across the foreshore. Bed elevation is found to vary at infragravity frequencies but is dominated by much larger (centimeter-scale) variations at lower frequencies in response to the time-varying balance of gravity and infragravity wave energy. No statistically significant relationship is observed between the change in bed elevation and the higher order moments of the velocity as would be expected from an energetics model for either bedload or suspended load. Balancing the bed elevation change with the suspension potential (u^3) provides an estimate of the advected sediment contribution, which is found to be on the same order of magnitude as the amount of locally suspended sediment. Accretion is associated with breaking on the innermost bar and lower foreshore, leading to swash bores with a relatively strong suspension potential during the uprush, and the landward advection of sediment with the time-averaged velocity. Erosion is associated with breaking on the foreshore and steeply faced swash bores that have a strong suspension potential during the uprush, but also have a strong seaward-directed transport of sediment with the backwash. In general, changes in bed elevation within the upper swash zone of this intermediate beach are a balance between the upward suspension potential (*S*) and the amount of sediment settling out of the water column after being advected landward with the advancing swash.

Keywords: Swash zone; bed elevation change; suspension potential; sediment advection

1. Introduction

The swash zone is the morphologically dynamic region landward of the surf zone where the shoreline sweeps back and forth across the beachface at both gravity and infragravity frequencies. Swash consists of an uprush as the shoreline moves landward and backwash when the shoreline retreats seaward. The large cross-shore velocities of the uprush and backwash are capable of mobilizing and transporting large quantities of sediment (Hughes et al., 1997; Masselink and Hughes, 1998; Butt and Russell, 1999; Osborne and Rooker, 1999; Puleo et al., 2000; Puleo et al., 2003; Aagaard and Hughes, 2006). Spatial gradients in the time-integrated transport drives morphological change and ultimately determine whether sediment is transported to the inner surf zone or stored on the upper beach. Sediment stored on the upper beach may become available for aeolian transport to the backshore, making the swash zone an important conduit between the surf zone and coastal dunes (Sherman and Bauer, 1993).

On gently sloped beaches, waves arrive at the beachface over a broad zone in which incident wave heights are depth limited and the amplitude of the swash does not increase in response to increases in the incident wave energy. Rather, increases in wave energy offshore lead to a linear increase in swash amplitudes at infragravity frequencies (e.g. Guza and Thornton, 1982; Holman and Sallenger, 1985), through either the nonlinear transfer of energy from offshore wave groups or through the modulation of the surf zone. On relatively steep beaches, with gradients >0.10, the swash motion is dominated by gravity waves (Waddell, 1976; Raubenheimer and Guza, 1996) and the swash cycle commences when the incoming bore reaches the exposed beachface and finishes before the next wave arrives. Low-frequency swash may also develop in response to standing infragravity waves in the surf zone, but also through the overtaking and capturing of bores in the lower swash zone (Carlson, 1984; Mase, 1988; Mase, 1995). Baldock et al. (1997) has also shown that low frequency swash motion can be directly induced by incident wave groups and are not necessarily due to standing infragravity waves or bore interaction.

The ability of gravity and infragravity waves to mobilize and transport sediment within the swash zone remains poorly understood, despite the considerable focus on swash zone morphodynamics in recent years (e.g. Puleo et al., 2000; Butt et al., 2002; Masselink et al., 2005; Aagaard and Hughes, 2006). Much of this research has been guided by the use of a Bagnold-type energetics model that relates bedload (I_b) to the third power of velocity and suspended load

(I_s) to the fourth power of velocity. In their most basic forms, the energetic formulae can be written for a given event as:

$$I_b = ku^3T \tag{1}$$

$$I_s = ku^3|u|T \tag{2}$$

where k is an empirical constant and T is the duration of the event. These models relate sediment transport to the cubed-velocity through a calibration coefficient (k) that is assumed to be constant for a given beach. In both the field and the laboratory, it has been found that uprush is more 'efficient' than the backwash due to larger mean bed shear stresses and friction factors (Masselink and Hughes, 1998; Puleo et al., 2000; Cox et al., 2000; Conley and Griffin, 2004 Aagaard and Hughes, 2006). Foreshore accretion occurs in opposition to the force of gravity and requires an asymmetry between the uprush and backwash velocity or in the amount of sediment in suspension. In general, suspended sediment concentrations tend to be larger during the uprush compared to the backwash (Puleo et al., 2000; Masselink et al., 2005), leading to a net onshore-directed transport that must be balanced by an offshore-directed velocity to have a net-offshore directed transport.

The use of an energetics model that is based on the local gradients in skewness (Equation 1) and kurtosis (Equation 2) does not account for the large amount of sediment advected landward from the point of bore collapse (Hughes et al., 1997, Jackson et al., 2004; Pritchard and Hogg, 2005). The models are also not able to account for sediment advected offshore by backwash containing hydraulic jumps, which are capable of advecting 2.5 times more sediment than 'normal' backwash (Butt and Russell, 2005). It is for this reason that Aagaard and Hughes (2006) argue that there is "little value in continuing to pursue energetics-type transport models much further". However, it is reasonable to expect that sediment is still resuspended by the higher order moments of the flow, but that the relationship between the local hydrodynamic gradients is masked by advected sediment. It is possible that the balance of locally suspended and (non-local) advected sediment may depend on the incident forcing and may even change from wave to wave.

Kobayashi and Johnson (2001) suggest that changes in bed elevation should be characterized as a balance between the upward suspension potential (*S*) and the amount of sediment settling out of the water column:

$$\frac{\partial(hC)}{\partial t} + \frac{\partial(hCU_s)}{\partial x} = S - wC \tag{3}$$

where h is the water depth, C is the depth-averaged sediment concentration including both bed and suspended load, U_s is the horizontal sediment velocity, and w is the sediment fall velocity. The horizontal sediment velocity is assumed to be equal to the difference between the horizontal fluid velocity and the settling velocity (U_s=U-w; Kobayashi and Johnson, 2001). The upward suspension potential is related to the wave energy dissipation rate:

$$S = \frac{e_b D_b + e_f D_f}{\rho g (s-1) h} \tag{4}$$

where D_b and D_f are the energy dissipation rates per unit horizontal area due to wave breaking and bottom friction, e_b and e_f are their respective efficiencies, ρ is the fluid density, g is acceleration due to gravity and s is the specific gravity of the sediment. The change in bed elevation can be calculated as the difference between the settling and suspension rates:

$$\frac{\partial z}{\partial t} = \frac{wC - S}{(1-n)} \tag{5}$$

where n is the porosity of the bed sediment. Kobayashi and Johnson (2001) numerically solved for the sediment concentration and change in bed elevation using a one-dimensional wave model and demonstrated that bed elevation changes are determined by small differences between the advected and locally suspended sediment. In this respect, the model can also be used to estimate the sediment balance if the local change in bed elevation resulting from each swash excursion is known.

While there has been considerable focus on the hydrodynamics and sediment transport of the swash zone in recent years, there are only a handful of studies to examine changes in bed elevation (e.g. Waddell, 1976; Sallenger and Richmond, 1984; Howd and Holman, 1987; Nordstrom and Jackson, 1990; Austin and Masselink, 2006; Turner et al., 2006; McDermott and Sherman, in review). The inability to examine wave-scale changes in bed elevation in past studies is a significant barrier to relating swash zone morphology and change to swash hydrodynamics.

Change in the morphology of the swash zone and the broader foreshore has been measured through traditional surveying and related to the incident forcing over a wide range of temporal scales, from days to years (e.g. Shepard**,** 1950**;** Strahler, 1966; Nordstrom, 1980**;** Short and Trembanis, 2004; Hsu et al., 2006). Other studies have also attempted to measured changes in swash morphology in response to individual gravity and infragravity waves using either erosion pins or electronic sensors (Waddell, 1976; Sallenger and Richmond, 1984; Howd and Holman, 1987; Nordstrom and Jackson, 1990; Horn and Li, 2006; Austin and Masselink, 2006; Turner et al., 2006; McDermott and Sherman, in press). Waddell (1976) observed changes in bed elevation by up to 0.05 m in response to individual swash excursions, but found that most changes in bed elevation had a low-frequency signal (~40 s) that was not related to the incident forcing. Oscillations between 6 and 15 minutes were observed by Sallenger and Richmond (1984), who suggested that the oscillations were associated with either shelf waves or seiche. McDermott and Sherman (in press) used photo-electric erosion pins (PEEP senors) and found evidence of cycles of erosion and accretion at a period of about 300 s and with a magnitude of about 1 to 1.5 cm. More recently, Turner et al. (2006) employed an ultrasonic sensor to measure bed elevation and found (for only a 40 s record) changes of ~0.02 m in response to a single swash excursion.

The hydrodynamic controls on both high and low-frequency variations in bed elevation remain poorly understood in response to the inability to quantify sediment gains and losses following individual swash events. The purpose of this study is to examine the change in bed elevation in response to individual swash bores within on an intermediate foreshore. The specific objectives are to relate changes in bed elevation to the depth-averaged Eularian velocity and its higher order moments and to estimate the relative importance of locally suspended and advected sediment in the upper swash zone.

2. Study Site

The instrumented field study was completed over a single tidal cycle on June 7, 2008 on Santa Rosa Island, near Pensacola Beach in northwest Florida. The study was completed within the Fort Pickens Unit of the Gulf Islands National Seashore where both the beach and dune systems are in a state of recovery following the 2004/2005 hurricane season in which the area experienced significant beach erosion and widespread overwash and breaching (Houser et al., 2008; Houser and Hamilton, in press). Santa Rosa Island is microtidal with an average diurnal tidal range of 0.43 m (Armbruster, 1997). The dominant wave approach is from the southeast (Balsillie, 1975), although it is not uncommon for storm waves to approach from the southwest or from the south with the sea-breeze. The time-averaged significant wave height (H_s) is ~1.0 m (Stone et al., 1992) with a peak spectral period (T) of ~5 s. The mean grain size is ~0.3 mm and has a settling velocity (*w*) of ~0.043 m s^{-1}. The dimensionless fall velocity ($\Omega=H_s/wT$) is ~4.6, which suggests a rhythmic bar and beach nearshore system. While the beach was fronted by a single nearshore bar prior to the 2004/2005 hurricane season, there is presently 2 subtidal bars that are slowly migrating landward. The foreshore is relatively steep (β=0.24), which permits for a wave-by-wave analysis of the swash motion and bed elevation change, with limited swash interaction or infragravity wave dominance.

3. Methodology

3.1 Data Collection

A total of 8 fixed stations were deployed across the narrow foreshore at a spacing of ~1 m (Fig. 1). Each station was equipped with a KPSI pressure transducer (KPSI 735T) and a Senix Toughsonic (ultrasonic) distance sensor (TS-30S) to measure changes in bed elevation. The transducers were initially placed flush with the bed and adjusted as the bed elevation changed greater than 2.5 cm relative to the sampling face after each sample burst. The ultrasonic distance sensors were deployed at the innermost stations (S1-S4) at an initial height of ~0.5 m and were oriented so that the sensor beam was perpendicular to the sediment surface. The sampling range

was set between a maximum distance of 1.0 m (10 volts) and a minimum of 0.15 m (0 volts); a 1 volt change in output is equivalent to a change in bed elevation by 6 cm. The resolution of the sensors is 0.086 mm, which is smaller than the mean grain size (~0.3 mm) and is at the lower limit of the grain sizes commonly found on the foreshore and inner surf zone (10^{th} percentile: 0.1 mm). All sensors were cabled linked to shore and monitored at 25 Hz using an Iotech datalogger (Personal DaqBook^{TM}) connected to a field laptop.

The ultrasonic distance sensors were calibrated before and after the field experiment in a series of bench tests. Grain scale changes in bed elevation were simulated by adding thin (~1 mm) layers of sediment to the test bed; changes in bed elevation were measured using a digital caliper at multiple locations and averaged relative to the starting distance between the bed and the sensor. Larger scale changes in distance from the sensor, to simulate the passage of individual waves beneath the station, were calibrated by adding water to the test bed. The calibration curve for both the sediment and water surface are presented in Fig. 2. The ability of the distance sensors to measure rapid water level fluctuations was also examined in the field (prior to this study) by comparing against the pressure transducer at the same station as a time series (Fig. 3a) and a scatterplot (Fig. 3b). Based on a sample size of 25,000 (1000 s), there is a strong correlation (r^2=0.93, ρ=0.001) between the pressure transducer and the distance sensor. In general, the pressure transducer underestimates shallow water depths as the sensor first becomes submerged or is exposed during the backwash. For many waves, the distance sensor shows the waves as larger (by up to 10 cm) than measured by the pressure transducers, which may reflect the foam and turbulence at the leading of the swash. As a consequence, wave heights and the depth-averaged velocity will be based on the pressure transducers and not the distance sensors throughout the remainder of this paper. The distance sensors will only be used to characterize changes in bed elevation.

Bed elevation changes were also measured at the start of each burst sample using the station posts like a traditional erosion pin. Grab samples of bed sediment were collected at 3 points during the rising tide (8:35), high tide (11:20) and falling tide (13:35) adjacent to S1, S3, S5 and S7. The sampling location was selected to avoid interference with the bed elevation. Samples were returned to the laboratory and sieved. Settling velocities were calculated using the method of Jimenez and Madsen (2003) and the mean grain size. The location of final wave breaking, the physical characteristics of the swash and the total swash excursion were monitored

using time-lapse cameras placed on either side of the instrumented transect. The cameras were set to record at 1 minute intervals and provide 3.1 MegaPixel color images.

3.1 Data Analysis

Swash depths at this site are typically <0.20 m, which precludes the use of current meters to directly measure flow velocities. The depth-averaged flow velocity *u(t)* at each of the stations (*x*) was therefore estimated (following Hughes and Baldock, 2004) through the mass balance of the swash discharge (Q):

$$Q = \frac{V}{t} = hu \tag{6}$$

where the volume of water (*V*) shoreward of a given station is calculated as:

$$V = \int_{x}^{X} h dx \tag{7}$$

Expressing Equation 5 in finite difference form provides an estimate of the depth-averaged flow velocity:

$$u = \frac{V(t+\Delta t) - V(t-\Delta t)}{2h(t)\Delta t} \tag{8}$$

The Eulerian velocity at each station is used to calculate the higher order moments of the flow (u^2u and u^3u), and the upward suspension potential (S, Equation 3) based on the local energy dissipation through bottom friction:

$$D_f = 0.5 f_b \left| u^3 \right| \tag{9}$$

where σ is the f_b is the constant bottom friction factor assumed to be 0.015 (Raubenheimer et al., 1995). This analysis assumes that friction for swash flows is primarily a function of grain roughness and does not account for resistance afforded by (1) bedforms, (2) sediment load or (3) infiltration and exfiltration; the source of bed resistance is beyond the scope of this paper.

4. Results

4.1 Bed Elevation Change

The slope of the beach became increasingly reflective over the course of the tidal cycle through accretion at the uppermost stations and erosion over the seaward portion of the profile (Fig. 4a). In this respect, the profile change exhibited a simple erosion-accretion couplet around a pivot point at S3. Approximately 0.16 m^3 of sediment was gained above the pivot point, while ~0.29 m^3 of sediment was lost lower on the profile; the net volume change was ~0.13 m^3 per m alongshore. It is not clear whether there was a net loss of sediment or whether sediment was stored landward of S1 along the beach scarp or seaward of S8 in the inner surf zone. The change at S8 was largely linear (-0.01 m hr^{-1}) except for a short period of accretion (~0.05 m) around high tide. Similarly, the change in S1 was also linear (0.02 m hr^{-1}), although most of the accretion occurred during the final 2 hours of the falling tide. The remaining stations exhibited a cyclical change (to varying degrees), with erosion through rising tide and accretion with falling tide, although all stations exhibited unexplained changes (both erosion and accretion) on the order of 0.03 m at various times over the tidal cycle (Fig. 4b). The cross-shore pattern of erosion and accretion was not associated with the migration of a distinct sediment lens, as noted by Duncan (1964), and more recently by Masselink and Russell (2006). Cross-correlation of elevation change suggests that there is no statistically significant lag in elevation change between the stations, although elevation change is inversely related on either side of the pivot point.

Bed elevation changes at S4 are plotted in Fig. 5 for representative burst samples collected at 25 Hz from the rising, high and falling tide. All time series exhibit low frequency undulations in bed elevation (running minimum of time series) at timescales ranging from 100 and 500 s. In some cases, these undulations are associated with incremental changes in bed elevation during each swash excursion (Fig. 5d), while others (Fig. 5a) are initiated by an individual swash excursions (Fig. 5a and 5b). For example, 75% of the total elevation change in the 9:45 sample (Fig. 5a) was associated with the large swash excursion that peaked at 108 s. The new elevation persisted until the large swash excursion at 610 s caused a loss of bed elevation by ~0.01 m that was reversed by the swash excursion that peaked at 655 s. Most

changes in bed elevation early in the tidal cycle were associated with individual swash excursions, particularly at the stations higher up on the beach. Through high tide, changes in bed elevation are increasingly associated with individual swash excursions, but are still punctuated by low-frequency swash excursions that cause rapid changes in bed elevation. The ~0.04 m accretion, that resulted (to varying degrees) from the 18 swash events that started at 417 s (11:00; Fig. 5b), was largely lost during the large swash excursion that peaked at 616 s.

Combining all bed elevation records together reveals further low frequency undulations in the bed elevation that are not captured by the less frequent erosion pin measurements (Fig. 4b). The maximum change in bed elevation measured using the station posts was ~0.08 m, approximately ½ of the change in bed elevation measured by the distance sensors. Throughout the first 1.5 hours of the sample period, the post measurements were fortuitously timed when the bed elevation was at a local minimum and the ~0.04 m oscillation in bed elevation was not recognized. Spectral analysis of the detrended variation in bed elevation reveals a statistically significant variation with a periodicity of ~978 s (16.3 minutes) and secondary variations with periods of 1100 and 1800 s (18.3 and 30 minutes respectively).

Histograms of bed elevation change at the uppermost stations (S1 to S4) are presented in Fig. 6. The range of bed elevation change is greatest at S4 with 33% of the 1094 waves recorded causing bed elevation changes greater than 0.01 m and 8% causing bed elevation changes greater than 0.02 m. While the range of elevation change decreases landward from S4 to S2, the range is greater at S1 due to an increase in the frequency of waves causing accretion ≥5 mm. Following these accretion events, the bed surface at S1 and only occasionally at S2 was covered by large pores, created by escaping air and suggestive of swash infiltration. Regardless of whether there were signs of infiltration at S1 or not, accretion across the upper-swash occurred as a sediment drape that ranged from a couple of grains thick to several centimeters.

Mean grain size and predicted settling velocity for grab samples collected at rising, falling, high and falling tide are presented in Table 1. During rising tide, there is a logarithmic fining of grain size present in the upper-foreshore, with little cross-shore change in grain size from S7 to S3. As the upper-foreshore is increasingly inundated by swash bores there is a fining of sediment particularly at S3. At S5 and S7, the high-tide boundary of the surf and swash zones, there is a coarsening of sediment followed by a refining of grain size as this region becomes increasingly dominated by swash. At both high and falling tide, the cross-shore

variation in grain size is best fit by a squared polynomial, which indicates greater cross-shore change in grain size lower in the lower foreshore.

4.2 Hydrodynamics

The cross-shore variation in average velocity, upward suspension potential (S), wave skewness (u^3) and kurtosis (u^3u) were examined for swash events that caused erosion and accretion at S4. Swash events that cause erosion tend to be associated with a stronger seaward-directed average velocity and a weaker suspension potential, while swash events that cause accretion tend to be associated with a landward-directed average velocity and a stronger suspension potential. As shown in Fig. 7, the leading face of a representative 'erosional' wave is quite turbulent and contains a high concentration of suspended sediment advected with the advancing bore. While there is a steep leading face, there is an early and sustained reversal of the flow, creating an asymmetry in the transport of advected sediment and resuspension of local sediment. In contrast, 'accretional' waves do not have a relatively steep leading face, but have a later and shorter duration reversal of the flow (Fig.s 7d-f).

Ensemble averaged time series of water depths predicted flow velocity and upward suspension potential (Equation 4) for Station 4 are plotted in Fig. 8. The time series have been normalized by the individual wave period and separated based on whether the wave was erosional or accretional. For both types of wave, maximum water depths occur at the start of the uprush and at the end of the backwash respectively, with flow reversal occurring at or close to the maximum swash depth. In general, the suspension potential was larger during the uprush in response to the steep leading face swash, but the relative strength of the uprush and backwash velocities appears to depend on the shape of the advancing bore. During accretional events, maximum velocities of 1.4 m s^{-1} were predicted during the uprush, leading to a larger suspension potential during the uprush and an onshore directed current. The onshore-directed current is partly determined by a volumetric imbalance between the uprush and backwash, suggesting infiltration in the upper-swash. Maximum velocities predicted during erosional events reached a maximum of ~1.0 m s^{-1} during the backwash leading to a weak but sustained suspension potential during the backwash and an offshore directed average current.

Based on the energetics model (Equations 1 and 2), changes in bed elevation should largely depend on the gradient in velocity skewness, kurtosis and the combination of these flow parameters. Scatterplots of bed elevation change and the gradients in the oscillatory skewness is presented in Fig. 9a; no statistically significant relationship could be identified for either skewness or kurtosis or their sum. While erosion events tend to be associated (but not significantly correlated) with a negative skewness and kurtosis, sediment accretion is associated with both positive and negative skewness and kurtosis. Both sediment accretion and erosion are found to be significantly correlated (ρ=0.01) to the local average velocity at the 95% confidence level (Fig. 9b). Accretion tends to be associated with a positive (landward) time-averaged velocity, which in turn tends to be associated with a landward directed skewness (see Fig. 8). Erosional events tend to be associated with a negative (offshore) average velocity that is associated with an offshore directed skewness and a sustained suspension potential during the backwash.

As noted, the change in bed elevation occurs at timescales ranging from 100 to 500 s that tend to be initiated or completed by large swash excursions. Through wavelet analysis it is found that periods of erosion tend to be associated with an increase in low frequency energy and a decrease in the gravity wave swash, while periods of accretion tend to be associated with an increase in gravity wave energy relative to the infragravity wave energy (Fig. 10). The rate of change in bed elevation appears to be dependent on both the relative importance of gravity and infragravity wave energy and the absolute amount of energy available. As noted, periods of erosion are associated with an offshore directed skewness and average velocity resulting from a weakened asymmetry in the swash depths. The swash excursion during these events tends to be dominated by the infragravity wave and not by the individual gravity waves that are relatively weak. As a consequence, larger backwash velocities develop in response to the retreat of the infragravity wave and the onshore directed velocities of the individual gravity waves is muted by their relatively small heights compared to the local depth. A plot of bed elevation change with the burst-averaged ratio of gravity to infragravity wave energy measured in each burst suggests that the tidal scale variation in bed elevation is also a response to the increase in infragravity wave energy through high tide (Fig. 11).

The relative importance of velocity skewness and sediment advection to bed elevation change was examined using the upward suspension potential through Equation 4. As expected

from the velocity skewness (see Fig. 9a), no statistically significant relationship was observed between the suspension potential and bed elevation change, suggesting that advected sediment may provide and sometimes dominant balance to the sediment suspended by the advancing and retreating swash. The predicted concentration of advected sediment required to balance the bed elevation change is plotted relative to the time-averaged velocity in Fig. 12. Larger concentrations of advected sediment tend to be predicted when the velocity average (and skewness) is directed onshore, while smaller concentrations of advected sediment tend to be predicted when the velocity average and skewness are directed offshore.

5. Discussion

The inability to directly measure changes in bed elevation following individual swash events has represented a significant barrier to relating beachface morphology and change to swash hydrodynamics and sediment transport. Wave-scale measurements of bed elevation change from a relatively steep beach reveals millimeter-scale variations at infragravity frequencies and centimeter-scale variations at far-infragravity frequencies. These variations in bed elevation are superimposed on larger (tidal-scale) variations in bed elevation in response to an increase in water depth and wave height at the seaward limit of the foreshore (S8). This caused a shift in the point of final wave breaking from the innermost bar to the base of the foreshore and an increase in the relative proportion of infragravity to gravity wave energy (Fig. 11). This control is most evident as the bed rapidly eroded (by ~0.06 m) with the rising tide and an increase in infragravity energy. This variation is consistent with the early observations of Strahler (1966) and the sediment transport ‘shape function’ described by Aagaard and Hughes (2006). An increase in water depth through high tide leads to the translation of the mid- to lower-swash zone, where offshore-directed sediment transport increases and a loss of bed elevation.

The bed elevation changes at both infragravity and far-infragravity frequencies (Fig. 10), appears to be associated with the time-varying balance of infragravity to gravity wave energy. Wavelet analysis suggests that erosion is associated with an increase in infragravity wave energy, which is in turn associated with an increase in water level and a landward translation of the swash zone. These observed low-frequency oscillations in bed elevation are similar to the oscillations described in previous studies of bed elevation change. McDermott and Sherman (in

press) present bed elevation oscillations on the order of 1 to 1.5 cm with periods of 300 s, while Sallenger and Richmond (1984) observed oscillations over much longer periods (6-15 minutes). In the latter study it was suggested that the oscillations were associated with either shelf waves or sieche waves with a period on the order of 10 minutes. The relationship between changes in bed elevation and the relative balance of infragravity and gravity wave energy in the present study suggests that these quasi-periodic oscillations are associated with (time-localized) changes in the incident wave field that leads to a translation of the swash zone.

The translation of the swash zone caused by the time-varying balance between infragravity and gravity wave energy leads to changes in the shape and velocity distribution of the advancing swash bore. Erosion is associated with steeply faced swash bores that have a strong suspension potential (u^3) during the uprush and a seaward-directed advection of sediment with the time-averaged velocity (Fig.s 8). In contrast, accretion tends to be associated with smaller more-symmetrical swash bores that have a relatively strong suspension potential during the uprush and a time-averaged velocity that would transport advected sediment landward. Balancing the bed elevation change with the suspension potential suggested that the amount of advected sediment to and from S4 was on the same order of magnitude as the amount of sediment estimated to be locally suspended. The importance of non-local sediment being advected from the point of bore collapse has been noted in several recent studies (e.g. Hughes et al., 1997; Puleo and Holland, 2003; Butt et al., 2004; Jackson et al., 2004; Pritchard and Hogg, 2005). Jackson et al. (2004) and Butt et al. (2005) argue that bore turbulence and sediment advection is more important on steep beaches, particularly when hydraulic jumps develop at the end of the preceding backwash. The landward decrease in the predicted fall velocity of bed sediment suggests that a large part of the sediment trapped in the upper swash (above S3) is advected from the point of bore collapse (see Jackson et al., 2004). This is consistent with the coarsening of bed sediment in the lower and mid-swash through high tide and a decrease in mean grain size as tide levels begin to fall.

The observed importance of advected sediment to bed elevation change is an obvious reason for the inability of traditional energetics-type transport models to predict sediment transport and morphological change. Butt et al. (2005) also noted stronger relationship between energetic model and actual transport during events on more gently sloped beaches and poor relationships on steep beaches where bore turbulence is important in sediment transport. In the present study it is found that the amount of advected sediment is more important under accretional waves when

the time-averaged velocity is onshore. The amount of advected sediment to balance bed elevation change under erosional waves is considerably less leading to an improved, but not statistically significant, relationship between the oscillatory skewness and the bed elevation change. The sediment that is advected landward by these "erosional" waves may be deposited with the decrease in flow velocity but are resuspend by the backwash and provide a partial balance to the sediment removed by the accelerating flow. The lack of free surface turbulence in the backwash makes it unlikely that sediment would be advected from the upper-swash during backwash and that steep beaches represent a balance between sediment advected with the uprush and locally resuspended sediment in the backwash. This partly supports the conclusion by Aagaard and Hughes (2006) that "there is little value in continuing to pursue energetics-type transport model". More importantly it suggests that bed elevation change is a balance between the upward suspension potential (S) and the amount of sediment settling out of the water column. In this respect, sediment is still locally resuspended by the higher order moments of the flow, but the relationship between the local hydrodynamic gradients and bed elevation change is masked by the advection of sediment.

6. Conclusions

This study examines the wave-scale changes in bed elevation in the high tide swash zone of an intermediate foreshore using ultrasonic distance sensors that are capable of measuring sub-millimeter changes in bed elevation. A number of conclusions can be made from the results of this field study:

1. Changes in bed elevation within the upper swash zone of this intermediate beach are a balance between the upward suspension potential (S) and the amount of sediment settling out of the water column after being advected landward with the advancing swash.
2. Bed accretion is associated with swash bores having a relatively strong suspension potential during the uprush and the landward advection of sediment with the time-averaged velocity. The advected sediment is able to balance the amount of sediment entrained and transported seaward by the backwash.
3. Erosion is associated with breaking at the seaward limit of the swash zone and steeply faced swash bores that have a strong suspension potential during the uprush but a seaward-directed

transport of sediment with the time-averaged velocity. The amount of sediment advected landward with the advancing swash is unable to balance the amount of sediment removed by the backwash.

4. The time-varying balance between gravity and infragravity wave energy within the swash zone leads to low-frequency oscillations in bed elevation that are not directly related to the incident wave field.

7. Acknowledgements

This study was supported by in part by grants from the National Park Service (P5320060026) and Florida Sea Grant (NA06OAR4170014**)**. Field assistance was provided by Gemma Barrett and Tim Brunk from Texas A&M and by Tanya Gallagher, Fritz Langerfeld and Klaus Meyer-Arendt from the University of West Florida. Jean Ellis is thanked for her insightful comments on early draft of the manuscript and assistance in the field.

8. References

Aagaard, T. and Hughes, M.G., 2006. Sediment suspension and turbulence in the swash zone of dissipative beaches. Marine Geology, 228(1-4): 117-135.

Armbruster, C.K., 1997. Morphologic responses of a low-energy, micro-tidal beach to winter cold front passages: north shore Santa Rosa Island, Florida. MS thesis, Department of Geography and Anthropology, Louisiana State University, Baton Rouge, La, 70803, 166 pp.

Austin, M.J. and Masselink, G., 2006. Observations of morphological change and sediment transport on a steep gravel beach. Marine Geology, 229(1-2): 59-77.

Baldock, T.E., Holmes, P. and Horn, D.P., 1997. Low frequency swash motion induced by wave grouping. Coastal Engineering, 32(2-3): 197-222.

Baisillie, J.H., 1975. Analysis and interpretation of LEO and profile data along the western Panhandle coast of Florida. CERC Tech. Mere., 49.

Beach, R.A. and Sternberg R.W., Infragravity-driven suspended sediment transport in the swash, inner and outer surf zones. In: N.C. Kraus, K.J. Gingerich and D.L. Kriebel, Editors, *Coastal Sediments '91*, ASCE, New York (1991), pp. 114–128

Butt, T. and Russell, P., 1999. Suspended sediment transport mechanisms in high-energy swash. Marine Geology, 161(2-4): 361-375.

Butt, T. and Russell, P., 2005. Observations of hydraulic jumps in high-energy swash. Journal of Coastal Research, 21(6): 1219-1227.

Butt, T., Russell, P., Puleo, J. and Masselink, G., 2005. The application of Bagnold-type sediment transport models in the swash zone. Journal of Coastal Research, 21(5): 887-895.

Butt, T., Russell, P., Puleo, J., Miles, J. and Masselink, G., 2004. The influence of bore turbulence on sediment transport in the swash and inner surf zones. Continental Shelf Research, 24(7-8): 757-771.

Carlson, C.T., 1984. Field studies of run-up on dissipative beaches. Proc. 19th Int. Conf. Coastal Eng., ASCE, New York, 399–414.

Conley, D.C. and Griffin, J.G., 2004. Direct measurements of bed stress under swash in the field. Journal of Geophysical Research-Oceans, 109(C3).

Cox, D.T. Hobensack W. and Sukumaran, A., 2000. Bottom stress in the inner surf and swash zone, *Proc. Int. Conf. Coastal Eng.*, ASCE, Sydney.

DUNCAN, J.R., JR., 1964. The effects of water table and tide cycle on swash-backwash sediment distribution and beach profile development. *Marine Geology*, 2, 186-197.

Guza, R.T. and Thornton, E.B., 1982. Swash Oscillations on a natural beach. Journal of Geophysical Research-Oceans and Atmospheres, 87(NC1): 483-491.

Holman, R.A. and Sallenger, A.H., 1985. Setup and swash on a natural beach. Journal of Geophysical Research-Oceans, 90(NC1): 945-953.

Horn, D. and Li, L., 2006. Measurement and modeling of gravel beach groundwater response to wave run-up: Effects on beach profile changes. Journal of Coastal Research, 22(5): 1241-1249.

Houser, C., and Hamilton, S., in press. Post-hurricane beach and dune recovery. Accepted to *Earth Surface Processes and Landforms*, April 2008.

Houser**,** C., Hapke, C. and Hamilton, S., 2008. Controls on Coastal Dune Morphology, Shoreline Erosion and Barrier Island Response to Extreme Storms. *Geomorphology*, 100, 223-240.

HOWD, P.A. and HOLMAN, R.A., 1987. A simple model of beach foreshore response to long period waves. *Marine Geology*, 79, 1-22.

Hughes, M.G. and Baldock, T.E., 2004. Eulerian flow velocities in the swash zone: Field data and model predictions. Journal of Geophysical Research-Oceans, 109(C8).

Hughes, M.G., Masselink, G. and Brander, R.W., 1997. Flow velocity and sediment transport in the swash zone of a steep beach. Marine Geology, 138(1-2): 91-103.

HSU, T.W., TSENG, I.F., and LEE, C.P., 2006. A new shape function for bar-type beach profiles. *Journal of Coastal Research*, 22, 728-736.

Jackson, N.L., Masselink, G. and Nordstrom, K.F., 2004. The role of bore collapse and local shear stresses on the spatial distribution of sediment load in the uprush of an intermediate-state beach. Marine Geology, 203(1-2): 109-118.

Kobayashi, N. and Johnson, B.D., 2001. Sand Suspension, Storage, Advection and Settling in Surf and Swash Zones, Journal of Geophysical Research, 106(C5), 9363-9376.

Mase, H., 1988. Spectral characteristics of random wave run-up. *Coastal Engineering* **12**, pp. 175–189

Mase, H., 1995. Frequency down-shift of swash oscillations compared to incident waves.

Journal of Hydraulic Research, 33(3): 397-411.

Masselink, G., Evans, D., Hughes, M.G. and Russell, P., 2005. Suspended sediment transport in the swash zone of a dissipative beach. Marine Geology, 216(3): 169-189.

Masselink, G. and Hughes, M., 1998. Field investigation of sediment transport in the swash zone. Continental Shelf Research, 18(10): 1179-1199.

Masselink, G. and Russell, P., 2006. Flow velocities, sediment transport and morphological change in the swash zone of two contrasting beaches. Marine Geology, 227(3-4): 227-240.

McDermott, J.P., and Sherman, D.J., in press. Using photo-electronic erosion pins for measuring bed elevation changes in the swash zone. Accepted to Journal of Coastal Research, May 2008.

NORDSTROM, K.F., 1980. Cyclic and seasonal beach response: a comparison of ocean and bayside beaches. *Physical Geography* 1, 177–196.

Nordstrom, K.F. and Jackson, N.L., 1990. Migration of swash zone, step and microtopographic features during tidal cycles on an estuarine beach, Delaware Bay, New Jersey, USA. Marine Geology, 92(1-2): 147-154.

Osborne, P.D. and Rooker, G.A., 1999. Sand re-suspension events in a high energy infragravity swash zone. Journal of Coastal Research, 15(1): 74-86.

Pritchard, D. and Hogg, A.J., 2003. On fine sediment transport by long waves in the swash zone of a plane beach. Journal of Fluid Mechanics, 493: 255-275.

Pritchard, D. and Hogg, A.J., 2005. On the transport of suspended sediment by a swash event on a plane beach. Coastal Engineering, 52(1): 1-23.

Puleo, J.A., Beach, R.A., Holman, R.A. and Allen, J.S., 2000. Swash zone sediment suspension and transport and the importance of bore-generated turbulence. Journal of Geophysical Research-Oceans, 105(C7): 17021-17044.

Puleo, J.A. and Holland, K.T., 2001. Estimating swash zone friction coefficients on a sandy beach. Coastal Engineering, 43(1): 25-40.

Puleo, J.A., Holland, K.T., Plant, N.G., Slinn, D.N. and Hanes, D.M., 2003. Fluid acceleration effects on suspended sediment transport in the swash zone. Journal of Geophysical Research-Oceans, 108(C11).

Raubenheimer, B. and Guza, R.T., 1996. Observations and predictions of run-up. *J. Geophys.*

Res. **101**, pp. 25575–2558

Raubenheimer, B., Guza, R.T., Elgar, S. and Kobayashi, N., 1995. Swash on a gently sloping beach. Journal of Geophysical Research-Oceans, 100(C5): 8751-8760.

SALLENGER, A.H. and RICHMOND, B.M., 1984. High-frequency sediment level oscillations in the swash zone. *Marine Geology*, 60, 155-164.

SHEPARD, F.P., 1950. *Beach Cycles in Southern California*. US Army Corps of Engineers, Beach Erosion Board Technical Memorandum No. 20, pp. 31.

Sherman, D.J. and Bauer, B.O., 1993. Dynamics of beach-dune systems. Progress in Physical Geography, 17, 413-447.

SHORT, A.D. and TREMBANIS, A.C., 2004. Decadal scale patterns in beach oscillation and rotation, Narrabeen Beach, Australia – time series, PCA and wavelet analysis. *Journal of Coastal Research*, 20, 523-532.

STRAHLER, A.N., 1966. Tidal cycle of changes in an equilibrium beach, Sandy Hook, New Jersey. *Journal of Geology*, 62: 1-12.

Stone, G.W., Stapor, F.W., Jr., May, J.P., Morgan, J.P., 1992. Multiple sediment sources and a cellular, non-integrated, longshore drift system: Northwest Florida and southeast Alabama coast, USA. Marine Geology 105, 141-154.

TURNER, I.L., RUSSELL, P., and BUTT, T., 2006. Swash zone bed-level measurements at wave-by-wave frequencies. International Conference on Coastal Engineering 2006, Submission 1427, 2 pp.

Waddell, E., 1976. Swash–groundwater–beach profile interactions. In: Davis, R.A., Etherington, R.L. (Eds.), Beach and nearshore sedimentation. SEPM Spec. Publ., 24, 115–125.

Table 4. Mean grain size (mm) and predicted fall velocity (m s^{-1}) for rising, high and falling tide collected adjacent to stations 1, 3, 5 and 7.

	Rising Tide (8:35)		High Tide (11:20)		Falling Tide (13:35)	
	d (mm)	*w* (m s^{-1})	d (mm)	*w* (m s^{-1})	d (mm)	*w* (m s^{-1})
S1	0.31	0.043	0.30	0.042	0.29	0.041
S3	0.34	0.046	0.31	0.044	0.30	0.042
S5	0.36	0.047	0.38	0.049	0.33	0.045
S7	0.37	0.048	0.48	0.057	0.40	0.050

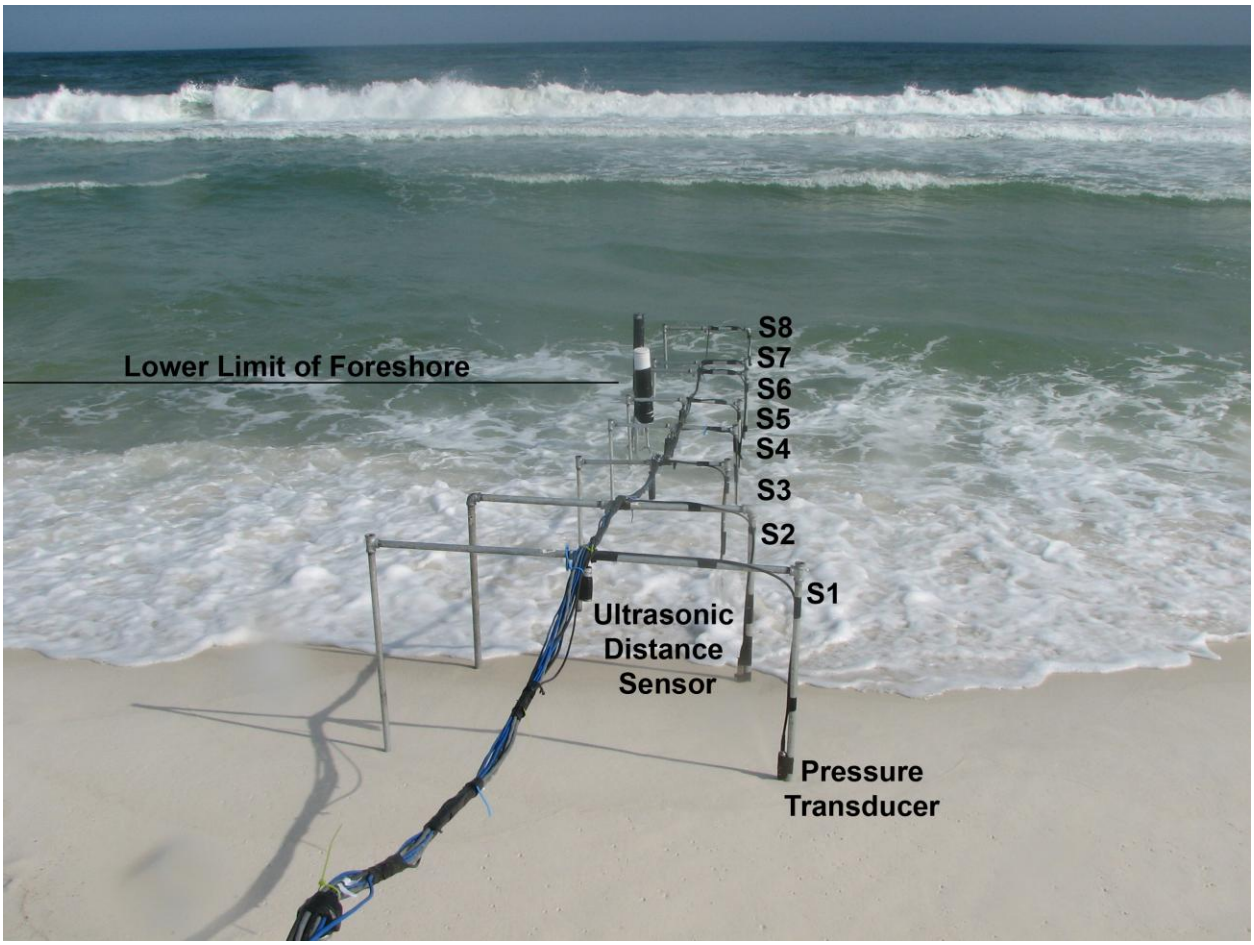


Figure 57. Photograph showing cross-shore deployment of pressure transducers (S1-S8) and ultrasonic distance sensors (S1-S4). Note that the stations are spaced at ~ 1 m intervals from the lower limit of the foreshore.

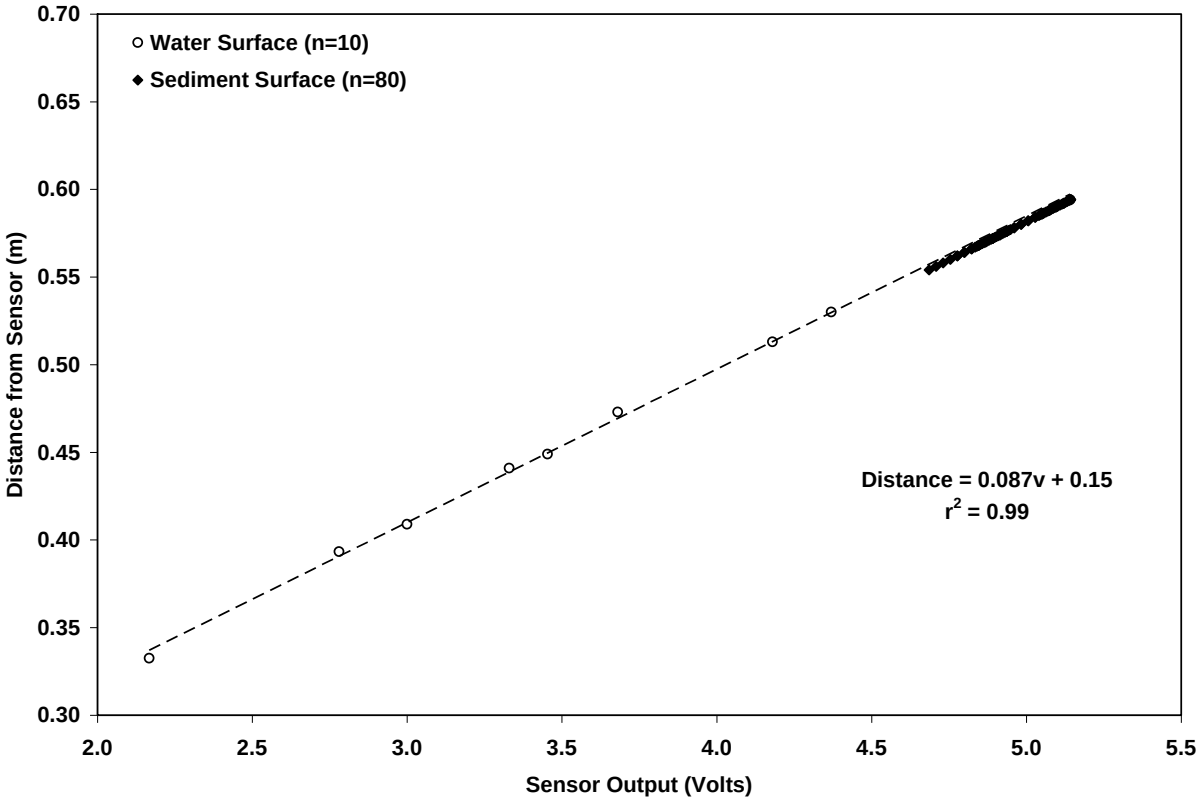


Figure 58. Scatterplot and combined calibration equation relating sensor output to measured distance between the ultrasonic distance sensor and sediment and water surface.

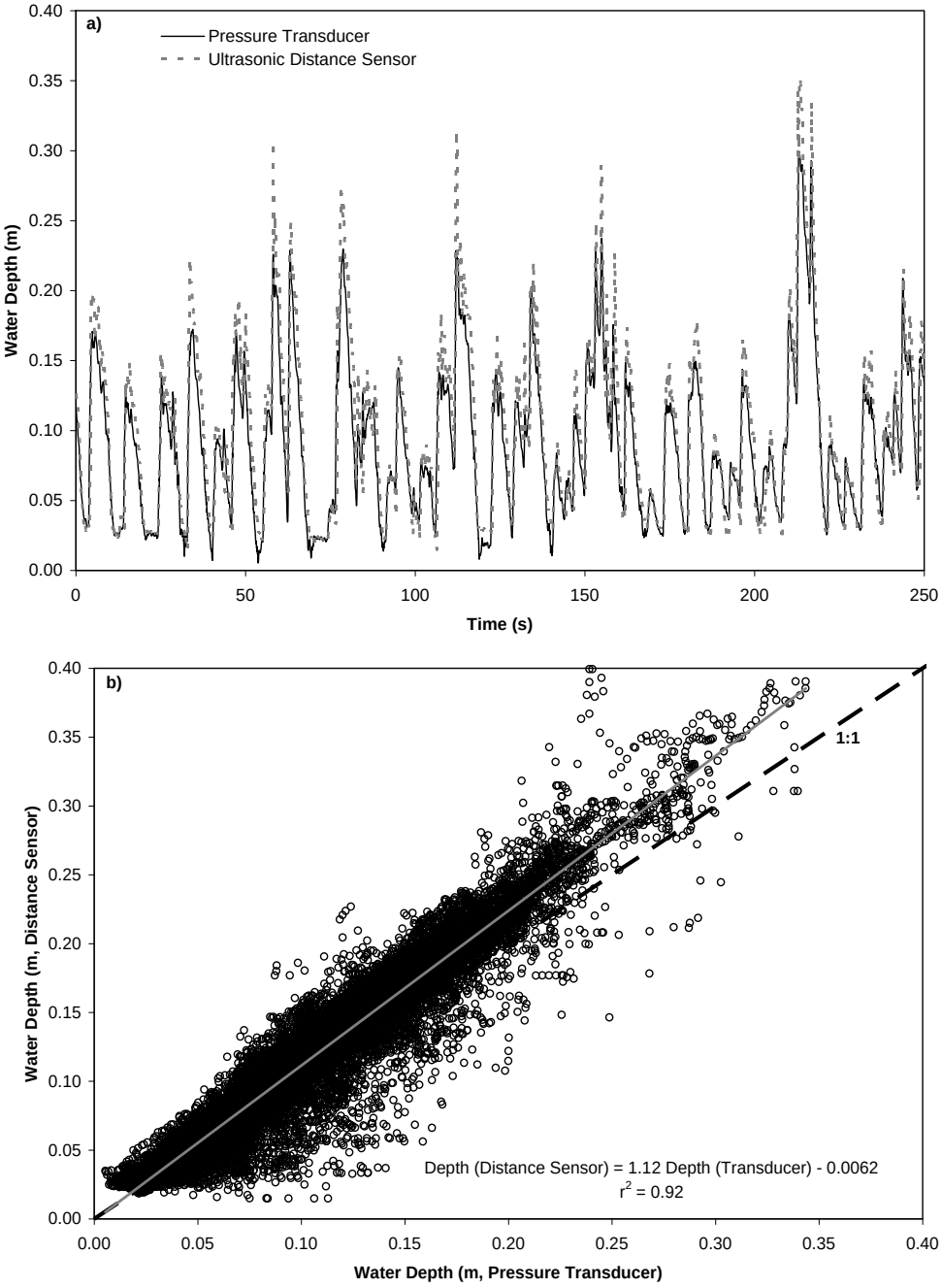


Figure 59. Time series of pressure transducer and ultrasonic distance sensor measurements of water depth. Also shown (b) is a scatterplot of the water depth measurements from both sensors over a representative burst sample.

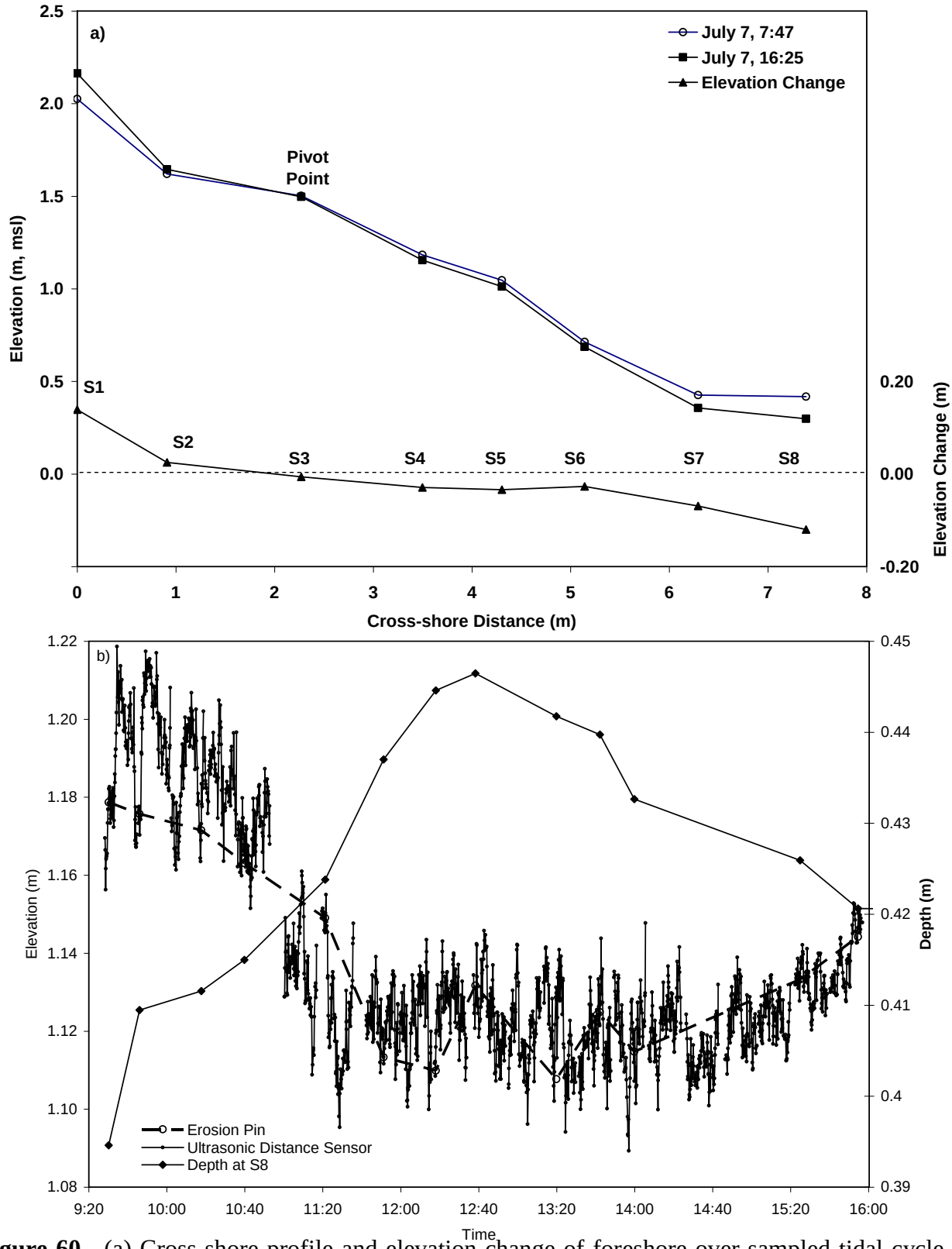


Figure 60. (a) Cross-shore profile and elevation change of foreshore over sampled tidal cycle and (b) time series of elevation changed at S4 as measured using the ultrasonic distance sensor and the station post.

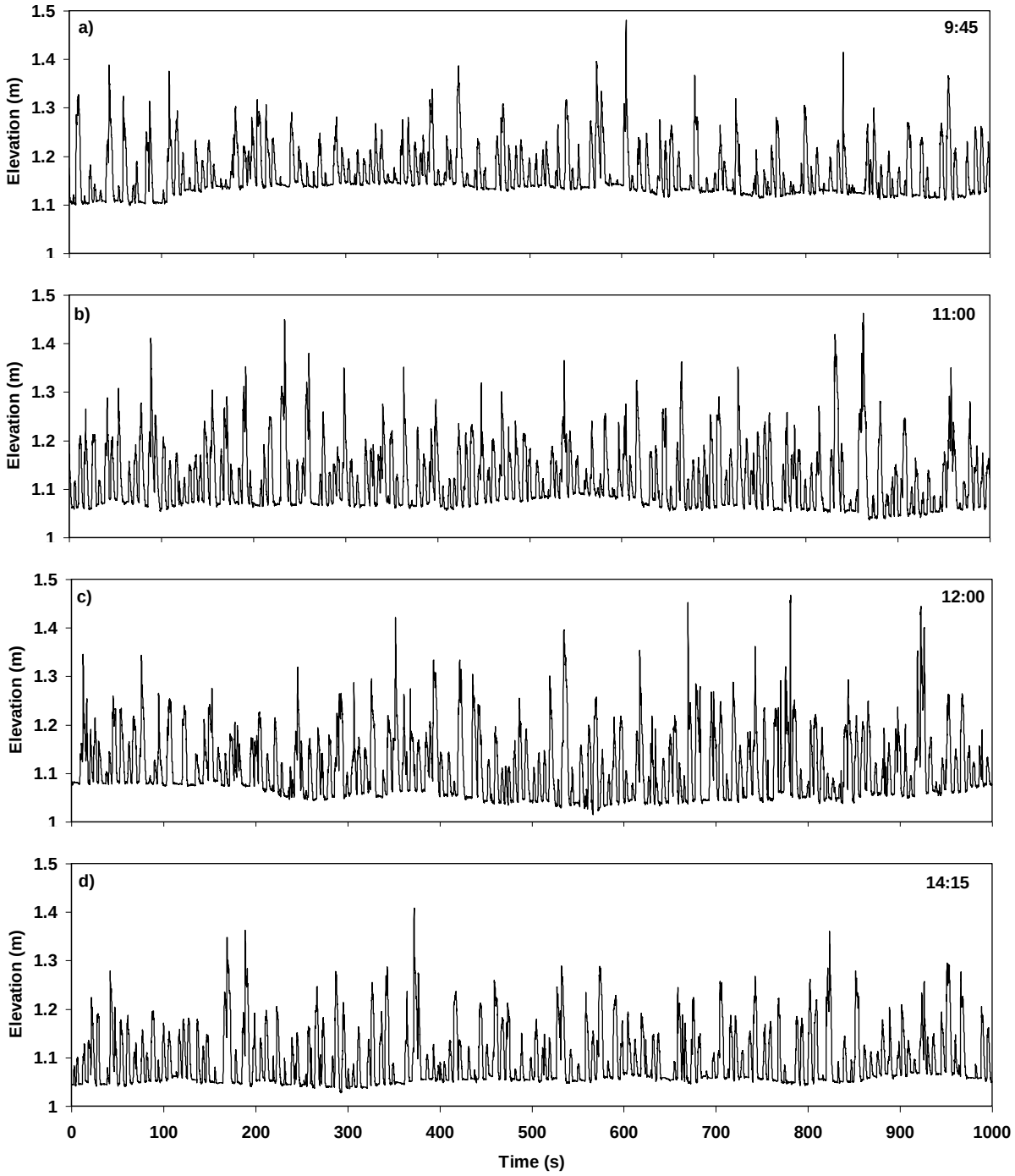


Figure 61. Representative time series of bed elevation and swash depths from ultrasonic distance sensor at Station 4 (S4). Shown are time series from (a) rising, (b,c) high and (d) falling tide.

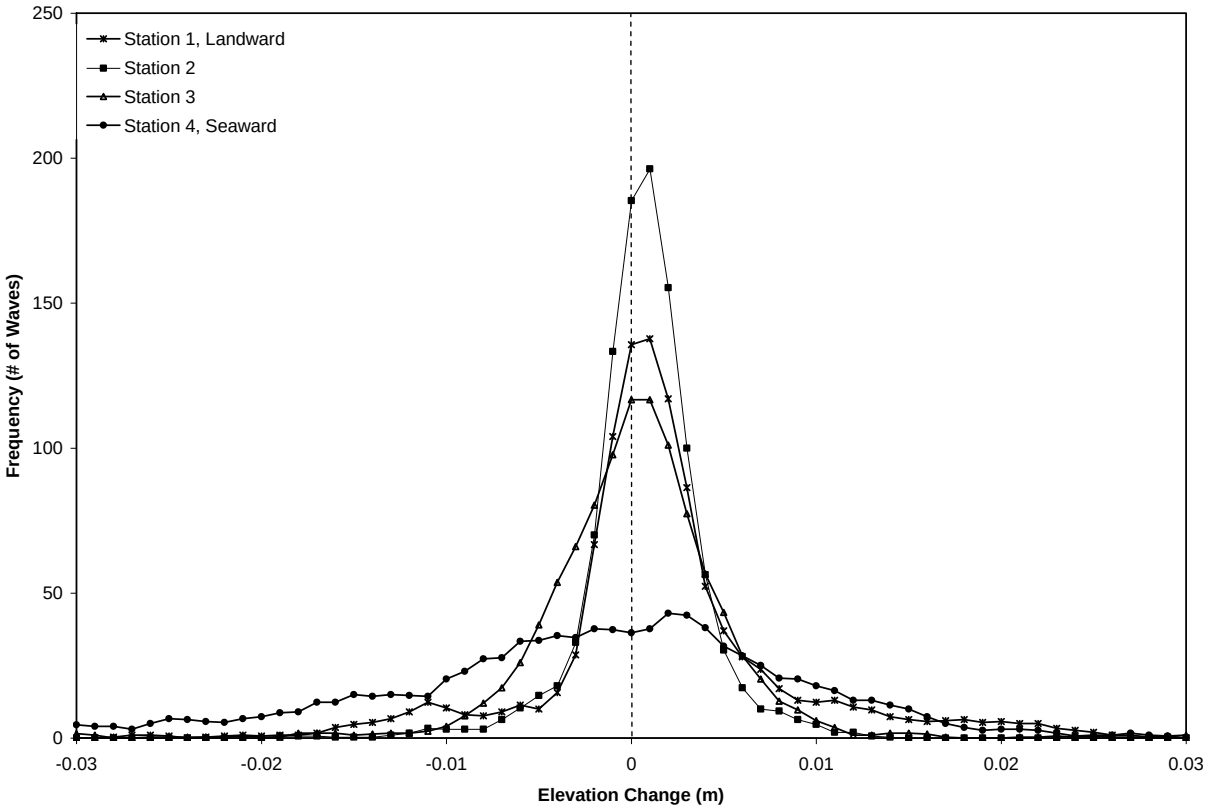


Figure 62. Histogram of elevation change measured by the ultrasonic distance sensors following passage of all swash events over the sampled tidal cycle.

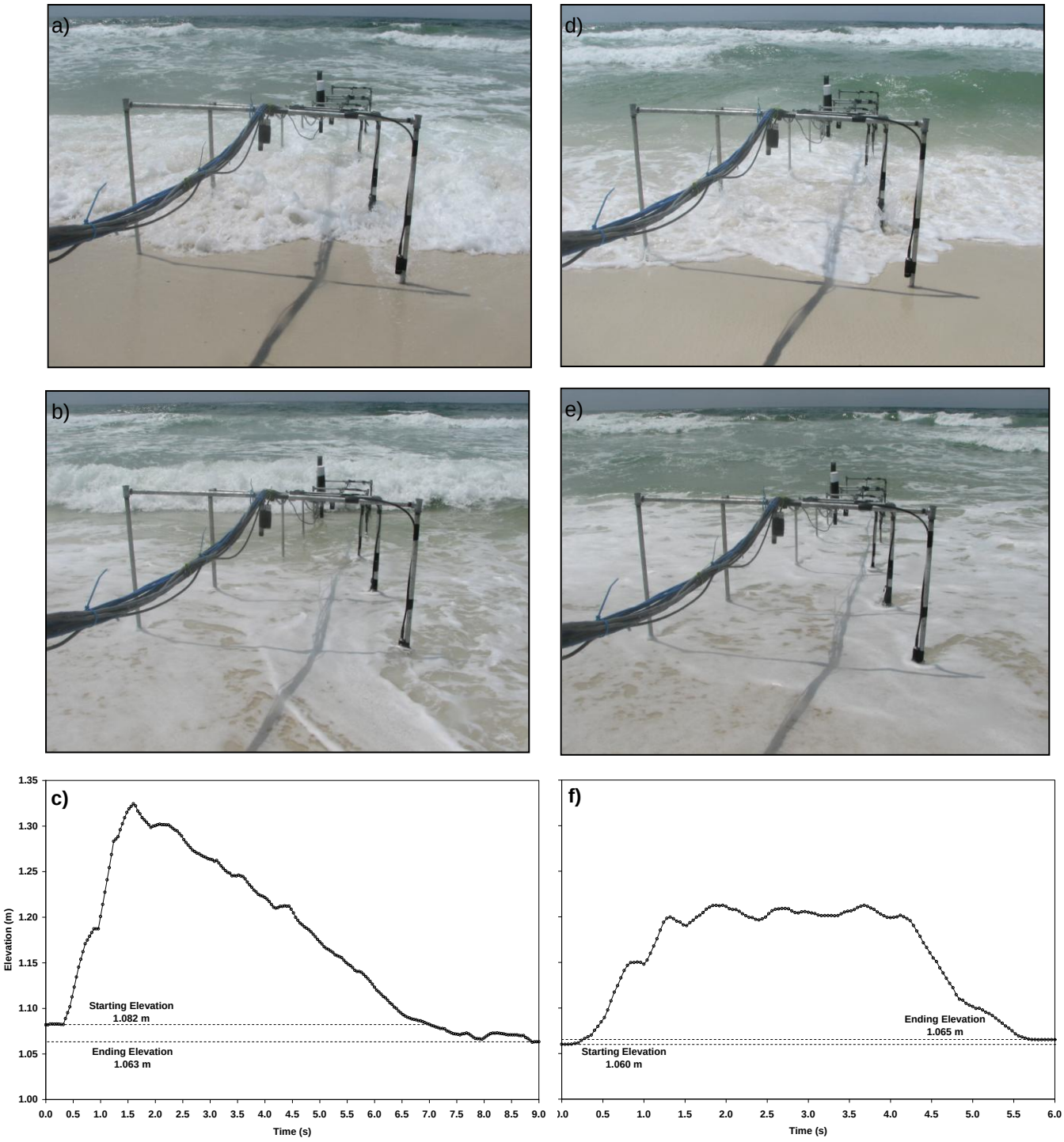


Figure 63. Sequential photographs showing uprush and start of backwash for (a,b) an erosional wave and (d,e) an accretional wave. Also shown are the time series of bed and water level elevation for both waves measured at high tide.

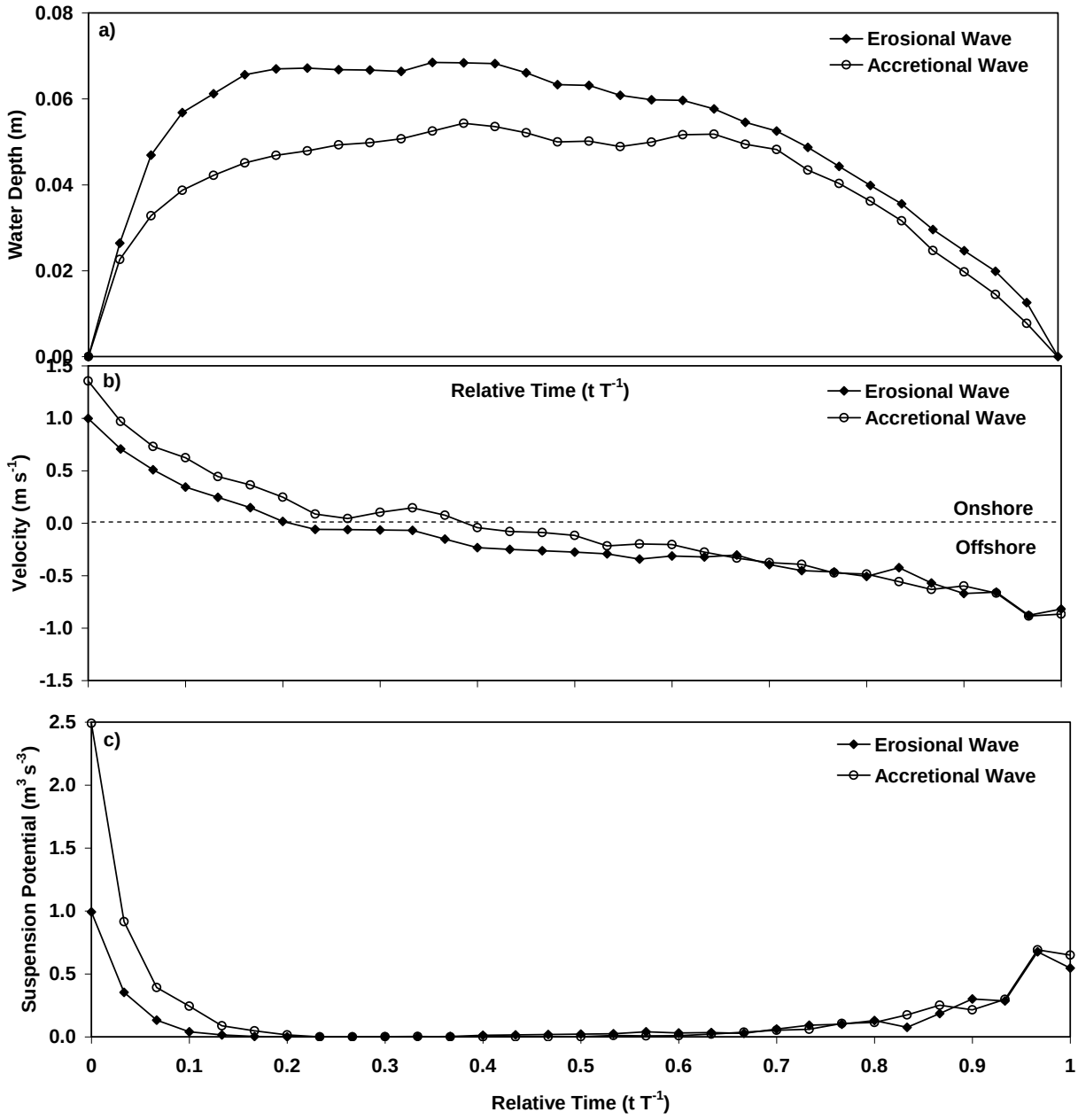


Figure 64. Normalized and ensemble averaged time series of (a) water depth, (b) depth-averaged velocity and (c) upward suspension potential at S4 averaged over 'erosional' and 'accretional' waves.

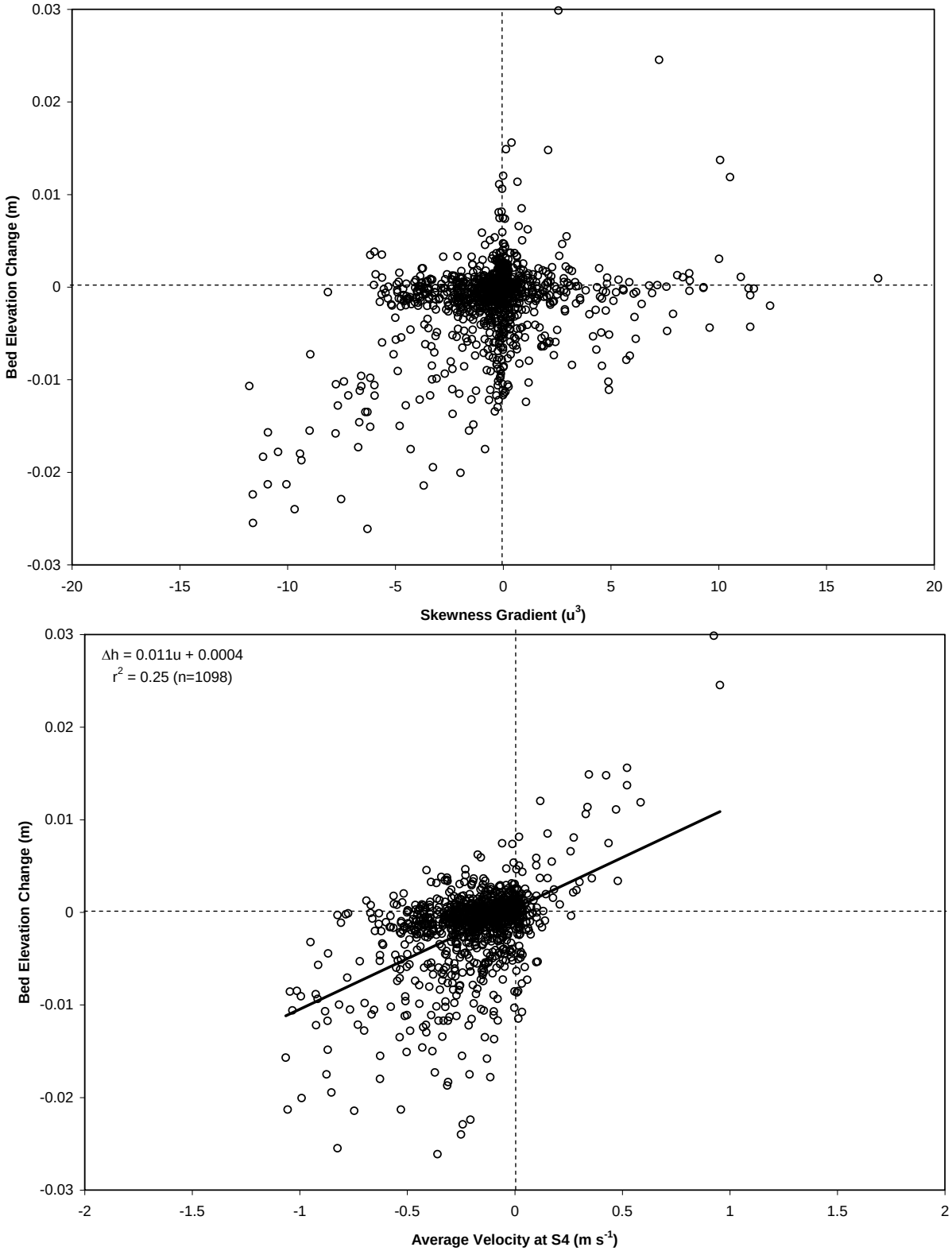
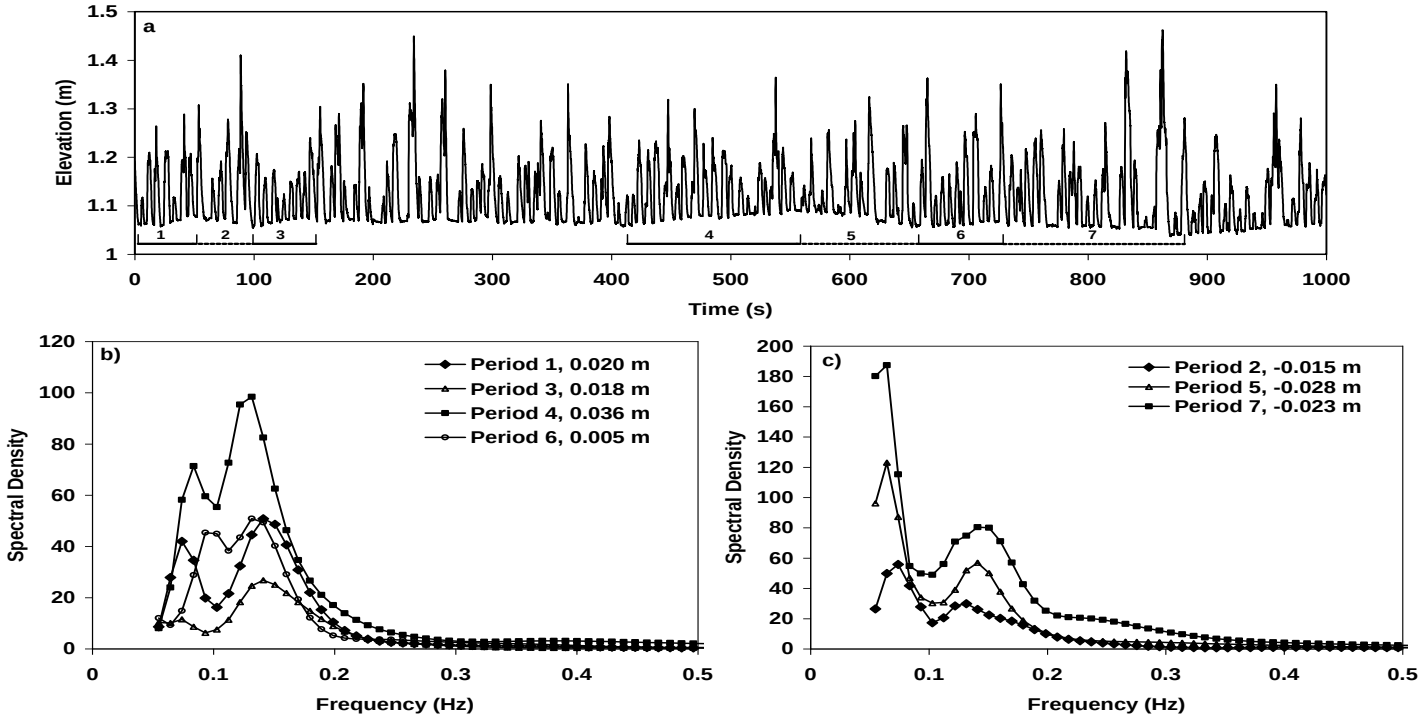


Figure 65. Scatterplots of bed elevation change relative to (a) skewness gradient across S4 and the local average velocity at S4.

Figure 66. Representative time series of bed elevation and swash excursion with wavelet spectra shown in the inset graphs.



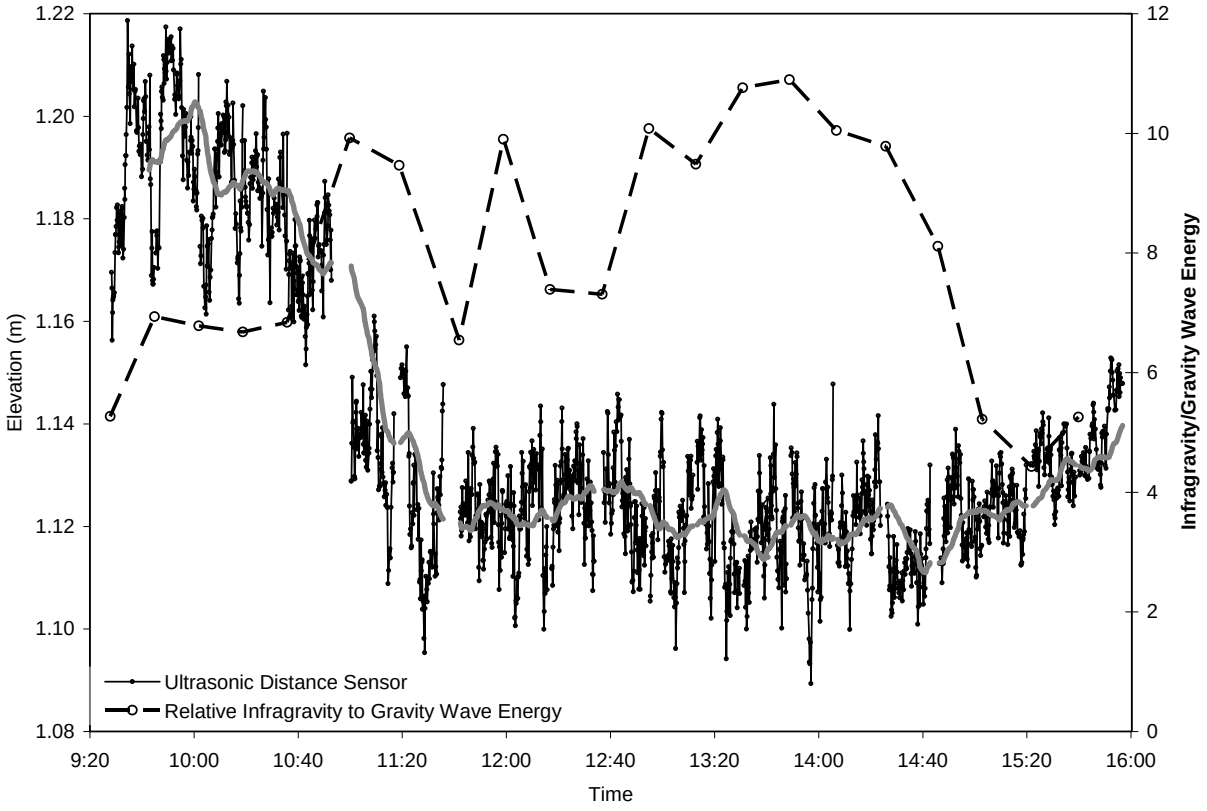


Figure 67. Variation in the relative importance of infragravity to gravity wave energy along with the variation in bed elevation and a 75 point running mean of bed elevation.

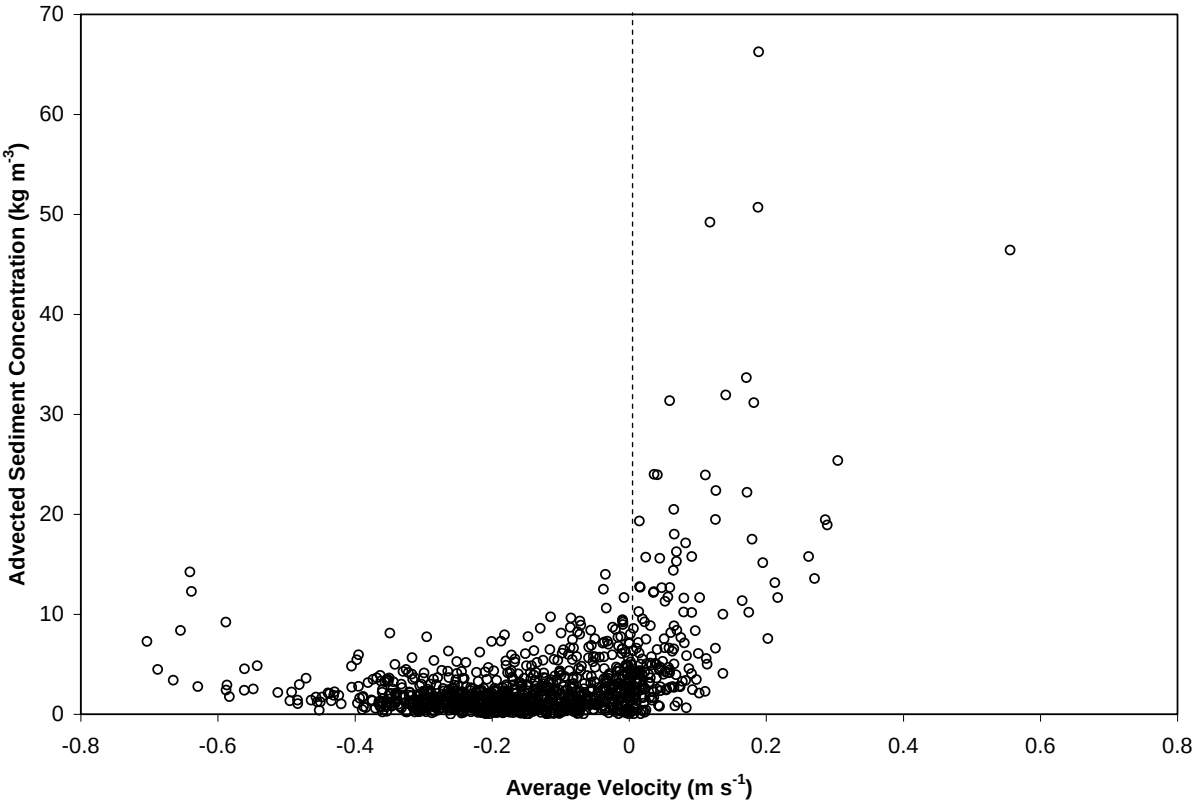


Figure 68. Scatterplot showing relationship between the local average velocity and the concentration of advected sediment predicted based on the balance of elevation change and upward suspension potential.

CHAPTER 6

Feedback between Ridge and Swale Bathymetry and Barrier Island Transgression

Chris Houser
Department of Geography
Texas A&M University
810 O&M Building
College Station, Texas
77843-3147

Abstract

As demonstrated in a number of recent studies, the shoreface of Santa Rosa Island in northwest Florida is characterized by a ridge and swale bathymetry that force an alongshore variation in beach and dune morphology. The alongshore variation in dune morphology in turn controls island response to and recovery from tropical storms and hurricanes, and is therefore, an important control on island transgression with relative sea level rise. A combination of field sampling, modeling and remote sensing is used in the present study to describe the geologic framework of Santa Rosa Island and to elucidate on the origins and maintenance of the shore-attached ridge and swale bathymetry. Shore-parallel seismic surveys reveal strong near-horizontal reflectors through the ridges at depths consistent with thick backbarrier muds extracted from vibracores taken across and along the ridges. Near-horizontal reflectors were also identified in ground-penetrating radar (GPR) surveys between the ridges and backbarrier cuspate headlands, but were not present in the narrow sections of the island landward of the swales. Continuation of the seismic surveys in the backbarrier also reveal near-horizontal reflectors at the cuspate headlands that are characterized by seagrass beds, salt marsh and maritime forest, and an absence of horizontal reflectors between headlands where the shoreline is dominated by washover deposits. Wave modeling suggests that the cuspate headlands are the littoral endpoints for sediment eroded from the washover fans during frontal storms and transported alongshore as transverse bars. It is argued that the ridge and swale bathymetry is a transgressive surface resulting from the cuspate headlands along the backbarrier shoreline. Results of the wave modeling further suggest that the ridge and swale bathymetry is maintained through the transport of sediment from the swales to the ridges during large storms. In this respect, maintenance of the ridge and swale morphology reinforces the position of the backbarrier cuspate headlands ultimately responsible for the development of the ridge and swale morphology of the shoreface. The alongshore variation in beach and dune morphology on this island is the expression of this large-scale feedback and suggests a tow-down model in which meso-scale processes and landforms depend on the geologic context.

Keywords: *Ridge and swale, Island transgression, Hurricane, Barrier Island*

1. Introduction

Barrier islands are elongated accumulations of sediment found along 13% of the world's coastlines (Dean and Dalrymple, 2002), mostly in areas with a small tidal range and an abundance of sediment (Davis and Fitzgerald, 2002). For the most part, modern barrier islands are inherited features that represent the time-integrated deposition of past beach, backshore and dune environments and are perched on older, eroding layers deposited by shelf and land-based processes (Riggs *et al.*, 1995). Pre-modern features on the inner shelf, such as ancient drainage systems and inlet channels, modify waves and currents, and thereby control patterns of sediment erosion, transport, and deposition along the barrier island shoreline (e.g. Schupp and McNinch, 2006). As a result, these inherited features also control barrier island response to extreme storms, and in turn the rate of island transgression to changes in sediment supply or an increase in mean sea level. Island transgression with rising sea levels is accomplished during storms capable of overtopping or breaching the dunes washing sediment to the backbarrier shoreline in the form of washover fans and terraces. As sea level rises, the threshold surge required for the dunes to be overtopped or breached decreases, and the probability of island overwash and island transgression increases. A lower threshold is also required for island transgression where dunes lack height, creating the potential for rapid transgression and even overstepping. Alongshore variability in dune height can lead to lateral dune erosion from the washover conduits that develop early in the storm where the dune height is low. Washover is limited and transgression becomes episodic where dunes are well developed and continuous alongshore, leading to extended periods of dune growth and island stability.

It follows from the above, that the rate of island transgression depends on the probability distribution and realized sequencing of storm surge events relative to the height and extent of the foredunes (see Sallenger, 2000; Masetti *et al.,* 2008). The height of the dune at storm landfall depends on the time since the last storm, the level of damage sustained in that storm and the rate of post-storm dune recovery (Houser and Hamilton, 2009). The rate of recovery is in turn dependent to varying degrees on the regional sediment budget (Psuty, 1992), and the ability of sediment to be transported from the beach and backshore to the dune (Short and Hesp, 1982). In general, dune development is promoted on wide dissipative beaches where boundary layer adjustment is at a minimum (Short and Hesp, 1982), and the aeolian fetch length is at a

maximum (Bauer and Davidson-Arnott, 2003). Dune recovery starts with the recovery of the beachface and backshore, through the landward migration of nearshore bars and their welding to the beachface (Leadon *et al.*, 1999), and possibly the recovery of burial tolerant vegetation (Stone *et al.*, 2004). The time required for dune recovery to its pre-storm height depends, in part, on the level of storm impact (Sallenger, 2000), and can take up to a decade where an island experiences extensive washover and erosion (Stone *et al.*, 2004). In this respect, rapid transgression can occur when and where storms occur in quick succession (see Houser and Hamilton, 2009).

This simple two-dimensional description of island transgression is often used for modeling purposes (e.g. Masetti *et al.*, 2008), but is complicated by alongshore variations in dune height, island width and storm surge. For example, the dunes at Cape Hatteras vary in height by up to 8 m at alongshore length scales from kilometers to tens of kilometers (Elko *et al.*, 2002), leading to an alongshore variable storm impact (Wetzell, 2003). While Stallins and Parker (2003) suggest that frequent and extensive overwash can reinforce a mosaic of dunes of varying age and composition through a biogeomorphic feedback, recent evidence suggests that the alongshore variability is forced by bathymetric variations on the inner-shelf (Houser *et al.*, 2008; Lentz and Hapke, 2011; Houser and Mathew, 2011). In a further example, the ridge and swale bathymetry fronting the dissipative beach of Padre Island, Texas is responsible for an alongshore variation in storm impact and post-storm recovery, with the largest dunes found landward of the swales and the smallest dunes landward of the ridges (Houser and Mathew, 2010). In contrast, the largest dunes on the more reflective Santa Rosa Island in northwest Florida are fronted by ridges, and the smallest dunes on the island are fronted by swales (Houser *et al.*, 2008). The ridge and swale topography of Padre Island affects the amount of sediment available to the backshore and dune, while a similar bathymetry determines the nearshore state and the aeolian transport potential on Santa Rosa Island. This bathymetric variation can also force alongshore variations in storm surge and creates erosion hotspots along the Outer Banks (Stockdon *et al.*, 2007), and locally supplies sediment to the shoreface at Fire Island (Lentz and Hapke, 2011).

Shoreface ridges and swales are common features on the continental shelf of the Atlantic seaboard (Duane *et al.*, 1972; Swift *et al.*, 1972; Field, 1980; Figueiredo *et al.*, 1981; Stubblefield *et al.*, 1984; Swift *et al.*, 1984; McBride and Moslow, 1991; Snedden and

Dalrymple, 1999; Snedden *et al.*, 1999; Robinson and McBride, 2008). In the majority of these studies, the ridge and swale topography has been described as near-perpendicular or oblique sand bodies forming topographic highs separated by swales composed of exposed muds. The transverse ridge and swale bathymetry fronting Santa Rosa Island in northwest Florida was first described by Hyne and Goodell (1967) and subsequently noted by Stone (1984). The ridges and swales are superimposed on lower order Pleistocene features, and appear to be reinforced and possibly even accrete during storms (Vaughan *et al.*, 2009). The features have been likened to the ridge and swale bathymetry of the US Atlantic shelf (see McBride, 1997; McBride *et al.*, 1999) that develop in response to storm waves and currents (Swift *et al.*, 1973). It is hypothesized that wind-forced set-up currents converge in the swale, leading to scour and headward erosion, while flow divergence across the ridge leads to localized sediment accretion. Hutchnance (1982) developed a similar model in which the sand ridge forms where there is an adequate supply of sand and active currents and some initial bathymetric irregularity is of sufficient size to disturb otherwise linear currents. Alternatively McBride and Moslow (1991) suggest that the shoreface sand ridges from New York to Miami Beach first develop as ebb-tidal deltas (see also Figueiredo, 1984), deposited by a tidal inlet that migrates alongshore as the island transgresses. While these different models have yielded significant insight into possible mechanisms for the formation of ridge and swale topography, they do not provide sufficient explanation of how the irregularity first developed, why in some cases the ridges are regularly spaced alongshore (see Houser *et al.*, 2008 and Houser and Mathew, 2010), and why many are not associated with tidal inlets.

Compared to the ridge and swale topography of the Atlantic Coast, the shoreface-attached oblique ridges and swales of northwest Florida have received relatively little attention. A recent survey by Vaughan *et al.* (2009) revealed sand deposition on the ridges and mud-draping in the relatively low-energy swales following Hurricane Ivan. These observations suggest that ridge and swale bathymetry is reinforced during the extreme storms that determine the rate of island transgression and its alongshore variability (see Houser and Hamilton, 2009). The purpose of this study is to use a combination of field sampling, hydrodynamic modeling and remote sensing to develop a conceptual model for the initial formation and persistence of the ridge and swale bathymetry. Based on the observed statistical relationship between the ridges and the backbarrier cuspate headlands (Houser *et al.*, 2008), it is hypothesized that the ridges

have a backbarrier origin and are maintained through storm deposition as the island transgresses over this initial topographic irregularity.

2. Study Site

Santa Rosa Island is a narrow sandy Holocene barrier island extending 96 km from Pensacola Pass in the west to East Pass near Destin (Figure 1). It is the second-longest barrier island on the U.S. Gulf Coast, and is separated from a higher standing barrier complex of late Pleistocene origin by Santa Rosa Sound. The origin of the island was originally attributed to the erosion of a central Pleistocene "core" and longshore redistribution of sediments (Otvos, 1982), but recent evidence suggests an origin from the longshore transport of sediment eroded from a Pleistocene headland east of Destin (Kwon, 1969, Stone, 1991, Stone *et al.,* 1992 and Stone and Stapor, 1996). The similarity of the beach sand to the Pleistocene sediments in grain size and mineralogy further suggests that they were not transported from the Apalachicola River as commonly believed, but from the reworking of the older Pleistocene sediments (Hsu, 1960). Landward transgression of the island through the Holocene draped a trailing sand sheet over the first-order Pleistocene surface (Parker *et al.,* 1992; McBride and Byrnes, 1995), which was reshaped by post-transgressive storm waves and currents. As previously noted, the transgressive sheet is dominated by shore-oblique shelf and shoreface sand ridges and swales lying on shelf-edge lobes formed during the Holocene.

The shoreline of Santa Rosa Island has been eroding at 0.7 and 0.1 m yr^{-1} at the eastern Santa Rosa and western Fort Pickens units respectively (Hapke and Christiano, 2007), in response to a an increase in fetch length and wave energy to the west (Stone *et al.*, 1992). The average annual retreat in both areas of the island is misleading, as the island's shoreline position remained relatively stable from 1920 to 1993, despite hurricanes in 1906, 1916, and 1926 (Foster *et al.*, 1999 and Stapor, 1975). During Hurricane Ivan (2004) alone, the shoreline eroded as much as ~60 m, and as much as ~88 m over the course of the 2005 storm season that included Tropical Storms Arlene and Cindy, and Hurricanes Ivan, Dennis and Katrina (Hapke and Christiano, 2007). Since 1851 northwest Florida has been impacted by 55 hurricanes, 12 of which have been major hurricanes (category 3 or higher). Just in the last 10 years, however, northwest Florida has been directly impacted by 5 hurricanes (Opal, Earl, George, Ivan and

Dennis) and indirectly impacted by Hurricanes Katrina and Rita. The historical and storm-driven retreat of the shoreline is not uniform alongshore, but exhibits a variation coherent with the near-island ridge and swale bathymetry (Houser *et al.*, 2008). The areas of greater erosion landward of the swales have an average retreat of ~1.3 m yr^{-1} in the same areas where the road damage is at a maximum (Houser, 2009) and overwash fans extend to the backbarrier shoreline. Washover deposits that develop during hurricanes and tropical storms are quickly eroded by the frontal winds (Stone *et al.*, 1992), with sediment transported alongshore as transverse bars towards the cuspate headlands.

The shoreface expression of the transverse ridge and swale bathymetry is quite visible in the position of the outermost nearshore bar along Santa Rosa Island (see Houser *et al.*, 2008). The shoreface profile is relatively steep in the swales, forcing the outermost bar closer to the shoreline and responsible for a transverse bar and rip morphology with a steep beachface. Not only does this beach and nearshore state limit the exchange of sediment from beach to dune, leading to small discontinuous dunes, but is a swimming hazard for beach users (Houser *et al.*, in press a,b). The beaches landward of the transverse ridges are more gently sloped and fronted by a relatively dissipative nearshore that promotes the development of larger dunes, which in turn limits washover penetration to the backbarrier shoreline (Houser *et al.*, 2008).

3. Methods

A geologic characterization of the entire Panhandle coastal region of western Florida has previously been carried out as part of a cooperative effort involving the Florida Department of Environmental Protection, the URS Corporation, Florida State University, and the University of South Florida (Balsillie and Clark, 1997; Locker *et al.*, 1988; Donoghue *et al.*, 2003). The data set includes over 3000 sand samples, more than 400 sediment cores, high resolution bathymetry, and over 3000 km of sub-bottom seismic lines. However, this survey is not of sufficient resolution to characterize the ridge and swale bathymetry that controls the response and recovery of the island to extreme storms and ultimately transgression with sea level rise. A combination of field sampling, modeling and remote sensing are used in the present study to describe the geologic framework of Santa Rosa Island and to elucidate on the origins and maintenance of the shore-attached ridge and swale bathymetry during storms.

3.1 Geophysical Survey

A digital sidescan-sonar survey was conducted in April 2005, using a Klein 100 kHz sidescan-sonar system in a shallow-draft vessel maintained by the University of West Florida. The survey provides continuous coverage of the sea floor over a 37 km^2 area of the shoreface and inner shelf. The swath width per trackline was 200 m and tracklines were spaced 100 m apart to provide overlapping coverage. The sidescan-sonar data were logged digitally at a sampling rate that provides a 0.1 m pixel size in the across-track direction following the methodology outlined in Danforth (1997). The data were processed using procedures described in Malinverno *et al.* (1990), Danforth (1997) and Paskevich (1992), resulting in an image-enhanced, geographically correct, sidescan-sonar mosaic of the study area. The short cable-out lengths and moderate wave activity created distinct artifacts in some of the sonar data with vessel heave, particularly in the nearshore (<2 m). To remove water depth variations due to vessel heave and tidal fluctuations, bathymetric data was collected using a hull-mounted fathometer. The vertical resolution of the bathymetric data was ±5 cm. A differential Global Positioning System (DGPS) with real-time correction was used for navigation during the survey resulting in a horizontal accuracy of ± 1 m for the bathymetric data and sample locations. To determine if the ridge and swales are dynamic or static features, the results of the survey are compared to the most recent (pre-Ivan) bathymetric data available from the National Oceanic and Atmospheric Administration (1983).

A high resolution seismic study was performed to characterize the deep geologic structure of the Gulf and sounds. The profiling will be completed with a Benthos Chirp II Subbottom Profiler and a Datasonics CAP-6600 Chirp II Acoustic Profiling System (processor and transceiver). This dual frequency sonar system produces high-resolution profiles of both the shallow and deep subbottom layers. Seismic lines and sonar images will both be processed using the GEO-STAR Full Spectrum Sonar computer program. The shoreface geology was examined on both the Gulf and Sound side of Santa Rosa Island, and was supplemented by ground-penetrating radar surveys along select transects in line with the dominant ridge and swale bathymetry.

3.2 Vibracores

The acoustic survey was supplemented by 84 sediment cores taken with a model 271 B Alpine Pneumatic Vibracore to an average depth of 20 feet. The vibracore were deployed on a boat with shallow-draft allowing samples to be taken within ~1 m of the shore. Vibracores were taken at 3 of the most prominent ridge and swale systems at Pensacola Beach and to the east and west in the Gulf Islands National Seashore. All cores were digitally scanned for sediment and facies analysis and sediment samples were taken at equal intervals along the core, with additional samples taken at changes in lithology and to ground truth the acoustic facies identified on the imagery. Grain size analyses of all sediment samples were conducted using a combination of wet sieve and Coulter Counter techniques following the methodology of Poppe *et al.* (1985).

3.3 Ground-penetrating Radar

The geophysical survey was extended across the barrier island using ground-penetrating radar (GPR). Specifically, a Geophysical Survey Systems Inc. SIR-3000 GPR with a 400 MHz antenna was used along representative transects landward of the ridge and swale features in the wide and narrow sections of the island respectively. The survey was conducted in summer 2009 when the dune field had yet to recover from the 2004/2005 hurricane season and the island morphology was near-horizontal with the exception of the beachface, berm and isolated hummocks with heights of <1 m. The GPR surveys were conducted from mean sea level along the Gulf of Mexico shoreline to the backbarrier shoreline in the narrow sections of the island and to the seaward (southern) edge of the maritime forest at the cuspate headlands.

3.4 Wave Model

The response of the transverse ridge and swale bathymetry to extreme storms and their role in controlling shoreline change is examined using a spectral wave and current model (MiKE21), which can also be used to predict sediment transport and morphological change. A nested modeling approach is used to produces boundary conditions (both spectral and parametric) at the seaward extent of the modeling area where the finer grid resolution is used.

The results of the model provides 2D spectra for all boundary points in the study area (on a computational grid), which is then used for finer scale transformations in the inshore area in order to consider wave convergence and divergence across the transverse ridge and swale topography. Specifically the model accounts for: (i) wave propagation in time and space, shoaling, and refraction due to current and depth, (ii) wave generation by wind, (iii) wave-current and wave-wave interactions, (iv) white-capping, bottom friction and depth-induced breaking and (v) wave-induced set-up and currents. In the present study, the model solves for wave transformation, wind and wave-forced currents and sediment transport over the NOAA bathymetric data that is interpolated to a flexible mesh with a maximum mesh area of 2 m^2 for a total of 61,184 nodes landward of the seaward nearshore bar. The wave and current model is run for a wide range of offshore wave boundary conditions and wind forcing based on long term meteorological and oceanographic records from two offshore wave buoys located near the study region (buoy 42039 and 42040). The model is also used to examine changes to the backbarrier shoreline and washover fans in the cold fronts immediately following the storm using a similar model framework (see Stone *et al.*, 2004).

3.5 Data Analysis

The locations of the cross-shore and alongshore transects used in the geophysical survey were based on the ridge and swale morphology, which was identified from the bathymetric data using Empirical Orthogonal Function (EOF) analysis. EOF analysis is used to identify common structures within a dataset and in this particular case it is used to identify shoreface profiles that account for the greatest percent of the variance. Only a limited number of factors are extracted from the cross-shore bathymetric data to explain most of the variance, and the variance explained by successive factors decreases monotonically. In this respect, EOFs can be used as a data reduction technique or a method to separate 'signal' and 'noise'. Data matrices X containing cross-island elevation and offshore bathymetric data (rows) from 486 transects (columns) are represented through matrices involving the eigenvalues and the spatial EOFs.

Due to the potentially non-stationary variation in the ridge and swale topography alongshore, wavelet analysis is used to quantify how the spectral signal of the eigenmodes varies over a range of spatial scales. Specifically, wavelets are designed to capture the behavior of non-

stationary stochastic signals, whereas Fourier spectra provide similar information in the frequency domain, but under the assumption of a stationary signal. The continuous wavelet transform (W_n^s) is defined as the convolution of the eigenmode (x_n) with a scaled and translated version of the normalized mother wavelet function. The one-dimensional sequence is expanded into a two-dimensional space (n,s) by varying the scale (s) and translating the function along n. As discussed by Torrence and Compo (1998), the complex Morlet mother wavelet provides a similar approximation to the Fourier wavelength ($\lambda = 1.03s$) and is used in this study. To avoid adding an artificial periodicity to the time series that is not periodic, the time series was padded with zeroes to the next power of 2. The global wavelet spectrum is calculated by averaging over all local wavelet spectra:

$$\overline{W}^2(s) = \frac{1}{N}\sum_{n=0}^{N-1}\left|W_n(s)\right|^2 \quad [1]$$

A further description on the methodology and interpretation of wavelet analysis is provided by Torrence and Compo (1998).

4. Results

4.1 Geophysical Survey

As previously described by Houser *et al.* (2008), the shoreface is dominated by shore-oblique ridges and swales of various size that are generally oriented at an angle of 65^o (SE) to the shoreline (see Figure 1). The shore-attached ridges extend ~1700 m offshore to a depth of ~15 m with an average height of 3 m. The shore-attached ridges are not discrete forms, but are part of a larger field of overlapping ridges and lobes extending from the modern shoreface to the shelf break. EOF analysis of the shoreface bathymetry reveals 2 significant eigenmodes (E1 and E2 respectively) that account for 67% of the variance and are associated with the ridge and swale respectively (Figure 2a). The ratio of eigenmodes (E1/E2) provides a simple estimate of the ridge locations, with local maxima representing the ridge crests and minima representing the swales (Figure 2). Wavelet analysis of the eigenmode ratio reveals statistically significant peaks at alongshore length scales of 750 and 1400 m, consistent with the spacing of the ridge and

bathymetry and the spacing of the cuspate headlands along Santa Rosa Sound (see also Houser *et al.*, 2008). In general, the cuspate headlands are located immediately landward of the ridges (large E1/E2), which are characterized by seagrass beds, backbarrier marsh and maritime forest (Figure 3). In contrast, the narrow sections of the island, which are susceptible to washover and breaching, are landward of the swales (small E1/E2). As shown in Figure 3, the narrow sections of the island are dominated by small discontinuous dunes that promote overwash and breaching, and a lack seagrass, backbarrier marsh and maritime forest along the backbarrier shoreline.

4.2 Seismic Survey

Representative sub-bottom surveys of the ridge and swale bathymetry at Pensacola Beach (Ridge 6) and within the Fort Pickens Section of Gulf Islands National Seashore (Ridge 4) are presented in Figures 4 and 5 respectively. The cross-ridge survey reveals multiple reflectors through both ridges and an absence of strong reflectors in the adjacent swales. Up to 5 strong reflectors are visible through Ridge 4, while only 2 strong reflectors can be identified through the larger ridge fronting Pensacola Beach (Ridge 6). In both cases, the near-horizontal reflectors transition to downward dipping structures along both the western and eastern ridge flanks and terminate at the swale. The along ridge surveys confirms that the reflectors are near-horizontal in the cross-shore, except at where they intersect with the ridge surface offshore. The abrupt termination of the reflectors along the ridges and the absence of any reflectors in the swales to a sediment depth of 10 m, suggest that the swales are texturally uniform.

Representative seismic profiles from along the backbarrier shoreline are presented in Figure 6 for the cuspate headland landward of Ridge 18. The seismic profile directly offshore of the headland (C-D) reveals several strong reflectors that are nearly horizontal, similar to the reflectors observed along the ridge crest (see Figures 4 and 5). Only a single near-horizontal reflector is visible in the profile offshore of the narrow section of the island (K-L) at a depth of ~0.25 m. The reflector develops at the waterline of the washover fans that were deposited during the 2004/2005 hurricane season and start to erode during cold fronts following the overwash events (see Houser *et al.*, 2008). As shown in the alongshore profile (G-H), the amount of sediment above the reflector increases towards the headland where it becomes buried beneath

almost 1 m of sand-sized sediment before rising to the surface at the headland. The surface layer at the headlands (ie. transect G-H) is dominated by seagrass beds and silty-sand.

4.3 Vibracores

Vibracore data for Ridge 6 (R6) fronting Pensacola Beach is presented in Figure 7. The landwardmost core (R6A) is dominated by dark gray mud with no shell fragments to a depth of ~6 m, with the exception of a thin (~0.10 m) dark-gray silty-mud at a depth of ~2 m. At R6B, the surface layer of mud is replaced by white medium to fine quartz sand with few scattered shell fragments to a depth of 2.8 m. The sand layer is underlain by a 0.75 m layer of grayish brown silty mud with trace of sand, a 0.84 m layer of grayish brown mud and a 1.5 m layer of brown silty sand. Further seaward at R6D, the sand layer extends to a depth of 3.4 m underlain by a thin (0.2 m) brownish gray medium quartz sand mixed with mud, and a thicker (>3 m) layer of dark gray to brownish gray silt/sand mud. A medium to fine sand layer extends the entire length of the core at R6E and is only interrupted by silty-sand layers containing medium to coarse shells at R6F and R6G. While the ridge core is composed of a mud layer overlain by either coarse sand or a silty-sand mixture, the swales do not have a mud layer (R6J) while the ridge flanks have a have a silty-sand layer that thins away from the ridge crest (R6I-R6B-R6H).

A similar stratigraphy is visible in the cores from Ridge 4 (R4) in the Fort Pickens Section of the study area (Figure 8). Along the ridge line (R4A-R4G), the ridge has a mud core that is increasingly overlain by a layer of sand with lens of silty-sand at depth. The thickness of the silt-sand lens appears to be sensitive to the relative location of the core to the ridge crest, with no lens present at R4E along the eastern ridge flank. Restriction of the mud core to the ridge crest is also apparent in the perpendicular transect (R4F-R4D-R4E), with a thin silty-sand lens along the ridge flank (R4F) and only sand within the swale (R4E). At both ridges 4 and 6, the depths of these reflectors are consistent with the alternating layers of mud and silty mud containing traces of sand visible in the seismic surveys (Figures 4 and 5).

4.4 Sediment samples

Grain size data from the ridge crest exhibits a seaward fining from moderately-sorted medium sands ($\phi \approx 1.5$) with a weak coarse-grained tail ($\phi_{sk} \approx -0.5$) to poorly-sorted fine sands ($\phi \approx 1.9$) with a more prominent coarse tail ($\phi_{sk} \approx -1.9$). Surficial sediment in the swales are well-sorted medium-grained ($\phi \approx 1.2$), and much coarser than the poorly sorted coarse-tailed sediment along the flanks of the ridge ($\phi \approx 1.8$). Along the ridge, the surficial sediment is again coarser-grained ($\phi \approx 1.5$) compared to the flanks and also well-sorted with a weak coarse-grained tail ($\phi_{sk} \approx -0.6$). Only at the landward extent of the ridge flanks, where the model predicts wave focusing through refraction, are the surficial sediments coarse-grained, well-sorted with a weak coarse-grained tail ($\phi \approx 1.3$; $\phi_{sk} \approx -0.5$). A similar pattern is observed over the ridge and swale to the west. The well-sorted coarse-grained swale ($\phi \approx 0.96$) is adjacent to a moderately sorted fine-grained ridge flank with a coarse-grained tail ($\phi \approx 2.3$) that grades into moderately-sorted medium sand at the ridge crest ($\phi \approx 1.7$). There is no statistically significant variation in the grain size distribution offshore on the relict ridge. The surficial sediment is poorly-sorted medium sand with a strong coarse-grained tail ($\phi \approx 1.4$; $\phi_{sk} \approx -1.9$).

Cores from the ridge, swale and flank regions exhibit a fining with depth. Even at depths of ~2.5 m below the surface, the grain size variation between these three zones persists. At 2.5 m below the surface, the swale sediment is well-sorted medium sand with a coarse tail ($\phi \approx 1.4$; $\phi_{sk} \approx -1.6$), while the same depth the flank sediment is moderately sorted fine-grained sand with a strong coarse tail ($\phi \approx 2.3$; $\phi_{sk} \approx -1.6$). At the ridge crest, the sediment at 2.5 m and below the mud/silt lens is well-sorted fine-grained sand with a moderate tail ($\phi \approx 1.4$; $\phi_{sk} \approx -1.9$). The observed differences in grain size between the ridge and swales are statistically significant at the 95% confidence level offshore. Unlike these offshore samples, there is no statistically significant difference in the grain size distributions between ridge and swale locations at the 95% confidence level within the nearshore (<5 m depths) and on the beachface and backshore. In all cases, the well-sorted medium-sized sand with a coarse-grained tail ($\phi \approx 1.2$; $\phi_{sk} \approx -0.53$) at mean sea level graded into a finer-grained moderately sorted sand with a coarse-grained tail ($\phi \approx 1.8$; $\phi_{sk} \approx -0.84$) at the 5 m bathymetric contour.

4.5 Terrestrial Survey

As described by Houser *et al.* (2008), washover during the 2004/2005 hurricane season exhibited an alongshore variability at a similar spacing to the cuspate headlands. Washover penetration was limited at the cuspate headlands in response to the wider island and larger dunes, but reached the backbarrier shoreline in the narrow sections of the island where dune heights are also at a minimum. A GPR survey was completed at representative wide and narrow sections of the island. Representative GPR survey transects from a cuspate headland and a narrow-section of island between headlands are provided in Figure 8. The headlands transect exhibits up to 1 m of beachface and backshore recovery with sub-horizontal stratification above a strong reflector at the post-Ivan surface. Numerous discrete hyperbolic reflections at the end of the transect suggest large woody stem and root material. The active surface above the near horizontal mud layer is characterized by sub-horizontal stratification characteristic of washover deposits. The thin mud layer caps steeply landward-dipping bedding with a slope of ~6^{o}, consistent with the break in slope for the shallow terrace fronting the cuspate headland. In contrast, the narrow sections of the island between headlands are dominated by near-horizontal bedding except for gently-sloped bedding at ~150 m from the Gulf of Mexico shoreline and at a depth of ~ 1 m. The near-horizontal bedding is consistent with washover deposits described by Wang *et al.* (2006) from other areas of Santa Rosa Island following Hurricanes Ivan and Dennis.

4.6 Wave Modeling

The structural similarity and statistically significant coherence between the transverse ridge and swale morphology and the backbarrier cuspate headlands suggests that the ridges and swales are not dynamic bedforms. Wave and transport modeling are used to describe the response of the ridge and swale morphology to Hurricane Ivan, which made landfall along the Florida-Alabama coastline on September 16, 2004 as a category 3 storm with a 3-4.5 m storm surge along Santa Rosa Island (Stewart, 2004). The National Data Buoy Center's (NDBC) buoy 42020 recorded a significant wave height of 15.96 m with the largest individual wave height recorded at 27.7 m (Wang *et al.*, 2005). These measurements were made when the storm was still a category 4 storm approaching the outer continental shelf. As described by Houser *et al.* (2008) the storm caused extensive shoreline erosion and overwash leading to a low-profile barrier that was inundated by Hurricanes Dennis and Katrina, despite these storms having locally

smaller storm surge. The predicted change in bed elevation for Hurricane Ivan (September 13-17, 2004) is presented in Figure 9. In general, the pattern of erosion and deposition closely mirrors the bathymetric variation, with accretion largely limited to the ridge crests and along the western flank of the ridges. Specifically, the model predicts ~0.03 m of sediment accretion along the centerline of Ridge 6 and ~0.05 m of accretion along its western flank. Erosion of the swales immediately southwest of the ridges suggests that wave shoaling and refraction move sediment from swale to ridge, thereby reinforcing the pre-existing ridge.

The predicted changes in bed elevation are compared to the measured change in bed elevation between the original NOAA survey in 1982 and the 2006 survey along 2 transects across the Pensacola Beach ridge and swale (Figure 10). Despite the very different timescales and the order of magnitude difference in the measured and predicted change over the respective timescales, there is a general agreement in the predicted and measured change. Along both transect the greatest accretion occurs at the topographic highs (ie. the ridges), while erosion is predicted in the topographic lows (the swales), where the measured amount of sediment accreted is at a local minimum. On average there was ~0.025 m of sediment accreted across the shoreface with up to 0.02 m of sediment accreted at the ridges and up to 0.04 m of sediment eroded from the swales. Claudino-Sales *et al.* (*in press*) estimate that approximately 50-100 m^3 m^{-1} of sediment was lost to the offshore during Hurricane Ivan. Assuming a 1450 m alongshore spacing of the ridge and swale topography, this would account for between 72,500 and 1,450,000 m^3 of sediment that if equally distributed to a depth of 15 m, this would lead to an accretion of between 0.03 and 0.06 m. This is of the same order of magnitude as predicted by the wave modeling for Hurricane Ivan. Whether this sediment is a partial source of the overall accretion is not clear, the change in bed elevation reinforces the morphology of the ridge and swale topography.

5. Discussion

Barrier island transgression is not a continuous process, but occurs episodically in response to storms capable of scarping the foredune (Davidson-Arnott, 2005), and/or transporting sediment to the backbarrier in the form of washover. Where dunes are well-developed and continuous alongshore, transgression tends to be episodic with extended periods

of dune growth and island stability. Recent evidence suggests that barrier island dune systems are not continuous alongshore, but exhibit considerable variability in height and extent (Elko *et al.*, 2002; Wetzell, 2003; Houser *et al.*, 2008). The height of the dune at storm landfall depends on the time since the last storm, the level of damage sustained in that storm and the rate of post-storm dune recovery (Houser and Hamilton, 2009), while the rate of recovery depends on the regional sediment budget (Psuty, 1992), and the ability of sediment to be transported from the beach and backshore to the dune (Short and Hesp, 1982). Barrier islands along the Atlantic Seaboard and the Gulf of Mexico have an alongshore variability in beach and dune form that is forced by bathymetric variations on the inner-shelf (Houser *et al.*, 2008; Lentz and Hapke, 2011; Houser and Mathew, *in press*). Specifically, the alongshore variation in beach and dune form at Santa Rosa Island in northwest Florida is forced by a transverse ridge and swale bathymetry that controls the aeolian transport potential and available sediment supply to the dunes (Houser and Hamilton, 2009). Results of the present study suggest that the ridges and swales are transgressive features and a response to the cuspate headlands along the backbarrier shoreline. Starting from an initial perturbation, such as a washover fan along the backbarrier shoreline, the cuspate headlands would have developed and self-organized in response to the near-oblique and bimodal wind and wave forcing of Santa Rosa Sound (see Ashton *et al.*, 2001). The backbarrier morphology and the alongshore variation in island response and recovery would be reinforced as the island transgressed and the backbarrier muds emerged as ridges on the Gulf of Mexico shoreface.

The cuspate headlands along Santa Rosa Sound are characterized by maritime forest, salt marsh and extensive seagrass beds that are responsible for the mud and silty-sand layers visible in the backbarrier seismic data (Figure 6). The continuation of the near-horizontal mud layers in the terrestrial survey and into the Gulf of Mexico suggests that the position of the headlands along the backbarrier shoreline has been relatively stable. Without invoking a symmetrical distribution of winds (see Ashton *et al.*, 2001), it is reasonable to expect that storm overwash through the narrow sections of the island reinforces the position of the littoral cells along the backbarrier shoreline. Persistence of overwash in the narrow sections of the island is in part reinforced by the alongshore variability of the dune system. Breaching and overwash penetration to the backbarrier shoreline are promoted in the narrow sections of the island by the small and discontinuous dunes (Houser *et al.*, 2008). The small discontinuous dunes are in turn forced by

the steep beachface and berm that limit aeolian transport (Short and Hesp, 1982), compared to the more gently sloped beachface along the wider sections of the island that promotes the development of larger and more continuous dunes (Houser *et al.*, 2009). The alongshore variation in beachface slope and dune morphology is forced by the transverse ridge and swale bathymetry (Houser and Hamilton, 2009), with the largest dunes fronted by ridges while the smallest dunes on the island are fronted by the swales (Houser *et al.*, 2008). In this respect, the stability of the cuspate headlands is a consequence of the transverse ridge and swale bathymetry, which forces an alongshore variation in dune height and the extent of washover penetration to the backbarrier shoreline.

Results of the seismic profiling and vibracores suggest that the transverse ridges are structurally similar to the cuspate headland and shoals along the backbarrier. The ridges contain near-horizontal mud and silty-sand layers separated by coarse sand lenses, while the swales do not have mud layers and dominated by relatively coarse sand similar to the washover fans. In this respect, the ridges can be interpreted as erosional remnants of Holocene transgressive sediments similar to those currently being deposited in Pensacola Bay and Santa Rosa Sound. The presence of coarse-sand lenses within the typically mud-dominated ridges may reflect periods with a greater frequency of extreme storms with washover penetration to the backbarrier shoreline, where the sediment is transported alongshore to the cuspate headlands (McNinch and Luettich, 2000). The supply of washover sediment would be depleted in the absence of storms, allowing for the expansion of seagrass and salt marsh, and the accretion of mud and organics. Nearby dune-lake sediment records suggest that the region experienced millennial scale periods of strong and weak storm activity caused by shifts in the position of the jet stream and the Bermuda High (Liu and Fearn, 2000). This raises the potential for episodic island transgression that may also be recorded in the alternating sand and mud layers of the tranvserve ridges.

Continuation of mud layers from the backbarrier to the Gulf of Mexico shoreline and the presence of mud layers at depth suggests that the ridges are not dynamic features that migrate alongshore in response to extreme storms. Similarity of the 1982 and 2006 bathymetric surveys suggests that the ridges are relatively stable features despite preferential accretion of sediment at the ridge crests. These results are supported by the wave modeling for Hurricane Ivan, which suggests a transfer of fine-grained sediment from the swales to the adjacent ridge crest. Depositional layers along the ridge flanks are visible in both the seismic and vibracore data as a

thickening sand layer away from the ridge crest as the mud layers abruptly terminate. The incident wave field is refracted towards the transverse ridges during Hurricane Ivan (Figure 9) and sediment would be transported swale to ridge with the shoaling wave. In this respect, extreme storms reinforce both the ridge and swale morphology as well the alongshore variation in beach-dune morphology and the backbarrier shoreline. Stallins and Parker (2003) have previously suggested that barrier islands are self-organized through a biogeomorphic feedback in which the vegetation of washover prone environments limits dune development and maintains the area as a washover conduit. While the results of the present suggest that the self-organization is initiated by the backbarrier headlands, it remains possible that the variations in vegetation type, or lack thereof, further reinforces the alongshore variation in island transgression.

In summary, the combined field and modeling results suggest that the transgression of Santa Rosa Island is not uniform alongshore and can be described by through the following model that is also shown conceptually in Figure 11. Cuspate headlands develop from an initial perturbation along the backbarrier shoreline such as a washover fan. As the headlands develop, the barrier island develops an alongshore variation in width that determines whether washover is able to penetrate to the backbarrier shoreline. Washover erosion in the narrow sections of the island and deposition at the headlands and shoal reinforces the alongshore variation in island width. Transgression of the island over the backbarrier deposits leads to shoreface ridges with a mud core separated by deeper swales. This alongshore variability in shoreface slope leads to an alongshore variation in the surf similarity parameter and beach state (Houser *et al.*, *in pressa,b*), which in turn controls the aeolian transport potential and sediment supply to the foredunes (Houser and Hamilton, 2010). A transverse bar and rip morphology with steep beachface and berm is common in the narrow sections of the island, while an intermediate longshore bar and trough morphology with a more gently sloped beachface is common in the wider sections of the island. Emergence of the ridge and swale bathymetry further reinforces the alongshore variation in dune morphology, overwash penetration and island width. In this respect, the contemporary response and recovery of the island to extreme storms and relative sea level rise is forced by the transgressive surface that is in turn forced by the development of cuspate headlands along the backbarrier shoreline early in the transgression. This feedback is expressed through the alongshore variation in beach and dune morphology and suggests a top-down model in which

advances in our understanding of beach-dune interaction (for example) depend on the broader geologic context.

The proposed model of transverse ridge formation is different from the model of McBride and Moslow (1991), which ascribes the initial development of the ridges to an alongshore migrating tidal inlet. The ridges examined by McBride and Moslow (1991) and cored by Figueiredo (1984) are compared of seaward dipping deltaic sediment and are not composed of a mud-core like the ridges at Santa Rosa Island. While also not formed by the storm waves and currents (Swift *et al.*, 1973), results of the wave model suggest that the ridges are reinforced are possibly accrete during storms as suggested by Vaughan *et al.* (2009) through the transport of sediment from swale to ridge. However, it is reasonable to expect that there is sediment transport within and between the nearshore and shoreface in response to the alongshore variable longshore transport (Stone *et al.*, 1992) that is also responsible for the redistribution of sediment from wide to narrow sections as the island recovers from an extreme storm (Figure 11). The results of the present study are also consistent with those of Otvos (1982) and Otvos (1985), who collected cores through a washover-dominated area just east of Pensacola Beach. The core data revealed no mud deposits within the tidal and barrier platform sands, similar to the seismic scans and core data from the swales and narrow-sections of the island. As this coring was only done along a single transect, a simple two-dimensional model of island transgression was developed. Only through the collection of multiple cores in relation to the transverse ridge and swales could the model of island transgression presented in this study be recognized.

6. Conclusions

Through a combination of field sampling, modeling and remote sensing the following conclusions can be made about the origins and maintenance of the shore-attached ridge and swale bathymetry:

1. The ridges are spatially coherent and structurally similar to the cuspate headlands along the backbarrier shoreline. Seismic surveys and vibracores reveal near-horizontal reflectors at the headlands and ridges, and an absence of horizontal reflectors between headlands where the shoreline is dominated by overwash. The mud-layers appear to be

associated with the development of seagrass beds, salt marsh and maritime forest at the headlands and associated shoals.

2. Emergence of the ridge and swale topography on the shoreface reinforces the backbarrier morphology through an alongshore variation in beach state and dune morphology. The ridges that develop from the cuspate headlands promote the development of larger and more continuous dunes, while a smaller discontinuous dune field develops at the swales. This allows for overwash penetration to the backbarrier shoreline between headlands and provides a source of sediment for the landward extension of the headlands.
3. Wave modeling further suggests that, once formed, the ridge and swale bathymetry is maintained through the transport of sediment from the swales to the ridges during large storms, which reinforces the backbarrier shoreline morphology.
4. The transgressive surface controls the response to and recovery from tropical storms and hurricanes and therefore future island transgression.

7. Acknowledgements

This study was supported by grants from the National Park Service (P5320060026 and J5320080001). LiDAR survey data were prepared by Nathan McKinney, Amber Bloechle and John Oravetz of the University of West Florida Geodata Center. Field assistance was variously provided by Kevin Bradley, Chasidy Hobbs and Gemma Barrett. Riley Hoggard, Resource Management Specialist for the Gulf Islands National Seashore, provided important background information to the site and was helpful in providing access to the site. Victor Thompson collected the GPR data and Al Browder provided access to additional cores and seismic profiles along the shoreface. The shorelines from the pre- and post-Ivan LiDAR were graciously provided by Asbury Sallenger, Hilary Stockdon and Laura Fauver of the US Geological Survey Coastal and Marine Geology Program. Additionally, post Katrina LiDAR coverage of Santa Rosa Island was made available by John Brock and Amar Nayegandhi of the US Geological Survey Center for Coastal and Watershed Studies and the July 2006 LiDAR data were provided by Escambia Count.

References

Ashton A., Murray A.B., Arnoult O., 2001. Formation of coastline features by large-scale instabilities induced by high-angle waves: Nature, v. 414, p. 296–300, doi: 10.1038/35104541.

Balsillie, J.H., Clark, R.R., 1997. Annotated and illustrated bibliography of marine subaqueous sand resources of Florida's Gulf of Mexico. Florida Geological Survey. Tallahassee.

Bauer, B.O., Davidson-Arnott, R.G.D., 2003. A general framework for modeling sediment supply to coastal dunes including wind angle, beach geometry, and fetch effects. Geomorphology 49, 89-108.

Danforth, W., 1997. Xsonar/Showimage: a complete system for rapid sidescan sonar processing and display. Open-File Report 97-686, US Geological Survey, Woods Hole Field Center, Quissett Campus, Woods Hole, MA, 02543.

Davis, R.A., Fitzgerald, D., 2002. Beaches and Coasts. Blackwell Science, 448pp.

Davidson-Arnott, R., 2005. Conceptual model of the effects of sea level rise on sand coasts. Journal of Coastal Research 21, 1166-1172.

Dean, R.G., Dalrymple, R.A., 2002. Coastal Processes with Engineering Applications. , Cambridge Univ. Press, Cambridge.

Donoghue, J.F., Niedoroda, A.W., Hatchett, L. , Locker, S. , Clark, R., Koch, J. , and Butler, K., 2003, Model for identifying and characterizing offshore sand sources using an interactive GIS: Proceedings, Coastal Sediments 2003, Fifth International Conference on Coastal Engineering and Science of Coastal Sediment Processes, St. Petersburg, FL.

Duane, D.B., Field, M.E., Meisburger, E.P., Swift, D.J.P., Williams, S.J., 1972. Linear shoals on the Atlantic inner continental shelf, Florida to Long Island. In: Swift, D.J.P., Duane, D.B., Pilkey, O.H. (Eds.), Shelf Sediment Transport: Process and Pattern. Dowden, Hutchinson and Ross, Stroudsburg, PA, pp. 447–498.

Elko, N.A., Sallenger, A.H., Guy, K., Morgan, K.L.M., 2002. Barrier island elevations relevant to potential storm impacts; 2, South Atlantic: U.S. Geological Survey, Open-File Report 2002-288, 1 folded sheet.

Field, M.E., 1980. Sand bodies on coastal plain shelves: Holocene record of the US Atlantic inner shelf of Maryland. Journal of Sedimentary Petrology 50, 505–528.

Figueiredo, A.G., Swift, D.J.P., Stubblefield,W.L., Clarke, T.L., 1981. Sand ridges on the inner Atlantic shelf of North America: morphometric comparisons with huthnance stability model. Geo-Marine Letters 1, 187–191.

Foster, E.R., Spurgeon, D.L., Cheng, J., 1999, Shoreline Change Rate Estimates: Escambia and Santa Rosa Counties. Report No. BCS-99-03. Tallahassee: Florida Department of Environmental Protection, Office of Beaches and Coastal Systems.

Hapke CJ, Christiano M. 2007, Long-term and Storm-related Shoreline Change Trends in the Florida Gulf Islands National Seashore. U.S. Geological Survey Open-file Report 2007-1392, 18p.

Houser, C., Hapke, C. Hamilton, S., 2008. Controls on Coastal Dune Morphology, Shoreline Erosion and Barrier Island Response to Extreme Storms. Geomorphology, 100, 223-240.

Houser, C., Mathew, S., 2011. Variability in foredune height depends on the alongshore correspondence of transport potential and sediment supply. Geomorphology, 125, 62-72.

Houser, C., Barrett, G., Labude, D., In Press a. Alongshore variation in the rip current hazard at

Pensacola Beach. Accepted to Natural Hazards, September 2010.

Houser, C., Caldwell, N., Meyer-Arendt, K., In Press b. Hot times at Hot spots: The rip current hazard at Pensacola Beach, Florida. Invited submission to refereed book **Rip Currents: Beach Safety, Physical Oceanography and Wave Modeling**, edited by Steven Leatherman and John Fletemeyer. Accepted August 2010.

Houser, C., Hamilton, S., 2009. Sensitivity of post-hurricane beach and dune recovery to event frequency. Earth Surface Processes and Landforms, 34, 613-628.

Huthnance, J.M., 1982. On one mechanism forming linear sand banks. Estuar. Coast. Shelf Sci. **14**, pp. 19–99.

Hsu, K. J., 1960. Texture and mineralogy of the Recent sands of the Gulf Coast: Jour. Sed. Petrology, v. 30, no. 3, p. 380-403.

Hyne, N.J., Goodell, H.G., 1967. Origin of the sediments and submarine geomorphology of the inner continental shelf off Choctawhatchee Bay, Florida. Marine Geology 5, 299-313.

Kwon, H.J., 1969. Barrier islands of the northern Gulf of Mexico coast: Sediment source and development. Coastal Studies Series 25. Baton Rouge: Louisiana State University Press.

Liu, K., Fearn, M.L., 2000. Reconstruction of prehistoric landfall frequencies of catastrophic hurricanes in northwestern Florida from lake sediment records. Quaternary Research 54, 238-245.

Leadon, M.E., Clark, R.R., Nguyen, N.T., 1999. Hurricane Earl and Hurricane Georges: Beach and dune erosion and structural damage assessment and post-storm recovery plan for Panhandle coast of Florida. Report No. BCS-99-01. Tallahassee: Florida Department of Environmental Protection, Office of Beaches and Coastal Systems.

Lentz, E.E., Hapke, C.J., 2011. Geologic framework influces on the geomorphology of an anthropogenically modified barrier island: Assessment of dune/beach changes at Fire Island, New York. Geomorphology 126, 82-96.

Malinverno, M.H. Edwards W.B.F. Ryan, 1990. Processing of SeaMARC swath sonar data. IEEE J. Ocean. Eng., 15. 14–23.

Masetti, R., Fagherazzi, S., Montanari, A., 2008. Application of a barrier island translation model to the millennial-scale evolution of Sand Key, Florida. Continental Shelf Research 28, 1116-1126.

McBride, R.A., Moslow, T.F., 1991. Origin, evolution and distribution of shoreface\ sand ridges, Atlantic inner shelf, USA. Marine Geology 97, 57–85.

McBride, R.A., Byrnes, M.R., 1995. Surficial sediments and morphology of the southwestern Alabama/western Florida Panhandle coast and shelf. Gulf Coast Association of Geological Societies Transactions 45, 392-404.

McBride, R.A., Anderson, L.C., Tudoran, A., Roberts, H.H., 1999. Holocene stratigraphic architecture of a sand-rich shelf and the origin of linear shoals: northeastern Gulf of Mexico. In Bergman, K.M., and Snedden, J.W., eds. Isolated Shallow Marine Sand Bodies: Sequence Stratigraphic Analysis and Sedimentologic Interpretation: SEPM Special Publications 64, 95-126.

McBride, R.A., 1997. Seafloor morphology, geologic framework, and sedimentary processes of a sand-rich shelf offshore Alabama and northwest Florida, northeastern Gulf of Mexico. Ph.D. Dissertation, Department of Oceanography and Coastal Sciences, Louisiana State University, 509pp.

McNinch, J.E., Luettich, R.A., 2000. Physical processes around a cuspate headland: implications to the evolution and long-term maintenance of a cape-associated shoal. Continental Shelf Research 20, 2367-2389.

Otvos, E.G., 1982. Santa Rosa Island, Florida panhandle: Origins of a composite barrier island. Southeastern Geology 23, 15-24.

Parker, S.J., Schultz, A.W., Schroeder, W.W., 1992. Sediment characteristics and seafloor topography of a palimpsest shelf, Mississippi-Alabama continental shelf. In Fletcher, C.H., and Wehmiller, J.F. eds. Quaternary coasta of the United States: Marine and Lacustrine Systems: SEPM Special Publication 48, 243-251.

Paskevich, V., 1992. Woods Hole image processing system software implementation: using NetCDF as a software interface for image processing. U.S. Geol. Surv. Open-File Rep. 92-25, 66 pp.

Poppe, L.J., Eliason, A.H., Fredericks, J.J., 1985. APSAS: an automated particle-size analysis system: U.S. Geological Survey Circular 963, 77 p.

Psuty, N.P., 1992. Spatial variation in coastal fordune development. In: R.W.G. Carter, T.G.F. Curtis and M.J. Sheehy-Skeffington (Eds), Coastal Dunes: Geomorphology, Ecology and Management for Conservation. Balkema Rotterdam, pp. 3-13.

Robinson, M.M., McBride, R.A., 2008. Anatomy of a shoreface sand ridge revisited using foraminifera: False Cape Shoals, Virginia/North Carolina inner shelf. Continental Shelf Research 28, 2428-2441.

Sallenger, A. H., 2000. Storm impact scale for barrier islands. Journal of Coastal Research, 16, 890-895.

Schupp, C.A., McNinch, J.E., List, J.H., 2006. Nearshore shore-oblique bars, gravel outcrops, and their correlation to shoreline change. Marine Geology 233, 63-79.

Short, A., Hesp, P.A., 1982. Wave–beach–dune interaction in southeast Australia, Marine Geology **48**, 259–284.

Snedden, J.W., Dalrymple, R.W., 1999. Modern shelf sand ridges: from historical perspective to a unified hydrodynamic and evolutionary model. In: Bergman, K.M., Snedden, J.W. (Eds.), Isolated Shallow Marine Sand Bodies: Sequence Stratigraphic Analysis and Sedimentologic Interpretation, vol. 64. SEPM, Special Publication, pp. 13–28.

Snedden, J.W., Kreisa, R.D., Tillman, R.W., Culver, S.J., Schweller, W.J., 1999. An expanded model for modern shelf sand ridge genesis and evolution on the New Jersey Atlantic shelf. In: Bergman, K.M., Snedden, J.W. (Eds.), Isolated Shallow Marine Sand Bodies: Sequence Stratigraphic Analysis and Sedimentologic Interpretation, vol. 64. SEPM, Special Publication, pp. 147–163.

Stallins, J.A., Parker, A.J., 2003. The influence of complex systems interactions on barrier island dune vegetation pattern and process. Annals of the Association of American Geographers, 93, 13-29.

Stapor, F.W., Jr., 1975. Shoreline changes between Phillips Inlet and Pensacola Inlet, northwest Florida coast, Transactions, Gulf Coast Association of Geological Societies 25: 373-378.

Stockdon, H.F., Sallenger, A.H., Holman, R.A, Howd, P,A., 2007. A simple model for the spatially-variable coastal response to hurricanes. Marine Geology 238, 1-20.

Stone, G.W., Liu, B., Pepper, D.A., Wang, P., 2004. The importance of extratropical and tropical cyclones on the short-term evolution of barrier islands along the northern Gulf of Mexico, USA. Marine Geology 210, 63-78.

Stone, G.W., 1991. Differential sediment supply and cellular nature of longshore sediment transport along coastal Northwest Florida and Southeast Alabama since the late Holocene. Ph.D. Dissertation, University of Maryland, College Park, MD.

Stone, G.W., Stapor, F.W., Jr., May, J.P., Morgan, J.P., 1992. Multiple sediment sources and a cellular, non-integrated, longshore drift system: Northwest Florida and southeast Alabama coast, USA, Marine Geology105: 141-154.

Stone, G.W., Stapor, F.W., Jr., 1996. A nearshore sediment transport model for the northeast Gulf of Mexico coast, USA, Journal of Coastal Research 12: 786-792

Stubblefield, W.L., McGrail, D.W., Kersey, D.G., 1984. Recognition of transgressive and post-transgressive sand ridges on the New Jersey continental shelf. In: Tillman, R.W., Siemers, C.T. (Eds.), Siliclastic Shelf Sediments. Society of Economic Paleontologists and Mineralogists (SEPM), Special Publication 34, Tulsa, OK, pp. 1–23.

Swift, D.J.P., Holliday, B., Avignone, N., Shideler, G., 1972a. Anatomy of a shoreface ridge system, False Cape, Virginia. Marine Geology 12, 59–84.

Swift, D.J.P., Duane, D.B., McKinney, T.F., 1973. Ridge and swale topography of the Middle Atlantic Bight, North America: Secular response to the Holocene hydraulic regime. Marine Geology 15, 227-247.

Swift, D.J.P., McKinney, T.F., Stahl, L., 1984. Recognition of transgressive and post transgressive sand ridges on the New Jersey continental shelf—discussion. In: Tillman, R.W., Siemers, C.T. (Eds.), Siliclastic Shelf Sediments. Society of Economic Paleontologists and Mineralogists (SEPM), Special Publication 34, Tulsa, OK, pp. 25–36.

Torrence, C., Compo, G.P., 1998. A practical guide to wavelet analysis. Bulletin of the American Meteorological Society 79, 61-78.

Vaughan, W.C., Briggs, K.B., Kim, J., Bianchi, T.S., Smith, R.W., 2009. Storm-generated sediment distribution along the Northwest Florida inner continental shelf. IEEE Journal of Oceanic Engineering 34, 495-515.

Wang, P., Kirby, J.H., Haber, J.D., Horwitz, M.H., Knorr, P.O., Krock, J.R., 2006. Morphological and Sedimentological Impacts of Hurricane Ivan and Immediate Poststorm Beach Recovery along the Northwestern Florida Barrier-Island Coasts. Journal of Coastal Research 22, 1382 – 1402.

Wang, D.W., Mitchell, D.A., Teague, W.J., Jarosz, E., Hulbert, M.S., 2005. Extreme waves under Hurricane Ivan. Science 309, 896.

Wetzell, L.M., 2003. Simple models for predicting dune erosion hazards along the Outer Banks of North Carolina. MS Thesis, University of South Florida.

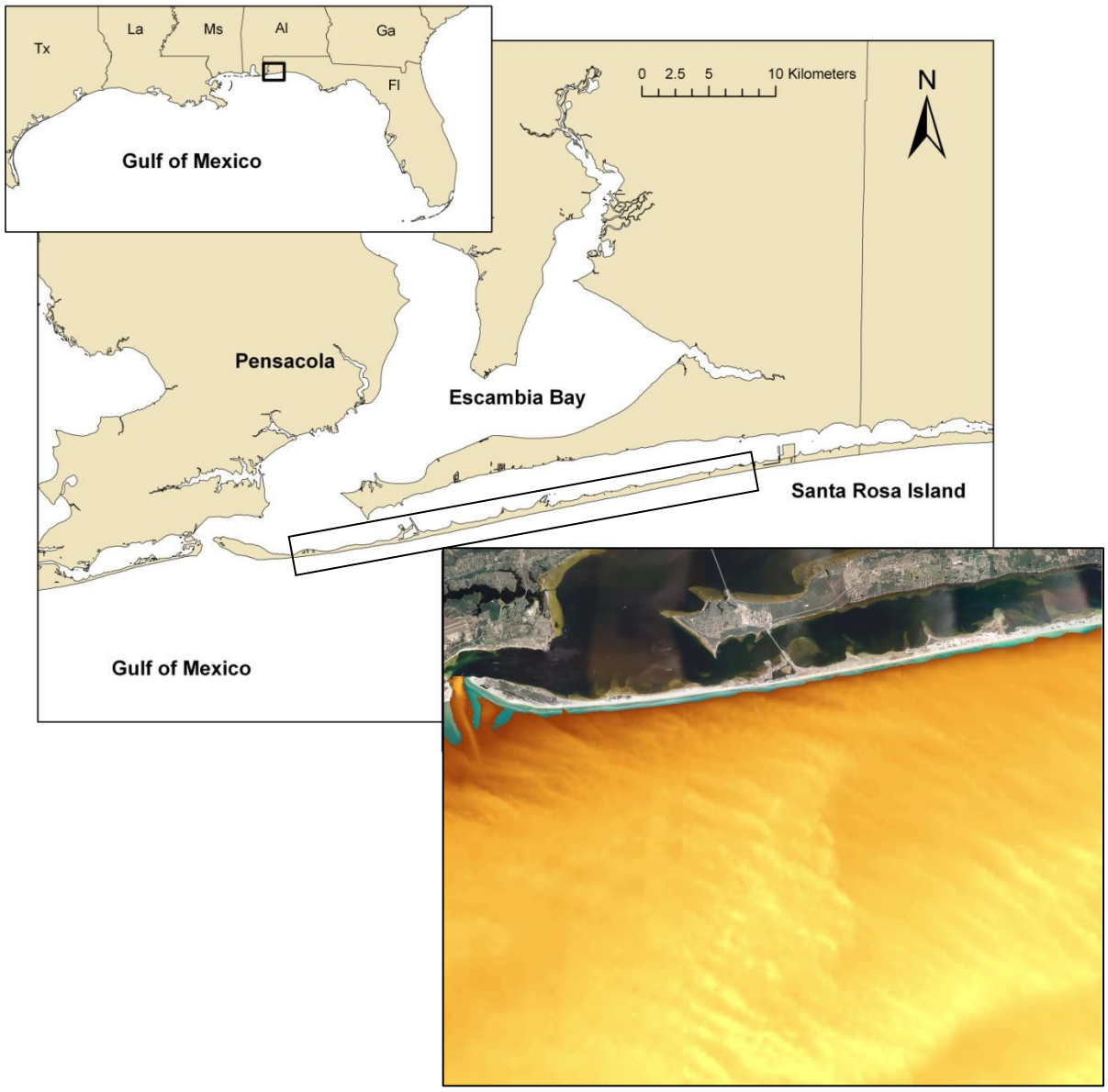


Figure 69. Santa Rosa Island, a narrow Holocene barrier island in northwest Florida, which extends from East Pass in Destin (just off map) to Pensacola Pass in the west. Also shown are the transverse ridge and swale features on the inner-shelf fronting Santa Rosa Island. The highlighted area on the regional map defines the extent of the study area presented in the remainder of the paper.

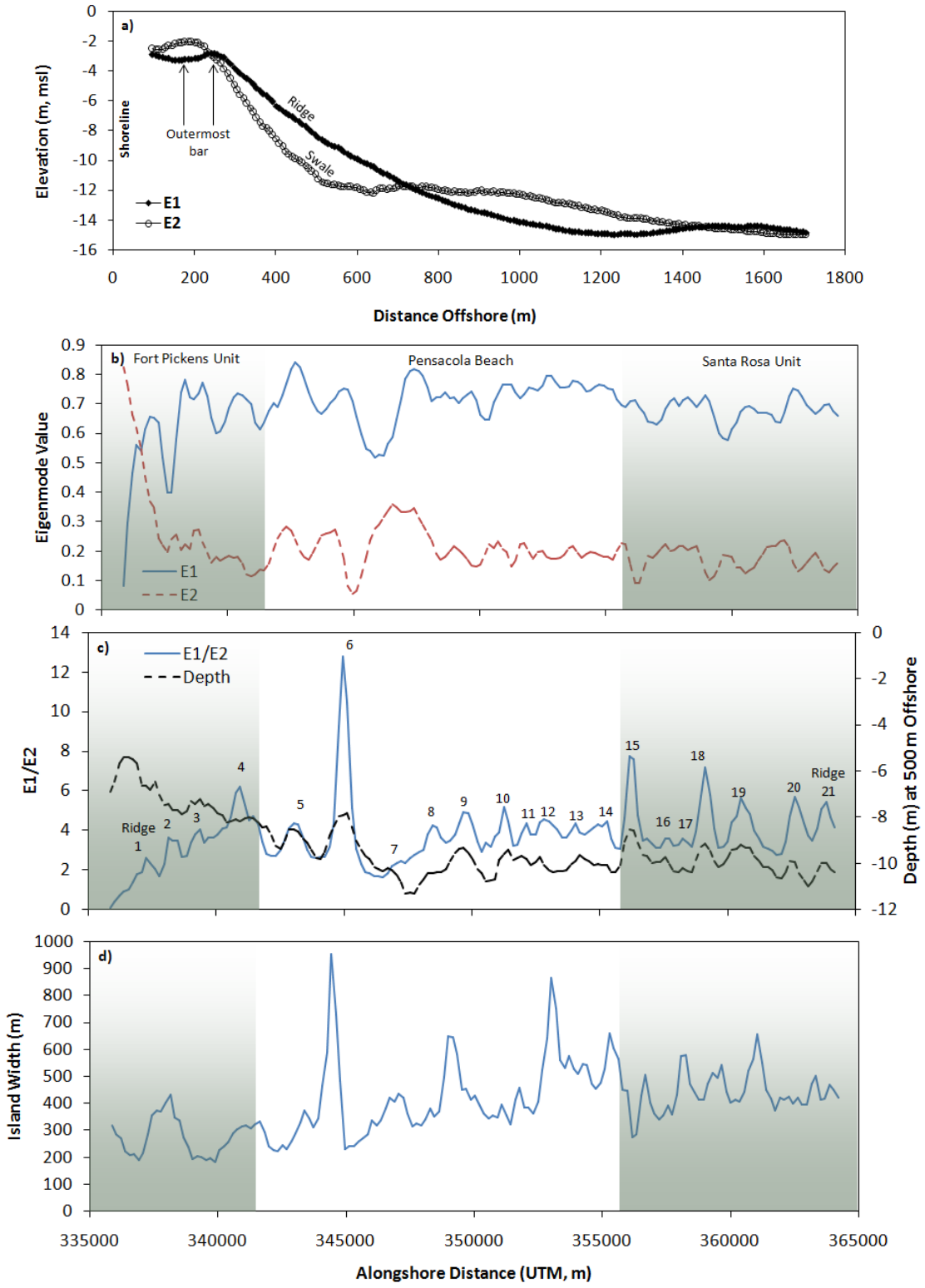


Figure 70. (a) Dominant eigenmodes (E1 and E2) of the shoreface bathymetry representing the average ridge and swale topography respectively. Also shown is the alongshore variation in (b) the eigenmodes, (c) the eigenmode ratio (E1/E2) and the depth at 500 m offshore, and (d) island width.

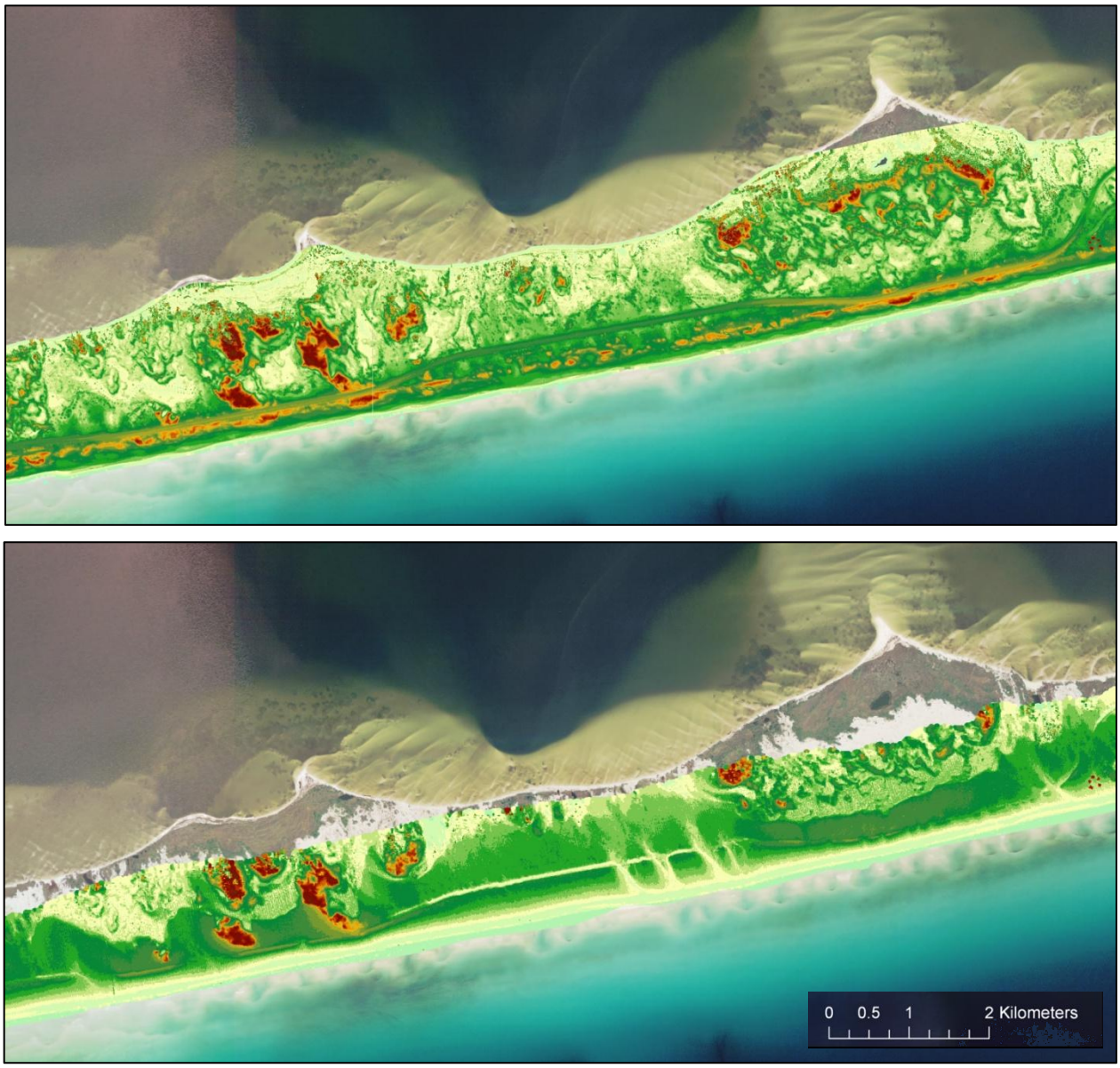


Figure 71. Pre- and post-Hurricane Ivan LiDAR imagery of cupate headlands in the Santa Rosa Unit with elevations ranging from 0 m (msl) in white to 5 m in dark red. Shown are the cuspate headlands directly landward of ridges 18 and 19 on Figure 2c.

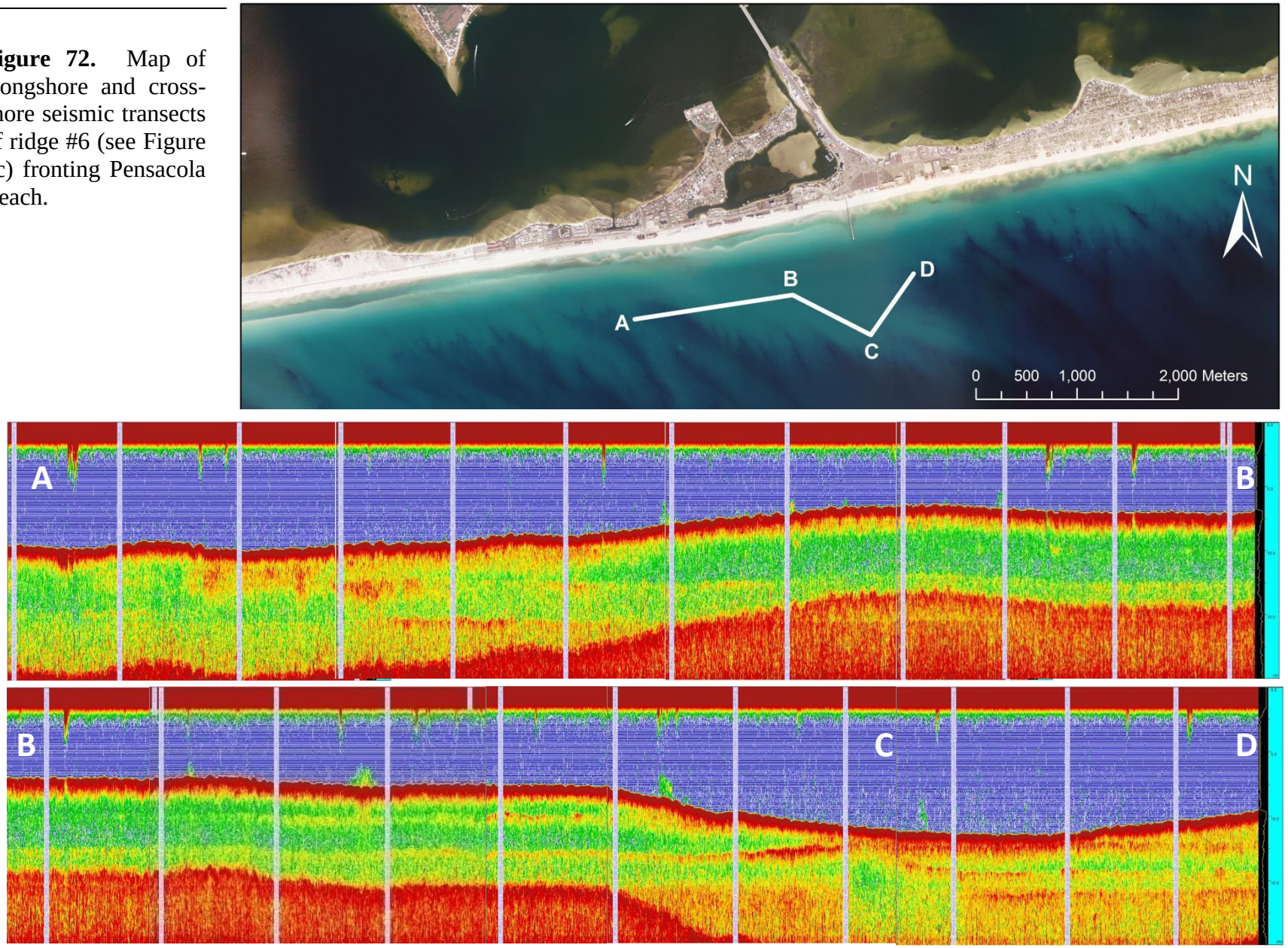
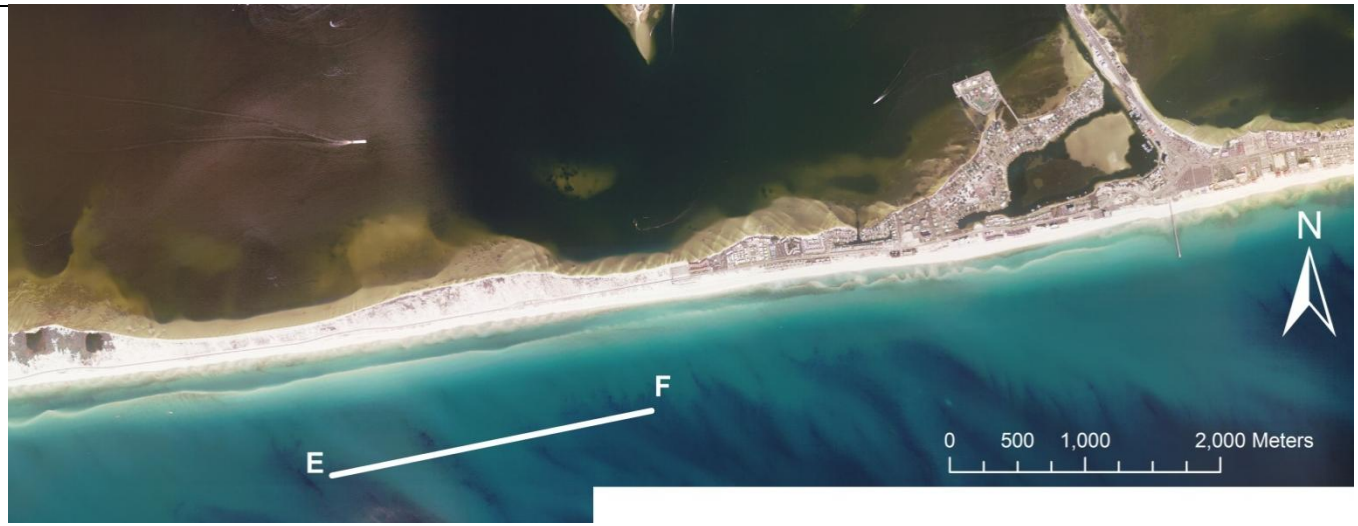


Figure 72. Map of alongshore and cross-shore seismic transects of ridge #6 (see Figure 2c) fronting Pensacola Beach.



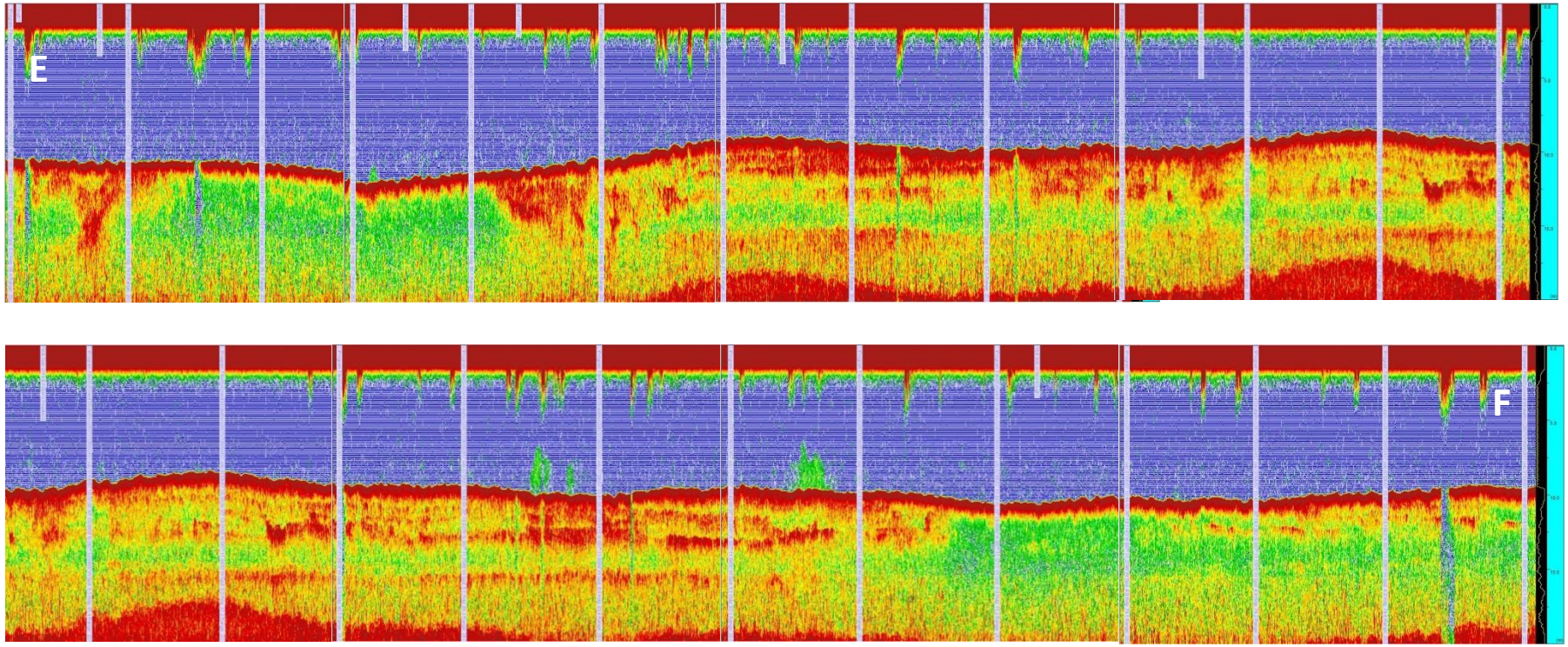


Figure 73. Map of alongshore and cross-shore seismic transects of ridge #4 (see Figure 2c) in the Fort Pickens Unit of the study area.

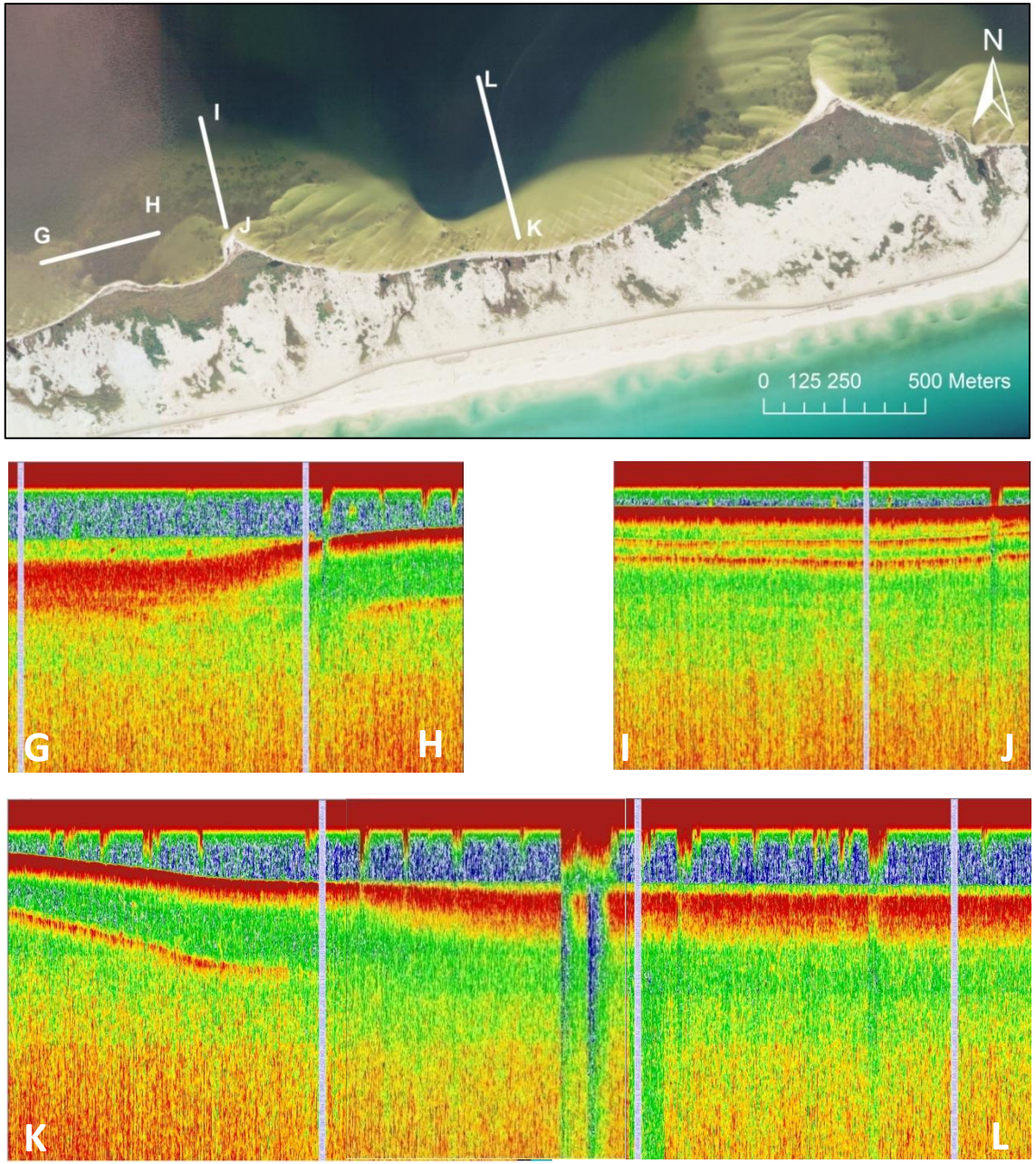


Figure 74. Map of alongshore and cross-shore seismic transects along backbarrier shoreline of ridge #18 (see Figure 2c) in the Santa Rosa Unit of the study area.

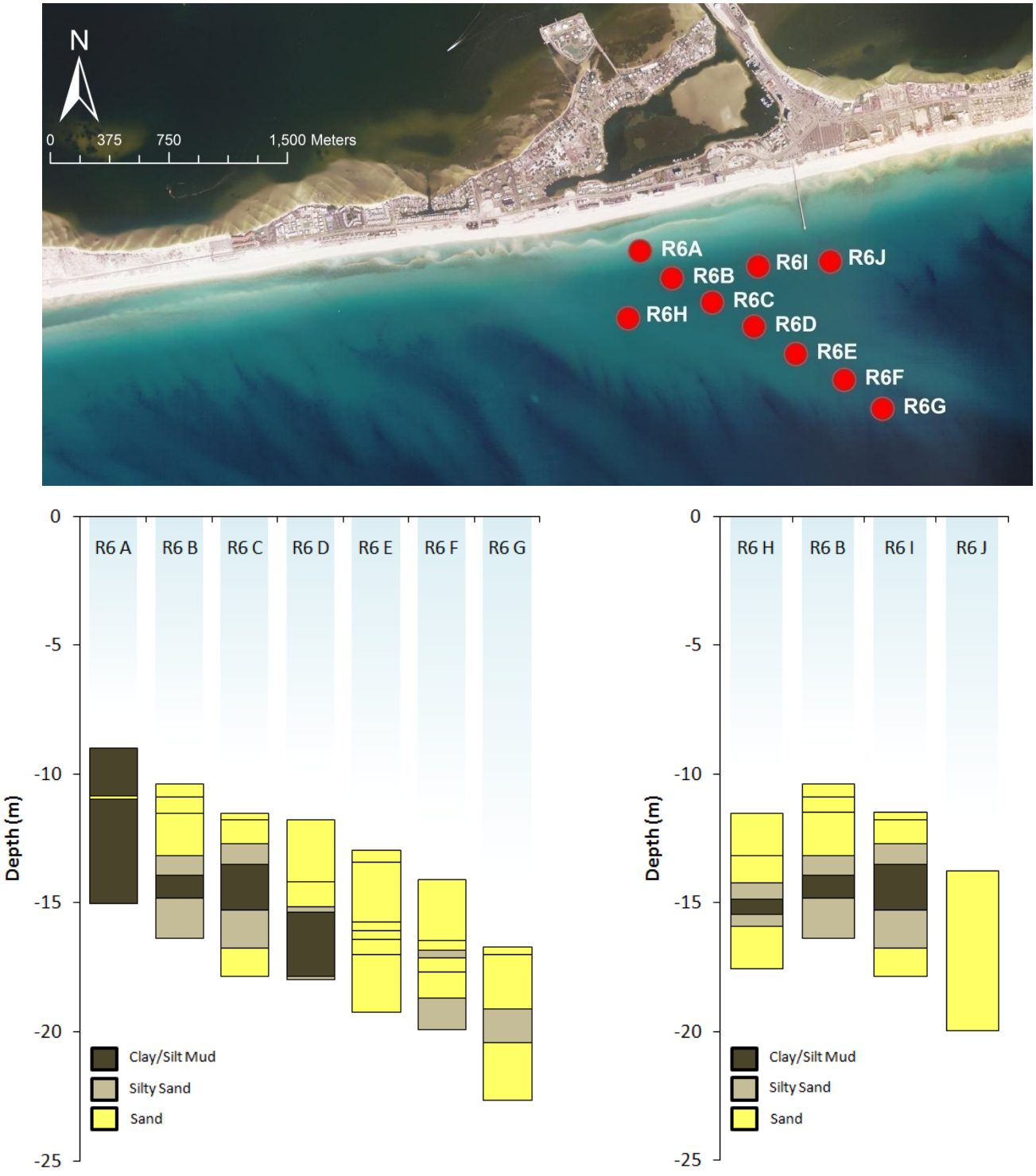


Figure 75. Vibracore data from Ridge 6 fronting Pensacola Beach. Shown are vibrabore data, shown in terms of broad textural classifications, from the cross-shore and alongshore transects shown on the satellite image above.

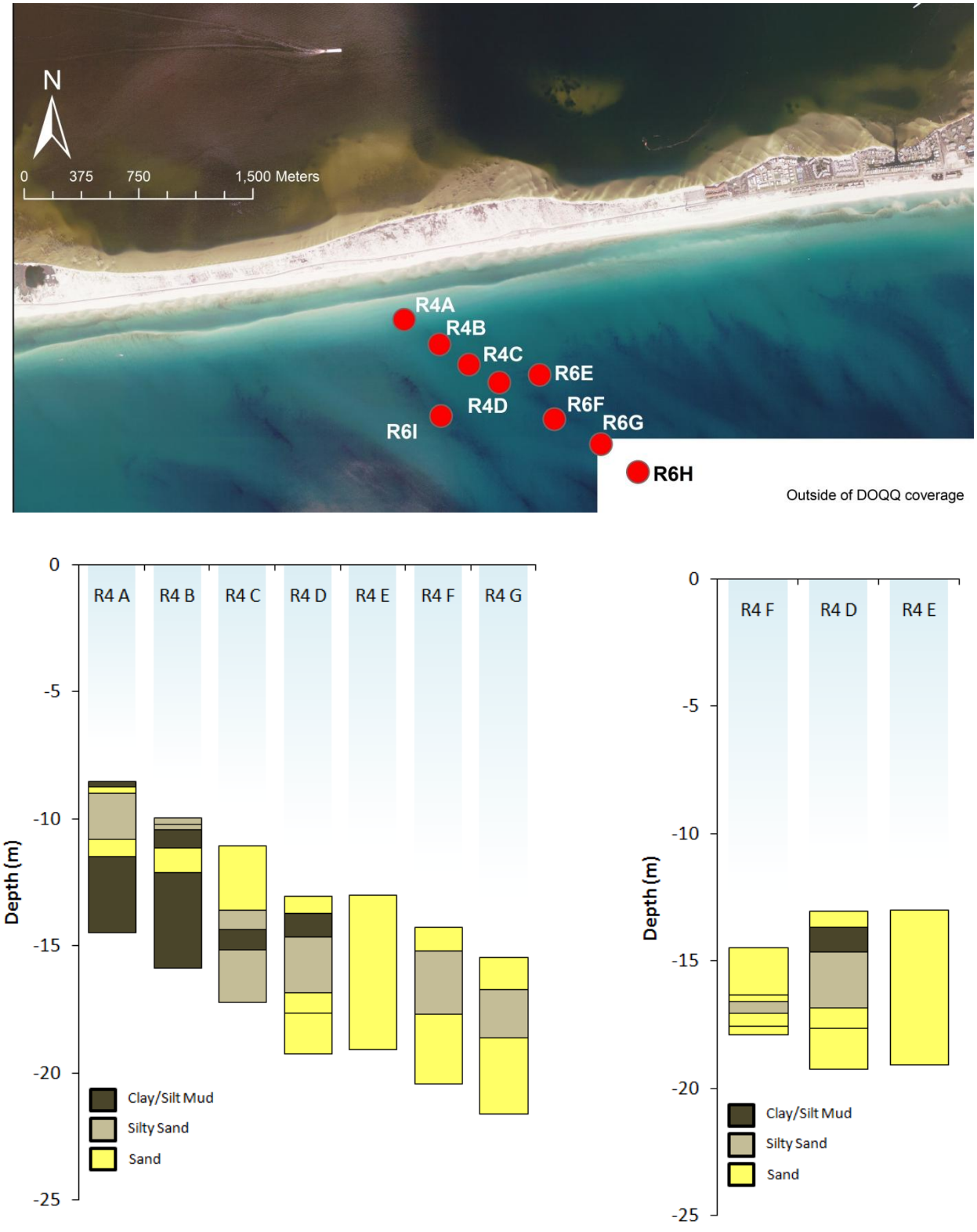


Figure 76. Vibracore data from Ridge 4 in the Fort Pickens Unit. Similar to Figure 7, the vicbracore data from the cross-shore and alongshore transects is presented in terms of broad textural classifications.

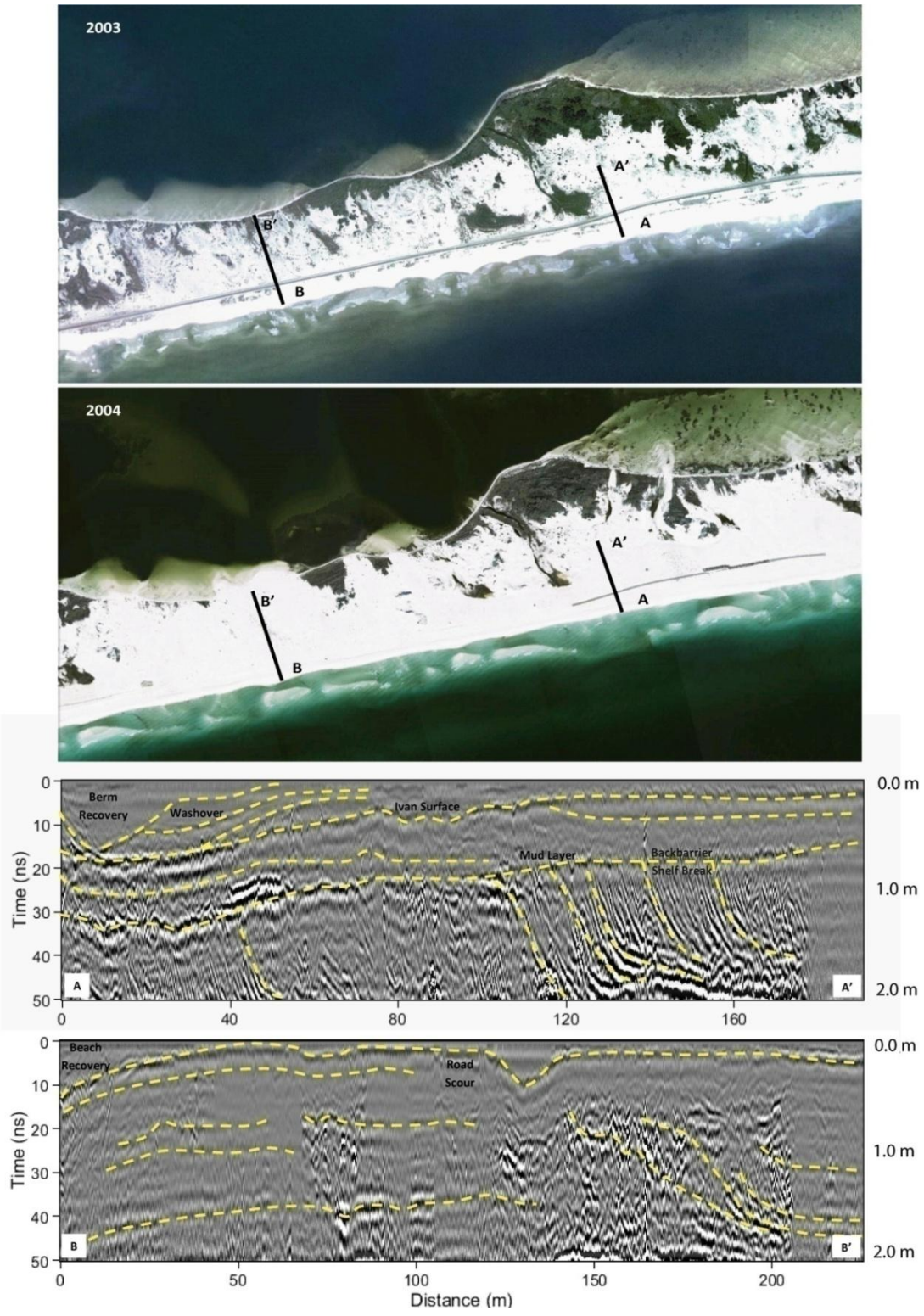


Figure 77. Ground-penetrating radar transects from the narrow and wide sections of the island in the Santa Rosa Island Unit of the study area. Note that the GPR surveys have not been corrected for the relatively small elevation variation of the transect areas.

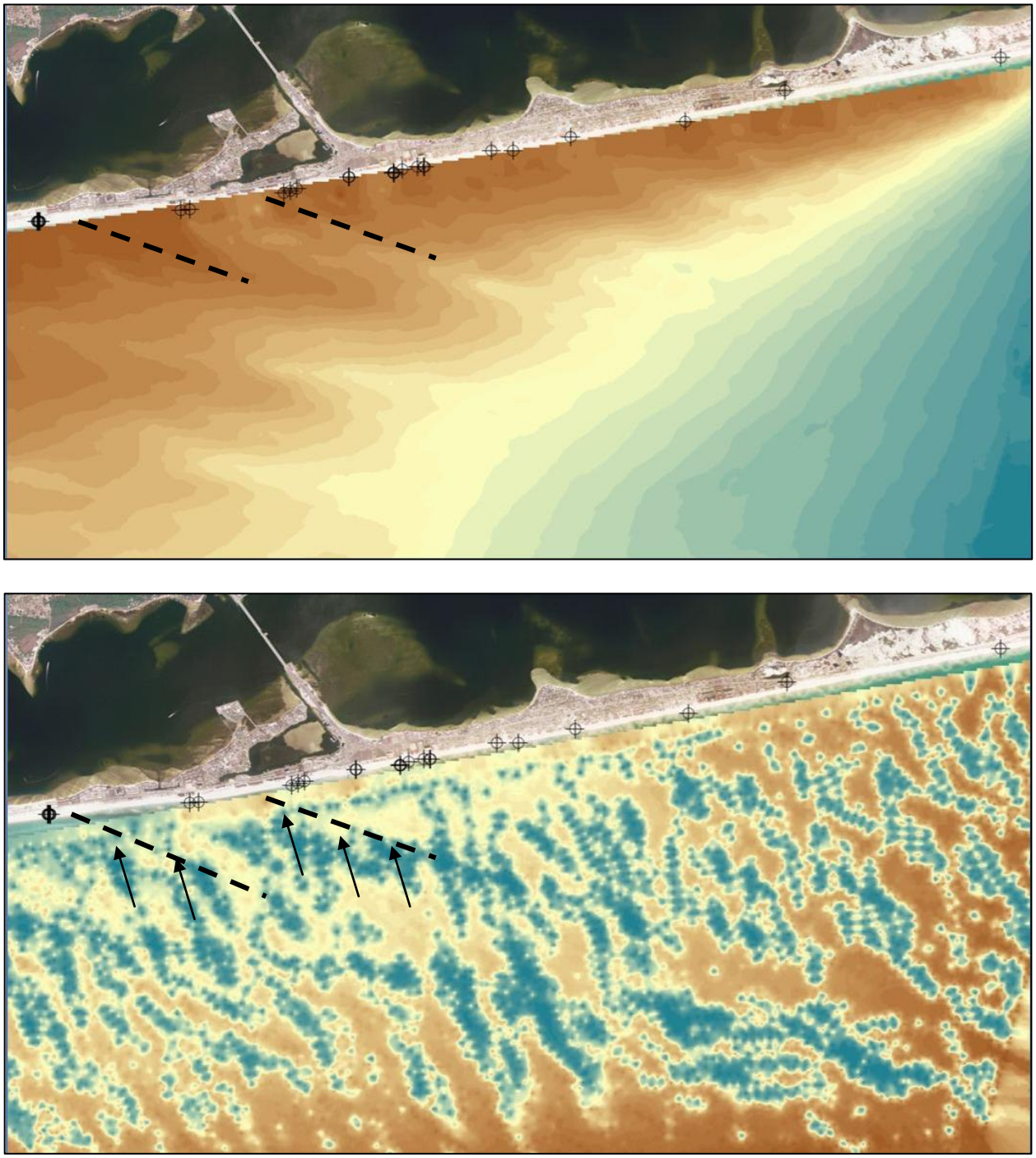


Figure 78. Modeled (a) average wave heights and (b) total bed elevation change for Hurricane Ivan (2004) in the Pensacola Beach section of the study area. The erosion data is presented only as erosion (blue) and deposition (brown).

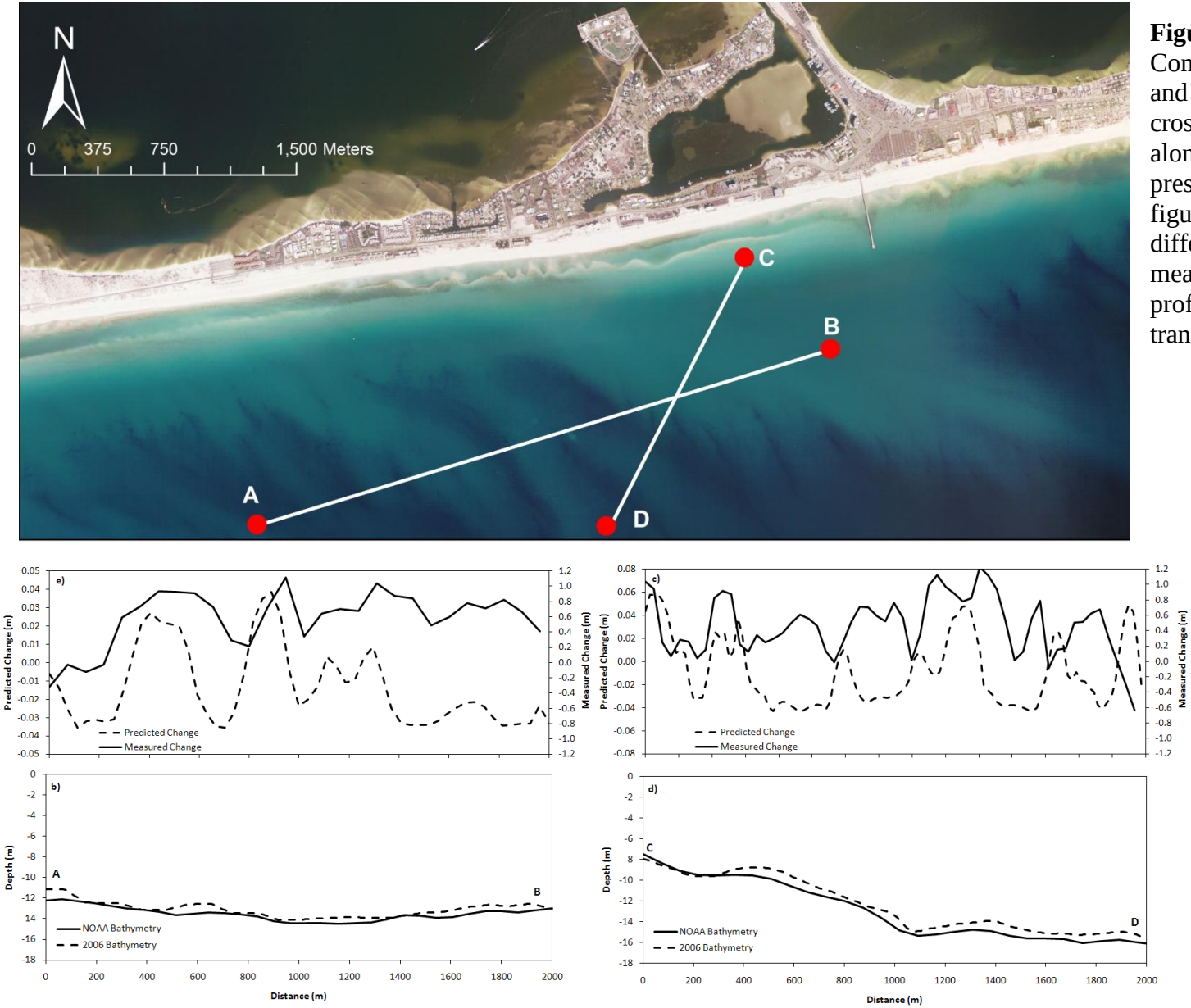


Figure 79. (a) Comparison of NOAA and 2006 bathymetry over cross-shore and alongshore transects presented in the above figure. Also shown is the difference between the measured and modeled profile change along both transect.

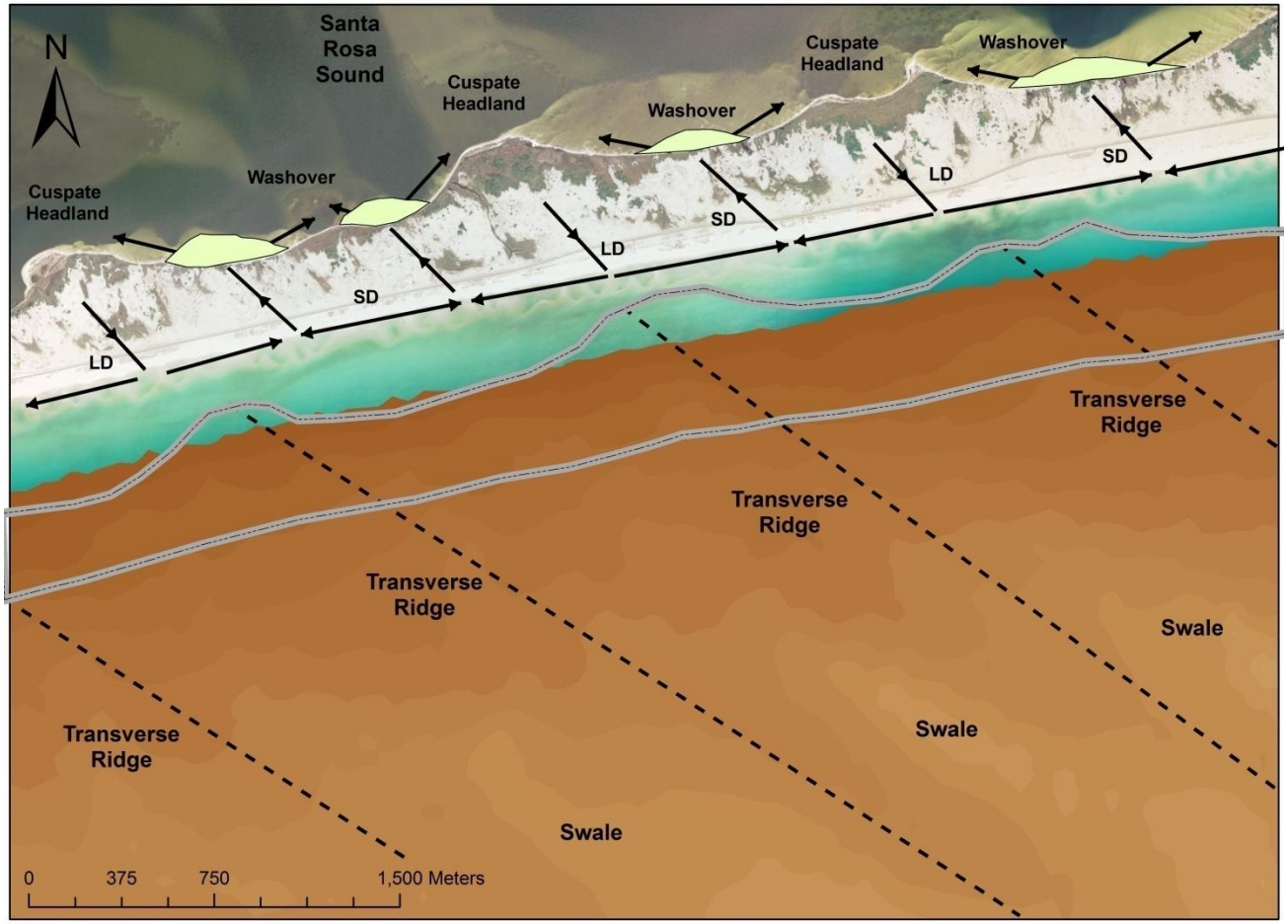


Figure 80. Conceptual model showing the translation of the island through with respect to the transverse ridges and swales. Also shown are transport vectors showing offshore erosion during extreme storms post-storm alongshore redistribution of sediment from areas of large dunes (LD) to small dunes (SD), and washover through the narrow sections of the island (Houser et al., 2008; Houser and Hamilton, 2010) responsible for the maintenance of island form.

99

100
101
102
103

CHAPTER 7

Impacts of Hurricane Katrina on the Geomorphology of the Mississippi Barrier Islands

Chris Houser
Department of Geography
Texas A&M University
810 O&M Building
College Station, Texas
77843-3147

SUMMARY OF RESULTS

On all three islands, the morphological impact of Hurricane Katrina depended on the pre-storm average elevation as predicted by the Sallenger (2000) model of hurricane impacts. Specifically, the shoreline change, overwash penetration (see Morton, 2007) and volume change were inversely related to the pre-storm average elevation (Figures 1 and 2). The sediment eroded from the areas of higher average elevation (during swash and dune impact) was deposited on the shoreface as a nearshore bar. In these areas, the backbarrier island morphology remained intact, fronted by a short overwash terrace. In areas where the average pre-storm elevation was at a local minimum, the island experienced overwash early in the storm (ie. limited swash and dune impact), leading to sediment losses to the backbarrier, with some sediment deposited in the sound. These areas had limited bar development.

Some of the greatest change in island morphology occurred at the eastern ends of Horn and Petit Bois Islands and at both ends of Ship Island. The eastern end of each islands were eroded and there was a reorientation of the island to the dominant wave direction (from the SE). One of the most dramatic changes (outside the loss of land on Ship Island) was the migration of the spit terraces on the eastern end of Petit Bois Island. Based on 2001 NOAA bathymetry data, it appears that the spit terrace decreased in elevation by ~1.5 m and migrated to the north by ~315 m (Figure 3). As the nearshore bar on this terrace continues to migrate landward (to the north), it is anticipated that a small spit will emerge on the terrace as was present in the 2001 bathymetry. In contrast, the western end of Petit Bois and Horn Islands accreted (in volume and shoreline position) through alongshore sediment delivery from the east.

Based on the results of this study, there was little change in the sediment volume for Petit Bois and Horn Islands. Most of the sediment eroded from the beachface and dune systems was deposited on the shoreface as bars and recovery will depend on the onshore migration of these features. The length of time for bar migration and beachface recovery along the Gulf Coast remains poorly understood. Sediment volume on Petit Bois and Horn Islands was only lost from the islands were the overwash terraces extended to backbarrier shoreline. This sediment is most likely lost from the system through cold front erosion, although it is possible that the sediment is distributed alongshore. In contrast, significant changes in volume were observed on Ship Island due to the lower elevation of the island were it was eroded during Hurricane Camille and only partly recovered and due to the higher storm surge and wave height on the island. The sediment was deposited along the backbarrier shoreline and into Mississippi Sound, which will limit the potential for post-storm recovery.

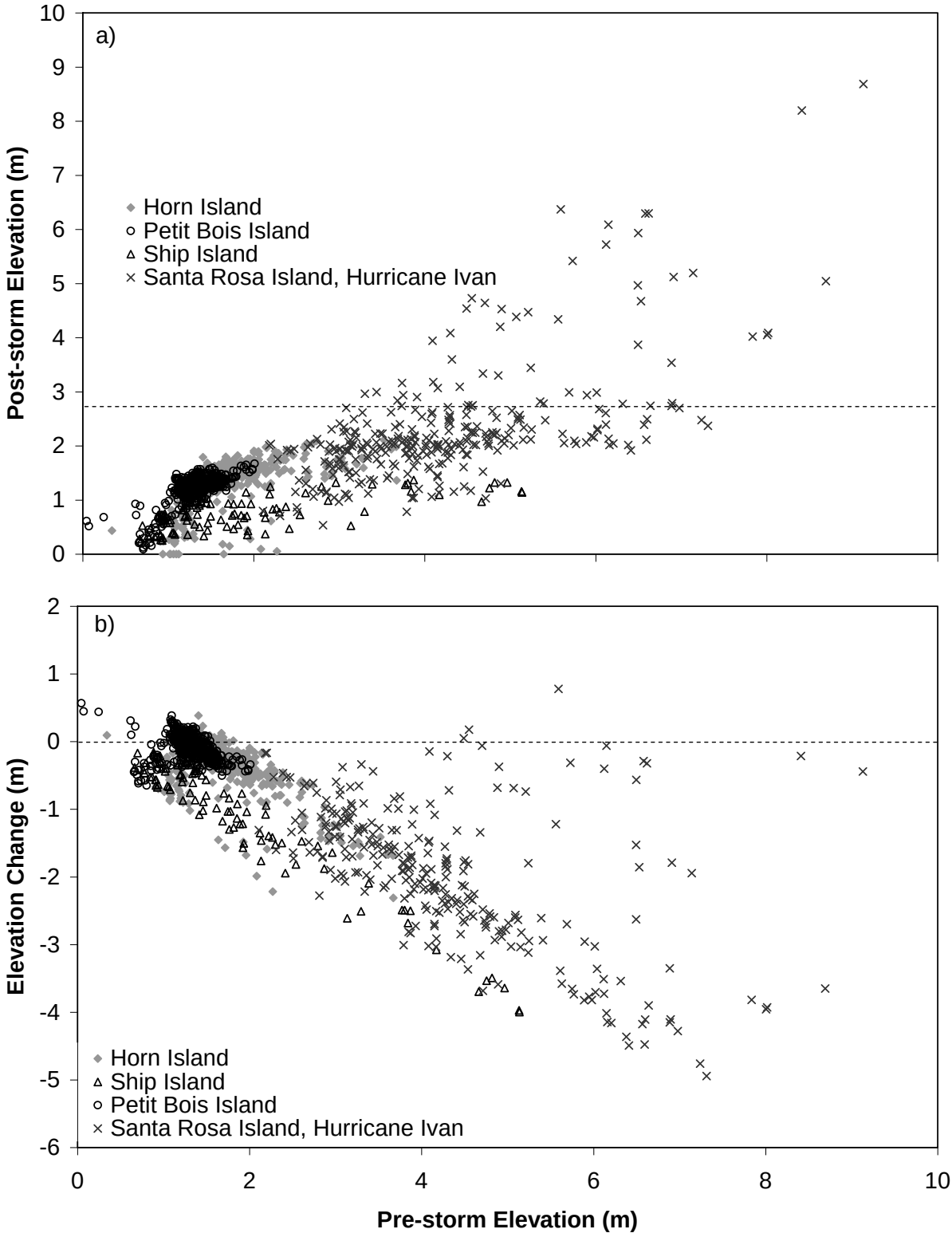


Figure 81. Relationship between average pre-storm elevation and (a) post-storm elevation and (b) elevation change (post-pre elevation) for Petit Bois, Ship and Horn Islands. Also shown is the relationship for Santa Rosa Island for Hurricane Ivan.

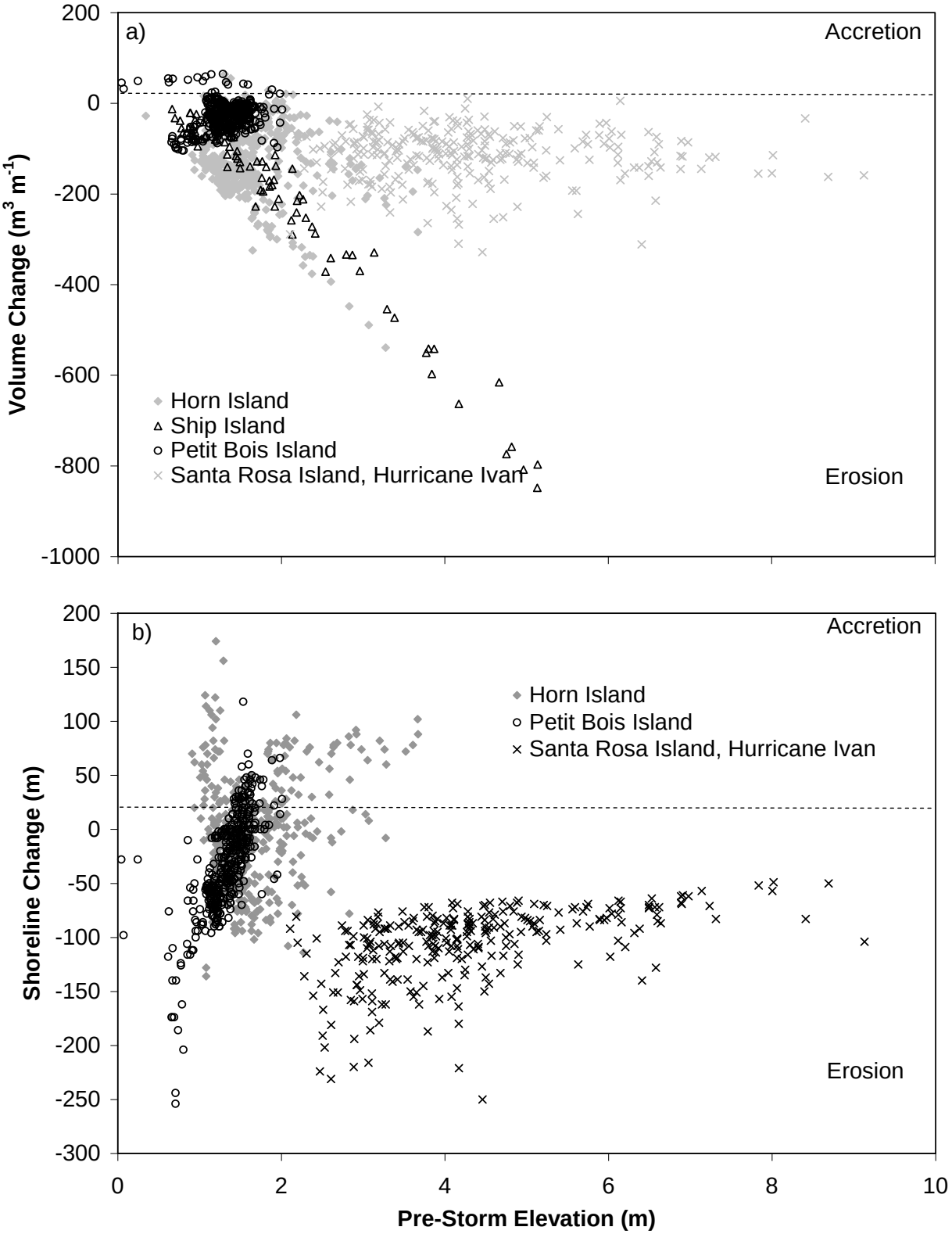


Figure 82. Relationship between average pre-storm elevation and (a) volume change and (b) shoreline change (post-pre elevation) for Petit Bois, Ship and Horn Islands. Also shown is the relationship for Santa Rosa Island for Hurricane Ivan.

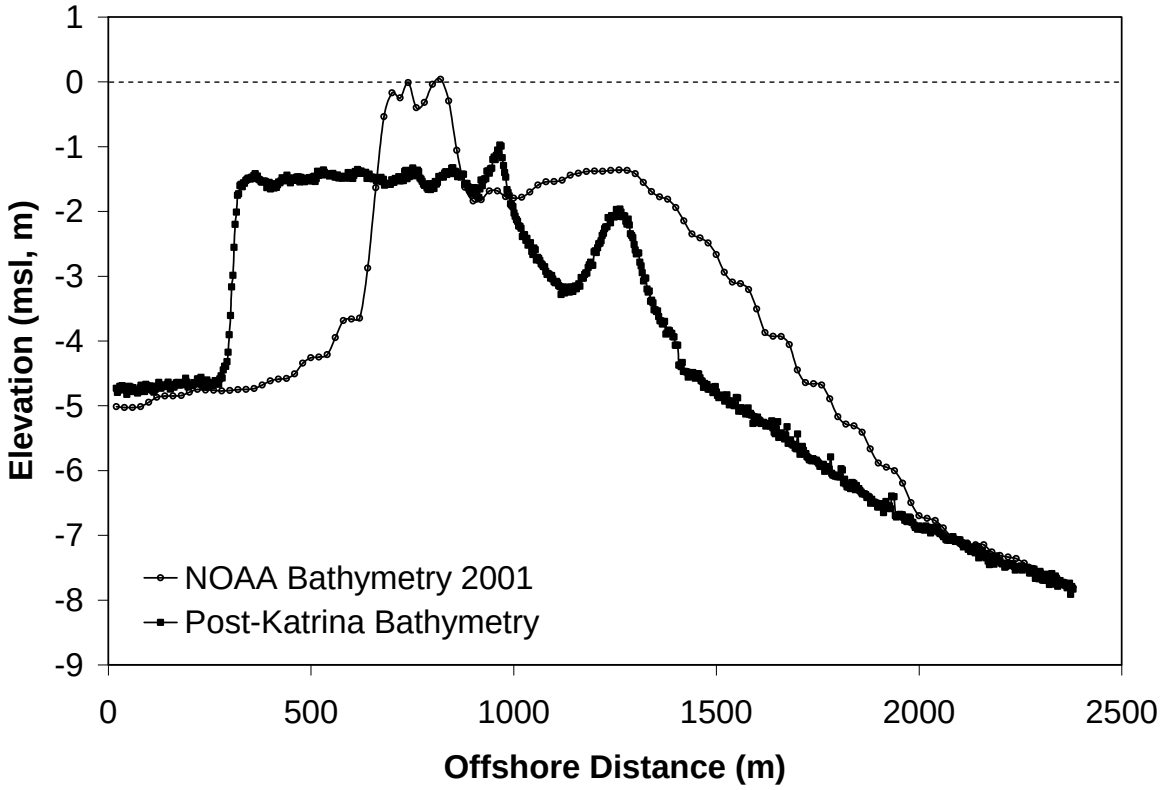


Figure 83. Pre- and post-storm bathymetry for the eastern end of Petit Bois Island showing the landward (northern) migration of the nearshore terrace and lose in elevation.

STUDY OVERVIEW

Hurricanes and tropical storms produce elevated water levels and large waves, capable of eroding the beachface and causing overwash and barrier breaching. In general, the morphological response of a barrier island can include:

1. shoreface erosion and bar formation and migration (also known as the Bruun Rule)
2. erosion alongshore by longshore transport
3. migration onshore via roll-over or over stepping (net sediment transfer landward)

The Bruun rule is a simple two-dimensional model of shoreline response to sea level change (including surge), in which the equilibrium profile remains unchanged as the shoreline moves in response to rising sea level (Cooper and Pilkey, 2004). Sand that moves from the upper portion of the beach profile accumulates at the lower portion of the profile, thus maintaining shoreline geometry. However, this type of response assumes that 1) geology does not play a role in shoreline shape, 2) sediment is only moved by waves, and 3) there is no significant movement beyond the depth of closure, the seaward limit of sediment transport. (USACE, 2002). When water levels exceed the height of the foredune or the beach ridge, the island experiences overwash. Sallenger (2000) describes this translation from offshore erosion during swash and impact regimes to overwash as a balance between the elevation of the storm surge relative to the vertical geometry of the coast, (Figure 4) which in turn depends on the extent and height of foredune or beach ridge development (Thieler and Young, 1991; Sallenger, 2000).

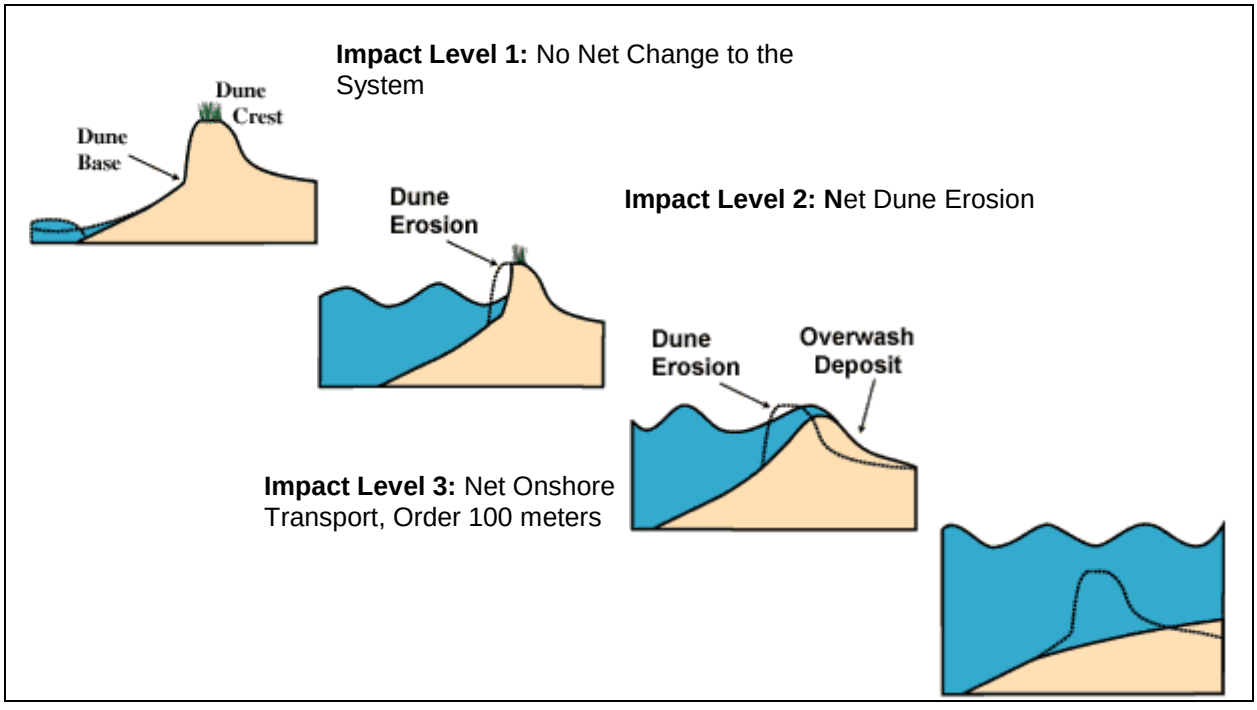


Figure 84. Hurricane Impact levels of Sallenger (2000).

The swash regime occurs during periods of low wave energy. Impacts in the swash regime are restricted to the swash zone, the zone between to the foreshore of the beach seaward of the foredune. As a consequence, the foreshore is eroded and sand transported offshore, and is returned (slowly) to the beach during periods of low wind and wave energy (Sallenger, 2000). When the storm tide (astronomical tide plus storm surge) increases, it will eventually collide with the base of the foredune (D_{low}), and sediment is eroded offshore. During particularly strong storms, sand can be moved offshore beyond the point where it will be transported under non-storm conditions (Sallenger, 2000).

The overwash regime occurs when the run-up height exceeds the dune crest ($R_{high} > D_{height}$), and water and sediment flow landward across the barrier. Although there is some loss of sediment offshore as the dune is first impacted, most of the sediment eroded from the dune is deposited landward as overwash (Sallenger 2000). This sediment can be only returned to the recovering foredune through aeolian transport from landward offshore winds originating on land and blowing offshore (Leatherman, 1979). If sediment is not returned to the beachface from the overwash or new sediment is made available from alongshore or the shelf, the island will experience a net landward migration or roll-over. The inundation regime occurs when surge levels greatly exceed the height of the foredune, such that the island is completely submerged. This can lead to island overstepping.

A good example of the importance of vertical geometry on the morphological response during an extreme storm is the impact of Hurricane Camille on Dauphin Island (Morton and Sallenger 2003). Prior to the storm, island elevation varied from 2 to 3 m with the largest dunes on the eastern end of the island. The maximum surge during Hurricane Camille reached 2.8 m; such that the eastern end of the island was in a "collision regime." Morphologic changes due to overwash gradually changed westward along the island where overwash and surge impacts progressively increased. The western end of the island not only had smaller dunes but also a steeper bathymetric gradient. In these areas, beach erosion via direct wave impact was magnified because storm waves energy was not dissipated offshore with the presence of shallow water or a nearshore bar (Thorton et al. 2006). The smaller dunes provided less protection and more sediment was transported landward as overwash (Morton and Sallenger 2003).

While the Sallenger model focuses on the foredune height, the alongshore extent and presence of secondary dunes can also be important. Topographic relief such as dunes and swales confine the surge into channels or low interdune areas and accelerate flow (Morton 2002; Leatherman 1977). Sediment transport within these areas can be further amplified by the shallow flows and high wind stress (Morton and Sallenger 2003). As found by Houser et al. (in press), overwash penetration and offshore erosion was increased in areas with discontinuous foredunes through lateral erosion, and decreased in areas where secondary dunes were present. Overwash penetration on Santa Rosa Island, Florida, following

Hurricane Ivan (2004) varied with the cross-island geometry and specifically with the presence of secondary dunes.

The shoreline of the Gulf Islands National Seashore along the Mississippi coast suffered significant beach erosion and widespread overwash and breaching. The impact of Hurricane Katrina on the barrier island chain depended on the vertical geometry of the coast, which in turn depends on the extent and height of foredune development (Sallenger, 2000). The erosion sustained by the islands during past extreme storms such as Hurricane Camille (1969) and more recently Hurricanes Ivan and Dennis has precluded growth of the islands. The anticipated increase in the frequency of extreme storms with the warming of Atlantic sea-surface temperatures (Keim *et al.*, 2004) will reduce the time available for the barrier island to recover. The erosion sustained by the barrier islands along the Mississippi coast during Hurricane Katrina will condition the response of the islands to future extreme storms and will therefore affect their longer-term evolution.

The ability of a barrier island to redevelop and the time required for that rebuilding depends on the availability of sediment. Recent evidence suggests that the barrier islands along the northern Gulf of Mexico can conserve mass during catastrophic hurricanes through the generation of overwash fans (Stone *et al.*, 2004). These overwash fans are, however, eroded during the passage of cold-fronts (Stone and Morgan, 1993; Armbruster *et al.*, 1995; Chaney and Stone, 1996; Armbruster, 1997; Stone *et al.*, 2004; McBride and Byrnes, 1997) that generate strong northerly winds and steep high-frequency waves (Kraus *et al.*, 1991). Despite recent studies documenting the immediate impact of extreme storms and the post-storm erosion of overwash deposits on the barrier islands of the Gulf of Mexico, the mechanisms responsible for post-storm changes in the island volume and the sediment transport pathways along the backbarrier have not been examined.

Island recovery can also occur through sediment delivery from alongshore and the onshore migration and eventual welding of nearshore bars created during the storm event. The model of Wright and Short (1984) is the most commonly cited morphometric model. It describes three basic forms and process signatures within a continuum of beach states from dissipative to reflective. In this model, beach states are differentiated with respect to the dimensionless fall velocity (Ω):

$$\Omega = \frac{H_b}{w_s T}$$

Wright and Short proposed that the beach would be dissipative when $\Omega > 6$, intermediate when $1 < \Omega < 6$, and reflective when $\Omega < 1$. To develop their model, Wright and Short (1984) used a morphological database spanning more than 6 years, consisting of pre- and post-storm surveys from a number of

environmentally different beaches in Australia. It was found that over the longer term, a given beach will tend to exhibit a *modal* (or most frequently recurrent) state, which depends on the modal wave conditions, around which a spread of higher or lower waves may prevail (Wright and Short, 1984). Recovery from the nearshore bar occurs via bar migration onshore when waves are shoaling and breaking landward of the bar crest (Plant *et al., 2*001; Houser and Greenwood, 2005). Transport of sediment onshore is associated with the oscillatory skewness and skewed accelerations that develop as the wave breaks (Houser and Greenwood, 2005). Unlike offshore migration during storms, beachface recovery requires an extended period of low-wave activity to enable bar migration onshore and ultimately bar attachment to the beachface.

Mississippi Barrier Islands

The Mississippi barrier islands are arranged east to west as follows: Petit Bois, Horn, East Ship, West Ship, and Cat Islands (Figure 5). Presently, these islands are part of the Gulf Islands National Seashore and are managed by the National Park Service. The National Park Service is currently updating its 1979 historical management plan to a plan that will adequately address issues facing the islands for the next 15-20 years (National Park Service 2006).

The islands originated during the Pleistocene period in response to water level changes (Otvos, 1979). The framework of the islands (from northwest Florida to the Mississippi delta) consists of numerous low-profile, well-preserved sand beach ridges and swales (Waller and Malbrough, 1976). The arrangement of these ridges and swales relates to the origins of sediment supply for the islands, suggesting that the beach ridge topography was formed during a period of abundant sediment supply. The present sand supplies are the result of spit growth supplied by sediments derived from the east by sediment discharged by the Apalachicola River, and locally by the Mobile River and Mississippi River (Schmid, 2003; Waller and Malbrough, 1976). Since formation, the islands have experienced significant lateral migration to the west while remaining approximately the same distance offshore. In systems with multiple subparallel barriers, longshore currents can transport sand from adjacent islands, which serve as a new source of sediment for recovery (Leatherman, 1979). However, the physical disconnect between islands and the dredging of the passes may have reduced or even completely removed the longshore source of sediment.

Island formation in Mississippi has been attributed to two mechanisms. The first suggests that sediment was transported from Mobile Bay area to an offshore continental shelf source (Shepard 1960). This offshore sediment source provided sediment supply to the islands via onshore bar progression (Shepard 1960). The second mechanism involves broad shoals composed of soft and unconsolidated sands between Mobile Bay and Pensacola which supplied sands to the west across the Mobile tidal inlet (Kwon,

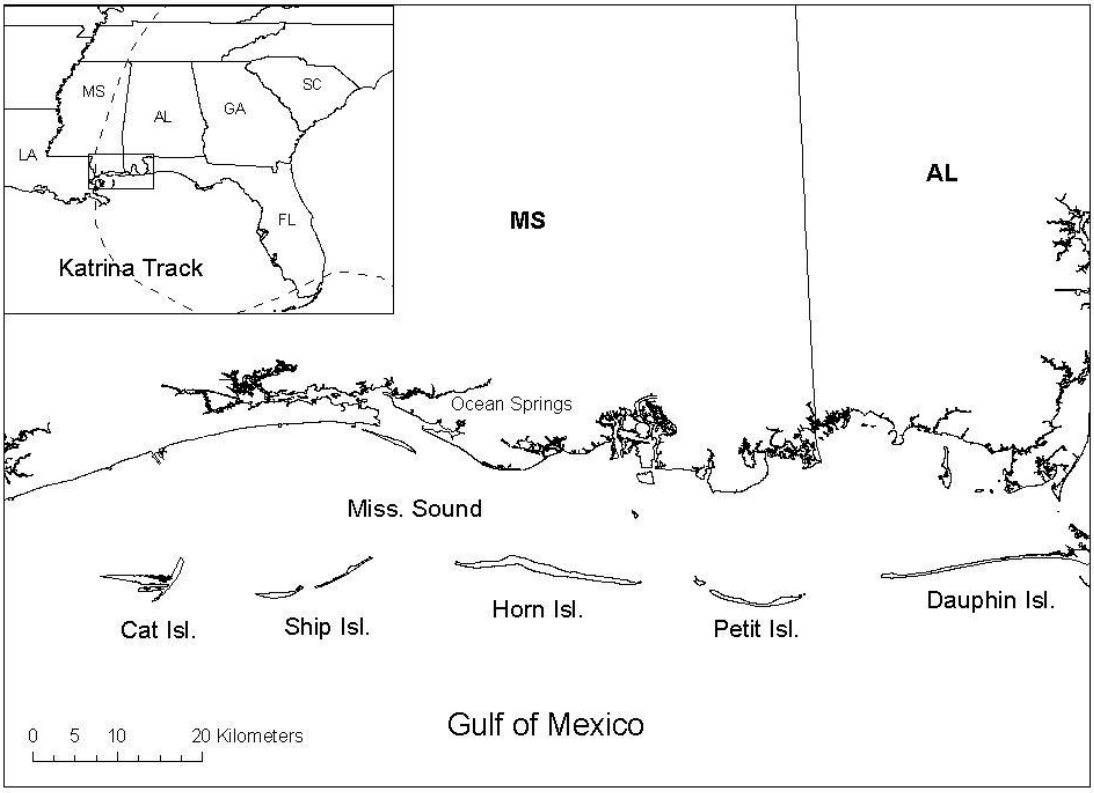
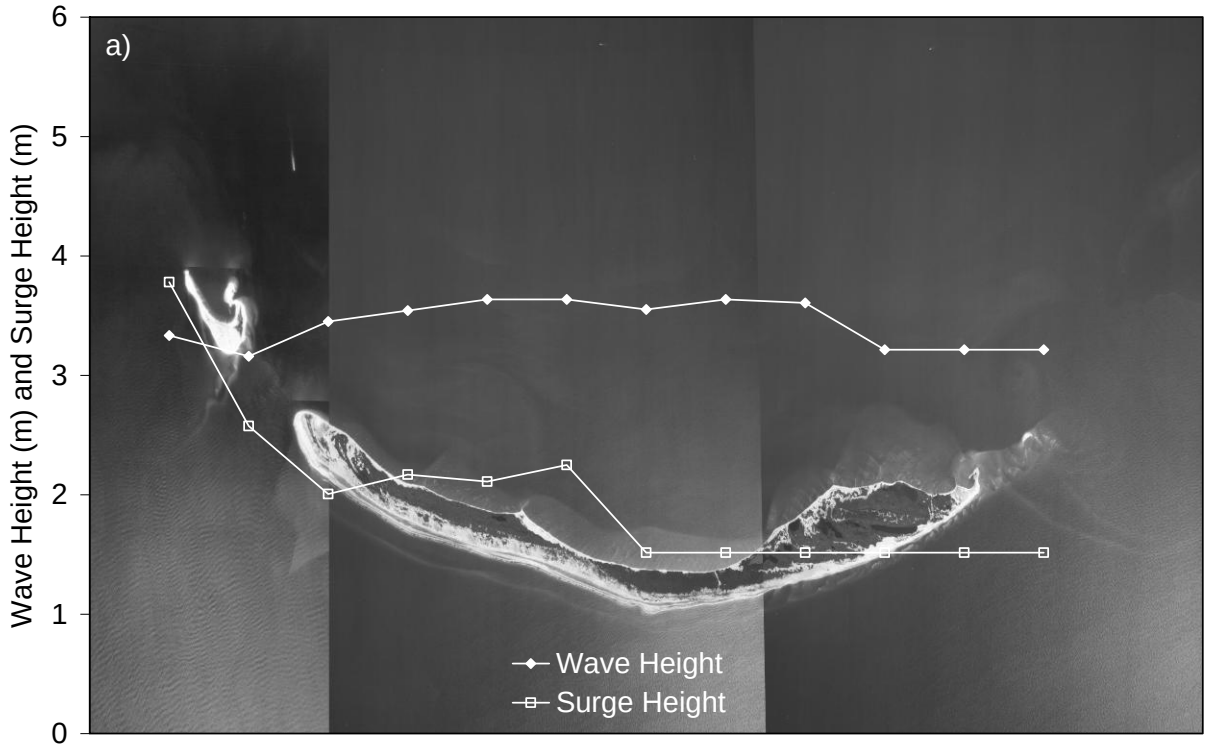


Figure 85. Map of the Mississippi barrier islands.

1975) as prevailing easterly winds enhanced longshore currents (Waller and Malbrough, 1976). Through time, silt and muddy sand layers originating from the Mobile Point Peninsula and Dauphin Island consolidated to form emerging islands formed between eastern Dauphin Island and New Orleans (Otvos, 1979). Otvos (1979) collect core-hole data and used comparisons of microfauna to demonstrate that the mainland shore of the islands remained unbarred in the Mid-Late Holocene period. This suggests that the Mississippi barrier islands emerged from shoals in their present locations and shifted west with longshore sediment transport over time (Otvos, 1979). In contrast to the Mississippi mainland coast, an acoustic survey of the Horn and Petit Bois shore found that present passes within the Mississippi Sound were not inherited from Late Pleistocene stream entrenchment (Otvos, 1979). Prevailing winds are out of the east and enhance longshore currents that move sediment westward (Waller and Malbrough, 1976). Soil samples from the islands reveal a progressive decrease in median grain size to the west (Waller and Malbrough, 1976). The combination of a decreasing sediment size and the westward lateral drift trend of the islands further enforces the idea of that sediment is transported alongshore from the Mobile Bay.

Six hurricanes (category 3 or greater on the Saffir-Simpson Scale) have made landfall in the Mississippi

area since 1969. These hurricanes include; Camile (1969), Frederic (1979), Elena (1985), Andrew (1992), and Ivan (2004) (NOAA, 2006). Most recently, Hurricane Katrina made landfall as a category 3 with sustained winds of 59.2 ms^{-1} near Buras, Louisiana, on August 29, 2005 (Knabb *et al.,* 2005). The storm had an eye wall radius of 13-48 km and hurricane force winds extending out 135 km to the east and west. Peak winds of 77.2 ms^{-1} were recorded on August 28 about 306 km southeast of the mouth of the Mississippi River (Knabb *et al.,* 2005). The storm created a storm surge that extended from Western Louisiana and into the Florida Panhandle (Knabb *et al.,* 2005); surge levels were between 3-5 m along the eastern Mississippi coast from Gulfport to Pascagoula (Knabb *et al.,* 2005). The extreme surge levels are attributed to the storm's large horizontal size, with the surge being further increased by the large waves (and set-up) created the previous day when the storm reached a category 5 level (Knabb *et al.,* 2005). Measurements taken by the National Data Buoy Center (NDBC, 2005) suggested a significant wave height (defined as the average of the one-third highest waves) of 9 m with a wave period of 17 s as early in the storm measured at buoy 42040, (approximately 115 km south of Dauphin Island, Alabama; Knabb *et al.,* 2005). The alongshore variation in predicted wave and surge heights are presented for each island in Figure 6.



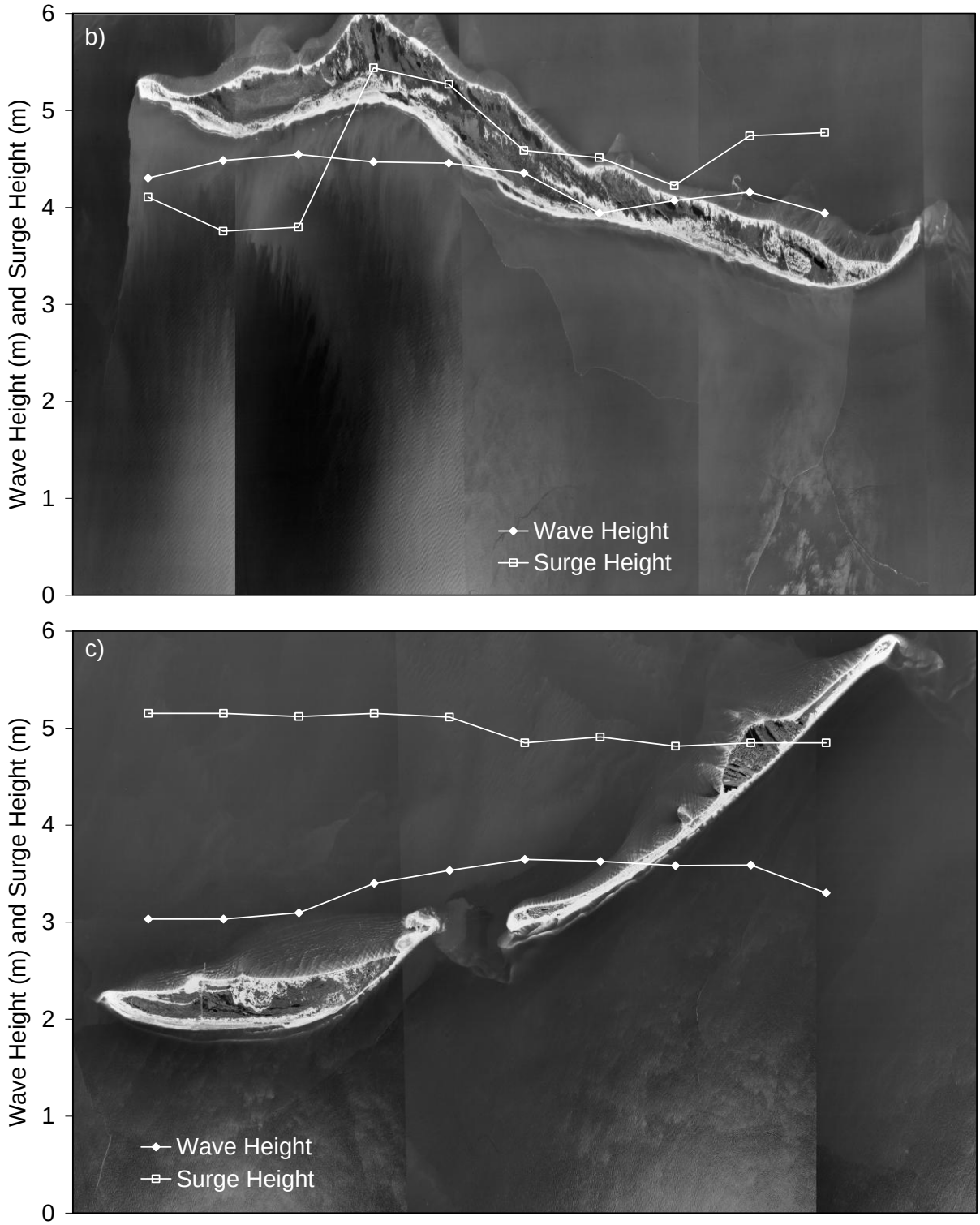


Figure 86. Alongshore variation in wave height and surge height at (a) Petit Bois Island, (b) Horn Island and (c) Ship Island.

METHODOLOGY

Changes to the barrier islands of the Gulf Islands National Seashore in Mississippi (Petit Bois, Horn, East Ship and West Ship) will be characterized by documenting conditions relative to the pre-storm morphology and the role of past extreme storms in shaping the morphology. This analysis will be completed through LIDAR elevation maps (pre- and post-storm) provided by the National Oceanographic and Atmospheric Administration (NOAA). In the past, research involving morphologic change to barrier islands was limited to data collected by surveying techniques and aerial photo interpretation. These methods produced coarse resolutions and were highly time-consuming (White and Wang, 2003). The Laser Imaging Detection and Ranging System (LiDAR) is an active remote sensing application (Zhang *et al.,* 2005), that uses a high-frequency laser directed at the earth's surface through an opening in the bottom of an overhead aircraft. The laser system records the time difference between emissions of the laser beam and the reception of the reflected laser signal in the aircraft (Meredith *et al.,* 1999). A rotating oscillatory mirror mounted to the front of the laser allows it to swath back and forth, providing a large coverage swath area below the plane (Zhang *et al.,* 2005). The system uses the combination of a high-speed scanning system and a high-repeating laser-pulse frequency to determine x, y, and z values across the terrain below, thus producing a data set of high spatial resolution in little time (White and Wang, 2003). The aircraft position is monitored by a GPS receiver mounted to the aircraft and a second GPS station mounted to the ground is used for differential corrections (Zhang *et al.,* 2005).

LiDAR elevation points were interpolated into digital elevation models (DEM), using the inverse distance weighted method (IDW) with a power of ten and using the six nearest neighbours. The IDW interpolation assumes that the interpolating surface should be influenced most by nearby points and should be less influenced by distant points. Specifically, the interpolated surface is a weighted average of the points, and the weight of each point decreases with distance. Because both elevation and depth are spatially autocorrelated, using a weighted distance interpolation method explicitly accounts for interrelationships between points. The interpolation yielded a root mean-square error of 0.16 for the pre-storm data set and a root mean square error (the difference between the interpolated value and the actual value) of 0.10 for the post-storm data set. Subaerial profiles were created from transects exported from DEMs. Elevation profiles were constructed through the use of the LiDAR Data Handler tool within ArcMap, which exports elevation data from the DEM. Points were exported from the DEM at 2 m intervals along transects. Transects were spaced at 40 m intervals along the island and provided a cross-shore elevation reference from the Gulf shoreline inland to the limit of the LIDAR data or tree line. Pre-storm LiDAR data for the island extended to transect 24 at the eastern tip of the island. Post-storm LiDAR data were limited in capturing the eastern end of the island and data was unavailable beyond transect 20.

Subaqueous changes to the island were examined through bathymetric profiles on both the Gulf and sound sides of the islands as well as the inlets between each island. Pre-storm bathymetric profiles were

constructed using bathymetric data from 1975 obtained from NOAA Hydrographic surveys; however, gulf-side data for the middle portion of the island were unavailable. The NOAA survey was collected using single beam sonar across the entire portion of the Mississippi Sound and for portions of the Gulf side of the Mississippi barrier islands. Bathymetry points were interpolated using the inverse distance weighted method, with a power of two, using the eight nearest neighbors. The interpolation yielded a root mean-square error of 0.59. Pre-storm bathymetric profiles were extracted at 7.5 m cross-shore intervals from the model using the NOAA LiDAR Data Handler tool within ArcMap. Post-storm bathymetric data were collected with the use of a Lowrance depth finder unit (model LMS-339) following the storm. Data were collected on June 1 and 2. Post-storm transects were collected at 400 m (ten times the distance of the land transects) intervals along the shoreline and extended from the shoreline to a distance of 1 km offshore on the Gulf side and to a distance of 500 m on the sound side. Transect intervals of 400 m provided a scale that indicated alongshore bathymetric variability, while offshore data collection distances of 1 km and 500 m indicated closure of pre- and post-storm bathymetric profiles. A similar bathymetric model was created using the post-storm sonar data. Tide variations during the collection of bathymetric data were subtracted from the data based on tide data collected at the NOAA Pascagoula tide station based on NAVD 1983.

Data Analysis

The analysis of pre-storm and post-storm data obtained from both the subaerial and subaqueous portions of the islands was examined through the use of empirical orthogonal functions (EOF) analysis. EOF analysis identified patterns in how the island responded to the storm and related changes to pre-storm morphology both subaerial and subaqueous. EOF analysis is similar to principal component analysis (PCA), except that the variable is examined through space rather than through time (Aubrey, 1979). The eigenvalues correspond to a statistically optimal description of the data with respect to how the variance is concentrated in the modes (Larson *et al.,* 2003). EOF analysis allows a user to reduce the number of variables and to detect structures in the interactions between variables. This allows variables to be classified and can identify redundancies and associations in the data (Houser *et al.,* in press). EOF analysis has previously been used in coastal geomorphology to describe nearshore bar behavior (Larson *et al.,* 2003; Houser and Greenwood 2005) and morphological controls on hurricane impacts (Houser et al. in press).

The relationships between pre- and post-storm topographies (bathymetric and aerial) were examined through canonical correlation analysis (CCA). This analysis identifies patterns that occur simultaneously in two different data sets and describes the nature of those patterns (Houser *et al.,* submitted).

IMPACTS TO PETIT BOIS ISLAND

Oblique aerial photographs of the post-storm morphology are presented in Figure 8, and the pre- and post-LiDAR images for Petit Bois Island are provided in Figures 9 and 10. The pre- and post-storm average elevation of the island across each of the survey transects are provided in Figure 12. While areas with large elevations were reduced in height, there were several areas of the island where the post-storm average elevation increased, suggesting accretion during or immediately following the storm. A review of the detailed analysis is provided in the following sections.

Volume Change

Over 460,000 m^3 of sediment was lost from the aerial portion of the island with an average volume loss of -28 m^3 m^{-1} length of shoreline (Figure 7). However, the volume change varied from an accretion of 63 m^3 m^{-1} length of shoreline to a loss of -100 m^3 m^{-1} at the eastern end of the island. In comparison, the net change in sediment volume along Santa Rosa Island ranged from an erosion of 238 to 43 m^3 per unit width of beach during Hurricane Ivan. Assuming that the nearshore profile maintained its shape, an additional 243,000 m^3 of sediment was lost from the sub-aqueous portion of the island. Assuming that the sediment losses from the island and the shoreface were equally distributed within the offshore survey area (15 million m^2), the sediment would only represent a change of 0.05 m which is within the sampling error of the depth sounder ($\pm$0.10 m).

Shoreline Change

On average the shoreline retreated by ~35 m but varied considerably from a gain (accretion) of 118 m to a loss (erosion) of 254 m. As shown in Figure 7, the change in shoreline position is related to the volume change. Areas of shoreline erosion are associated with the largest losses of sediment, while areas of shoreline accretion are associated with the smallest loss of sediment and sometimes a volume gain. Shoreline accretion was observed along the western end of the island despite the general loss of island volume, while both shoreline and volume loss were observed at the eastern end of the island. In the centre of the island there is an increase in island volume and little change (<5 m) in shoreline position. Consistent with Morton (2007), Petit Bois narrowed and the eastern shore rotated counterclockwise as a result of wave refraction and associated differential erosion and overwash along the eastern Gulf beach. This rotation is associated with a change towards a swash-alignment caused by a loss of updrift sediment.

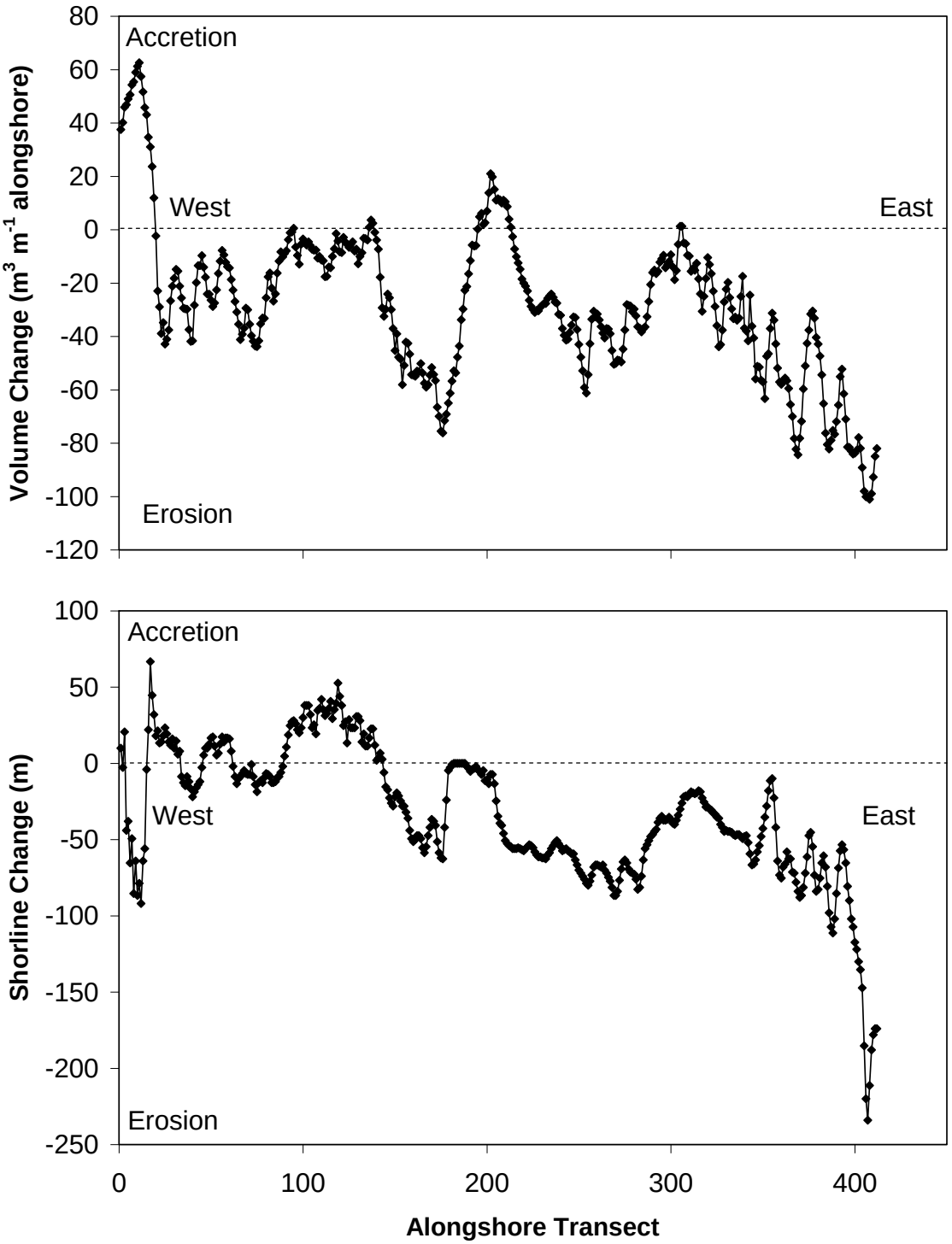


Figure 87. (A) Alongshore variation (by transect) in volume change for Petit Bois Island from West to East. The alongshore variation has been smoothed using a 3-point moving average. Positive change represents accretion and negative change represents erosion. (B) Alongshore variation (by transect) in shoreline position for Petit Bois Island from West to East. The alongshore variation has been smoothed using a 3-point moving average. Positive change represents accretion and negative change represents erosion.



Figure 88. Oblique aerial photographs of morphological change to Petit Bois Island following Hurricane Katrina. Photographs were taken November 30, 2005 and all photographs from the aerial survey are provided on the accompanying compact disc.

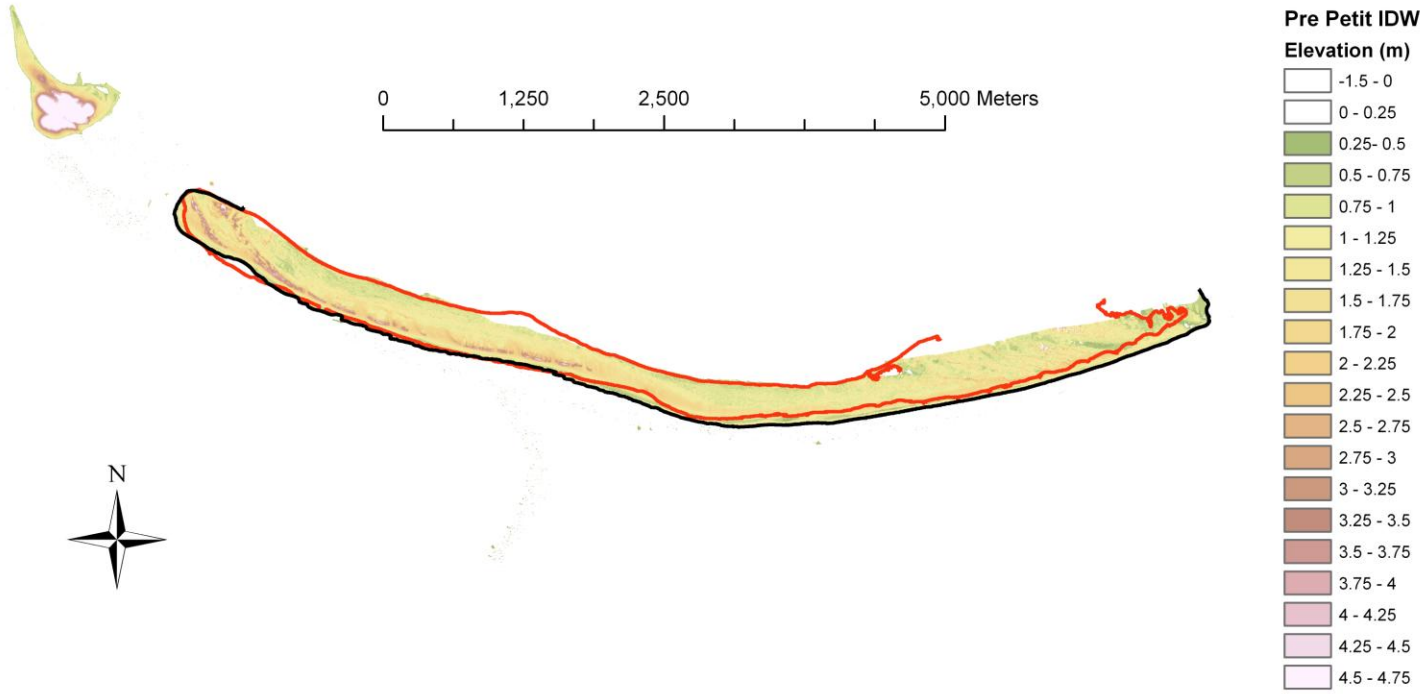


Figure 89. Pre-storm LiDAR data for Petit Bois Island.

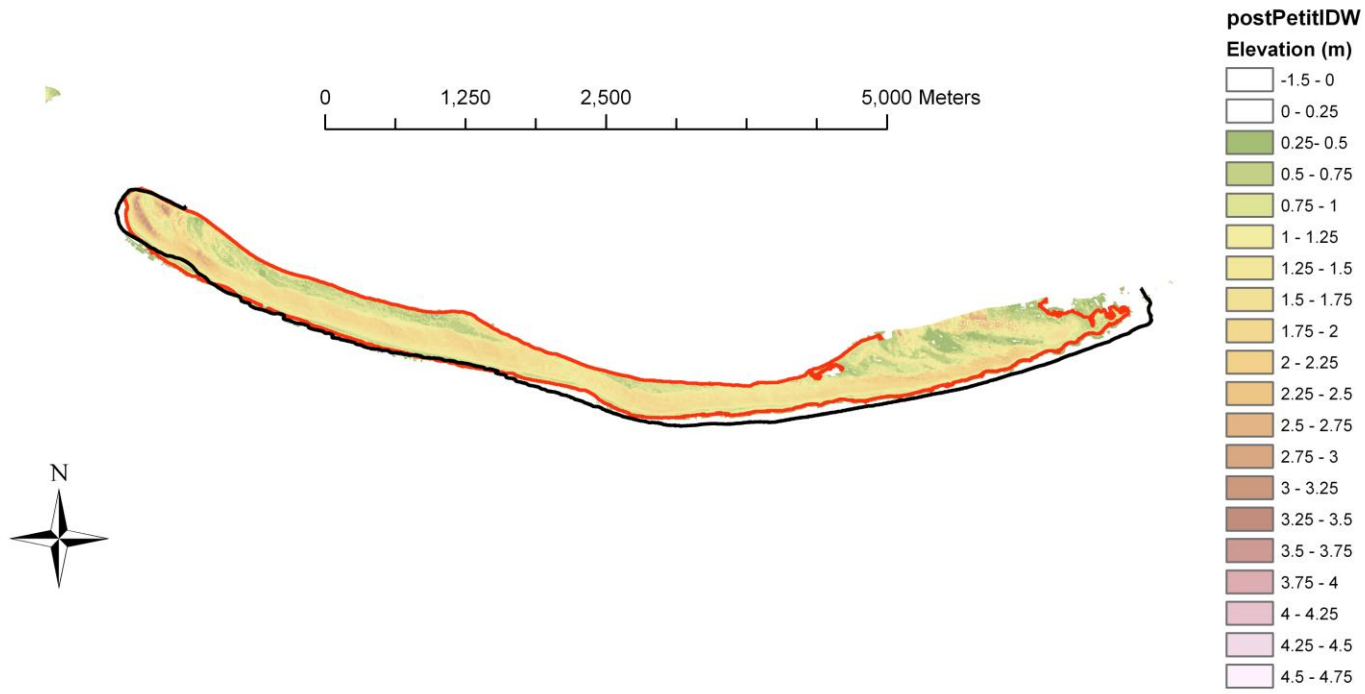


Figure 90. Post-storm LiDAR data for Petit Bois Island.

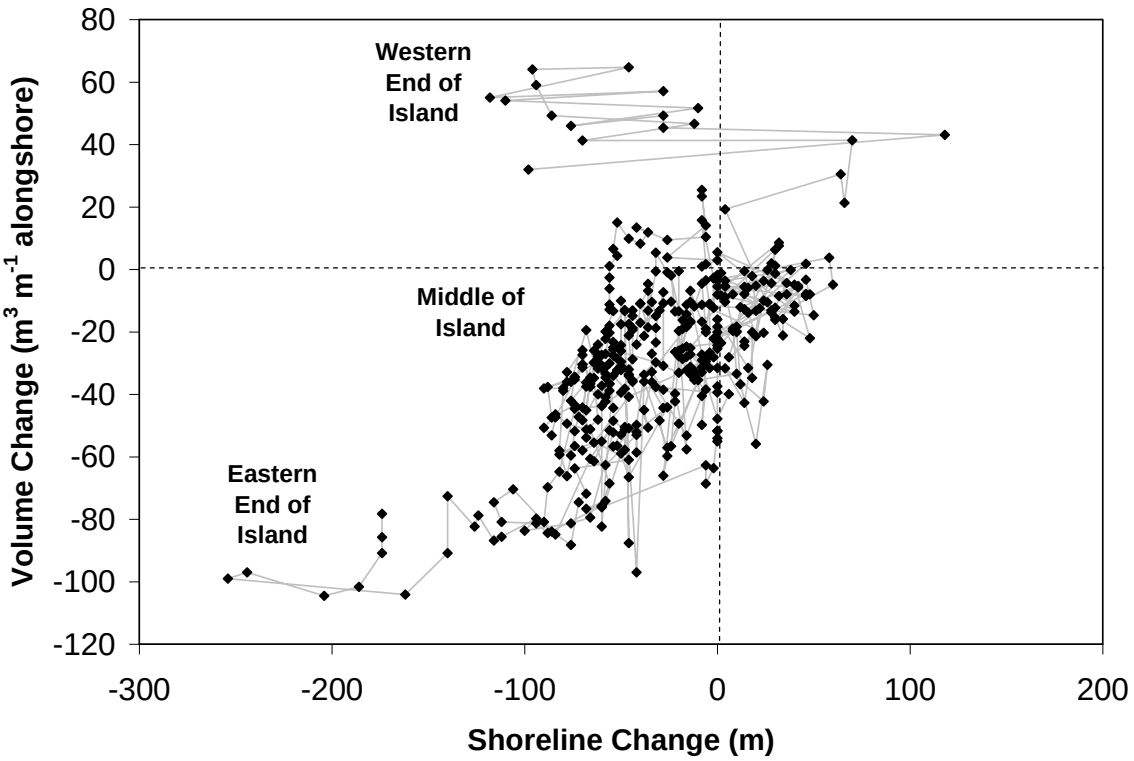


Figure 91. Scatter plot of alongshore variation (by transect) in island volume change with shoreline position for Petit Bois. For both variables, a positive change represents accretion and negative represents erosion.

Elevation Change

The alongshore variation in average elevation based on the pre- and post-storm LiDAR data are provided in Figure 12. In contrast to the considerable change in elevation observed along Santa Rosa Island during Hurricane Ivan (>2 m), the average elevation change on Petit Bois was 0.10 m. The change in average elevation varied from a loss of 0.64 m to a gain of 0.57 m in the centre part of the island where island accretion was observed for both the shoreline and the island volume. A scatter plot of the alongshore variation in island volume change and average elevation change is also provided in Figure 12.

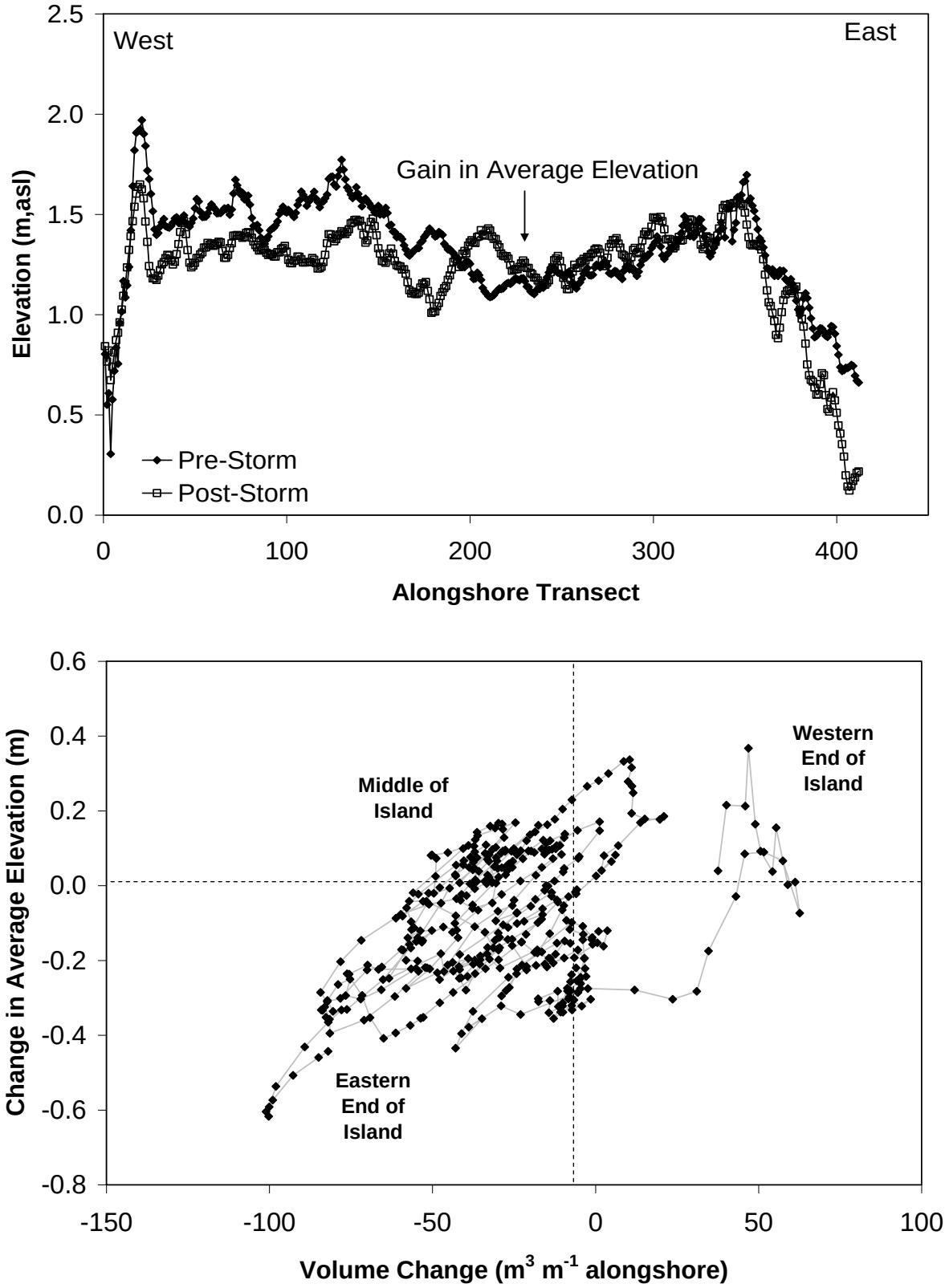


Figure 92. (a) Alongshore variation in pre- and post-storm elevation and (b) the relationship between volume change and the change in average elevation (post-pre-storm elevation).

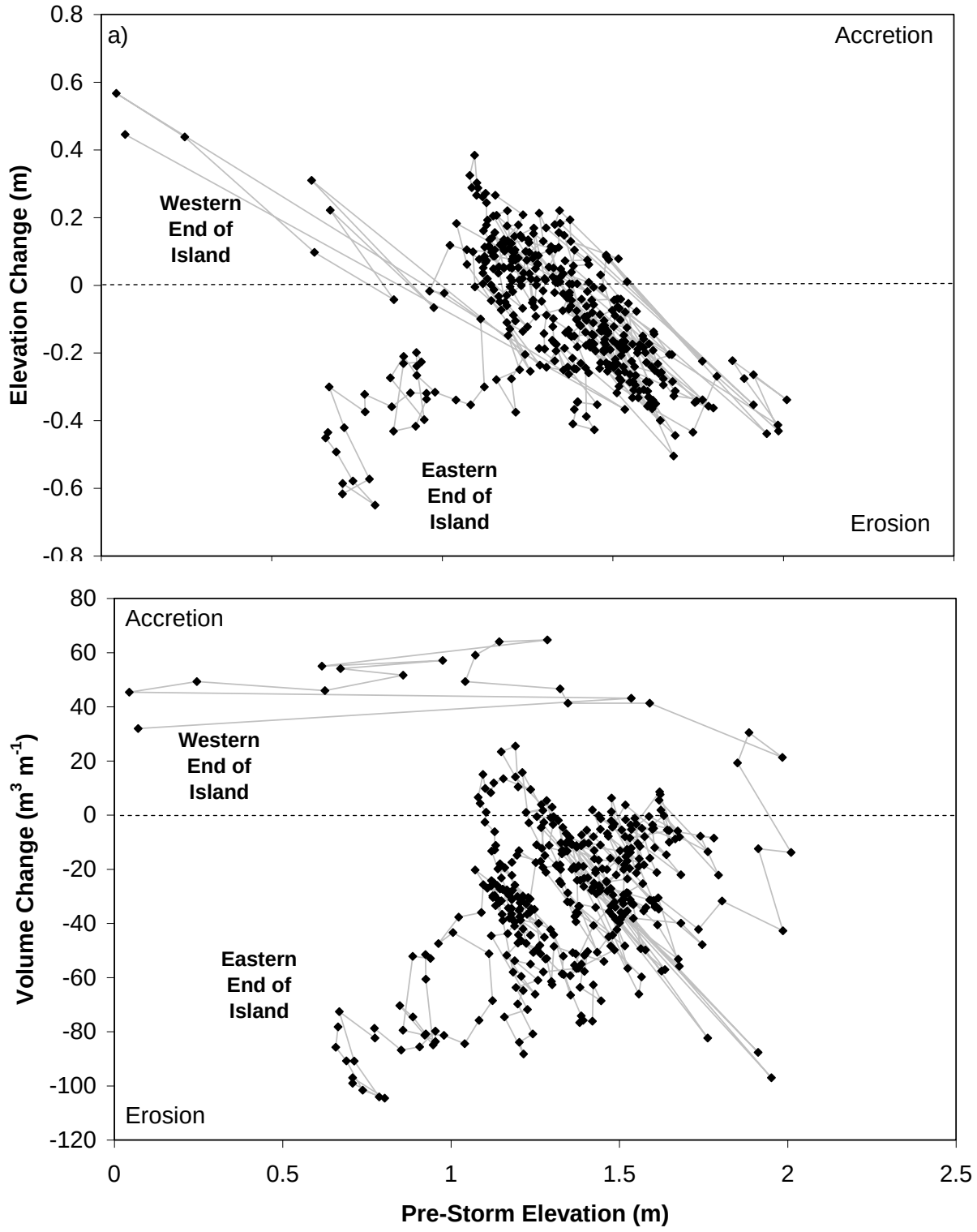


Figure 93. (a) Relationship between pre-storm elevation and elevation change. Also shown (b) is the relationship between pre-storm elevation and change in profile volume.

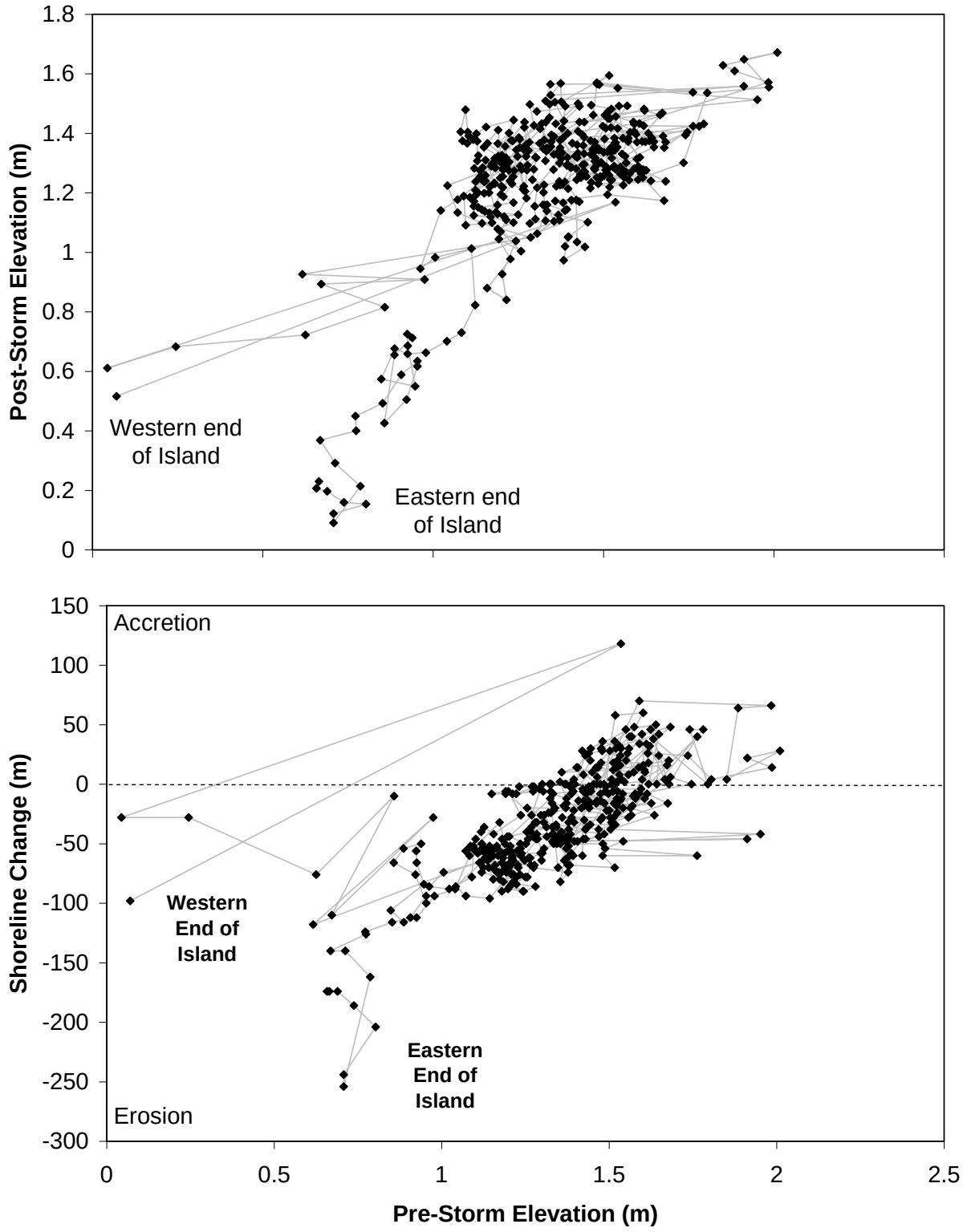


Figure 94. (a) Relationship between pre-storm elevation and post-storm elevation. Also shown (b) is the relationship between pre-storm elevation and shoreline change.

Morphology Change

Based on the scree plots, both the pre- and post-storm data sets found six eigenmodes to be statistically significant with the percent of total variance explain at 81% and 92%, respectively. The primary eigenmode (E1) for the pre-storm morphology explains 31% of the variance and shows a large and wide ridge ~150 m landward of the average shoreline (Figure 15a). The second eigenmode (E2) explains 28% of the variance and exhibits a small ridge ~120 m from the shoreline with a higher than average backbarrier elevation. The third eigenmode (E3) exhibits a large ridge ~90 from the shoreline, which is dominated by a large berm and swale ~40 from the average shoreline. The fourth eigenmode (E4) exhibits a large ridge ~120 from the shoreline, and a secondary ridge with greater elevation ~250 m from the average shoreline. The fifth eigenmode (E5) also exhibits a large ridge ~120 from the shoreline, and a secondary ridge with greater elevation ~320 m from the average shoreline. The sixth eigenmode (E6) is characterized by the largest ridge at ~120 m from the shoreline.

In contrast to the pre-storm morphology, the post-storm morphology (for all eigenmodes) is characterized by a single ridge at different distances from the new average shoreline. The primary eigenmode (E1) for the post-storm morphology explains 65% of the variance and shows a large and wide ridge ~188 m landward of the average post-storm shoreline (Figure 15a). The second eigenmode (E2) explains 34% of the variance and exhibits a small ridge ~190 m from the shoreline with a small ridge ~375 m landward. The third eigenmode (E3) exhibits a large ridge ~276 from the shoreline. The fourth eigenmode (E4) exhibits a large ridge ~190 from the shoreline that grades into a higher than average shoreline elevation that suggests accretion. The fifth eigenmode (E5) also exhibits a large ridge ~190 from the shoreline, and a secondary ridge with greater elevation ~330 m from the average shoreline. The sixth eigenmode (E6) is characterized by the largest ridge at ~242 m from the shoreline.

The alongshore variation in the pre- and post-storm eigenmodes is presented as factor scores in Figure 16. Consistent with the shoreline, volume and elevation data, there appears to be 3 parts to the island: western, middle and eastern. The western section of the island (transects 1-164) is characterized by pre-storm E1, E6 and E4, while the eastern section of the island (transects 289-400) is characterized by pre-storm E2, E3 and E5. The middle section of the island is characterized by pre-storm E3. Canonical correlation analysis between the factor scores for the pre- and post-storm morphology yields a correlation of 0.73 (ρ<0.05). Results of the analysis are presented in Table 1 below. The correlated pairs are plotted in Figure 17.

Table 5. Canonical correlation coefficients (*r*) between the pre- and post-storm profiles for Petit Bois Island, with the largest coefficients (strongest relationships) highlighted.

		Post-storm Profiles					
		E1	**E2**	**E3**	**E4**	**E5**	**E6**
Pre-Storm Profiles	**E1**	0.48	-0.11	0.11	0.22	-0.11	0.18
	E2	0.21	0.82	-0.11	-0.07	0.02	0.01
	E3	0.42	-0.15	-0.32	-0.25	-0.30	0.07
	E4	0.26	0.02	0.60	-0.06	0.03	-0.07
	E5	0.17	0.13	0.17	-0.11	0.55	0.01
	E6	0.35	0.00	0.02	0.53	-0.09	-0.08

Bathymetry Changes

The characteristic post-storm bathymetry profiles are shown in Figure 18a and the alongshore variation (as factor scores) is shown in Figure 18b. In general, there is a change from a relatively steep offshore profile at the western end of the island to a more dissipative profile at the eastern end of the island. This change in profile shape is accompanied by a change in bar position from far offshore and deep (Bathy E4) to close onshore and shallow (E1). Each of the bars exhibited a steep onshore face suggesting some onshore migration during or following Hurricane Katrina.

The distance of the bar offshore and the depth to the bar crest were positively correlated, such that water depths over the bar increased as the distance between the bar and the shoreline increased. The position of the bar exhibits an alongshore variation at a spacing of ~72 transects. In general, the bar is offshore where the average pre-storm elevation is at a local minimum. At these locations the shoreline was observed to retreat and there was net loss of sediment volume. In contrast, shoreline retreat and volume loss were at a local minimum and some accretion was observed where the average pre-storm elevation was relatively large. At these locations, the post-storm bar was relatively close to shore and the depth to the bar crest was at a local minimum. These results suggest that where the average pre-storm elevation was large, sediment was deposited on the inner-shoreface as a nearshore bar. Intervening areas also suggest that sediment was deposited from these areas on the shoreface. The sediment lost in the intervening (low elevation) areas was deposited in the backbarrier as overwash fans that in some locations extended into the sound (see Figure 8). The overwash and loss of shoreline and profile volume was worst at the eastern end of the island, which was the updrift end of the island.

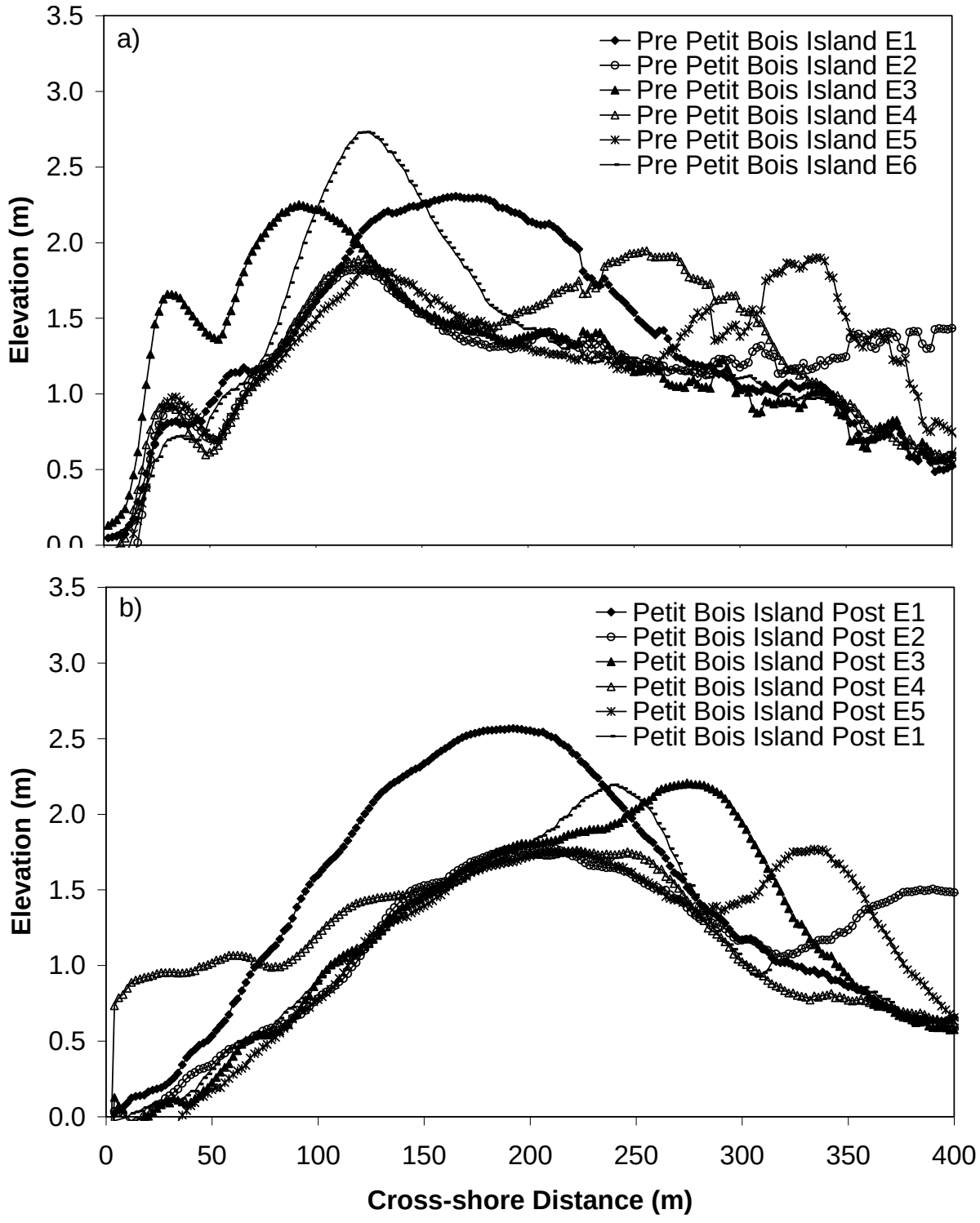


Figure 95. Characteristic (a) pre-storm and (b) post-storm cross-shore profiles for Petit Bois Island.

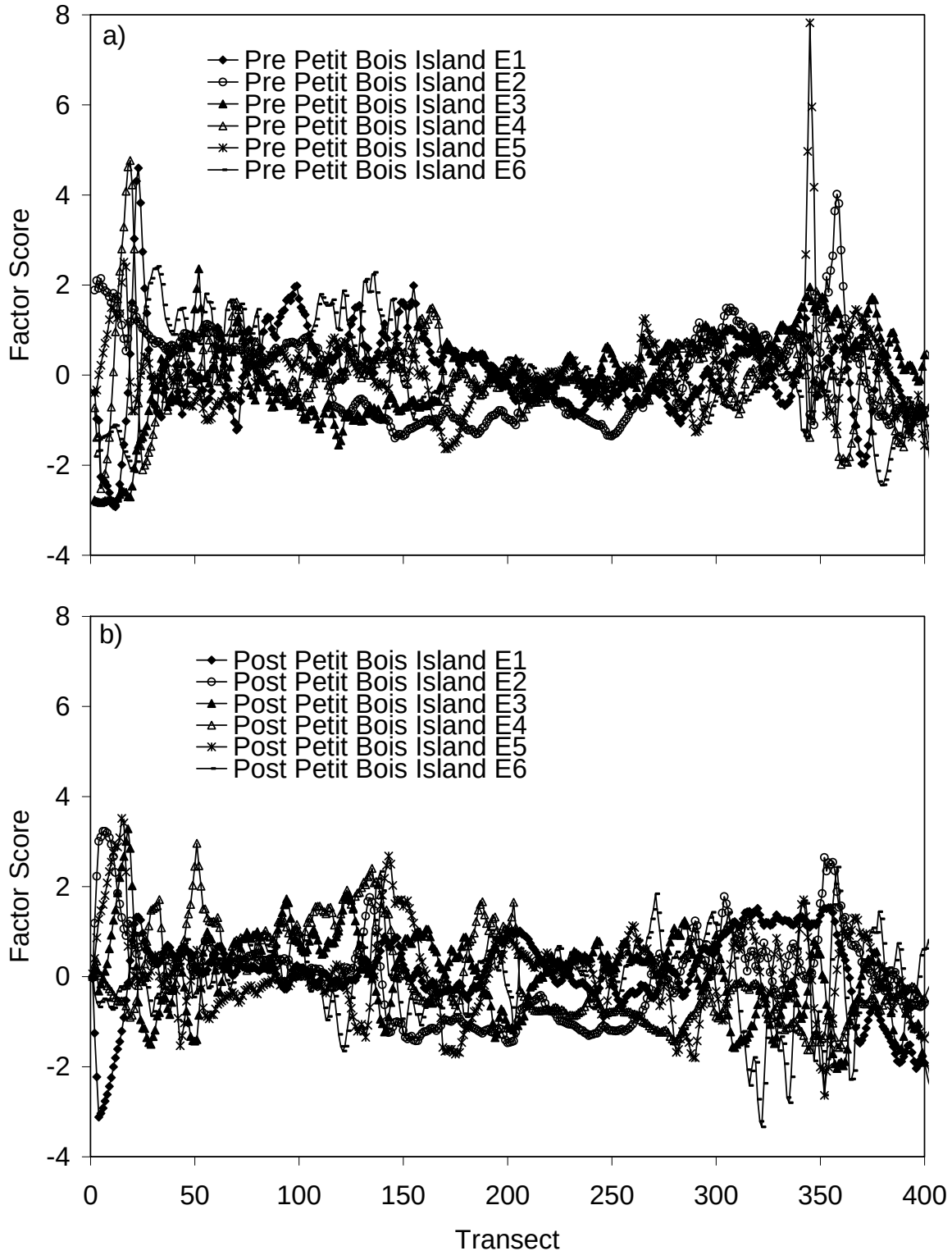


Figure 96. Alongshore factor scores for the pre-storm and post-storm characteristic profiles.

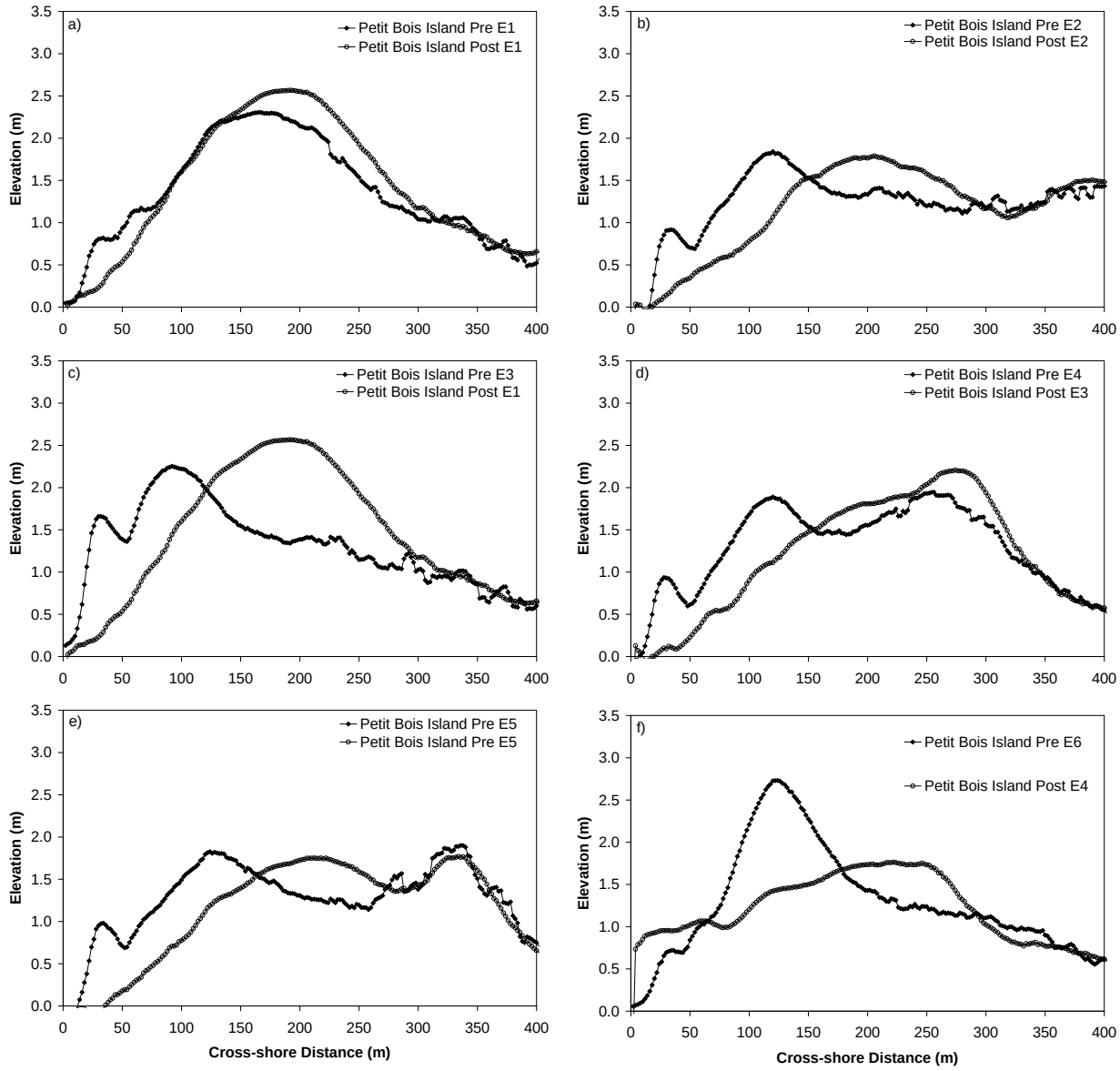


Figure 97. Comparison of cross-island profiles (factor scores) for the pre- and post-storm eigenvalues with strong correlations identified through canonical correlation analysis.

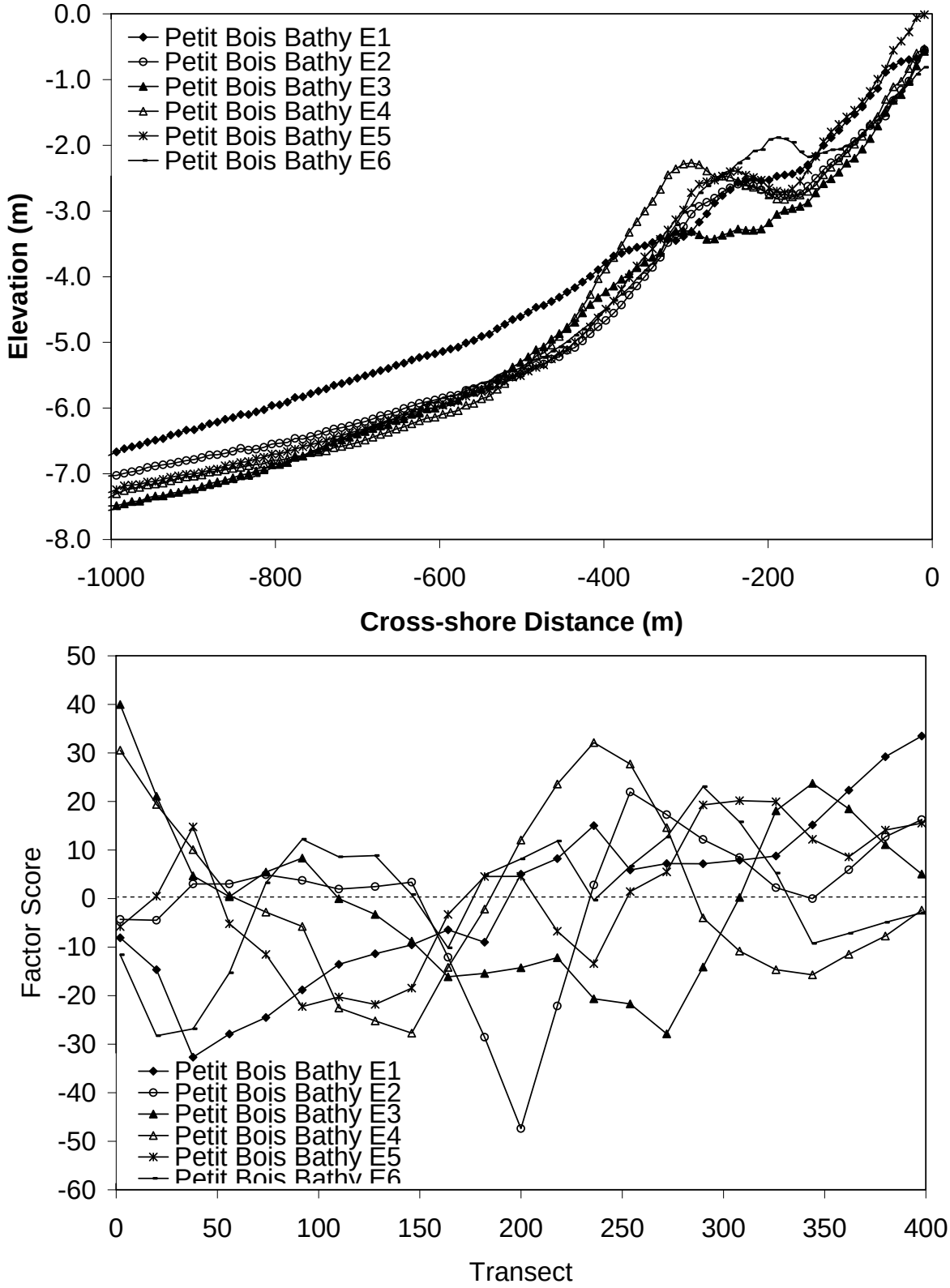


Figure 98. (a) Characteristic offshore profiles for Petit Bois Island and (b) alongshore factor scores for the characteristic profiles.

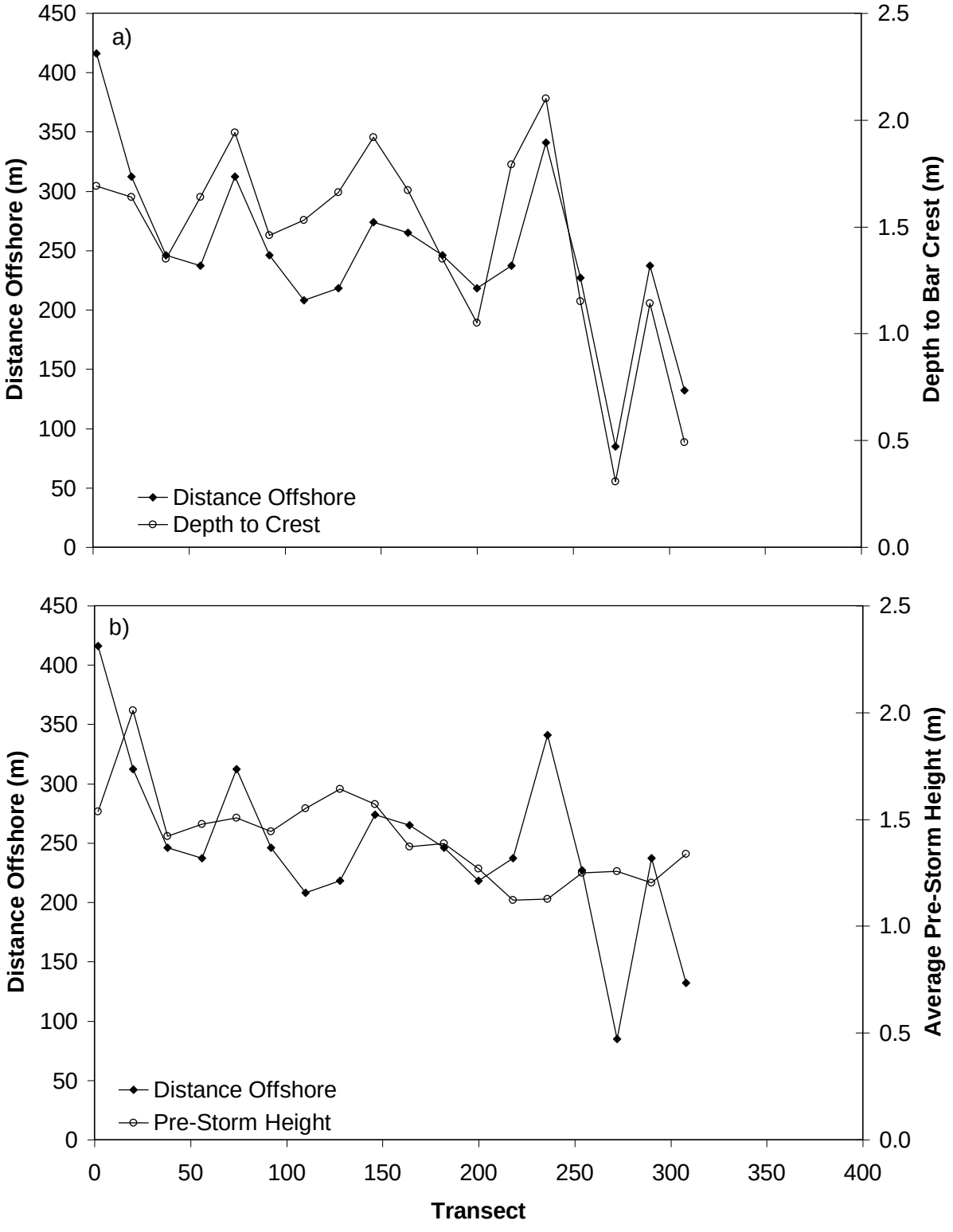


Figure 99. Alongshore variation in the distance of the nearshore bar offshore relative to (a) the depth to the bar crest and (b) the average pre-storm elevation of the island.

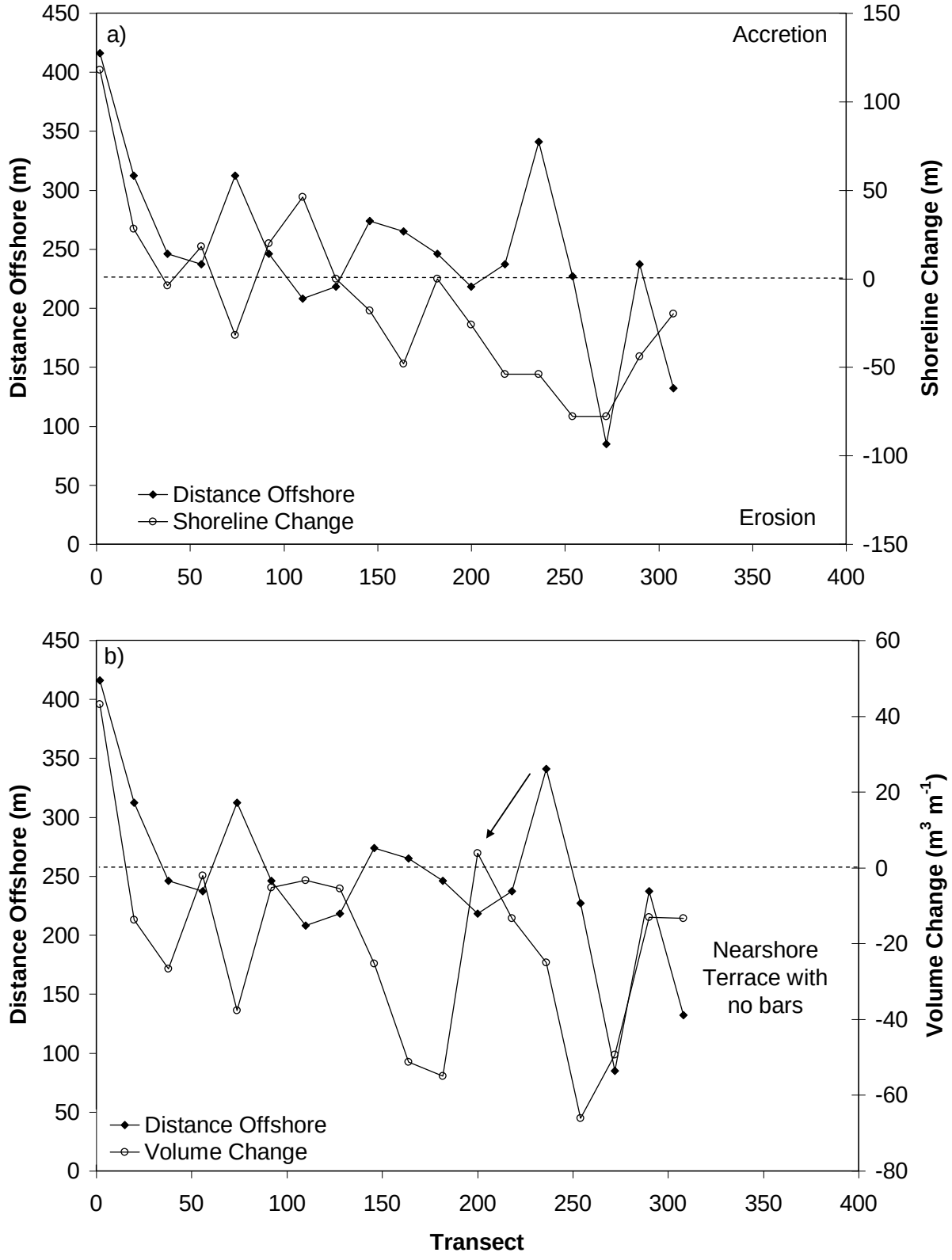


Figure 100. Alongshore variation in the distance of the nearshore bar offshore relative to (a) shoreline change and (b) the change in profile volume.

IMPACTS TO HORN ISLAND

Oblique aerial photographs of the post-storm morphology are presented in Figure 22, and the pre- and post-LiDAR images for Horn Island are provided in Figures 23 and 24. Similar to Petit Bois Island, areas with large elevations were reduced in height, but there were several areas of the island where the post-storm average elevation increased, suggesting accretion during or immediately following the storm. A review of the detailed analysis is provided in the following sections.

Volume Change

Over 2,270,000 m^3 of sediment was lost from the aerial portion of the island with an average volume loss of -120 m^3 m^{-1} length of shoreline (Figure 24). However, the volume change varied from an accretion of 64 m^3 m^{-1} length of shoreline near the eastern end of the island to a loss of -539 m^3 m^{-1} at transect 159. Assuming that the nearshore profile maintained its shape, an additional 360,000 m^3 of sediment was lost from the sub-aqueous portion of the island. Assuming that the sediment losses from the island and the shoreface were equally distributed within the offshore survey area (15 million m^2), the sediment would only represent a change of 0.09 m which is within the sampling error (±0.10 m) of the depth sounder.

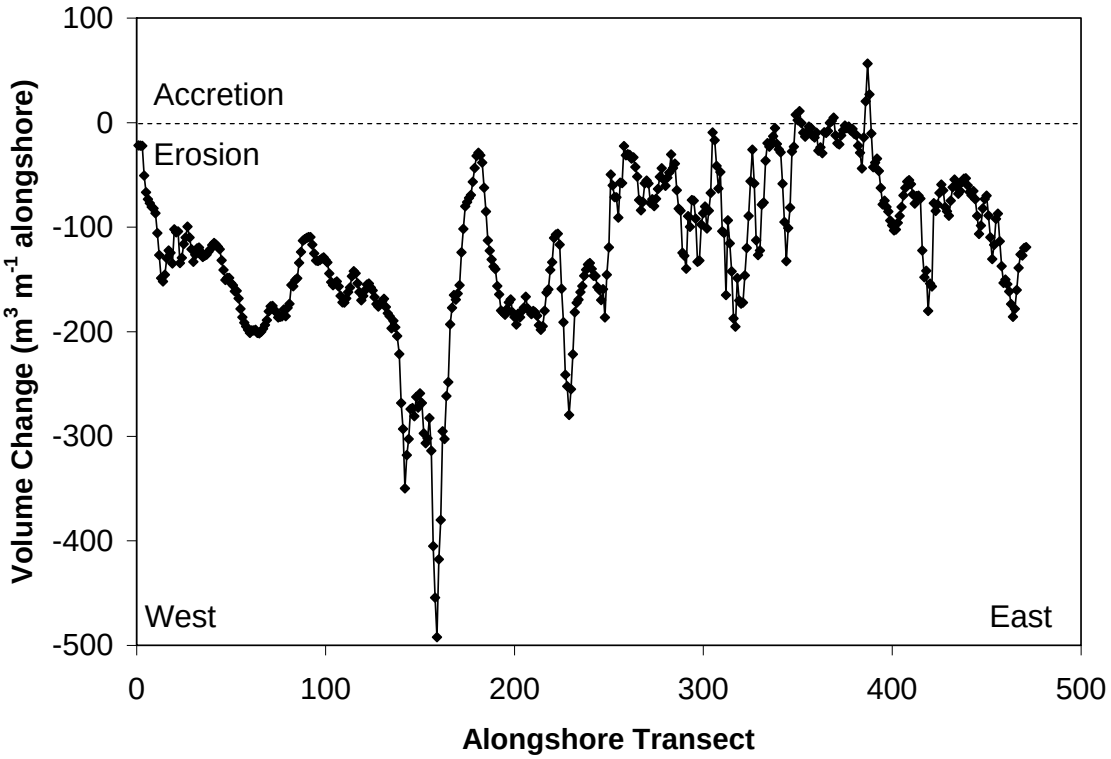


Figure 101. Alongshore variation (by transect) in volume change for Horn Island from West to East. The alongshore variation has been smoothed using a 3-point moving average. Positive change represents accretion and negative change represents erosion.

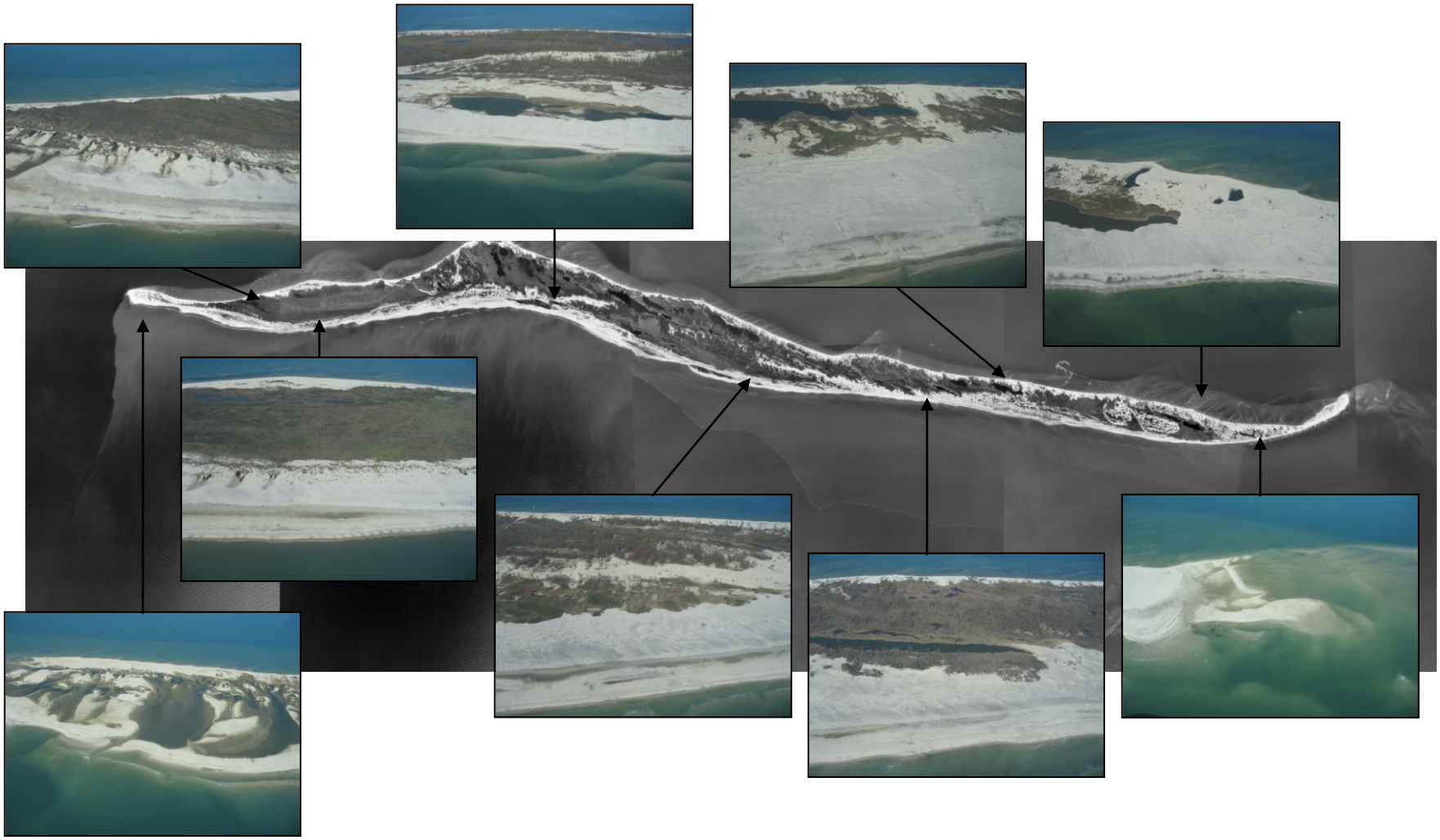


Figure 102. Oblique aerial photographs of morphological change to Horn Island following Hurricane Katrina. Photographs were taken November 30, 2005 and all photographs from the aerial survey are provided on the accompanying compact disc.

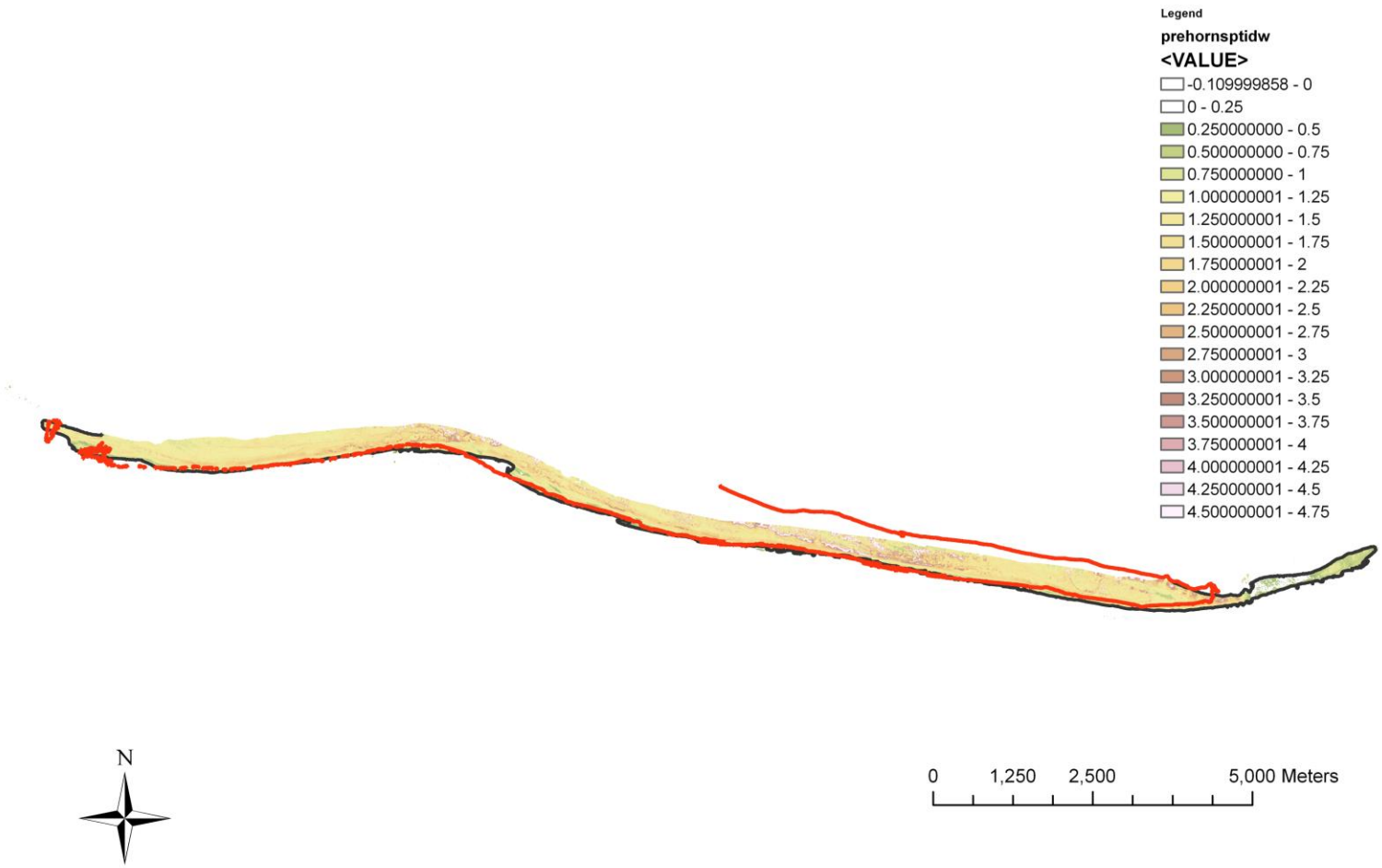


Figure 103. Pre-storm LiDAR data for Horn Island.



Figure 104. Post-storm LiDAR data for Horn Island.

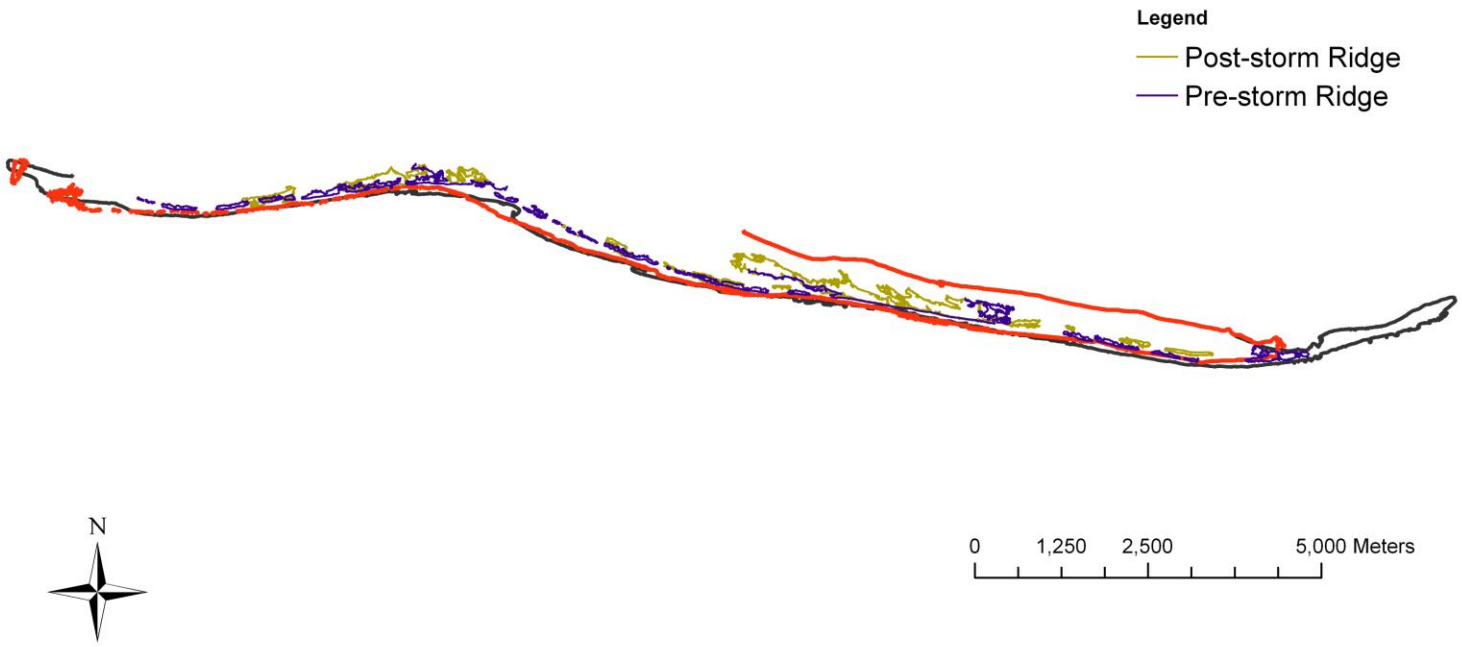


Figure 105. Pre- and post-storm locations of beachface ridges.

Shoreline Change

On average the shoreline retreated by ~3 m but varied considerably from a gain (accretion) of 174 m to a loss (erosion) of 136 m (Figure 26). Unlike Petit Bois, the change in shoreline position is not related to the volume change. Areas of shoreline erosion are not consistently associated with the largest losses of sediment, while areas of shoreline accretion are not associated with the smallest loss of sediment and sometimes a volume gain. Whereas Petit Bois had an alongshore trend from erosion (in the east) to accretion (in the west), Horn Island exhibits some erosion in the east and accretion in the west, with considerable (and almost periodic) variability through the middle transects. Both shoreline change and volume change exhibit statistically significant variations at alongshore length scales of ~3000 and 1700 m. At the 3000 m length scale, volume and shoreline change are in-phase (and positively correlated), but the variables are in quadrature (out-of-phase) at the 1700 m length scale. In other words, areas of large volume change are to the east of areas with large shoreline change at the 1700 m length scale.

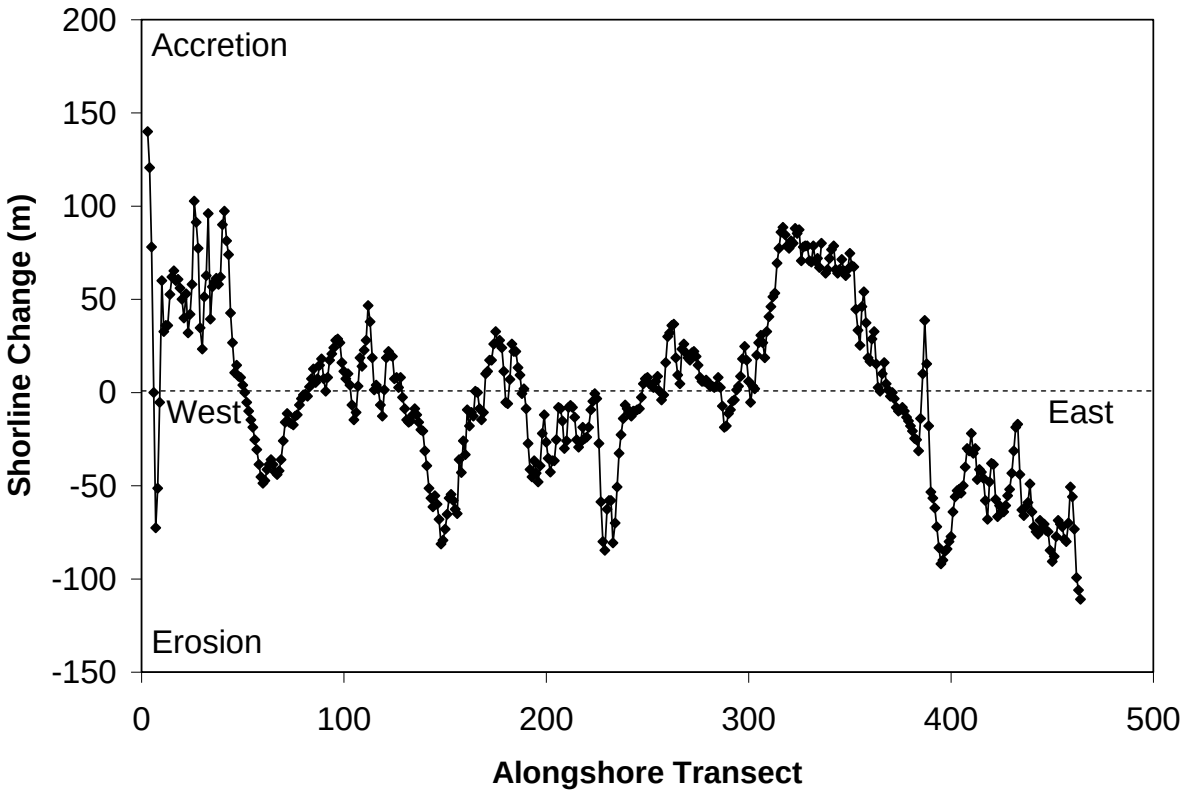


Figure 106. Alongshore variation (by transect) in shoreline position for Horn Island from West to East. The alongshore variation has been smoothed using a 3-point moving average. Positive change represents accretion and negative change represents erosion.

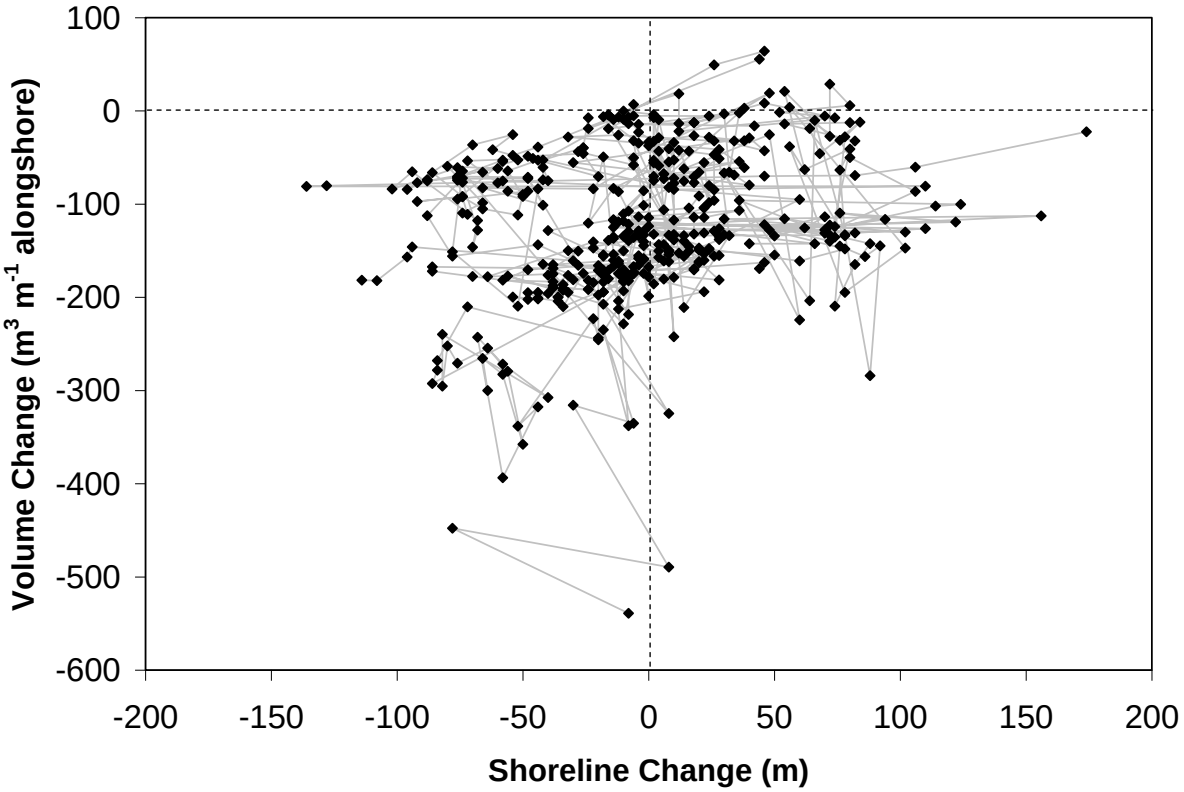


Figure 107. Scatter plot of alongshore variation (by transect) in island volume change with shoreline position for Horn Island. For both variables, a positive change represents accretion and negative represents erosion.

Elevation Change

The alongshore variation in average elevation based on the pre- and post-storm LiDAR data are provided in Figure 28. The change in average elevation varied from a loss of 2.3 m to a gain of 0.38 m at the eastern end of the island. The loss in average elevation tended to be greatest at the western end of the island and near the middle (transects 250-350) where large dune features had been present before the storm. A scatter plot of the alongshore variation in island volume change and average elevation change is provided in Figure 28. While there appears to be 2 separate populations, both suggest that a greater loss in average elevation is associated with larger volume losses. In this respect, change in elevation is coherent and in-phase with changes in volume change at all length scales.

.

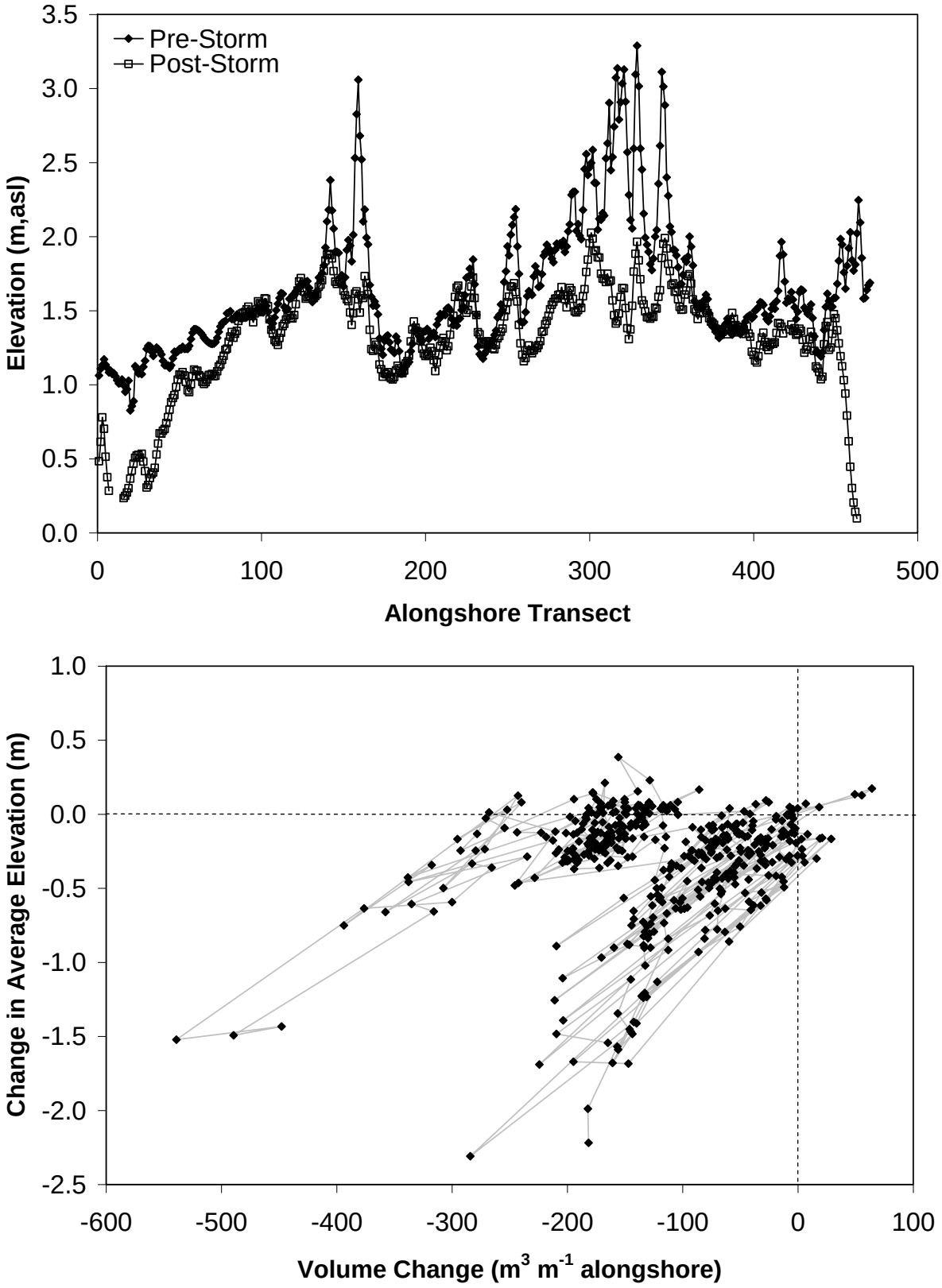


Figure 108. (a) Alongshore variation in pre- and post-storm elevation and (b) the relationship between volume change and the change in average elevation (post-pre-storm elevation).

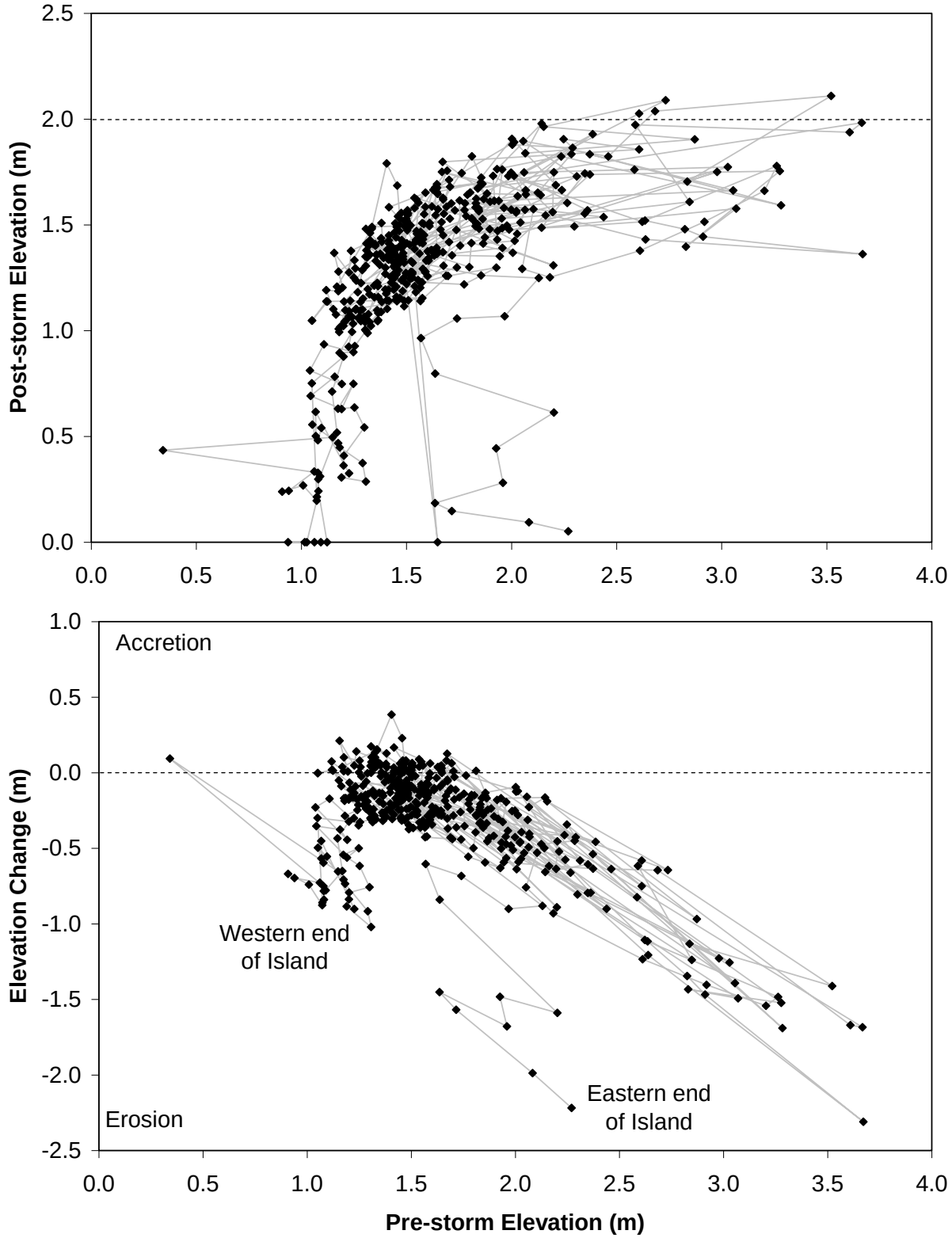


Figure 109. (a) Relationship between pre-storm elevation and elevation change. Also shown (b) is the relationship between pre-storm elevation and change in profile volume.

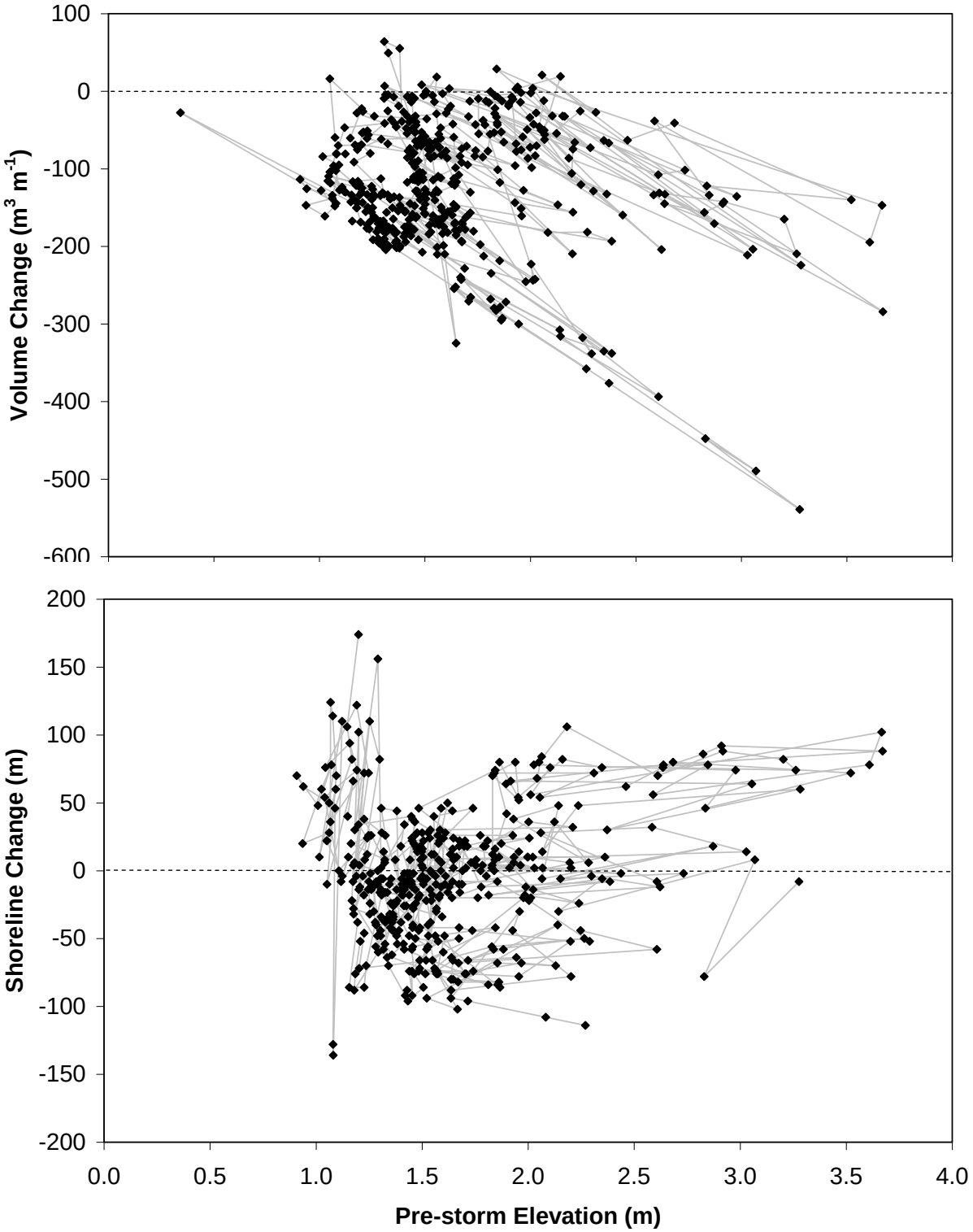


Figure 110. (a) Relationship between pre-storm elevation and post-storm elevation. Also shown (b) is the relationship between pre-storm elevation and shoreline change.

Morphology Change

Based on the scree plots, both the pre- and post-storm data sets found six eigenmodes to be statistically significant with the percent of total variance explain at 75% and 86%, respectively. The primary eigenmode (E1) for the pre-storm morphology explains 32% of the variance and shows a large and wide ridge ~260 m landward of the average shoreline (Figure 31a). The second eigenmode (E2) explains 28% of the variance and exhibits a small ridge ~86 m from the shoreline with a large berm and swale at ~30 m from the shoreline. The third eigenmode (E3) exhibits a large ridge 170 m from the shoreline while the fourth and sixth eigenmodes (E4 and E6) only exhibit secondary ridges ~370 and 350 m from the shoreline. The fifth eigenmode (E5) exhibits a large ridge ~125 m from the average shoreline.

In contrast to the pre-storm morphology, but similar to Petit Bois, the post-storm morphology (for all eigenmodes) is characterized by a single ridge at different distances from the new average shoreline. The primary eigenmode (E1) for the post-storm morphology explains 62% of the variance and shows a large and wide ridge ~182 m landward of the average post-storm shoreline (Figure31b). The second eigenmode (E2) explains 32% of the variance and exhibits a small ridge ~134 m from the shoreline. The third eigenmode (E3) exhibits a large ridge ~392 from the shoreline. The fourth eigenmode (E4) exhibits a large ridge ~288 while the fifth eigenmode (E5) has no ridge. The sixth eigenmode (E6) is characterized by the largest ridge at ~322 m from the shoreline.

The alongshore variation in the pre- and post-storm eigenmodes is presented as factor scores in Figures 32. Unlike Petit Bois, there does not seem to be a well-defined alongshore pattern Canonical correlation analysis between the factor scores for the pre- and post-storm morphology yields a correlation of 0.73 (ρ<0.05). Results of the analysis are presented in Table 2 below and the correlated pairs are plotted in Figure 33.

Table 6. Canonical correlation coefficients (*r*) between the pre- and post-storm profiles for Horn Island, with the largest coefficients (strongest relationships) highlighted.

		Post-storm Profiles					
		E1	**E2**	**E3**	**E4**	**E5**	**E6**
Pre-Storm Profiles	**E1**	0.11	0.22	0.47	0.25	0.14	0.01
	E2	0.04	-0.11	0.03	-0.18	0.17	-0.07
	E3	0.07	-0.16	-0.10	0.51	-0.08	0.15
	E4	0.58	-0.09	-0.15	0.00	-0.12	0.06
	E5	0.12	-0.04	0.12	0.06	-0.14	0.01
	E6	0.01	-0.06	0.03	0.17	-0.10	0.40

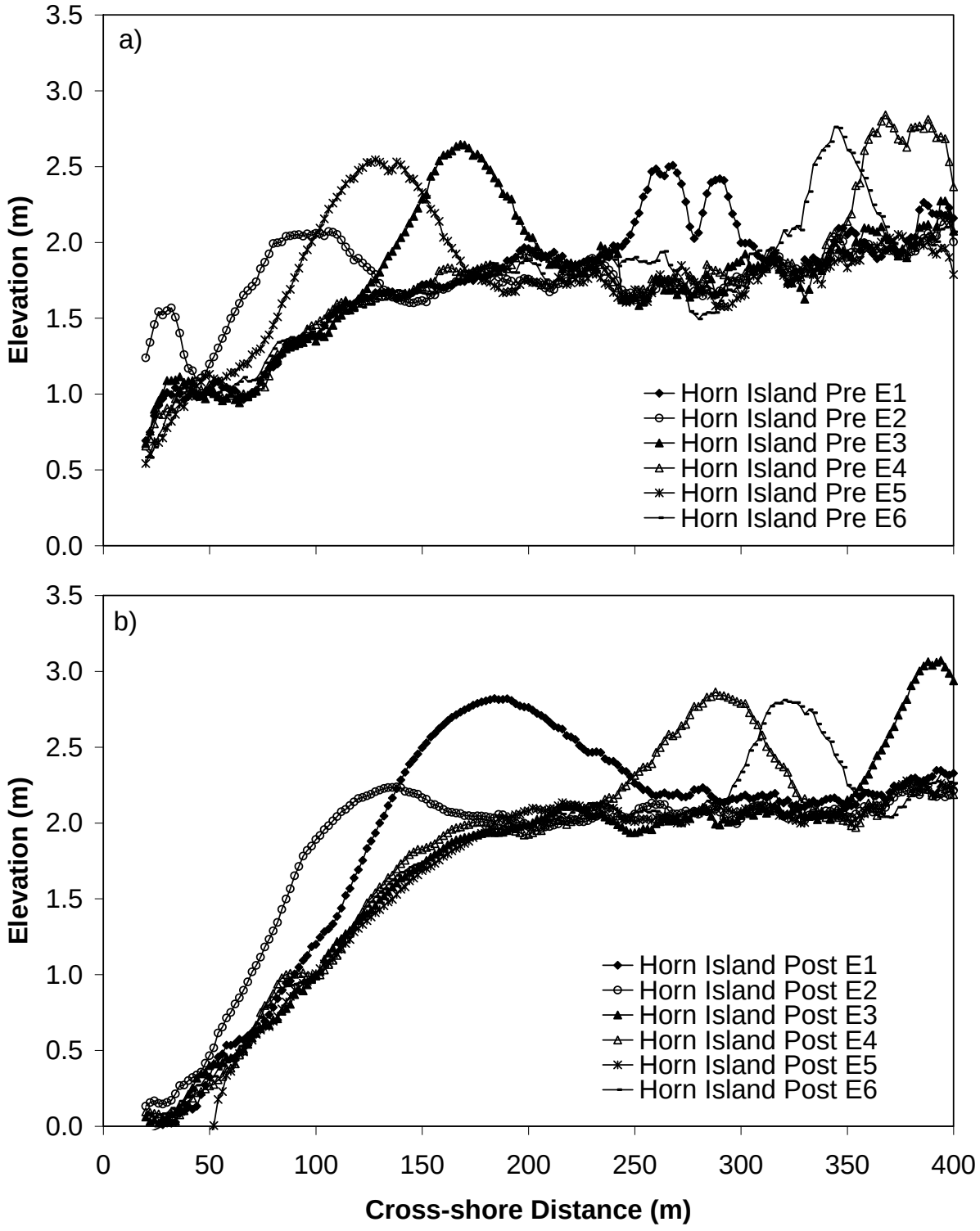


Figure 111. Characteristic (a) pre-storm and (b) post-storm cross-shore profiles for Horn Island.

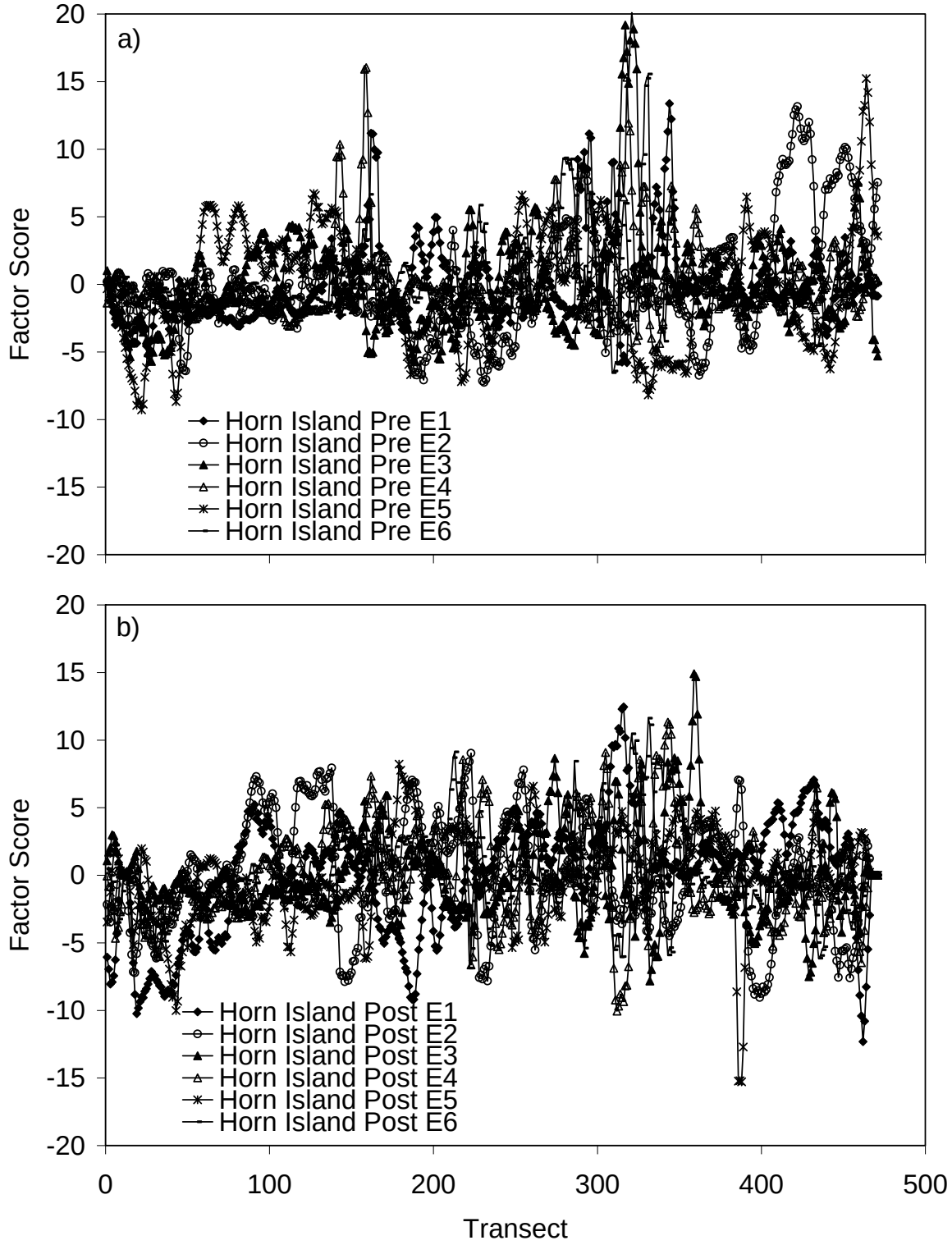


Figure 112. Alongshore factor scores for the pre-storm and post-storm characteristic profiles.

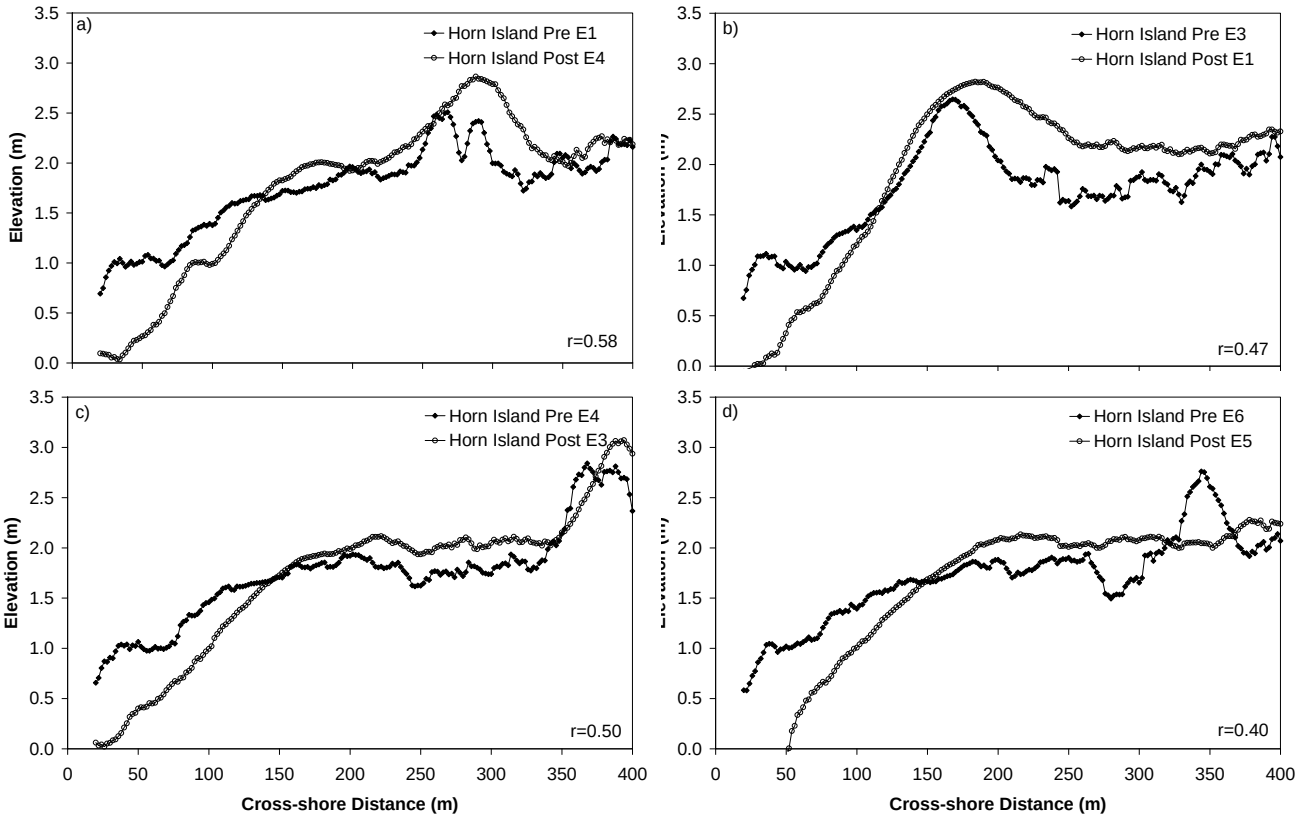


Figure 113. Comparison of cross-island profiles (factor scores) for the pre- and post-storm eigenvalues with strong correlations identified through canonical correlation analysis.

Bathymetry Changes

The characteristic post-storm bathymetry profiles are shown in Figure 34a and the alongshore variation (as factor scores) is shown in Figure 34b. In general, there is a change from a relatively dissipative (gentle) offshore profile at the western end of the island to a more reflective profile at the eastern end of the island with a large prominent bar. This change in profile shape is accompanied by a change in bar morphology from no bar (Bathy E1) to a pronounced bar that is distant from the shoreline (E4). Each of the bars exhibited a steep onshore face suggesting some onshore migration during or following Hurricane Katrina.

Similar to the average pre-storm elevation and shoreline and volume change, the distance and depth of the bar crest offshore exhibit an alongshore variation at a spacing of ~120 transects. Within a distance of 30 transects (from west to east), the bar increases in height by ~1.4 m at which point it moves inshore by ~130 m. When the bar is further offshore it is relatively symmetric but becomes increasingly asymmetric as it approaches the shore. Where the bar is relatively far offshore and well developed (large in height

and asymmetric), the shoreline accreted during the storm (Figure 35a), the volume loss is at a local minimum (Figure 36b) and the average pre-storm elevation is at a local maximum (Figure 35b). Where the bar is close to shore and depth over the crest is relatively deep (a small bar), the shoreline tended to erode, the volume loss is at a local maximum and the average pre-storm elevation is at a local minimum. Similar to Petit Bois, these results suggest that where the average pre-storm elevation was large, sediment was deposited on the inner-shoreface as a nearshore bar. Like Petit Bois Island, the sediment lost in the intervening (low elevation) areas was deposited in the backbarrier as overwash fans that in some locations extended into the sound (see Figure 22). The overwash and loss of shoreline and profile volume was worst at the eastern end of the island, which was the updrift end of the island.

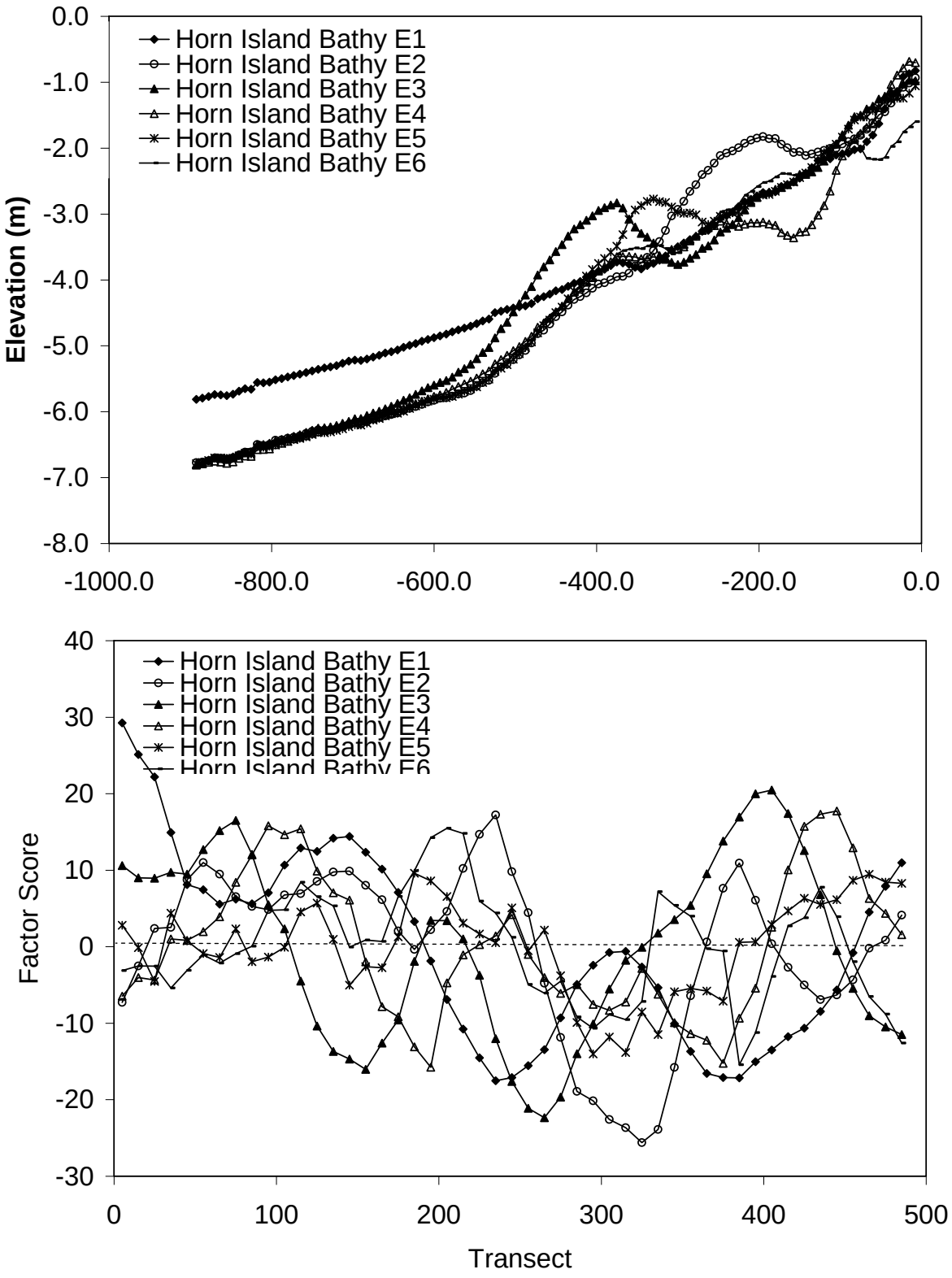


Figure 114. (a) Characteristic offshore profiles for Horn Island and (b) alongshore factor scores for the characteristic profiles.

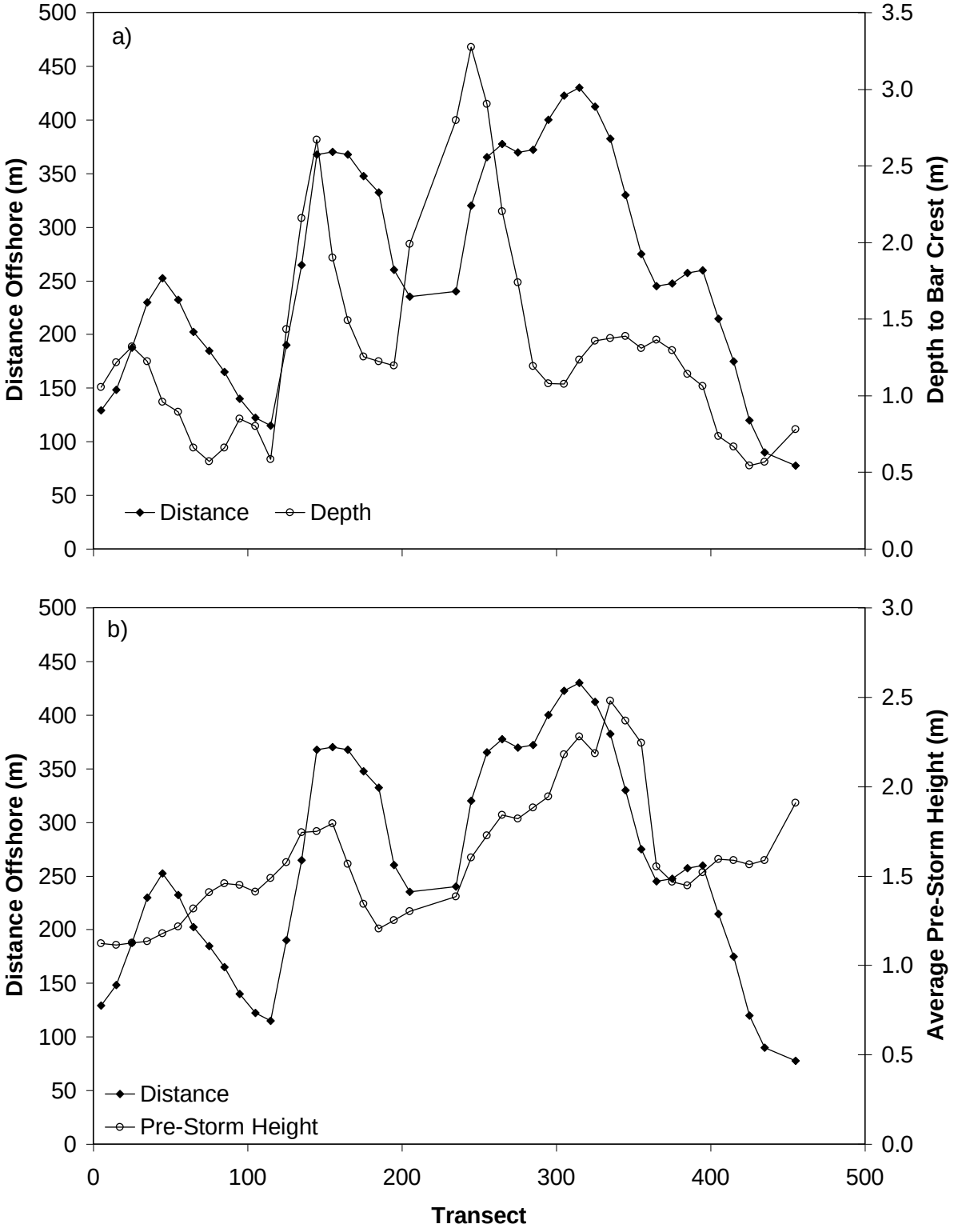


Figure 115. Alongshore variation in the distance of the nearshore bar offshore relative to (a) the depth to the bar crest and (b) the average pre-storm elevation of the island.

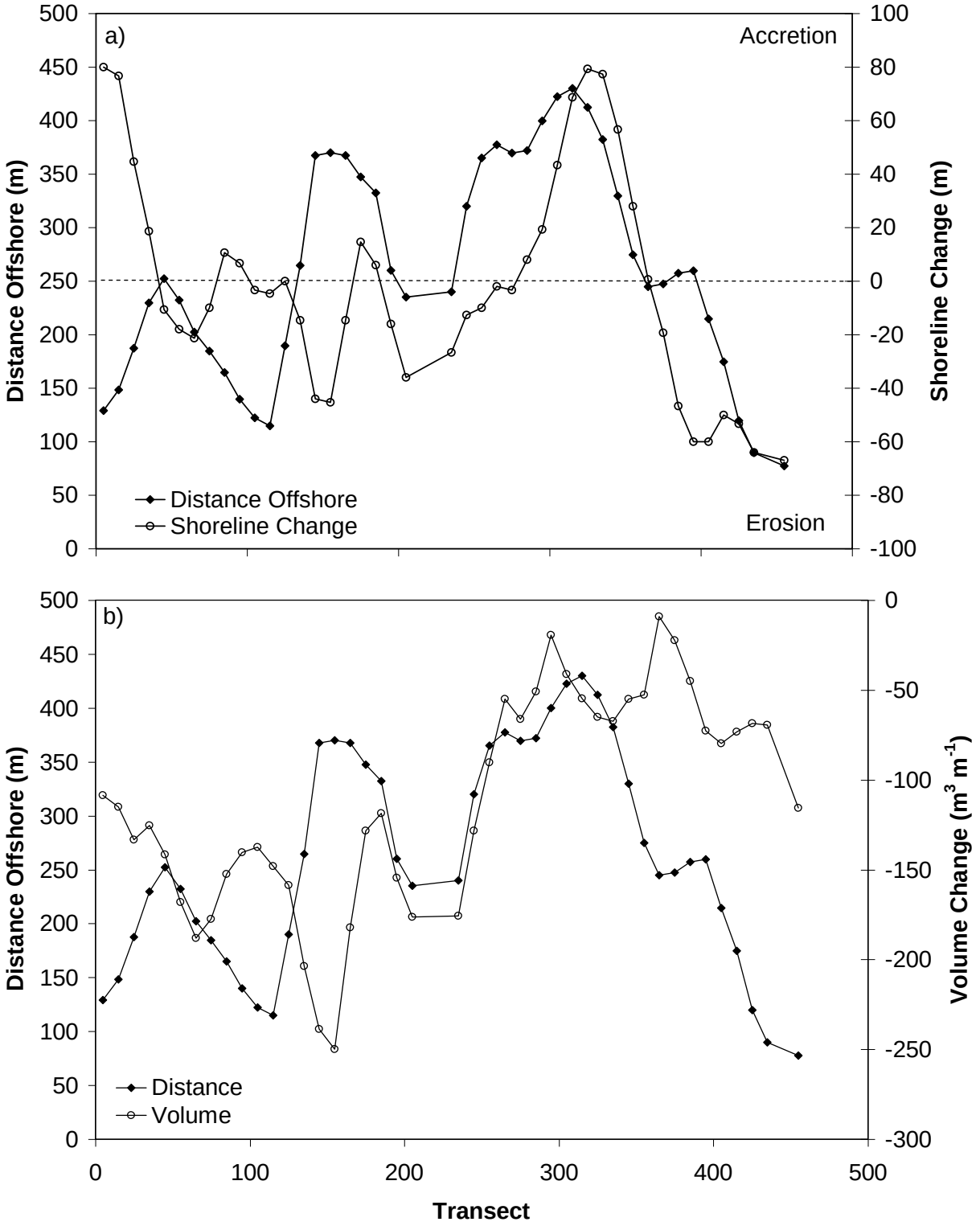


Figure 116. Alongshore variation in the distance of the nearshore bar offshore relative to (a) shoreline change and (b) the change in profile volume.

IMPACTS TO SHIP ISLAND

Oblique aerial photographs of the post-storm morphology are presented in Figure 38, and the pre- and post-LiDAR images for Ship Island are provided in Figures 39 and 40. While areas with large elevations were reduced in height, there were several areas of the island where the post-storm average elevation increased, suggesting accretion during or immediately following the storm. A review of the detailed analysis is provided in the following sections. However, due to limited data from West Ship Island and on the post-storm location of the shoreline the following discussion will focus largely on East Ship Island.

Volume Change

Over 680,000 m^3 of sediment was lost from the aerial portion of East Ship Island, with an average volume loss of 245 m^3 m^{-1} length of shoreline (Figure 37). However, the volume change varied from a minimum of 20 m^3 m^{-1} to a maximum of 848 m^3 m^{-1} length of shoreline near the centre of the island. In contrast, some accretion was observed on West Ship Island, although there was an average loss of 42 m^3 m^{-1} length of shoreline.

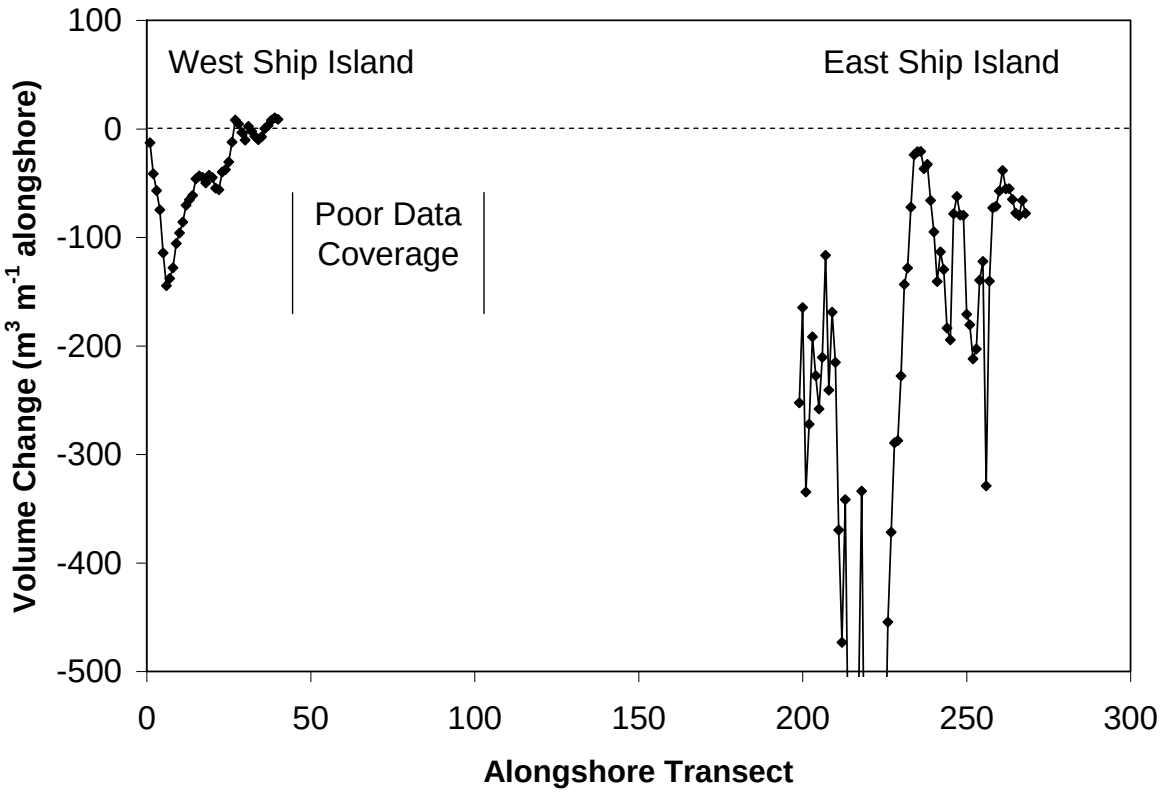


Figure 117. Alongshore variation (by transect) in volume change for Ship Island from West to East. The alongshore variation has been smoothed using a 3-point moving average. Positive change represents accretion and negative change represents erosion.



Figure 118. Oblique aerial photographs of morphological change to Ship Island Island following Hurricane Katrina. Photographs were taken November 30, 2005 and all photographs from the aerial survey are provided on the accompanying compact disc.

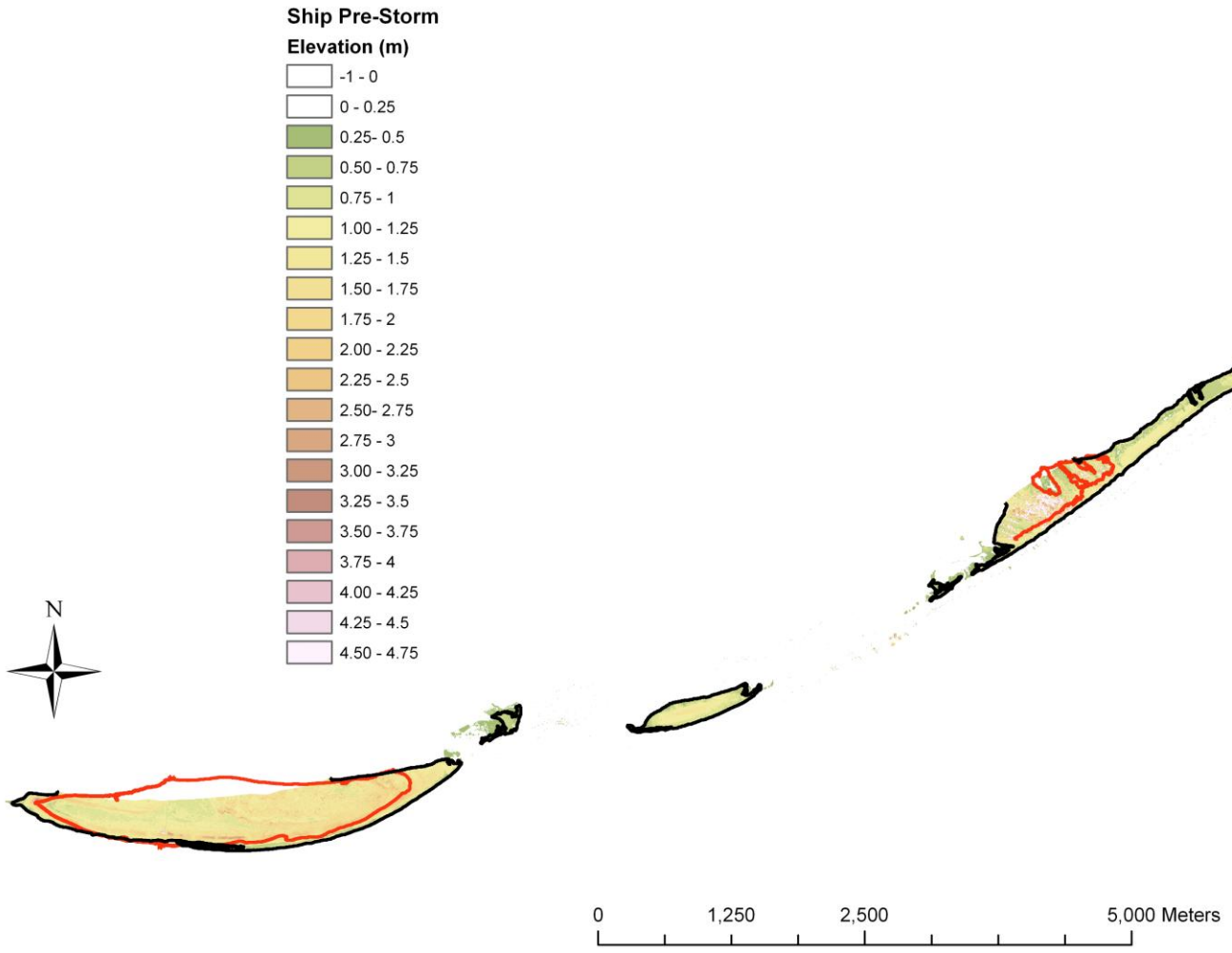


Figure 119. Pre-storm LiDAR data for Ship Island.

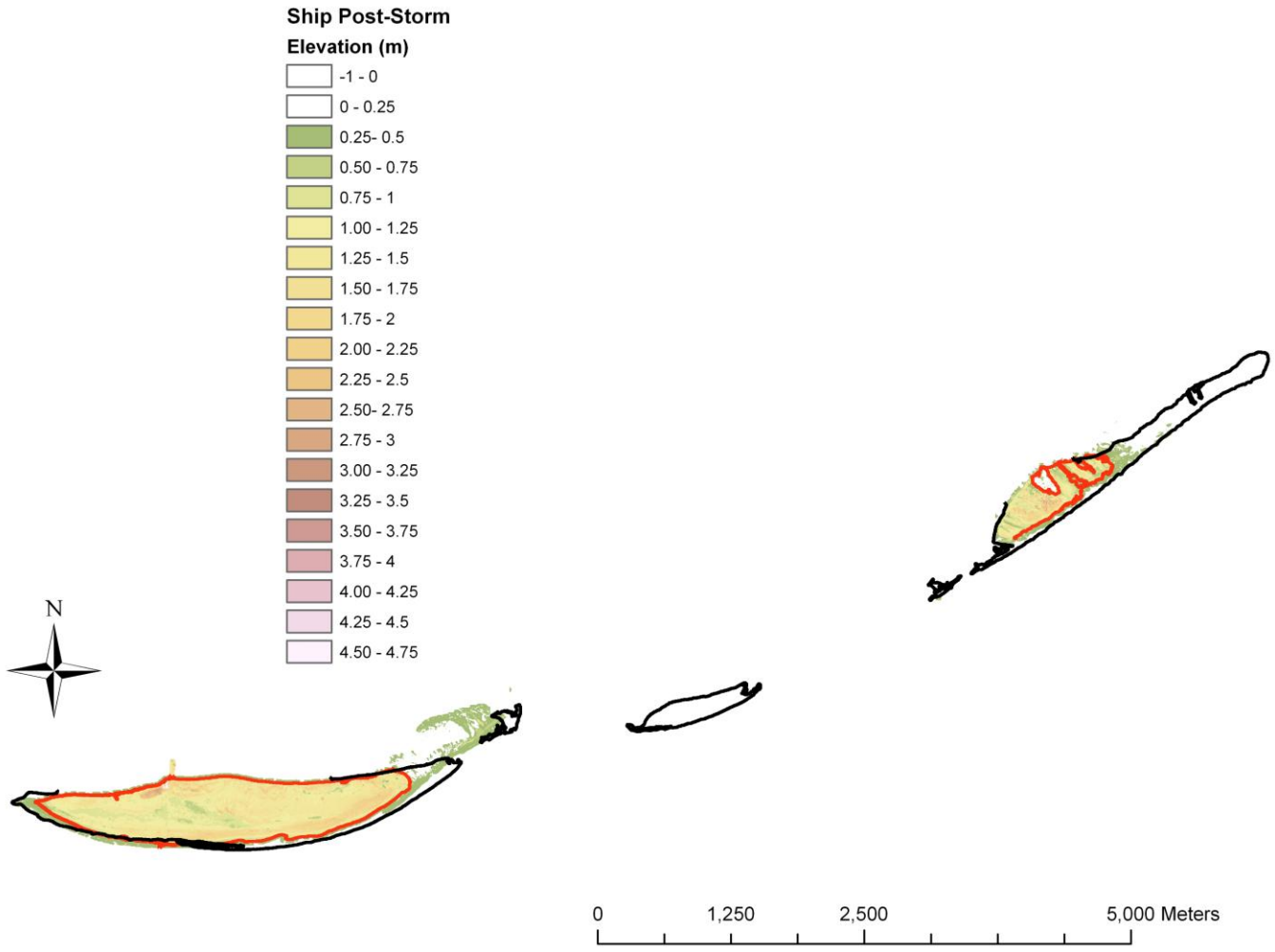


Figure 120. Post-storm LiDAR data for Ship Island.

Elevation Change

The alongshore variation in average elevation based on the pre- and post-storm LiDAR data are provided in Figure 41. The change in average elevation on East Ship Island varied from a loss of 3.9 m to a loss of 0.17 m. The loss in average elevation was greatest on East Ship Island where large dune features had been present before the storm. A scatterplot of the alongshore variation in island volume change and average elevation change is provided in Figure 42.

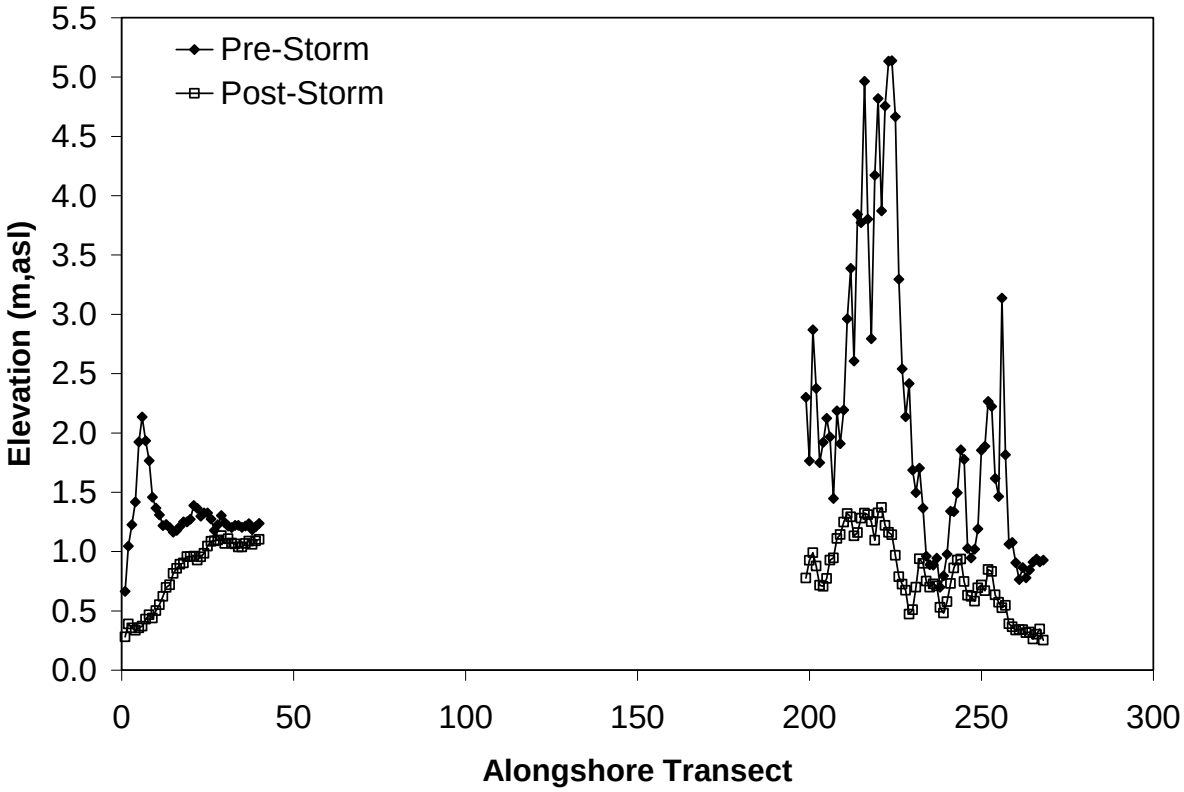


Figure 121. (a) Alongshore variation in pre- and post-storm elevation for Ship Island.

Morphology Change

Based on the scree plots, both the pre- and post-storm datasets have six eigenmodes that are statistically significant, with the percent of total variance explained at 74% and 76% respectively. The primary eigenmode (E1) for the pre-storm data explains 43% of the variance and shows a large and side ridge in the centre of the island at ~225 m from the shoreline. All eigenmodes exhibit this same ridge, but with smaller amplitude and with other ridges landward and seaward of this central ridge.

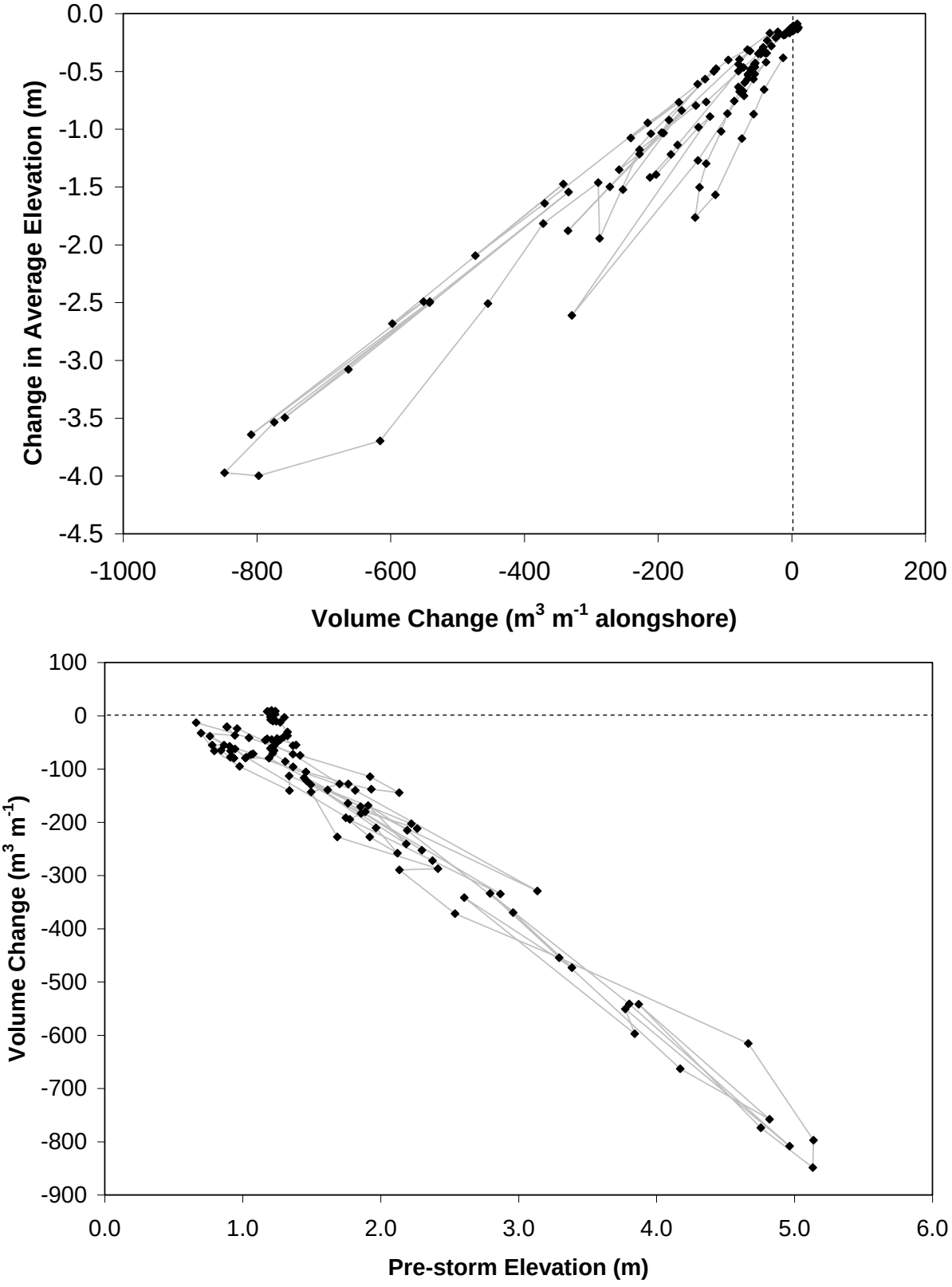


Figure 122. Relationship between (a) profile volume change and the change in average elevation (post-pre storm average elevation), and (b) pre-storm average elevation and volume change.

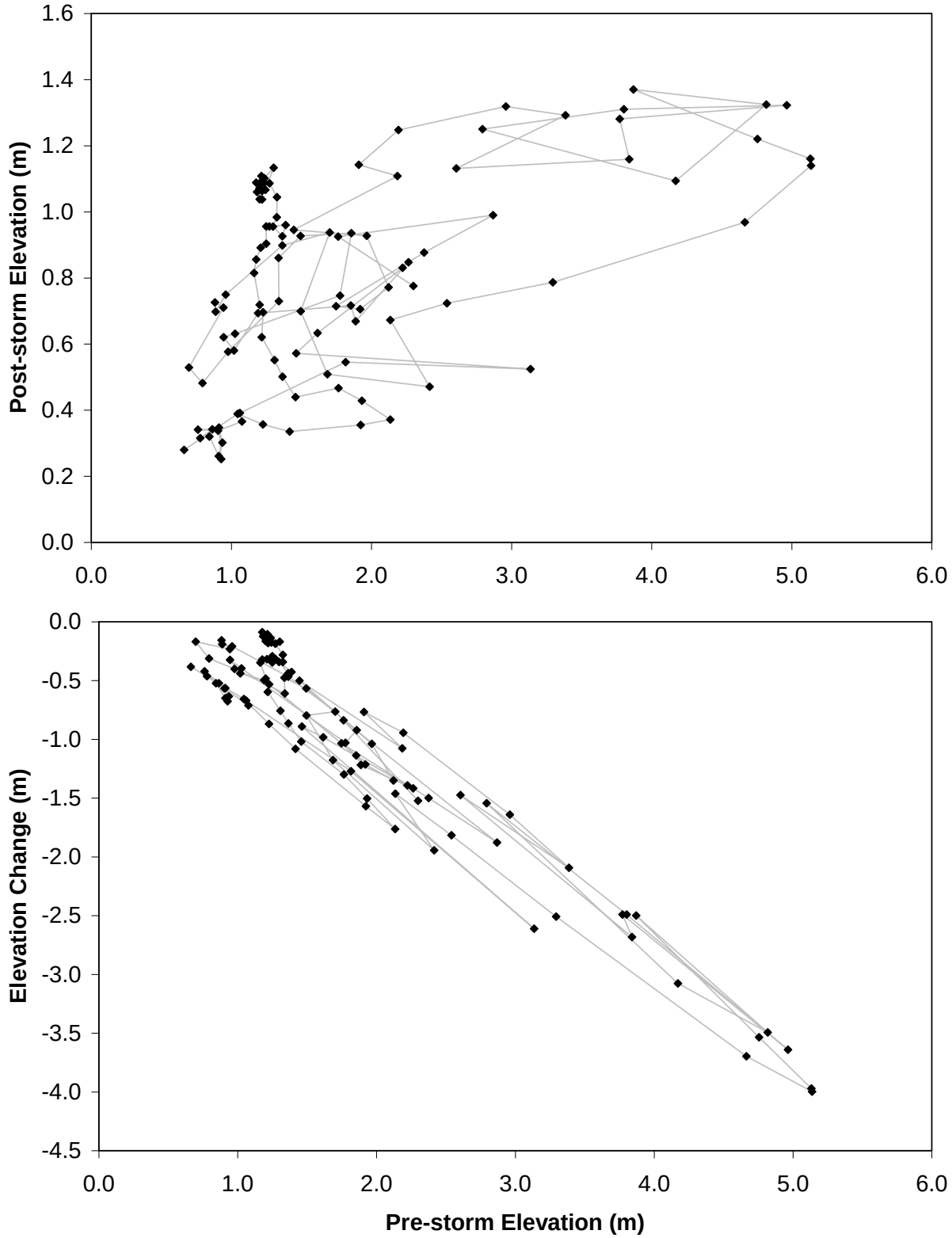


Figure 123. (a) Relationship between pre-storm elevation and elevation change. Also shown (b) is the relationship between pre-storm elevation and change in profile volume.

Similar to the other islands and in sharp contrast with the pre-storm morphology, the post-storm eigenmodes are characterized by a single storm ridge at varying distances from the shoreline. The primary eigenmode (E1) is characterized by a single ridge at a distance of 125 m from the pre-storm shoreline. The second eigenmode is characterized by a ridge ~375 m from the pre-storm shoreline, while E3 is characterized by a ridge at the shoreline. The remaining eigenmodes (E4, E5 and E6) have ridges at 225, 125 and 325 m from the pre-storm shoreline respectively.

No discernable alongshore patterns were observed in either the pre-storm or the post-storm morphology for Ship Island in general or East Ship Island alone. No statistically significant relationships were observed using Canonical Correlation Analysis between the pre- and post-storm characteristic profiles.

Bathymetry Changes

Unlike Petit Bois and Horn Islands, the offshore bathymetry of Ship Island is not characterized by a nearshore system and the analysis used for the other islands could not be used for Ship Island. The offshore bathymetry transects for both West and East Ship Island are presented in Figure 45.

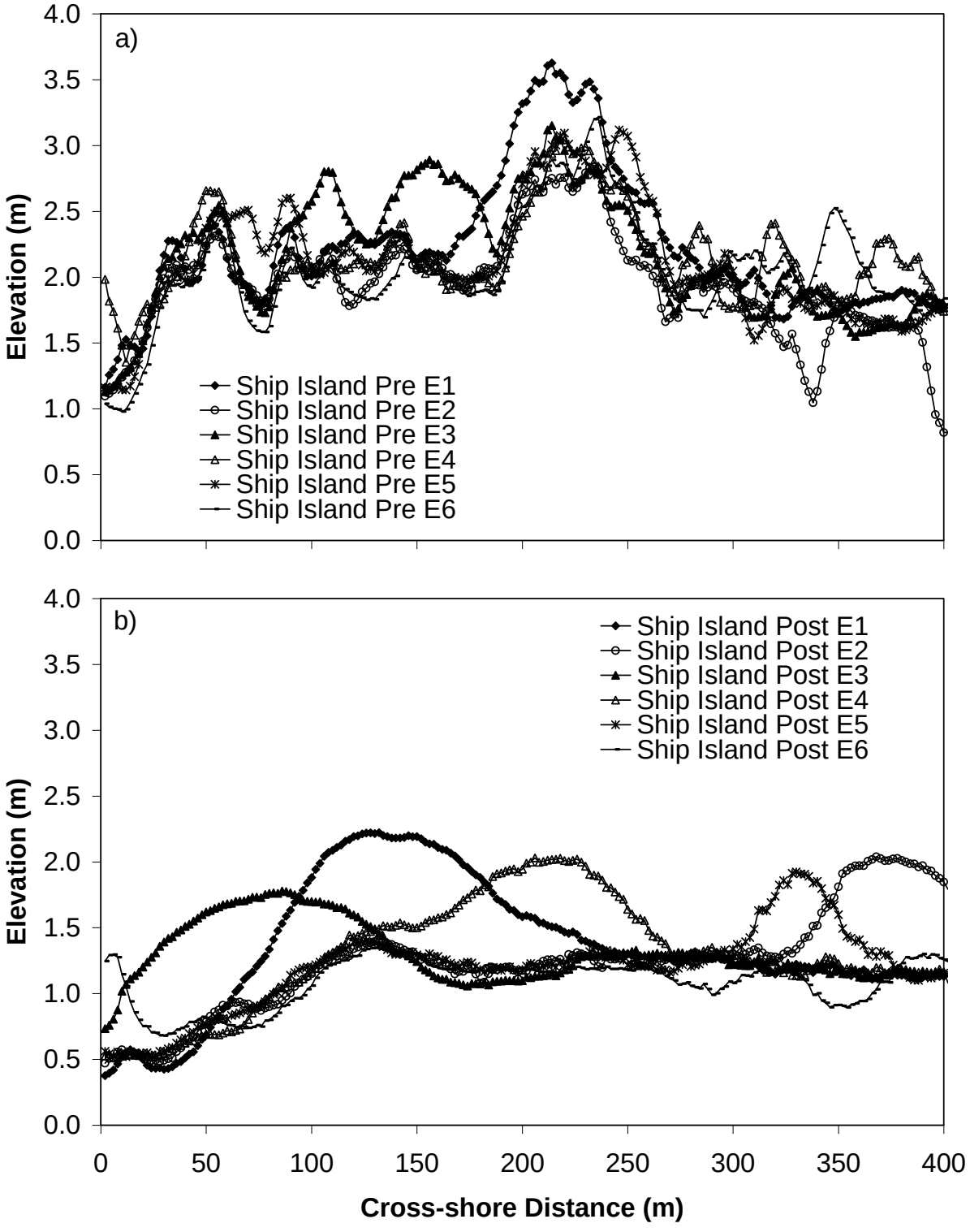


Figure 124. Characteristic (a) pre-storm and (b) post-storm cross-shore profiles for Ship Island.

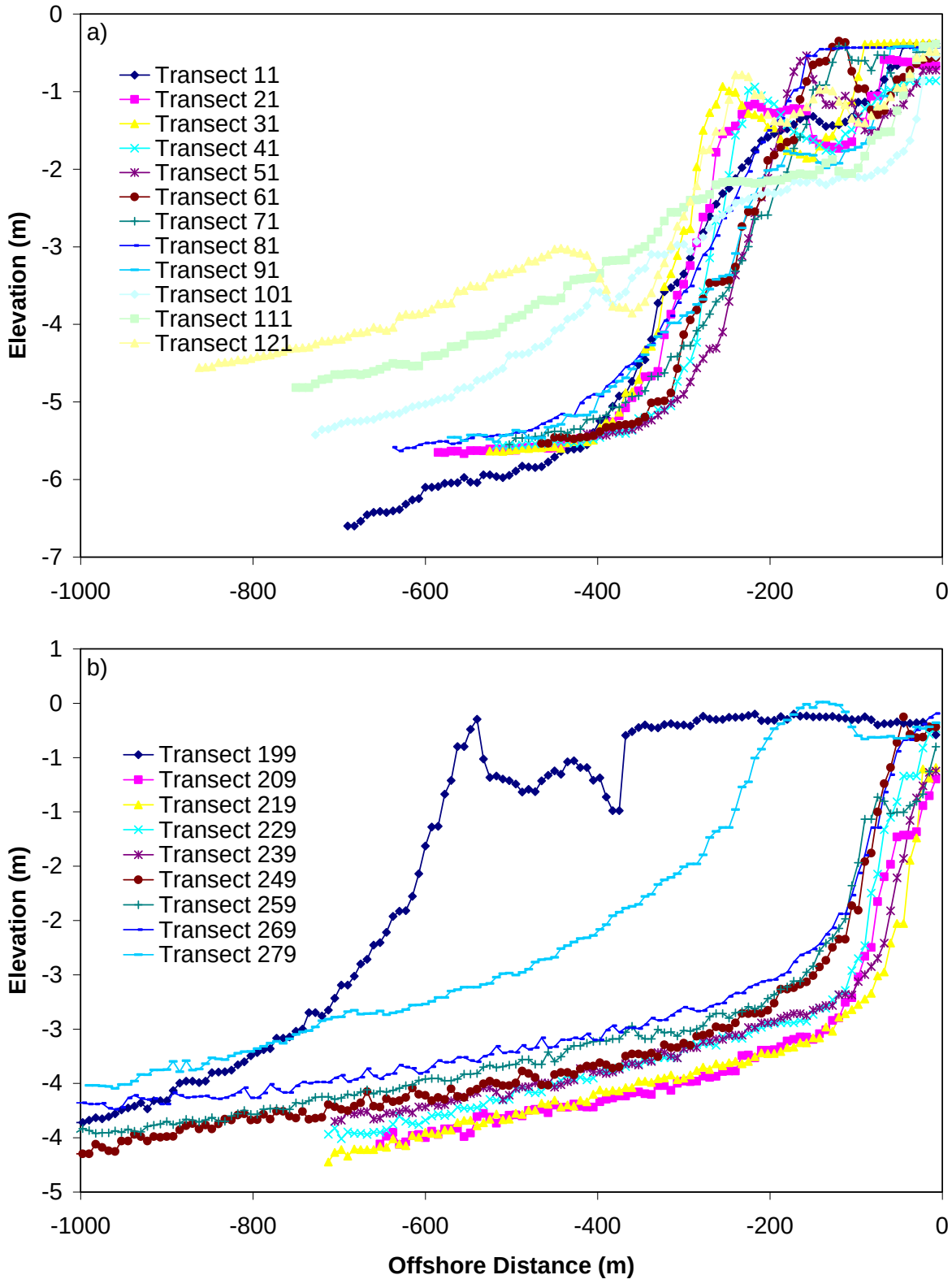


Figure 125. Post-storm cross-shore profiles for Ship Island.

REFERENCES

Armbruster, C.K., 1997 Morphologic responses of a low-energy micro-tidal beach to winter cold front passages: north shore Santa Rosa Island, Florida. M. S. Thesis, Department of Geography and Anthropology, Louisiana State University, Baton Rouge, Louisiana, 166 pp.

Armbruster, C.K., Stone, G.W., Xu, J.P., 1995. Episodic atmospheric forcing and bayside foreshore erosion: Santa Rosa Island Florida. Transactions-Gulf Coast Association of Geological Societies XLV, 31-37.

Aubrey D., 1979. Seasonal patterns of Onshore/Offshore Movement. Journal of Geophysical Research 84: 6347-6354.

Chaney, P.L and Stone, G.W., 1996. Soundside shoreline erosion and implications for winter cold front forcing: West Ship Island, Mississippi. *Shore and Beach,* 64, 27-33.

Cooper, J. A and Pilkey, O., 2004. "Sea-level Rise and Shoreline Retreat: Time to Abandon the Bruun Rule." Global and Planetary Change 43: 157-171.

Houser, C. and Greenwood, B., 2005. "Hydrodynamics and Sediment Transport Within the Inner Surf Zone of a Lacustrine Multiple Barred Nearshore." Marine Geology 218 (2005): 37-63.

Houser, C., Hamilton, S., Meyer-Arendt, K., and Oravetz, J., 2007. EOF Analysis of Morphological response to Hurricane Ivan. Coastal Sediments, 2007.

Keim, B.D., Muller, R.A., and Stone, G.W., 2004. Spatial and temporal variability of coastal storms in the North Atlantic Basin. *Marine Geology*, 210, 7-15.

Knabb, R, Rhome, J., and Brown, D., 2005. "Tropical Cyclone Report: Hurricane Katrina 23-30 August 2005." Miami: National Hurricane Center, 2005

Kraus, N.C., Larson, M., and Kriebel, D.L., 1991. Evaluation of beach erosion and accretion predictors. Proceedings of Coastal Sediments 1991. ASCE Press, New York, 572-587.

Kwon, D. "Barrier Islands of the Northern Gulf of Mexico Coast: Sediment Sources and Development." Louisiana State University, Coastal Studies Series 25 (1975): 51.

Larson, M., Capobianco, M., Jansen, H., Rozynski, G., Southgate, H., Stive, M., Wijnberg, K., and Hulscher, S., "Analysis and Modeling of Field Data on Coastal Morphological Evolution Over Yearly and Decadal Time Scales. Part 1: Background and Linear Techniques." Journal of Coastal Research 19.4 (2003): 760-775.

Leatherman, S., 1977. Overwash Hydraulics and Sediment Transport." Coastal Sediments:135-148.

Leatherman, S.P., 1979. Landward Migration of Nauset Spit: Relative Rates and Mechanisms. NPS-CRU-UMass Report.

McBride, R.A. and Byrnes, M.R., 1997. Regional variations in shore response along barrier island systems of the Mississippi River Delta Plain; historical change and future prediction. *Journal of Coastal Research*, 13, 628-655.

Meredith, A., .Eslinger, D., Aurin, D. 1999. An evaluation of Hurricane Induced Erosion Along the North Carolina Coast Using Airborne LiDAR Surveys. Charleston: Coastal Service Center Technical Report CSC/99031-PUB, 1999.

Morton, R. 2002. Factors controlling Storm Impacts on Coastal Barrier and Beaches: A Preliminary Basis for Real Time Forecasting. Journal of Coastal Research 18.3: 486-501.

Morton, R.A., and Sallenger, A.H., 2003. Morphological impacts of extreme storms on sandy beaches and barriers. *Journal of Coastal Research*, 19, 560-573.

Otvos, E., 1979, Barrier island evolution and history of migration, North Central Gulf Coast, *in* S. P. Leatherman, ed., Barrier Islands: New York, Academic Press, 325 p.

Plant, M. Freilich, and R. Holman. "The role of morphological feedback in surf zone sand bar response." Journal of Geophysical Research 106 (2001): 959-971.

Sallenger, A. H., 2000, Storm impact scale for barrier islands. *J. Coastal Research*, 16, 890-895.

Schmidt, Keil "East Ship Island Evolution, Morphology, and Hurricane Response 1994 to 2001." Mississippi Department of Environmental Quality, Open File Report 134. 2003.

Shepard, F. "Gulf Coast Barriers.*"* Recent Sediments Northwest Gulf of Mexico. American Association of Petroleum Geologists, 1960. 197-220.

Stone, G.W. and Morgan, J.P., 1993. Implications for a constant rate of relative sea-level rise during the last millennium along the Northern Gulf of Mexico: Santa Rosa Island, Florida. Shore and Beach, 61, 24-28.

Stone, G.W., Liu, B., Pepper, D.A., and Wang, P., 2004. The importance of extratropical and tropical cyclones on the short-term evolution of barrier islands along the northern Gulf of Mexico, USA. *Marine Geology*, 210, 63-78.

Thieler, E.R., and Young, R. S. 1991. "Quantitative evaluation of coastal geomorphic changes in South Carolina After Hurricane Hugo." In: Finkl, C.W. and Pilkey, O.H. (eds.), *Impacts of Hurricane Hugo: September 10-22, 1989, Journal of Coastal Research* Special Issue #8: 187-200.

Thorton, E., Sallenger, A., Conforto Sesto, J., Egley, L., McGee, T., and Parons. R., 2006. Sand Mining Impacts on Long-term Dune Erosion in Southern Monterey Bay. Marine Geology 229 (2006): 45-58.

U.S. Army Corps of Engineers. Coastal Engineering Manual: Engineer Manual 1110-2-1100. USACE: Washington, D.C. 2002.

Waller, T. and L. Malbrough, 1976. “Temporal Changes in the Offshore Islands of Mississippi.” Water Resources Research Institute, Mississippi State University.

White, S., and Wang, Y., 2003. “Utilizing DEMs derived from LiDAR data to analyze morphologic change in the North Carolina coastline.” Remote Sensing of Environment 85: 39-47.

Zhang, K., Whitman, D., Leatherman, S., and Robertson, W., 2005. “Quantification of Beach Changes Caused by Hurricane Floyd Along Florida's Atlantic Coast Using Airborne Laser Surveys.” Journal of Coastal Research 21.1: 123.

APPENDIX I

The following papers were not funded through contracts with the National Park Service but were nonetheless developed and based on the data collected in this study and provide greater insight into the geologic control of geomorphic processes on Santa Rosa Island.

Houser, C., Barrett, G., and Labude, D. (*In Press*) Alongshore variation in the rip current hazard at Pensacola Beach. Accepted to *Natural Hazards*, September 2010.

Houser, C., Caldwell, N., and Meyer-Arendt, K. (*In Press*) Hot times at Hot spots: The rip current hazard at Pensacola Beach, Florida. Invited submission to refereed book *Rip Currents: Beach Safety, Physical Oceanography and Wave Modeling*, edited by Steven Leatherman and John Fletemeyer. Accepted August 2010.

Houser, C., and Sojan, M. (*2011*) Variability in foredune height depends on the alongshore correspondence of transport potential and sediment supply. *Geomorphology*, 125, 62-72.

Houser, C. (2009) Synchronization of transport and supply in beach-dune interaction. *Progress in Physical Geography*, 33, 733-746. doi:10.1177/0309133309350120

Nat Hazards (2011) 57:501–523
DOI 10.1007/s11069-010-9636-0

ORIGINAL PAPER

Alongshore variation in the rip current hazard at Pensacola Beach, Florida

Chris Houser · Gemma Barrett · Daniel Labude

Received: 2 March 2010 / Accepted: 28 September 2010 / Published online: 17 October 2010
© Springer Science+Business Media B.V. 2010

Abstract Many drowning and near drownings at Pensacola Beach, Florida are attributed to rip currents, the strong seaward-flowing currents that extend from the shoreline to the line of breakers and sometimes beyond. While surf forecasts assume that the rip hazard is uniform alongshore and that the (erosion) rips are ephemeral features, evidence is presented to suggest that the rip hazard at Pensacola Beach is not uniform alongshore. Rather the rip current "hotspots" develop as a consequence of an alongshore variation in the surf similarity parameter and nearshore state on the order of ~1,450 m. The variation is forced by transverse ridges on the inner shelf that force wave refraction and focusing at the ridge crests. This creates a more dissipative, rhythmic bar and beach morphology at the ridges and rougher surf. Between ridges, where wave heights and periods are smaller and the outermost bar is forced closer to the shoreline, the nearshore is in a (more reflective) bar and rip state during red flag conditions. Drownings between 2000 and 2009 are shown to be clustered between transverse ridges and in the years following a hurricane or tropical storm (2000–2003 and 2005–2008) when the bar and rip morphology first develops as the shore face recovers. This continues until the innermost bar attaches to the beach face unless the bar system is reset by another tropical storm or hurricane. It is argued that the rip hazard is dependent on the alongshore covariation of the environmental forcing with the individual and group behavior in both time and space, even on what appears to be a relatively uniform beach environment.

Keywords Rip current · Drownings · Coastal hazards

1 Introduction

It is estimated that between 100 and 150 beach users drown in rip currents in the United States each year (Fletemeyer and Leatherman 2010), and more than 80% of lifeguard rescues are necessary because of these shore-normal currents (Lushine 1991; Lascody

C. Houser (✉) · G. Barrett · D. Labude
Department of Geography, Texas A&M University, 810 O&M Building, College Station, TX, USA
e-mail: chouser@geog.tamu.edu

1998). The State of Florida has one of the highest rates of drowning in the United States (Florida Department of Health 2003), and the United States Lifesaving Association identified the Florida panhandle "as the worst in the nation for beach drowning" (The Tuscaloosa News 2002). In Pensacola, drownings and near drowning (submersions) tend to occur between March and October, when the surf is strong (Lascody 1998), and involve inexperienced or vulnerable swimmers that may not have heeded warning signs (Morgan et al. 2009; Fletemeyer and Leatherman 2010). More broadly across the southeastern United States, submersions and rescues tend to be clustered during busy summer weekends and are associated with strong onshore winds generated by a high pressure systems (Gensini and Ashley 2009). Similar patterns have been seen on Galveston Island, where the greatest number of submersions occurs in May, when there remains a strong potential for frontal storms and a substantial increase in beach users as the school year ends (Davis, Pers. Comm.). Submersions are more frequent in the late afternoon, coincident with the peak in the number of beach users as well as the strength of the landward component of the sea breeze (Nielsen-Gammon 2001).

The United States National Weather Service (NWS) is required to provide forecasts of the rip current potential for much of the continental United States coastline. The forecasts largely depend on wind and wave forcing, with the greatest likelihood of rip formation associated with storm winds and waves (see Mollere et al. 2001). It is (implicitly) assumed that heavy surf will lead to erosional rips (see Short 1985), which develop with a quasi-regular spacing as a consequence of flow and morphological instabilities (Hino 1974; Dalrymple and Lozano 1978; Deigaard et al. 1999; Falques et al. 1999; Holman et al. 2006; Turner et al. 2007). As these instabilities grow, the longshore pressure gradients are enhanced through a topographic feedback. This leads to more intense wave energy dissipation and setup occurring across barred areas compared to the adjacent erosional rip channels (Aagaard et al. 1997). The alongshore spacing of the rip channels is associated with the fastest growing instability. Several studies suggest a spacing that scales with the width of the surf zone (Hino 1974; Falques et al. 1999; Brander and Short 2000), or the distance to the offshore bar (Deigaard et al. 1999). As a consequence, rip current velocities increase in response to increasing wave heights and decreasing tidal elevations (Sonu 1972; Bowman et al. 1988a, b; Aagaard et al. 1997; Brander 1999; Brander and Short 2000, 2001; Drønen et al. 2002; Haller et al. 2002; MacMahan et al. 2005). Due to the strong flows and the mobility of the channel alongshore (Holman et al. 2006; Reniers et al. 2004; Turner et al. 2007), these rips pose a significant hazard to those on the beach during storms. Once formed, these erosional rips can become topographically controlled following a large (reset) storm, such that the location is determined as much by the evolving morphology as the incident forcing (Ranasinghe et al. 2000; Turner et al. 2007).

In addition to erosion rips, Short (1985) also describes accretion and topographically controlled rip current systems. Topographically controlled rips are forced by the local geology or shelf bathymetry that controls the refraction patterns and wave focusing, which in turn determines the location and number of rip currents. An offshore control on rip currents was first noted by Shepard et al. (1941) at La Jolla, California, where waves are refracted over an offshore submarine canyon. Maximum velocities are reached during storm winds and waves. In contrast, accretion rips develop in response to decreasing wind and wave energy that drives shoreface recovery and a transition from a dissipative to a reflective profile (Wright and Short 1984). The change in morphological state is driven by a change in the surf scaling parameter (ε) described by Guza and Inman (1975):

$$\varepsilon = \frac{a_b \omega^2}{g \tan^2 \beta} \quad (1)$$

where a_b is the breaker amplitude ($H_b/2$), ω is the radian frequency of the incident waves ($2\pi/T$, $T = period$), g is acceleration due to gravity and β is the gradient of the beach/surf zone. As wave energy decreases following a storm, the beach changes from dissipative ($\varepsilon > 20$) to reflective ($\varepsilon < 2.5$) by passing through each of four intermediate states: longshore bar-trough, rhythmic bar-beach, bar-rip and low-tide terrace ($2.5 > \varepsilon < 20$). Each of these intermediate states is characterized (to varying degrees) by the presence of accretion rips. As the shoreface evolves, there is an increase in the rip current velocity as the cross-sectional rip channel area decreases and the ability of the bar system to block return flows increases (Brander 1999), until the innermost bar completely welds to the beachface. These rips do not have the characteristic form and may be difficult to identify from the perspective of a beach user. Further, they persist through both storm and non-storm conditions.

In low-energy (accretional) environments, current velocities in a rip channel are on the order of 0.8–1.2 m s^{-1} (Sonu 1972; Bowman et al. 1988a, b; Sherman et al. 1993; Smith and Largier 1995; Aagaard et al. 1997; Brander 1999). Such velocities are potentially problematic for a non-swimmer. Velocities in high-energy environments can reach a peak of 2 m s^{-1} (Brander and Short 2000). There is not necessarily a direct correlation between the number of submersions and the presence of storm waves, since fewer people choose to enter the water or are prevented by lifeguards during storm events. In fact, the greatest hazard to beach users may occur under low to moderate conditions (green to yellow flag) when more people enter the water with greater confidence (Lascody 1998). In particular, as winds subside and wave heights decrease, beach users reenter the water (prematurely), despite the presence of long period (swell) waves that are capable of generating strong rip velocities (Lascody 1998; Bob West, Pers. Comm.). The stage is set for a beach user to experience problems. The degree to which there is a potential for someone to drown or be in need of rescue depends on a number of variables including alcohol consumption, gender, age, swimming ability (Morgan et al. 2009; Gensini and Ashley 2009). At Pensacola Beach, Florida, approximately 25% of drownings in the last decade were by good Samaritans trying to rescue others or parents going into the surf to rescue their children (Bob West, Pers. Comm.). In this respect, the hazard posed by heavy surf and rip currents along with the number of rescues and submersions is dependent on the covariation in environmental forcing with personal and group behavior (Fig. 1).

As noted, the beaches of the Florida Panhandle have been described by the United States Lifesaving Association "as the worst in the nation for beach drowning" (The Tuscaloosa News 2002). Based on the NWS forecast, beach users in places such as Pensacola Beach (Fig. 2) are warned of the rip and surf hazards through warning flags (Table 1). Erosion rips are common during storm events (red or double red flag conditions), typical of fall through spring, but they tend to be ephemeral (as described by Holman et al. 2006) and migrate rapidly alongshore with the prevailing current (West, Pers. Comm.). Despite the presence of erosion rips, beach rescues and submersions tend to be clustered around what appears to be "semi-permanent" accretion rip areas that persist during both storm and non-storm conditions and are not necessarily related to primary access points (Vaughan, pers comm). It is unclear whether rip currents are responsible for the high number of rescues and submersions at Pensacola Beach. The purpose of this study is to confirm the clustering of rescues and drowning, as well as to identify the forcing mechanism responsible and the likely role of rip currents.

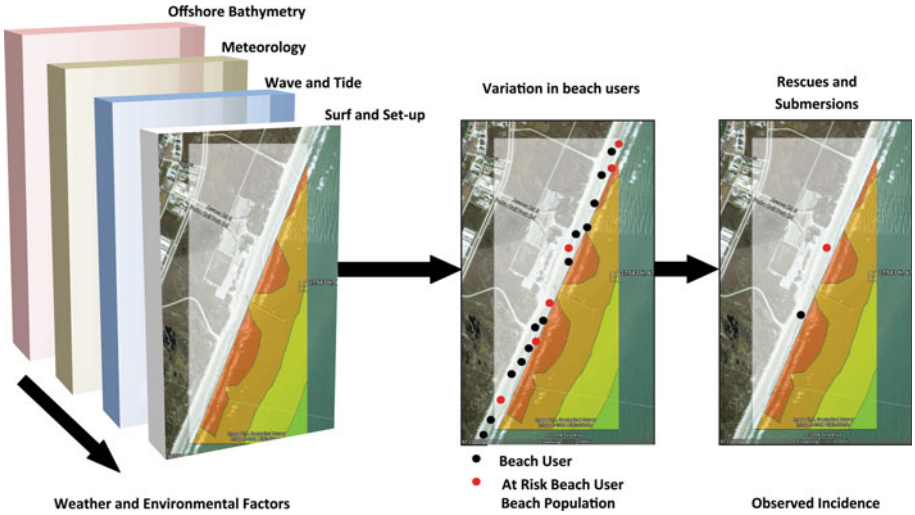
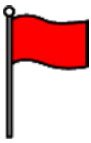
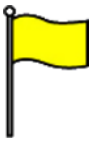


Fig. 1 The number and location of rescues and submersions on a given day depend on the spatial variation of beach users (including those at risk to drowning) and the spatial variation in surf and rip current potential from low (*orange*) to high (*red*)



Fig. 2 Location of Pensacola Beach in northwest Florida

Table 1 Description of flagging system used at Pensacola Beach to describe surf and rip current hazard based on National Weather Service forecast

Flag		Description	# Days	Drownings	Prevents	Assists	Rescues
	Double Red	Water closed to public	1	2	0	0	0
	Red	High hazard, strong surf and/or currents	160	2	17,000	214 (46%)	113 (47%)
	Yellow	Med. hazard, moderate surf and/or currents	538	0	20,596	1106 (38%)	582 (44%)
	Green	Low hazard, calm conditions	693	0	5,993	258 (41%)	64 (47%)

Also shown are the number of such events during the lifeguard season (March to October) between 2004 and 2009. The percentage of assists and rescues in unguarded sections are listed parenthetically next to the total count

Table 2 Average coherency and phase relationship between the depth 250 m offshore with the position of the outermost bar, the significant wave height (H_s) and the surf similarity parameter (ε)

Length scale (m)	Bar	H_s	ε
1468			
Coherence	0.44	0.66	0.98
Phase (m)	−75	36	−42
2038			
Coherence	0.52	0.73	0.99
Phase (m)	−123	294	−71
4205			
Coherence		0.79	0.96
Phase (m)		1071	136
8041			
Coherence	0.72	0.33	0.93
Phase (m)	−2443	5379	629

2 Study site

2.1 Socioeconomic setting

Pensacola Beach is an important tourist destination in northwest Florida (Fig. 2), supporting over 4000 local jobs and contributing ~$277 million to the local economy annually (Livingston and Arthur 2002). Bed tax revenue indicates that there are ~1.8 million visitors annually in addition to the more than 270,000 day visitors and 670,000 visitors staying at unpaid lodging sites. While there was a decrease in the number of visitors following Hurricane Ivan, there has been a steady increase in visitors in recent years, although levels remain below pre-Hurricane Ivan levels. Toll data suggests that visits to the island reach a maximum in July (>400,000 vehicles) and a minimum in December (around 200,000 vehicles). Over 87% of visitors to the Pensacola area indicate that the beach is an "extensive influence" or "moderate influence" on their decision to visit the area (Livingston and Arthur 2002). Visitors indicate that cleanliness, climate, natural beauty and (beach) safety are their most important concerns.

As discussed by Meyer-Arendt (1990), the lack of overland access and devastating hurricanes limited the development of Pensacola Beach in the 19th century. An increase in the number of day users ultimately led to the development of permanent structures, bridge access and the establishment of lifeguards at Casino Beach in 1931. The recreational business district developed in the 1950s in the form of cottages, motels and other tourist-oriented businesses. Today, commercial and residential development at Pensacola Beach occupies ~13 km of shoreline and is bounded to the east and west by the Gulf Islands National Seashore. Access for day users of the beach is provided at the main Casino Beach (30.331006°N, 87.140842°W) as well as at Fort Pickens Gate (30.324764°N, 87.180515°W), and Park East (30.347154°N, 87.056521°W). Access is also possible via a walkover at 'the cross' (30.329132°N, 87.153533°W), and at the end of streets in the residential area east of Casino Beach, such as 23rd Avenue (30.339142°N, 87.097929°W). Between March and October, lifeguards are stationed at Casino Beach, Fort Pickens Gate and Park East, with the rest of the beach patrolled by foot and vehicle. Lifeguards are permanently stationed at Casino Beach between March and October, and only between May and August at Fort Pickens Gate and Park East.

2.2 Physical setting

Santa Rosa Island is a narrow sandy Holocene barrier island extending 96 km from East Pass near Destin to Pensacola Pass in the west. Formation of the island is attributed to the erosion of a central Pleistocene core and the redistribution of sediment alongshore (Otvos 1982), although bluff erosion east of Destin is also cited as being important to the development of the island (Kwon 1969; Stone 1991; Stone et al. 1992; Stone and Stapor 1996). Fronting the island on the inner shelf is a series of offshore sinusoidal ridges and troughs oriented northwest-southeast in alignment with the De Soto submarine canyon to the east (Stone 1984). Although these features were also described by Hyne and Goodell (1967), little is known about how these shore-transverse ridges developed. As shown by Houser et al. (2008), the ridges are an important control on island response and recovery to extreme storms, and the alongshore variation in shoreline erosion. Specifically, the alongshore variation in dune morphology and hurricane impact in 2004/2005 was coherent with transverse ridges on the inner shelf. Large foredunes and the backbarrier dunes were observed at the widest sections of the island (the cuspate headlands), which also

corresponds to the crest of the transverse ridges. The ridges create a more dissipative shoreface that promotes dune development, while the more reflective shoreface between ridges limits aeolian transport and dune development (Houser and Hamilton 2009). Browder (2001), and Browder and Reilly (2008) also note that the relict beach ridge fronting Casino Beach focuses wave energy to create erosion hotspots and variations in nearshore state.

The beach and dune system of Santa Rosa Island site are recovering from Hurricanes Ivan, Dennis and Katrina during the 2004/2005 hurricane season, when the island experienced widespread shoreline retreat and widespread overwash and breaching (Houser et al. 2008; Houser and Hamilton 2009). The area has an average tidal range of 0.43 m (Armbruster 1997) and the dominant wave approach is from the southeast (Balsillie 1975). However, it is not uncommon for storm waves to approach from the southwest or from the south with the sea breeze or with tropical activity. The time-averaged significant wave height (H_s) offshore is $\sim$1.0 m (Stone et al. 1992) with a mean period (T) of $\sim$5 s. While the beach was fronted by a single nearshore bar and a relatively steep foreshore (average tan β of 0.15) prior to the 2004/2005 hurricane season, there are presently 2 subtidal bars that are migrating landward.

3 Methodology

3.1 Flagging system

Based on the National Weather Service rip forecast, the Santa Rosa Island Authority maintains a flagging system to alert beach users about the heavy surf and rip hazard. The highest flag color for that day is recorded by the Island Authority along with the number of prevents, assists and rescues. As defined by the Santa Rosa Island Authority, prevents are when a lifeguard takes a preventative action, such as moving people away from a rip current prior to them needing to be rescued (West, Pers. Comm). Assists occur when a lifeguard enters the water and makes physical contact with a distressed swimmer and helps them to shore. While this would be considered a rescue by the definitions set by the United States Lifeguard Association, the Island Authority reserve the rescue definition for those persons in extreme difficulty who are in the opinion of the lifeguard would have drowned without assistance. Rescues, assists and prevents are identified as being either in a 'guarded' area, a designated swimming area where there are typically a large number of beach users (Casino Beach, Fort Pickens Gate Beach and Park East), or along the $\sim$13 km stretch of unguarded beach where lifeguards nonetheless conduct regular patrols and respond to emergency calls, or when lifeguards are not provided. Location-specific drowning data are available for the period 2000–2009, while the number of location-specific rescues, assists and prevents are only available for the period 2004–2009. Standard archival techniques are used to obtain media reports that provide further detail as to the circumstances surrounding each drowning.

3.2 Offshore bathymetry

The most recent and extensive bathymetric data for Santa Rosa Island that detail the form and location of the transverse ridges were collected by NOAA in 1982. Following recent hurricane activity in 2004 and 2005, a series of shore-parallel and shore-perpendicular surveys were conducted in spring 2007 using a 200 kHz fathometer to determine whether

the inner-shelf morphology changed. Transects were spaced 175 m alongshore, extending 1.5 km into the Gulf of Mexico. All data were spatially referenced in real time using a ship-based GPS, and the seafloor depths were heave and tide-corrected to mean low water (MLW) using measured tides. Comparison to the bathymetry data, collected by NOAA in 1982, suggests that the ridges have changed little (if at all) during the recent increase in hurricane activity and that the post-storm bathymetry data collected for this study is appropriate to examine the (pre- and post-storm) controls on dune morphology. The grouped bathymetric data were combined with the NOAA data and interpolated using inverse distance weighting at a spacing of 1 m.

3.3 Wave model

The wave climate in northwest Florida is a combination of wind waves that are locally generated and swells propagating into the region from the Gulf of Mexico. To account for the resulting double-peaked wave spectra, the spectral wave model Mike21 is used to examine the alongshore variation in wave forcing and the surf similarity parameter (Eq. 1), between 2000 and 2009. The model accounts for (1) wave propagation in time and space, shoaling, and refraction due to current and depth, (2) wave generation by wind, (3) wave interactions, (4) white-capping, bottom friction and depth-induced breaking and (5) wave-induced set-up. A nested modeling approach produces boundary conditions (both spectral and parametric) for fine grid resolution models. The results of the model provide 2D spectra for all boundary points in the study area (on a computational grid), which is then used for finer scale transformations in areas of wave convergence and divergence. Offshore wave boundary conditions and wind forcing function are based on long-term meteorological and oceanographic records from two offshore wave buoys located near the study region (buoy 42039 and 42040).

3.4 Data analysis

Cross-shelf profiles of the shelf bathymetry were extracted from 1,500 m long shore-normal transects spaced at 250 m alongshore over a distance of 25 km. Empirical orthogonal function (EOF) analysis is used to characterize alongshore recurring patterns in the bathymetry data. EOF analysis is similar to principal component analysis (PCA), except that the variability in the data is examined through space rather than over time (Aubrey 1979; Houser and Hamilton 2009). Since the analysis is used to identify a limited number of profiles to explain the variation in the data, the variance explained by each successive factor decreases. In this respect, EOF is commonly used as a data reduction technique or a method to separate ‘signal’ and ‘noise’. The orthogonal functions are obtained by solving an eigenvalue problem for the data matrix (X) containing the bathymetry data (columns) from the 95 transects (rows). The alongshore variation in the factors and their ability to explain the profile shape are examined using the spatial amplitudes (factors scores) calculated for each transect. The number of statistically significant factors is determined from the scree plot as the point where the eigenvalues for each factor start to level off and there is very little random (unexplained) variability left.

The alongshore variation in wave forcing, bathymetry and the surf scaling parameter is decomposed using wavelet analysis, an increasingly used approach to time and spatial series that cannot be assumed to be statistically stationary (see Short and Trembanis 2004; Coco et al. 2005; Ruessink et al. 2006). Specifically, wavelet analysis quantifies how the spectral signal varies alongshore, rather than the overall spatially averaged strength of the

signal considered using traditional Fourier analysis. Wavelets are designed to capture the behavior of non-stationary stochastic signals, whereas Fourier spectrum provides similar information in the frequency domain, but under the assumption of a stationary signal. The continuous wavelet transform $\left(W_n^s\right)$ is defined as the convolution of the alongshore series (x_n) with a scaled and translated version of the normalized mother wavelet function. The one-dimensional sequence is expanded into a two-dimensional space $(n,\ s)$ by varying the scale (s) and translating the function along n. As discussed by Torrence and Compo (1998), the complex Morlet mother wavelet provides a similar approximation to the Fourier wavelength $\lambda = 1.03$ s and is used in this study. To avoid adding an artificial periodicity to the spatial series that is not periodic, the time series was padded with zeroes to the next power of two (128 in the present study). The global wavelet spectrum is calculated by averaging over all local wavelet spectra:

$$\overline{w^2}(s) = \frac{1}{N}\sum_{n=0}^{N-1} |w_n(s)|^2 \tag{2}$$

A further description on the methodology and interpretation of wavelet analysis are provided by Torrence and Compo (1998).

Cross-wavelet analysis is a bivariate extension of the continuous wavelet transform that compares two series (x_n *and* y_n) to produce the cross-wavelet spectrum:

$$w_n^{xy}(s) = w_n^x(s) w_n^y(s) \tag{3}$$

The magnitude of the W_n^{xy}, the cross-wavelet power, is the covariance between the series $\mathrm{x_n}$ and $\mathrm{y_n}$ in $(n,\ s)$ space. To avoid large power spikes associated with spikes in the individual series, the wavelet squared coherency $R_n^2(s)$ is used instead of the simple cross-wavelet transform. The coherency is similar to the squared correlation coefficient, in which $R_n^2(^\circ s) = 1$ is obtained for a perfect linear relationship between the series and $R_n^2(s) = 0$ represents no correlation. The coherency phase difference $\phi_n(s)$ is calculated as:

$$\phi_n = \tan^{-1}\left[\frac{I(S(s^{-1} w_n^{xy}(s)))}{R(S(s^{-1} w_n^{xy}(s)))}\right] \tag{4}$$

where I and R are the imaginary and real parts of the cross-wavelet transform, respectively. The phase difference describes the spatial lag between the series for a given longshore distance (n) and scale (s). There is a potential for strong power when only one variable exhibits a strong variation at a given scale. To avoid this problem, only those length scales in which there is power in both variables, a statistically significant coherence (relative to white noise), and a consistent phase relationship will be considered as exhibiting a discrete covariance.

4 Results

4.1 Lifeguard statistics

Between 2004 and 2009, lifeguards performed 43,589 preventative acts, assisted 1,578 swimmers in distress and rescued 759 swimmers who would have drowned without assistance (Table 1; Fig. 3). Over this period, 80% of assists and 65% of rescues occurred within the $\sim$550 m of guarded beach, for an average of 1.4 rescues per m of guarded

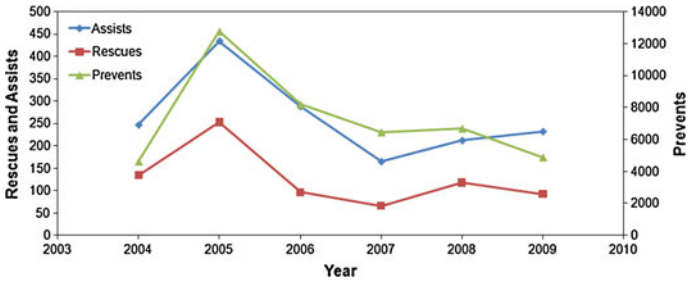


Fig. 3 Variation in the number of assists, rescues and prevents between 2004 and 2009 at Pensacola Beach

beach, compared to 0.04 rescues per m of unguarded beach. As shown in Fig. 3, there is a substantial increase in the number of prevents, assists and rescues in 2005, despite fewer beach users and an expanded beach patrol (Bob West, Pers Comm.). Chi-square analysis suggests that prevents and assists are overrepresented on red flag days and to a lesser extent on yellow flag days ($\chi^2 = 681$, $p < 0.001$), while rescues tend to be more common on yellow flag days.

As shown in Table 1, there were only 4 drownings between 2004 and 2009, partly in response to the expanded beach patrol, but over the entire study period (2000–2009) there were a total of 25 drownings. The significantly lower number of drownings between 2005 and 2009 is partly attributed to the expanded beach patrol (Bob West, Pers. Comm.). Regardless, all drownings within the expanded period were attributed to rip currents by the lifeguards and in the media:

> "She said the waves kept pulling her back out there……They drowned in an area that had several drop-offs and sandbars where currents or waves can suddenly pull a swimmer into deeper water" (Sarasota Herald-Tribune, June 6, 2000, "Alabama men drown at Pensacola Beach after lifeguards leave area")

> "The last two (drownings) occurred March 27, when a teenager from nearby Milton vanished after a riptide swept him into deep water….." (Sarasota Herald-Tribune, April 15, 2003, "Most beaches still unguarded on deadly island)

The location of drownings between 2000 and 2010 are presented in Fig. 4a. While most drownings were concentrated within about 3.5 km of the central and popular Casino Beach, more than 90% of the drownings occurred in the unguarded sections of the beach or at times when lifeguards were not on duty. Rip currents are identified as the primary cause in all drownings, but both the lifeguard and media reports suggest that other mitigating factors (age, fatigue, heavy surf, lack of concern, etc.) may have also been important:

> "Hundreds of people swam despite red flags warning them to keep out of the water…" (Herald Tribune, June 11, 2003; "Panhandle drowning toll climbs to nine")

> "Another problem is that few of the warning flags and signs are in the unguarded areas……" (Sarasota Herald-Tribune, April 15, 2003, "Most beaches still unguarded on deadly island")

Most drownings occurred when a red flag was the highest flag flown on that day and all but one involved a male swimmer. The average age was 35, but ranged from 16 to 66 and available newspaper articles suggest a number of different reasons for the person entering the rough surf although all identify rip currents as the primary cause of drowning. With a

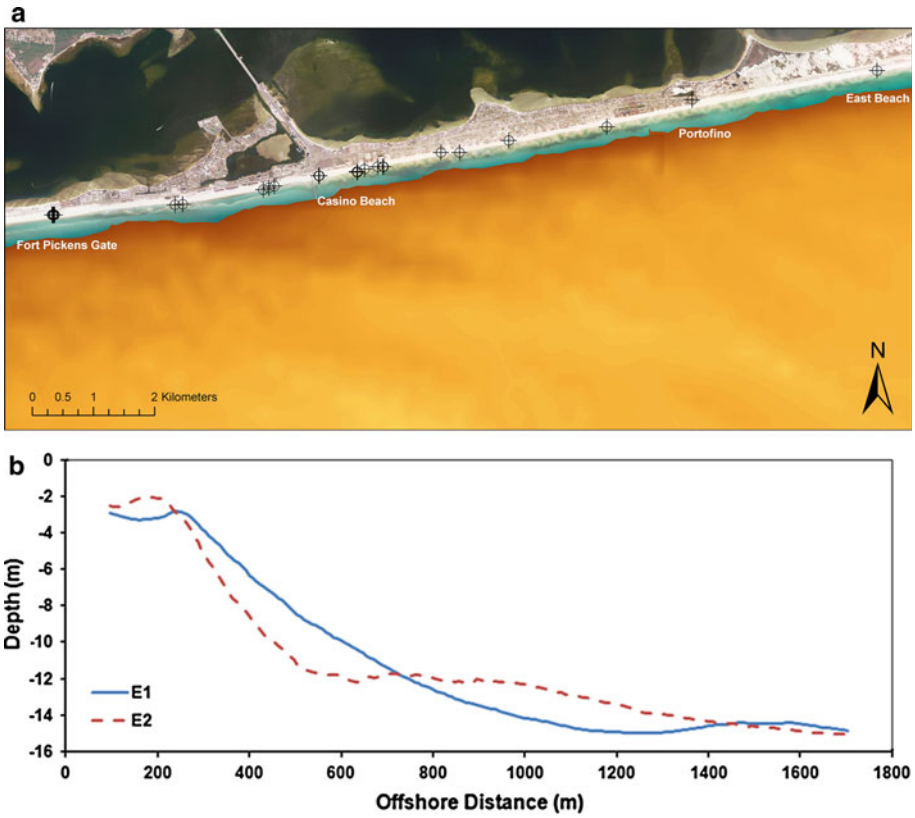


Fig. 4 **a** Shelf bathymetry and transverse ridges fronting Pensacola Beach showing location of drownings between 2000 and 2009 and **b** the primary eigenmodes (E1 and E2) of the cross-shelf bathymetry

few exceptions (e.g. December 17, 2001, November 10, 2002 and August 3, 2003), the majority of drownings at Pensacola Beach have occurred in spring and fall when the time-averaged significant wave height exceeds 1.5 m, and yellow and red flags are more common.

Notwithstanding the preceding, there has also been some debate in the media about whether the drownings are in fact associated with rip currents as demonstrated by these quotes from an article in The Tuscaloosa News (2003) following the 21 drownings between 2000 and 2003:

> "I've never seen a rip current of any significant magnitude on the stretch of Pensacola Beach that I frequent and I swim in, that I surf in, that I walk along"
>
> "I've flown over that beach dozens upon times and I could count on one or two fingers the number of times I've seen well-developed rip currents"
>
> "This rip current issue or whatever mechanism is causing the problem is something that is endemic to the wave climate….It's a mystery"
>
> "….Douglass….is convinced rip currents are rampant in the Panhandle…."

Regardless of this debate, chi-square analysis (using 1 km bins starting at Fort Pickens Gate) reveals that the alongshore distribution in drownings is significantly clustered ($\chi^2 = 23$, $p < 0.001$). However, all the drownings have occurred within unguarded sites without direct or signed access. The drownings since the year 2000 also exhibit a statistically significant clustering in time ($\chi^2 = 26.6$, $p = 0.02$), with most drownings occurring between 2000 and 2003 and again between 2005 and 2008. The number of drownings may have been significantly higher in the 2005–2008 season if not for expanded and more frequent beach patrols along the unguarded sections of beach (Bob West, Pers. Comm.). With few exceptions, the majority of drownings at Pensacola Beach have occurred in late spring and early fall, when wave heights and periods are larger but crowds smaller than the busier summer month.

4.2 Alongshore variation in shoreface bathymetry and forcing

The inner-shelf bathymetry fronting Pensacola Beach is presented in Fig. 4a. As discussed by Houser et al. (2008), the shelf is dominated by transverse ridges oriented to the southeast, extending ~1,700 m offshore to a depth of ~15 m. The ridges have a maximum relief of ~3 m, but are part of a larger field of overlapping ridges on the inner shelf. EOF analysis of the demeaned data reveals 2 significant eigenmodes (E1 and E2) that represent steep and relatively gently sloped profiles (Fig. 4b). Wavelet analysis suggests that the alongshore variation in the ratio of the E1 to E2 factor scores (E1 score/E2 score) exhibits statistically significant length scales of ~1,450, 2,038, 4,205 and 8,041 m (Fig. 5). The peak length scale is at the 1,450 m length scale, consistent with the ridges visible in the bathymetric data, and consistent with the length scales described by Houser et al. (2008) and Houser and Hamilton (2009). As would be expected, these length scales are also expressed in the depth at a distance of 250 m seaward of the shoreline, which has a

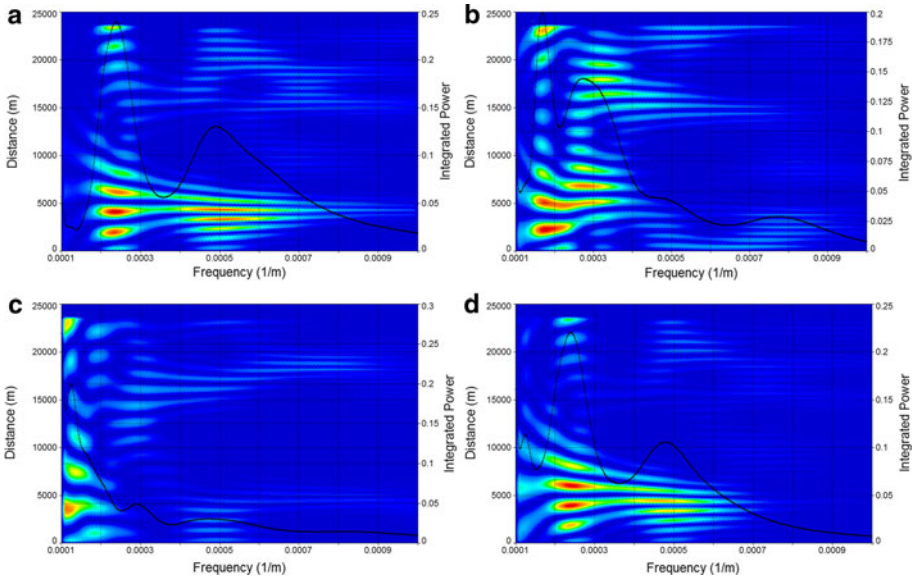


Fig. 5 Global and mother wavelets for the **a** surf similarity parameter, **b** average red flag significant wave height between 2000 and 2009, **c** position of the outermost bar, and **d** depth at 250 m offshore

more direct and physical relationship with the wave heights estimated from the spectral wave model.

A representative output of the wave model is presented in Fig. 6 for the wind and wave forcing on March 15, 2008 when there was a drowning in an unguarded section east of Casino Beach. On this red flag day, offshore waves from the SSE reached an average height of 1.96 m and period of 7 s from winds that reached an hourly peak of 11.4 m s^{-1}. These conditions are similar to those on September 14, 2008 when there were 2 drownings near the entrance to the Fort Pickens section of the Gulf Islands National Seashore. On this day, there were an additional 4 assists and 12 rescues in response to 8 s waves of 1.82 m from the SSE. The alongshore variations in wave height and period shown in Fig. 6 are consistent with the ensemble-averaged forcing for each flag level between 2000 and 2009 (Fig. 7). In addition to an increase in the wind and wave forcing with each flag level, there is a statistically significant increase in the alongshore variance in wave height and period at 250 m offshore (Table 3). The variation in wave height and period exhibits a statistically significant variation alongshore at the same length scales, indicating that the transverse ridges are capable of refracting the incident wave field to create an alongshore variation in the wave forcing. The statistically significant phase relationships between the wave field and the depth at 250 m offshore are presented in Table 2. In general, wave heights and periods are at a maximum at the crest of the transverse ridge and at a minimum between ridges where offshore depths are greater.

The alongshore variation in wave height and period leads to variations in both the similarity parameter (Eq. 1) and the position of the outermost bar. Both variables exhibit statistically significant coherence at the 95% confidence level with the transverse ridges, with a more dissipative profile (larger similarity parameter) at the ridge crest. Based on the satellite images from 1999 to 2010 (Fig. 8), these sections of the coast tend to be characterized by a rhythmic bar and beach profile (Wright and Short 1984), particularly during the initial recovery period following an extreme storm (2000–2003 and 2005–2008). Between ridges, the outermost bar is forced closer to the shoreline in response to the smaller surf similarity parameter. This in turn forces the innermost bar closer to the beachface and greater potential for the development of a bar and rip morphology as the shoreface recovers from an extreme storm. Continued recovery, however, causes the innermost bar to weld with the beachface (Fig. 8b) until the outermost bar moves into a bar and rip morphology (Fig. 8d, e). The bars are then moved offshore with the next extreme storm (Fig. 8c), starting the bar and hazard cycle over. The alongshore variation in the surf similarity parameter is at a minimum for green flag days with nearshore states ranging from reflective ($\varepsilon = 1.5$) between ridges to bar and rip ($\varepsilon = 8.7$) at the headlands. The variation is greater for both yellow and red flag days with nearshore states ranging from low-tide terrace ($\varepsilon \approx 3.1$) between ridges to longshore bar-trough ($\varepsilon \approx 18.5$). For all flags combined, the surf similarity parameter varies from a low-tide terrace ($\varepsilon \approx 2.3$) to rhythmic bar and beach ($\varepsilon \approx 13.8$). In this respect, the rip hazard is not uniform alongshore; there is a greater potential for (accretion) rip currents to develop between transverse ridges than at the crest.

4.3 Relationship between drownings and wave forcing

The data presented in Figs. 6 and 7 suggest that the drowning clusters alongshore are coherent with the bar and rip morphology between transverse ridges where both wave heights and periods during storms are at a local minimum. Results of a *t*-test between the drowning locations ($n = 25$) and the population of shoreline sampling points ($n = 95$)

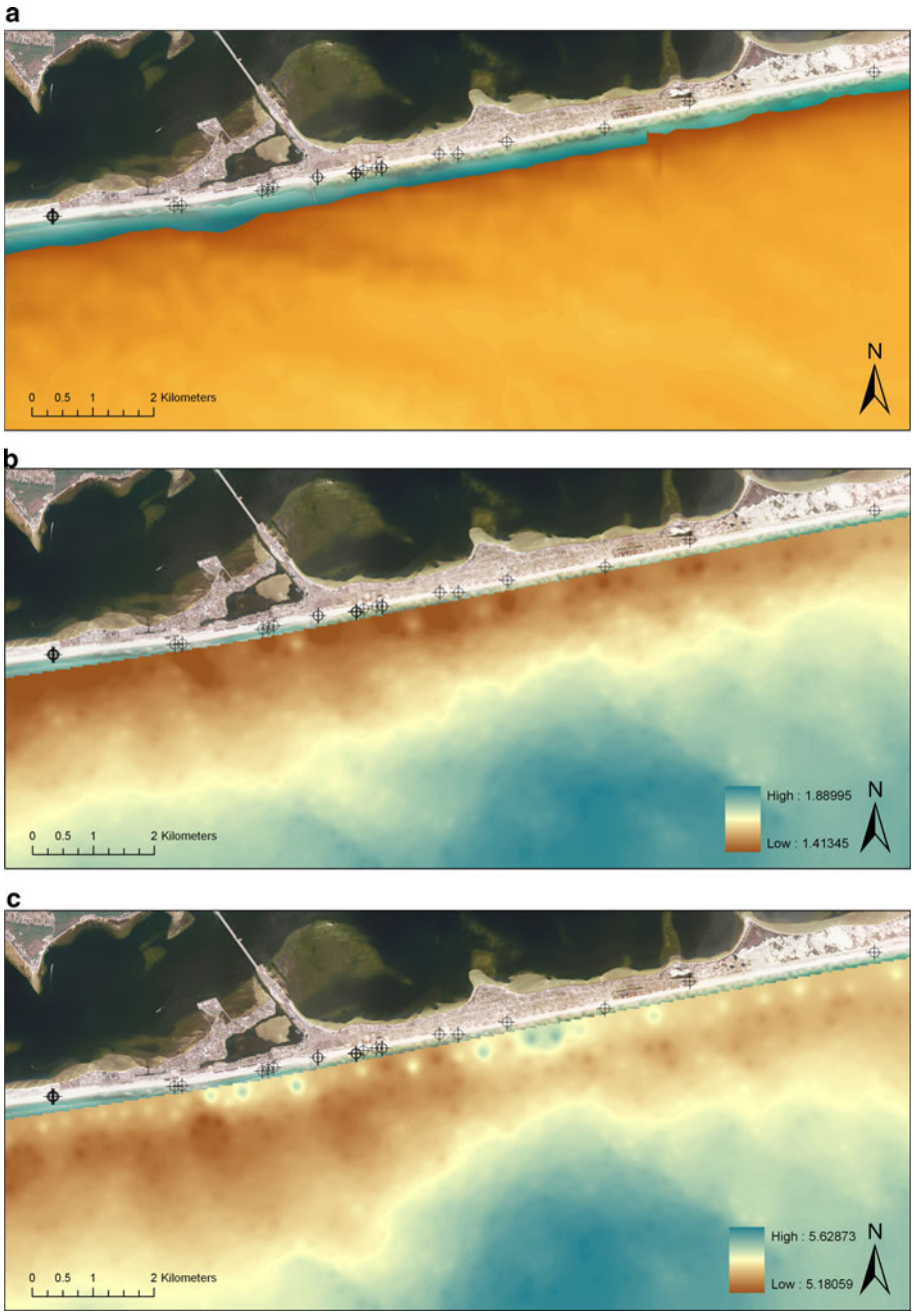


Fig. 6 Shelf bathymetry and drownings locations (**a**), and representative wave model output (**b** and **c**). Shown are the spatial variation in (**b**) the significant wave height and (**c**) the mean wave period for the wind and wave forcing on March 15, 2008 when there was a drowning in an unguarded section east of Casino Beach

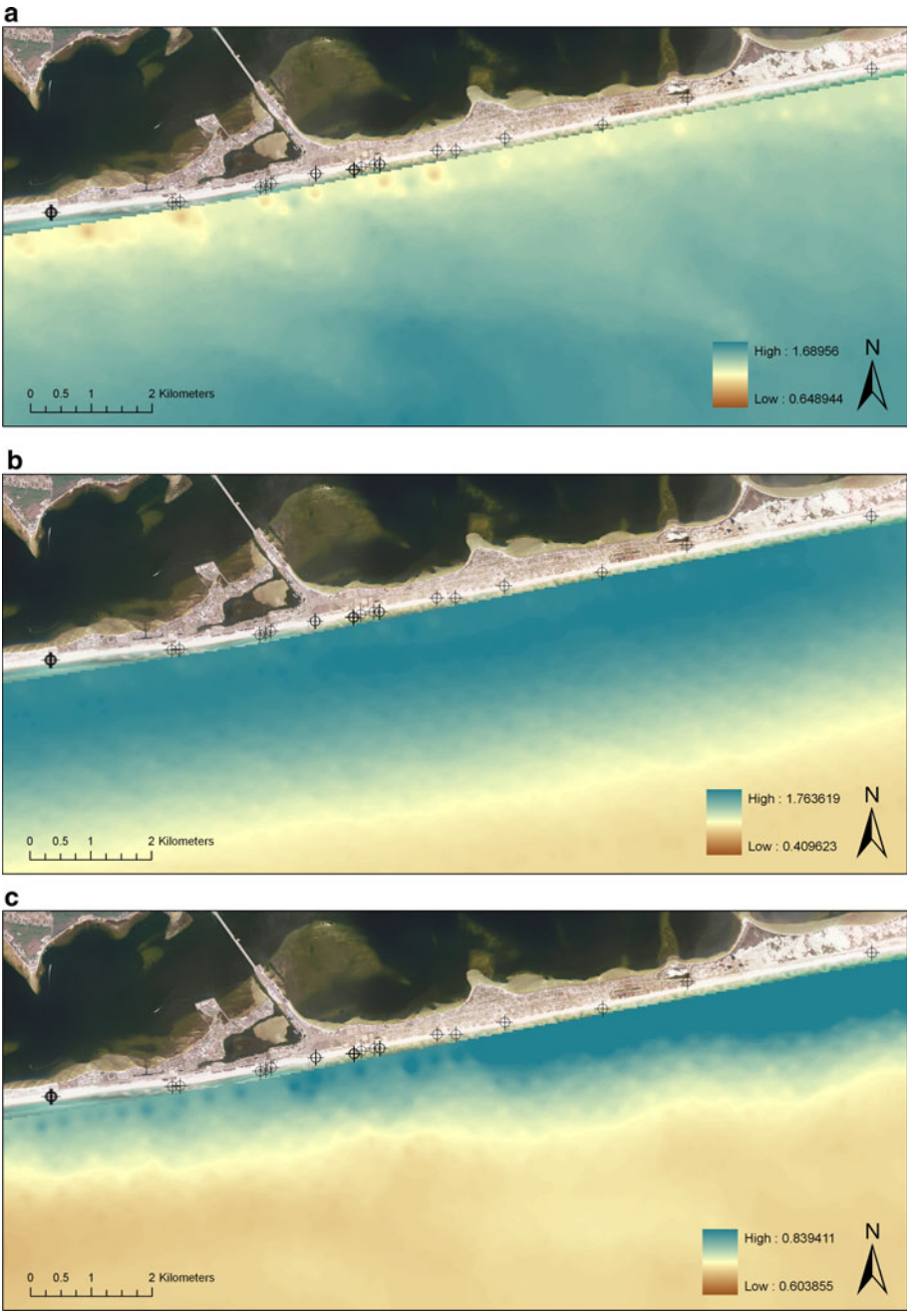


Fig. 7 Modeled wave heights for **a** green, **b** yellow and **c** red flag days at Pensacola Beach

reveal a statistically significant difference in the surf similarity parameter (Table 4). Drownings tend to occur between transverse ridges (small E1/E2 ratio) where wave heights and periods are smaller just offshore of an outermost bar that is closer to the shoreline by

Table 3 Incident wave and wind forcing for green, yellow and red flag days at Pensacola Beach, and the alongshore variance in the modeled wave height and period

	H_s (m)	T (s)	θ (°)	S (m s^{-1})	h (m)	H_s SD	T SD	Min ε	Max ε
Green flag	0.63	5.31	182	4.13	0.10	0.04	0.1	1.5	8.7
Yellow flag	1.02	5.93	141	5.63	0.07	0.1	0.2	3.3	19.7
Red flag	1.73	6.97	139	7.45	0.06	0.2	0.7	2.9	17.3
All flags	0.90	5.69	159	5.06	0.08	0.1	0.2	2.3	13.8

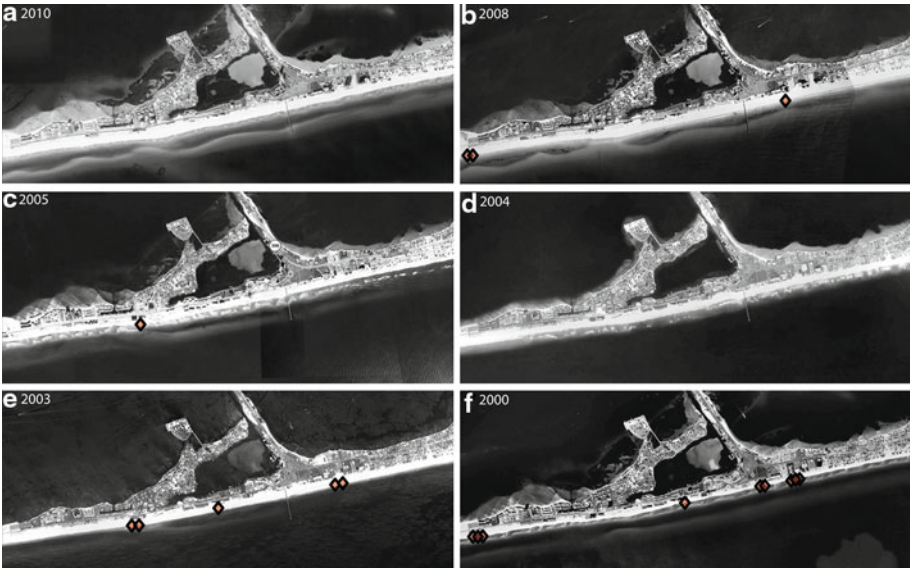


Fig. 8 Location of drownings between Casino Beach and Fort Pickens Gate between 2000 and 2009 on the satellite image for that period showing change in nearshore morphology. Not shown are drownings to the east of satellite image

an average of 36 m. As evidenced by the surf similarity parameter, drownings tend to be clustered in sections of the beach where a bar and rip morphology is predicted on red flag days. However, Fig. 8 suggests that the outermost bar and the nearshore state are not static, but rather evolve through a bar cycle (see Shand 2003; Houser and Greenwood 2007) that is initiated by a large storm capable of moving the outermost bar offshore. As the bar system recovers, the rip-prone areas evolve from bar and rip morphology immediately following a storm to a rhythmic bar morphology and eventually to a nearshore terrace. An example of the later is seen in an oblique aerial photograph of Casino Beach looking west (Fig. 9). The outermost bar has attached to the beachface to create a wide nearshore terrace that appears to be absent of persistent rip channels. The satellite image from April 2004 (Fig. 8d) also suggests that there was a broad nearshore terrace before Hurricane Ivan forced the outermost bar offshore and a new inner-bar was formed (Fig. 8a–c). In this respect, the drownings from 2000 to 2003 and 2005 to 2008 are associated with the recovery of the shoreface from hurricanes in 1998 (Earl and George) and 2004 (Ivan, Dennis and Katrina), respectively.

Table 4 Results of a *t*-test, assuming unequal variance, between drowning locations and the total length of beach at Pensacola Beach for red flag days

	n	*E1/E2*	Bar (m)	tan(β)	H_s (m)	ε
All transects	95	3.96	252	0.10	3.18	12 (rhythmic bar and beach)
Drowning locations	25	3.16	216	0.12	2.96	7 (bar and rip)
t-Statistic		2.06	4.11	3.40	2.24	2.92
ρ ($T \leq t$) *one-tailed*		0.02	<0.01	<0.01	0.02	<0.01

The analysis considered the location of the transverse ridges (E1/E2), the position of the outermost bar, the beachface slope, the significant wave height and the surf similarity parameter



Fig. 9 Oblique aerial photograph of nearshore morphology, looking east from the Fort Pickens Gate on March 6, 2007. Also shown are the locations of drownings (in the immediate field of view) between 2000 and 2009. Photography courtesy of *A. Browder*

5 Discussion

Since 2000, there have been 25 drownings at Pensacola Beach, with most clustered at a small number of locations along the beach, when the surf was rough and red flags were flying. While the cause of drowning in each case is attributed to rip currents, there has been debate over whether rip currents are the cause or are even present at these sites (The Tuscaloosa News 2003). The results of the present study suggest that rip currents are indeed present and are a probable cause of most, if not all the recorded drownings between 2000 and 2009. The study further confirms that the hazard is not uniform alongshore. Transverse ridges on the inner shelf are shown to be capable of refracting the incident wave field to create alongshore variation in wave height and mean period, which combined with

the beachface slope of the transverse ridges creates an alongshore variation in the surf similarity parameter and nearshore state. The alongshore variation in nearshore state is clear in Fig. 9, which is annotated to show the location of drownings within the immediate field of view. Drownings are clustered between these transverse ridges where the shoreface is forced into a bar and rip morphology on red flag days (Table 3). Further, wave heights and periods are smaller than at the crest of the transverse ridge. While seemingly ephemeral, the bar and rip morphology has rip channels that persist over a wide range of incident forcing and are close to the beachface. The modal nearshore state is low-tide terrace ($\varepsilon \approx 2.3$) between the transverse ridges. A rhythmic bar and beach ($\varepsilon \approx 13.8$) occurs coincident with at the transverse ridges. It is reasonable to expect that erosion rips can develop at the relatively dissipative ridge crests, but they would only develop during storms and would not be as close to the shoreline. The accretion rips between transverse ridges pose a more significant hazard to beach users because they are not only persistent over a range of storm conditions, but are directly against the beachface. A beach user would not have to enter far into the water before getting caught in the rip channel and needing assistance.

The accretion rips at Pensacola Beach tend to be considered a transitional state between dissipative (large ε) and reflective (small ε) profiles (Wright and Short 1984) in which the nearshore can evolve from a longshore bar-trough to a low-tide terrace by passing through rhythmic bar-beach and bar-rip morphologies. This transition occurs as the shoreface recovers from a storm and is accompanied by an increase in the rip current velocity as the cross-sectional rip channel area decreases and the ability of the bar system to block return flows increases (Brander 1999). Only as the innermost bar attaches completely to the beachface and a low-tide terrace develops do the rip channels disappear and the currents weaken. These accretion rips do not have the characteristic form modeled of erosion rips and may prove difficult to identify from the low oblique angle of a beach user. While surveying the bar and rip morphology at "the cross" access point (Houser et al. 2010), the surveyed rip was repeatedly photographed using a remote camera (Fig. 10a) and the location of the rip was identified using a time stack of the images (Fig. 10b). A sample photograph from June 10, 2008, shows several beach users (including small children) at the rip head and in the rip channel. While this was a green flag day, the velocity (V) in the pre-existing rip channel was estimated (in the field and numerically) to be ~ 0.29 m s^{-1} from:

$$V = \left(Q_{drift} + Q_{roller}\right)\lambda / R \tag{5}$$

where λ is the distance between rip channels (surveyed at ~ 110 m), R is the cross-sectional area of the rip (surveyed at 31 m^2), and Q_{drift} and Q_{roller} are the mass transports in the waves (i.e. Stokes drift) and rollers respectively. These are calculated as:

$$Q_{drift} = \frac{CBH^2}{h} \tag{6}$$

$$Q_{roller} = A/T \tag{7}$$

where C is the wave celerity (~ 3.13 m s^{-1}), B is a coefficient equal to 1/12 for saw-tooth waves, H is the wave height (~ 0.4 m), h is the water depth over the innermost bar (~ 0.69 m), A is the cross-sectional area of the roller ($\sim 0.9H^2$; Fredsoe and Deigaard 1992) and T is the wave period (~ 3.5 s). While this velocity does not pose a significant hazard to an adult, it does suggest that the velocities can be quite strong during yellow and red flag days when conditions are much more intense and a bar and rip morphology is predicted between ridges.

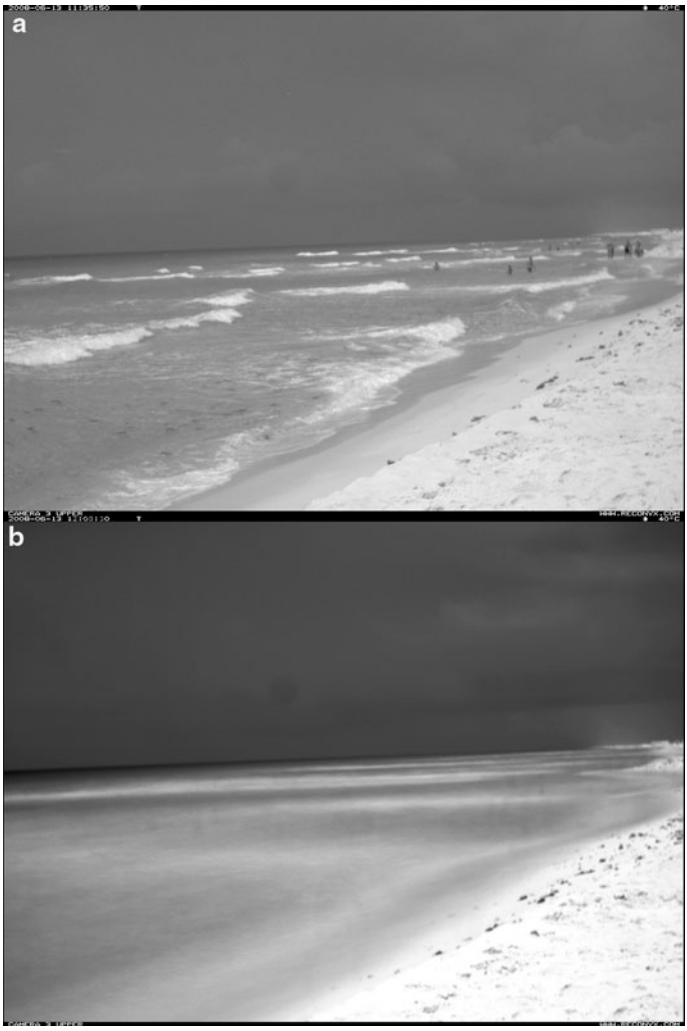


Fig. 10 Representative photograph (a) of an accretion rip from the perspective of a beach user showing 8 people swimming in the rip channel and 2 children playing in the feeder channel flowing west to east. Also shown (b) is a time stack of the same channel taken over 15 min showing accretion rip and complex topography of the bar and rip morphology

The satellite images presented in Fig. 8 suggest that both the inner and the outermost bars are not static, but rather migrate seaward in response to storms and landward as they recover (Houser and Greenwood 2007). The bar cycle at Pensacola Beach is largely driven by tropical storms and hurricanes, capable of moving the outermost bar offshore from the modal beach state with only a single bar as observed in 2003 (Fig. 8e). The outermost bar had almost attached to the beachface following Hurricanes Earl and Georges in 1998, before being moved offshore during Hurricanes Ivan (2004), Dennis (2005), Katrina (2005) and tropical storms Arlene (2005) and Cindy (2005). Recovery from a double-bar system (Fig. 8c) and transition to rhythmic bar-beach and then bar-rip occur first between the transverse ridges. In this respect, the accretion rip hazard first develops and persists

between the transverse ridges. The clustering of the drownings between 2000 and 2003, and again between 2005 and 2008 confirms that the rip hazard is also not uniform in time and varies with the development of the bar and rip morphology following a tropical storm or hurricane. Ultimately, the hazard may be reduced in these areas as the innermost bar completely attaches to the beachface to form a nearshore terrace without defined rip channels, which may explain the lack of drownings in 2004 (before Hurricane Ivan) and in 2009. Complete recovery of the beachface and the development of a nearshore terrace would, however, require the persistence of green flag (non-storm) conditions to allow for the relatively slow landward migration of the innermost bar (Houser and Greenwood 2007). The relative lack of drownings through the busy summer season may reflect the absence of strong reset storms and the inability for the channels to be maintained by the weak currents. Despite the large number of days with green flags through a typical summer, the modal beach state is predicted to be bar and rip between ridges, and rhythmic bar and beach at the ridge crests. The predominance of drownings in the spring and fall is partly a reflection of a higher frequency of red and yellow flag conditions in which a bar and rip morphology is the equilibrium state between ridges and the beaches are still heavily populated.

It is important to note that the results of this study do not suggest that drowning is inevitable at specific places and times, as it is recognized that rip hazard depends not only on environmental forcing but also individual and group behavior and susceptibility (Fig. 1). Rather, it is argued that the hazard is dependent on the covariation in the environmental forcing and individual and group behavior in both time and space, even on what appears to be a relatively uniform beach environment. As noted, the degree to which the potential for someone to drown or be in need of rescue depends on a number of variables including alcohol consumption, gender, age and swimming ability (Morgan et al. 2009; Gensini and Ashley 2009). It is also possible that beach users are attracted to the area between transverse ridges because the surf is not as strong as it is at the ridge crests. The ridge crests are incidentally the most popular spots for surfers along this coast.

The present flagging system assumes a uniform hazard potential alongshore in response to storm winds and waves. The results of the present study show that there are times and locations when the rip hazard is greater, even during green and yellow flag days when the potential for erosion rips is low. As noted, the accretion rips between transverse ridges are persistent features that still have a current on days when the forecast suggests that rips have a low potential to develop. More importantly, accretion rips do not have the characteristic shape associated with erosion rips that are posted on warning signs on most beaches (Fletemeyer and Leatherman 2010). This suggests a need for different warning flags being distributed alongshore and a modification to existing warning signs so that they are more representative of the local rip morphology. Previous studies have looked at the dominant beach states for an area and produced warning signs for beach visitors upon entry to the beach identifying the specific hazardous areas associated with the current beach state. However, increased emphasis on the area between transverse ridges should not come at the expense of the areas between ridges where surf and the potential for erosion rips on yellow and red flag days remain.

6 Conclusions

A number of conclusions can be made from this study that examines the rip current hazard at Pensacola Beach, Florida:

1. While the present warning system from the National Weather Service assumes that the rip hazard is uniform along the entire length of Santa Rosa Island, drownings between 2000 and 2009 exhibit a statistically significant clustering alongshore. The drowning hotspots are found between transverse ridges on the inner shelf that cause an alongshore variation in the nearshore state as estimated by the surf similarity parameter. In these locations, the backshore tends to be flatter and more easily accessible, the waves appear to be smaller and possess less energy, and conditions appear safer.
2. Drownings are also found to be clustered in the first couple of years following an extreme storm and related to the bar cycle and during the spring and fall months. The accretion rips at Pensacola Beach are a transitional state between dissipative (large) and reflective (small) profiles (Wright and Short 1984) in which the nearshore can evolve from a longshore bar-trough to a low-tide terrace by passing through rhythmic bar-beach and bar-rip morphologies. This transition occurs as the shoreface recovers from a storm and is accompanied by an increase in the rip current velocity as the cross-sectional rip channel area decreases and the ability of the bar system to block return flows increases. Only as the innermost bar attaches completely to the beachface and a low-tide terrace develops do the rip channels disappear and the currents weaken.
3. The clustering of the drownings between 2000 and 2003 and again between 2005 and 2008 suggests that the rip hazard is also not uniform in time and may vary with the development of the bar and rip morphology. Ultimately, the hazard may be reduced in these areas as the innermost bar completely attaches to the beachface to form a nearshore terrace without defined rip channels, which may explain the lack of drownings in 2004 (before Hurricane Ivan) and in 2009.
4. The hazard posed by rip currents is not uniform alongshore or in time, but is dependent on how personal and group behavior covaries alongshore with the wave forcing and through time. It is also possible that beach users are attracted to the area between transverse ridges, because the surf is not as strong as it is at the ridge crests during yellow and red flag days. The beach users are seemingly unaware of the accretion rips directly against the shore.

Acknowledgments This study was supported in part by grants from the National Park Service (P5320060026) and Florida Sea Grant (R/C–S-50). Field assistance was provided by Tim Brunk and Jack Walker from Texas A&M, and by Tanya Gallagher, Fritz Langerfeld and Klaus Meyer-Arendt from the University of West Florida. Bob West of the Santa Rosa Island Authority is also thanked for his support and contributions to this study.

References

Aagaard T, Greenwood B, Nielsen J (1997) Mean currents and sediment transport in a rip channel. Mar Geol 140:25–45

Aubrey DG (1979) Seasonal patterns of onshore/offshore sediment movement. J Geophys Res 84: 6347–6354

Balsillie JH (1975) Analysis and interpretation of LEO and pro-file data along the Western Panhandle coast of Florida. CERC Tech Memo 49:72p

Bowman D, Arad D, Rosen DS, Kit E, Goldbery R, Slavicz A (1988a) Flow characteristics along the rip current system under low-energy conditions. Mar Geol 82:149–167

Bowman D, Rosen DS, Kit E, Arad D, Slavicz A (1988b) Flow characteristics at the rip current neck under low energy conditions. Mar Geol 79:41–54

Brander RW (1999) Field observations on the morphodynamic evolution of a low-energy rip current system. Mar Geol 157:199–217
Brander RW, Short AD (2000) Morphodynamics of a large-scale rip current system at Muriwai Beach, New Zealand. Mar Geol 165:27–39
Brander RW, Short AD (2001) Flow kinematics of low-energy rip current systems. J Coastal Res 17:468–481
Browder AE (2001) Bathymetrically-induced erosional hot spots: Pensacola Beach, L. Report prepared by Olsen Associates, Inc., Jacksonville, FL, for Santa Rosa Island Authority
Browder AE, Reilly WL (2008) Observations of large-scale beach cusps in the Florida Panhandle and Alabama. Annual National Conference on Beach Preservation Technology, pp 1–16
Coco G, Bryan MO, Green BG, Ruessink IL, Turner I, van Enckevort I (2005) Video observations of shoreline and sandbar coupled dynamics. Proceedings of coasts and ports 2005, Adelaide, pp 471–476
Dalrymple RA, Lozano CJ (1978) Wave-current interaction models for rip currents. J Geophys Res 83:6063–6072
Deigaard R, Drønen N, Fredsøe J, Jensen JH, Jørgensen MP (1999) A morphological stability analysis for a long straight barred coast. Coastal Eng 36:171–195
Drønen N, Karunarathna H, Fredsøe J, Mutlu Sumer B, Deigaard R (2002) An experimental study of rip channel flow. Coastal Eng 45:223–238
Falques A, Montoto A, Vila D (1999) A note on hydrodynamic instabilities and horizontal circulation in the surf zone. J Geophys Res 104(20):615
Fletemeyer J, Leatherman S (2010) Rip currents and beach safety education. J Coastal Res 26:1–3
Fredsoe J, Deigaard R (1992) Mechanics of coastal sediment transport. Advanced Series on Ocean Engineering, 367 pp
Gensini V, Ashley W (2009) An examination of rip current fatalities in the United States. Nat Hazards 54:159–175
Guza RT, Inman DL (1975) Edge waves and beach cusps. J Geophys Res 80:2997–3012
Haller MC, Dalrymple RA, Svendsen IA (2002) Experimental study of nearshore dynamics on a barred beach with rip channels. J Geophys Res C: Oceans 107: 14-1-14-21
Hino M (1974) Theory on formation of rip-current and cuspidal coast. Coastal Eng Japan 17:23–37
Holman RA, Symonds G, Thornton EB, Ranasinghe R (2006) Rip spacing and persistence on an embayed beach. J Geophys Res C: Oceans 111
Houser C, Greenwood B (2007) Onshore migration of a swash bar during a storm. J Coastal Res 23:1–14
Houser C, Hamilton S (2009) Sensitivity of post-hurricance beach and dune recovery to event frequency. Earth Surf Proc Land 34:613–628
Houser C, Hapke C, Hamilton S (2008) Controls on coastal dune morphology, shoreline erosion and barrier island response to extreme storms. Geomorphology 100:223–240
Houser C, Caldwell N, Meyer-Arendt K (2010) Hot times at hot spots: the rip current hazard at Pensacola Beach, Florida. In: Leatherman S, Fletemeyer J (eds) Rip currents: beach safety, physical oceanography and wave modeling. CRC Press
Hyne NJ, Goodell HG (1967) Origin of the sediments and submarine geomorphology of the inner continental shelf off Choctawhatchee bay, Florida. Mar Geol 5:299–313
Kwon HJ (1969) Barrier islands of the northern Gulf of Mexico coast: sediment source and development, coastal studies series 25, Louisiana State University Press, Baton Rouge
Lascody LL (1998) East central Florida rip current program. Nat Weather Dig 22(2):25–30
Livingston G, Arthur K (2002) The economic impact of Pensacola Beach. Unpublished report by the Haas Center for Business Research and Economic Development, University of West Florida. 49 pp
Lushine JB (1991) A study of rip current drownings and weather related factors. Nat Weather Dig 16:13–19
MacMahan JH, Thornton EB, Stanton TP, Reniers AJHM (2005) RIPEX: observations of a rip current system. Mar Geol 218:113–134
Meyer-Arendt KJ (1990) Recreational business districts in Gulf of Mexico seaside resorts. J Cult Geogr 11:39–55
Mollere GJ, Watson AI, Goree RC (2001) A rip current assessment of the Florida Panhandle coastal waters. National Weather Service SR-210
Morgan D, Ozanne-Smith J, Triggs T (2009) Self-reported water and drowning risk exposure at surf beaches. Risk Prevention 33:180–188
Nielsen-Gammon JW (2001) The tropical sea Breeze. Ninth conference on mesoscale processes, pp 4
Ranasinghe R, Symonds G, Black K, Holman R (2000) Processes governing rip spacing, persistence, and strength in a swell dominated, microtidal environment. In: Coastal engineering 2000–proceedings of the 27th international conference on coastal engineering, ICCE, 454–467

Reniers AJHM, Roelvink JA, Thornton EB (2004) Morphodynamic modeling of an embayed beach under wave group forcing. J Geophys Res C: Oceans 109: C01030 1–22
Ruessink BG, Coco G, Ranasinghe R, Turner IL (2006) A cross-wavelet study of alongshore nonuniform nearshore sandbar behavior. In: IEEE international conference on neural networks–conference proceedings, pp 4310–4317
Shand RD (2003) Relationships between episodes of bar switching, cross-shore bar migration and outer bar degeneration at Wanganui, New Zealand. J Coastal Res 19(1):157–170
Shepard FP, Emery KO, LaFond EC (1941) Rip currents: a process of geological importance. J Geol 49:337–369
Sherman DJ, Short AD, Takeda I (1993) Sediment mixing depth and bedform migration in rip channels. J Coastal Res 15:39–48
Short AD (1985) Rip-current type, spacing and persistence, Narrabeen Beach, Australia. Mar Geol 65:47–71
Short AD, Trembanis AC (2004) Decadal scale patterns in beach oscillation and rotation Narrabeen beach, Australia–Time series, PCA and wavelet analysis. J Coastal Res 20:523–532
Smith JA, Largier JL (1995) Observations of nearshore circulation: rip currents. J Geophys Res 100:10,967–10,975
Sonu CJ (1972) Field observations of nearshore circulation and meandering currents. J Geophys Res 77:3232–3247
Stone GW (1984) Mathematical modeling of the nearshore and implications for coastal management, Northwest Florida. Unpublished MSc thesis, Department of Environmental Studies, University of West Florida, 140 pp
Stone GW (1991) Differential sediment supply and cellular nature of longshore sediment transport along coastal Northwest Florida and Southeast Alabama since the late Holocene. PhD Dissertation, University of Maryland, College Park
Stone GW, Stapor FW Jr (1996) A nearshore sediment transport model for the northeast Gulf of Mexico Coast USA. J Coastal Res 12:786–792
Stone GW, Stapor FW Jr, May JP, Morgan JP (1992) Multiple sediment sources and a cellular, non-integrated, longshore drift system: Northwest Florida and southeast Alabama coast, USA. Mar Geol 105:141–154
Torrence C, Compo GP (1998) A practical guide to wavelet analysis. Bull Am Meteorol Soc 79:61–78
Turner IL, Whyte D, Ruessink BG, Ranasinghe R (2007) Observations of rip spacing, persistence and mobility at a long, straight coastline. Mar Geol 236:209–221
Wright LD, Short AD (1984) Morphodynamic variability of surf zones and beaches: a synthesis. Mar Geol 56:93–118

11 Rip Current Hazards at Pensacola Beach, Florida

Chris Houser, Nicole Caldwell, and Klaus Meyer-Arendt

CONTENTS

Introduction 175
Study Area 180
Methods 180
Results 183
Drownings 183
Rescues 190
Water Level 191
Discussion 193
Conclusions 195
Acknowledgments 196
References 196

INTRODUCTION

Rip currents are approximately shore-normal channels of seaward-directed flows, driven by alongshore variations in wave height and associated variations in the mean water surface elevation. The resulting circulation cells play an important role in nearshore processes through offshore sediment transport and shoreline change (Shepard et al., 1941; McKenzie, 1958; Greenwood and Davidson-Arnott, 1979; Short, 1985; Smith and Largier, 1995; Aagaard et al., 1997; Thornton et al., 2007), but also represent significant hazards to beach users (Short, 1985; Lushine, 1991; Short and Hogan, 1994). Current velocities within a rip channel are on the order of 0.2 to 0.65 ms^{-1} in low-energy environments (Sonu, 1972 ; Bowman et al., 1988; Sherman et al., 1993; Smith and Largier, 1995; Aagaard et al., 1997; Brander, 1999; MacMahan et al., 2008), but can reach peak velocities in excess of 1 and up to 2 ms^{-1} in higher energy environments (Sonu, 1972; Brander and Short, 2000).

The potential for drowning or rescue depends on the presence of a strong rip current at a specific time and place and also on personal behavior including alcohol consumption, gender, age, swimming ability, panic, and exhaustion (Morgan et al., 2009; Gensini and Ashley, 2009). Wilks et al. (2007) suggest that a rip hazard also depends on whether beach users (particularly tourists) recognize and obey safety information and warning flags. At Pensacola Beach, an important tourist destination

K11772_C011.indd 175 1/4/11 10:03:12 AM

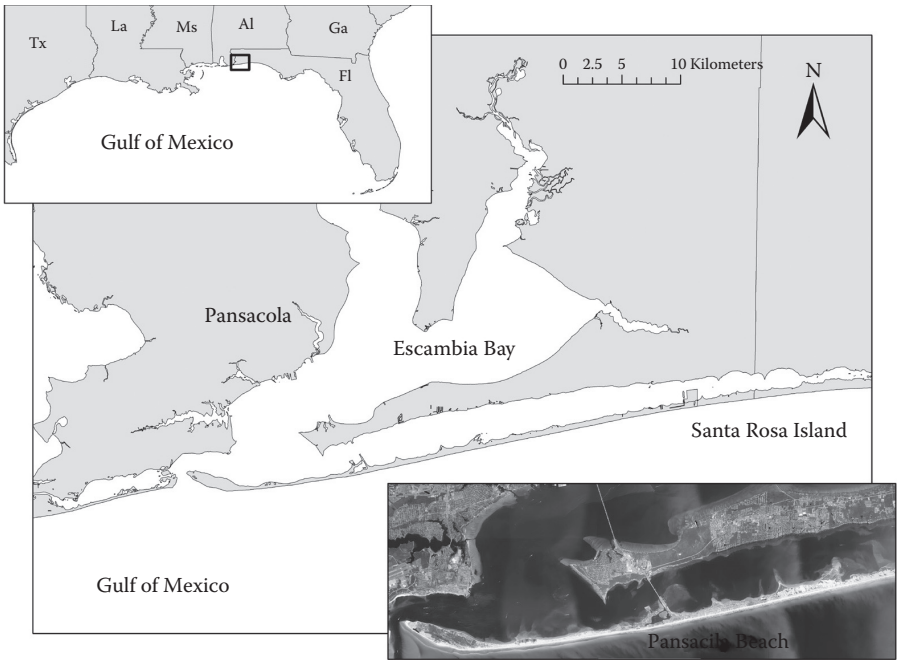


FIGURE 11.1 Location of Pensacola Beach in northwest Florida.

in northwest Florida (Figure 11.1), approximately 25% of drowning victims in the last decade were Good Samaritans trying to rescue others or parents going into the surf to rescue their children (Bob West, personal communication). Drownings and near-drownings usually cluster during summer weekends when strong onshore winds are associated with high pressure systems and large beach population are present (Gensini and Ashley, 2009).

Florida has the highest drowning rate in the United States (Lascody, 1998; Florida Department of Health, 2003), and the United States Lifesaving Association identified the Florida Panhandle as the nation's worst area for beach drownings. Drownings and near-drownings at Pensacola Beach tend to occur between March and October when the surf is strong (Lascody, 1998) and involve inexperienced swimmers who may not have heeded warning signs (Morgan et al., 2009; Fletemeyer and Leatherman, 2010).

Signage warns beach users of rip hazards at all access points along Pensacola Beach. Despite these clearly marked warning signs, beach users at Pensacola are unable to identify rip currents before entering the water and tend to swim in rip "hot spots" (Figure 11.2). A survey of 121 beach users during the summer of 2008 recreating at a persistent rip channel showed that 95% could not identify the active rip current. Additionally, only 3 of the 13 respondents who had previously been caught in rip currents could identify the rip channel, even during yellow flag conditions when the rip channel was clearly defined by a breaking wave pattern. This may be due to the fact that the Florida Panhandle rips are more variable and appear closer to the shore (Figure 11.3) than the simple rip diagrams depicted on the warning signs.



FIGURE 11.2 (a) Representative photograph of accretion rip from perspective of a beach user showing eight people swimming in the rip channel and two children playing in the feeder channel that flows west to east. (b) Time stack (15-min) of same channel showing rip and complex topography of the bar and rip morphology.

Sonu (1972) examined a similar rip current system to the east of Pensacola Beach (Seagrove) that he described as alternating shoals and seaward-trending troughs. These accretion rips most commonly form during the recovery period following large storms as the shore face transitions from a dissipative to a reflective profile (Wright and Short, 1984; Short, 1985). The authors characterized the morphological state through a dimensionless fall velocity (Ω) given by:

$$\Omega = \frac{H_b}{\omega_s T} \tag{11.1}$$

where H_b is the breaking wave height, ω_s is the average fall velocity of the beach sediment, and T is the wave period. As wave energy decreases following a storm, the beach changes from dissipative ($\Omega > 6$) to reflective ($\Omega < 1$) by passing through each

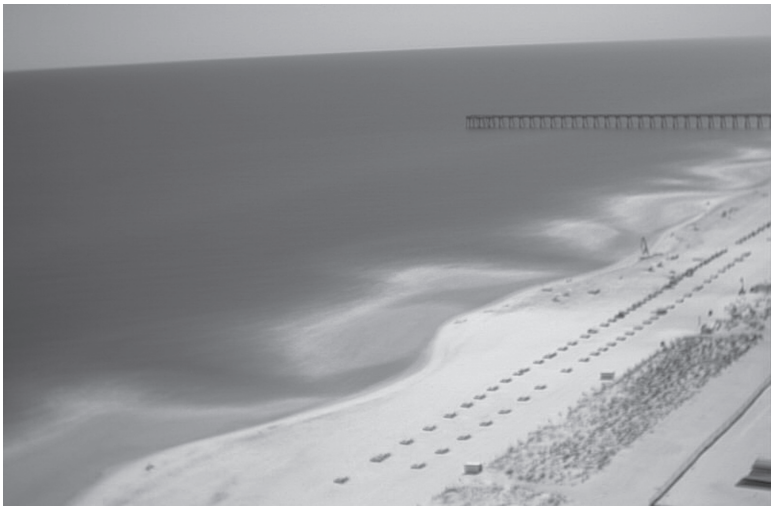


FIGURE 11.3 Representative time exposure of rhythmic rip and shoal morphology at Pensacola Beach.

of four intermediate states: longshore bar–trough, rhythmic bar–beach, transverse bar–rip and low tide–terrace. Each intermediate state is characterized by the presence of rip currents, with the strength of the current in the feeder channel and neck varying in response to the landward migration and welding of the innermost bar. The current velocity increases as the cross-sectional area of the feeder channel decreases and the bar (or shoal) is more effective at blocking the return flow (Brander, 1999). As the feeder currents tend to be directly adjacent to the beach face (Figures 11.2 and 11.3), a beach user would not have to venture too far into the water before getting caught in rip channel and potentially needing assistance.

After development, rip channels induce an alongshore pressure gradient, leading to a strong current of 0.2 to 0.3 ms^{-1} across the shoal that contribute to feeder and rip current speeds of 0.4 to 0.6 ms^{-1} (Sonu, 1972; Mei and Liu, 1977). Over a rip and shoal system at Pensacola Beach, Houser et al. (in review) used a mass balance approach to estimate a depth-averaged current velocity of 0.2 ms^{-1} under green flag (low hazard, calm) conditions. While this velocity would not necessarily pose a significant hazard to an adult, it suggests that the velocities can be very strong during yellow and red flag days when wave breaking and set-up across the shoal would be more intense.

With increasing wave height, more water may enter a rip directly from the steep sides of the shoal rather than through the feeder channel (McKenzie, 1958; Sonu, 1972; Short, 2007), potentially leading to weaker currents near the shore. However, superimposed on the mean current are oscillatory currents at both gravity and infragravity frequencies that can more than double the seaward current (Sonu, 1972; Aagaard et al., 1997; Brander and Short, 2001; MacMahan et al., 2004). These currents can also create a pulsed flow, significantly contributing to drownings (Bob West, personal communication). Wave heights tend to be greater in rip channels than over shoals due

to interactions with the seaward-flowing current and the deeper bathymetry (Sonu, 1972; Haller et al., 1998). This strong current can also cause seaward-migrating mega-ripples and possibly unstable footing that may be responsible for the "collapsing sand bar" phenomenon described by beach users as a sudden collapse of the bed and loss of footing (Short, 2007).

Rip currents at Pensacola Beach are morphologically controlled by transverse ridges on the inner shelf (Houser and Hamilton, 2009; Houser et al., 2008). The ridges are capable of refracting the incident wave field to create an alongshore variation in wave height that causes an alongshore variation in the breaking wave height [Equation (11.1)]. Between ridges, where the breaking wave heights are smaller, the nearshore tends to be forced into a rhythmic transverse bar and rip state (TBR; Wright and Short, 1984) as shown in Figure 11.3, creating hot spots of rip current activity and drowning events. It is also possible that beach users are attracted to these areas because the surf is not as strong as along the ridge crests during yellow and red flag conditions—meaning that they may be unaware of the rips directly at the shore.

The TBR morphology develops soon after a reset storm detaches the innermost bar from the beach face. As the nearshore recovers from the storm, it progresses through a range of intermediate beach states, whereby the innermost bar becomes more crescentic and eventually attaches to the shoreline, and topographically-forced rips develop rhythmically along the shoreline (Turner et al., 2007). Due to wave refraction over the transverse ridges, the rhythmic bar and rip state and the rip channels form first and persist longest between ridges, but will eventually be replaced by a nearshore terrace. The TBR beach state will develop nearer the (higher energy) ridge crests if low energy recovery conditions are maintained for a sufficiently long period.

The Santa Rosa Island Authority responsible for Pensacola Beach safety maintains a flag system to alert beach users about heavy surf and rip hazards based on the National Weather Service forecasts. The highest flag color for that day (green, yellow, red, or double-red) is recorded by the authority, along with the number of prevents, assists, rescues, and contacts. Between March and October, lifeguards are stationed at Casino Beach, Fort Pickens Gate, and Park East; the remainder of the beach is patrolled by foot and vehicle. Lifeguards are permanently stationed at Casino Beach from March to October, and only between May and August at Fort Pickens Gate and Park East. Between 2004 and 2009, lifeguards performed 43,589 preventative acts, assisted 1,578 swimmers in distress, and rescued 759 swimmers who would have drowned without assistance.

Chi-square analysis suggests that prevents and assists are over-represented on red flag days and to a lesser extent on yellow flag days ($\chi 2 = 681$, $p < 0.001$), while rescues tend to be more common on yellow flag days. Due to expanded beach patrols and the hiring of additional lifeguards in 2004 and 2005, only four drownings occurred—many fewer than the 21 drownings between 2000 and 2004. While most rescues concentrated within about 3.5 km of the central and popular Casino Beach, all the drownings occurred at unguarded sections of the beach or at times when lifeguards were not on duty; all occurred during red or double-red flag conditions. Rip currents are identified by lifeguards and the media as the primary causes of drowning, although it is reasonable to expect that other factors (age, health, fatigue, heavy surf, etc.) also played a role.

While it has been demonstrated that drownings at Pensacola Beach tend to cluster between transverse ridges, little information is available about the current velocities during these events. The specific combinations of wind, wave, and tidal conditions causing drownings are not clear. A spectral wave and current model (MiKE21) was used to estimate the depth-averaged velocities and inshore wave heights of a representative rip and shoal system (Figure 11.2).

STUDY AREA

Development of Santa Rosa Island was initially limited by a lack of overland access and devastating hurricanes in the late 19th century, but fewer storms and the placement of permanent structures led to the construction of a bridge and the establishment of lifeguards at Casino Beach in 1931 (Meyer-Arendt, 1990). The recreational business began to develop following World War II as a small core of cottages, motels and other tourist-oriented businesses. Now commercial and residential development occupies about 13 km of shoreline and is bounded to the east and west by the Gulf Islands National Seashore.

Pensacola Beach receives 1.8 million visitors annually, in addition to the more than 270,000 day visitors and 670,000 visitors who stay at unpaid lodging sites. Toll data suggests that visits to the island are at a maximum during the summer holiday season (>400,000 vehicles per month) and at a minimum through the winter season (~200,000 vehicles per month). Most visitors indicate that the beach and its recreational opportunities served as an "extensive influence" or "moderate influence" on their decisions to visit the area (Livingstone and Arthur, 2002). Visitors also indicate that cleanliness, climate, natural beauty, and beach safety are their most important concerns.

Based on a survey of beach users completed in 2008, most day visitors use the beach within a short distance of primary access points. Access is provided at the main Casino Beach (30.331006°N, 87.140842°W), Fort Pickens Gate (30.324764°N, 87.180515°W), and Park East (30.347154°N, 87.056521°W). Access is also possible via a walkover at "the cross" (30.329132°N, 87.153533°W) and at the ends of streets in the residential area east of Casino Beach, such as 23rd Avenue (30.339142°N, 87.097929°W). All the access points are between transverse ridges where rip currents are common and drownings occurred (Figure 11.4). The high probability of rips and concentrations of beach users at these access points make them the most hazardous areas at Pensacola Beach.

METHODS

Since 2000, the Santa Rosa Island Authority has maintained a detailed rescue log listing the highest flag color for each day (green, yellow, red, or double-red) along with the number of drownings, prevents, assists, rescues, and contacts. To examine the wave and tidal forcing responsible for drownings, rescues and assists, a spectral wave and current model (MiKE21) was used to estimate the depth-averaged velocities and inshore wave heights over a rip and shoal morphology (Wright and Short, 1984); this is representative of areas where drownings and most rescues and assists occurred at Pensacola Beach.

K11772_C011.indd 180 1/4/11 10:03:13 AM

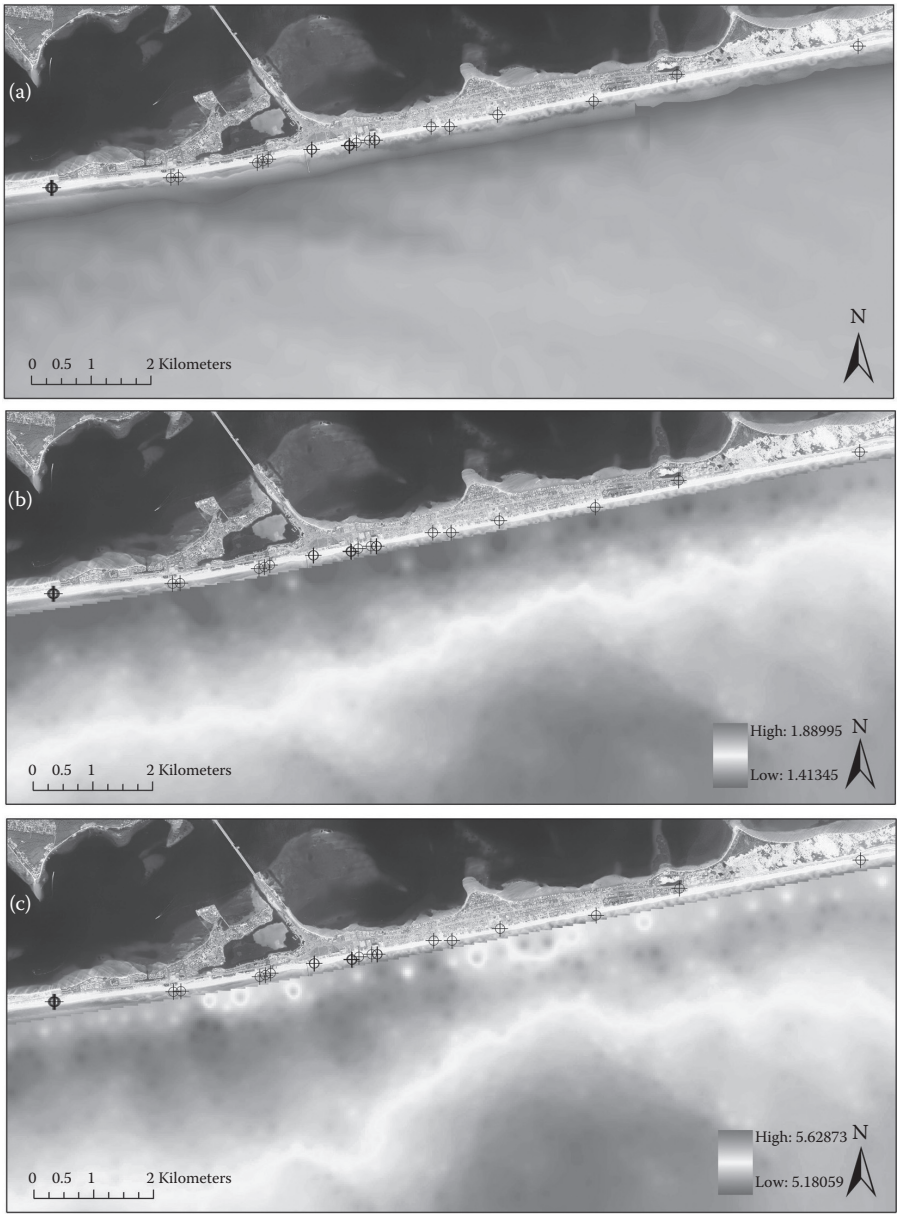


FIGURE 11.4 (*See color insert following page XXX.*) (a) Shelf bathymetry and drowning locations. (b) and (c) Representative wave model outputs. Shown are spatial variations of significant wave height (b) and mean wave period for wind and wave forcing (c) on March 15, 2008 when a drowning occurred at an unguarded section east of Casino Beach.

Au: What "feature"?

The rip-and-shoal and nearshore morphologies within 200 m east and west of the feature was surveyed on June 16, 2008. While the specific morphology associated with each drowning, rescue, assist, and prevent differs, the results of this modeling analysis provide a first approximation of the conditions under which the events may have occurred. No observable changes in the morphology were noted within a week of the survey, and two rescues at this location involved use of U.S. Coast Guard helicopters to locate missing bathers. The survey was extended offshore using a fathometer to a depth of 15 m (~1.5 km offshore). The xyz survey data were interpolated to a flexible mesh with a maximum mesh area of 2 m^2 for a total of 61,184 nodes landward of the outermost bar.

The wave and current model was run using offshore wave boundary conditions and wind forcing function based on long-term meteorological and oceanographic records from two offshore wave buoys (42039 and 42040) located near the study region. A nested modeling approach was used to produce boundary conditions (both spectral and parametric) at the seaward extent of the modeling area where the finer grid resolution was used (Figure 11.5). Modeling results provide two-dimensional spectra for all boundary points in the study area (on a computational grid). The spectra were then used for finer scale transformations of the inshore area in order to analyze wave convergence and divergence across the shoal and rip. The model accounts for (1) wave propagation in time and space, shoaling, and refraction due to current and depth, (2) wave generation by wind, (3) wave–current and wave–wave interactions, (4) white capping, bottom friction and depth-induced breaking, and (5) wave-induced set-up and currents. The model utilized output from this wave transformation

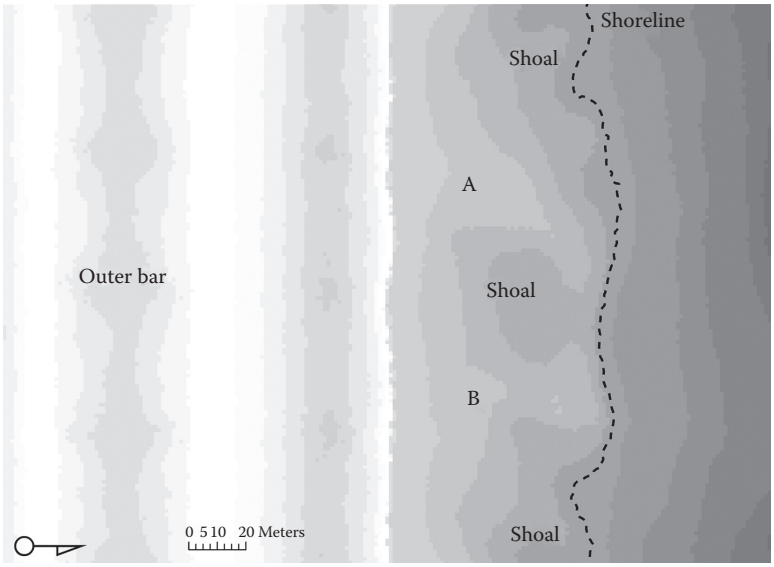


FIGURE 11.5 Interpolated bathymetry of the representative rip and shoal morphology used to model inshore wave heights and currents. This is the same rip and shoal complex shown in Figure 11.3.

module to generate currents resulting from the alongshore and cross-shore variations in wave set-up and set-down.

The inshore wave and current fields were generated for wave and tidal forcing at the time of each drowning (Table 11.1). Lifeguard records of times of drowning allowed the use of specific wave, wind, and tidal forcing in the model: the forcing for flag type, rescues, assists, and contacts was calculated as an average over daylight hours. The wave and current data were also generated for weighted average wave and tidal forcings for drownings, rescues, assists, prevents, and contacts (Table 11.2), for average green, yellow and red flag conditions, and for flag conditions weighted by the number of rescues.

RESULTS

Drownings

Twenty-five drownings occurred at Pensacola Beach over a range of wave and tidal conditions between 2000 and 2009, and all were assumed by lifeguards and reporters to be associated with rip currents (Table 11.1). Some drownings were described as follows

- "Lifeguards went on duty over the weekend……but they arrived 5 days too late." (*Ocala Star Banner*, April 11, 2000)
- "Two men drowned about 2 hours after lifeguards went off duty…. She said the waves kept pulling her back out there…. They drowned in an area that has several drop-offs and sand bars where currents and waves can suddenly pull a swimmer into deep water…." (*Lakeland Ledger*, June 6, 2000)
- "Drowned while swimming…in an unguarded area under [yellow] surf warnings." (*Lakeland Ledger*, May 12, 2002)
- "[Tropical Storm] Hannah was presumed to have claimed the life of a body surfer…after getting caught in a rip current…. No lifeguards were on duty, but red flags and signs were posted, warning people to keep out of the water due to high surf and rip currents." (*USA Today*, September 15, 2002)
- "Rip currents apparently swept away a 19-year-old man wading in waist-deep water… [with] yellow caution flags but no lifeguards." (*Daily News*, March 29, 2003)

In other cases, reported rip drownings appear to have occurred during rough surf capable of toppling bathers:

- "Drowned in an unguarded area while swimming in rough conditions… in 6- to 8-ft waves kicked up by Tropical Storm Gordon." (*The Advocate*, September 22, 2000)
- "Being roiled by Tropical Storm Allison…several firefighters tried to reach Bill Thomas but they too were swept away by riptides." (*Sarasota Herald Tribune,* June 9, 2001)

TABLE 11.1
Incident Forcing for Submersions at Pensacola Beach, 2000 to 2008

Date	Location	Time	Tide Direction	Tidal Range (ft)	Water Depth (m)	Wind Direction	Wind Speed (ms^{-1})	Wave Height (m)	Wave Period (sec)	Wave Direction (°)	Atmospheric Pressure (bar)
4/3/00	Ave. 21	—	—	—	0.15	148.0	10.4	1.6	6.7	1014.2	
6/4/00	FPG	1600	Out	2.5	0.05	238.6	2.9	0.4	6.0	1017.8	
6/4/00	FPG	1830	Out	2.5	0.12	229.4	3.5	0.4	6.4	1017.5	
9/17/00	Casino Beach	1930	In	0.8	0.25	41.7	9.3	3.7	9.0	1011.3	
9/20/00	Beach Resort	1930	In	1.5	0.05	122.7	6.7	1.0	5.0	1014.2	
10/27/00	Casino Beach	1330	In	1.0	0.13	—	—	—	—	—	
4/3/01	Five Flags	1330	In	1.5	0.10	160.7	7.5	1.3	5.2	153.4	1018.3
6/6/01	304 Ariola	1441	Out	2.0	0.20	132.1	7.0	1.6	7.5	186.6	1017.2
12/17/01	Clarion	1130	In	2.0	–0.10	159.1	8.7	1.6	6.6	165.1	1016.2
5/10/02	FPG	1300	Out	1.0	0.15	113.6	3.5	0.7	6.2	173.4	1019.8
5/13/02	BWJ	1125	Out	1.8	0.30	182.9	4.1	1.1	7.0	150.9	1018.0
7/5/02	1000 Ariola	—	—	—	0.05	239.6	7.7	0.7	6.1	239.6	1016.1
9/14/02	WPE	—	—	—	0.50	147.4	11.6	2.9	8.3	191.1	1012.9

K11772_C011.indd 184 1/4/11 10:03:14 AM

11/10/02	Emerald Isle	0900	Out	2.0	0.13	206.7	7.8	1.8	7.0	159.6	1012.2
3/27/03	Seahorse	1440	In	1.5	0.25	95.9	5.3	1.5	6.7	140.7	1008.5
4/7/03	Holiday Inn	1050	In	1.3	0.26	135.1	3.5	1.0	5.7	174.0	1015.2
5/11/03	BWJ	1700	In	0.5	0.15	185.0	4.6	1.0	5.8	192.0	1016.9
6/9/03	Sans Souci	1400	Out	0.5	–0.03	260.1	3.1	0.8	7.1	187.9	1015.5
8/30/03	Emerald Isle	1230	In	0.3	0.38	100.9	6.6	1.6	8.7	164.0	1018.2
8/30/03	Portofino	1400	In	0.3	0.33	95.4	6.5	1.5	8.8	162.6	1018.6
8/31/03	Ave. 14–16	1030	Out	0.5	0.28	97.9	7.3	1.5	6.4	160.9	1017.2
3/15/05	BWDI	1623	In	2.2	0.15	—	—	1.0	4.4	30.7	1014.5
9/25/05	S of SYR	1623	Out	1.8	0.21	141.3	8.0	1.8	9.0	246.1	1017.5
9/14/08	PL 18 E of FPG	1620	Out	1.0	0.33	186.0	3.5	1.3	8.7		1016.1
9/14/08	PL 18 E of FPG	1800	Out	1.0	0.25	188.6	2.9	1.2	8.2		1015.7
Average				1.3	0.19	157	6.2	1.4	6.9	169	1016

Note: FPG = Fort Pickens Gate. BWJ = Beachside Windjammer. WPE = West of Park East. DWDI = Best Western Days Inn. SYR = Sabine Yacht & Racquet Club.

K11772_C011.indd 185 1/4/11 10:03:14 AM

TABLE 11.2
Average Incident Wave, Wind, and Tidal Forcing for Drownings, Rescues, Assists, Prevents, and Contacts

	Speed (ms^{-1})	Wind Direction (°)	Height (m)	Period (sec)	Water Level (m)
Drownings	6.21 ± 0.94	157 ± 8	1.41 ± 0.19	6.90 ± 0.71	0.19 ± 0.04
Rescues	6.70 ± 0.16	154 ± 7	1.16 ± 0.06	5.46 ± 0.21	0.04 ± 0.02
Assists	6.12 ± 0.09	150 ± 5	0.97 ± 0.04	5.18 ± 0.16	0.06 ± 0.01
Prevents	6.72 ± 0.02	152 ± 1	1.30 ± 0.01	5.97 ± 0.04	0.07 ± 0.002
Contacts	5.88 ± 0.01	171 ± 1	0.81 ± 0.003	4.54 ± 0.01	0.08 ± 0.0005

Note: Weighted by the number of each event.

- "Got caught in the surf…." (*The Advocate*, December 19, 2001)
- "Disappeared after she was hit by a wave in waist-deep water." (*South Florida Sun*, May 22, 2002)
- "Red flag conditions, meaning swimming is extremely dangerous…. Lifeguards said they rescued [an additional] 15 swimmers caught in rip currents off the guarded beach." (*USA Today*, August 31, 2003)

In some cases, Good Samaritans drowned while trying to rescue others:

- "Would be rescuers died trying to save children from drowning…. Both children were rescued by other beachgoers. … apparently drowned Sunday while going to the aid of his granddaughter who was struggling in rough surf….died when he tried to rescue a 10-year old boy…. Neither [area] had lifeguards." (*Fredericksburg Free Lance Star*, April 8, 2001)
- "Drowned while trying to help other swimmers who were struggling with rough surf… under a yellow flag at the time." (*Gainesville Sun*, November 12, 2002)
- "Georgia man drowned Monday while trying to rescue his 12-year-old son struggling in rough surf… plunges into 3-ft waves to try to reach children…. The red flag at the end of the Pensacola Beach Gulf Pier warned of dangerous surf." (*Pensacola News Journal*, April 9, 2003)

The offshore significant wave height during these drownings averaged 1.4 m and ranged from 0.4 to 3.7 m (Table 11.3). The peak spectral wave period averaged 7 sec, with range from 4 to 9 sec. Water levels at the time of drowning averaged 0.2 m [above mean sea level (msl)], but ranged from –0.1 to 0.5 m. In all cases, the observed tide was greater than would have been expected from tide alone, with an average deviation of 0.1 m in response to storm winds from the south southeast. Bivariate plots of offshore significant wave height versus peak spectral period and significant wave height versus water depth are presented in Figure 11.6. There is no statistically significant difference in the wind and wave conditions between the periods when drowning did and did not occur.

TABLE 11.3
Predicted Significant Wave Height, Mean Current, Peak Oscillatory Current, and Combined Mean and Oscillatory Current for Shoal and Rip Channel Over Representative Morphology for Each Submersion

		Shoal				Rip Channel			
Date	**Location**	H_s	C_{mean}	C_{osc}	C_{total}	H_s	C_{mean}	C_{osc}	C_{total}
4/3/00	Ave. 21	0.55	0.29	0.79	1.08	0.62	0.24	0.85	1.09
6/4/00	FPG	0.41	0.25	0.62	0.87	0.47	0.19	0.69	0.88
6/4/00	FPG	0.43	0.24	0.63	0.87	0.49	0.20	0.70	0.90
9/17/00	Casino Beach	0.76	0.37	1.09	1.46	0.86	0.33	1.11	1.44
9/20/00	Beach Resort	0.47	0.27	0.70	0.97	0.55	0.20	0.77	0.98
10/27/00	Casino Beach								
4/3/01	Five Flags	0.51	0.28	0.74	1.02	0.59	0.22	0.82	1.04
6/6/01	304 Ariola	0.56	0.28	0.80	1.09	0.63	0.25	0.86	1.10
12/17/01	Clarion	0.47	0.32	0.77	1.09	0.55	0.23	0.79	1.02
5/10/02	FPG	0.46	0.25	0.67	0.92	0.53	0.21	0.75	0.95
5/13/02	BWJ	0.54	0.25	0.74	0.99	0.61	0.23	0.83	1.06
7/5/02	1000 Ariola	0.43	0.26	0.66	0.92	0.50	0.20	0.72	0.92
9/14/02	WPE	0.77	0.30	1.00	1.31	0.86	0.31	1.08	1.39
11/10/02	Emerald Isle	0.56	0.30	0.82	1.12	0.64	0.25	0.87	1.12
3/27/03	Seahorse	0.57	0.27	0.79	1.06	0.64	0.24	0.87	1.11
4/7/03	Holiday Inn	0.53	0.25	0.72	0.97	0.60	0.22	0.82	1.03
5/11/03	BWJ	0.49	0.26	0.71	0.97	0.57	0.21	0.79	1.00
6/9/03	Sans Souci	0.41	0.28	0.67	0.95	0.47	0.21	0.70	0.91
8/30/03	Emerald Isle	0.61	0.27	0.82	1.09	0.67	0.26	0.89	1.15
8/30/03	Portofino	0.58	0.27	0.81	1.07	0.64	0.26	0.86	1.12
8/31/03	Ave. 14-16	0.58	0.27	0.79	1.06	0.66	0.24	0.88	1.12
3/15/05	BWDI	0.50	0.26	0.70	0.96	0.59	0.20	0.81	1.01
9/25/05	S of SYR	0.57	0.30	0.84	1.13	0.64	0.27	0.86	1.13
9/14/08	PL 18 E of FPG	0.56	0.26	0.78	1.04	0.62	0.25	0.84	1.09
9/14/08	PL 18 E of FPG	0.53	0.26	0.76	1.02	0.59	0.24	0.81	1.05
	Average	0.53	0.27	0.77	1.04	0.61	0.24	0.83	1.07

Note: Predicted significant wave height = H_s (m). Mean current = C_{mean} (ms^{-1}). Peak oscillatory current = C_{osc} (ms^{-1}). Combined mean and oscillatory current = C_{total} (ms^{-1}). FPG = Fort Pickens Gate. BWJ = Beachside Windjammer. WPE = West of Park East. DWDI = Best Western Days Inn. SYR = Sabine Yacht & Racquet Club.

Au:Missing data for Casino Beach?

Drownings are significantly over-represented for water levels greater than mean sea level and for tidal ranges larger than the mean. With the relatively small ranges and drownings equally distributed between incoming and outgoing tides, it is reasonable to expect that they are not associated with an additional current as the tide drains, but arise from a change in transformation of storm waves over the nearshore morphology. Model results suggest that for every 0.1 m increase in water level and

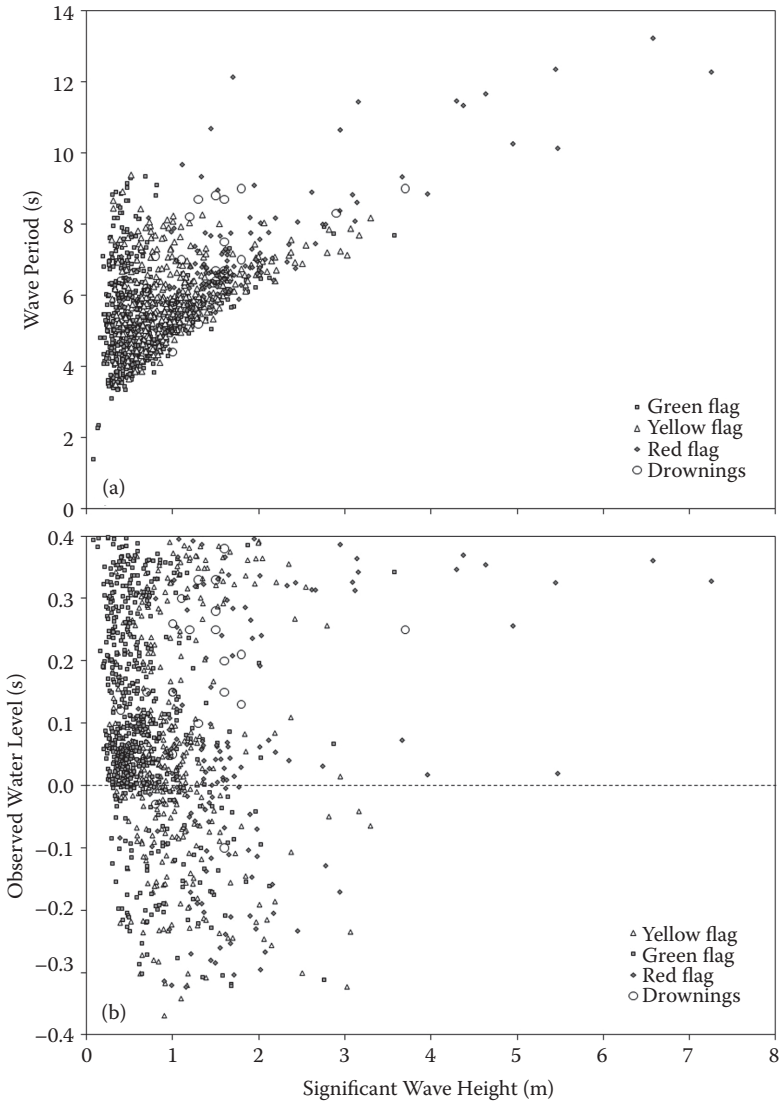


FIGURE 11.6 Scatter plots of (a) offshore significant wave height and wave period and (b) observed water levels for all flag types and for drowning events.

constant wave height and period, a 0.03 m increase in wave height appears along the seaward edge of the shoal. The 0.1 m increase in water level has a negligible effect on the inshore wave heights for green flag (small wave and period) conditions. An almost 0.05 m increase in inshore wave height creates red flag conditions (large wave and period). While seemingly small, a 0.05-m increase in wave height is enough to lift bathers and cause them to lose footing in a channel with depths of 1 to 1.5 m and both mean and oscillatory currents moving them seaward.

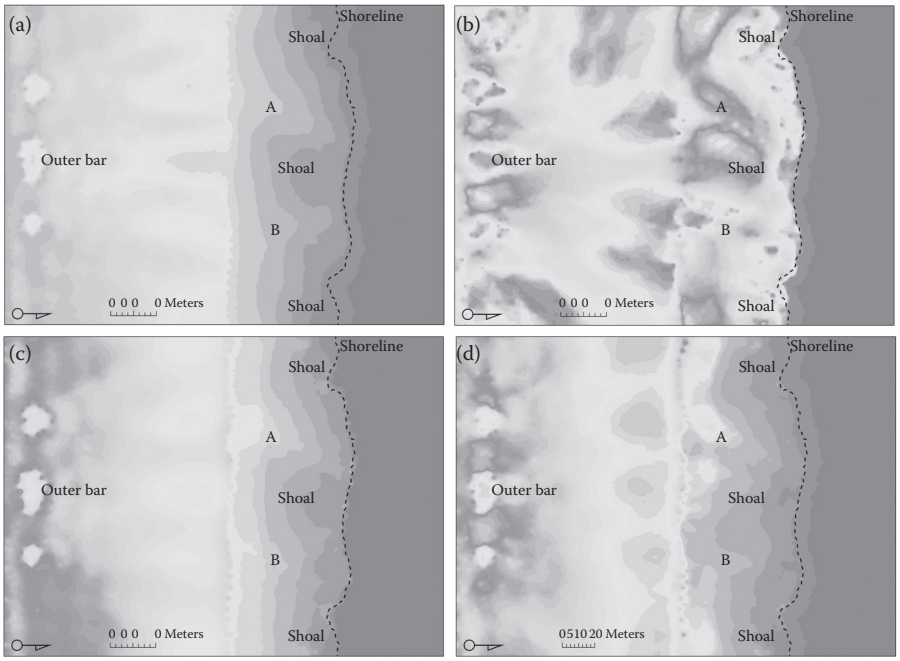


FIGURE 11.7 Spatial variations in (a) significant wave height, (b) mean current, (c) oscillatory current, and (d) maximum combined current speed for average of all drowning events at Pensacola Beach.

Model results showing spatial variations in mean current speed, peak oscillatory velocity, and significant wave height are presented in Figure 11.7 for average wind, wave, and tidal conditions during drowning events (Table 11.1). Significant wave height closely follows nearshore bathymetry (Figure 11.5), with larger waves closer to shore in the rip channels (A and B), consistent with the observations of Sonu (1972). Wave breaking through spilling across the shoal creates a wide zone of relatively small waves (<0.2 m) compared to the >0.3-m unbroken waves within the rip channel. Despite the greater depths of the rip channel, the larger waves are responsible for peak oscillatory velocities (>0.4 ms^{-1}) within the feeder current approximately 5 m of the shoreline (Figure 11.7c). Within 30 m of the shoreline, the peak oscillatory velocities exceed 0.6ms^{-1} at depths of 1 m. Comparatively, the mean current within the feeder current is only 0.1 ms^{-1} and increases to a maximum of 0.24 ms^{-1} approximately 50 m seaward of the shore. The landward-directed currents across the shoal reach a maximum of 0.28 ms^{-1} about 50 m from the shoreline, but remain 0.2 ms^{-1} along the seaward edge of the feeder channel. The maximum combined mean and oscillatory current is >0.4 ms^{-1} within 7 m of the shoreline and exceeds >0.7 ms^{-1} in the rip channel about 50 m from the shoreline.

The mean current in the rip channel ranged from 0.19 to 0.33 ms^{-1} over a wide range of incident wave and tidal conditions. In comparison, the peak oscillatory current within the rip channel varied from 0.69 to 1.11 ms^{-1} in response to significant

wave heights of 0.47 and 0.86 m, respectively. The combination of the mean and peak oscillatory currents caused a pulsing flow within the rip channel, reaching maximum velocities between 0.88 and 1.44 ms^{-1}. The oscillatory current accounts for 78% of the maximum current in the rip channel—consistent with Sonu's observation (1972) of an oscillatory current accounting for 70% of the maximum current in the rip channel. This estimation does not include pulses in current speed at infragravity frequencies (Sonu, 1972; Aagaard et al., 1997; Brander and Short, 2001; MacMahan et al., 2003; Reniers et al., 2004).

The oscillatory current also accounts for 70% of the maximum current across the shoal for all of the drowning events. The mean current varied from a minimum of 0.24 ms^{-1} to a maximum of 0.37 ms^{-1}. The peak oscillatory currents varied from a maximum of 1.09 ms^{-1} to 0.62 ms^{-1} with maxima located along the seaward edge of the shoal. Within about 25 m of the shoreline, the oscillatory current was only 0.4 ms^{-1}, but combined with the mean landward current reached >0.6 ms^{-1} with broken wave heights of 0.2 m in depths of ~0.25 m.

Rescues

Green flag rescues are generally associated with an offshore wave height of 0.70 m, wave period of 6 sec, and a tidal elevation of 0.04 m (Table 11.4). The rescue-weighted wave height and period are significantly greater than the average height (0.63 m) and period (5 sec) for all green flag days (with and without rescues), while the water level is significantly lower than the green flag average of 0.1 m. The mean current in the rip channel reaches a maximum of 0.18 ms^{-1} at a distance of 40 m from the shoreline. The inshore wave height is 0.46 m within the rip channel and 0.37 m along the seaward edge of the shoal, with peak oscillatory currents of 0.71 and 0.56 ms^{-1}, respectively. The combined current reaches a maximum of 0.89 ms^{-1} in the rip channel, which is significantly different at the 95% confidence level ($p = 0.03$) from the predicted current for all green flag days combined (0.85 ms^{-1}). With no statistically significant difference in the peak

TABLE 11.4
Average and Incident Wave Forcing[a] for Green, Yellow, and Red Flag Days, Mean Current, Oscillatory Current, Total Current and Maximum Inshore Wave Height

Color	H_s (m)	T (sec)	H (m)	C_{mean} (ms^{-1})	C_{osc} (ms^{-1})	C_{total} (ms^{-1})	H_s (m)
Green	0.70	5.74	0.01	0.18	0.71	0.89	0.46
Yellow	0.93	6.58	0.04	0.23	0.68	0.91	0.49
Red	1.69	7.62	0.09	0.24	0.81	1.05	0.61
Green	0.63	5.31	0.10	0.14	0.72	0.85	0.51
Yellow	1.02	5.93	0.07	0.14	0.70	0.84	0.50
Red	1.73	6.97	0.05	0.15	0.69	0.84	0.48

[a] Weighted by number of rescues for flags with and without rescues.

oscillatory current and smaller wave heights on rescue days, it appears that green flag days with rescues are dependent on the strength of the mean current in the rip channel.

Yellow flag rescues are generally associated with an offshore significant wave height of 0.93 m, wave period of 6.6 sec, and water depth of 0.01 m. The wave period is significantly greater than all yellow flag days combined (5.9 sec), while the wave height and water depth are significantly lower than the wave height (1.02 m) and depth (0.07 m) for all yellow flag days combined. Despite smaller wave heights offshore, the combination of longer period waves in shallower water leads to greater dissipation across the shoal and a significantly stronger mean current of 0.23 ms^{-1} in the rip channel. The combined oscillatory and mean current reached 0.91 ms^{-1} within the rip current, although the oscillatory current alone was not significantly different from all yellow flag days combined (0.84 ms^{-1}). Similar to green flag conditions, yellow flag days with rescues appear to depend on the strength of the mean current in the rip channel.

Red flag days with rescues tend to be associated with offshore wave heights of 1.69 m, wave periods of 7.6 sec, and water depths of 0.09 m. The wave period and tidal elevation are significantly different from all red flag days (5.9 sec and 0.05 m), and the offshore wave height is significantly below 1.73 m for all red flag days combined. As a result of smaller wave height and larger tidal elevation, wave height in the rip channel was significantly larger at 0.61 m, leading to a greater oscillatory current. While the mean current in the rip channel was significantly larger than for all red flag days (0.24 versus 0.15 ms^{-1}), it was not significantly different from that on yellow flag days with rescues (0.23 ms^{-1}). The combined oscillatory and mean current of >1.0 ms^{-1} is significantly larger than for all red flag days and yellow flag days with rescues, suggesting that red flag days with rescues depend on inshore wave height and oscillatory currents.

Water Level

Dangerous rip currents are often linked to lower tidal elevations (Shepard et al., 1941; McKenzie, 1958; Short and Hogan, 1994; Lushine, 1991; Lascody, 1998; Engle et al., 2002). However, most drownings at Pensacola Beach occurred during periods of elevated water level, averaging 0.19 m above msl (Table 11.1). Similarly, rescues during yellow and red flag conditions are associated with water levels greater than msl, while green flag rescues are associated with water levels close to 0 m msl.

To examine the role of water level in controlling rip development, cross-shore variations in significant wave height are plotted for green, yellow, and red flag conditions in Figure 11.8. Wave height is unaffected by the outermost bar during green flag conditions (Figure 11.8a). There is slightly greater dissipation over the shoal with decreasing water levels, until the shoal is exposed as the water level approaches 0.3 m. As a consequence, maximum set-up at the shoreline is inversely related to water depth, leading to stronger rip currents at low water levels. In contrast, wave heights are attenuated by the outermost bar during yellow and red flag conditions, leading to an opposite relationship between maximum set-up and water depth. Increasing depths allow for larger waves inshore and greater dissipation across the shoal. This

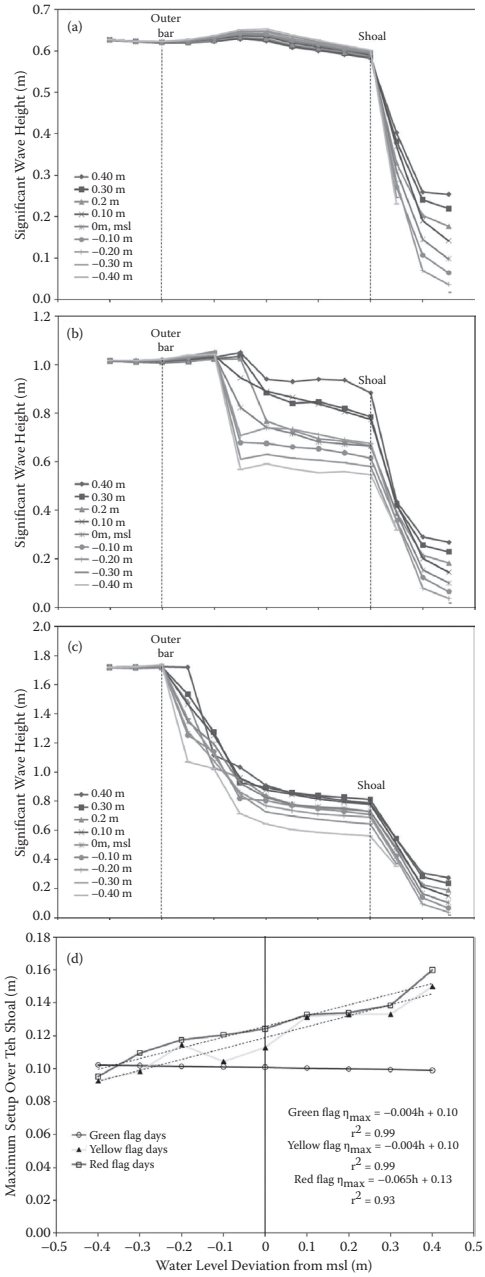


FIGURE 11.8 (*See color insert following page XXX.*) Modeled cross-shore transformation of incident wave fields for (a) green, (b) yellow, and (c) red flag conditions with respect to inner and outermost bars; (d) is variation in maximum set-up across the shoal with respect to water level.

does not necessarily lead to increased rip speeds as there is also an increase in wave heights in the rip channel under red flag conditions.

Tides at Pensacola Beach are diurnal; high tide occurs around 8 am at the onset of spring tides, 10 am at the height of spring tides, and 12 am at the transition to neap tides. To examine the daily variations in rip hazard in response to this consistent water level, water depths, wave heights, and predicted rip current speeds were ensemble-averaged by hour of day between March and September 2000 to 2008 (Figure 11.9). While the offshore significant wave height reached a late afternoon (4 pm) maximum due to developing sea breezes, the inshore significant wave height tended to reach maximum around 11 am in response to maximum sea level. Rip speed is predicted to reach a sustained maximum from 11 am to 1 pm in response to the greater water depths and larger inshore wave heights.

As the water levels increase and breaking over the outermost bar is reduced, more frequent wave sets come ashore, creating a flash rip effect (Bob West, personal communication). This suggests that in addition to the stronger mean current resulting from dissipation of larger inshore waves, additional pulsation of the current at infragravity frequencies (Sonu, 1972; Aagaard et al., 1997; Brander and Short, 2001; MacMahan et al., 2003; Reniers et al., 2004) cannot be addressed by the model. However, the times of above-average wave heights and rip speeds overlap significantly with heaviest beach use and account for 84% of all drownings.

DISCUSSION

The Florida panhandle is "… the worst [area] in the nation for beach drownings" (*Tuscaloosa News*, April 6, 2002). Santa Rosa Island was designated the "Drowning Capital" (*Lakeland Ledger*, April 3, 2002) after 11 drownings in 2001 (3 at Pensacola Beach). Between 2000 and 2008, 25 drownings occurred at Pensacola Beach. The drowning hot spots are situated between transverse ridges where the waves appear smaller and conditions safer. In addition, rip hot spots are coincident with the primary beach access points and resulting clusters of beach users at those locations.

Model results suggest that the average rip current speed on days with rescues ranges from 0.18 to 0.24 ms^{-1} and from 0.19 to 0.33 ms^{-1} for drowning events. In comparison, predicted current speeds for periods without rescues or drownings are on the order of 0.15 ms^{-1} regardless of the flag color flying that day. The days with drownings and rescues exhibit no statistically significant dependence on wind and wave forcing, but are significantly over-represented for water levels greater than msl and for tidal ranges exceeding the mean tidal range. An increase in rip speeds at high tide is contrary to previous studies linking rip current danger to lower tidal elevations (Shepard et al., 1941; McKenzie, 1958; Short and Hogan, 1994; Lushine, 1991; Lascody, 1998; Engle et al., 2002). Lower tides during storm waves increase wave dissipation and set-up across the bar and drive larger rip current velocities until the bar emerges and the currents are driven only by water trapped landward of the bar.

At Pensacola Beach, rip current speed is inversely related to water level during green flag conditions (Figure 11.8d), while low water levels during yellow and red flag conditions are associated with an increase in wave breaking and attenuation over

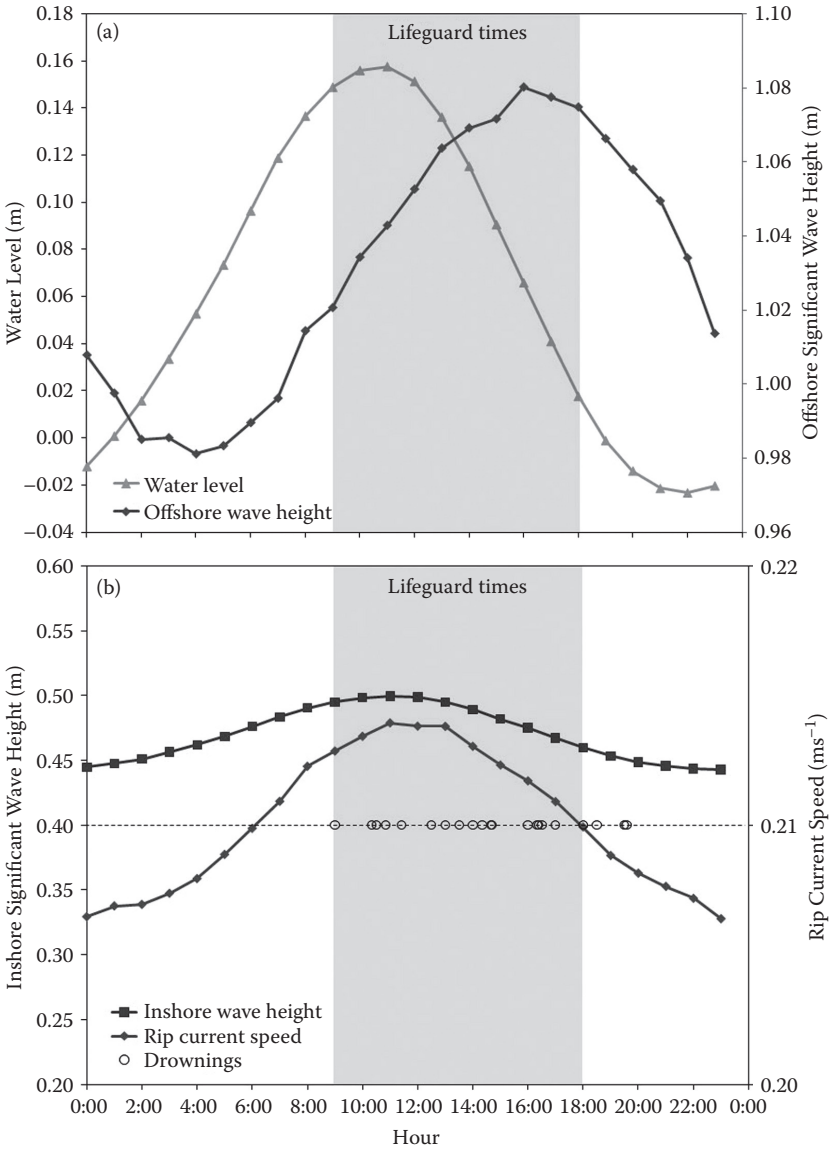


FIGURE 11.9 Ensemble-averaged hourly variation in (a) water level and offshore significant wave height and (b) inshore significant wave heights, rip current speeds, and drowning times.

the outermost bar. This limits the heights of inshore waves breaking on the shoal. Therefore, the morphology and behavior of the innermost bar and its rip channels are partly controlled by position and relative depth of the outermost bar (Ruessink and Terwindt, 2000; Masselink, 2004; Houser and Greenwood, 2005; Castelle et al., 2006; Castelle et al., 2010).

While drownings tend to occur on red flag days, lifeguards at Pensacola Beach regularly perform rescues, assists, and prevents on green and yellow days. This in part reflects the semi-permanent nature of the channels that allows rip current development under the right combination of waves and tides. On green flag days, the current begins to develop in late afternoons, with falling tide and an increase in sea breeze (Figure 11.9). The strength of the rip under green flag conditions is surprisingly close to conditions for both red and yellow flags (Table 11.4), which may reflect more water entering the channel from the side of the shoal and a less focused current (McKenzie, 1958; Sonu, 1972; Short, 2007).

Rip current speeds cited in this study do not include an infragravity component that can make a current stronger (Sonu, 1972; Aagaard et al., 1997; Brander and Short, 2001; MacMahan et al., 2003; Reniers et al., 2004). As noted by West (personal communication), "more frequent wave sets" create a strong "flash rip current effect" as the water level increases and breaking over the outermost bar is reduced. Houser and Barrett (2009, 2010) also noted a strong infragravity signal in the elevation of the swash zone during high tide on a yellow flag day. While the infragravity signal was dominant throughout high tide, it was at a maximum with the incoming and outgoing tides in response to the decrease in water level. MacMahan et al. (2006) suggested that the infragravity component of the current can be double that of the mean current, suggesting that the rip velocities at Pensacola Beach may reach 0.72 ms^{-1} under yellow and red flag conditions.

Bathers are also subject to relatively large waves and oscillatory currents within the rip channel. Specifically, the model predicts wave heights between 0.47 and 0.86 m within the channel, consistent with the observations of Sonu (1972) at a similar site. The larger waves within the channel are in part responses to shoaling through the deeper rip channel, but also wave–current interactions that, while weak (Froude number of 0.06 to 0.11 for drownings), nonetheless increase wave heights. The presence of larger, unbroken waves in the rip channel may limit further current development through opposing radiation stress (Yu and Slinn, 2003) that forces a counter torque that opposes the pressure gradient from shoal to rip (Haller et al., 2002; Haas et al., 2003). Nonetheless, a pressure gradient exists between the shoal and the rip channel since the waves in the rip channel break and set up closer to shore. A bather entering a rip channel would encounter rapid changes in depth and short but very strong oscillatory pulses (0.7 to 1.1 ms^{-1}), possibly leading to unstable and lost footing in depths of 1 to 1.5 m.

Strong tidal dependence of rips at Pensacola Beach and the tendency of high tides to occur at mid-day through the summer season mean that these dangerous currents reach maximum speed when most people are at the beach (Figure 11.9). This explains why rip currents at Pensacola Beach and elsewhere along Santa Rosa Island are responsible for so many drownings and rescues.

CONCLUSIONS

The primary access points at Pensacola Beach are located where semi-permanent rip channels exist, and model results indicate that rips can occur over a wide range of wave and tidal conditions. Rip strength is controlled by wave breaking over the

outermost bar and reaches a maximum at high tide, which occurs mid-day for spring tides; red and yellow flags are flown at these times. Rip currents can still develop during green flag days; their strength increases during late afternoons in response to greater dissipation over the shoal caused by falling tide and onset of sea breezes.

The model predicts that the mean rip current velocity on rescue days is relatively weak (0.2 to 0.3 ms^{-1}), but this does not include pulsing flows resulting from infragravity waves. Direct measurements of rip speeds, locations, and timings are required to confirm the model results and estimate the relative importance of infragravity waves.

ACKNOWLEDGMENTS

This study was supported by in part by grants from the National Park Service (P5320060026) and Florida Sea Grant (R/C-S-50). Field assistance was provided by Tim Brunk and Jack Walker of Texas A&M University and by Tanya Gallagher, Fritz Langerfeld, and Klaus Meyer-Arendt from the University of West Florida. Bob West of the Santa Rosa Island Authority is also thanked for his support and contributions to this study.

REFERENCES

Aagaard, T., B. Greenwood, and J. Nielsen. 1997. Mean currents and sediment transport in a rip channel. *Marine Geol.,* 140: 25–45.

Bowman, D., D. Arad, D.S. Rosen et al. 1988. Flow characteristics along the rip current system under low energy conditions. *Marine Geol.,* 82: 149–167.

Brander, R.W. 1999. Field observations on the morphodynamic evolution of a low energy rip current system. *Marine Geol.,* 157: 199–217.

Brander, R.W., and A.D. Short. 2000. Morphodynamics of a large-scale rip current system at Muriwai Beach, New Zealand. *Marine Geol.,* 165: 27–39.

Brander, R.W., A.D. Short, P.D. Osborne et al. 1999. Field measurements of a large-scale rip current system. In *Coastal Sediments,* Kraus, N.C. and McDougal, W.G., Eds.

Castelle, B., P. Bonneton, and R. Butel. 2006. Modeling of crescentic pattern development of nearshore bars: Aquitanian Coast, France. *Compt. Rend. Geosci.,* 338: 795–801.

Castelle, B., B.G. Ruessink, P. Bonneton et al. 2010. Coupling mechanisms in double sandbar systems 1: Patterns and physical explanation. *Earth Surface Proc. Landforms,* 35: 476–486.

Engle, J., J. MacMahan, R.J. Thieke et al. 2002. Formulation of a rip current predictive index using rescue data. *Proc. 15th Annu. Conf. on Beach Preservation Technology,* Tait, L., Ed.

Fletemeyer, J. and S. Leatherman. 2010. Rip currents and beach safety education. *J. Coastal Res.,* 26: 1–3.

Gensini, V. and W. Ashley. 2009. An examination of rip current fatalities in the United States. *Natural Hazards*, in press.

Greenwood, B. and P.R. Mittler. 1979. Structural indexes of sediment transport in a straight, wave-formed nearshore bar. *Marine Geol.,* 32: 191–203.

Haas, K.A., I.A. Svendsen, M.C. Haller et al. 2003. Quasi three-dimensional modeling of rip current systems. *J. Geophys. Res. Oceans,* 108: C7.

Haller, M.C., R.A. Dalrymple, and I.A. Svendsen. 2002. Experimental study of nearshore dynamics on a barred beach with rip channels. *J. Geophys. Res. Oceans,* 107: C6.

Haller, M.C., R.A. Dalrymple, and I.A. Svendsen. 1998. Experimental modeling of a rip current system. In *Ocean Wave Measurement and Analysis,* Edge, B.L. and Hemsley, J.M., Eds.

Houser, C. and B. Greenwood. 2005. Profile response of a lacustrine multiple barred nearshore to a sequence of storm events. *Geomorphology,* 69: 118–137.
Lascody, R.L. 2009. East Central Florida rip current program. *Natl. Weather Dig.,* 22: 25–30.
Livingston, G. and K. Arthur. 2002. The economic impact of Pensacola Beach (unpublished report). Haas Center for Business Research and Economic Development, University of West Florida. Pensacola.
Lushine, J.B. 1991. A study of rip current drownings and related weather factors. *Natl. Weather Dig.,* 16: 13–19.
MacMahan, J., A.J.H.M. Reniers, E.B. Thornton et al. 2004. Infragravity rip current pulsations. *J. Geophys. Res. Oceans,* 109: C1.
MacMahan, J.H., E.B. Thornton, and A.J.H.M. Reniers. 2006. Rip current review. *Coastal Eng.,* 53: 191–208.
MacMahan, J.H., E.B. Thornton, A.J.H.M. Reniers et al. 2008. Low-energy rip currents associated with small bathymetric variations. *Marine Geol.,* 255: 156–164.
Masselink, G. 2004. Formation and evolution of multiple intertidal bars on macrotidal beaches: application of a morphodynamic model. *Coastal Eng.,* 51: 713–730.
Mei, C.C., and P.L.F. Liu. 1977. Effects of topography on circulation in and near surf zone: linear theory. *Est. Coastal Marine Sci.*, 5: 25–37.
Meyer-Arendt, K.J. 1990. Recreational business districts in Gulf of Mexico seaside resorts. *J. Cultural Geogr.,* 11: 39–55.
Morgan, D., J. Ozanne-Smith, and T. Triggs. 2009. Self-reported water and drowning risk exposure at surf beaches. *Austral. New Zeal. J. Public Health,* 33: 180–88.
Reniers, A.J.H.M., J.A. Roelvink, and E.B. Thornton. 2004. Morphodynamic modeling of an embayed beach under wave group forcing. *J. Geophys. Res. Oceans,* 109: C1.
Ruessink, B.G. and J.H.J. Terwindt. 2000. The behaviour of nearshore bars on the time scale of years: a conceptual model. *Marine Geol.,* 163: 289–302.
Shepard, F.P., K.O. Emery, and E.C. Lafond. 1941. Rip currents: a process of geological importance. *J. Geol.*, 49: 338–369.
Short, A.D. 1985. Rip current type, spacing and persistence, Narrabeen Beach, Australia. *Marine Geol.,* 65: 47–71.
Short, A.D., and C.L. Hogan. 1994. Rip currents and beach hazards: their impact on public safety and implications for coastal management. *J. Coastal Res.,* 12: 197–209.
Smith, J.A. and J.L. Largier. 1995. Observations of nearshore circulation: rip currents. *J. Geophys. Res. Oceans,* 100: 10967–10975.
Sonu, C.J. 1972. Field observation of nearshore circulation and meandering currents. *J. Geophys. Res.,* 77: 3232.
Thornton, E.B., J. MacMahan, and A.H. Sallenger. 2007. Rip currents, mega-cusps, and eroding dunes. *Marine Geol.,* 240: 151–167.
Turner, I.L., D. Whyte, B.G. Ruessink et al. 2007. Observations of rip spacing, persistence and mobility at a long, straight coastline. *Marine Geol.*, 236: 209–221.
Wright, L.D. and A.D. Short. 1984. Morphodynamic variability of surf zones and beaches: a synthesis. *Marine Geol.*, 56: 93–118.
Yu, J. and D.N. Slinn. 2003. Effects of wave–current interaction on rip currents. *J. Geophys. Res. Oceans,* 108: C3.

Geomorphology 125 (2011) 62–72

Contents lists available at ScienceDirect

Geomorphology

journal homepage: www.elsevier.com/locate/geomorph

Alongshore variation in foredune height in response to transport potential and sediment supply: South Padre Island, Texas

Chris Houser [a,*], Sojan Mathew [b]

[a] Department of Geography, Texas A&M University, College Station, TX 77843-3147, United States
[b] The University of Texas at Austin, Bureau of Economic Geology, Austin, TX 78713-8924, United States

ARTICLE INFO

Article history:
Received 20 October 2009
Received in revised form 29 June 2010
Accepted 2 July 2010
Available online 17 September 2010

Keywords:
Beach
Foredune
Barrier island
Wavelet analysis
LiDAR
South Padre Island

ABSTRACT

The height and extent of coastal dune development can exhibit considerable variability over short distances, leading to variable storm impact alongshore. The source of this variation is not well understood in general, and in many cases is not easily explained by models that ascribe dune height and development to regional variations in sediment availability and foreshore slope. In this paper, LiDAR data collected in 2000 and 2005 from South Padre Island, Texas are used to characterize the alongshore variation in dune morphology, and to identify how the variation is related to foreshore morphology and nearshore state. Results of cross-wavelet analysis suggest that foredune height exhibits a statistically significant coherence with the surf similarity parameter at length scales of ~1300 of 2300 m. The resulting variation in beach state alongshore, from intermediate to dissipative, is the consequence of wave refraction and focusing by transverse ridges on the inner shelf. Dune height reaches a local maximum approximately halfway between the more intermediate and dissipative sections of the coast, where the volume of sediment in the backshore and in the foreshore bars are also at a maximum. The greater elevation of the foreshore and backshore also provides a wider fetch and potential for aeolian transport during the storm surge that tends to accompany storm winds. It is argued that the variation in dune morphology is not strictly the result of transport limitations as suggested by the fetch model, but rather depends on the alongshore coincidence of transport potential with an available supply of sediment in the backshore and on the foreshore.

© 2010 Elsevier B.V. All rights reserved.

1. Introduction

Shoreline erosion and washover during an extreme storm depends on the height and extent of foredune development relative to the elevation of the storm surge (Thieler and Young, 1991; Sallenger, 2000; Morton, 2002; Houser et al., 2008). As the storm surge increases above the elevation of the backshore (D_{low}), the impact changes from beach erosion to erosion of the dune face and ultimately washover as the surge exceeds the elevation of the dune crest (D_{high}). This model is complicated by alongshore variations in dune height as large dunes adjacent to smaller dunes can be eroded through lateral erosion (Houser et al., 2008). Variations in dune height and localized shoreline response is well documented (e.g. Elko et al., 2002; Schupp et al., 2006; Stockdon et al., 2007), but the source of the variation is not well understood. Localized coastal response can be forced by wave refraction over the inner-shelf bathymetry (Demarest and Leatherman, 1985; Kraft et al., 1987; Pilkey et al., 1993; Riggs et al., 1995; Schwab et al., 2000; McNinch, 2004; Browder and McNinch, 2006; Schupp et al., 2006; Stockdon et al., 2007). Alternatively, Stallins and Parker (2003) argue that a patchwork of dunes and washover conduits can develop freely in response to random variations in height and a preferential selection of dune-building dunes. Regardless of the mechanism, alongshore variations in dune morphology are reinforced by the different levels of storm impact (Stockdon et al., 2007; Houser et al., 2008) and the availability of sediment for post-storm recovery (Houser and Hamilton, 2009).

Following storm erosion, dune recovery first requires that the beach recovers through the onshore migration and welding of the innermost nearshore bar, followed by accretion in the backshore to create a wide flat backshore that promotes the aeolian transport of the newly available sediment into the dune (Morton et al., 1994; Aagaard et al., 2004). Despite the recognized importance of nearshore and intertidal bars to dune recovery, most field studies on beach–dune interaction focus on the limits to aeolian transport across the foreshore and backshore. Limits to transport has been variously ascribed to the presence of moisture (Hotta et al., 1985; Sarre, 1989; Nordstrom and Jackson, 1992; Arens, 1996; Sherman et al., 1998; Wiggs et al., 2004; Yang and Davidson-Arnott, 2005; Davidson-Arnott et al., 2005; Bauer et al., 2009), boundary layer adjustments (Houser et al., 2008), and lag deposits (Nickling and McKenna Neuman, 1995; McKenna Neuman, 1998). Each of these controls influences the length of the required fetch for transport to reach a maximum (Bauer and Davidson-Arnott, 2003; Davidson-Arnott et al., 2005; Hesp et al., 2005), which can be further

* Corresponding author.
E-mail addresses: chouser@geog.tamu.edu (C. Houser), sojan.mathew@beg.utexas.edu (S. Mathew).

0169-555X/$ – see front matter © 2010 Elsevier B.V. All rights reserved.
doi:10.1016/j.geomorph.2010.07.028

reduced through inundation by tidal excursions, storm surge, and wave set-up and run-up. Jackson and Cooper (1999) have shown that the critical fetch is not an important constraint on sediment transport for beaches with a large supply of dry sand in the backshore. In response, it has been argued that the primary control on transport and sediment delivery to coastal foredunes in dissipative environments is the availability of sediment and not the fetch effect (Christiansen and Davidson-Arnott, 2004; Saye et al., 2005; Lynch et al., 2006).

The lack of clarity about the relative importance of supply and transport limitations on aeolian transport is mirrored in the oft-cited models of beach–dune interaction that ascribe regional variations in dune morphology to the fixed constraints of beach slope (Short and Hesp, 1982) and local sediment budget (Psuty, 1993). Short and Hesp (1982) argue that aeolian transport rates are potentially the greatest on a dissipative beach, moderate on an intermediate beach and lowest on reflective beaches due to greater flow disturbance and a shorter fetch. Psuty (1993) suggests that dune development is dependent on the availability of sediment from the beach, which is in turn dependent on the availability of sediment from littoral drift. The dune budget reaches a maximum and heights are greatest where the beach is slightly erosional. Pye (1990) presents an alternative model that accounts for (i) the rate of littoral sand supply, (ii) the wind energy available for transport and (iii) the effectiveness of sand-trapping vegetation. A single foredune ridge develops if the vegetation is sufficient to trap sediment, and the amount of sediment transferred from beach to dune balances the littoral supply. Houser and Hamilton (2009) found supporting evidence for these models along Santa Rosa Island in northwest Florida. Historically and following the 2004/2005 hurricane season, the authors present evidence to suggest that the exchange of sediment between beach and dune in erosional areas with a relatively reflective foreshore is limited by the steep gradient and limited fetch of the beach berm, while the larger beach width and lack of berm development in intermediate sections of the island are more conducive to the transport of sediment from beach to dune (Short and Hesp, 1982; Hesp, 1988). The alongshore variations in beach type and dune morphology in northwest Florida are the result of transverse ridges on the inner shelf that create an alongshore variation in wave energy and beach state (Houser et al., 2008).

The beach–dune interaction described by Houser and Hamilton (2009) suggest that alongshore variation in dune development in an intermediate to reflective environment is controlled by an alongshore variation in the width and slope of the foreshore. While this is consistent with the beach–dune interaction model of Short and Hesp (1982) it is not clear whether this would also be true for more dissipative environments where sediment supply has been identified as a primary control on dune development (cf. Jackson and Cooper, 1999; Christiansen and Davidson-Arnott, 2004; Saye et al., 2005; Lynch et al., 2006). In the present study, LiDAR data from 2000 and 2005 are used to describe the alongshore variation in beach and dune morphology along South Padre Island in south Texas, which has a relatively dissipative shoreface and exhibits considerable variability in dune height alongshore. The alongshore coherency and phase relationship amongst dune, beach and beach state is quantified using cross-wavelet analysis.

2. Study site

South Padre Island is the southernmost part of a large arcuate system of barrier islands and spits that extends approximately 600 km from the Bolivar Peninsula at the mouth of Galveston Bay (Fig. 1). South Padre Island is microtidal with a mean diurnal tidal range of 0.49 m. Low tide exposes a foreshore width of ~70 m that is typically characterized by a storm-generated supra-tidal bar and berm (Fig. 2). Sediment to the barrier is largely supplied by sediment from the Rio Grande River Delta to the south, but reductions in the flow of the Rio Grande and reservoir sedimentation have lead to a substantial loss of sediment supply (Morton and Pieper, 1975; Mathewson and Minter, 1976). As a consequence, the island has been experiencing widespread erosion, particularly during hurricanes capable of breaching the dunes and moving sediment into Laguna Madre through washover channels (Shideler and Smith, 1984).

Beach sediments consist of quartz-rich sand that is moderately to well sorted and has a mean grain diameter of ~0.2 mm. Hunter and Richmond (1988) estimated that the aeolian transport threshold for the sediment in the backshore is ~5 m s^{-1}. Hourly average wind speeds for onshore events reached 21 m s^{-1} in 2008, with an annual average of 5.6 m s^{-1}. The summer sea breeze is superimposed on a synoptic anticyclonic flow around the Azores-Bermuda high-pressure cell (Yu and Wagner, 1970), reinforcing the sea breeze and suppressing the land breeze (Hunter and Richmond, 1988). The aeolian sediment drift potential, calculated from the modified Fryberger method (Lettau and Lettau, 1978), suggests that the resultant drift potential from 1990 to 2008 is oriented onshore from the SW (140°). Accounting for the sediment input per unit length of dune, which varies with the cosine of the wind direction to the beach (Bauer and Davidson-Arnott, 2003), winds between 120° and 140° represent the greatest (potential) source of sediment to the dune. With the exception of extreme storms, the events with the largest transport potential occur through fall and winter in response to frontal storms that tend to be accompanied by a storm surge that also narrows the available fetch. Shideler and Smith (1984) argue that the larger dunes on South Padre Island, compared to those of northern Texas, are the consequence of a progressive southward increase in mean wind speed and aridity that enhance aeolian transport. Thus, despite the narrowing of the fetch, storm winds are still capable of providing sediment to the foredune.

3. Methodology

LiDAR is an active remote sensing technology which involves the collection of spatially dense and accurate topographic data using aircraft mounted lasers capable of recording elevations measurements with a vertical precision of ~0.15 m. Airborne LiDAR topographic mapping (ALTM) systems consists of three basic components namely, the laser scanner, a kinematical Global Positioning System (GPS), and the Inertial Measurement Unit (IMU). The laser scanner detects the range from the aircraft to a ground object. A rotating or oscillating mirror mounted in front of the laser causes it to scan back and forth, allowing for coverage of a wide swath beneath the flight path. Aircraft positions are recorded continuously by a GPS receiver mounted in the aircraft. A second GPS station at a known ground position provides differential corrections for more accurate estimation of the aircraft trajectory. Aircraft orientation is measured by the IMU on the aircraft. The IMU consists of a set of gyroscopes and accelerometers that continuously measure the roll, pitch, and yaw of the aircraft from 10 to 100 times per second.

3.1. Data processing

Post-processed ASCII data sets with *X*, *Y*, *Z* and intensity values corresponding to last return were used in this study. The output from the Optech REALM software generates horizontal coordinates (*X*, *Y*) in UTM, and vertical coordinate (*Z*) referenced to ellipsoid WGS84. Since the WGS84 reference frame uses the Earth's center of mass as its origin, ellipsoidal heights (*Z*) of ground points are different from the most often-used orthometric height reference to the geoidal surface. This height is commonly referred to as height above sea level. Therefore, ellipsoidal heights of LiDAR measurements were converted into orthometric heights to detect beach topographic changes. The LiDAR data included subaquaeous measurements to the depth covered by the bathymetric data, providing complete data coverage for both years. For efficient processing, the data were split into quarter-quad tiles. The same tile boundaries were used for both surveys. A buffer with a size of 50 m was created at the boundaries to ensure seamless gridding.

Airborne LiDAR surveys produce a cloud of points with irregular spacing because of the zigzag scanning pattern. It is difficult to compare

beach elevation changes from two different surveys because the horizontal coordinates of data points are not exactly matched directly. Therefore, point data were converted into a grid based digital elevation model (DEM) for topographic comparison. In this study, point elevation data were interpolated into binary raster grids with 1 m cell size using the inverse distance weighted (IDW) algorithm method for each tile with a search radius of 10 m. The root-mean-square error (RMSE) was 0.32 m and 0.24 m for 2000 and 2005 surveys, respectively. Note that the RMSE should not be confused with the accuracy of the LiDAR sensor. Vertical accuracy of LiDAR is approximately ±0.15 m and horizontal accuracy is <1 m (Sallenger et al., 2004).

3.2. Analysis of cross shore morphology

The shorelines of South Padre Island in 2000 and 2005 were generated using a datum-based mean sea level (MSL) line from the respective LiDAR data. Cross-shore profiles were generated using Digital Shoreline Analysis System (DSAS; Thieler et al., 2005) producing shore-perpendicular transects at a spacing of 20 m from the inlet at Port Mansfield to southern extent of the undeveloped island. Elevations were extracted at 1-m intervals along each cross-shore transect, which extended 200 m inland from the shoreline. The dune crest was identified as the point of maximum elevation landward of the dune toe, which was identified as the point of maximum slope change landward of the shoreline. The elevation of the dune crest (D_{high}), or the beach berm in the absence of a dune, and the elevation of the backshore at the dune toe (D_{low}) were extracted from the cross-shore profiles (Fig. 2). The beach width was calculated as the slope distance from MSL to D_{low} and the extent of bar development on the foreshore was calculated as the standard deviation of the detrended profile. While the extent of the LiDAR data for both years extended almost the entire length of the island (2350 profiles; 47 km), this study only examines the northernmost 40 km of shoreline (2000 profiles). The beach and dune system south of the study area have been modified (to varying degrees) by heavy day-use, over-sand vehicles impacts and development in the resort town of South Padre.

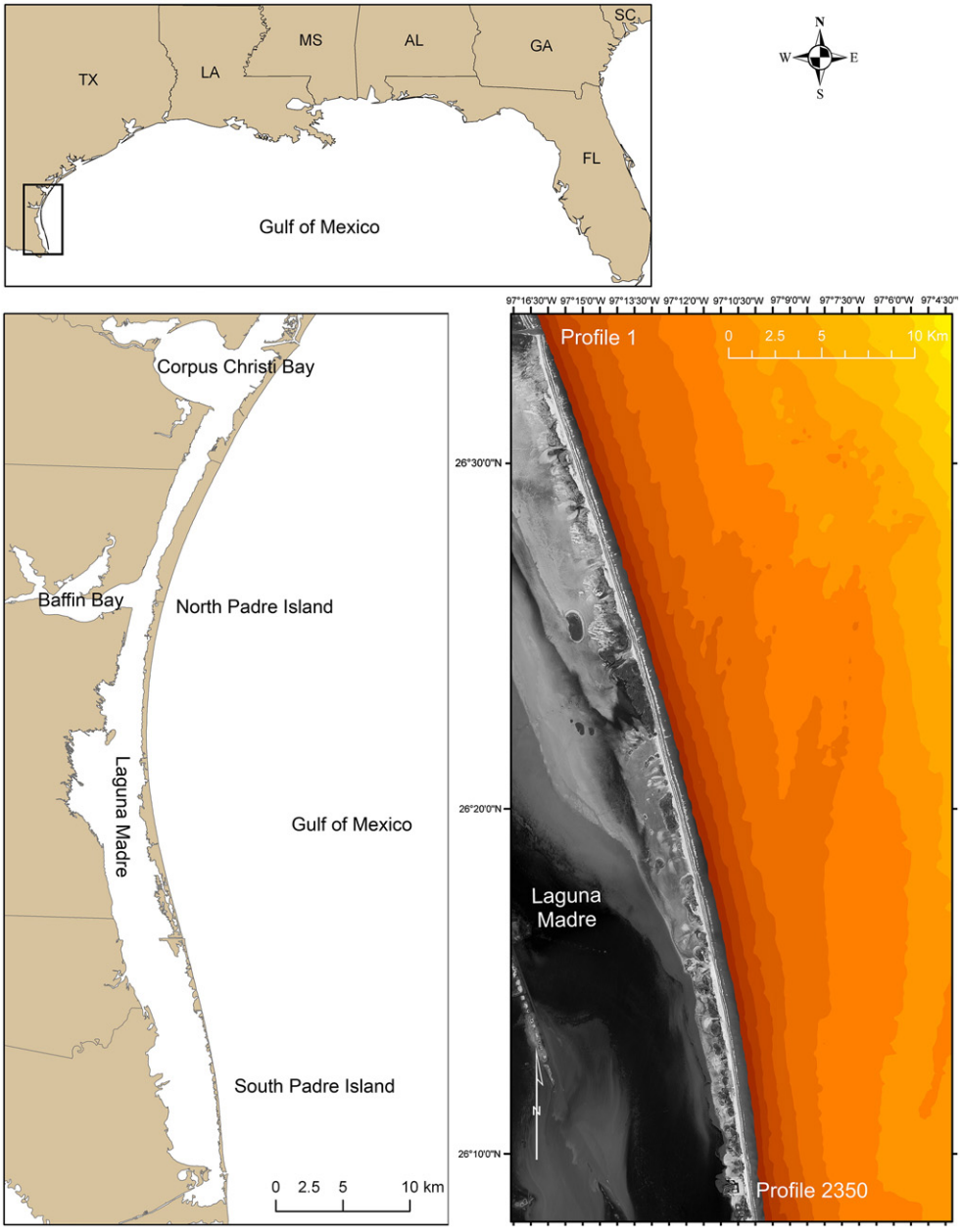


Fig. 1. Location map and satellite image of South Padre Island, Texas showing offshore bathymetry and LiDAR images from 2000 and 2005.

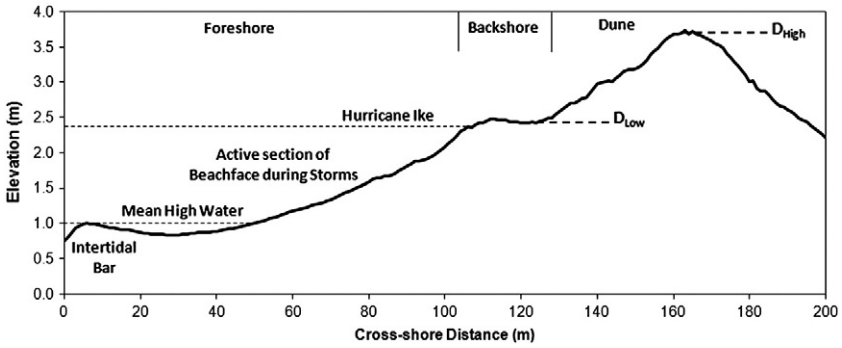


Fig. 2. Representative profile showing morphological features of a typical cross-shore profile including the dune crest (D_{high}), the dune toe (D_{low}), mean high water and the documented elevation of the storm surge during Hurricane Ike (2008), the most recent storm.

3.3. Wave height and period

A commercially available wave model (MIKE21) was used to characterize the alongshore variation in wave activity. The wave climate of South Padre Island is a combination of locally generated wind waves and swells propagating into the region from the Gulf of Mexico. The model accounts for (i) wave propagation in time and space, shoaling, refraction due to current and depth, (ii) wave generation by wind, (iii) wave interactions, (iv) white-capping, bottom friction and depth-induced breaking, and (v) wave-induced set-up. A nested modeling approach was used to produce boundary conditions (both spectral and parametric) for fine grid resolution models. The results of the MIKE21 model provide directional spectra for all boundary points in the study area (on a computational grid), which are then be used to finer scale transformations by the inner-shelf bathymetry. Hourly average wave heights and periods were calculated at 20-m intervals at the 10-m depth contour directly offshore of the cross-shore profiles derived from the LiDAR data. The model was driven by wind speed, direction and wave spectra data from NOAA buoys 42045 and 42020 and tide data from an NOAA tide station on South Padre Island. Buoy 42020 is approximately 74 km northeast of the northern boundary of the study site and Buoy 42045 is approximately 68 east of the southern boundary of the study site. The hourly wave data at each sample point were averaged for the time period between the 2000 and 2005 LiDAR surveys. All available bathymetry data for South Padre Island were obtained from the NOAA Hydrographic Services to create a fine element mesh with nodes at the end of each LiDAR transect.

The wave and bathymetry data are used to calculate the dimensionless ratio used by Wright and Short (1984) and developed by Guza and Inman (1975) to distinguish between beach states:

$$\varepsilon = \frac{2\pi^2 H_b}{gT^2 S^2} \tag{1}$$

where H_b is the breaker height (m), g is acceleration due to gravity, T is the wave period and S is the foreshore slope (Wright and Short, 1984). Dissipative beaches have ratio values <30, while intermediate beaches have ratio values between 30 and 1 with an associated change in morphology from longshore-bar trough to low-tide terrace. Inversely related to the Iribarren number, the surf scaling parameter can be used as a proxy estimate of run-up on the foreshore. However, an estimate of the 2% exceedence level for the run-up (including wave set-up and swash) is calculated following the model of Stockdon et al. (2007):

$$R_2 = 1.1\left(0.35S(H_oL_o)^{1/2} + \frac{\sqrt{H_oL_o(0.563S^2 + 0.004)}}{2}\right) \tag{2}$$

where H_o and L_o are the offshore wave height and length, respectively. This equation does not include variation in water level due to tide or the rise in water due to pressure and wind.

3.4. Wavelet and cross-wavelet analysis

Wavelet analysis is an increasingly used approach to time and spatial series that cannot be assumed to be statistically stationary. While this approach is commonly used to analyze oceanographic data sets (e.g. Farge, 1992; Mak, 1995; Goring and Bell, 1999; Torrence and Webster, 1999; Jevrejeva et al., 2003), it has only been used in a handful of nearshore studies (Short and Trembanis, 2004; Coco et al., 2005; Li et al., 2005; Ruessink et al., 2006). Wavelet analysis quantifies how the spectral signal varies over a range of temporal or spatial scales, rather the overall strength of the signal at specific frequencies as calculated using traditional Fourier analysis. Wavelets are designed to capture the behavior of non-stationary stochastic signals, whereas Fourier spectra provide similar information in the frequency domain, but under the assumption of a stationary signal.

The continuous wavelet transform (W_n^s) is defined as the convolution of the alongshore series (x_n) with a scaled and translated version of the normalized mother wavelet function. The one-dimensional sequence is expanded into a two-dimensional space (n,s) by varying the scale (s) and translating the function along n. As discussed by Torrence and Compo (1998), the complex Morlet mother wavelet provides a similar approximation to the Fourier wavelength ($\lambda = 1.03s$) and is used in this study. To avoid adding an artificial periodicity to the spatial series that is not periodic, the spatial series was padded with zeroes to the next power of two (4096 in the present study). The global wavelet spectrum is calculated by averaging over all local wavelet spectra:

$$\overline{W^2}(s) = \frac{1}{N}\sum_{n=0}^{N-1}\left|W_n(s)\right|^2 \tag{3}$$

A further description on the methodology and interpretation of wavelet analysis is provided by Torrence and Compo (1998).

Cross-wavelet analysis is a bivariate extension of the continuous wavelet transform that compares two series (x_n and y_n) to produce the cross-wavelet spectrum:

$$W_n^{xy}(s) = W_n^x(s)W_n^y(s) \tag{4}$$

The magnitude of the W_n^{xy}, the cross-wavelet power, is the covariance between the series x_n and y_n in (n,s) space. To avoid large power spikes associated with spikes in the individual series, the wavelet squared coherency $R_n^2(s)$ is used instead of the simple cross-wavelet

transform. The coherency is similar to the squared correlation coefficient, in which $R_n^2(s)=1$ is obtained for a perfect linear relationship between the series and $R_n^2(s)=0$ represents no correlation. The coherency phase difference $\phi_n(s)$ is calculated as:

$$\phi_n = \tan^{-1}\left[\frac{I\left(S\left(s^{-1}W_n^{xy}(s)\right)\right)}{R\left(S\left(s^{-1}W_n^{xy}(s)\right)\right)}\right] \quad (5)$$

where I and R are the imaginary and real parts of the cross-wavelet transform, respectively. The phase difference describes the spatial lag between the series for a given longshore distance (n) and scale (s). There is a potential for strong power when only one variable exhibits a strong variation at a given scale. To avoid this problem, only those length scales in which there is power in both variables, a statistically significant coherence (relative to white noise), and a consistent phase relationship will be considered as exhibiting a discrete covariance.

4. Results

South Padre Island exhibits considerable variability in dune morphology alongshore, ranging from well-developed foredunes with crest elevations approaching 12 m above sea level, to washover channels completely devoid of vegetation that extend to the back-barrier shoreline at a maximum elevation of just over 1 m in 2000. The washover channels were re-occupied by Tropical Depression Bertha (2002), Hurricane Claudette (2003) and Hurricane Emily (2005) between the 2000 and 2005 LiDAR surveys. Despite erosion of the beachface and backshore and a shoreline retreat of ~27 m, the foredune height increased over most of the study area and washover was limited to the pre-existing channels. The histograms for D_{high} presented in Fig. 3 show an increase in the elevation of the washover channels (D_{high} ~1.5 m) and for the mid-range of dune elevations (5.5 to 8.5 m). The increase in D_{high} elevations is inversely correlated with the shoreline retreat and the volume of sediment lost from the foreshore and backshore. The washover channels experienced a net gain of sediment (as overwash), while the mid-elevation dunes gained in height but not enough to balance the loss of profile volume that reached a maximum with the largest dunes. A z-test for difference of means suggests that there was a statistically significant increase in dune height between 2000 and 2005 at the 95% confidence level. The increase in dune height is associated with a relatively small (~0.5 m) accumulation of sediment in the vicinity of the dune crest, particularly for dune with heights greater than 5 m.

The morphology of the beachface for both years was ensemble-averaged based on the backshore elevation (D_{low}) and normalized by beach width. While the lower swash bar is a common feature across the entire range of profiles, it is not visible in the profiles from 2005 (Fig. 4). In both surveys, the average elevation of the dune toe, and the height and number of bars increases with increasing dune height. The presence of distinct bar-like features in the average profiles suggests that there is a degree of similarity in the position of the bars and backshore deposits between profiles of similar dune height in different sections of the study area. The relationship between foredune height classes, the elevation of the backshore (D_{low}) and the standard deviation of the foreshore profile are presented in Fig. 5a. The loss in backshore elevation between 2000 and 2005 resulted from erosion of the foreshore and scarping of the dune. While it is reasonable to expect that some of the sediment would have been deposited in the inner nearshore as a bar, the standard deviation for the 2005 profiles, a surrogate for supratidal bars and berms, suggests that most sediment was lost offshore or deposited as washover in the low elevation sections of the island. Despite storm erosion of the beachface and backshore, the largest dunes in both years were associated with the largest supratidal volume (Fig. 5b) and width (Fig. 5c). The supratidal volume increases over the entire range of dune heights in response to the increase in backshore elevation, while the supratidal width increases by only 8 m for dunes with heights greater than 5 m.

The shelf bathymetry fronting the barrier island is not uniform alongshore. Transverse ridges extend to the NNW (10°) or about 40° off the shoreline with an apparently regular spacing. Based on studies from the Outer Banks (McNinch and Luettich, 2000; McNinch, 2004; Schupp et al., 2006) and Dundrum Bay, Northern Ireland (Cooper and Navas, 2004), it is hypothesized that these bathymetric features affect the wave energy incident to the coast through attenuation, and refraction and diffraction. While these transverse features are only a couple of meters in height and the foreshore slope only varies between 0.06 and 0.08, the combination of slope and wave focusing is responsible for a cyclical variation in the surf similarity parameter (Fig. 6a) between an intermediate beach state ($\varepsilon \approx 20$)and a dissipative beach state ($\varepsilon \approx 35$). Regression analysis suggests that 67% of the variation in the surf similarity parameter is associated with the foreshore slope ($p<0.001$), and that the alongshore variation in wave height accounts for 31% of the variation ($p<0.001$). Based on Eq. (2), the alongshore variation in wave height and foreshore slope is responsible for an alongshore variation in run-up that would be in addition to the tide and the surge resulting from the wind and atmospheric pressure. The time-averaged run-up varies between 0.68 m for the more intermediate sections of the island and 0.52 m for the more dissipative sections. Despite the small difference in the time-averaged run-up, the addition of the run-up to the mean high water results in a significant variation in the width of foreshore and a simple estimate of the available fetch for aeolian transport (Fig. 6b). The available fetch is at a local maximum in the more intermediate sections of the beach, where the elevation of the

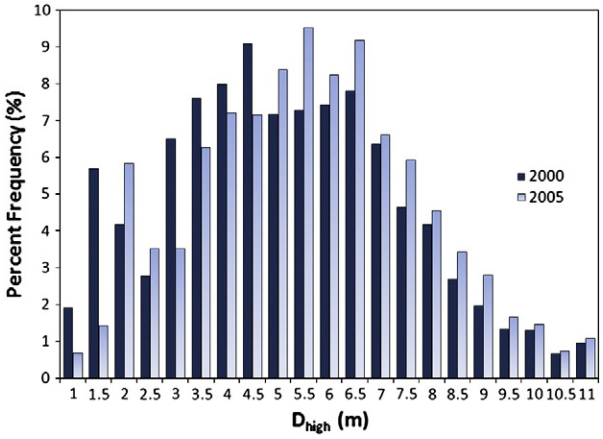


Fig. 3. Histograms of dune height ($D_{high}-D_{low}$) for 2000 and 2005.

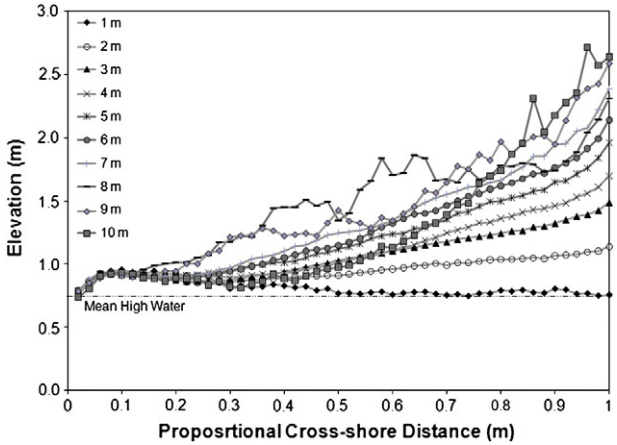


Fig. 4. Ensemble-averaged beachface profile normalized by distance between shoreline and dune toe (D_{low}). Profiles were ensemble-averaged based on foredune or berm height ($D_{high}-D_{low}$) in 1 m bins.

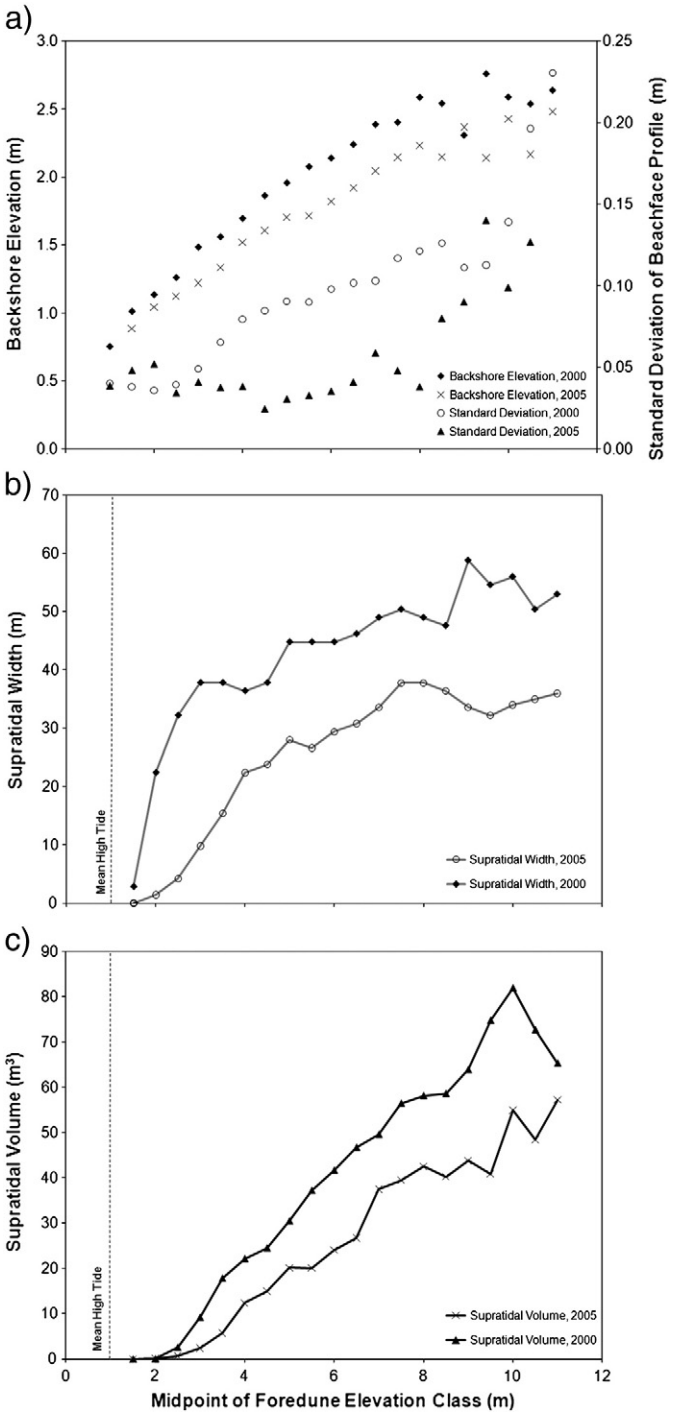


Fig. 5. (a) Ensemble-averaged elevation of the backshore (D_{low}) and the standard deviation of the detrended foreshore profile in 1-m bins of foredune height ($D_{high} - D_{low}$) for 2000 and 2005. Also shown are the ensemble-averaged (b) supratidal volume and (c) supratidal width for both years.

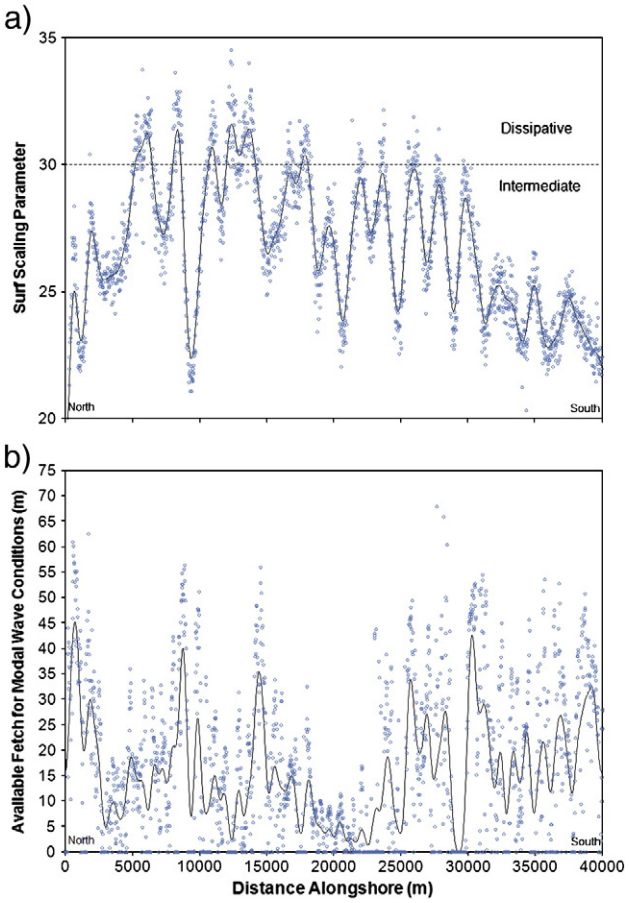


Fig. 6. Spatial series of (a) the surf scaling parameter (ε) and (b) the available aeolian fetch length of the foreshore based on the modal wave conditions (between 2000 and 2005) and the LiDAR data for 2005. Shown are the individual transect values and a 50-point Hamming smoothing function.

backshore is also at a local maximum. In contrast, the lower run-up elevations predicted for the more dissipative areas are capable of inundating a large part of the beach and even reoccupy the lowest elevation washover conduits. The variation in beach width is not a response to an alongshore variation in shoreline retreat as observed by Houser et al. (2008), but rather reflects an alongshore variation in the volume and elevation of the beachface and backshore, respectively. The average shoreline retreat between 2000 and 2005 was 27 m and was not statistically significant different over the range of dune heights at the 95% confidence level.

4.1. Wavelet and cross-wavelet analysis

The alongshore variation in D_{high}, D_{low}, foredune height ($D_{high} - D_{low}$), beach width, and standard deviation of the foreshore, are presented in Fig. 7. The variables exhibit considerable variability alongshore over a range of different length scales, but with a visually dominant variation at a length scale of over 2000 m that reflects the average spacing between washover channels. The surf scaling parameter varies by over 10 at the 2000-m length scale, which is half of the total variation between 20 (intermediate) at the north and south ends of the island to 35 (dissipative) near the center of the study area. Although visually dominant in each of the spatial series, the local and global wavelets (Fig. 8) suggest that there is also a small but significant variation at a length scale of ~1300 m. These 'high-frequency' variations are superimposed on lower frequency (regional) variations at length scales of ~5300 m and ~8200 m. The presence of common length scales in the wavelet data suggests that the beach–dune system of South Padre Island exhibits a characteristic alongshore pattern/interaction that can be quantified. Due to the uniform shoreline change and increase in dune heights between 2000 and 2005, the identified length scales are visible in the LiDAR data for both years, which suggests that these alongshore patterns and relationships are forced.

The alongshore coherency and phase between foredune height and the other variables at the above length scales is quantified using cross-wavelet analysis and the results are presented in Table 1. The

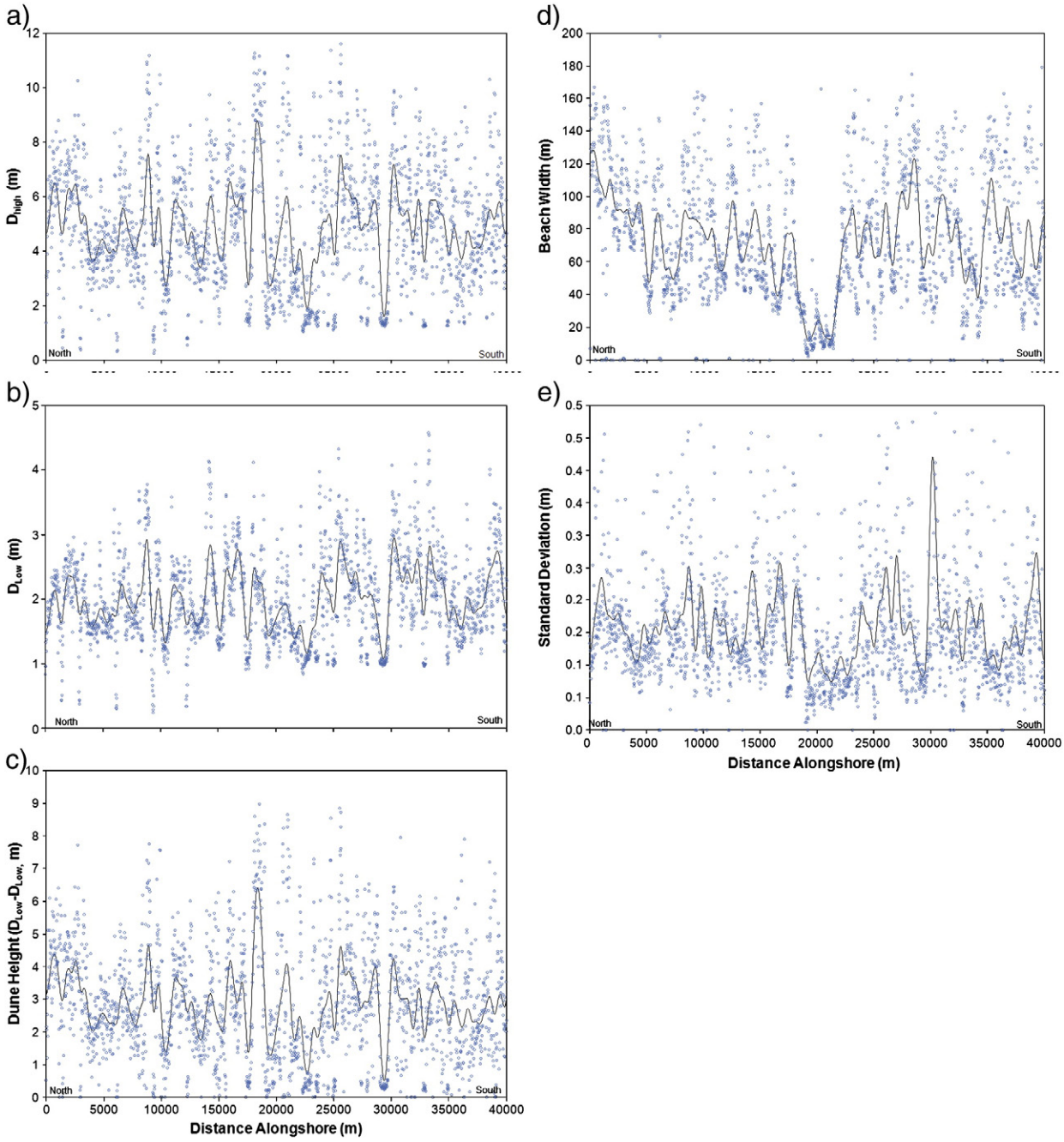


Fig. 7. Spatial series of (a) D_{high}, (b) D_{low}, (c) dune height, (d) beach width, and (e) standard deviation of the foreshore profile.

foredune height exhibits statistically significant coherence with the other variables at 1300 and 2300 m length scales, but only D_{high}, D_{low}, surf similarity and depth at 50 m offshore at the 5300- and 8200-m length scales. At the 5300- and 8200-m length scales, the foredune height is in phase ($\phi(\pi) = 0.09$ to 0.16) with D_{high} with the largest crest and backshore elevations ~100 and 328 m south of the largest dunes respectively. At the 1300- and 2300-m length scales, the foredune height are in phase (± 40 m alongshore) with D_{high}, D_{low}, the standard deviation of the foreshore and the available width of foreshore. The alongshore coherence of dune height, D_{low} and foreshore standard deviation suggests that sediment accretion in the backshore and dune is the result of a similar process. While fetch models suggest that dune height is dependent on the width of the beach, dune height and backshore elevation are out-of-phase with beach width, which is at a minimum in front of the largest dunes and approaches a maximum at the washover channels. Rather, dune height and backshore elevation appear to be dependent on the beach state. Specifically, they are ~440 m ($\phi(\pi) \approx -1.14$) out of phase with the dissipative areas of the coast, or ~170 m north of the less dissipative (intermediate) sections of the coast at the 1300-m length scale. A similar pattern is observed at the 2300-m length scale, where the local maxima in dune height are ~658 m south of the dissipative areas ($\phi(\pi) \approx -1.12$) or ~481 m north of intermediate sections.

At all length scales, the largest dunes are positioned approximately a third of the distance between the more dissipative and intermediate beach states ($\phi(\pi) \approx -1.12$ to -1.20). While the surf scaling parameter is partly dependent on the offshore bathymetry through foreshore slope (S), it is not necessarily in phase with the transverse ridges on the inner shelf. To examine the role of the transverse ridges, the depth at 50 m from the shoreline was extracted from the bathymetry data and compared to the alongshore variation in foredune height and the surf similarity parameter. The trough between transverse ridges is ~125 m ($\phi(\pi) \approx -0.38$) and 300 m ($\phi(\pi) \approx -0.52$) south of the largest dunes, at the 1300- and 2300-

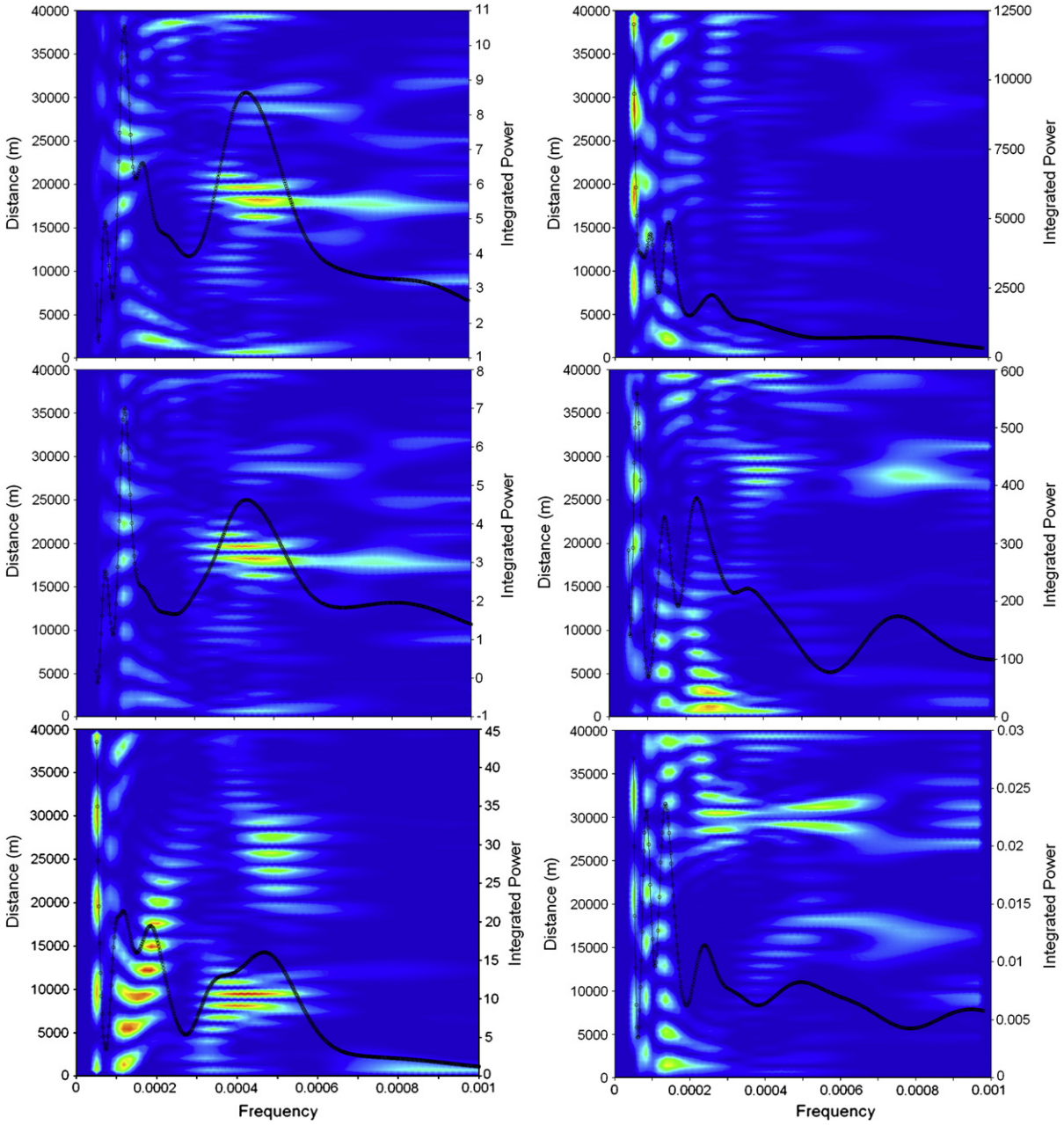


Fig. 8. Local and global wavelets for (a) D_{high}, (b) D_{low}, (c) dune height, (d) beach width, (e) standard deviation of the foreshore profile and (f) surf scaling parameter (ε).

m length scales, respectively. In this respect, the washover channels and areas with limited dune development are 125 and 300 north of the transverse ridges, respectively, and 170 and 481 m north of the most dissipative sections of the coast. The wave height is in-phase with the surf similarity parameter at both length scales, suggesting that the variation in beach state and the location of the washover conduits are a consequence of wave focusing through refraction over the transverse ridges, further suggesting that the alongshore variation in the surf similarity parameter is a response to both the foreshore slope and the variation in wave height.

5. Discussion

The impact of an extreme storm on a barrier island and the rate of island transgression depend on the relative elevation of the storm surge to the height of the foredune. This simple two-dimensional model is complicated by considerable variability in foredune height alongshore over a range of spatial scales. Ultimately, the height of a dune depends on the frequency of storm events that erode and overwash the dune, relative to the rate at which sediment is returned to the backshore and dune since the last storm. The recovery depends on the extent of storm damage and the availability of sediment from nearshore sources to be transported by the wind from the beach and backshore to the dune. In this respect, variations in dune height at both regional and local scales are a reflection of similar scale changes in the supply of sediment and the competence of the wind for transport. The Short and Hesp (1982) model suggests that supply and transport potential are at a maximum on dissipative beaches and are at a minimum on reflective beaches. The correspondence of transport potential and sediment supply is supported by Houser and Hamilton (2009) in their examination of a reflective to intermediate beach ($\bar{\varepsilon}$= 5.6), but is not supported in the present study of beach–dune interaction on South Padre Island, which has an intermediate to dissipative beach ($\bar{\varepsilon}$ = 26.8). Local peaks in dune height ($D_{high} - D_{low}$) on Padre Island are found midway between the intermediate and dissipative sections of the coast (from south to

Table 1
Statistically significant coherency and phase relationship of foredune height ($D_{high} - D_{low}$) with D_{high}, D_{low}, beach width, standard deviation of the foreshore, the surf scaling parameter, the available fetch for the time-averaged run-up and the depth at 50 m from the shoreline. A negative phase relationship indicates that the largest dunes are (locally) south of the other variables.

	1300 m		2300 m		5300 m		8200 m	
	b_{xy}	$\phi(\pi)$	b_{xy}	$\phi(\pi)$	b_{xy}	$\phi(\pi)$	b_{xy}	$\phi(\pi)$
D_{high}	0.96	−0.08	0.97	−0.02	0.93	−0.09	0.98	−0.16
D_{low}	0.70	−0.07	0.73	−0.07	0.57	−0.52	–	–
Beach Width	0.34	−1.90	0.30	−1.77	–	–	–	–
St. Deviation	0.51	−0.06	0.57	−0.03	–	–	–	–
Surf Similarity	0.43	−1.14	0.45	−1.12	0.38	−1.10	0.33	−1.21
Fetch	0.61	−0.06	0.65	−0.05	–	–	–	–
Depth at 50 m	0.42	−1.20	0.43	−1.15	0.39	−1.12	0.36	−1.20

north), where the development of storm-generated intertidal bars and the backshore elevation are at a maximum. This characterization of beach–dune interaction is dependent on the consistency of the patterns observed in both the 2000 and 2005 LiDAR data that appear to be forced by the transverse ridges on the inner shelf. Once formed, and in the absence of complete inundation and total loss of all dunes (Sallenger, 2000), washover and erosion are largely dependent on the pre-existing dune morphology and, thereby, reinforce the alongshore variation (Houser et al., 2008; Houser and Hamilton, 2009). This may not hold in environments where the beach and dune system are not geologically forced, although Stallins and Parker (2003) suggest that variations in the vegetation burial can create a complex feedback in which storm response and recovery are further reinforced.

The variation in beach and dune morphology appears to be directly forced by wave refraction over the inner-shelf bathymetry, which exhibits statistically significant variations at length scales of 1300, 2300 and 8200 m. This is consistent with a growing body of literature in which localized coastal response is shown to be forced by wave refraction by offshore features (Demarest and Leatherman, 1985; Kraft et al., 1987; Pilkey et al., 1993; Riggs et al., 1995; Schwab et al., 2000; McNinch, 2004; Browder and McNinch, 2006; Schupp et al., 2006; Stockdon et al., 2007; Houser et al., 2008; Houser and Hamilton, 2009). While the geologic framework responsible for the transverse ridges off South Padre Island is beyond the scope of this paper, the results of this study suggest that the beach–dune interaction on this island is also geologically forced. The phase relationship between the offshore ridges and the inshore wave height at all length scales suggests that the waves are refracted and focused immediately south of where the foreshore slope is at a local minimum. The inshore wave height is predicted to reach a local minimum south of areas with a steeper foreshore slope and in the lee of the northeast-trending ridges. If the variation in beach and dune morphology was simply the result of past storm impact and the alongshore variation in surge height, then the washover channels should be found where the combined inshore wave height and the surf scaling factor are at a maximum (with a phase of 0). Rather, the washover channels are ~170 and 480 m north of the most dissipative sections of the coast at the 1300- and 2300-m length scales, respectively. The lack of in-phase relationship suggests that the position of the channels reflects the ability of the dunes (or lack thereof) to develop and recover in height following a storm and not the storm surge potential. Once formed, this alongshore pattern would be reinforced by subsequent storms; the impact would be less and recovery faster in the areas with the largest dunes compared to washover and inundation in the washover channels.

Dune recovery following a storm depends first on the welding of nearshore bar to the foreshore and the expansion of the backshore. The newly deposited sediment on the foreshore and in the backshore is then transported into the dune by winds above the entrainment threshold. In this respect, the recovery of a dune is limited by both the availability of sediment and the competency of the wind. According to Short and Hesp (1982), transport potential is greatest on dissipative beaches where the wide, gently sloped foreshore allows for boundary development and the maximum fetch. As noted, the most gently sloped and widest beaches on South Padre Island are in-phase with the washover channels, while the largest dunes tend to be fronted by a foreshore that is relatively steep and short. However, run-up during storm winds inundates more of the gently sloped foreshore in the more dissipative areas and may even reoccupy the lowest elevation washover conduits. In the presence of storm waves and wind, the available fetch is at a local maximum in the more intermediate sections of the island due to the higher elevations of the upper-foreshore and backshore. Not only does the larger fetch mean that the transport potential is at a maximum, a higher elevation backshore will contain a greater volume of sediment that will not be limited by presence of moisture (e.g. Yang and Davidson-Arnott, 2005; Davidson-Arnott et al., 2005; Bauer et al., 2009; Anthony et al., 2009) and shell lag deposits. In this respect, the alongshore variation in dune height results from the correspondence of the available sediment supply on the foreshore and in the backshore, and the transport potential. Since the fetch length is dependent on the elevation of the backshore, it is reasonable to argue that the primary control on dune development on South Padre is the availability of sediment rather than transport potential (cf. Jackson and Cooper, 1999). Moreover, the increase in available fetch with increasing dune height is relatively minor compared to the increase in the amount of sediment readily available for aeolian transport. In this respect, the availability of transportable sediment on the foreshore and in the backshore appears to be the primary constraint on sediment delivery on intermediate and dissipative beaches. In contrast, dunes on intermediate to reflective beaches, such as those in northwest Florida (Houser and Hamilton, 2009), are limited by the transport potential and not by the available supply of sediment.

Consistent with the beach–dune models of Pye (1990) and Psuty (1993) dune growth was observed in response to beachface erosion and shoreline retreat, but these models are unable to account for the alongshore variation in dune height. The alongshore variation is also not consistent with the Short and Hesp (1982) model, which suggests larger dunes backing the more dissipative parts of the coast. In general and between different coastal regions, it is reasonable to expect larger dunes in dissipative environments that are characterized by storm winds and more sediment compared to reflective beaches. The results of this study suggest that intra-site variability in dune height depends on the alongshore correspondence of sediment supply and transport potential, which varies with the beach state. In this respect, the beach–dune interaction models described in this study and that of Houser and Hamilton (2009) reflect a different balance between transport and supply limitations alongshore. Dissipative beaches are limited by the availability of sediment on beach and in the backshore, while more reflective beaches are transport limited as a result of the steeper foreshore. While intermediate beaches, have both transport and supply in bars and in the backshore, they are potentially limited by their more dynamic nature and the greater potential for erosion of the dune base. Further study, particularly at the process-scale is need to characterize the relative importance of transport and supply limitations over a range of beach profiles.

6. Conclusions

The results of this study suggest that the alongshore variation in dune morphology is a reflection of the alongshore correspondence between transport potential and sediment availability. The largest dunes on South Padre Island are not found where the beach is wide and gently sloped, but rather are found in the vicinity of an intermediate beach with a larger supply of sediment in the backshore and on the foreshore. The higher elevation of the backshore fronting the largest dunes also limits inundation by run-up and surge, thereby maintaining the transport potential during storm winds. The greater elevation of the

backshore during storms means that the sediment within these areas will not be less likely to be limited by moisture and lag deposits. In this respect, the largest dunes are found where the backshore sediment is relatively unlimited and the transport potential is also at a maximum. Since both the available sediment supply and the transport potential are dependent on the backshore volume, it is argued that alongshore variations in sediment supply forced by the transverse ridges are the primary control on beach and dune interaction at South Padre Island. When combined with the recent results of Houser and Hamilton (2009), it is further argued that dune development on intermediate to dissipative beaches is largely limited by the availability of sediment rather than the transport potential, in contrast to reflective and intermediate beaches that have a readily available supply of sediment but limited transport potential.

Acknowledgements

This work was supported in part by the National Science Foundation under award number GSS-0920851, and by the National Park Service under contract number J5320 08 001. The authors would like to thank Tiffany L. Caudle and Reuben Reyes from Bureau of Economic Geology, University of Texas at Austin for providing access to the raw LiDAR data.

References

Aagaard, T., Davidson-Arnott, R., Greenwood, B., Nielsen, J., 2004. Sediment supply from shoreface to dunes: linking sediment transport measurements and long-term morphological evolution. Geomorphology 60, 205–224.
Anthony, E.J., Ruz, M.-H., Vanhée, S., 2009. Aeolian sand transport over complex intertidal bar-trough beach topography. Geomorphology 105, 95–105.
Arens, S.M., 1996. Patterns of sand transport on vegetated foredunes. Geomorphology 17, 339–350.
Bauer, B.O., Davidson-Arnott, R.G.D., 2003. A general framework for modeling sediment supply to coastal dunes including wind angle, beach geometry, and fetch effects. Geomorphology 49, 89–108.
Bauer, B.O., Davidson-Arnott, R.G.D., Hesp, P.A., Namikas, S.L., Ollerhead, J., Walker, I.J., 2009. Aeolian sediment transport on a beach: surface moisture, wind fetch and mean transport. Geomorphology 105, 106–116.
Browder, A.G., McNinch, J.E., 2006. Linking framework geology and nearshore morphology: correlation of paleo-channels with shore-oblique sandbars and gravel outcrops. Marine Geology 231, 141–162.
Christiansen, M.B., Davidson-Arnott, R., 2004. Rates of landward sand transport over the Foredune at Skallingen, Denmark and the role of dune ramps. Geografisk Tidsskrift-Danish Journal of Geography 104, 31–43.
Coco, G., Bryan, K.R., Green, M.O., Ruessink, B.G., van Enckevort, I.M., Turner, I.L., 2005. Video observations of shoreline and sandbar coupled dynamics. Proceedings of Coasts and Ports: Coastal Living- Living Coast, Australasian Conference 2005, Australia, pp. 471–476.
Cooper, J.A.G., Navas, F., 2004. Natural bathymetric change as a control on century-scale shoreline behavior. Geology 32, 513–516.
Davidson-Arnott, R.G.D., MacQuarrie, K., Aagaard, T., 2005. The effect of wind gusts, moisture content and fetch length on sand transport on a beach. Geomorphology 68, 115–129.
Demarest, J.M., Leatherman, S.P., 1985. Mainland influence on coastal transgression—Delmarva Peninsula. Marine Geology 63, 19–33.
Elko, N.A., Sallenger, A.H., Guy, K., Morgan, K.L.M., 2002. Barrier island elevations relevant to potential storm impacts; 2, South Atlantic. U.S. Geologic Survey Open-File Report 2002-208, 1 folded sheet.
Farge, M., 1992. Wavelet transforms and their applications to turbulence. Annual Review of Fluid Mechanics 24, 395–458.
Goring, D.G., Bell, R.G., 1999. El Nino and decadal effects on sea-level variability in northern New Zealand: a wavelet analysis. New Zealand Journal of Marine and Freshwater Research 33, 587–598.
Guza, R.T., Inman, D.L., 1975. Edge waves and beach cusps. Journal of Geophysical Research 80, 2997–3012.
Hesp, P.A., 1988. Foredune morphology, dynamics and structures. Journal of Sedimentary Geology Special Issue: Aeolian Sediments 55, 17–41.
Hesp, P.A., Davidson-Arnott, R., Walker, I.J., Ollerhead, J., 2005. Flow dynamics over a foredune at Prince Edward Island, Canada. Geomorphology 65, 71–84.
Hotta, S., Kubota, S., Katori, S., Horikawa, K., 1985. Sand transport by wind on a wet sand surface. Proceedings of the Coastal Engineering Conference, pp. 1265–1281.
Houser, C., Hamilton, S., 2009. Sensitivity of post-hurricane beach and dune recovery to event frequency. Earth Surface Processes and Landforms 34, 613–628.
Houser, C., Hapke, C., Hamilton, S., 2008. Controls on coastal dune morphology, shoreline erosion and barrier island response to extreme storms. Geomorphology 100, 223–240.
Hunter, R.E., Richmond, B.M., 1988. Daily cycles in coastal dunes. Sedimentary Geology 55, 43–67.
Jackson, D.W.T., Cooper, J.A.G., 1999. Beach fetch distance and aeolian sediment transport. Sedimentology 46, 517–522.
Jevrejeva, S., Moore, J.C., Grinsted, A., 2003. Influence of the Arctic Oscillation and El Niìfo-Southern Oscillation (ENSO) on ice conditions in the Baltic Sea: the wavelet approach. Journal of Geophysical Research D: Atmospheres 108 ACL 10-1-ACL 10-11.
Kraft, J.C., Chrzastowski, M.J., Belknap, D.F., Toscano, M.A., Fletcher, C.H., 1987. The transgressive barrier-lagoon coast of Delaware: morphostratigraphy, sedimentary sequences and responses to relative rise in sea level. In: Nummedal, D., Pilkey, O.H., Howard, J.D. (Eds.), Sea-Level Fluctuation and Coastal Evolution Society of Economic Paleontologists and Mineralogists, Tulsa, Oklahoma, pp. 129–143.
Li, Y., Lark, M., Reeve, D., 2005. Multi-scale variability of beach profiles at duck: a wavelet analysis. Coastal Engineering 52, 1133–1153.
Lettau, K., Lettau, H.H., 1978. Experimental and micrometeorological studies of dune migration. In: Lettau, K., Lettau, H.H. (Eds.), Exploring the World's Driest Climate. University of Wisconsin Institute of Environmental Sciences, Madison, Wisconsin, pp. 110–147.
Lynch, K., Jackson, D.W.T., Cooper, J.A.G., 2006. A remote-sensing technique for the identification of aeolian fetch distance. Sedimentology 53, 1381–1390.
Mak, M., 1995. Orthogonal wavelet analysis: interannual variability in the sea surface temperature. Bulletin of the American Meteorological Society 76, 2179–2186.
Mathewson, C.C., Minter, L.L., 1976. Impact of water resource development on coastal erosion, Brazos River, Texas. Texas A&M University, Texas Water Resources Institute: Tech. Rept., 77, p. 85.
McKenna Neuman, C., 1998. Particle transport and adjustments of the boundary layer over rough surfaces with an unrestricted, upwind supply of sediment. Geomorphology 25, 1–17.
McNinch, J.E., 2004. Geologic control in the nearshore: shore-oblique sandbars and shoreline erosional hotspots, Mid-Atlantic Bight, USA. Marine Geology 211, 121–141.
McNinch, J.E., Luettich Jr., R.A., 2000. Physical processes around a cuspate foreland: implications to the evolution and long-term maintenance of a cape-associated shoal. Continental Shelf Research 20, 2367–2389.
Morton, R.A., 2002. Factors controlling storm impacts on coastal barriers and beaches: a preliminary basis for near real-time forecasting. Journal of Coastal Research 18, 486–501.
Morton, R.A., Pieper, M.J., 1975. Shoreline changes on Brazos Island and South Padre Island (Mansfield Channel to Mouth of the Rio Grande). An Analysis of Historical Changes of the Texas Gulf Shoreline: Univ. Texas, Bur. Econ. Geology, Geol. Circ., 75(2), p. 39.
Morton, R.A., Paine, J.G., Gibeaut, J.C., 1994. Stages and durations of post-storm beach recovery, Southeastern Texas Coast, U.S.A. Journal of Coastal Research 10, 884–908.
Nickling, W.G., Neuman, C.M., 1995. Development of deflation lag surfaces. Sedimentology 42, 403–414.
Nordstrom, K.F., Jackson, N.L., 1992. Effect of source width and tidal elevation changes on aeolian transport on an estuarine beach. Sedimentology 39, 769–778.
Pilkey, O.H., Young, R.S., Riggs, S.R., Sam Smith, A.W., Wu, H., Pilkey, W.D., 1993. The concept of shoreface profile of equilibrium: a critical review. Journal of Coastal Research 9, 255–278.
Psuty, N.P., 1993. Foredune morphology and sediment budget, Perdido Key, Florida, USA. Geological Society, London, Special Publications 72, 145–157.
Pye, K., 1990. Physical and human influences on coastal dune development between the Ribble and Mersey estuaries, northwest England. In: K.F. Nordstrom, N.P. Psuty and R.W.G. Carter, Editors, Coastal Dunes: Form and Process, Wiley, Chichester (1990), pp. 339–359.
Riggs, S.R., Cleary, W.J., Snyder, S.W., 1995. Influence of inherited geologic framework on barrier shoreface morphology and dynamics. Marine Geology 126, 213–234.
Ruessink, B.G., Coco, G., Ranasinghe, R., Turner, I.L., 2006. A cross-wavelet study of alongshore nonuniform nearshore sandbar behavior. IEEE International Conference on Neural Networks—Conference Proceedings, pp. 4310–4317.
Sallenger Jr., A.H., 2000. Storm Impact Scale for Barrier Islands. Journal of Coastal Research 16, 890–895.
Sallenger, A., Wright, C.W., Guy, K., Morgan, K., 2004. Assessing storm-induced damage and dune erosion using airborne lidar: Examples from Hurricane Isabel. Shore and Beach 72, 3–7.
Sarre, R.D., 1989. Aeolian sand drift from the intertidal zone on a temperate beach: potential and actual rates. Earth Surface Processes and Landforms 14, 247–258.
Saye, S.E., van der Wal, D., Pye, K., Blott, S.J., 2005. Beach–dune morphological relationships and erosion/accretion: an investigation at five sites in England and Wales using LIDAR data. Geomorphology 72, 128–155.
Schupp, C.A., McNinch, J.E., List, J.H., 2006. Nearshore shore-oblique bars, gravel outcrops, and their correlation to shoreline change. Marine Geology 233, 63–79.
Schwab, W.C., Thieler, E.R., Allen, J.R., Foster, D.W., Swift, B.A., Denny, J.F., 2000. Influence of inner-continental shelf geologic framework on the evolution and behavior of the barrier-island system between fire island inlet and Shinnecock Inlet, Long Island, New York. Journal of Coastal Research 16, 408–422.
Sherman, D.J., Jackson, D.W.T., Namikas, S.L., Wang, J., 1998. Wind-blown sand on beaches: an evaluation of models. Geomorphology 22, 113–133.
Shideler, G.L., Smith, K.P., 1984. Regional variability of beach and foredune characteristics along the Texas Gulf Coast barrier system. Journal of Sedimentary Research 54, 507–526.
Short, A.D., Hesp, P.A., 1982. Wave, beach and dune interactions in southeastern Australia. Marine Geology 48, 259–284.
Short, A.D., Trembanis, A.C., 2004. Decadal scale patterns in beach oscillation and rotation Narrabeen beach, Australia—time series, PCA and wavelet analysis. Journal of Coastal Research 20, 523–532.
Stallins, J.A., Parker, A.J., 2003. The influence of complex systems interactions on barrier island dune vegetation pattern and process. Annals of the Association of American Geographers 93, 13–29.
Stockdon, H.F., Sallenger, A.H., Holman, R.A., Howd, P.A., 2007. A simple model for the spatially-variable coastal response to hurricanes. Marine Geology 238, 1–20.

Thieler, E.R., Young, R.S., 1991. Quantitative evaluation of coastal geomorphological changes in South Carolina after Hurricane Hugo. Journal of Coastal Research 8, 187–200.
Thieler, E.R., Martin, D., Ergul, A., 2005. Digital Shoreline Analysis System (DSAS) version 3.0—An ArcGIS extension for calculating shoreline change: U.S. Geological Survey Open-File Report 03-076.
Torrence, C., Compo, G.P., 1998. A practical guide to wavelet analysis. Bulletin of the American Meteorological Society 79, 61–78.
Torrence, C., Webster, P.J., 1999. Interdecadal changes in the ENSO-monsoon system. Journal of Climate 12, 2679–2690.
Wiggs, G.F.S., Baird, A.J., Atherton, R.J., 2004. The dynamic effects of moisture on the entrainment and transport of sand by wind. Geomorphology 59, 13–30.
Wright, L.D., Short, A.D., 1984. Morphodynamic variability of surf zones and beaches: a synthesis. Marine Geology 56, 93–118.
Yang, Y., Davidson-Arnott, R.G.D., 2005. Rapid measurement of surface moisture content on a beach. Journal of Coastal Research 21, 447–452.
Yu, T.-W., Wagner, N.Y., 1970. Diurnal variation of onshore wind speed near a coastline. Journal of Applied Meteorology 9, 760–766.

Progress in Physical Geography 33(6) (2009) pp. 733–746

Synchronization of transport and supply in beach-dune interaction

Chris Houser*

Department of Geography, Texas A&M University, College Station, Texas 77843-3147, USA

Abstract: This review considers the role of nearshore processes and morphological change as a flexible and dynamic constraint on the supply and transport of sediment between beach and dune. It is argued that the lack of information in this regard remains a central barrier to the development of a theory of beach-dune interaction that can be translated across scales and between field sites. Existing beach-dune models do not consider how and when sediment gets transferred to the backshore where it becomes available for transport by wind. Rather, existing models largely ascribe regional variations in dune morphology to fixed constraints on beach slope and sediment budget, without explicit recognition of processes involved. Recent (process-scale) transport studies have shown that the transfer of sediment is both spatially variable and temporally intermittent as a result of transport limitations across the beachface. While these studies have identified varied controls on sediment transport and exchange, there remains a limited capacity to predict the evolution of beach-dune systems, largely because the beachface tends to be viewed as a static transport surface without regard to supply or to the changing limits to transport. Following storm erosion, dune recovery first requires that the beach recovers through the onshore migration and welding of nearshore bars, followed by accretion in the backshore to create a supply of sediment for transport by the wind. The dependence of dune recovery on the synchronization of transport events with the recovery of sediment supply in the backshore creates a strong asymmetry in dune recovery that makes barrier island susceptible to widespread erosion and breaching if a change in the frequency or grouping of storm events is capable of resetting the bar system (offshore) before the next extreme storm.

Key words: beach, dune, sediment supply, synchronization.

I Introduction

Barrier islands and spits have become an important part of the cultural and economic landscape throughout much of the world, and development to support recreation and navi-gation has in turn become a dominant factor in barrier island landscape change (Meyer-Arendt, 1990; Ehlers and Kunz, 1993; Nordstrom, 2000). Most barrier islands and spits are in a state of transgression (landward retreat) in response to a combination of eustatic sea-level rise and local land

*Email: chouser@geog.tamu.edu

© The Author(s), 2009. Reprints and permissions:
http://www.sagepub.co.uk/journalsPermissions.nav

DOI: 10.1177/0309133309350120

subsidence. Barrier islands transgress during extreme storms capable of breaching the fronting dunes and distributing sediment to the back of the island in the form of washover fans. The redistribution of sediment during an extreme storm and the rate of island transgression depends on the height and alongshore extent of coastal dunes relative to the elevation of the storm surge (Thieler and Young, 1991; Sallenger, 2000; Morton, 2002; Nott, 2006; Houser *et al.*, 2008a), which over longer timescales can be dependent on the availability of sediment from alongshore and offshore sources (Hequette and Ruz, 1991; Psuty, 1992; Schwab *et al.*, 2000; Hansom, 2001; Houser *et al.*, 2008a). Independent of sediment availability, the height and extent of the dunes depends on the impact of the previous storm and the ability of the dunes to recover. This is most evident in the Gulf of Mexico, where a high frequency of hurricanes and tropical storms has left many barrier islands and spits vulnerable to washover and rapid transgression. For example, Santa Rosa Island in northwest Florida suffered beach erosion and widespread overwash and breaching during Hurricane Katrina (2005), despite the storm making landfall along the border of Louisiana and Mississippi (Houser and Hamilton, 2009). The relatively large impact of Katrina in this specific area was conditioned by the lack of a fronting dune, which had largely been eroded during Hurricane Ivan (2004). In turn, the dunes eroded during Ivan were still recovering from Hurricane Opal (1995) and had not achieved substantial height or extent. Similarly, the impact of Hurricane Alicia on Galveston Island, Texas, was magnified by the absence of a protective foredune that had been eroded three years earlier during Hurricane Allen and had not had sufficient time to recover (Morton and Paine, 1985). A magnified storm impact was most recently observed during Hurricane Ike (2008) on sections of Galveston Island and the Bolivar Peninsula lacking well-developed dunes. Alterations to island morphology (specifically dune height and extent) can reinforce and even amplify, to varying degrees, the vulnerability of a barrier island, and commercial and residential development, to storm waves and surge (Nordstrom, 2000).

Dune morphology and barrier island form exhibits a strong dependence on the frequency of storm events (Stallins and Parker, 2003; Christiansen and Davidson-Arnott, 2004). Barrier islands that are impacted infrequently by extreme storms tend to have larger dunes covered by burial-intolerant vegetation. A high frequency of storms limits dune recovery, leading to low-profile dunes covered by burial-tolerant vegetation. An increase in the frequency of extreme storms or even the grouping of storms can lead to the preferential selection of burial-tolerant vegetation in washover and breach areas. A change in vegetation leads to a significant change in island morphology through the development dunes with limited relief separated by overwash conduits and breaches that are reinforced with each storm (Wright *et al.*, 1979; Morton, 2002; Gares and White, 2005; Stallins and Parker, 2003). Alongshore variation in dune morphology can also be forced by wave refraction/diffraction around bathymetric highs and lows (O'Reilly and Guza, 1993; Bender and Dean, 2003; Schupp *et al.*, 2006; Houser *et al.*, 2008b), leading to alongshore variations in beach morphology. Since beach width and sediment budget affect the availability of sediment to the foredune, it is reasonable to expect that local-scale variations along the beachface will be mirrored in the dune morphology (see Psuty, 1992; Bauer and Davidson-Arnott, 2003; Houser and Hamilton, 2009). The ability of dunes to recover following an extreme storm exhibits the same alongshore pattern visible in the pre-storm dune morphology (see Houser and Hamilton, 2009). In this respect, the pre-storm dunefield conditions beach and dune recovery and the resiliency of the barrier island to storms and sea-level rise.

Storm erosion of the backshore and dunes leads to a scarped seaward dune slope that

promotes sediment transport to the lee slope and the migration of the dune landward (Bauer and Sherman, 1999; Davidson-Arnott, 2005). This behaviour is recognized to varying degrees in beach-dune models (eg, Psuty, 1992) and through observations on Lake Erie (Davidson-Arnott and Law, 1990; 1996) and at Skallingen, Denmark (Aagaard *et al*., 1998a; 1998b). An increase in sea level will also lead to the landward migration of the nearshore and beach profile, creating the potential for the dune system to retreat landward without loss of height (Davidson-Arnott, 2005). Migration of the beach-dune system requires sediment eroded offshore by the storm surge to be delivered first to the beachface by nearshore (surf and swash) processes and then transported to the backshore by the wind. This transfer of sediment requires that the distribution of storms and the relative balance of aeolian transport potential and storm surge (see below) are unchanged (see Ruz and Meur-Ferec, 2004). Storm activity is not stationary, but varies at seasonal and decadal timescales (Viles and Goudie, 2003), and has the potential to further vary in response to a change in climate. An increase in the number of storms capable of eroding and breaching the dunes must be accompanied by an increase in the length of the intervening period for the beach to recover and sediment be redelivered to the backshore and to dunes.

The impact of a tropical storm or hurricane depends on the height and alongshore extent of the dune system, which in turn depends on the frequency of storms relative to the rate of recovery from the last storm (Christiansen and Davidson-Arnott, 2004). Despite the importance of dune recovery to the impact of subsequent storms, little attention has been paid to dune recovery following storms. Recovery of dunes following a storm requires sediment to be delivered first to the beachface by nearshore (surf and swash) processes and then transported to the backshore by the wind. Recent evidence from northwest Florida following Hurricanes Opal and Ivan (Stone *et al*., 2004; Houser *et al*., 2008b; Houser and Hamilton, 2009), suggests that dune recovery does not occur immediately and continuously following a storm. The mechanisms and rate of dune recovery following storms have received relatively little attention in the literature, with the exception of Morton *et al*. (1994), McLean and Shen (2006) and Houser and Hamilton (2009). Despite the relative lack of attention, dune recovery through the exchange of sediment between the beach and dune is an integral part of a 'robust conceptual framework or grand, unifying theory' of beach-dune systems. Sherman and Bauer (1993) identified several areas of research that required further study before such a framework can be developed. The authors identified the need to: (1) quantify the role of nearshore processes on beach-dune system behaviour; (2) link dune morphology and change to the littoral sediment budget model; (3) quantify the role of short-timescale events in the long-term evolutionary trends; (4) link microscale aeolian sediment transport processes with mesoscale investigations of beach morphology and dune evolution; and (5) develop high accuracy monitoring methods for measuring sediment supply to the dune system. This can be summarized as a need to examine both the supply and transport limitations on the exchange of sediment from beach to dune.

II Supply limitations

As noted, the primary source of sediment to the coastal dune is aeolian transport from the subaerial beachface, which can be defined as the intertidal zone between the upper limit of the swash at high tide and the lower limit of wave run-down (backwash) at low tide. Depending on the storm tide range, the foreshore is affected by wave shoaling, breaking and swash and can be divided into 4 tidal zones: (1) a subtidal zone largely influenced by shoaling wave processes; (2) a lower intertidal zone controlled by surf zone and shoaling wave processes; (3) a mid-intertidal

zone dominated by swash and surf processes; and (4) an upper intertidal zone across which swash and aeolian transport dominate (Masselink and Short, 1993). The width of each zone depends on the tidal range and the slope of the shoreface, which in turn depends on the sediment size, modal wave height and wave period (Wright and Short, 1984), and the availability of sediment from alongshore or offshore. During non-storm (accretional) conditions, the beach develops a prominent berm with a relatively steep foreshore slope characteristic of a reflective beach. A longer, flatter profile is required for dissipation of storm-wave energy and is achieved during storms that erode the beachface and dune, and build sediment in the form of intertidal and offshore bars (eg, Thom and Hall, 1991), creating a more dissipative beach (Wright and Short, 1984).

Erosion and scarping of the beachface occurs during storms with elevated water levels and wave heights. In addition to gravitational tide, water levels during storms (the storm tide) are the result of wind-push, wave set-up and atmospheric pressure. Wave set-up is caused by the shoreward transport of wave-induced momentum. Water piles up against the coast until the hydrostatic pressure gradient under the now tilting mean water surface balances the radiation stress gradient. The resulting set-up varies between 0.15 and 0.45 of the breaking wave height, a significant increase in water level that, depending on the local bed slope, leads to the generation of a bed-return flow (undertow) capable of transporting sediment offshore through the surf zone. The further migration of the surf and swash zones onto the beach and into the backshore leads to a lower (more dissipative) beach slope, scarping of the dune and the formation of a nearshore bar in the inner surf zone (Lee *et al.*, 1998). The sand moves back onshore and the beach undergoes gradual accretion as the innermost bar welds to the beachface during low-energy conditions, providing a wide low-gradient berm (Thom and Hall, 1991). Erosion of a beachface during a storm (the reaction) can occur over several hours, but the landward migration of the bar (the recovery) takes a significantly longer time. The disparate timescales of storm response and relaxation leads to a significant dependence of beach and dune recovery on the frequency and grouping of storm events (Christiansen and Davidson-Arnott, 2004). The rate of beach recovery and incipient dune formation tends to be faster and of greater magnitude when beachface erosion is most severe (Thom and Hall, 1991), but there appear to be no general mechanisms in which the transport of this material to the backshore and dune is coordinated with the nearshore bar system.

The landward migration of intertidal bars under calm wave conditions is a primary mechanism in which the beachface accretes (Masselink *et al.*, 2006), and sediment becomes available in the backshore for delivery to the dunes (Aagaard *et al.*, 1998a; Christiansen and Davidson-Arnott, 2004). Since storm winds capable of entraining sediment are usually accompanied by elevated water levels, it is reasonable to assume that sediment only becomes available to the dunes when the intertidal bar reaches and expands the backshore and allows for the development/recovery of the dune ramp (Christiansen and Davidson-Arnott, 2004). Bar migration capable of moving sediment to the backshore tends to be greater for slip-faced ridges (swash bars) common on dissipative beaches with a small relative tide range. Storm waves are dissipated through breaking on these intertidal bars, thereby reducing the amount of wave energy available to erode the backshore and dunes (Masselink *et al.*, 2006). At Skallingen, the landward migration of swash bars during storms is a result of relatively weak undertow currents (Aagaard *et al.*, 2004). The gently sloping dissipative shoreface leads to a persistent onshore-directed transport, particularly within the intertidal zone (Houser *et al.*, 2006; Houser and Greenwood, 2007). As a consequence there is a persistent onshore

migration of the subtidal and intertidal bars, and a relatively simple model of beach-dune interaction. The bar behaviour at this site is not representative of the persistent offshore migration of bars further south on the Dutch coast (see Ruessink and Kroon, 1994; Wijnberg and Terwindt, 1995) and in New Zealand (Shand, 2003), or the cyclical (storm-dominated) bar migration observed at Duck, North Carolina (Lippmann and Holman, 1990), and northwest Florida (Houser, unpublished data). Along the storm-dominated North Sea coast of France, Anthony *et al*. (2006) found that differences in net upper beach–dune sand budget patterns between the three monitored sites are, over timescales of years, primarily controlled by the availability of sand from the tide- and storm-dominated shoreface. Such marine sand supply depends on the local onshore welding of shoreface tidal banks that create a large upper beach fetch favourable to dune development.

Unlike Skallingen, very few beach-dune systems in the United States have a large offshore sand supply to permit continued dune development, meaning that there is a finite potential for dune development if there is not a supply of sediment from alongshore. The sediment required for beach and dune recovery comes from the landward migration and welding of the bar(s) formed during the last storm(s) (Aagaard *et al*., 2006) or from sediment transported from alongshore sources and deposited by swash (Lapinskis, 2005). How the supply of sediment is synchronized with the aeolian transport responsible for accumulation in the dunes is not clear. In general, as the wind speed increases and more sediment can potentially be delivered to the dune, water levels also increase and there is a greater chance for the beach supply to be eroded. This asynchronous relationship would not permit dune development, except under strong alongshore winds entraining a readily available supply of sediment seaward of the dune (Bauer and Davidson-Arnott, 2002). Haxel and Holman (2004) describe dune development by summer winds over a beachface that has recovered from winter storms, in the absence of storm surges capable of eroding the backshore and dune. Synchronization in coupled systems results in collective coherent states (Pikovsky *et al*., 2001) and the degree to which beach and dune systems are synchronized will ultimately determine the height and extent of dune development. As will be discussed later, in-phase synchronization is expected on wide dissipative beaches where erosion of the backshore is infrequent and there is wide backshore, consistent with the Short and Hesp (1982) model of beach-dune interaction. However, dune development may be limited in ultra-dissipative systems, characterized by sand waves or ridge and runnel intertidal bars that are not dynamic features and storm winds are typically weak. Only as the beachface accretes and extends seaward does new sediment become available, so long as the transport of sediment to the dune can keep pace with the accretion of the beachface (Psuty, 1992).

III Transport limitations

Aeolian transport rates are potentially the greatest on a dissipative beach, moderate on an intermediate beach and lowest on reflective beaches (Short and Hesp, 1982). Dissipative beaches are characterized by high wave energy, a wide surf zone with numerous parallel bars and troughs and a low gradient wide beach (fetch). This beach presents the least flow disturbance and the greatest potential for large foredunes. With increasing beach slope, there is greater flow disturbance, and less wind and wave energy available for beach for dune development (Short and Hesp, 1982). For steep (reflective) beaches, sediment transport to the dunes depends on a sustained period with a wide, low gradient backshore landward of the berm crest (Hesp, 1988). The amount of sediment delivered to the incipient foredune

depends on the width of the berm that builds through bar welding and/or swash deposition (Thom and Hall, 1991).

As wind velocity increases, the drag and lift forces on surface particles exceed the forces holding the particle to the surface and the particle is entrained. The fluid threshold is dependent on the turbulent structure of the boundary layer resulting from coherent structures (bursts and sweeps) that lead to 'flurries of activity' (Lyles and Kraus, 1971). As the entrained particles impact the bed they are able to further dislodge particles at lower shear velocities than that required for entrainment by the time-average fluid drag and lift. As more particles are dislodged, there is a cascade of sediment downwind and an exponential increase in sediment (Nickling, 1988). As a consequence, there is a minimum distance, the critical fetch length, required for equilibrium saltation to develop and sediment transport to be at a maximum (Owen, 1964; Bauer and Davidson-Arnott, 2002). If the available beach width is less than the critical fetch, the amount of sediment transported and delivered to the dunes does not reach its full potential. The available fetch length is strongly influenced by tidal excursions, storm surge, and wave set-up and run-up (Bauer *et al*., 2009). As water levels increase and more of the beach is inundated, the transport system begins to shut down unless the wind angle is oblique to the shore. While the larger fetch and lower gradient slope associated with an oblique wind enhances the transport flux (Nordstrom and Jackson, 1993), less sediment is delivered per unit length of the dune (Bauer and Davidson-Arnott, 2002).

On most beaches, the critical fetch length is dependent on the spatial distribution of surface moisture resulting from precipitation and tide, which have been shown to be the primary control on aeolian transport (eg, Hotta *et al*., 1984; Sarre, 1989; Bauer *et al*., 1990; Nordstrom and Jackson, 1992; Arens, 1996; Sherman *et al*., 1998; Atherton *et al*., 2001; Wiggs *et al*., 2004; Yang and Davidson-Arnott, 2005). In general, surface moisture varies from the wet and variable foreshore and berm to the dry backshore (Yang and Davidson-Arnott, 2005). As tide recedes, the water table falls and the beach dries, leading to a wider expanse of dry sediment. Following a high tide and precipitation event, drying is greatest mid-beach where the water table is more than 500 mm below the surface and slowest where the water table lies close to the surface (Yang and Davidson-Arnott, 2005). Based on the spatial and temporal variability in surface moisture, Jackson and Nordstrom (1997) identified five transport states that can exist on a beach: (1) direct entrainment of moist sediment; (2) *in situ* drying of sediment and entrainment of upper grain layer; (3) entrainment of dry sediment in bedforms on the moist sediment; (4) entrainment of sediment from upwind and saltation across a moist surface; and (5) entrainment and transport on a completely dry surface. As a consequence, surface moisture results in poor correspondence between measured transport rates and model predictions that depend on both beach slope and gravimetric water content (Sherman *et al*., 1998).

In general, beachface moisture is a response to a range of oceanographic and atmospheric forcing including wave set-up and wave run-up (Hanslow and Nielsen, 1993), barometric pressure changes (Dominick *et al*., 1971), and ocean tides (Turner, 1993). The sloping beachface acts as a non-linear filter that causes the exit point (the intersection of the water table and the beachface) to rise with the storm tide, but lag behind as the tide starts to ebb (Turner and Masselink, 1998). This results in a seepage face above the mean water level where the water table intersects the beachface and groundwater flow is vertically outward. The length of the seepage face varies inversely with the beach slope, and directly with the hydraulic conductivity, tidal period, and tidal extent (Turner, 1993). Through capillary action, the beach landward of the seepage face can still be wet as

a result of capillary action that can create a capillary fringe that extends between 0.2 and 0.5 m above the water table (Dingman, 1984; Turner and Nielsen, 1997). The moisture content of sediments above the capillary fringe are largely dependent on the rate of evaporation, while surface moisture within the capillary fringe can be highly variable, leading to intermittent transport (Darke and McKenna Neuman, 2008), particularly when the wind is just above threshold (Davidson-Arnott and Bauer, 2009). Intermittent transport can also result from unsteadiness in the wind field leading to spatially variable phenomena such as sand streamers (Gares *et al*., 1996; Baas and Sherman, 2005). In addition to surface moisture, transport can be limited by the presence of surface lags (Nickling and McKenna Neuman, 1995; Arens, 1996; McKenna Neuman, 1998), surface crusts (Nickling and Ecclestone, 1981), variation in available grain size (Bauer, 1991), and the adjustment of the boundary layer as the surface roughness evolves from swash to beach to the steep stoss slope of the dune (eg, Wal and McManus, 1993; van der Wal, 1998; Davidson-Arnott *et al*., 2005; Bauer *et al*., 2009). It is reasonable to expect that intermittent transport, while frequent, does not provide sufficient sediment to the dune to explain the mesoscale evolution of the system.

Many of these limitations on transport are dependent on the morphology of the foreshore and backshore, the beach state. Intertidal bar morphology leads to damp troughs and a segmented beach that limits sediment supply to the backshore by limiting aeolian sediment transport across most of the intertidal profile (Anthony *et al*., 2009). The authors note that the cross-shore reduction in fetch as a result of the troughs is mitigated by oblique winds, which means that most of the sediment delivered to the dunes is coming from the existing supply within the backshore, except when storm winds are coincident with neap tide that creates a wide upper foreshore. Anthony *et al*. (2009) also note microscale variability in aeolian transport resulting from topographic modulation of the wind over the intertidal bars, a boundary adjustment that was secondary to the effects of the fetch segregation by moisture. It is reasonable to expect that the sediment contained in the intertidal bars is only available to the dunes when the intertidal bar reaches the upper foreshore and expands the backshore (Aagaard *et al*., 2004). Landward bar migration appears only possible for the slip-faced ridges (swash bars) described by Aagaard *et al*. (2004) and not the ridge and runnel bars examined by Anthony *et al*. (2009). In both cases, the beachface can provide a source of sediment if the profile is flattened through trough infilling by swash, but this may also lead to greater surface moisture and reduced transport (Anthony *et al*., 2009).

Jackson and Cooper (1999) have shown that the critical fetch is not an important constraint on sediment transport for beaches with a large supply of dry sand in the backshore. This led Lynch *et al*. (2006) to argue that the availability of sediment rather than the fetch effect is the primary control on the transport rate and amount of sediment delivered to the dunes (see also Christiansen and Davidson-Arnott, 2004; Saye *et al*., 2005). The contemporary view is that as sediment is supplied to the beachface during calm waves (see above) it must be then transported into the dunes by onshore winds. These onshore winds, however, tend to be accompanied by storm surge and a restricted fetch that limits transport. Lynch *et al*. (2009) argue that offshore winds are largely responsible (at their study site) for sediment accumulation in the upper foreshore through a flow-reversal that causes near-bed winds to be directed landward. This offshore wind model depends first on sediment being delivered to the backshore by nearshore (surf and swash) processes and then transported to the dune by the wind,

a lagged coupling that can limit dune development depending on the frequency of storm events capable of eroding the backshore and dune.

The importance of the synchronization between transport potential and the availability of sediment in the backshore was recently described by Ruz and Meur-Ferec (2004) in an examination of volume change along the French coast. Although 'optimal' transport conditions (strong winds) were observed during in the winter and spring, sand accumulation in the dunes was only observed during the summer period (see also Haxel and Holman, 2004). The increase in transport potential during the fall and winter was associated with an increase in storm tides that led to a lowering of the upper beach and a retreat of the dune through scarping. The most severe erosion was observed when high spring tides coincided with periods of strong onshore winds (Ruz and Meur-Ferec, 2004). During such storm events, the level of the upper beach was lowered and sand was transferred towards the lower foreshore and nearshore zone as deposited as bars. Following storm events, the upper beach displayed a planar, low-angle form, and the foot of the dunes could be reached by waves during subsequent but smaller tides. While it is reasonable to expect that aeolian transport occurred during these periods, it is as likely that the high water levels that flooded the upper beach limited sediment accumulation. Accumulation in the dunes occurred during the summer season when the beach and backshore had recovered and there was only a moderate transport potential. Nordstrom and Jackson (1992) also observed that sediment deposited in the upper beach by the wind was subsequently eroded during high tide by the large waves and storm surge generated by the winds responsible for entraining and transporting the sediment. As a consequence, there was a net loss of sediment from the backshore and dune despite the large transport potential.

IV Synchronization of transport and supply

The link between small-scale transport processes and the mesoscale evolution of landforms represents a major challenge in geomorphology (Sherman, 1995; Church, 1996; Bauer and Davidson-Arnott, 2002). The summary of supply and transport limiting conditions builds an argument that the evolution and recovery of dunes results from the spatial and temporal coupling of nearshore and aeolian processes. Delivery of sediment from the beach to the dune is dependent on a specific combination of transport potential and transitional beach state. Sediment delivered to the beachface and backshore by nearshore processes is delivered to the dune through aeolian transport. The transfer of sediment has been shown to be both spatially variable and temporally intermittent as a result of transport limitations (eg, moisture, lag) across the beachface. While process-scale studies have identified varied controls on sediment transport, there is still a very limited capacity to predict the evolution of beach-dune systems. An argument is developed in this section that sediment accumulation in the dune depends on the synchronization of transport potential (wind speed and direction) with the availability of sediment deposited on the beachface and in the backshore by nearshore and aeolian processes (see Christiansen and Davidson-Arnott, 2004). As defined by Pikovsky *et al*. (2001), synchronization is the adjustment of rhythms of oscillating objects and systems as a result of a weak interaction, which in a beach-dune system is the landward and seaward exchange of sediment. Specifically, synchronization requires that:

(1) Beaches and dunes are active systems that oscillate (erode and accrete around some equilibrium morphology) independently in response to a feedback between some driving force (wind and wave) and their respective morphology before the

event. For a given distribution of wind and wave forcing, the coupled system will continue to oscillate until the source of energy is expired.

(2) The phase and amplitude of the oscillation and synchronization are determined by the geologic and climatological parameters of the system and are independent of storm sequencing.

(3) The phase and amplitude of the oscillation and synchronization are stable to small perturbations (changes in sediment supply and climate forcing) and will soon return to the pre-disturbance state.

(4) If the oscillation of either the beach or the dune is slowly varied through the loss of sediment, the second system will eventually respond and adjust.

Synchronization of beach-dune systems is supported by Guillén *et al*. (1999) who identified oscillatory behaviour at a decadal scale in bar migration and the position of the dune toe. Specifically, the authors found that the evolution of the dune on a decadal scale was correlated with cross-shore migration of the bar system and the alongshore variation in the beach state. Even the offshore wind model of Lynch *et al*. (2009) requires that sediment be first delivered to the backshore by surf and swash processes where it can be transported to the dune by the reverse flow in the lee of the dune.

Sediment emplacement in the backshore by surf and swash can either occur between storms, when winds tend to be below the transport threshold, or through the ('unexpected') landward migration of subtidal and intertidal bars during storms (Houser and Greenwood, 2005; 2007). As wind speeds increase above threshold it is reasonable to expect that there is a narrow spatial or temporal window in which sediment can be transported to the dune before the storm surge extends into the backshore and the transport system begins to shut down. In response, Bauer and Davidson-Arnott (2002) present an elegant model to show that oblique winds are largely responsible for transport of sediment from beach to dune, assuming that there is an unlimited supply of sediment in the backshore and across the beach. This fixed-state model does not account (at present) for changes in the morphology of the beachface and variations in the supply of sediment that define the absolute amount of sediment contributed to the backshore and dune. It is not clear whether dunes can develop in response to the gradual supply of sediment from a limited source. Since beachface accretion tends to be dominated by landward migration and welding of nearshore bars, the concept of synchronization suggests that dune development is dependent on the episodic delivery of a sediment supply from the nearshore at the scale of the bar cycle.

Synchronization in coupled systems results in collective coherent states (Pikovsky *et al*., 2001) and the degree to which beach and dune systems are synchronized will ultimately determine the height and extent of dune development. An in-phase or near in-phase relationship between aeolian transport and sediment supply will lead to greater dune development, while an asynchronous relationship will limit dune development for given amplitudes of transport and supply. This importance of the phase relationship between transport and supply is consistent with the beach-dune model of Psuty (1992), in which dune development is greatest when a positive dune budget (transport) and neutral beach budget (supply) are synchronized. The primary difference between the synchronization introduced in this review and the beach-dune model of Psuty (1992) is that synchronization is defined here as a complex dynamical process rather than a fixed state. Since both models depend on the balance of transport and supply, the proposed synchronization model and the fixed-state model of Psuty (1992) would eventually converge over larger spatial and temporal scales.

The concept of synchronization also overlaps with the oft-cited beach-dune model of Short and Hesp (1982). This model

predicts that the greatest potential for aeolian sediment transport occurs on wide, low-angle dissipative beaches, which tend to be backed by large transgressive dunefields. It further ascribes that narrow reflective beaches have limited dune development due to the short steep fetch that limits aeolian transport. In this respect, the model accounts only for the relative strength (amplitude) of aeolian transport for different beach states; a fixed state model also does not account for the dynamic exchange of sediment between beach and dune, which can account for differences in dune height and morphology for similar beach states. The perpetual onshore migration of the nearshore bars at Skallingen leads to an almost in-phase synchronization of the large supply with strong onshore winds (Aagaard *et al*., 2004), allowing the dunes to maintain height and extent as the barrier spit transgresses. Reflective beaches are limited by transport despite the potential for a large supply of sediment, unless sediment is delivered to the dunes through offshore winds across washover deposits (Houser and Hamilton, 2009). More dissipative ridge and runnel beaches are also transport limited by the segmentation of the beach (Anthony *et al*., 2009) and the greater extent of surface within the capillary fringe during falling tide. This leaves only a narrow but morphologically static backshore to supply sediment to the dune that expands at large timescales in retrogressive environments.

V Summary

This review considers the role of nearshore processes and morphological change as a flexible and dynamic constraint on the supply and transport of sediment between beach and dune. It is argued that the lack of information in this regard remains a central barrier to the development of a theory of beach-dune interaction that can be translated across scales and between field sites. Existing beach-dune models do not consider how and when sediment gets transferred to the backshore, where it becomes available for transport by the wind. Rather, existing models largely ascribe regional variations in dune morphology to fixed constraints on the beach slope and sediment budget, without explicit recognition of the processes involved. Recent (process-scale) transport studies have shown that the transfer of sediment is both spatially variable and temporally intermittent as a result of transport limitations across the beachface. While these studies have identified varied controls on sediment transport and exchange, there remains a limited capacity to predict the evolution of beach-dune systems, largely because the beachface tends to be viewed as a static transport surface without regard to supply or to the changing limits to transport. Following storm erosion, dune recovery first requires that the beach recovers through the onshore migration and welding of nearshore bars, followed by accretion in the backshore to create a supply of sediment for transport by the wind. It is further argued that the dependence of dune recovery on the synchronization of transport events with the recovery of sediment supply in the backshore creates a strong asymmetry in dune recovery that makes barrier islands susceptible to widespread erosion and breaching if a change in the frequency or grouping of storm events is capable of resetting the bar system (offshore) before the next extreme storm. Synchronization of transport and supply suggests that dune evolution is quasi-periodic (in response to changes in the beach and nearshore state) and predictable by considering the dune within the broader context of the beach-nearshore system.

Acknowledgements

This work was supported in part by the National Science Foundation under award number GSS-0920851, and by the National Park Service under contract number J5320 08 001.

References

Aagaard, T., Davidson-Arnott, R.G.D., Greenwood, B. and **Nielsen J.** 2004: Sediment

supply from shoreface to dunes – linking sediment transport measurements and long term morphological evolution. *Geomorphology* 60, 205–24.

Aagaard, T., Hughes, M, Møller-Sørensen, R. and **Andersen, S.** 2006: Hydrodynamics and sediment fluxes across an onshore migrating intertidal bar. *Journal of Coastal Research* 22, 247–59.

Aagaard, T., Nielsen, J., Davidson-Arnott, R., Greenwood, B. and **Nielsen, N.** 1998a: Coastal morphodynamics at Skallingen, SW Denmark: high-energy conditions. *Danish Journal of Geography* 98, 20–30.

Aagaard, T., Nielsen, J. and **Greenwood, B.** 1998b: Suspended sediment transport and nearshore bar formation on a shallow intermediate-state beach. *Marine Geology* 148, 203–25.

Anthony, E.J., Ruz, M.H. and **Vanhee, S.** 2006: Morphodynamics of intertidal bars on a megatidal beach, Merlimont, northern France. *Marine Geology* 208, 73–100.

— 2009: Aeolian sand transport over complex intertidal bar-trough topography. *Geomorphology*, in press.

Arens, S.M. 1996: Rates of aeolian transport on a beach in a temperate humid climate. *Geomorphology* 17, 3–18.

Atherton, R.J., Baird, A.J. and **Wiggs, G.F.S.** 2001: Intertidal dynamics of surface moisture content on a meso-tidal beach. *Journal of Coastal Research* 17, 482–89.

Baas, A.C.W. and **Sherman, D.J.** 2005: Formation and behavior of aeolian streamers. *Journal of Geophysical Research* 110, F03011, DOI: 10.1029/2004JF000270.

Bauer, B.O. 1991: Aeolian decoupling of beach sediments. *Annals of the Association of American Geographers* 81, 290–303.

Bauer, B.O. and **Davidson-Arnott, R.G.D.** 2002: A general framework for modeling sediment supply to coastal dunes including wind angle, beach geometry, and fetch effects. *Geomorphology* 49, 89–108.

Bauer, B.O. and **Sherman, D.J.** 1999: Coastal dune dynamics: problems and prospects. In Goudie, A.S., Livingstone, I. and Stokes, S., editors, *Aeolian environments, sediments and landforms*, Chichester: Wiley, 71–104.

Bauer, B.O., Davidson-Arnott, R.G.D., Hesp, P.A., Namikas, S.L., Ollerhead, J. and **Walker, I.J.** 2009: Aeolian sediment transport on a beach: surface moisture, wind fetch and mean transport. *Geomorphology*, in press.

Bauer, B.O., Sherman, D.J., Nordstrom, K.F. and **Gares, P.A.** 1990: Aeolian transport measurement and prediction across a beach and dune at Castroville, California. In Nordstrom, K.F., Psuty, N.P. and Carter, R.W.G., editors, *Coastal dunes: form and process*, Chichester: Wiley, 38–55.

Bender, C.J. and **Dean, R.G.** 2003: Wave field modification by bathymetric anomalies and resulting shoreline changes: a review with recent results. *Coastal Engineering* 49, 125–53.

Christiansen, M.B. and **Davidson-Arnott, R.** 2004: Rates of landward sand transport over the foredune at Skallingen, Denmark and the role of dune ramp. *Danish Journal of Geography* 104, 31–43.

Church, M. 1996: Space time and the mountain – how do we order what we see? In Rhoads, B.L. and Thorn, C.E., editors, *The scientific nature of geomorphology*, Chichester: Wiley, 147–70.

Darke, I. and **McKenna Neuman, C.** 2008: Field study of beach water content as a guide to wind erosion potential. *Journal of Coastal Research* 24, 1200–208.

Davidson-Arnott, R.G.D. 2005: Conceptual model of the effects of sea level rise on sandy coasts. *Journal of Coastal Research* 21, 1166–72.

Davidson-Arnott, R.G.D. and **Bauer, B.O.** 2009: Aeolian sediment transport on a beach: thresholds, intermittency, and high frequency variability. *Geomorphology*, in press.

Davidson-Arnott, R.G.D. and **Law, M.N.** 1990: Seasonal patterns and controls on sediment supply to coastal foredunes, Long Point, Lake Erie. In Nordstrom, K., Psuty, N. and Carter, R.W.G., editors, *Coastal dunes: processes and geomorphology*, New York: Wiley, 177–200.

— 1996: Measurement and prediction of long-term sediment supply to Coastal Foredunes. *Journal of Coastal Research* 12, 654–63.

Davidson-Arnott, R.G.D., MacQuarrie, K. and **Aagaard, T.** 2005: The effect of wind gusts, moisture content and fetch length on sand transport on a beach. *Geomorphology* 68, 115–29.

Dingman, S.L. 1984: *Fluvial hydrology*. San Francisco: Freeman, 383 pp.

Dominick, T.F., Wilkins, B. and **Roberts, H.** 1971: Mathematical model for beach groundwater fluctuations. *Water Resources Research* 7, 1626–35.

Ehlers, J. and **Kunz, J.** 1993: Morphology of the Wadden Sea: natural processes and human interference. In Hillen, R. and Verhagen, H.J., editors, *Coastlines of the Southern North Sea*, New York: American Society of Civil Engineers, 65–84.

Gares, P. and **White, S.A.** 2005: Volumetric analysis of overwash fans resulting from tropical storms on North Hatteras Island, North Carolina. *Southeastern Geographer* 45, 1–15.

Gares, P.A., Davidson-Arnott, R.G.D., Bauer, B.O., Sherman, D.J., Carter, R.W.G., Jackson, D. and **Nordstrom, K.F.** 1996: Longshore variations in aeolian sediment transport, sediment size and moisture at Carrick Finn Strand, Ireland. *Journal of Coastal Research* 12, 673–82.

Guillén, J., Stive, M.J.F. and **Capobianco, M.** 1999: Shoreline evolution of the Holland coast on a decadal scale. *Earth Surface Processes and Landforms* 24, 517–36.

Hanslow, D. and **Nielsen, P.** 1993: Shoreline setup on natural beaches. *Journal of Coastal Research* 15, special issue, 1–10.

Hansom, J.D. 2001: Coastal sensitivity to environmental change: a view from the beach. *Catena* 42, 291–305.

Haxel, J.H. and **Holman, R.A.** 2004: The sediment response of a dissipative beach to variations in wave climate. *Marine Geology* 206, 73–99.

Hequette, A. and **Ruz, M.-H.** 1991: Spit and barrier island migration in the southeastern Canadian Beaufort Sea. *Journal of Coastal Research* 7, 677–98.

Hesp, P.A. 1988: Surf zone, beach and foredune interactions on the Australian southeast coast. *Journal of Coastal Research* SI3, 15–25.

— 2002: Foredunes and blowouts: initiation, geomorphology and dynamics. *Geomorphology* 48, 245–68.

Hotta, S., Kubota, S., Katori, S. and **Horikawa, K.** 1984: Sand transport by wind on a wet sand surface. In Edge, B.L., editor, *Coastal Engineering 1984, Proceedings of the 19th International Conference, Houston, Texas, September 1984, American Society of Civil Engineers* 2, 1265–81.

Houser, C. and **Greenwood, B.** 2005: Profile response of a lacustrine multiple-barred nearshore to a sequence of storm events. *Geomorphology* 69, 118–37.

— 2007: Onshore migration of a swash bar during a storm. *Journal of Coastal Research* 23, 1–14.

Houser, C. and **Hamilton, S.** 2009: Post-hurricane beach and dune recovery. *Earth Surface Processes and Landforms* 34, 613–28.

Houser, C., Greenwood, B. and **Aagaard, T.** 2006: Divergent response of an intertidal swash bar. *Earth Surface Processes and Landforms* 31, 1775–91.

Houser, C., Hapke, C. and **Hamilton, S.** 2008a: Controls on coastal dune morphology, shoreline erosion and barrier island response to extreme storms. *Geomorphology* 100, 223–40.

Houser, C., Hobbs, C. and **Saari, B.** 2008b: Post-hurricane airflow and sediment transport over a recovering dune. *Journal of Coastal Research* 4, 944–53.

Jackson, D.W.T. and **Cooper, A.G.** 1999: Beach fetch distance and aeolian sediment transport. *Sedimentology* 46, 517–22.

Jackson, N.L. and **Nordstrom, K.F.** 1997: Effects of time-dependent moisture content of surface sediments on aeolian transport rates across a beach, Wildwood, New Jersey, USA. *Earth Surface Processes and Landforms* 22, 611–21.

Lapinskis, J. 2005: Long-term fluctuations in the volume of beach and foredune deposits along the coast of Latvia. *Baltica* 18, 38–43.

Lee, G., Nicholls, R.J. and **Birkemeier, W.A.** 1998: Storm-driven variability of the beach-nearshore profile at Duck, North Carolina, USA, 1981–1991. *Marine Geology* 148, 163–77.

Lippmann, T.C. and **Holman, R.A.** 1990: The spatial and temporal variability of sand bar morphology. *Journal of Geophysical Research* 95, 11,575–90.

Lyles, L. and **Krauss, R.K.** 1971: Threshold velocities and initial particle motion as influenced by air turbulence. *Transactions of the ASAE* 14, 563–66.

Lynch, K., Jackson, D.W.T. and **Cooper, J.A.G.** 2006: A remote-sensing technique for the identification of aeolian fetch distance. *Sedimentology* 53, 1381–90.

— 2009: Foredune accretion under offshore winds. *Geomorphology*, in press.

Masselink, G. and **Short, A.D.** 1993: The effect of tide range on beach morphodynamics and morphology: a conceptual beach model. *Journal of Coastal Research* 9, 785–800.

Masselink, G., Kroon, A. and **Davidson-Arnott, R.G.D.** 2006: Morphodynamics of intertidal bars in wave-dominated coastal settings – a review. *Geomorphology* 73, 33–49.

McKenna-Neuman, C. 1998: Particle transport and adjustments of the boundary layer over rough surfaces with an unrestricted, upwind supply of sediment. *Geomorphology* 25, 1–17.

McLean, R. and **Shen, J.S.** 2006: From foreshore to foredune: foredune development over the last 30 years at Moruya Beach, New South Wales, Australia. *Journal of Coastal Research* 22, 28–36.

Meyer-Arendt, K.J. 1990: Recreational business districts in Gulf of Mexico seaside resorts. *Journal of Cultural Geography* 11, 39–55.

Morton, R.A. 2002: Factors controlling storm impacts on coastal barriers and beaches – a preliminary basis for near real-time forecasting. *Journal of Coastal Research* 18, 486–501.

Morton, R.A. and **Paine, J.G.** 1985: *Beach and vegetation-line changes at Galveston Island, Texas: erosion, deposition, and recovery from Hurricane Alicia*. The University of Texas at Austin, Bureau of Economic Geology Geological Circular 85-5, 39 pp.

Morton, R.A, Paine, J.G. and **Gibeaut, J.C.** 1994: Stages and durations of post-storm beach recovery, southeastern Texas coast. *Journal of Coastal Research* 10, 884–908.

Nickling, W.G. 1988: The initiation of particle movement by wind. *Sedimentology* 35, 499–511.

Nickling, W.G. and **Ecclestone, M.** 1981: The effects of soluble salts on the threshold shear velocity of fine sand. *Sedimentology* 28, 505–10.

Nickling, W.G. and **McKenna-Neuman, C.** 1995: Development of deflation lag surfaces. *Sedimentology* 42, 403–14.

Nordstrom, K.F. 2000: *Beaches and dunes of developed coasts.* Cambridge: Cambridge University Press, 356 pp.

Nordstrom, K.F. and **Jackson, N.L.** 1992: Effect of source width and tidal elevation changes on aeolian

transport on an estuarine beach. *Sedimentology* 39, 769–78.

— 1993: The role of wind direction in eolian transport on a narrow sandy beach. *Earth Surface Processes and Landforms* 18, 675–86.

Nott, J. 2006: Tropical cyclones and the evolution of the sedimentary coast of northern Australia. *Journal of Coastal Research* 22, 49–62.

O'Reilly, W.C. and **Guza, R.T.** 1993: A comparison of two spectral wave models in the Southern California Bight. *Coastal Engineering* 19, 263–82.

Owen, P.R. 1964: Saltation of uniform sand grains in air. *Journal of Fluid Mechanics* 20, 225–42.

Pikovsky, A., Rosenblum, M. and **Kurths, J.** 2001: *Synchronization: a universal concept in nonlinear sciences*. Cambridge: Cambridge University Press, 432 pp.

Psuty, N.P. 1992: Spatial variation in coastal fordune development. In Carter, R.W.G., Curtis, T.G.F. and Sheehy-Skeffington, M.J., editors, *Coastal dunes: geomorphology, ecology and management for conservation*, Rotterdam: Balkema, 3–13.

Ruessink, B.G. and **Kroon, A.** 1994: The behaviour of a multiple bar system in the nearshore zone of Tershelling, the Netherlands: 1965–1993. *Marine Geology* 121, 187–97.

Ruz, M.H. and **Meur-Ferec, C.** 2004: Influence of high water levels on aeolian sand transport: upper beach/dune evolution on a macrotidal coast, Wissant Bay, northern France. *Geomorphology* 60, 73–87.

Sallenger, A.H. 2000: Storm impact scale for barrier islands. *Journal of Coastal Research* 16, 890–95.

Sarre, R.D. 1989: The morphological significance of vegetation on relief of coastal foredune processes. *Zeitschrift für Geomorphologie*, Supplement Band 73, 17–31.

Saye, S.E., van der Wal, D., Pye, K. and **Blott, S.J.** 2005: Beach–dune morphological relationships and erosion/accretion: an investigation at five sites in England and Wales using LIDAR data. *Geomorphology* 72, 128–55.

Schupp, C.A., McNinch, J.E. and **List, J.H.** 2006: Nearshore shore-oblique bars, gravel outcrops, and their correlation to shoreline change. *Marine Geology* 233, 63–79.

Schwab, W.C., Thieler, E.R., Allen, J.R., Foster, D.S., Swift, B.A. and **Denny, J.F.** 2000: Influence of inner-continental shelf geologic framework on the evolution and behavior of the barrier-island system between Fire Island inlet and Shinnecock Inlet, Long Island, New York. *Journal of Coastal Research* 16, 408–22.

Shand, R.D. 2003: Relationships between episodes of bar switching, cross-shore bar migration and outer bar degeneration at Wanganui, New Zealand. *Journal of Coastal Research* 19, 157–70.

Sherman, D.J. 1995: Problems of scale in the modeling and interpretation of coastal dunes. *Marine Geology* 124, 339–49.

Sherman, D.J. and **Bauer, B.O.** 1993: Dynamics of beach-dune systems. *Progress in Physical Geography* 17, 413–47.

Sherman, D.J., Jackson, D.W.T., Namikas, S.L. and **Jinkang, W.** 1998: Wind-blown sand on beaches: an evaluation of models. *Geomorphology* 22, 113–33.

Short, A. and **Hesp, P.A.** 1982: Wave–beach–dune interaction in southeast Australia. *Marine Geology* 48, 259–84.

Stallins, J.A. and **Parker, A.J.** 2003: The influence of complex systems interactions on barrier island dune vegetation pattern and process. *Annals of the Association of American Geographers* 93, 13–29.

Stone, G.W., Liu, B., Pepper, D.A. and **Wang, P.** 2004: The importance of extratropical and tropical cyclones on the short-term evolution of barrier islands along the northern Gulf of Mexico, USA. *Marine Geology* 210, 63–78.

Thieler, E.R. and **Young, R.S.** 1991: Quantitative evaluation of coastal geomorphological changes in South Carolina after Hurricane Hugo. *Journal of Coastal Research* 8, 187–200.

Thom, B.G and **Hall, W.** 1991: Behavior of beach profiles during accretion and erosion dominated periods. *Earth Surface Processes and Landforms* 16, 113–27.

Turner, I.L. 1993: The total water content of sandy beaches. *Journal of Coastal Research* SI15, 11–26.

Turner, I.L. and **Masselink, G.** 1998: Swash infiltration-exfiltration and sediment transport. *Journal of Geophysical Research* 103, 30,813–24.

Turner, I.L. and **Nielsen, P.** 1997: Rapid water table fluctuations within the beach face: implications for swash zone sediment mobility? *Coastal Engineering* 32, 45–59.

van der Wal, D. 1998: The impact of the grain-size distribution of nourishment sand on aeolian sand transport. *Journal of Coastal Research* 14, 620–31.

Viles, H.A. and **Goudie, A.S.** 2003: Interannual, decadal and multidecadal scale climatic variability and geomorphology. *Earth-Science Reviews* 61, 105–31.

Wal, A. and **McManus, J.** 1993: Wind regime and sand transport on a coastal beach-dune complex, Tentsmuir, eastern Scotland. In Pye, K., editor, *The dynamics and environmental context of aeolian sediment systems*, Geological Society of London Special Publication 72, 159–72.

Wiggs, G.F.S., Baird, A.J. and **Atherton, R.J.** 2004: The dynamic effects of moisture on the entrainment and transport of sand by wind. *Geomorphology* 59, 13–30.

Wijnberg, K.M. and **Terwindt, J.H.J.** 1995: Extracting decadal morphological behavior from

high-resolution, long-term bathymetric surveys along the Holland coast using eigenfunction analysis. *Marine Geology* 126, 301–30.

Wright, L.D. and **Short, A.D.** 1984: Morphodynamic variability of surf zones and beaches: a synthesis. *Marine Geology* 56, 93–118.

Wright, L.D., Chappell, J., Thom, B.G., Bradshaw, M.P. and **Cowell, P.** 1979: Morphodynamics of reflective and dissipative beach and inshore systems: southeastern Australia. *Marine Geology* 70, 251–85.

Yang, Y. and **Davidson-Arnott, R.** 2005: Rapid measurement of surface moisture content on a beach. *Journal of Coastal Research* 21, 447–52.

APPENDIX II

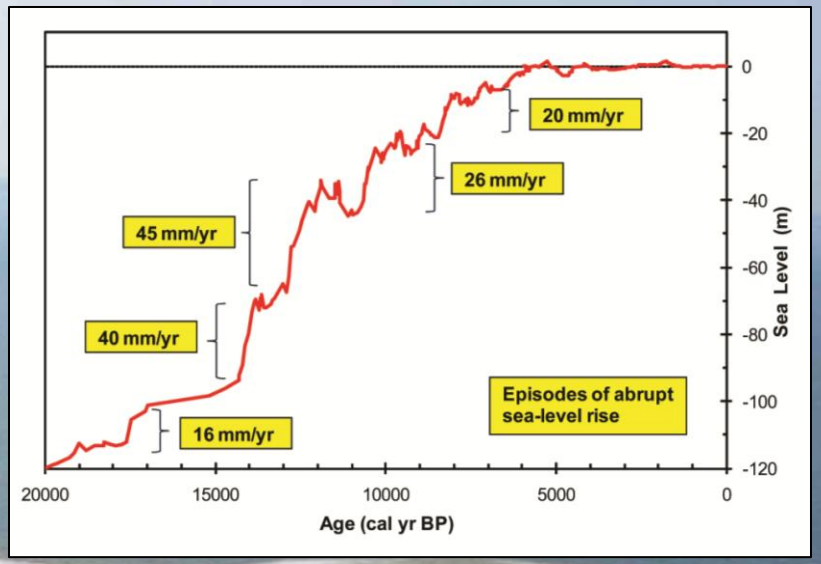
National Park Service Webinar: Linking Island Transgression and Storm Response with Beach-Dune Interaction, April 2011.



Linking Island Transgression and Storm Response with Beach-Dune Interaction

Chris Houser
Texas A&M University

Depending on the rate of sea level rise, barrier islands will either rollover (transgress) or be overstepped and drowned





Implications for park infrastructure and management



Island transgression is accomplished during storms capable of overwashing the foredunes or through the development of blowouts



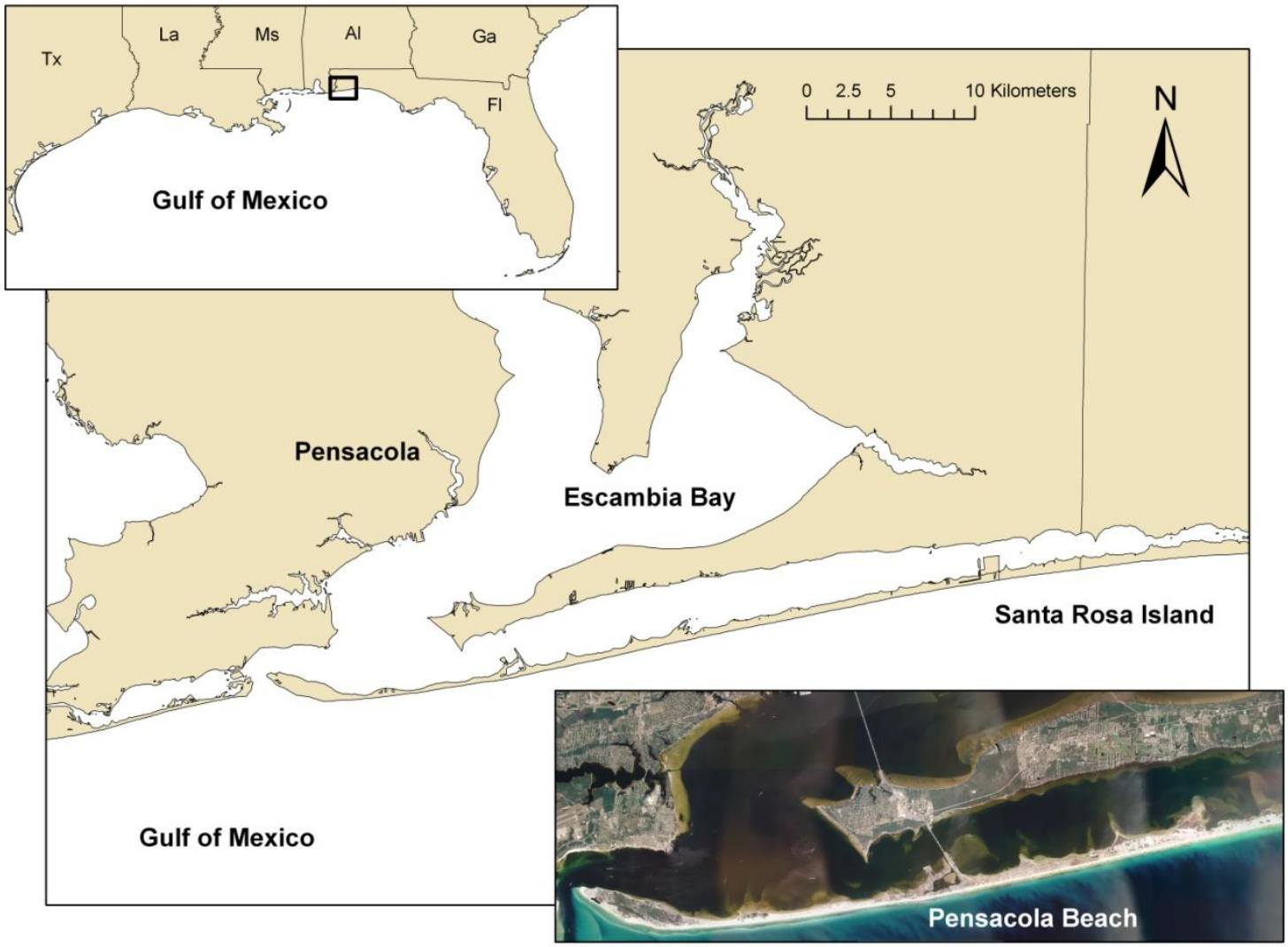
Overwash depends on the elevation of the surge relative to the dune, and the duration of the storm



Resiliency of a barrier island depends on the ability of the dunes to recover in height and extent



Dune recovery depends on the recovery of the beach and backshore, the return of vegetation and winds to transport sediment landward


Tx
La
Ms
Al
Ga
Fl
Gulf of Mexico
0 2.5 5 10 Kilometers
N
Pensacola
Escambia Bay
Santa Rosa Island
Gulf of Mexico
Pensacola Beach



Pre-Ivan (May 2004)



Houser, C., Hapke, C. and Hamilton, S., (2008). Controls on Coastal Dune Morphology, Shoreline Erosion and Barrier Island Response to Extreme Storms. *Geomorphology*, 100, 223-240.

TEXAS A&M UNIVERSITY

Beach-dune interaction and transgression



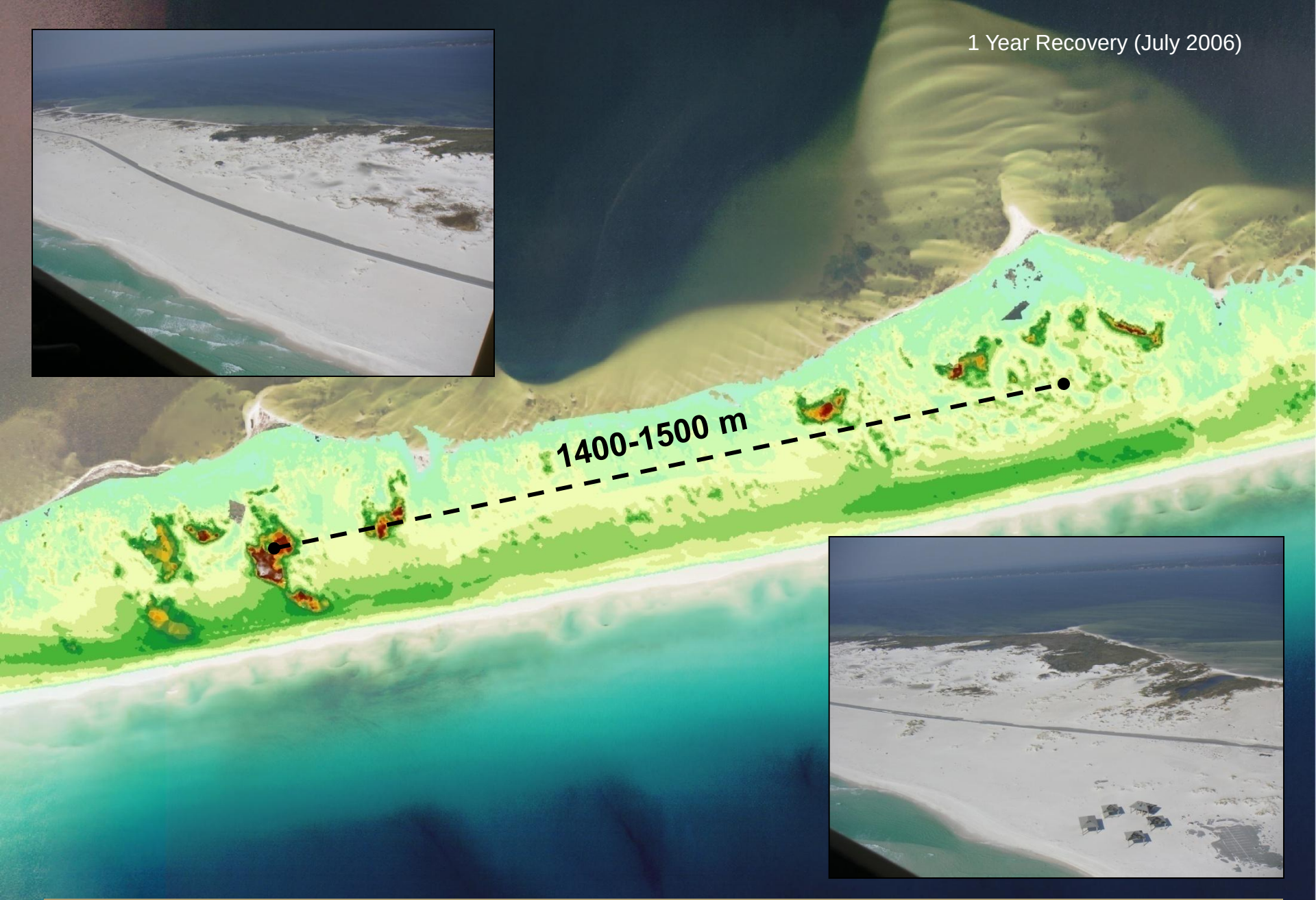
Post-Ivan (September 2004)



Houser, C., Hapke, C. and Hamilton, S., (2008). Controls on Coastal Dune Morphology, Shoreline Erosion and Barrier Island Response to Extreme Storms. *Geomorphology*, 100, 223-240.

TEXAS A&M UNIVERSITY

Beach-dune interaction and transgression

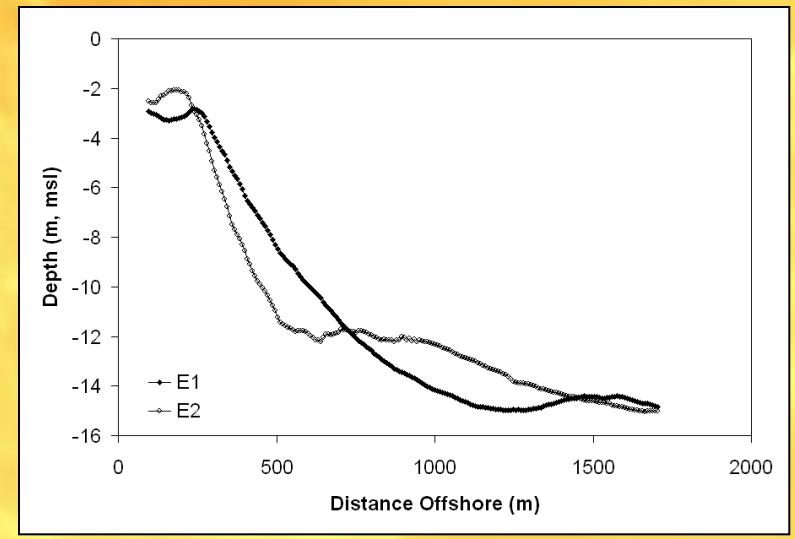


TEXAS A&M UNIVERSITY

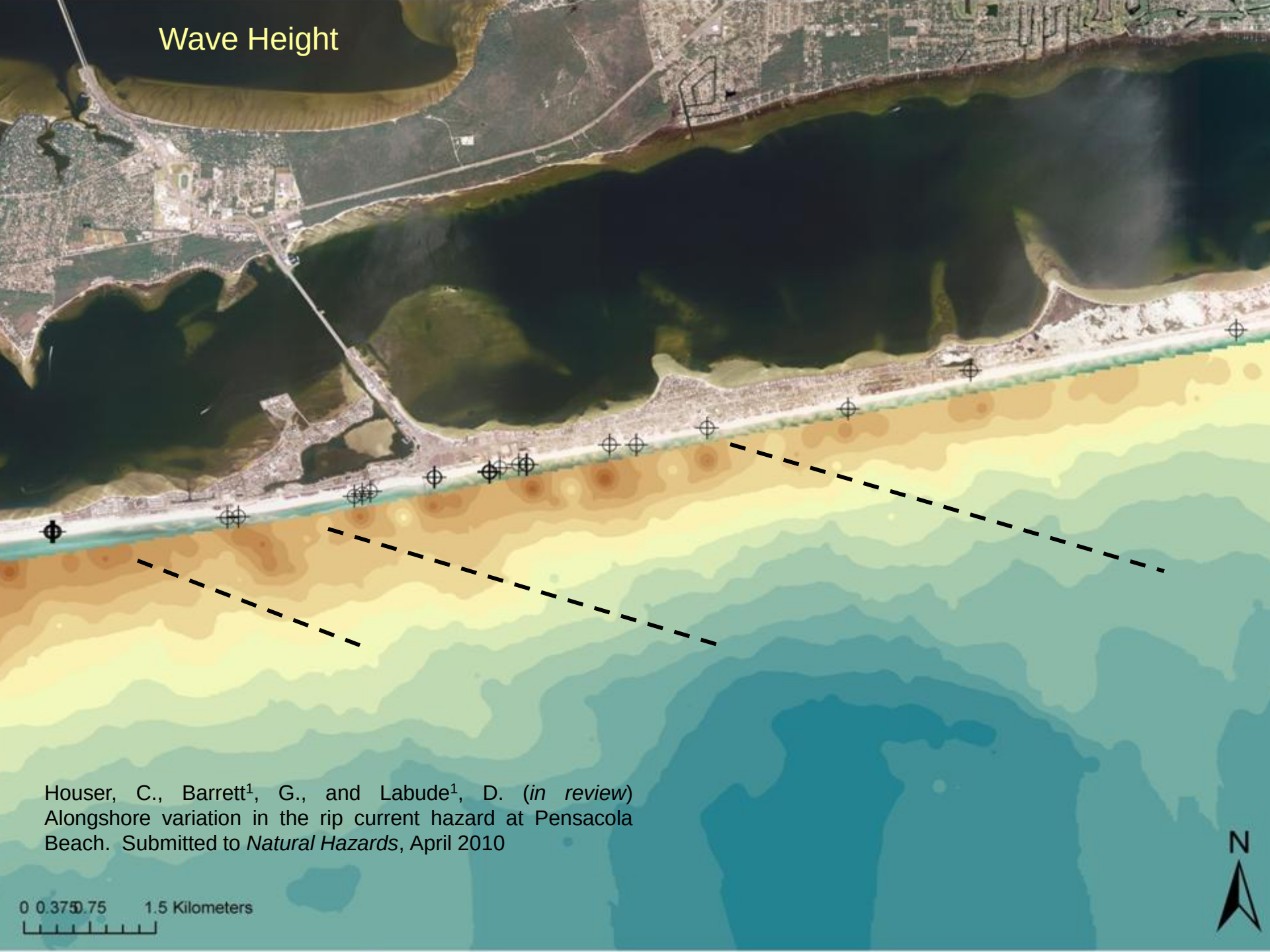
Alongshore Variation in Storm Impact and Dune Morphology


6 MARCH 2007
1400-1500 m

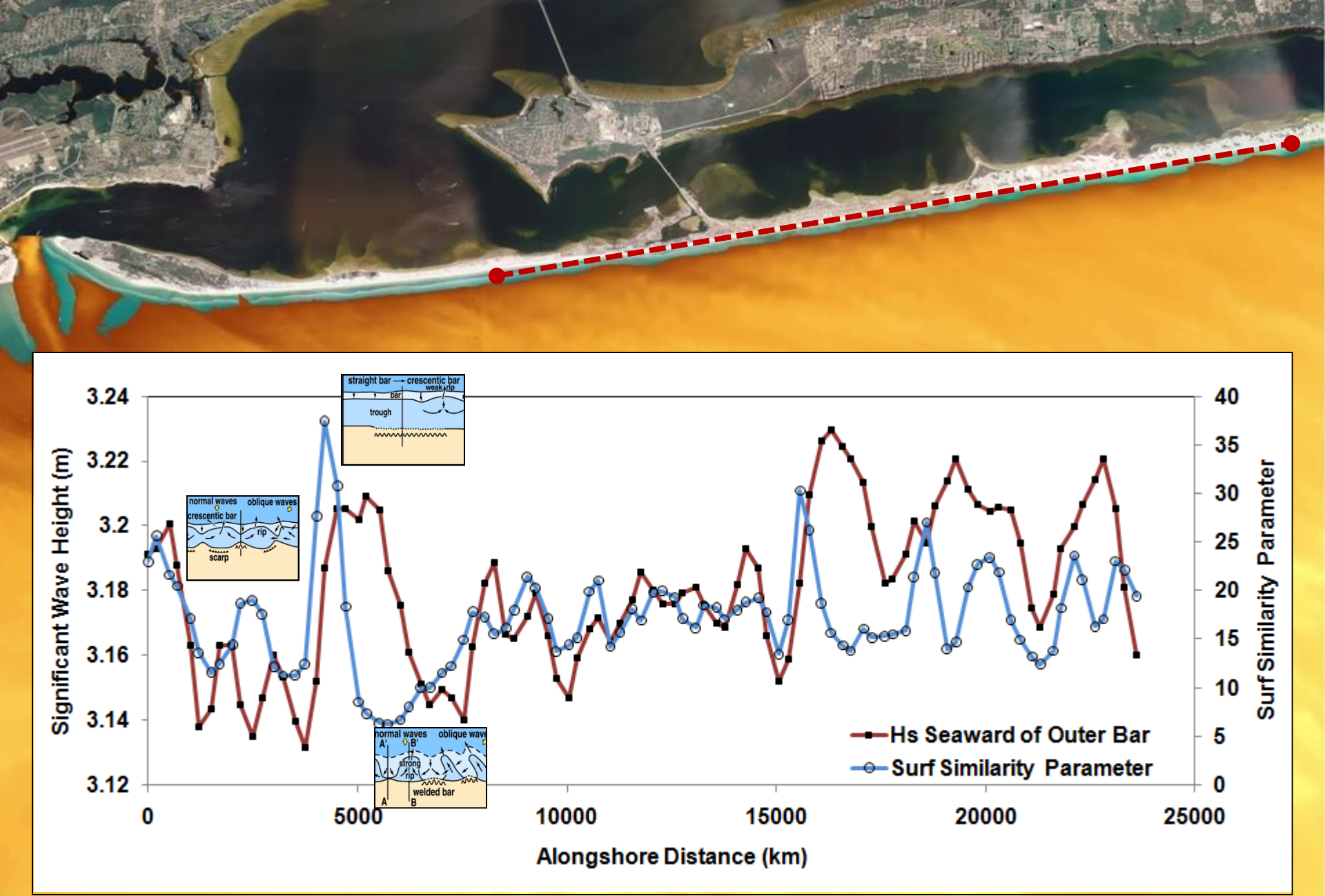
>20).



Alongshore patterns in island response and recovery are controlled and reinforced by ridge and swale topography on the inner-shelf

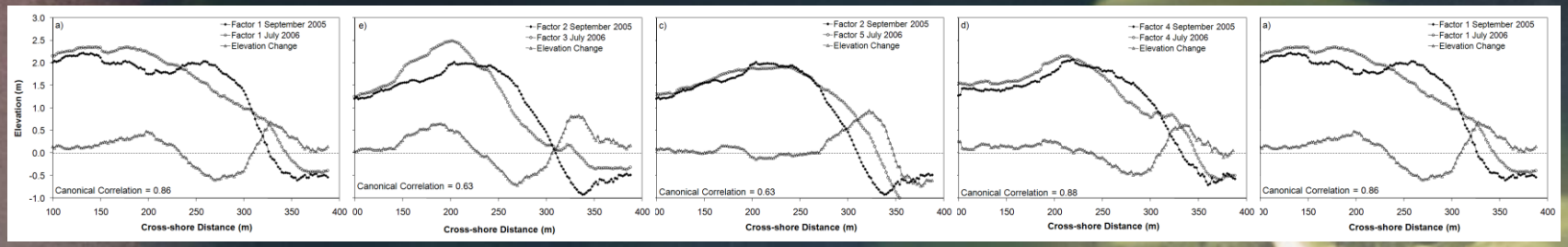


Houser, C., Barrett[1], G., and Labude[1], D. (*in review*) Alongshore variation in the rip current hazard at Pensacola Beach. Submitted to *Natural Hazards*, April 2010


Significant Wave Height (m)
3.24
3.22
3.2
3.18
3.16
3.14
3.12
Surf Similarity Parameter
40
35
30
25
20
15
10
5
0
0
5000
10000
15000
20000
25000
Alongshore Distance (km)
Hs Seaward of Outer Bar
Surf Similarity Parameter
straight bar → crescentic bar
weak rip
bar
trough
normal waves
oblique waves
crescentic bar
rip
scarp
normal waves
oblique wave
A'
B'
strong rip
welded bar
A
B




4B
SATURDAY, APRIL 6, 2002 | THE TUSCALOOSA NEWS
Florida island deemed worst in nation for beach drownings



Not Transport Limited

Transport Limited

Not Transport Limited



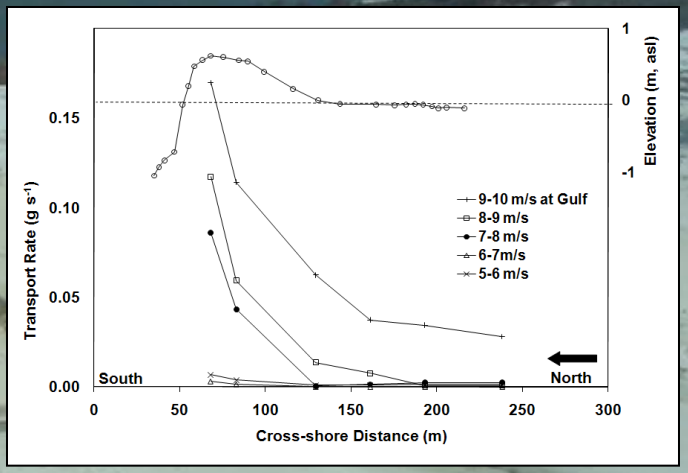




TEXAS A&M UNIVERSITY

Beach-dune interaction and transgression

Limited sediment supply maintains transport cascade across barrier and limits role of vegetation

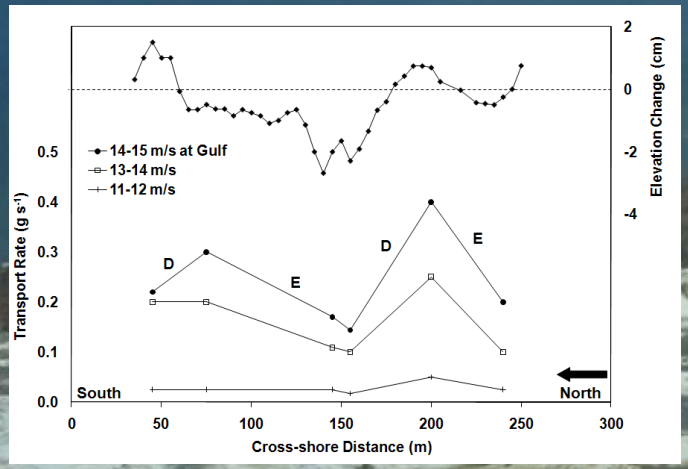




TEXAS A&M UNIVERSITY

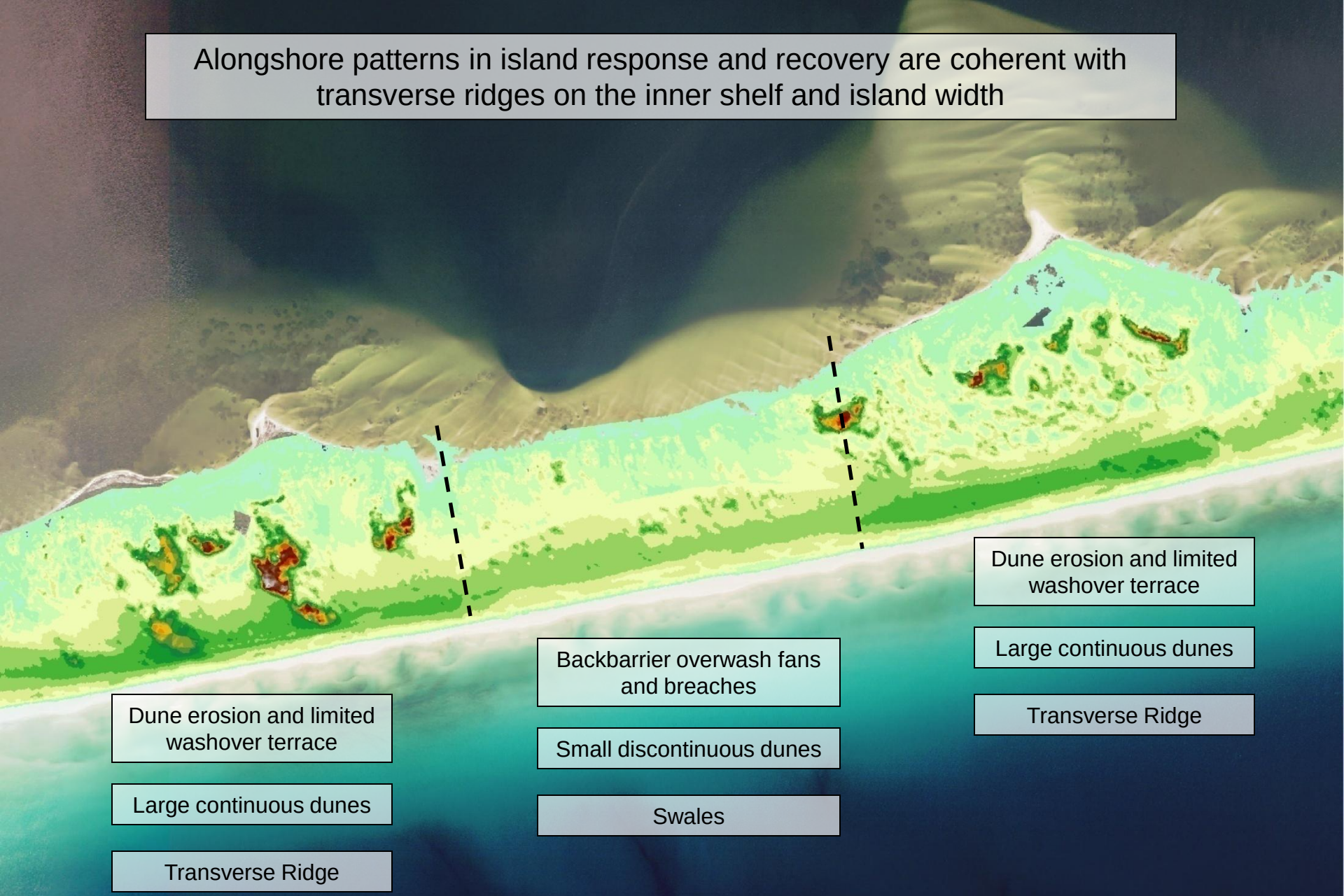
Beach-dune interaction and transgression

Ample supply of sediment, but a lack of dune grass to promote new dune development





Alongshore patterns in island response and recovery are coherent with transverse ridges on the inner shelf and island width

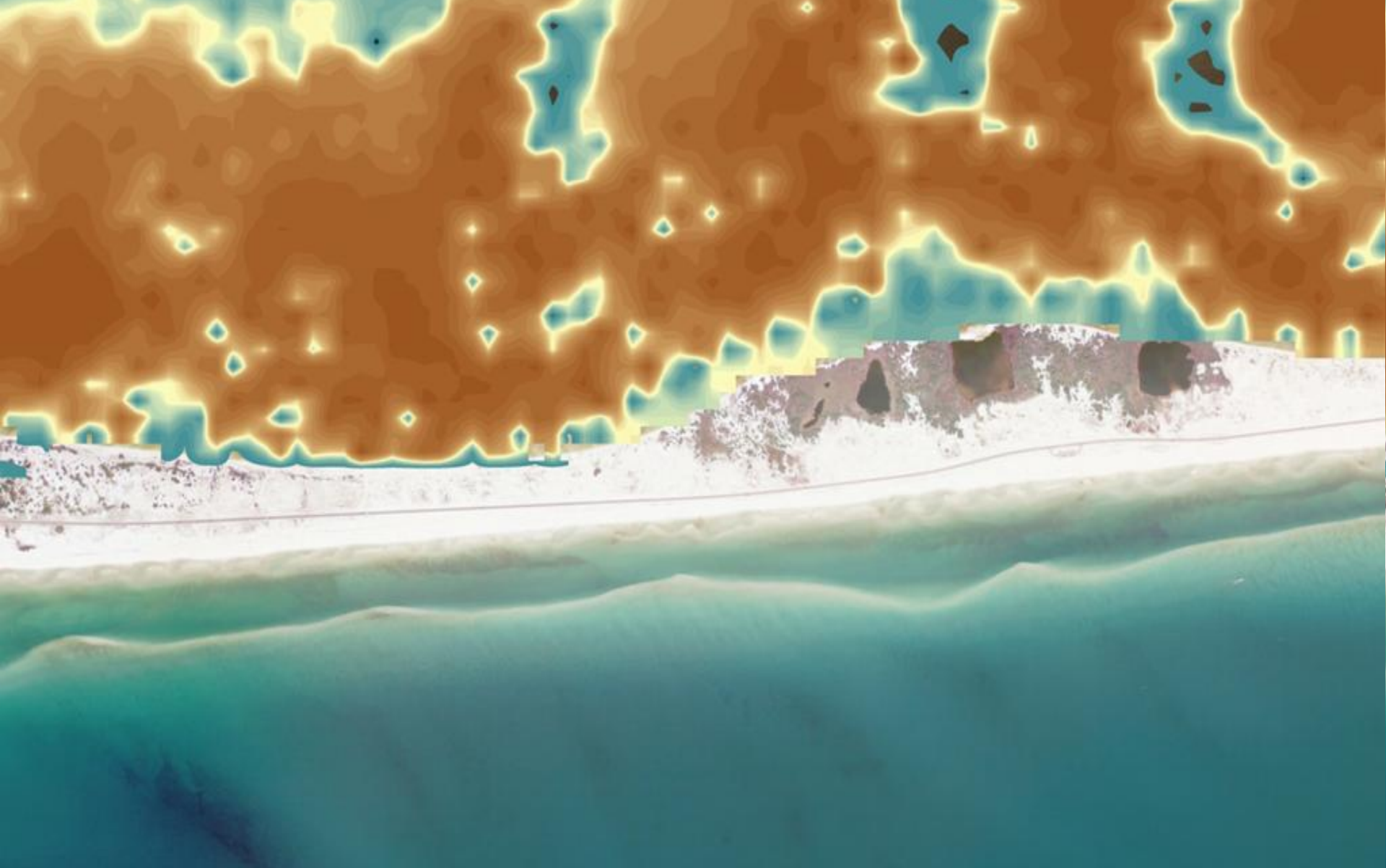




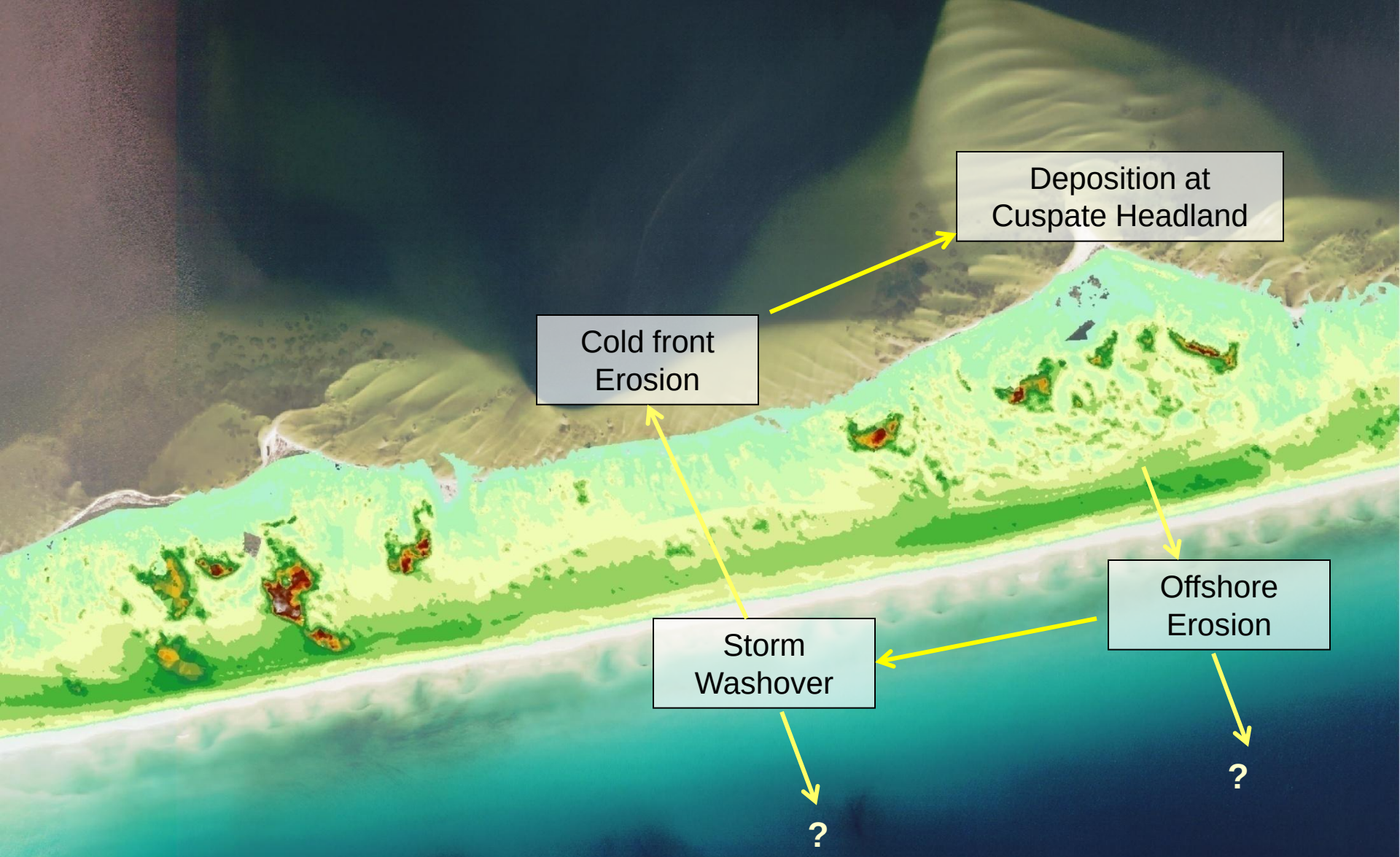


TEXAS A&M UNIVERSITY

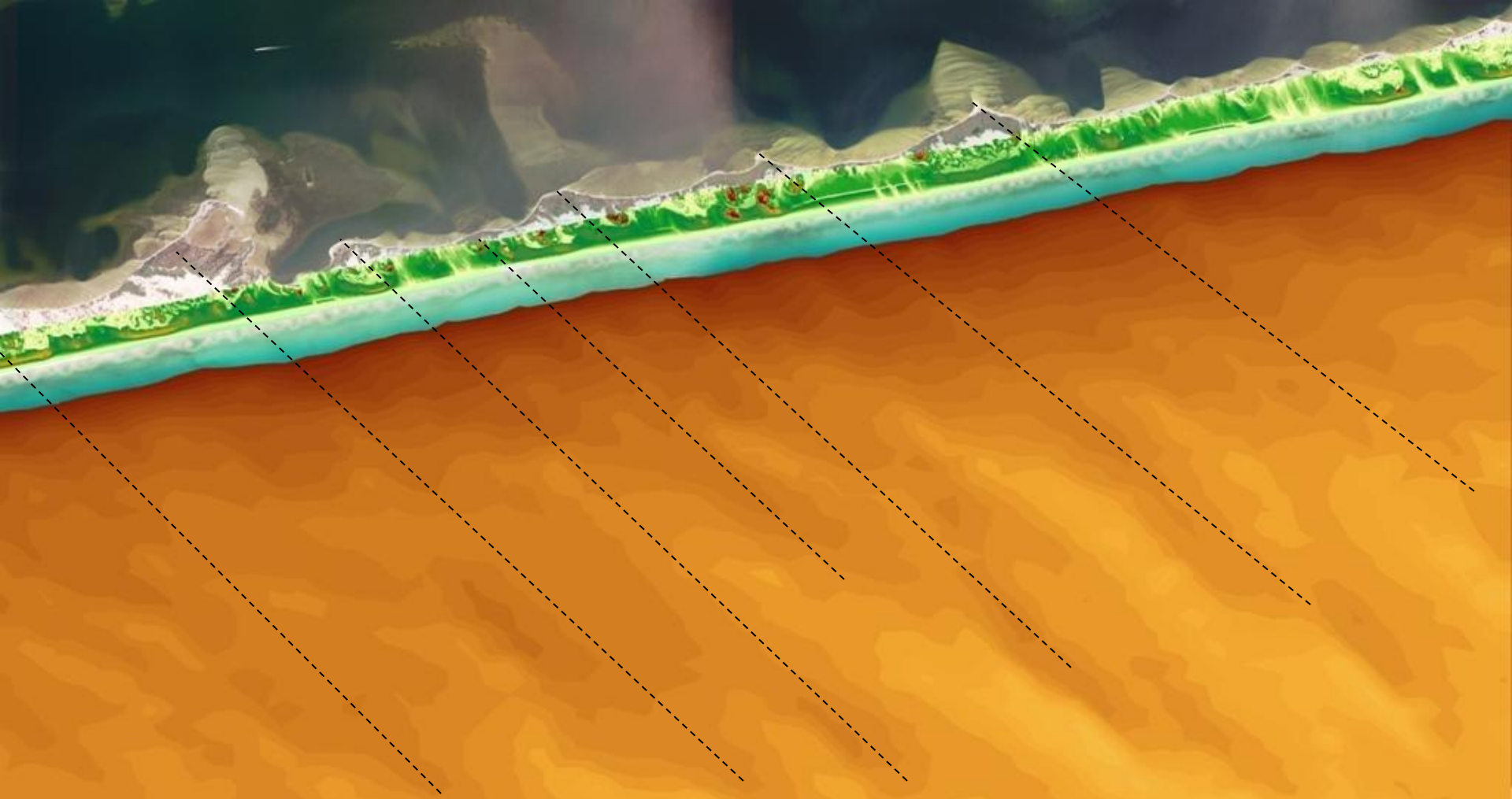
Beach-dune interaction and transgression

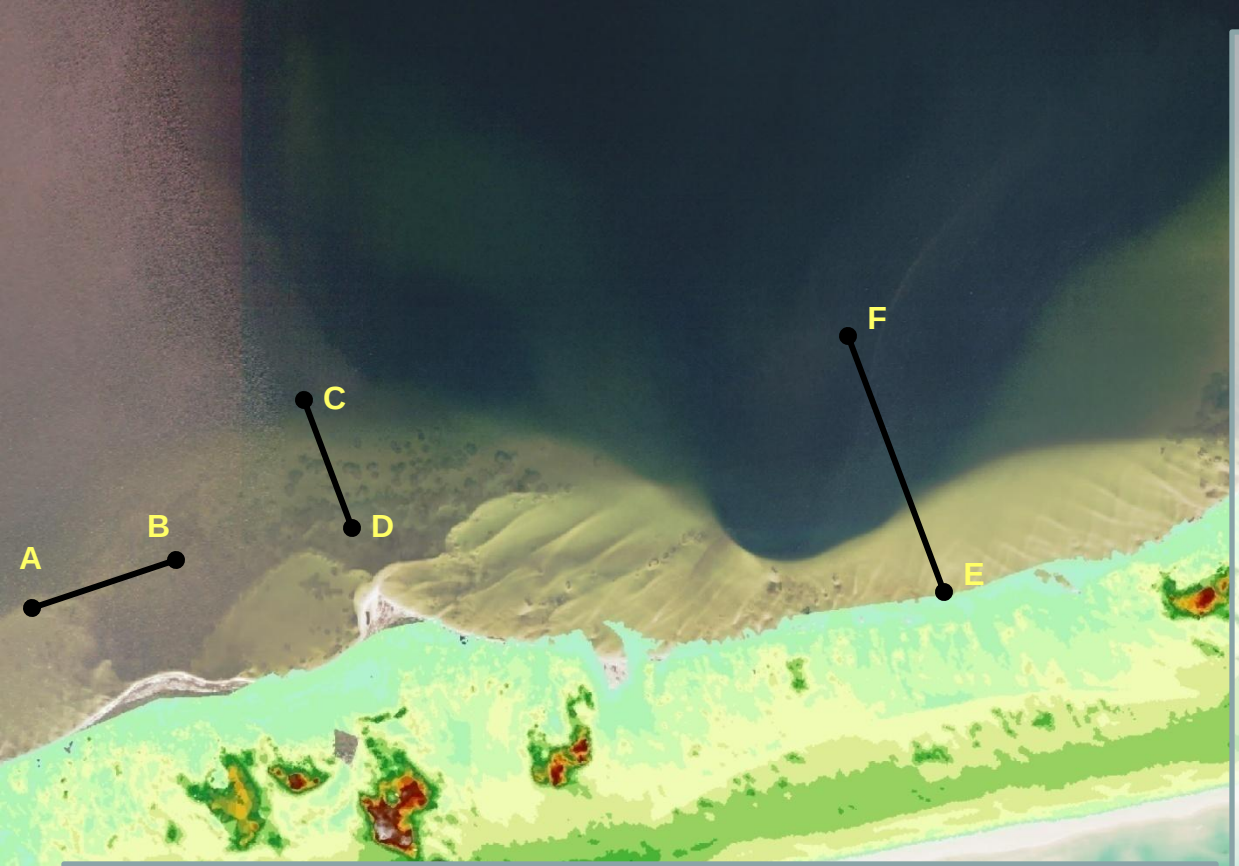


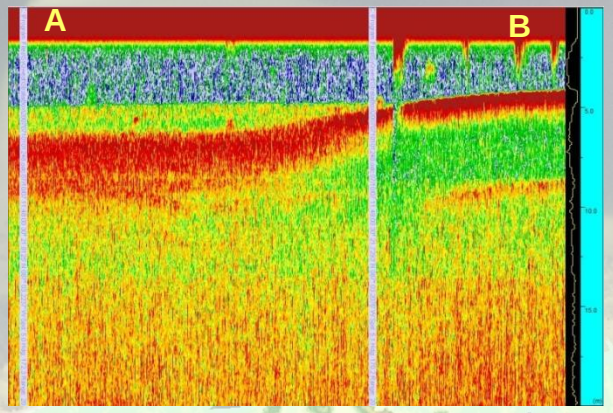
Erosion of washover fans extending into the Sound and deposition at the cuspate headlands by frontal winds



Transgression controlled by
alongshore variation in dune height

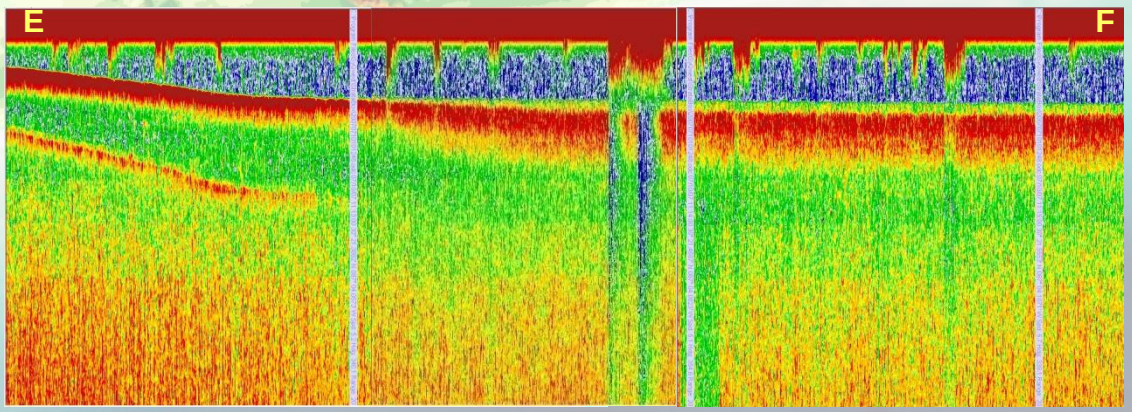


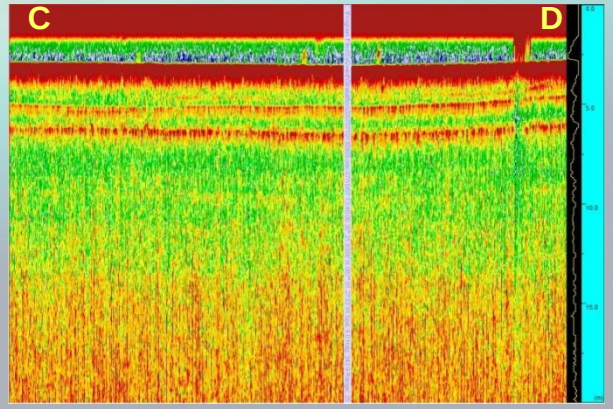




Multiple mud layers layered separated by sand at headlands

Single sand layer between headlands

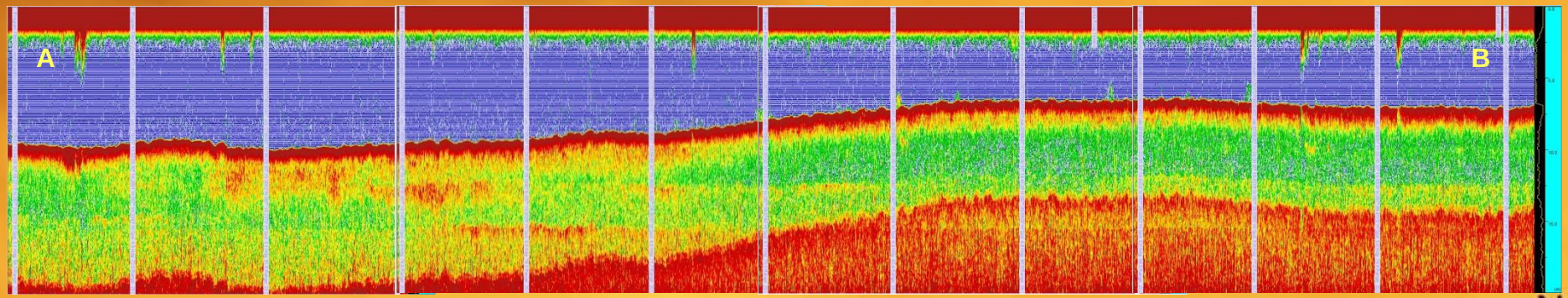




TEXAS A&M UNIVERSITY

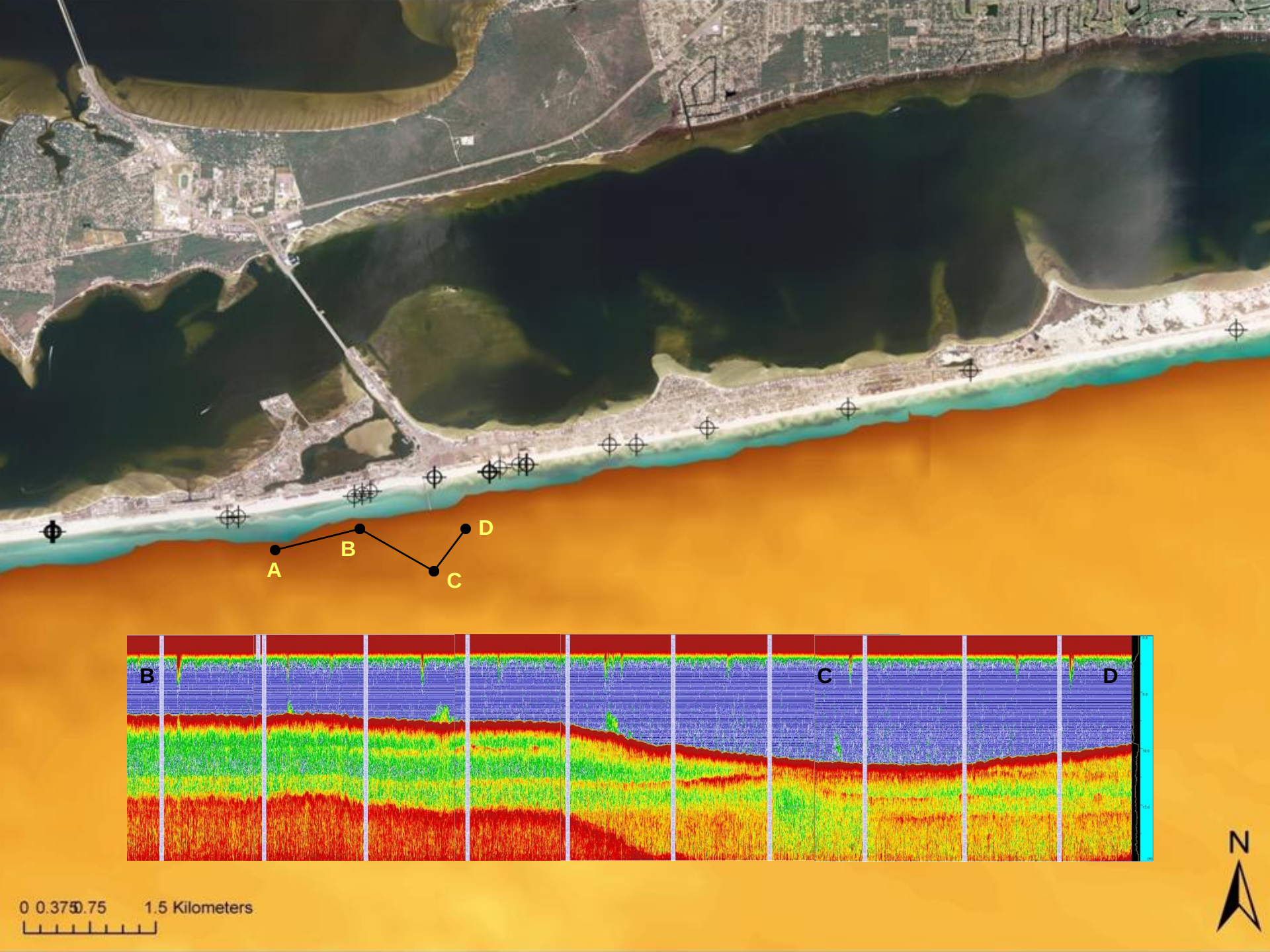
Alongshore Variation in Island Response





N

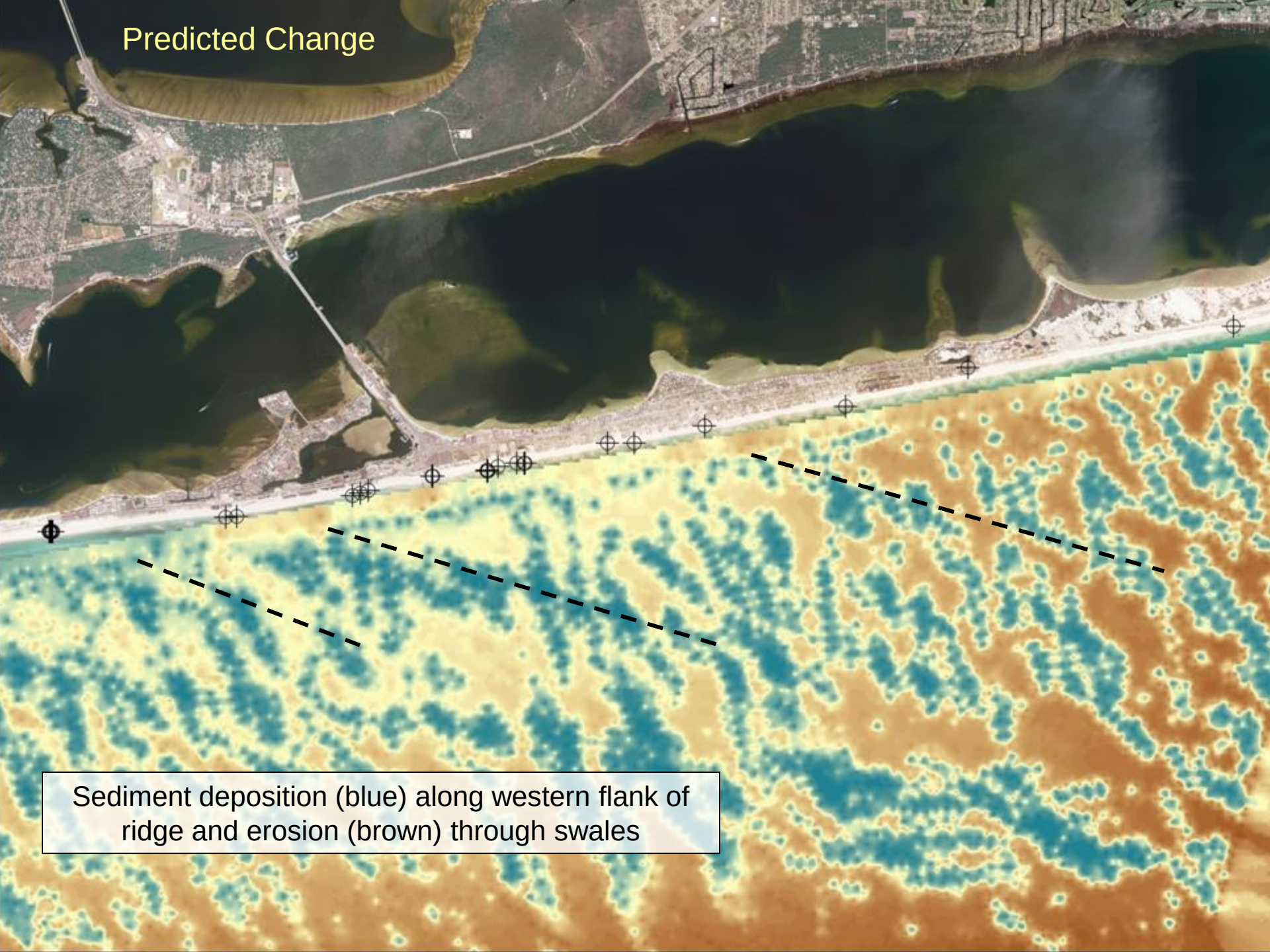
0 0.375 0.75 1.5 Kilometers

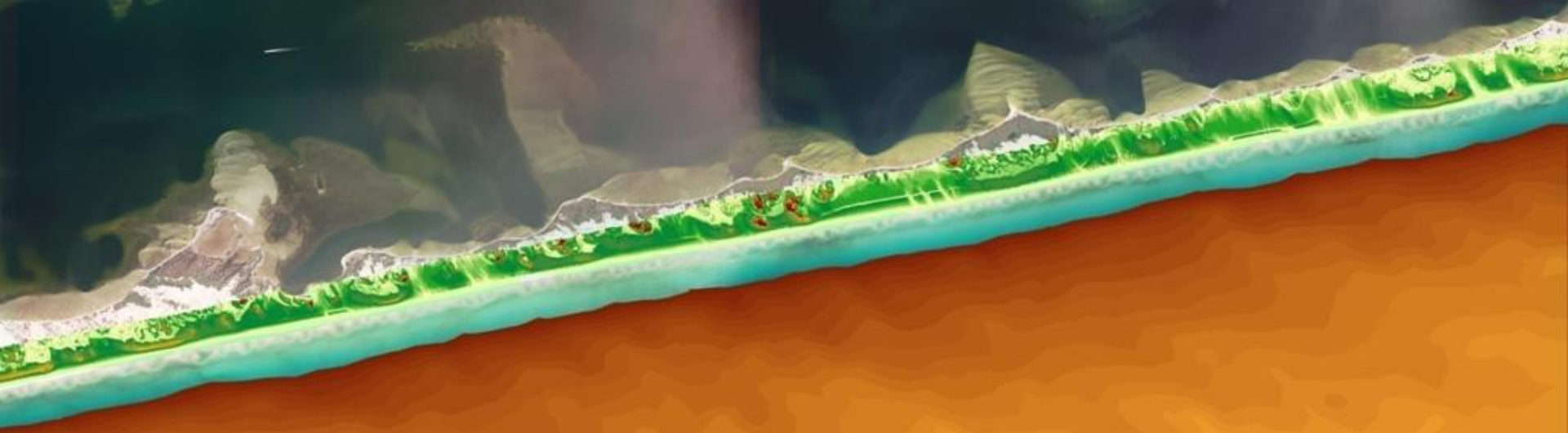

A
B
C
D
B
C
D
0 0.375 0.75 1.5 Kilometers
N

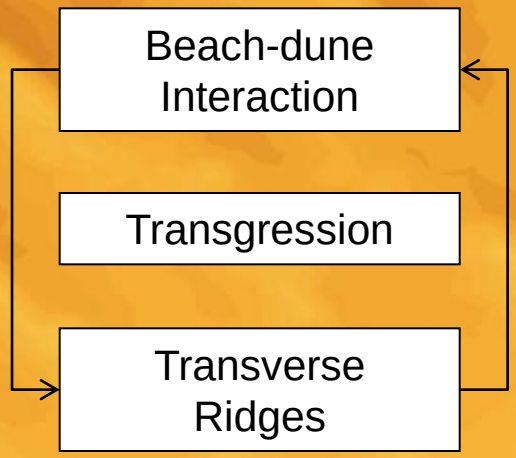


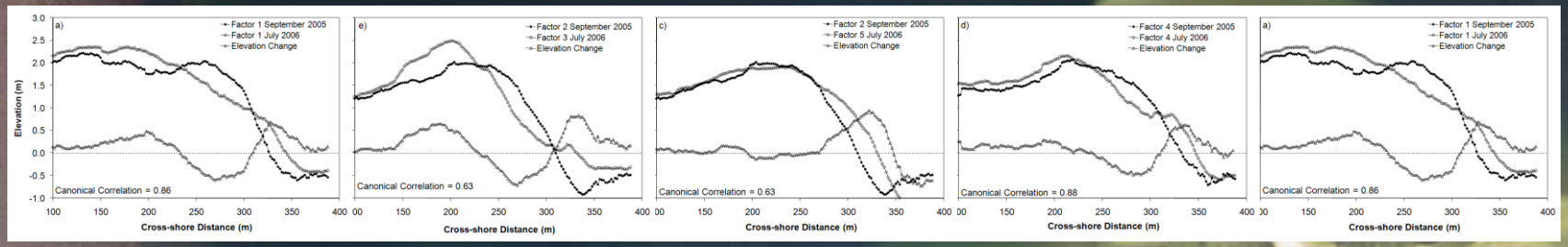
TEXAS A&M UNIVERSITY

Beach-dune interaction and transgression


Predicted Change
Sediment deposition (blue) along western flank of ridge and erosion (brown) through swales




Beach-dune Interaction
Transgression
Transverse Ridges



Not Transport Limited

Transport Limited

Not Transport Limited







TEXAS A&M UNIVERSITY

Beach-dune interaction and transgression


Baia
de Ste Maria
de Galle.
Canal de Bocaynes
Mexicane.



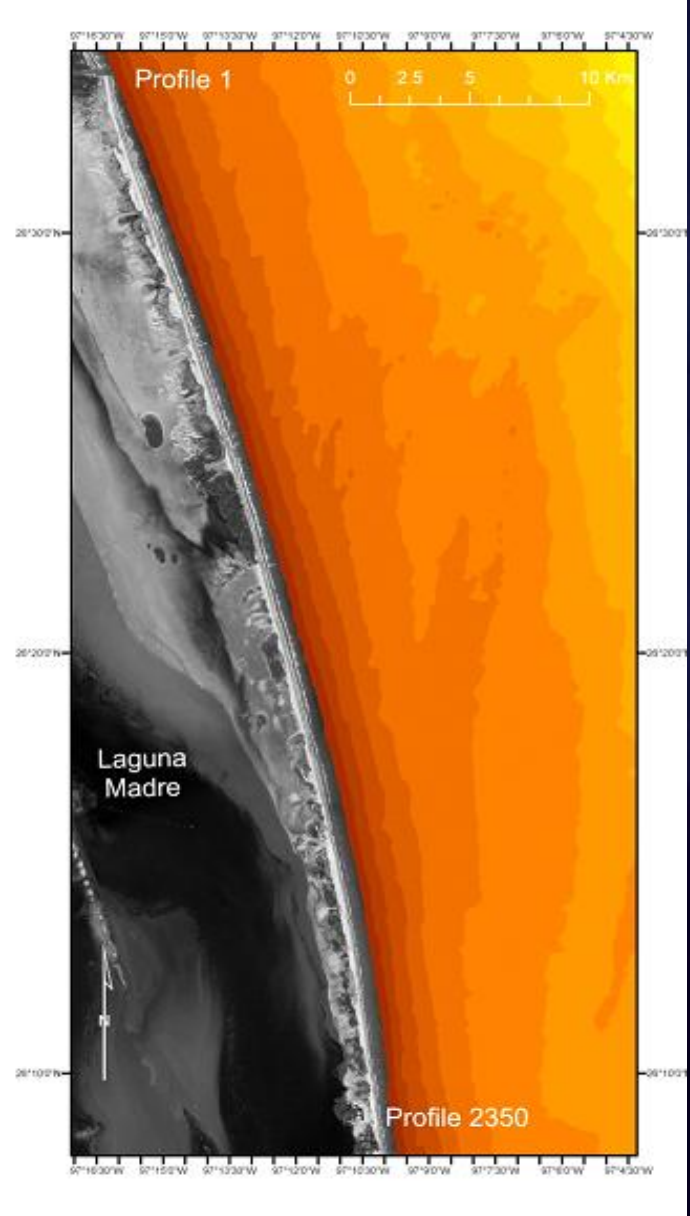
Summary of GUIS

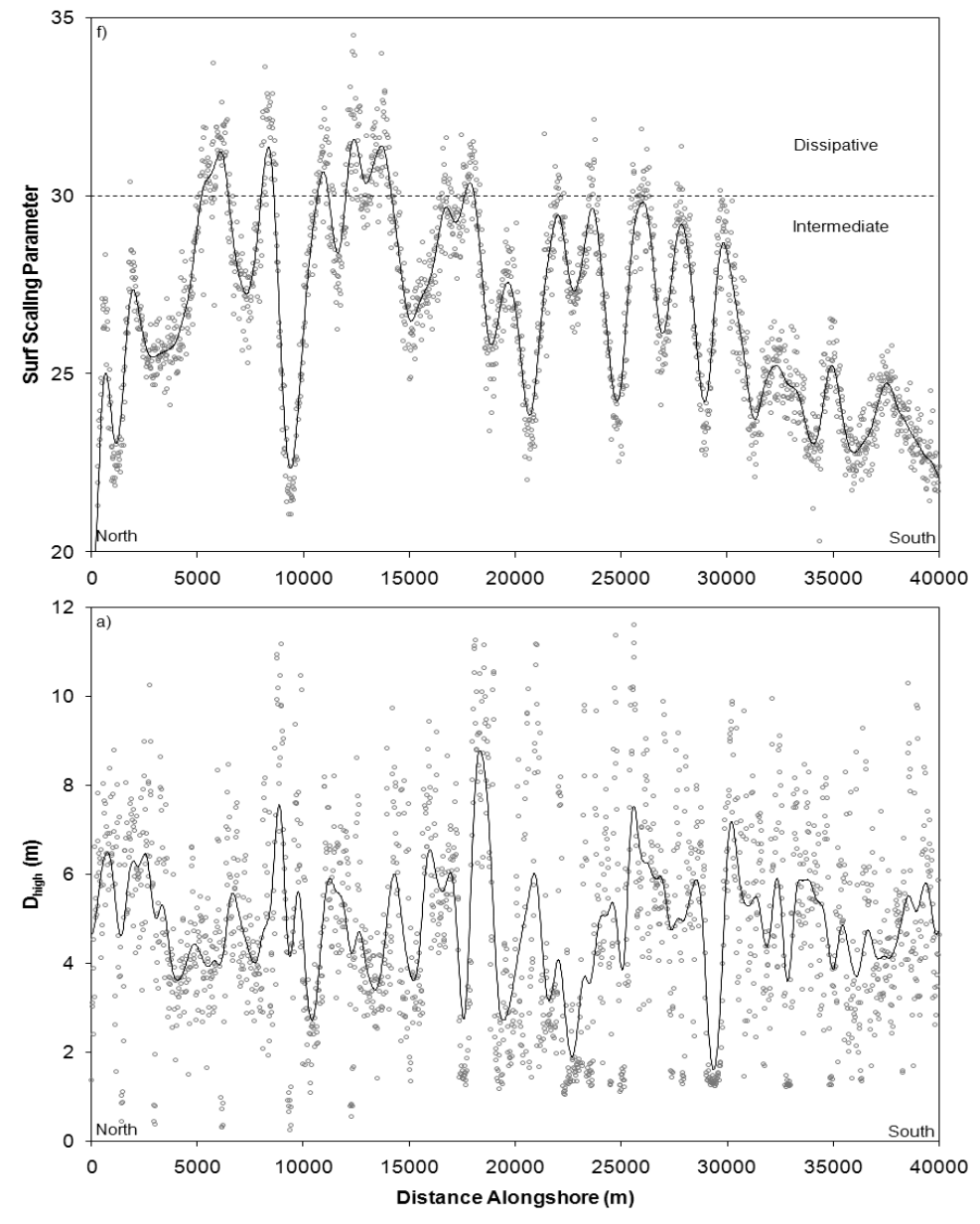
- Alongshore variation in dune morphology and storm response forced by transverse ridges on inner-shelf
- Ridges force wave refraction and focusing that determines local nearshore/beachface state
- Determines both the supply of sediment to the backshore and the aeolian transport potential
- Feedback of short-term aeolian and storm processes with island transgression

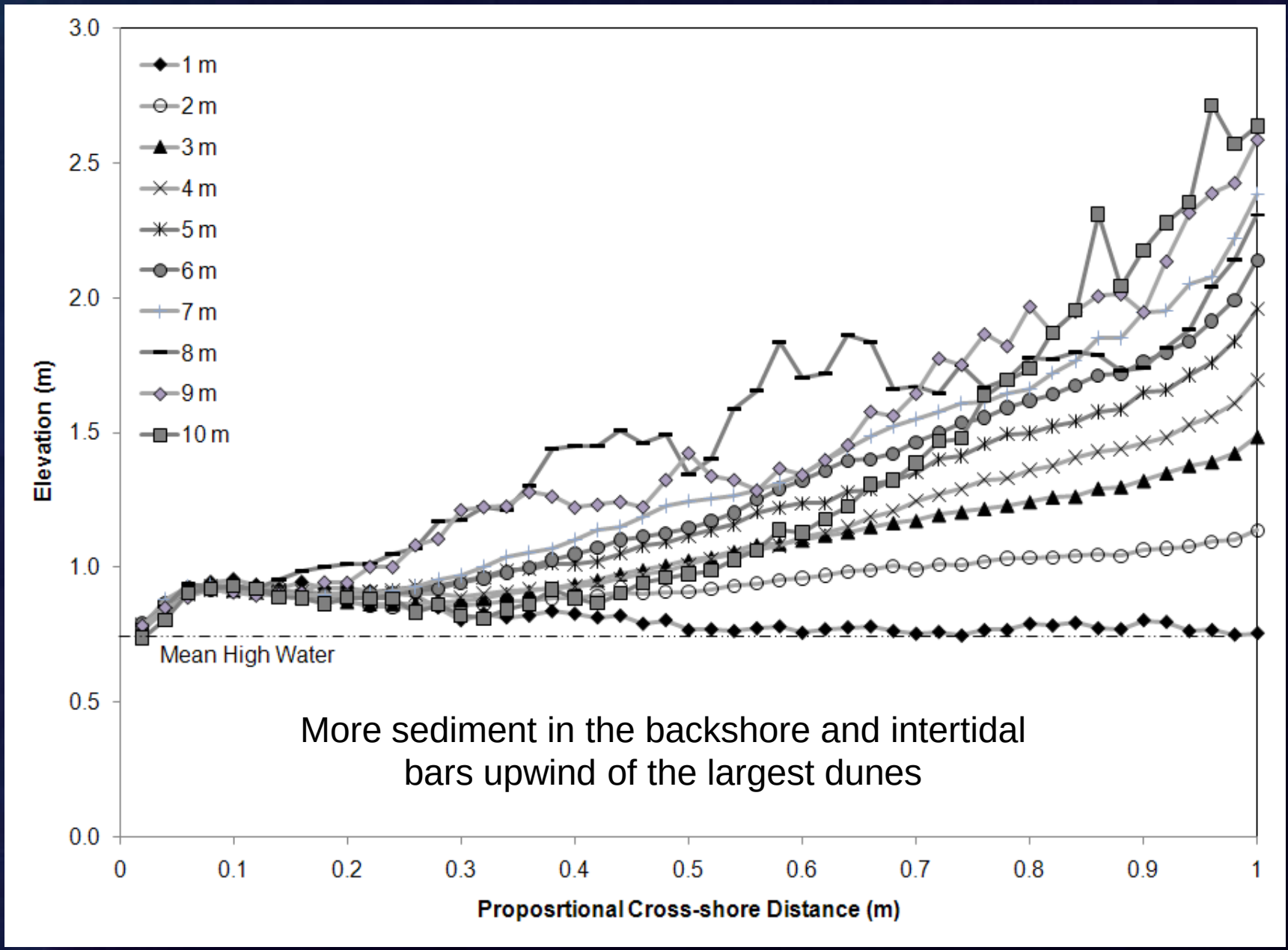
South Padre Island

- Alongshore variation in dune height and extent creates alongshore variations in storm impact and recovery

Houser, C., and Sojan, M. (*in review*) Variability in foredune height depends on the alongshore correspondence of transport potential and sediment supply. Submitted to *Geomorphology*, October 2009.


Profile 1
0 2.5 5 10 Km
Laguna Madre
Profile 2350


f)
Surf Scaling Parameter
Dissipative
Intermediate
North
South
a)
D_{high} (m)
Distance Alongshore (m)


1 m
2 m
3 m
4 m
5 m
6 m
7 m
8 m
9 m
10 m
Elevation (m)
3.0
2.5
2.0
1.5
1.0
0.5
0.0
Mean High Water
More sediment in the backshore and intertidal bars upwind of the largest dunes
0
0.1
0.2
0.3
0.4
0.5
0.6
0.7
0.8
0.9
1
Proposrtional Cross-shore Distance (m)

Summary

Gulf Islands National Seashore

Reflective to Intermediate profile

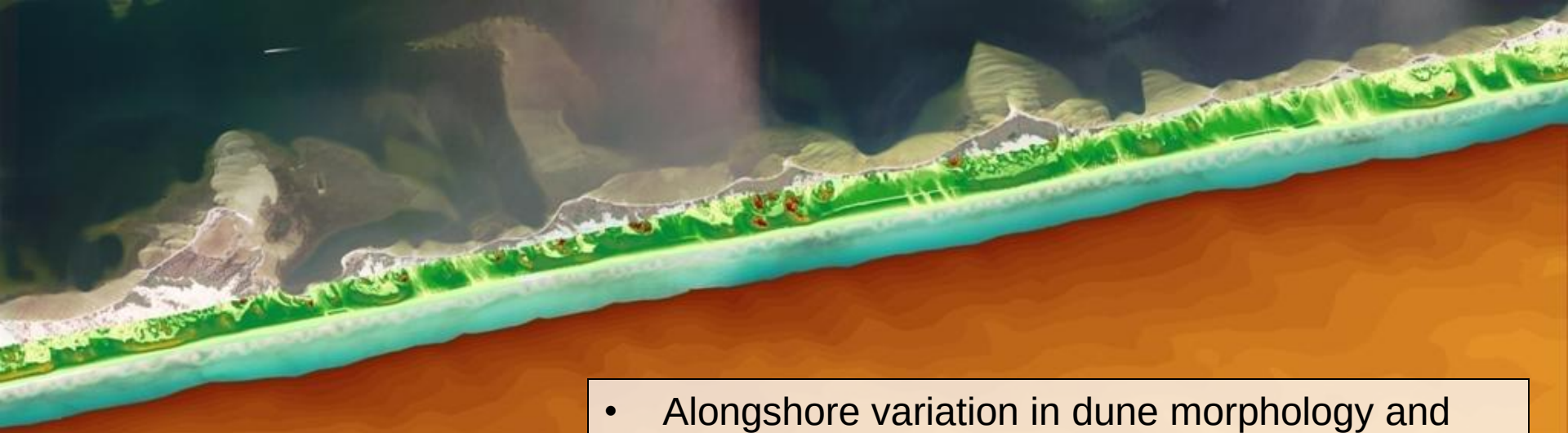
- Largest dunes where the beachface is more gently sloped at ridges
- Smallest dunes where beachface is relatively steep between ridges
- **Transport limited environment**
- Depends on gentle slope to permit transport from beach to dune

Padre Island National Seashore

Intermediate to Dissipative profile

- Largest dunes where the beachface is intermediate between ridges
- Smallest dunes where beachface is dissipative at ridges
- **Supply limited environment**
- Depends on intertidal bar migration and backshore accretion

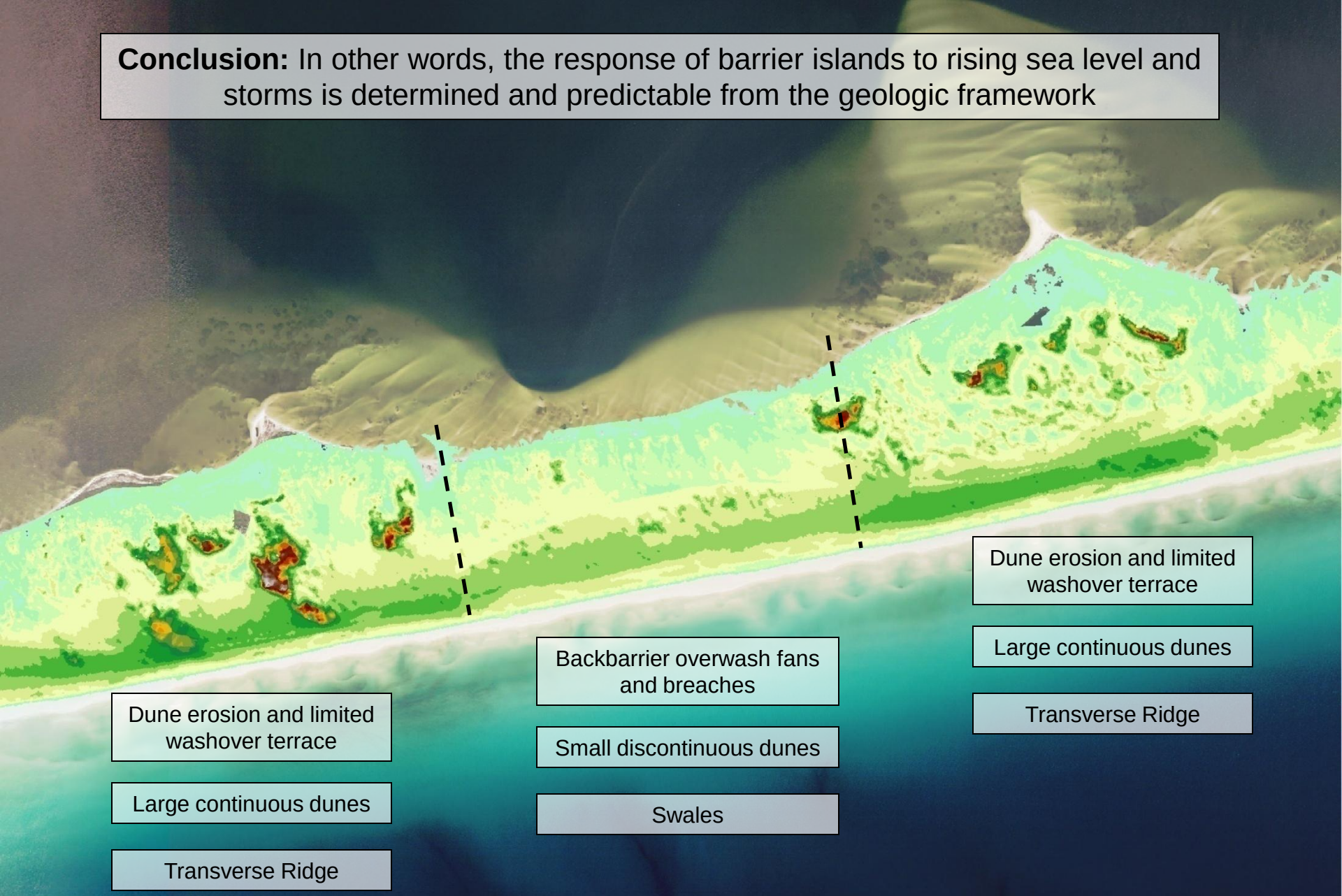
Alongshore alternation between transport and supply limited sites



Summary

- Alongshore variation in dune morphology and storm response forced by transverse ridges on inner-shelf
- Ridges force wave refraction and focusing that determines local nearshore/beachface state
- Determines both the supply of sediment to the backshore and the aeolian transport potential
- Alongshore variable response to sea level rise that is averaged out through alongshore redistribution of sediment

Conclusion: In other words, the response of barrier islands to rising sea level and storms is determined and predictable from the geologic framework



Next Steps

Beach-dune interaction at a range of spatial and temporal scales




Short-term sediment transport



Alongshore variability in beach-dune interaction

Ground-penetrating radar



Next Steps

Synchronization of Transport and Supply PAIS





Linking Island Transgression and Storm Response with Beach-Dune Interaction

Chris Houser
Texas A&M University